BIRKHÄUSER

Integral Methods in Science and Engineering

Techniques and Applications

C. Constanda
S. Potapenko
Editors

Birkhäuser
Boston • Basel • Berlin

C. Constanda
University of Tulsa
Department of Mathematical
and Computer Sciences
600 South College Avenue
Tulsa, OK 74104
USA

S. Potapenko
University of Waterloo
Department of Civil
and Environmental Engineering
200 University Avenue West
Waterloo, ON N2L 3G1
Canada

Cover design by Joseph Sherman, Hamden, CT.

Mathematics Subject Classification (2000): 45-06, 65-06, 74-06, 76-06

Library of Congress Control Number: 2007934436

ISBN-13: 978-0-8176-4670-7 e-ISBN-13: 978-0-8176-4671-4

9 8 7 6 5 4 3 2 1

www.birkhauser.com (IBT)

Contents

Preface

The international conferences with the generic title of Integral Methods in Science and Engineering (IMSE) are a forum where academics and other researchers who rely significantly on (analytic or numerical) integration methods in their investigations present their newest results and exchange ideas related to future projects.

The first two conferences in this series, IMSE1985 and IMSE1990, were held at the University of Texas at Arlington under the chairmanship of Fred Payne. At the 1990 meeting, the IMSE consortium was created for the purpose of organizing these conferences under the guidance of an International Steering Committee. Subsequently, IMSE1993 took place at Tohoku University, Sendai, Japan, IMSE1996 at the University of Oulu, Finland, IMSE1998 at Michigan Technological University, Houghton, MI, USA, IMSE2000 in Banff, AB, Canada, IMSE2002 at the University of Saint-Étienne, France, and IMSE2004 at the University of Central Florida, Orlando, FL, USA. The IMSE conferences have now become recognized as an important platform for scientists and engineers working with integral methods to contribute directly to the expansion and practical application of a general, elegant, and powerful class of mathematical techniques.

A remarkable feature of all IMSE conferences is their socially enjoyable atmosphere of professionalism and camaraderie. Continuing this trend, IMSE2006, organized at Niagara Falls, ON, Canada, by the Department of Civil and Environmental Engineering and the Department of Applied Mathematics of the University of Waterloo, was yet another successful event in the history of the IMSE consortium, for which the participants wish to express their thanks to the Local Organizing Committee:

Stanislav Potapenko (University of Waterloo), *Chairman;*

Peter Schiavone (University of Alberta);

Graham Gladwell (University of Waterloo);

Les Sudak (University of Calgary);

Siv Sivaloganathan (University of Waterloo).

The organizers and the participants also wish to acknowledge the financial support received from the Faculty of Engineering and the Department of Applied Mathematics, University of Waterloo and the Department of Mechanical Engineering, University of Alberta.

The next IMSE conference will be held in July 2008 in Santander, Spain. Details concerning this event are posted on the conference web page, http://www.imse08.unican.es.

This volume contains 2 invited papers and 30 contributed papers accepted after peer review. The papers are arranged in alphabetical order by (first) author's name.

The editors would like to record their thanks to the referees for their willingness to review the papers, and to the staff at Birkhäuser-Boston, who have handled the publication process with their customary patience and efficiency.

Tulsa, Oklahoma, USA *Christian Constanda, IMSE Chairman*

List of Contributors

Mario Ahues
Université de Saint-Étienne
23 rue du Docteur Paul Michelon
42023 Saint-Étienne, France
mario.ahues@univ-st-etienne.fr

Vladimir Ajaev
Southern Methodist University
3200 Dyer Street
Dallas, TX 75275-0156, USA
ajaev@smu.edu

Andrey Amosov
Moscow Power Engineering Institute
(Technical University)
Krasnokazarmennaya 14
Moscow 111250, Russia
amossovandrey@yandex.ru

David M. Barnett
Stanford University
416 Escondido Mall
Stanford, CA 94305-2205, USA
barnett@stanford.edu

Barbara S. Bertram
Michigan Technological University
1400 Townsend Drive
Houghton, MI 49931-1295, USA
bertram@mtu.edu

Bardo E.J. Bodmann
Universidade Federal do Rio Grande
do Sul
Av. Osvaldo Aranha 99/4
Porto Alegre, RS 90046-900, Brazil
bardo.bodmann@ufrgs.br

Daniela Buske
Universidade Federal do Rio Grande
do Sul
Rua Sarmento Leite 425/3
Porto Alegre, RS 90046-900, Brazil
buske@mecanica.ufrgs.br

Haroldo F. de Campos Velho
Instituto Nacional de Pesquisas
Espaciais
PO Box 515
São José dos Campos, SP 12245-970,
Brazil
haroldo@lac.inpe.br

Mariana Cassol
Istituto di Scienze dell'Atmosfera e
del Clima
Str. Prov. di Lecce-Monteroni, km
1200
Lecce I-73100, Italy
cassol@le.isac.cnr.it

Roma Chakrabarti
University of Brighton
Lewes Road
Brighton BN2 4GJ, UK
r.chakrabarti@brighton.ac.uk

David Chappell
University of Brighton
Lewes Road
Brighton BN2 4GJ, UK
d.j.chappell@brighton.ac.uk

Saïd Chergui
Entreprise Nationale des Travaux aux Puits, Direction Engineering
BP 275
Hassi-Messaoud 30500, Algeria
sadchergui@yahoo.fr

Igor Chudinovich
University of Tulsa
600 S. College Avenue
Tulsa, OK 74104-3189, USA
igor-chudinovich@utulsa.edu

Christian Constanda
University of Tulsa
600 S. College Avenue
Tulsa, OK 74104-3189, USA
christian-constanda@utulsa.edu

Dale R. Doty
University of Tulsa
600 S. College Avenue
Tulsa, OK 74104-3189, USA
dale-doty@utulsa.edu

Liselott Flodén
Mittuniversitetet
Akademigatan 1
Östersund, S-831 25, Sweden
lotta.floden@miun.se

Vladimir Gerasik
University of Waterloo
200 University Avenue West
Waterloo, ON N2L 3G1, Canada
vgerasik@uwaterloo.ca

Salim Haidar
Grand Valley State University
1 Campus Drive
Allendale, MI 49401, USA
haidars@gvsu.edu

William Hamill
University of Tulsa
600 S. College Avenue
Tulsa, OK 74104-3189, USA
william-hamill@utulsa.edu

Carl Hardwidge
Princess Royal Hospital
Lewes Road
Haywards Heath RH16 4EX, UK
carl.hardwidge@bsuh.nhs.uk

Paul J. Harris
University of Brighton
Lewes Road
Brighton BN2 4GJ, UK
p.j.harris@brighton.ac.uk

David Henwood
University of Brighton
Lewes Road
Brighton BN2 4GJ, UK
davidhenwood@talk21.com

John W. Hilgers
Signature Research, Inc.
56905 Calumet Avenue
Calumet, MI 49913, USA
jwhilgers@mtu.edu

Anders Holmbom
Mittuniversitetet
Akademigatan 1
Östersund, S-831 25, Sweden
anders.holmbom@miun.se

Huaxiong Huang
York University
4700 Keele Street
Toronto, ON M3J 1P3, Canada
hhuang@yorku.ca

Jukka Kemppainen
University of Oulu
PO Box 4500
90550 Oulu, Finland
jukemppa@oulu.fi

Kunquan Lan
Ryerson University
350 Victoria Street
Toronto, ON M5B 2K3, Canada
klan@ryerson.ca

Alain Largillier
Université de Saint-Étienne
23 rue du Docteur Paul Michelon
42023 Saint-Étienne, France
largillier@univ-st-etienne.fr

Balmohan V. Limaye
Indian Institute of Technology
Bombay
Powai
Mumbai 400076, India
bvl@iitb.ac.in

Sergey E. Mikhailov
Brunel University West London
John Crank Building
Uxbridge UB8 3PH, UK
sergey.mikhailov@brunel.ac.uk

Dorina Mitrea
University of Missouri
202 Math Science Building
Columbia, MO 65211-4100, USA
dorina@math.missouri.edu

Davidson M. Moreira
Universidade Federal de Pelotas
Rua Carlos Barbosa s/n
Bagé, RS 96412-420, Brazil
davidson@mecanica.ufrgs.br

Marianne Olsson
Mittuniversitetet
Akademigatan 1
Östersund, S-831 25, Sweden
marianne.olsson@miun.se

M. Eugenia Pérez
Universidad de Cantabria
Av. de los Castros s/n
39005 Santander, Spain
meperez@unican.es

Gianpietro Del Piero
Università di Ferrara
Via Saragat 1
Ferrara 44100, Italy
dlpgpt@unife.it

Peter M. Pinsky
Stanford University
496 Lomita Mall
Stanford, CA 94305-4040, USA
pinsky@stanford.edu

Shirley Pomeranz
University of Tulsa
600 S. College Avenue
Tulsa, OK 74104-3189, USA
pomeranz@utulsa.edu

Stanislav Potapenko
University of Waterloo
200 University Avenue West
Waterloo, ON N2L 3G1, Canada
spotapen@civmail.uwaterloo.ca

María-Luisa Rapún
Universidad Politécnica de Madrid
Cardinal Cisneros 3
Madrid 28040, Spain
marialuisa.rapun@upm.es

William R. Reynolds
Signature Research, Inc.
56905 Calumet Avenue
Calumet, MI 49913, USA
reynolds@signatureresearchinc.com

Raffaella Rizzoni
Università di Ferrara
Via Saragat 1
Ferrara 44100, Italy
rzzrfl@unife.it

Keijo Ruotsalainen
University of Oulu
PO Box 4500
90550 Oulu, Finland
keijo.ruotsalainen@ee.oulu.fi

Francisco-Javier Sayas
Universidad de Zaragoza
CPS María de Luna 3
Zaragoza 50018, Spain
jsayas@unizar.es

Patrick Selvadurai
McGill University
817 Sherbrooke Street West
Montreal, QC H3A 2K6, Canada
patrick.selvadurai@mcgill.ca

Yongxing Shen
Stanford University
496 Lomita Mall
Stanford, CA 94305-4040, USA
shenyx@stanford.edu

Lili Shi
Chengdu University of Information Technology
Xue Fu Road 24, Block 1
Chengdu, Sichuan 610225, PR China
shili119@126.com

Elena Shmoylova
Tufts University
200 College Avenue
Medford, MA 02155, USA
elena.shmoylova@tufts.edu

Marianna Shubov
University of New Hampshire
33 College Road
Durham, NH 03824, USA
marianna.shubov@euclid.unh.edu

Ronald M.C. So
Hong Kong Polytechnic University
Hung Hom, Kowloon
Hing Kong
mmmcso@polyu.edu.hk

Marek Stastna
University of Waterloo
200 University Avenue West
Waterloo, ON N2L 3G1, Canada
mmstastn@uwaterloo.ca

Shu Takagi
University of Tokyo
7-3-1 Hongo, Bunkyo-ku
Tokyo 113-8656, Japan
takagi@mech.t.u-tokyo.ac.jp

Johannes Tausch
Southern Methodist University
3200 Dyer Street
Dallas, TX 75275-0156, USA
tausch@smu.edu

Tiziano Tirabassi
Istituto di Scienze dell'Atmosfera e del Clima
Via P. Gobetti 101
Bologna 40129, Italy

Naveen K. Vaidya
York University
4700 Keele Street
Toronto, ON M3J 1P3, Canada
nvaidya@mathstat.yorku.ca

Marco T. de Vilhena
Universidade Federal do Rio Grande do Sul
Rua Sarmento Leite 425/3
Porto Alegre, RS 90046-900, Brazil
vilhena@pq.cnpq.br

Sergio Wortmann
Universidade Federal do Rio Grande do Sul
Rua Ramiro Barcelos 2777-Santana
Porto Alegre, RS 90035-007, Brazil
wortmann@mat.ufrgs.br

Wei-Chau Xie
University of Waterloo
200 University Avenue West
Waterloo, ON N2L 3G1, Canada
xie@uwaterloo.ca

Guanchong Yang
Chengdu University of Information Technology
Xue Fu Road 24, Block 1
Chengdu, Sichuan 610225, PR China
gcyang@cuit.edu.cn

Jinyu Zhu
University of Waterloo
200 University Avenue West
Waterloo, ON N2L 3G1, Canada
j7zhu@engmail.uwaterloo.ca

1

Superconvergence of Projection Methods for Weakly Singular Integral Operators

M. Ahues[1], A. Largillier[1], and A. Amosov[2]

[1] Université de Saint-Étienne, France; mario.ahues@univ-st-etienne.fr, largillier@univ-st-etienne.fr
[2] Moscow Power Engineering Institute (Technical University), Moscow, Russia; amossovandrey@yandex.ru

1.1 Introduction

In [AALT05], the authors proposed error bounds for the discretization error corresponding to the Kantorovich projection approximation $\pi_h T$ of a linear, compact, weakly singular integral operator T defined in the functional Lebesgue space $L^p(0, \tau_*)$ for some $p \in [1, +\infty]$. The equation to be solved is $\varphi = T\varphi + f$, where f is a given function lying in the space $L^p(0, \tau_*)$. Here, π_h is a family of projections onto the piecewise constant function subspace of $L^p(0, \tau_*)$ and it is pointwise convergent to the identity operator. The error estimates in that article were significant for sufficiently regular grids in the sense that they grew to infinity if the ratio between the biggest and the smallest step of the mesh went to zero. In this chapter, we discuss four numerical solutions based on such a family of projections. We obtain accurate error estimates that are independent of the length τ_* of the interval where f and the solution φ are defined, and we suggest global superconvergence phenomena in the sense of [Sloa82]. Particular attention is given to the transfer equation occurring in astrophysical mathematical models of stellar atmospheres. In that context, τ_* represents the optical depth of the star's atmosphere and the operator T has a multiplicative factor ω_0 representing the albedo. The error bounds are given explicitly in terms of this parameter.

1.2 General Facts

We state the problem in the following terms: Given $\tau_* > 0$, $\omega_0 \in [0, 1[$, g such that

$g(0^+) = +\infty$,
g is continuous, positive and decreasing on $]0, \infty[$,
$g \in L^r(\mathbb{R}) \cap W^{1,r}(\delta, +\infty)$ for all $r \in [1, \infty[$ and all $\delta > 0$,
$\|g\|_{L^1(\mathbb{R}^+)} \leq \frac{1}{2}$,

and a function f, find a function φ such that

$$\varphi(\tau) = \omega_0 \int_0^{\tau_*} g(|\tau - \tau'|)\varphi(\tau')\, d\tau' + f(\tau), \quad \tau \in [0, \tau_*].$$

As an example, we consider the transfer equation

$$\varphi(\tau) = \frac{\omega_0}{2} \int_0^{\tau_*} E_1(|\tau - \tau'|)\varphi(\tau')\, d\tau' + f(\tau), \quad \tau \in [0, \tau_*],$$

where

$$E_1(\tau) := \int_0^1 \mu^{-1} e^{-\tau/\mu}\, d\mu, \quad \tau > 0,$$

the source term f belongs to $L^1(0, \tau_*)$, the optical depth τ_* is a very large number, and the albedo ω_0 may be very close to 1. For details, see [Busb60].

The goal of this chapter is as follows: For a class of four numerical solutions based on projections, find accurate error estimates that

1. are independent of the grid regularity,
2. are independent of τ_*,
3. depend on ω_0 in an explicit way,
4. suggest global superconvergence phenomena in the sense of [Sloa82].

As an abstract framework for the subsequent development, we choose the following: Set

$$(\Lambda\varphi)(\tau) := \int_0^{\tau_*} g(|\tau - \tau'|)\varphi(\tau')\, d\tau', \quad \tau \in [0, \tau_*],$$

and let X and Y be suitable Banach spaces. The problem reads as follows: For $f \in Y$, find $\varphi \in X$ such that

$$\varphi = \omega_0 \Lambda\varphi + f.$$

We remark that

$$\|(I - \omega_0 \Lambda)^{-1}\| \leq \gamma_0 := \frac{1}{1 - \omega_0},$$

where the equality is attained for $X = Y = L^2(0, \infty)$.

1.3 Projection Approximations

We consider a family of projections onto piecewise constant functions. Let be a grid of $n+1$ points in $[0,\tau_*]$:

$$0 =: \tau_0 < \tau_1 < \ldots < \tau_{n-1} < \tau_n := \tau_*,$$

and define

$$\begin{aligned} h_i &:= \tau_i - \tau_{i-1}, \quad i \in [\![1,n]\!], \\ h &:= (h_1, h_2, \ldots, h_n), \\ \mathcal{G}^h &:= (\tau_0, \tau_1, \ldots, \tau_n), \\ \hat{h} &:= \max_{i\in[\![1,n]\!]} h_i, \\ \mathcal{I}_{i-\frac{1}{2}} &:=]\tau_{i-1}, \tau_i[, \quad i \in [\![1,n]\!], \\ \tau_{i-\frac{1}{2}} &:= (\tau_{i-1}+\tau_i)/2, \quad i \in [\![1,n]\!]. \end{aligned}$$

The approximating space $\mathbb{P}^h_{\,0}(0,\tau_*)$ is characterized by

$$f \in \mathbb{P}^h_{\,0}(0,\tau_*) \iff \forall i \in [\![1,n]\!], \forall \tau \in \mathcal{I}_{i-\frac{1}{2}}, f(\tau) = f(\tau_{i-\frac{1}{2}}).$$

In what follows,

$$p \in [1,+\infty] := [1,+\infty[\cup \{+\infty\}$$

is arbitrary but fixed once for all.

The family of projections

$$\pi_h : L^p(0,\tau_*) \to L^p(0,\tau_*)$$

is defined as follows:

For all $i \in [\![1,n]\!]$ and all $\tau \in \mathcal{I}_{i-\frac{1}{2}}$,

$$(\pi_h\varphi)(\tau) := \frac{1}{h_i}\int_{\tau_{i-1}}^{\tau_i} \varphi(\tau')\,d\tau'.$$

Hence

$$\pi_h(L^p(0,\tau_*)) = \mathbb{P}^h_{\,0}(0,\tau_*).$$

Four approximations based on π_h are considered:

1. The classical Galerkin approximation φ_h^{G}, which solves

$$\varphi_h^{\mathrm{G}} = \omega_0 \pi_h \Lambda \varphi_h^{\mathrm{G}} + \pi_h f.$$

2. The Sloan approximation φ_h^{S} (iterated Galerkin), which solves

$$\varphi_h^{\mathrm{S}} = \omega_0 \Lambda \pi_h \varphi_h^{\mathrm{S}} + f.$$

3. The Kantorovich approximation φ_h^{K}, which solves
$$\varphi_h^{\mathrm{K}} = \omega_0 \pi_h \Lambda \varphi_h^{\mathrm{K}} + f.$$
4. The authors' approximation φ_h^{A} (iterated Kantorovich), which solves
$$\varphi_h^{\mathrm{A}} = \omega_0 \Lambda \pi_h \varphi_h^{\mathrm{A}} + f + \omega_0 \Lambda (I - \pi_h) f.$$

Remark 1. The following relationships and facts are important and easy to check:

$\varphi_h^{\mathrm{G}} \in \mathbb{P}_0^h(0, \tau_*)$.
φ_h^{G} is computed through an algebraic linear system.
$\varphi_h^{\mathrm{S}} = \omega_0 \Lambda \varphi_h^{\mathrm{G}} + f$.
If $\psi_h = \omega_0 \pi_h \Lambda \psi_h + \pi_h \Lambda f$, then $\varphi_h^{\mathrm{K}} = \omega_0 \psi_h + f$.
If $\phi_h = \omega_0 \Lambda \pi_h \phi_h + \Lambda f$, then $\varphi_h^{\mathrm{A}} = \omega_0 \phi_h + f$.

1.4 Superconvergence

Superconvergence is understood with respect to $\mathrm{dist}(\varphi, \mathbb{P}_0^h(0, \tau_*))$.

Theorem 1. *In any Hilbert space setting, there exists α such that*
$$\|\varphi - \pi_h \varphi\| \le \|\varepsilon_h^{\mathrm{G}}\| \le \alpha \|\varphi - \pi_h \varphi\|.$$

We now present some useful technical notions and the main result. Define
$$\begin{aligned}
\Delta_\epsilon g(\tau) &:= g(\tau + \epsilon) - g(\tau), \\
\omega_r(g, \delta) &:= \sup_{0 < \epsilon \le \delta} \|\Delta_\epsilon g(|\cdot|)\|_{L^r(\mathbb{R})}, \\
\omega_\infty(g, \delta) &:= \operatorname*{essup}_{|\tau - \tau'| \le \delta} |g(\tau) - g(\tau')|,
\end{aligned}$$
and for $\alpha \in [0,1]$ and $i \in [\![1, n]\!]$:
$$\begin{aligned}
\Delta_\alpha^h f(\tau) &:= \begin{cases} \Delta_{\alpha h_i} f(\tau) & \text{for } \tau \in [\tau_{i-1}, \tau_i - \alpha h_i], \\ 0 & \text{for } \tau \in]\tau_i - \alpha h_i, \tau_i], \end{cases} \\
\omega_p(f, \mathcal{G}^h) &:= 2^{\frac{1}{p}} \Big[\int_0^1 \|\Delta_\alpha^h f\|_p^p \, d\alpha \Big]^{\frac{1}{p}}, \\
\widehat{\omega}_p(g, \mathcal{G}^h) &:= \sup_{0 < \tau' < \tau_*} \omega_p(g(|\cdot - \tau'|, \mathcal{G}^h) \text{ for } p \in [1, \infty[, \\
\omega_\infty(f, \mathcal{G}^h) &:= \max_{i \in [\![1,n]\!]} \operatorname*{essup}_{\tau, \tau' \in \mathcal{I}_{i-\frac{1}{2}}} |f(\tau) - f(\tau')|.
\end{aligned}$$

For $\mathrm{N} \in \{\mathrm{G}, \mathrm{K}, \mathrm{S}, \mathrm{A}\}$, we consider the absolute discretization error
$$\varepsilon_h^{\mathrm{N}} := \varphi_h^{\mathrm{N}} - \varphi.$$

The main result is as follows.

Theorem 2. *If $0 \neq f \in L^p(0,\tau_*)$ for some $p \in [1,+\infty]$, then a unique solution φ exists and satisfies $0 \neq \varphi \in L^p(0,\tau_*)$. Moreover, the discretization errors are such that*

$$\frac{\|\varepsilon_h^{\mathrm{K}}\|_p}{\|\varphi\|_p} \leq 4 \cdot 3^{\frac{1}{p}} \omega_0 \gamma_0 \int_0^{\hat{h}} g(\tau)\, d\tau,$$
$$\frac{\|\varepsilon_h^{\mathrm{S}}\|_p}{\|\varphi\|_p} \leq 12 \cdot 3^{-\frac{1}{p}} \omega_0 \gamma_0 \int_0^{\hat{h}} g(\tau)\, d\tau,$$
$$\frac{\|\varepsilon_h^{\mathrm{A}}\|_p}{\|\varphi\|_p} \leq 48 \omega_0^2 \gamma_0 \Big[\int_0^{\hat{h}} g(\tau)\, d\tau \Big]^2.$$

A proof of this result may be given considering four steps:

1. Establish the following estimate:
   For all $f \in L^p(0,\tau_*)$,

$$\|(I-\pi_h)f\|_p \leq \omega_p(f, \mathcal{G}^h).$$

   The proof is technical.
   Let $f \in L^p(0,\tau_*)$. For all $i \in [\![1,n]\!]$ and $\tau \in \mathcal{I}_{i-1/2}$,

$$(I-\pi_h)f(\tau) = \frac{1}{h_i} \int_{\tau_{i-1}}^{\tau_i} (f(\tau) - f(\tau'))\, d\tau'.$$

   If $p < \infty$, then

$$\begin{aligned}
\int_{\tau_{i-1}}^{\tau_i} |(I-\pi_h)f(\tau)|^p\, d\tau &\leq \int_{\tau_{i-1}}^{\tau_i} \Big[\frac{1}{h_i} \int_{\tau_{i-1}}^{\tau_i} |f(\tau') - f(\tau)|\, d\tau' \Big]^p d\tau \\
&\leq \frac{1}{h_i} \int_{\tau_{i-1}}^{\tau_i} \Big[\int_{\tau_{i-1}}^{\tau_i} |f(\tau') - f(\tau)|^p d\tau' \Big] d\tau \\
&= \frac{2}{h_i} \int_{\tau_{i-1}}^{\tau_i} \Big[\int_{\tau}^{\tau_i} |f(\tau') - f(\tau)|^p d\tau' \Big] d\tau \\
&= 2 \int_{\tau_{i-1}}^{\tau_i} \Big[\int_0^{(\tau_i - \tau)/h_i} |f(\tau + \alpha h_i) - f(\tau)|^p d\alpha \Big] d\tau \\
&= 2 \int_0^1 \Big[\int_{\tau_{i-1}}^{\tau_i - \alpha h_i} |\Delta_{\alpha h_i} f(\tau)|^p d\tau \Big] d\alpha.
\end{aligned}$$

   As a consequence,

$$\|(I-\pi_h)f\|_p^p \le 2\sum_{i=1}^{n}\int_0^1 \Big[\int_{\tau_{i-1}}^{\tau_i-\alpha h_i} |\Delta_{\alpha h_i} f(\tau)|^p d\tau'\Big] d\alpha = \omega_p(f,\mathcal{G}^h)^p.$$

If $p=\infty$, the proof is elementary.

2. Show that

$$\frac{\|\varepsilon_h^{\mathrm{K}}\|_p}{\|\varphi\|_p} \le \|(I-\pi_h)\Lambda\|_p,$$
$$\frac{\|\varepsilon_h^{\mathrm{S}}\|_p}{\|\varphi\|_p} \le \|\Lambda(I-\pi_h)\|_p,$$
$$\frac{\|\varepsilon_h^{\mathrm{A}}\|_p}{\|\varphi\|_p} \le \|\Lambda(I-\pi_h)\Lambda\|_p.$$

3. Prove that

$$\|(I-\pi_h)\Lambda\|_p \le \omega_1(g,\hat{h})^{1-\frac{1}{p}}\widehat{\omega}_1(g,\mathcal{G}^h)^{\frac{1}{p}},$$
$$\|\Lambda(I-\pi_h)\|_p \le \omega_1(g,\hat{h})^{\frac{1}{p}}\widehat{\omega}_1(g,\mathcal{G}^h)^{1-\frac{1}{p}},$$
$$\|\Lambda(I-\pi_h)\Lambda\|_p \le \omega_1(g,\hat{h})\widehat{\omega}_1(g,\mathcal{G}^h).$$

4. Demonstrate that

$$\omega_1(g,\hat{h}) \le 4\int_0^{\hat{h}} g(\tau)\,d\tau,$$
$$\widehat{\omega}_1(g,\mathcal{G}^h) \le 12\int_0^{\hat{h}} g(\tau)\,d\tau.$$

Remark 2. If the kernel is $g := \frac{1}{2}E_1$, then, as $\hat{h}\to 0^+$,

$$\int_0^{\hat{h}} g(\tau)\,d\tau = O(\hat{h}\ln\hat{h}).$$

1.5 Numerical Evidence

Let us consider the following data:

1. The kernel: $g := \frac{1}{2}E_1$.
2. The albedo: $\omega_0 = 0.5$.
3. The optical depth: $\tau_* = 500$.
4. A constant source term: $f(\tau) = 0.5$ for all $\tau \in [0,\tau_*]$.
5. The number of grid points: $n = 1000$.
6. The first 5 points equally spaced by 0.1.
7. The last 5 points equally spaced by 0.1.

8. A uniform grid with 990 points between 0.5 and 499.5 so

$$\hat{h} = 0.5\overline{04}.$$

Figure 1.1 shows the residual functions

$$\varrho_h^{\mathrm{N}} := \varphi_h^{\mathrm{N}} - \omega_0 \Lambda \varphi_h^{\mathrm{N}} - f, \quad \mathrm{N} \in \{\mathrm{K}, \mathrm{A}\},$$

in the subinterval $[0, 5]$ of the whole atmosphere $[0, 500]$.

Since in any normed linear context the relative residuals $\dfrac{\|\varrho_h^{\mathrm{N}}\|}{\|f\|}$ are of the order of the relative errors $\dfrac{\|\varepsilon_h^{\mathrm{N}}\|}{\|\varphi\|}$, the numerical results show that the theoretical majorizations are sharp enough.

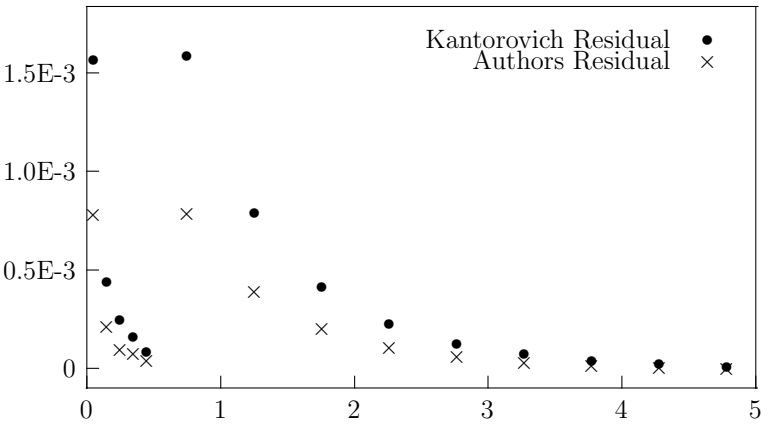

Fig. 1.1. Plotting residuals on $[0, 5]$.

References

[AALT05] Ahues, M., Amosov, A., Largillier, A., Titaud, O.: L^p error estimates for projection approximations. *Appl. Math. Lett.,* **18**, 381–386 (2005).

[Busb60] Busbridge, I.W.: *The Mathematics of Radiative Transfer,* Cambridge University Press, Cambridge New York (1960).

[Sloa82] Sloan, I.H.: Superconvergence and the Galerkin method for integral equations of the second kind. In: *Treatment of Integral Equations by Numerical Methods,* Academic Press, New York, 197–206 (1982).

2

On Acceleration of Spectral Computations for Integral Operators with Weakly Singular Kernels

M. Ahues[1], A. Largillier[1], and B. Limaye[2]

[1] Université de Saint-Étienne, France; mario.ahues@univ-st-etienne.fr, largillier@univ-st-etienne.fr
[2] Indian Institute of Technology Bombay, Mumbai, India; bvl@math.iitb.ac.in

2.1 Introduction

Let T be a compact integral operator on a Banach space X over the complex scalars $\mathbb{C}$. Consider the eigenvalue problem for T of finding a nonzero $\varphi \in X$ and a nonzero $\lambda \in \mathbb{C}$ such that $T\varphi = \lambda\varphi$. More generally, we may consider the spectral subspace problem for T of finding linearly independent elements $\varphi_1, \ldots, \varphi_m$ in X and a nonsingular $m \times m$ matrix Θ with complex entries such that

$$[T\varphi_1, \ldots, T\varphi_m] = [\varphi_1, \ldots, \varphi_m]\Theta.$$

Here, Θ represents the restricted operator $T_M : M \to M$, $x \mapsto Tx$, where $M := \mathrm{Span}\,[\varphi_1, \ldots, \varphi_m]$. If M is the spectral subspace corresponding to a isolated spectral value λ of T, then the spectrum of Θ is $\{\lambda\}$ and m is the algebraic multiplicity of λ.

If we let $\underline{X} = X^{1\times m}$ and $\underline{\varphi} = [\varphi_1, \ldots, \varphi_m] \in \underline{X}$, then the above equation can be written as $\underline{T}\,\underline{\varphi} = \underline{\varphi}\,\Theta$. Since finding exact solutions of such problems is a tall order, one often finds an approximation $\widetilde{T}$ of T and attempts to solve the problem $\underline{\widetilde{T}}\,\underline{\widetilde{\varphi}} = \underline{\widetilde{\varphi}}\,\widetilde{\Theta}$. If an approximate solution $(\underline{\widetilde{\varphi}}, \widetilde{\Theta})$ is not sufficiently accurate, one may employ an iterative refinement technique or use an acceleration technique as described in Chapter 3 of [ALL01] for improving the accuracy. In this procedure, the question of implementation of these techniques on a computer is of paramount importance. For this purpose, we must be able to reduce this procedure to (finite-dimensional) matrix computations. If the approximating operator $\widetilde{T}$ is of finite rank, then the spectral subspace problem $\underline{\widetilde{T}}\,\underline{\widetilde{\varphi}} = \underline{\widetilde{\varphi}}\,\widetilde{\Theta}$ as well as iterative refinement and acceleration can in fact be reduced to matrix computations (see Chapter 5 of [ALL01]).

If $X := C^0([0,1], \mathbb{C})$, the space of all complex-valued continuous functions on the interval $[0,1]$, and if the kernel of a compact integral operator T on X is weakly singular, then one may resort to singularity subtraction (see [Ans81]

and [ALL01].) Here one obtains a sequence (T_n) of the so-called Kantorovich–Krylov approximations, which converges to T in the following manner:

(1) $\|T_n x - Tx\| \to 0$ as $n \to \infty$ for each $x \in X$,
(2) $\|(T_n - T)T\| \to 0$ as $n \to \infty$,
(3) $\|(T_n - T)T_n\| \to 0$ as $n \to \infty$

(see Proposition 4.18 and Theorem 4.19 of [ALL01]). The approximating operator T_n in this case is not of finite rank. Yet in [AL04] it was shown that the spectral subspace problem $\underline{T_n}\,\underline{\varphi_n} = \underline{\varphi_n}\Theta_n$ for each T_n can be reduced to finite-dimensional computations. In addition, in [ALL06] it was shown that iterative refinement based on T_n can also be reduced to finite-dimensional considerations. Two such iterative refinement schemes are known as "elementary iteration" and "double iteration" (see Chapter 3 of [ALL01]). However, it turns out that the acceleration technique based on T_n is not in general amenable to such a reduction. We, therefore, consider an approximate implementation of the acceleration technique.

2.2 Approximate Acceleration

Let T be a bounded operator on a complex Banach space X, and let a bounded operator $\widetilde{T}$ on X serve as an approximation of T. The acceleration technique involves the following framework (see Section 3.2 of [ALL01]). Fix a positive integer q greater than 1, and let $\mathbf{X} := X^{q\times 1} = \{\mathbf{x} = [x_1, \ldots, x_q]^\top : x_1, \ldots, x_q \text{ in } X\}$ denote the product space of X consisting of the columns of length q with entries in X. Define the operators $\mathbf{T}$ and $\widetilde{\mathbf{T}}$ from $\mathbf{X}$ to $\mathbf{X}$ by

$$\mathbf{Tx} := \begin{bmatrix} Tx_1 \\ x_1 \\ \vdots \\ x_{q-1} \end{bmatrix} \text{ and } \widetilde{\mathbf{T}}\mathbf{x} := \begin{bmatrix} \sum_{k=0}^{q-1}(T-\widetilde{T})^k\widetilde{T}x_{k-1} \\ x_1 \\ \vdots \\ x_{q-1} \end{bmatrix} \text{ for } \mathbf{x} = \begin{bmatrix} x_1 \\ \vdots \\ x_q \end{bmatrix} \text{ in } \mathbf{X}.$$

They are represented by $q \times q$ matrices of operators on X as given below:

$$\mathbf{T} = \begin{bmatrix} T & O & \cdots & \cdots & O \\ I & O & \cdots & \cdots & O \\ O & I & O & \cdots & O \\ \vdots & \ddots & \ddots & \ddots & \vdots \\ O & \cdots & O & I & O \end{bmatrix} \quad \text{and} \quad \widetilde{\mathbf{T}} = \begin{bmatrix} \widetilde{T} & (T-\widetilde{T})\widetilde{T} & \cdots & \cdots & (T-\widetilde{T})^{q-1}\widetilde{T} \\ I & O & \cdots & \cdots & O \\ O & I & O & \cdots & O \\ \vdots & \ddots & \ddots & \ddots & \vdots \\ O & \cdots & O & I & O \end{bmatrix}.$$

The nonzero spectral values of T and $\mathbf{T}$ are the same. But this is not the case in general for the nonzero spectral values of $\widetilde{T}$ and $\widetilde{\mathbf{T}}$. In fact, if $\|(T-\widetilde{T})T\|$ and $\|(T-\widetilde{T})\widetilde{T}\|$ are small, then the nonzero spectral values of finite type of T are better approximated by the nonzero spectral values of finite type of $\widetilde{\mathbf{T}}$ as

compared with those of $\widetilde{T}$. Also, a basis for a spectral subspace of T is better approximated by the first components of a basis for the corresponding spectral subspace of $\widetilde{\mathbf{T}}$. However, if X is infinite-dimensional, then $\widetilde{\mathbf{T}}$ is not of finite rank (even if $\widetilde{T}$ is of finite rank) and it may not be possible to implement the spectral calculations for $\widetilde{\mathbf{T}}$ on a computer. This is the case, in general, when T is a weakly singular integral operator on $C^0([0,1],\mathbb{C})$ and $\widetilde{T}$ is a Kantorovich–Krylov approximation of T. In such a situation, we may attempt to employ the iterative refinement technique based on the operator $\widetilde{\mathbf{S}} : \mathbf{X} \to \mathbf{X}$ given by

$$\widetilde{\mathbf{S}} := \begin{bmatrix} \widetilde{T} & O & \cdots & \cdots & O \\ I & O & \cdots & \cdots & O \\ O & I & O & \cdots & O \\ \vdots & \ddots & \ddots & \ddots & \vdots \\ O & \cdots & O & I & O \end{bmatrix}$$

to obtain approximations of spectral values and spectral subspaces of $\widetilde{\mathbf{T}}$. In this connection, we prove the following result.

Theorem 1. *Let $\widetilde{\Lambda}$ be a spectral set of finite type for $\widetilde{T}$ such that $0 \notin \widetilde{\Lambda}$. Assume that it is possible to implement an iterative refinement scheme based on $\widetilde{T}$ and $\widetilde{\Lambda}$ to obtain approximation of spectral elements of operators defined on X. Then it is possible to implement such an iterative refinement scheme based on $\widetilde{\mathbf{S}}$ and $\widetilde{\Lambda}$ to obtain approximations of spectral elements of operators defined on $\mathbf{X}$.*

Proof. Let m denote the rank of the spectral projection associated with $\widetilde{T}$ and $\widetilde{\Lambda}$. Our assumption says that we can compute (using finite-dimensional matrix calculations) (i) an ordered basis $\underline{\widetilde{\varphi}}$ of the spectral subspace associated with $\widetilde{T}$ and $\widetilde{\Lambda}$, (ii) an adjoint basis $\underline{\widetilde{\varphi}}^*$ of the spectral subspace associated with $\widetilde{T}^*$ and $\widetilde{\Lambda}^*$ satisfying $\langle \underline{\widetilde{\varphi}}, \underline{\widetilde{\varphi}}^* \rangle = I_m$, and (iii) a solution of any Sylvester equation of the following type:

$$\widetilde{T}\,\underline{\widetilde{x}} - \underline{\widetilde{x}}\,\widetilde{\Theta} = \underline{\widetilde{y}}, \text{ subject to } \langle \underline{\widetilde{x}}, \underline{\widetilde{\varphi}}^* \rangle = O,$$

where the nonsingular $m \times m$ matrix $\widetilde{\Theta}$ satisfies $\widetilde{T}\,\underline{\widetilde{\varphi}} = \underline{\widetilde{\varphi}}\,\widetilde{\Theta}$ and $\underline{\widetilde{y}} \in \underline{X}$ satisfies $\langle \underline{\widetilde{y}}, \underline{\widetilde{\varphi}} \rangle = O$. Here $\widetilde{T}^*$ denotes the adjoint of $\widetilde{T}$ defined on the adjoint space X^* consisting of all conjugate-linear continuous functionals on X, $\widetilde{\Lambda}^*$ is the set of all complex conjugates of points in $\widetilde{\Lambda}$, and $\langle \underline{x}, \underline{f} \rangle$ denotes the $m \times m$ Gram matrix associated with $\underline{x} \in \underline{X}$ and $\underline{f} \in \underline{X}^*$, whose (i,j)th element is equal to the complex conjugate of $f_i(x_j)$, $1 \le i, j \le m$.

We note that $\widetilde{\Lambda}$ is a spectral set for $\widetilde{\mathbf{S}}$ and the rank of the spectral projection associated with $\widetilde{\mathbf{S}}$ and $\widetilde{\Lambda}$ is equal to m (see part (b) of Proposition 3.9 of [ALL01]). Let $\underline{\mathbf{X}} := \mathbf{X}^{1\times m}$ denote the product space of $\mathbf{X}$ consisting of the rows of length m with entries in $\mathbf{X}$. An element of $\underline{\mathbf{X}}$ can be written as

$$\underline{\mathbf{x}} = [\mathbf{x_1}, \ldots, \mathbf{x_m}], \text{ where } \mathbf{x_1}, \ldots, \mathbf{x_m} \text{ are in } \mathbf{X},$$

and also as

$$\underline{\mathbf{x}} = [\underline{x}_1, \ldots, \underline{x}_q]^\top, \text{ where } \underline{x}_1, \ldots, \underline{x}_q \text{ are in } \underline{X}.$$

First, it can be seen that

$$\widetilde{\underline{\boldsymbol{\varphi}}} = \begin{bmatrix} \widetilde{\underline{\varphi}} \\ \widetilde{\underline{\varphi}}\,\widetilde{\Theta}^{-1} \\ \vdots \\ \widetilde{\underline{\varphi}}\,\widetilde{\Theta}^{-q+1} \end{bmatrix}$$

forms an ordered basis for the spectral subspace associated with $\widetilde{\mathbf{S}}$ and $\widetilde{\Lambda}$ and $\widetilde{\underline{\mathbf{S}}}\,\widetilde{\underline{\boldsymbol{\varphi}}} = \widetilde{\underline{\boldsymbol{\varphi}}}\,\widetilde{\Theta}$. (See pages 168 and 169 of [ALL01].) Clearly, $\widetilde{\underline{\boldsymbol{\varphi}}}$ is computable since $\widetilde{\underline{\varphi}}$ and $\widetilde{\Theta}$ are given to be computable.

Second, if we let

$$\widetilde{\underline{\boldsymbol{\varphi}}}^* := \begin{bmatrix} \widetilde{\underline{\varphi}}^* \\ \underline{0} \\ \vdots \\ \underline{0} \end{bmatrix} \in \underline{\mathbf{X}}^*,$$

then $\widetilde{\underline{\boldsymbol{\varphi}}}^*$ is an adjoint basis for the spectral subspace associated with $\widetilde{\mathbf{S}}^*$ and $\widetilde{\Lambda}^*$; that is, $\widetilde{\underline{\mathbf{S}}}^*\,\widetilde{\underline{\boldsymbol{\varphi}}}^* = \widetilde{\underline{\varphi}}^*\,\widetilde{\Theta}^*$ and $\langle\, \widetilde{\underline{\boldsymbol{\varphi}}}, \widetilde{\underline{\boldsymbol{\varphi}}}^* \,\rangle = I_m$. This can be seen as follows:

$$\widetilde{\underline{\mathbf{S}}}^*\,\widetilde{\underline{\boldsymbol{\varphi}}}^* = \begin{bmatrix} \widetilde{\underline{T}}^* & \underline{I}^* & \underline{O} & \cdots & \underline{O} \\ \underline{O} & \underline{O} & \underline{I}^* & \cdots & \underline{O} \\ \vdots & \vdots & \underline{O} & \ddots & \underline{O} \\ \vdots & \vdots & \vdots & \ddots & \underline{I}^* \\ \underline{O} & \underline{O} & \underline{O} & \cdots & \underline{O} \end{bmatrix} \begin{bmatrix} \widetilde{\underline{\varphi}}^* \\ \underline{0} \\ \vdots \\ \underline{0} \end{bmatrix} = \begin{bmatrix} \widetilde{\underline{T}}^*\,\widetilde{\underline{\varphi}}^* \\ \underline{0} \\ \vdots \\ \underline{0} \end{bmatrix} = \begin{bmatrix} \widetilde{\underline{\varphi}}^*\,\widetilde{\Theta}^* \\ \underline{0} \\ \vdots \\ \underline{0} \end{bmatrix} = \widetilde{\underline{\boldsymbol{\varphi}}}^*\,\widetilde{\Theta}^*$$

and

$$\begin{aligned} \langle\, \widetilde{\underline{\boldsymbol{\varphi}}}, \widetilde{\underline{\boldsymbol{\varphi}}}^* \,\rangle &= \langle\, [\widetilde{\underline{\varphi}}, \widetilde{\underline{\varphi}}\,\widetilde{\Theta}^{-1}, \ldots, \widetilde{\underline{\varphi}}\,\widetilde{\Theta}^{-q+1}]^\top, [\widetilde{\underline{\varphi}}^*, \underline{0}, \ldots, \underline{0}]^\top \,\rangle \\ &= \langle\, \widetilde{\underline{\varphi}}, \widetilde{\underline{\varphi}}^* \,\rangle + \langle\, \widetilde{\underline{\varphi}}\,\widetilde{\Theta}^{-1}, \underline{0} \,\rangle + \cdots + \langle\, \widetilde{\underline{\varphi}}\,\widetilde{\Theta}^{-q+1}, \underline{0} \,\rangle \\ &= I_m + O + \cdots + O = I_m. \end{aligned}$$

Again, it is clear that $\widetilde{\underline{\boldsymbol{\varphi}}}^*$ is computable since $\widetilde{\underline{\varphi}}^*$ is given to be computable.

Finally, let $\widetilde{\underline{\mathbf{y}}} \in \underline{\mathbf{X}}$ be such that $\langle\, \widetilde{\underline{\mathbf{y}}}, \widetilde{\underline{\boldsymbol{\varphi}}}^* \,\rangle = O$. If $\widetilde{\underline{\mathbf{y}}} = [\widetilde{\underline{y}}_1, \ldots, \widetilde{\underline{y}}_q]^\top$ with $\widetilde{\underline{y}}_1, \ldots, \widetilde{\underline{y}}_q$ in $\underline{X}$, then

$$\langle\, \widetilde{\underline{\mathbf{y}}}, \widetilde{\underline{\boldsymbol{\varphi}}}^* \,\rangle = \langle\, \widetilde{\underline{y}}_1, \widetilde{\underline{\varphi}}^* \,\rangle + \langle\, \widetilde{\underline{y}}_2, \underline{0} \,\rangle + \cdots + \langle\, \widetilde{\underline{y}}_q, \underline{0} \,\rangle = \langle\, \widetilde{\underline{y}}_1, \widetilde{\underline{\varphi}}^* \,\rangle.$$

Hence $\langle \widetilde{\underline{y}}_1, \widetilde{\underline{\varphi}}^* \rangle = O$. By our assumption, we can compute $\widetilde{\underline{x}}_1 \in \underline{X}$ such that

$$\widetilde{\underline{T}}\,\widetilde{\underline{x}}_1 - \widetilde{\underline{x}}_1\widetilde{\Theta} = \widetilde{\underline{y}}_1 \text{ and } \langle \widetilde{\underline{x}}_1, \widetilde{\underline{\varphi}}^* \rangle = O.$$

For $i = 2, \ldots, q$, define

$$\widetilde{\underline{x}}_i := \left(\widetilde{\underline{x}}_{i-1} - \widetilde{\underline{y}}_i\right)\widetilde{\Theta}^{-1},$$

so that $\widetilde{\underline{x}}_{i-1} - \widetilde{\underline{x}}_i\widetilde{\Theta} = \widetilde{\underline{y}}_i$ for $i = 2, \ldots, q$. If we let $\widetilde{\underline{\mathbf{x}}} = [\widetilde{\underline{x}}_1, \ldots, \widetilde{\underline{x}}_2]^\top$, then

$$\widetilde{\mathbf{S}}\,\widetilde{\underline{\mathbf{x}}} - \widetilde{\underline{\mathbf{x}}}\widetilde{\Theta} = \begin{bmatrix} \widetilde{\underline{T}}\,\widetilde{\underline{x}}_1 \\ \widetilde{\underline{x}}_1 \\ \vdots \\ \widetilde{\underline{x}}_{q-1} \end{bmatrix} - \begin{bmatrix} \widetilde{\underline{x}}_1\widetilde{\Theta} \\ \widetilde{\underline{x}}_2\widetilde{\Theta} \\ \vdots \\ \widetilde{\underline{x}}_q\widetilde{\Theta} \end{bmatrix} = \begin{bmatrix} \widetilde{\underline{y}}_1 \\ \widetilde{\underline{y}}_2 \\ \vdots \\ \widetilde{\underline{y}}_q \end{bmatrix} = \widetilde{\underline{\mathbf{y}}}.$$

Also,

$$\langle \widetilde{\underline{\mathbf{x}}}, \widetilde{\underline{\boldsymbol{\varphi}}}^* \rangle = \langle \widetilde{\underline{x}}_1, \widetilde{\underline{\varphi}}^* \rangle + \langle \widetilde{\underline{x}}_2, \underline{0} \rangle + \cdots + \langle \widetilde{\underline{x}}_q, \underline{0} \rangle = O + O + \cdots + O = O.$$

Thus, a solution $\widetilde{\underline{\mathbf{x}}}$ of a Sylvester equation

$$\widetilde{\underline{\mathbf{S}}}\,\widetilde{\underline{\mathbf{x}}} - \widetilde{\underline{\mathbf{x}}}\,\widetilde{\Theta} = \widetilde{\underline{\mathbf{y}}}, \text{ subject to } \langle \widetilde{\underline{\mathbf{x}}}, \widetilde{\underline{\boldsymbol{\varphi}}}^* \rangle = O,$$

is also computable. This implies that an iterative refinement scheme based on $\widetilde{\mathbf{S}}$ and $\widetilde{\Lambda}$ is implementable for obtaining approximations of spectral elements of operators defined on $\mathbf{X}$, as described in Section 5.2 of [ALL01].

The above result allows us to compute approximately the nonzero spectral values of finite type and the corresponding spectral subspaces of the acceleration operator $\widetilde{\mathbf{T}}$ defined on $\mathbf{X}$.

2.3 Numerics for a Weakly Singular Kernel

We consider a weakly singular kernel

$$g(t) := \ln 2 - \ln(1 - \cos 2\pi t), \quad t \in [0, 1],$$

and the corresponding integral operator T defined on $X := C^0([0, 1], \mathbb{C})$ by

$$(Tx)(s) := \int_0^1 g(|s - t|)x(t)dt, \quad x \in X, \quad s \in [0, 1].$$

This operator has $2\ln 2$ as a simple eigenvalue and $1, 1/2, 1/3, \ldots$ as double eigenvalues (see [Wan76] and [ALL06]). The approximating operator $\widetilde{T}$ is taken as a Kantorovich–Krylov approximation T_n built by considering

$$g_n(t) := \begin{cases} g(h_n) \text{ if } 0 \le t \le h_n, \\ g(t) \quad \text{otherwise,} \end{cases}$$

where $0 < h_n < 1$, and by using a compound trapezoidal quadrature rule with n nodes. Since we need to solve a spectral subspace problem for T_n initially, the number n of nodes is kept moderate. On the other hand, since evaluations involving the operator T are difficult, the operator T is replaced by its Kantorovich–Krylov approximation T_N of a very high order; that is, N is taken to be much larger than n. Our computations use $n = 40$ and $N = 625$.

For approximate acceleration, we consider $q = 2$ and implement the iterative refinement scheme known as the "double iteration" based on the operator

$$\mathbf{S}_n := \begin{bmatrix} T_n & O \\ I & O \end{bmatrix}$$

defined on $\mathbf{X} := X^{2\times 1}$ in order to obtain approximate spectral element of the acceleration operator

$$\mathbf{T}_n := \begin{bmatrix} T_n & (T - T_n)T_n \\ I & O \end{bmatrix}.$$

We consider the four double eigenvalues 1, 1/2, 1/3, and 1/4 of T and their corresponding spectral subspaces of dimension 2. The natural logarithm of the norm of the residual after each step of the iterative refinement is shown in Figure 2.1.

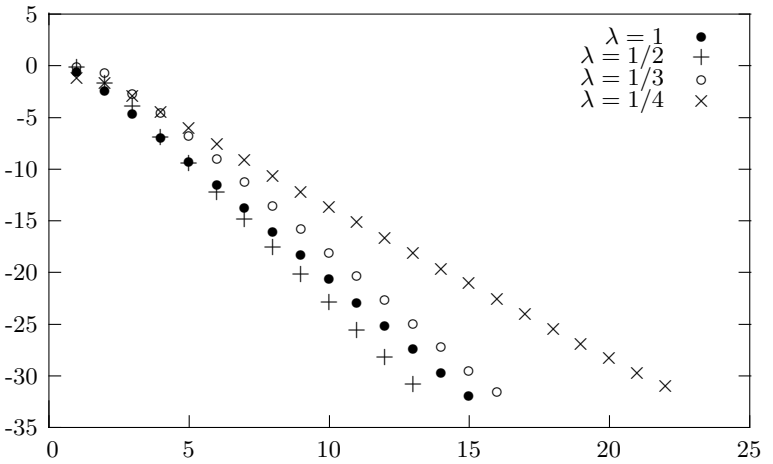

Fig. 2.1. Approximate acceleration convergence with double iteration for refinement: $k \mapsto \ln(\|\text{Residual of iterate number } k\|)$.

It is clear from Figure 2.1 that the convergence of the double iteration for the double eigenvalue 1/4 is slower than the convergence for the other three double eigenvalues 1, 1/2, and 1/3. The residuals considered here are calculated with respect to the "final" operator $\mathbf{T}_n$. The accuracy given by this approximate acceleration cannot be better than the accuracy given by the acceleration operator $\mathbf{T}_n$ itself. This is borne out in Figure 2.2, which depicts the natural logarithms of the norms of the residuals calculated with respect to the "final" operator T.

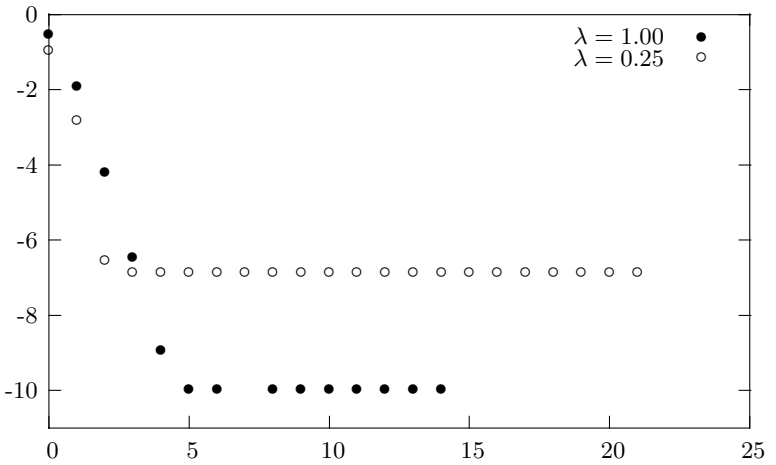

Fig. 2.2. Natural logarithm of the norm of the residuals with respect to T.

In the case of the double eigenvalue 1 of T, the norms of the residuals are stationary after the fifth iterate, and in the case of the double eigenvalue 1/4 of T they are stationary after the third iterate itself, whereas the accuracy attained for the eigenvalue 1 of T is much better than the one for the eigenvalue 1/4 of T.

We remark that the implementation of the approximate acceleration technique requires a much larger amount of computation compared with the usual iterative refinement technique. As such, the latter should be preferred whenever its stability is not in doubt.

References

[AL04] Ahues, M., Limaye, B.V.: Computation of spectral subspaces for weakly singular integral operators. *Numer. Functional Anal. Optim.,* **25**, 1–14 (2004).

[ALL01] Ahues, M., Largillier, A., Limaye, B.V.: *Spectral Computation for Bounded Operators.* Chapman & Hall/CRC, Boca Raton, FL (2001).

[ALL06] Ahues, M., Largillier, A., Limaye, B.V.: A singularity subtraction iterative refinement scheme for spectral subspaces of weakly singular integral operators. *J. Anal.,* (in press).

[Ans81] Anselone, P.M.: Singularity subtraction in the numerical solution of integral equations. *J. Austral. Math. Soc. Ser. B,* **22**, 408–418 (1981).

[Wan76] Wang, J.Y.: On the numerical computation of eigenvalues and eigenfunctions of compact integral operators using spline functions. *J. Inst. Math. Appl.,* **18**, 177–188 (1976).

3

Numerical Solution of Integral Equations in Solidification and Melting with Spherical Symmetry

V.S. Ajaev and J. Tausch

Southern Methodist University, Dallas, TX, USA; ajaev@smu.edu, tausch@smu.edu

3.1 Introduction

Mathematical modeling of solidification and melting is important for many technological applications [Dav01]. Numerical studies of moving interfaces between phases employ both finite-difference [JT96] and finite element [FO00] approaches. However, these standard approaches have to address the difficult issue of maintaining the accuracy of the method in situations when the domain shape is changing: This requires dealing with complicated deforming meshes or some interface tracking algorithms for situations when the mesh is fixed. To avoid these difficulties, alternative methods have been proposed. Phase field methods treat interfaces as regions of rapid change in an auxiliary order parameter, or phase field [AMc98]. The phase field takes two different constant values in the two phases away from the interface. Evolution of the phase field in time is followed in the simulation, as opposed to the evolution of a free boundary. Another related approach used to avoid direct tracking of the interface is the level-set method [OF01]. It involves solving an equation for a level-set function; the information about the interface motion is then recovered by following a zero contour of this function.

Integral equation methods have been used in several studies of solidification and melting [Wro83], [BM92]. However, they are rarely applied to practical simulations, in part because in many situations competing approaches, e.g., phase field methods, turn out to be more efficient. In recent years, substantial progress has been made in the development of fast boundary integral methods for the heat equation [GL99], [Tau06]. Application of such methods to problems in melting and solidification allows one to develop a new class of efficient, accurate, and robust methods for numerical simulations of evolving solid–liquid interfaces. The goal of this chapter is to discuss some numerical issues in the development of fast methods for simulations of solidification and melting in three-dimensional configurations. Computational examples are limited here to cases with spherical symmetry, but the approach can be extended to a variety of more complicated situations.

3.2 Model Formulation

Let us first formulate a general physical problem of interest for many applications of solidification. Consider a region of solid phase Ω surrounded by the undercooled liquid, i.e., liquid at the temperature T_∞ below the melting temperature T_M. The interface between the two phases is moving because the two heat fluxes at the solid and liquid sides of the interfacial region do not balance each other. We account for unsteady heat conduction in both phases, but we neglect the flow in the liquid in the current model.

It is convenient to define nondimensional temperatures according to

$$u_l = \frac{T_l - T_\infty}{T_M - T_\infty}, \quad u_s = \frac{T_s - T_\infty}{T_M - T_\infty},$$

where T_l and T_s are the dimensional temperatures in the liquid and solid phases, respectively. We assume that the temperature at the solid-liquid interface is equal to the melting temperature, which in nondimensional terms implies that

$$u_s = u_l = 1 \quad \text{on } \partial\Omega. \tag{3.1}$$

The scaled equations for unsteady heat conduction in the two phases can be then written in the form

$$\partial_t u_i = \alpha_i \Delta u_i, \quad i = s, l. \tag{3.2}$$

Here the nondimensional coefficients α_i are defined in terms of the thermal diffusivities α_i^* of the two phases according to

$$\alpha_i = \alpha_i^* t_{ch}/R^2,$$

where R is the length scale (e.g., the initial size of the domain of the solid phase) and t_{ch} is the characteristic time scale. A convenient choice of an expression for t_{ch} is based on the energy balance at the interface, which can be written in the form

$$\frac{\rho \mathcal{L} R}{t_{ch}} V_n = \frac{T_M - T_\infty}{R} \left(k_s \frac{\partial u_s}{\partial n} - k_l \frac{\partial u_l}{\partial n} \right), \tag{3.3}$$

where V_n is the scaled normal velocity of the interface, ρ is the liquid density, $\mathcal{L}$ is the latent heat per unit mass, and k_i are the thermal conductivities of the two phases. Clearly, choosing $t_{ch} = \rho \mathcal{L} R^2/k_l(T_M - T_\infty)$ reduces the equation to the form

$$V_n = k \frac{\partial u_s}{\partial n} - \frac{\partial u_l}{\partial n}, \tag{3.4}$$

where k is the ratio of the thermal conductivities. To complete the formulation, we note that the nondimensional temperature approaches zero as the distance from the solidified part of the material approaches infinity.

For the case of melting, the scales, governing equations, and the boundary conditions at the interface remain the same, but the interior of the finite domain Ω is now the liquid phase, and the exterior is solid. In addition, heat sources may need to be introduced inside Ω to model localized heating, as discussed in more detail in Section 3.6.

3.3 Integral Equations

Depending on whether we consider the melting problem or the solidification problem, the liquid phase is either inside or outside the interface. In what follows, subscripts i and e will denote a quantity in the interior and exterior phase, and subscripts l and s will denote the same quantity in the liquid and solid phases.

By Green's formula, the system of equations in the previous section can be recast in the boundary integral form, resulting in the system of two integral equations

$$1/2 = \alpha_e \mathcal{K}_e[1] - \alpha_e \mathcal{V}_e \left[\frac{\partial u_e}{\partial n} + \frac{1}{\alpha_e} V_n \right] + \mathcal{A}_e + \mathcal{F}_e, \tag{3.5}$$

$$1/2 = -\alpha_i \mathcal{K}_l[1] + \alpha_i \mathcal{V}_i \left[\frac{\partial u_i}{\partial n} + \frac{1}{\alpha_i} V_n \right] + \mathcal{A}_i + \mathcal{F}_i, \tag{3.6}$$

where $\mathcal{V}_a$ is the single-layer and $\mathcal{K}_a$ is the double-layer heat potential in phase $a \in \{i, e\}$, and $\mathcal{A}_a$ and $\mathcal{F}_a$ represent contributions from nonhomogeneous initial conditions and source terms.

The heat potentials are defined by

$$\mathcal{V}_a[f] = \int_0^t \int_S G_a(x - y, t - \tau) f(y, \tau) dS_y d\tau,$$

$$\mathcal{K}_a[f] = \int_0^t \int_S \frac{\partial}{\partial n} G_a(x - y, t - \tau) f(y, \tau) dS_y d\tau,$$

$$\mathcal{A}_a = \int_{B_a} \frac{\partial}{\partial n} G_a(x - y, t) u_0(y) d^3 y,$$

where $a \in \{i, e\}$, S is the solid–liquid interface, B_i is the domain inside, B_e is the domain outside the initial interphase, u_0 is the initial nondimensional temperature, and G_a denotes the standard free-space Green's function

$$G_a(z, \delta) = \frac{1}{(4\pi\alpha_a \delta)^{3/2}} \exp\left(-\frac{|z|^2}{4\alpha_a \delta} \right), \quad a \in \{e, i\},$$

for the three-dimensional unsteady heat equation in each phase. Our focus is on the case where the interface at time t is a sphere of radius $r(t)$ and the

density is independent of the spatial variable. Simple integration shows that the heat potentials reduce to

$$\mathcal{V}_a[f] = \int_0^t \frac{1}{\sqrt{t-\tau}} K_a^v(t-\tau, r(\tau)) f(\tau)\, d\tau, \tag{3.7}$$

$$\mathcal{K}_a[f] = \int_0^t \frac{1}{\sqrt{t-\tau}} K_a^d(t-\tau, r(\tau)) f(\tau)\, d\tau, \tag{3.8}$$

where the kernels K_a^v and K_a^d are defined by

$$K_a^v(t,\tau) = \frac{1}{\sqrt{4\pi\alpha_a}} \left[\exp\left(-\frac{(r-R)^2}{4\alpha_a d} \right) - \exp\left(-\frac{(r+R)^2}{4\alpha_a d} \right) \right] \frac{R}{r},$$

$$K_a^d(t,\tau) = \frac{1}{\sqrt{4\pi\alpha_a}} \left[\exp\left(-\frac{(r-R)^2}{4\alpha_a d} \right) \left(-1 + \frac{R(r-R)}{2\kappa d} \right) + \exp\left(-\frac{(r+R)^2}{4\alpha_a d} \right) \left(1 + \frac{R(r+R)}{2\kappa d} \right) \right] \frac{1}{r},$$

where $r = r(t), R = r(\tau)$, and $d = t - \tau$. If the radius is positive and a smooth function of t, then both kernels are smooth functions as well. The normal velocity is the time derivative of the radius; that is,

$$r'(t) = V_n; \tag{3.9}$$

therefore, the problem at hand is to find the functions $\frac{\partial u_i}{\partial n}(t)$, $\frac{\partial u_e}{\partial n}(t)$, and $r(t)$ that satisfy (3.5), (3.6), and (3.3). These three equations constitute a nonlinear initial value problem for the unknown radius. To make this relationship more obvious, we define the functions

$$w_a = \frac{\partial u_a}{\partial n} + \frac{1}{\alpha_a} V_n, \quad a \in \{i, e\}.$$

From (3.5) and (3.6), it follows that

$$\mathcal{V}_e w_e = -\frac{1}{2\alpha_e} + \mathcal{K}_e[1] + \frac{1}{\alpha_e} \mathcal{A}_e, \tag{3.10}$$

$$\mathcal{V}_i w_i = \frac{1}{2\alpha_i} - \mathcal{K}_i[1] - \frac{1}{\alpha_i} \mathcal{A}_i. \tag{3.11}$$

For a given radius $r(\tau), 0 \le \tau \le t$, (3.10) and (3.11) are Volterra integral equations of the first kind with unknowns w_e and w_i. The derivative $r'(t)$ can be obtained from (3.9) and (3.3):

$$r'(t) = F(r(t)) := \left(1 - \frac{k}{\alpha_l} + \frac{1}{\alpha_s} \right)^{-1} \left(\frac{k}{\alpha_l} w_l - \frac{1}{\alpha_s} w_s \right). \tag{3.12}$$

In this initial value problem, the function F depends on the complete time history of r.

3.4 Discretization Method

To integrate the initial value problem, we use the implicit Euler method. The right-hand side in (3.12) involves two integral equations which are discretized with the Nyström method. We discuss briefly the quadrature for the heat potentials. Because of the singularity at $t = \tau$, the convergence rate of standard quadrature rules will be of low order. To overcome this problem, we subtract the singularity:

$$\int_0^t \frac{1}{\sqrt{t-\tau}} K(t-\tau, r(\tau)) f(\tau)\, d\tau$$
$$= \int_0^t \frac{1}{\sqrt{t-\tau}} \Big(K(t-\tau, r(\tau)) f(\tau) - K(0, r(t)) f(t) \Big)\, d\tau + 2\sqrt{t} K(0, r(t)) f(t).$$

Here K is one of the kernels in (3.7) or (3.8). The singularity has been reduced to $O\left((t-\tau)^{1/2}\right)$, and therefore, the error of composite trapezoidal rule is $O(h^{3/2})$, where h is the stepsize. After some simplifications we obtain the rule

$$\int_0^t \frac{1}{\sqrt{t-\tau}} K(t-\tau, r(\tau)) f(\tau)\, d\tau$$
$$\approx \sum_{j=0}^{i-1} \frac{w_j}{\sqrt{t_i - t_j}} K(t_i - t_j, r(t_j)) f(t_j) \; + \; m_i K(0, r(t_i)) f(t_i),$$

where $t_j = jh$, $w_0 = w_i = h/2$, $w_j = h$, and

$$m_i = 2\sqrt{t_i} - \sum_{j=0}^{i-1} \frac{w_j}{\sqrt{t_i - t_j}}\,.$$

Replacing the integrals in (3.10) and (3.11) by the above quadrature rule results in a recurrence formula for the unknowns. Specifically, the ith timestep involves the approximations w_j^s, w_j^l, r_j for $0 \le j \le i$. Solving the resulting equations for w_i^s, w_i^l defines the discrete right-hand side $F_h(r_i, r_{i-1}, \ldots, r_0)$ of (3.12). Solving the discretized initial value problem with the implict Euler method gives

$$r_i = r_{i-1} + hF_h(r_i, r_{i-1}, \ldots, r_0)\,.$$

To solve this equation, Newton's method is employed.

3.5 Solidification Problem

We start with the classical problem of a spherical nucleus of a solid phase growing into the undercooled liquid [Dav01]. The initial temperature distribution is given by

$$u_0(r') = \begin{cases} 1 & r' \le r(0), \\ 0 & r' > r(0). \end{cases}$$

We note that the nucleus can become unstable when it is sufficiently large, but investigation of such instability is beyond the scope of this work. In the simulations here and below we use the values of the nondimensional parameters $\alpha_s = 65.31$, $\alpha_l = 40.82$, and $k = 1.47$, calculated based on the material properties of copper.

To test the validity of our approach, we compute the solution of the solidification problem where the evolution of the radius as a function of time is known analytically. The solution (sometimes referred to as a Frank sphere) is based on the assumption of self-similarity, i.e., u_l being a function of $r/t^{1/2}$. Then the radius of the growing sphere is given by

$$r(t) = S\sqrt{t},$$

where S is a constant that depends on α_l and is found from

$$\alpha_l S F(S) = 2F'(S) \tag{3.13}$$

and

$$F(S) = \frac{1}{S} e^{-S^2/4} - \frac{\sqrt{\pi}}{2} \operatorname{erfc}\left(\frac{S}{2}\right).$$

Because the velocity is singular at $t = 0$, we initialize the radius with a small positive value $r(0)$ and solve the initial value problem with a certain stepsize Δt. To improve the approximation, we then halve the initial radius and the stepsize several times. Table 3.1 displays the exact discretization values and the computed radius for $t = 1$. We observe that the convergence with respect to the stepsize is rapid and that the initial radius has little influence on the long-term solution. Figure 3.1 displays the normalized radii $r(t)/\sqrt{t}$. We also verified that the radius at $t = 1$ is in good agreement with the value S obtained by solving (3.13) in *Matlab*.

Table 3.1. Discretization parameters and radius data for the solidifying sphere.

# time steps	$r(0)$	$r(1)$	Error
600	0.2	1.5758716	0.003732
1200	0.1	1.5739710	0.001830
2400	0.05	1.5731524	0.001012
4800	0.025	1.5727139	0.000574

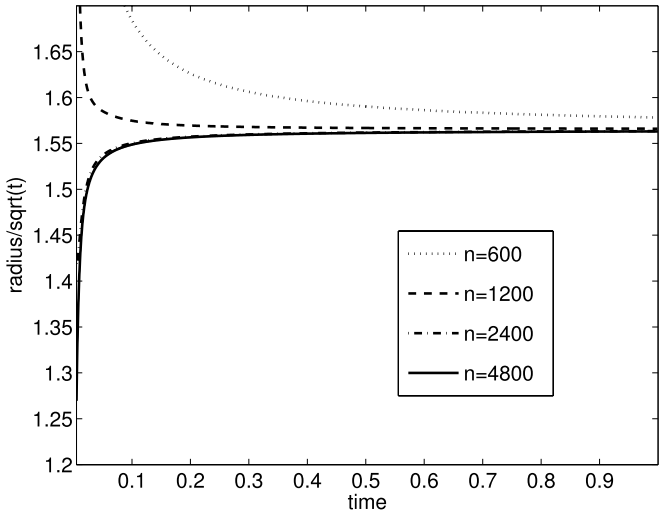

Fig. 3.1. Normalized radius of the interface as a function of time for the solidification problem. The discretization parameters of the curves are those of Table 3.1.

3.6 Laser-Induced Melting

We consider a laser focused on the surface of an initially solid metal that occupies the lower half-space (modeling a situation when the size of the sample is large compared with other relevant length scales in the problem). Melting of the solid material is a result of localized laser-induced heating. A simplified treatment of this physical effect involves prescribing the normal derivative of the temperature on the metal–air interface in the form of a delta-function. By reflectional symmetry, the problem can be cast in the form (3.5,3.6), where $\mathcal{F}_e = 0$ and

$$\mathcal{F}_i = \frac{Q}{4\pi\alpha_l r}\left(1 - \operatorname{erf}\left(\frac{r}{\sqrt{4\alpha_l t}}\right)\right),$$

and Q measures the intensity of the laser. To obtain the initial condition, we solve the heat equation in the solid phase without melting for some short interval $t \in [-T_0, 0]$. This problem has a closed-form solution. The initial radius $r(0)$ is the radius of the sphere with temperature above the melting temperature.

Figure 3.2 shows the radius as a function of time for several initial radii. The plot shows that the long-time propagation of the interface is insensitive to the initial radius.

The time step has been varied over a wide range, resulting in different curves shown in Figure 3.3.

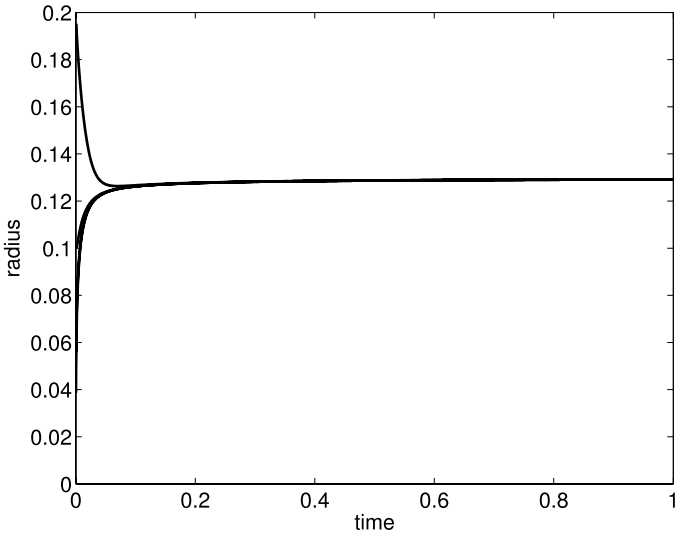

Fig. 3.2. Radius of the interface as a function of time for the melting problem. The initial radius is $r = 0.2$ (top curve) $r = 0.1$, $r = 0.05$, and $r = 0.025$ (bottom curve). The lowest three curves overlap.

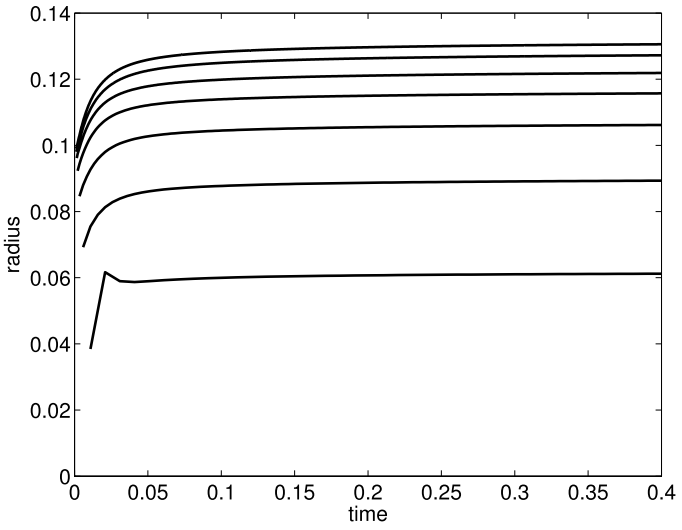

Fig. 3.3. Radius of the interface as a function of time for the melting problem. The initial radius is 0.025, and the curves are for the 600 timesteps (bottom) to 6400 timesteps (top).

3.7 Conclusions

We have derived an integral formulation for melting and solidification problems. Because of spherical symmetry, the heat potentials appear as weakly singular Volterra integral operators, which are discretized by a singularity corrected quadrature rule. The resulting initial value problem was solved effectively using the Euler scheme. The computation times even for the finest meshes are of order of only a few seconds. Numerical examples used to illustrate the approach include growth of a solid nucleus in the undercooled melt and laser-induced melting of a solid material.

The methodology can be extended to interfaces with arbitrary shapes. In this case surface integrals appear in addition to time convolutions, which dramatically increases the complexity of the heat potential approach. To speed up computations, we will incorporate our recently-developed fast heat equation solver [Tau06]. The results will be reported elsewhere.

Acknowledgement. This work was supported by the NSF.

References

[Dav01] Davis, S.H.: *Theory of Solidification.* Cambridge University Press, Cambridge (2001).

[JT96] Juric, D., Tryggvason, G.: A front-tracking method for dendritic solidification. *J. Comput. Phys.,* **123**, 127–148 (1996).

[FO00] Fukai, J., Ozaki, T., Asami, H., Miyatake, O.: Numerical simulation of liquid droplet solidificaion on substrates. *J. Chem. Engng Japan,* **33**, 630–637 (2000).

[AMc98] Anderson, D.M., McFadden, G.B., Wheeler, A.A.: Diffuse-interface methods in fluid mechanics. *Ann. Rev. Fluid Mech.,* **30**, 139–165 (1998).

[OF01] Osher, S., Fedkiw, F.: Level set methods: an overview and some recent results. *J. Comput. Phys.,* **169**, 463–502 (2001).

[Wro83] Wrobel, L.C.: A boundary element solution to Stefan's problem. In: *Boundary Elements,* V. Springer-Verlag, Berlin (1983).

[BM92] Brattkus, K., Meiron, D.: Numerical simulations of unsteady crystal growth. *SIAM J. Appl. Math.,* **52**, 1303–1320 (1992).

[GL99] Greengard, L., Lin, P.: Spectral approximation of the free-space heat kernel. *Appl. Comput. Harmon. Anal.,* **9**, 83–97 (1999).

[Tau06] Tausch, J.: A fast method for solving the heat equation by layer potentials. *J. Comput. Phys.,* **224**, 956–969 (2007).

4

An Analytic Solution for the Steady-State Two-Dimensional Advection–Diffusion–Deposition Model by the GILTT Approach

D. Buske[1], M.T. de Vilhena[1], D. Moreira[2], and B.E.J. Bodmann[1]

[1] Universidade Federal do Rio Grande do Sul, Porto Alegre, RS, Brazil;
buske@mecanica.ufrgs.br, vilhena@mat.ufrgs.br, bardo.bodmann@ufrgs.br
[2] Universidade Federal de Pelotas, Bagé, RS, Brazil;
davidson@mecanica.ufrgs.br

4.1 Introduction

The Eulerian approach for modeling the concentration of contaminants in a turbulent flow as the planetary boundary layer (PBL) is widely used in the field of air pollution studies. The simplicity of the K-theory of turbulent diffusion has led to the frequent use of this theory as the mathematical basis for simulating air pollution dispersion. Dry deposition refers to the transfer of air pollution (gas and particles) to the ground, where it is removed. The various transfer mechanisms leading to dry deposition are complex and involve micrometeorological characteristics of the atmospheric surface layer [SP97]. The deposition flux is usually parameterized in terms of deposition velocity, which is either specified empirically or estimated from appropriate theoretical relations. Moreover, the integral mass conservation equation is modified to account for the amount of material deposited on the surface.

The advection–diffusion equation can be written in finite-difference form, thus paving the way to a wide variety of numerical solutions. When the gradient transport (K-theory) is used, dry deposition is included by specifying the deposition flux as the surface boundary condition. Therefore, numerical solutions to the advection–diffusion equation with variable eddy diffusivities are used in order to take into account the effects of dry deposition as well as of gravitational settling for heavier particles [Ary99].

Analytic solutions of equations are of fundamental importance in understanding and describing physical phenomena [PS83]. Many operative models (using an analytic formula for the air pollution concentration) adopt empirical algorithms for describing dry deposition. The Gaussian plume equation was modified to include source depletion models ([Cha53], [Ove76]) and surface depletion model algorithms ([Hor77], [Hor84]). The solution proposed by

[Erm77] and [Rao81] also retained the framework of invariant wind speed and eddies with height (as the Gaussian approach). More recently, analytic solutions of the advection–diffusion equation with dry deposition at the ground have used height-dependent wind speed and eddy duffusivities (see [Chr92] and [LH97]). However, these solutions are restricted to the specific case where the source is located at the ground level and/or with restriction to the vertical profiles of the wind speed and eddy diffusivities.

We present an analytic solution of the advection–diffusion equation obtained by the GILTT (Generalized Integral Laplace Transform Technique) method (see [Mor05] and [Wor05]), describing dry deposition with a boundary condition of a nonzero flux to the ground and without any restriction to the above profiles and the source position. Recently, the GILTT method has been applied for the simulation of pollutant dispersion in the atmosphere by solving analytically the multidimensional advection–diffusion equation. The steps of this methodology are as follows: construction of an auxiliary Sturm–Liouville problem, expansion of the contaminant concentration in a series in terms of the obtained eigenfunctions, replacing of this equation in the original, and finally taking moments. The result is a set of ordinary differential equations that are then solved analytically by the Laplace transform technique. For more details, see [Wor05] and [Mor05].

In this chapter, a step forward is taken toward solving the two-dimensional, steady-state advection–diffusion–deposition equation by the above methodology. The novelty depends on the construction of the auxiliary Sturm–Liouville problem. Indeed, for this type of problem, the eigenvalues and eigenfunctions must be determined assuming boundary conditions of the third type, which include the contaminant deposition speed. At this point it is worth noting that the mentioned works ([Mor05] and [Wor05]) assume boundary conditions only of the second type. To validate the results obtained, numerical comparison is undertaken with results available in the literature.

4.2 The Analytic Solution

For a Cartesian coordinate system in which the x direction coincides with that of the average wind, the steady-state, two-dimensional advection–diffusion equation with dry deposition to the ground, valid for any variable vertical eddy diffusivity coefficients and wind profile (without lateral dispersion), is written as

$$u(z)\frac{\partial C(x,z)}{\partial x} = \frac{\partial}{\partial z}\left(K_z(z)\frac{\partial C(x,z)}{\partial z}\right), \tag{4.1}$$

subjected to the boundary conditions

$$K_z(z)\frac{\partial C(x,z)}{\partial z} = V_g C(x,z), \quad z = 0,$$

$$K_z(z)\frac{\partial C(x,z)}{\partial z} = 0, \quad z = h,$$

and a continuous source condition

$$u(z)C(0,z) = Q\delta(z - H_s), \quad x = 0.$$

Here C denotes the pollutant concentration, K_z is the turbulent eddy diffusivity coefficient assumed to be a function of the variable z, u is the mean wind oriented in the x direction, V_g is the deposition velocity, h is the height of PBL, Q is the emission rate, H_s is the height of the source, and δ is the Dirac delta distribution.

To solve this problem by the GILTT method, (4.1) is rewritten as

$$u(z)\frac{\partial C(x,z)}{\partial x} = K_z(z)\frac{\partial^2 C(x,z)}{\partial z^2} + K_z'(z)\frac{\partial C(x,z)}{\partial z},$$

where it should be noted that the first term on the right-hand side satisfies the Sturm–Liouville problem

$$\begin{aligned} \zeta_i''(z) + \lambda_i^2\zeta_i(z) = 0, \quad & 0 < z < h, \\ -K_z(z)\zeta_i'(z) + V_g\zeta_i(z) = 0, \quad & z = 0, \\ \zeta_i'(z) = 0, \quad & z = h. \end{aligned} \tag{4.2}$$

The solution of (4.2) is a well-known set of orthogonal eigenfunctions $\zeta_i(z) = \cos(\lambda_i(h - z))$, whose eigenvalues satisfy the ensuing transcendental equation

$$\lambda_i \tan(\lambda_i h) = H_1,$$

where $H_1 = \frac{V_g}{K_z}$. The eigenvalues are calculated solving the transcendental equation by the Newton–Raphson method.

It is now possible to apply the GILTT approach. For this purpose, the pollutant concentration is expanded in the series ([Mor05], [Wor05])

$$C(x,z) = \sum_{i=0}^{\infty} \overline{c_i}(x)\,\zeta_i(z). \tag{4.3}$$

Replacing the above equation in (4.1) and taking moments, the following equation is obtained:

$$\sum_{i=0}^{\infty}\left[\overline{c_i}(x)\int_0^{z_i} K_z'(z)\,\zeta_i'(z)\,\zeta_j(z)dz \;-\; \lambda_i^2\overline{c_i}(x)\int_0^h K_z(z)\,\zeta_i(z)\,\zeta_j(z)dz \right.$$
$$\left. -\; \overline{c_i'}(x)\int_0^h u(z)\,\zeta_i(z)\,\zeta_j(z)dz\right] = 0.$$

The above equation can be written in matrix form as

$$Y'(x) + F \,.\, Y(x) = 0, \tag{4.4}$$

where $Y(x)$ is the column vector whose components are $\overline{c_i}(x)$, the matrix F is defined as $F = B^{-1}E$, and the matrices B and E are given by

$$b_{i,j} = -\int_0^h u(z)\,\zeta_i(z)\,\zeta_j(z)dz,$$

$$e_{i,j} = \int_0^h K_z'(z)\,\zeta_i'(z)\,\zeta_j(z)dz - \lambda_i^2 \int_0^h K_z(z)\zeta_i(z)\zeta_j(z)dz.$$

Following the procedure in [Wor05] and [Mor05], one obtains the following solution for (4.4):

$$Y(x) = X \,.\, G(x) \,.\, \xi, \tag{4.5}$$

where X is the eigenfunction matrix of F, G is the diagonal matrix whose entries have the form $e^{-d_i x}$, d_i are the eigenvalues of F, and ξ is the vector given by $\xi = X^{-1}Y(0)$. Knowing the coefficients of the concentration series expansion, the solution of problem (4.1) is well determined by (4.3), where $\overline{c_i}(x)$ is the solution of the transformed problem given by (4.5), and $\zeta_i(z)$ comes from the solution of the Sturm–Liouville problem given in problem (4.2), where $\zeta_i(z) = \cos(\lambda_i(h - z))$.

No approximations are made in the derivation of this solution and so, the solution is analytic except for the round-off error. The number of terms considered in the series summation is established so that a prescribed accuracy is achieved. In this problem, 30 terms were sufficient to ensure the derived percentage error of 0.5%.

4.3 Experimental Data Analysis

To show an example of the application of the obtained solution (4.3), the dataset of the Hanford diffusion experiment was used. This experiment was conducted in May–June 1983 on a semi-arid region of southeastern Washington on generally flat terrain. The detailed description of the experiment was provided by Doran and Horst (1985). Data were obtained from six dual-tracer releases located at 100, 200, 800, 1600, and 3200 m from the source during moderately stable to near-neutral conditions. However, the deposition velocity was evaluated only for the last three distances. The release time was 30 min except in run five, when it was 22 min. The terrain roughness was 3 cm.

Two tracers, one depositing and one nondepositing, were released simultaneously from a height of 2 m. Zinc sulfide (ZnS) was chosen for the depositing tracer, whereas sulfur hexafluoride (SF_6) was the nondepositing tracer. The lateral separation between the SF_6 and ZnS release points was less than 1 m. The near-surface release height and the atmospheric stability conditions were chosen to produce differences between the depositing and nondepositing tracer concentrations that could be measured easily. The data collected during the

field tests were tabulated (as crosswind-integrated tracer concentration data) and presented in Doran et al. (1984). The meteorological data and crosswind-integrated tracer concentration data, normalized by the release rate Q, are listed in Table 4.1. Note that in Table 4.1, C_d and C_{nd} are, respectively, the crosswind-integrated concentrations of ZnS and SF_6 normalized by the emission rate Q. For more details about the way that the effective deposition velocities and wind speed are calculated, see [DR85].

Table 4.1. Tracer and meteorological data for six dual-tracer releases. Tracer data are normalized by the emission Q. L (m), u_* (cm.s^{-1}), and h (m) are the Monin–Obukhov length scale, the friction velocity, and the PBL height, respectively. u is the wind velocity, and V_g is the deposition velocity. Subscript d refers to depositing material, and subscript nd refers to nondepositing material.

Exp.	Arc (m)	ZnS/Q $(s.m^{-2})$	SF_6/Q $(s.m^{-2})$	u $(m.s^{-1})$	V_g $(cm.s^{-1})$	C_d/C_{nd}
$u_* = 40$	800	0.00224	0.00373	7.61	4.21	0.601
$L = 166$	1600	0.00098	0.00214	8.53	4.05	0.459
$h = 325$	3200	0.00059	0.00130	9.43	3.65	0.451
$u_* = 26$	800	0.00747	0.0129	3.23	1.93	0.579
$L = 44$	1600	0.00325	0.00908	3.59	1.80	0.358
$h = 135$	3200	0.00231	0.00722	3.83	1.74	0.320
$u_* = 27$	800	0.00306	0.00591	4.74	3.14	0.518
$L = 77$	1600	0.00132	0.00331	5.40	3.02	0.399
$h = 182$	3200	0.00066	0.00179	6.32	2.84	0.370
$u_* = 20$	800	0.00804	0.0201	3.00	1.75	0.400
$L = 34$	1600	0.00426	0.0131	3.39	1.62	0.325
$h = 104$	3200	0.00314	0.00915	3.75	1.31	0.343
$u_* = 26$	800	0.00525	0.0105	3.07	1.56	0.500
$L = 59$	1600	0.00338	0.00861	3.24	1.47	0.393
$h = 157$	3200	0.00292	0.00664	3.46	1.14	0.440
$u_* = 30$	800	0.00723	0.0134	3.17	1.17	0.540
$L = 71$	1600	0.00252	0.00615	3.80	1.15	0.410
$h = 185$	3200	0.00125	0.00311	4.37	1.10	0.402

To use the above solution (4.3), it was necessary to select wind and eddy coefficient vertical profiles. The reliability of each model strongly depends on the way that turbulent parameters are calculated and related to the current understanding of the PBL [SP97].

The vertical eddy diffusivity used in this work is given by [Deg00]:

$$K_z = \frac{0.3(1 - z/h)u_* z}{1 + 3.7(z/\Lambda)},$$

where z is the height, u_* is the friction velocity, $\Lambda = L(1 - z/h)^{\frac{5}{4}}$, and L is the Monin–Obukhov length.

The wind velocity profile was described by a power law expressed as follows [PD88]:

$$\frac{u_z}{u_1} = \left(\frac{z}{z_1}\right)^n,$$

where u_z and u_1 are the mean wind velocity at the heights z and z_1, whereas n is an exponent that is related to the intensity of turbulence for rural terrain [Irw79].

4.4 Numerical Results

The model was evaluated with the ratio C_d/C_{nd}, where C_d and C_{nd} are the crosswind-integrated concentrations of ZnS and SF_6 measured at 1.5 m above the ground and normalized, respectively, by the emission rate Q. A comparison of predicted and observed values C_d/C_{nd} are shown in Figure 4.1 for approach (4.3), with vertical eddy diffusivity given by [Deg00] and power profile of wind [PD88]. In this respect, it is possible to note that the model reproduce fairly well the observed concentration.

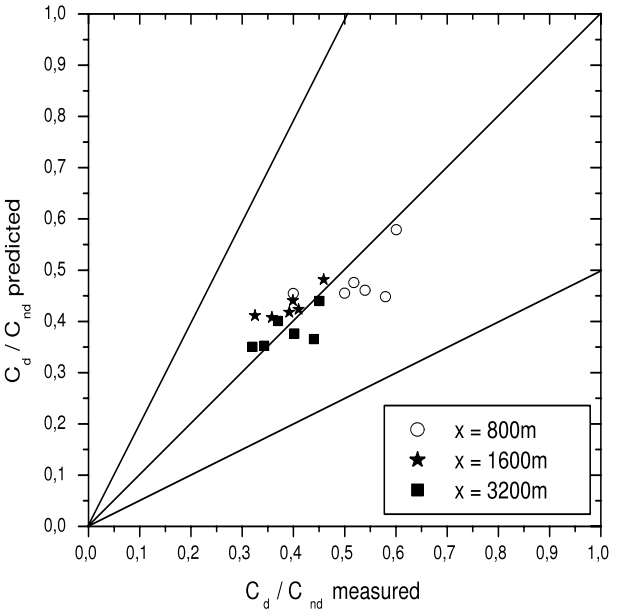

Fig. 4.1. Scatter diagram of observed C_d/C_{nd} vs C_d/C_{nd} predicted data. Data between lines correspond to a factor of two.

Doran and Horst (1985) presented four different models that evaluate the dry deposition at the ground with four different approaches: the source depletion approach of Chamberlain (1953), the corrected source depletion model of

Horst (1983), the K model proposed by Ermak (1977) and Rao (1981), and the corrected K model of Rao (1981). Finally, to compare the results with the four models above, statistical parameters were calculated (used in the paper [DR85]) described in [Fox81] and [Wil82]:

Mean bias $(\overline{d}) = \sum_{i=1}^{N} d_i/N$.

Variance $(S^2) = \sum_{i=1}^{N}(d_i - \overline{d})^2/(N-1)$.

Mean absolute error (MAE) $= \sum_{i=1}^{N} |Cp_i - Co_i|/N$.

Index of agreement (I) $= 1 - [\sum_{i=1}^{N}(P_i' - O_i')/\sum_{i=1}^{N}(|P_i'| + |O_i'|)^2]$, where d_i is the difference between observed (Co_i) and predicted (Cp_i) values, $P_i' = Cp_i - \overline{Co_i}$, $O_i' = Co_i - \overline{Co_i}$, the overbar indicates an average, and $0 < I < 1$ and N is the data number.

In Table 4.2, comparisons between the GILTT approach and the above models ([Cha53], [Erm77], [Hor83], [Rao81]) are reported, and it is possible to see the good performance of the solution.

Table 4.2. Statistical measures of model performance.

Parameter	GILTT	Source depletion	Corrected source depletion	K model	Corrected K model
Mean bias	0.02	0.11	0.01	0.21	0.07
MAE	0.04	0.11	0.05	0.21	0.07
S	0.06	0.05	0.06	0.08	0.05
COR	0.77	0.82	0.70	0.63	0.78
I	0.81	0.64	0.83	0.42	0.76

4.5 Final Remarks

A new exact general solution of the two-dimension steady-state advection–diffusion equation has been presented, considering dry deposition to the ground, which can be applied for describing turbulent dispersion of many scalar quantities, such as air pollution, radioactive material, heat, and so on. To show the performances of the solution in actual scenarios, a parameterization of the PBL has been introduced, and the values predicted by the solutions have been compared with the Hanford diffusion experiment dataset. The analysis of the results shows a reasonably good agreement between the computed values against the experimental ones. The discrepancies with the experimental data do not depend on the solution of the advection–diffusion equation, but on the equation itself, which is only a model of the reality. Moreover, a source of discrepancies between the predicted and the measured values lies in

the PBL parameterization used (i.e., vertical wind and eddy diffusivity profiles). Finally, the solution results were compared with those of four different models.

Although models are sophisticated instruments that ultimately reflect the current state of knowledge on turbulent transport in the atmosphere, the results they provide are subject to a considerable margin of error. This is due to various factors, including in particular the uncertainty of the intrinsic variability of the atmosphere. Models, in fact, provide values expressed as an average, i.e., a mean value obtained by the repeated performance of many experiments, whereas the measured concentrations are a single value of the sample to which the ensemble average provided by models refers. This is a general characteristic of the theory of atmospheric turbulence and is a consequence of the statistical approach used in attempting to parameterize the chaotic character of the measured data.

In the light of the above considerations, an analytic solution is useful for evaluating the performances of sophisticated numerical dispersion models (which numerically solve the advection–diffusion equation), yielding results that could be compared, not only against experimental data but, in an easy way, with the solution itself, in order to check numerical errors without the uncertainties presented above.

Acknowledgement. The authors thank to CNPq (Conselho Nacional de Desenvolvimento Científico e Tecnológico) and CAPES (Coordenação de Aperfeiçoamento de Pessoal de Nível Superior) for the partial financial support of this work.

References

[Ary99] Arya, S. Pal: *Air Pollution Meteorology and Dispersion.* Oxford University Press, New York (1999).

[Cha53] Chamberlain, A.C.: Aspects of travel and deposition of aerosol and vapour clouds. UKAEA Report No. AERE-HP/R-1261, Harwell, Berkshire, England (1953).

[Chr92] Chrysikopoulos, C.V., Hildemann, L.M., Roberts, P.V.: A three-dimensional atmospheric dispersion–deposition model for emissions from a ground-level area source. *Atmos. Environ.,* **26A**, 747–757 (1992).

[Deg00] Degrazia, G.A., Anfossi, D., Carvalho, J.C., Mangia, C., Tirabassi, T., Campos Velho, H.F.: Turbulence parameterisation for PBL dispersion models in all stability conditions. *Atmos. Environ.,* **34**, 3575–3583 (2000).

[Dor84] Doran, J.C., Abbey, O.B., Buck, J.W., Glover, D.W., Horst, T.W.: *Field Validation of Exposure Assessment Models,* vol. 1. Data Environmental Science Research Lab, Research Triangle Park, NC, EPA/600/384/092A (1984).

[DR85] Doran, J.C., Horst, T.W.: An evaluation of Gaussian plume-depletion models with dual-tracer field measurements. *Atmos. Environ.,* **19**, 939–951 (1985).

[Erm77] Ermak, D.L.: An analytical model for air pollution transport and deposition from a point source. *Atmos. Environ.,* **11**, 231–237 (1977).

[Fox81] Fox, D.G.: Judging air quality model performance: a summary of the AMS workshop on dispersion model performance. *Bull. Am. Meteorol. Soc.,* **62**, 599–609 (1981).

[Hor77] Horst, T.W.: A surface depletion model for deposition from a Gaussian plume. *Atmos. Environ.,* **11**, 41–46 (1977).

[Hor83] Horst, T.W.: A correction to the Gaussian source depletion model. In: Pruppacher, H.R., Semonin, R.G., Slinn, W.G.N. (eds.), *Precipitation Scavenging, Dry Deposition, and Resuspension.* Elsevier North-Holland, Amsterdam (1983), pp. 1205–1218.

[Hor84] Horst, T.W.: The modification of plume models to account for dry deposition. *Boundary-Layer Meteorol.,* **30**, 4413–430 (1984).

[Irw79] Irwin, J.S.: A theoretical variation of the wind profile power-low exponent as a function of surface roughness and stability. *Atmos. Environ.,* **13**, 191–194 (1979).

[LH97] Lin, J.S., Hildemann, L.M.: A generalized mathematical scheme to analytically solve the atmospheric diffusion equation with dry deposition. *Atmos. Environ.,* **31**, 59–71 (1997).

[Mor05] Moreira, D.M., Vilhena, M.T., Tirabassi, T., Buske, D., Cotta, R.M.: Near source atmospheric pollutant dispersion using the new GILTT method. *Atmos. Environ.,* **39**, 6289–6294 (2005).

[Ove76] Overcamp, T.J.: A general Gaussian diffusion–deposition model for elevated point source. *J. Appl. Meteorol.,* **15**, 1167–1171 (1976).

[PD88] Panofsky, A.H., Dutton, J.A.: *Atmospheric Turbulence.* Wiley, New York (1988).

[PS83] Pasquill, F., Smith, F.B.: *Atmospheric Diffusion.* Wiley, New York (1983).

[Rao81] Rao, K.S.: Analytical solutions of a gradient-transfer model for plume deposition and sedimentation. NOAA Tech. Mem. ERL ARL-109, Air Resources Laboratories, Silver Spring, MD (1981).

[SP97] Seinfeld, J.H., Pandis, S.N.: *Atmospheric Chemistry and Physics.* Wiley, New York (1997).

[Wil82] Wilmott, C.J.: Some comments on the evaluation of model performance. *Bull. Am. Meteorol. Soc.,* **63**, 1309–1313 (1982).

[Wor05] Wortmann, S., Vilhena, M.T., Moreira, D.M., Buske, D.: A new analytical approach to simulate the pollutant dispersion in the PBL. *Atmos. Environ.,* **39**, 2171–2178 (2005).

5

Analytic Two-Dimensional Atmospheric Pollutant Dispersion Simulation by Double GITT

M. Cassol[1,2], S. Wortmann[2], M.T. de Vilhena[2], and H.F. de Campos Velho[3]

[1] Istituto di Scienze dell'Atmosfera e del Clima, Lecce, Italy;
cassol@le.isac.cnr.it
[2] Universidade Federal do Rio Grande do Sul, Porto Alegre, RS, Brazil;
wortmann@etcom.ufrgs.br, vilhena@mat.ufrgs.br
[3] Instituto Nacional de Pesquisas Espaciais, São José dos Campos, SP, Brazil;
haroldo@lac.inpe.br

5.1 Introduction

In the generalized integral transform technique (GITT) [Cot93], [Cot97], the solution is expressed as a truncated series, in which the orthogonal function basis are obtained by solving the associated Sturm–Liouville problem. The expanded equation is transformed into an ordinary differential equation system. Once the transformed problem solution is found, the inverse formula is applied to compute the solution.

Application of the GITT to the atmospheric pollutant dispersion for one dimensional problem has been addressed in [Mor06], [WVM00], [WVMB05], and [WVCVS05].

The goal here is to apply the GITT approach to a two-dimensional (2D) atmospheric pollutant dispersion problem, with the use of a mathematical filter for dealing with nonhomogeneous boundary conditions. The turbulence is modeled by Taylor's statistical approach. In the GITT approach, it is possible to control the truncated error, computing the number of eigenfunctions for the final solution, according to the desired accuracy.

5.2 Two-Dimensional Pollutant Dispersion Model

The stationary, two-dimensional diffusion–advection equation in the atmosphere can be expressed as

$$u\frac{\partial C}{\partial x}+w\frac{\partial C}{\partial z}=\frac{\partial}{\partial x}\left(K_{xx}\frac{\partial C}{\partial x}\right)+\frac{\partial}{\partial z}\left(K_{zz}\frac{\partial C}{\partial z}\right),\ (x,z)\in(0,\infty)\times(0,h),\ (5.1)$$

where $C(x,z)$ is the pollutant concentration, $u(x,z)$ and $w(x,z)$ are the horizontal and vertical wind velocities, K_{xx} and K_{zz} are the eddy diffusivities in the horizontal and vertical components, respectively, and h is the atmospheric boundary layer height. The boundary conditions are given by

$$C(x,z) = \frac{Q\,\delta(z-h_f)}{u(x,z)} \quad \text{at} \quad x=0,$$
$$\frac{\partial C}{\partial x} = 0 \quad \text{as} \quad x \to \infty, \quad \frac{\partial C}{\partial z} = 0 \quad \text{at} \quad z=0 \ \text{ and } \ z=h,$$

where $\delta(z)$ is the delta distribution and h_f is the height at which the pollutant is released.

In (5.1), a first-order closure for turbulence transport was employed, where $\langle u_i' \phi' \rangle \approx K_{ii} \partial\phi/\partial x_i$ $(i = x, z)$, with $\Phi = \phi + \phi'$. In this approach, the Reynolds turbulent flux $\langle u_i' \phi' \rangle$ is taken as the product between the gradient of the Reynolds average quantity ($\phi = (1/\Delta t) \int \Phi\, dt$) and the eddy diffusivity.

To solve (5.1) by GITT, a mathematical filter will be introduced.

5.3 Mathematical Filter Definition

The theory for the GITT is applied for problems with homogeneous boundary conditions. The first boundary condition associated with the advection–diffusion equation is nonhomogeneous. A mathematical filter will now be defined to deal with this condition. Let us consider the function $F(x,z)$, which is a solution of a simplified version of (5.1), namely,

$$\bar{u}\frac{\partial F(x,z)}{\partial x} = \bar{K}_{xx}\frac{\partial^2 F(x,z)}{\partial x^2} + \bar{K}_{zz}\frac{\partial^2 F(x,z)}{\partial z^2} \tag{5.2}$$

with the same boundary conditions as for (5.1):

$$F(x,z) = \frac{Q\,\delta(z-h_f)}{u(x,z)} \quad \text{at} \quad x=0,$$
$$\frac{\partial F}{\partial x} = 0 \quad \text{at} \quad x \to \infty, \quad \frac{\partial F}{\partial z} = 0 \quad \text{at} \quad z=0 \ \text{ and } \ z=h,$$

where $\bar{u}$, $\bar{K}_{xx}$, and $\bar{K}_{zz}$ are constant coefficients representingthe average values of $u(x,z)$, K_{xx}, and K_{zz}, respectively. The classical integral transform technique (CITT) [Ozi80] is now applied to (5.2). The first step of this technique is to choose a good auxiliary problem (in general, this means a *well-known* one). For CITT and GITT, the auxiliary problem is a Sturm–Liouville problem, which requires homogeneous boundary conditions. Hence, the transformation is applied with respect to the z-coordinate, because the boundary conditions in this direction are homogeneous. Performing the transformation in this coordinate, the chosen variable of the Sturm–Liouville problem is also the z-coordinate. Therefore, the selected auxiliary problem is

$$\frac{d\Psi_r^2(z)}{dz^2} + \lambda_r^2 \Psi_r(z) = 0 \quad \text{at} \quad z \in [0, h];$$
$$\frac{d\Psi_r(z)}{dz} = 0 \quad \text{at} \quad z = 0 \text{ and } z = h.$$

The auxiliary problem solution is

$$\Psi_r(z) = \begin{cases} 1 & \lambda_r = 0 \quad \text{for } r = 0\ ; \\ \cos(\lambda_r z) & \lambda_r = r\pi/h \quad \text{for } r = 1,\ 2,\ \ldots . \end{cases}$$

The function $F(x, z)$ is given by an expansion considering the solution of the auxiliary problem. The expansion is defined by the Sturm–Liouville eigenfunctions and its respective eigenvalues. The inverse transform formula is just the expansion cited above. It is defined as follows:

$$F(x, z) = \sum_{r=0}^{\infty} \frac{\overline{F}_r(x)\Psi_r(z)}{N_r^{1/2}}, \tag{5.3}$$

where $\overline{F}_r(x)$ is the transformed potential and N_r is the *norm,* given by

$$N_r \equiv \int_0^h \Psi_r^2(z)\, dz\ .$$

The result of the CITT application is

$$\bar{u}\overline{F}'_r(x) = \bar{K}_{xx}\overline{F}''_r(x) - \lambda_r^2 \overline{F}_r(x), \tag{5.4}$$

where $\overline{F}'_r(x)$ and $\overline{F}''_r(x)$ are the first and second derivatives, respectively. The same procedure is applied to the boundary conditions

$$\overline{F}_r(0) = \frac{Q}{N_r^{1/2}} \frac{\cos(\lambda_r h_f)}{u(0, h_f)}\ ;$$
$$\overline{F}'_r(x) = 0 \quad \text{as} \quad x \to \infty\ .$$

Equation (5.4) is solved, and the result is substituted in (5.3), completing the solution for the mathematical filter.

5.4 Double GITT Application for 2D Dispersion Model

After computing the filter solution, a new variable (called filtered potential) is defined, to produce a problem with homogeneous boundary conditions, as follows:

$$C_f(x, z) \equiv C(x, z) - F(x, z)\ .$$

By analogy with (5.3), the filtered solution is given by the inverse formula

$$C_f(x,z) = \sum_{r=0}^{\infty} \frac{\overline{C}_{f,r}(x)\Psi_r(z)}{N_r^{1/2}}, \tag{5.5}$$

where $\overline{C}_{f,r}(x)$ is the transformed potential. The associated Sturm–Liouville problem for the variable $C_f(x,z)$ is the same as that for $F(x,z)$, because the boundary conditions are identical. Substituting (5.5) and the filter function in (5.1), we arrive at the differential equation

$$\sum_{i=0}^{\infty} \left[\overline{C}_{f,i}\left(B_{ij} - G_{ij} + \lambda_i^2 H_{ij}\right)\right] + \sum_{i=0}^{\infty} \left[\frac{\partial \overline{C}_{f,i}}{\partial x}\left(A_{ij} - E_{ij}\right)\right] - \sum_{i=0}^{\infty} \left[\frac{\partial^2 \overline{C}_{f,i}}{\partial x^2} J_{ij}\right] = V_j,$$

where

$$A_{ij} = \int_0^h u \frac{\Psi_i \Psi_j}{\sqrt{N_i N_j}} dz \; ; \qquad B_{ij} = \int_0^h w \frac{\Psi_i \Psi_j}{\sqrt{N_i N_j}} dz \; ;$$

$$H_{ij} = \int_0^h K_{xx} \frac{\Psi_i \Psi_j}{\sqrt{N_i N_j}} dz \; ; \qquad J_{ij} = \int_0^h K_{zz} \frac{\Psi_i \Psi_j}{\sqrt{N_i N_j}} dz \; ;$$

$$E_{ij} = \int_0^h \left(\frac{\partial K_{xx}}{\partial x}\right) \frac{\Psi_i \Psi_j}{\sqrt{N_i N_j}} dz \; ; \quad G_{ij} = \int_0^h \left(\frac{\partial K_{zz}}{\partial z}\right) \frac{\Psi_i \Psi_j}{\sqrt{N_i N_j}} dz \; ;$$

$$V_j = \int_0^h u \frac{\partial F}{\partial x} \frac{\Psi_j}{N_j^{1/2}} dz - \int_0^h w \frac{\partial F}{\partial z} \frac{\Psi_j}{N_j^{1/2}} dz + \int_0^h K_{xx} \frac{\partial^2 F}{\partial x^2} \frac{\Psi_j}{N_j^{1/2}} dz + \int_0^h \frac{\partial K_{xx}}{\partial x} \frac{\partial F}{\partial x} \frac{\Psi_j}{N_j^{1/2}} dz + \int_0^h K_{zz} \frac{\partial^2 F}{\partial z^2} \frac{\Psi_j}{N_j^{1/2}} dz + \int_0^h \frac{\partial K_{zz}}{\partial z} \frac{\partial F}{\partial x} \frac{\Psi_j}{N_j^{1/2}} dz.$$

For computing $\overline{C}_{f,r}(x)$ in (5.5), GITT is applied again on the variable x, and the associated Sturm–Liouville problem can be expressed as

$$\frac{d^2\phi_m(x)}{dx^2} + \beta_m^2 \phi_m(x) = 0 \quad \text{with} \quad x \in [0,\ x_{\max}]; \tag{5.6}$$

$$\left.\frac{d\phi_m(x)}{dx}\right|_{x\to\infty} = 0 \quad \text{and} \quad \phi_m(x)|_{x\to 0} = 0.$$

The solution of problem (5.6) is given by

$$\phi_m(x) = \sin(\beta_m x), \quad \beta_m = \frac{(2m-1)\pi}{2x_{\max}}, \quad (m = 1, 2, \ldots).$$

For GITT transformation on the direction x, the following inverse formula is used:

$$\overline{C}_{f,r}(x) = \sum_{m=1}^{\infty} \frac{\overline{\overline{C}}_{f,r,m}\phi_m(x)}{N_m^{1/2}}, \tag{5.7}$$

where $\overline{\overline{C}}_{f,r,m})$ is the double transformed potential. In matrix notation, this is written as

$$\mathbf{P}\,\mathbf{T} = \mathbf{V}, \tag{5.8}$$

where

$$\mathbf{T} = \left[\overline{\overline{C}}_{f,r,m}\right] \; ; \qquad \mathbf{V} = \left[\int_0^{x_{\max}} V_j \frac{\phi_m(x)}{N_m^{1/2}} dx\right] \; ;$$

$$\mathbf{P} = \int_0^{x_{\max}} \left[\left(B_{ij} - G_{ij} - \lambda_i^2 H_{ij}\right) + \beta_m^2 J_{ij} + \left(A_{ij} - E_{ij}\right)\right] \frac{\phi_m \phi_n}{\sqrt{N_m\, N_n}}\, dx \; .$$

The matrix $\mathbf{P}$ has order $(\eta_x \eta_z) \times (\eta_x \eta_z)$. Parameters η_z and η_x are the truncation order of the summation in (5.5) and (5.7), respectively. The algebraic equation system (5.8) is solved by Gaussian elimination. The filtered potential is calculated using the *modified inverse formula*. Such a formula was proposed by Wortmann [Wo03] for obtaining better function approximations by trigonometric expansions (see related references for more details). The mathematical expression for the modified inverse formula is [Cas06]

$$\begin{aligned} C_f(x,z) \approx & \sum_{i=0}^{\eta_z}\sum_{m=1}^{\eta_x} \overline{\overline{C}}_{f,i,m} \frac{\Psi_i\, \phi_m}{\sqrt{N_i\, N_m}} - \frac{1}{2}\sum_{i=0}^{\eta_z} \overline{\overline{C}}_{f,i,\eta_x} \frac{\Psi_i\, \phi_{\eta_x}}{\sqrt{N_i\, N_{\eta_x}}} \\ & - \frac{1}{2}\sum_{m=1}^{\eta_x} \overline{\overline{C}}_{f,\eta_z,m} \frac{\Psi_{\eta_z}\, \phi_m}{\sqrt{N_i\, N_m}} + \frac{1}{4}\overline{\overline{C}}_{f,\eta_z,\eta_x} \frac{\Psi_{\eta_z}\, \phi_{\eta_x}}{\sqrt{N_{\eta_z}\, N_{\eta_x}}} \; . \end{aligned} \tag{5.9}$$

Finally, the expression $C(x,z) = C_f(x,z) - F(x,z)$ is used to calculate the original potential.

5.5 Experimental Data and Model Evaluation

A permanent feature in the atmospheric flow is the high Reynolds number, indicating that turbulent regime can always be found. The turbulent fluxes can be parameterized using the first-order closure, where such fluxes are represented by the product of the gradient of the average quantity and the eddy diffusivity: $\langle v_i' \phi' \rangle = K_{\alpha\alpha} \partial\bar{\phi}/\partial x_i$, where $\langle f \rangle \equiv (1/\Delta t)\int_t^{t+\Delta t} f(\tau)\, d\tau$, with $i = u, v, w$ and $\alpha = x, y, z$. The Taylor statistical theory can be employed to derive a model for the convective atmospheric boundary layer (see [DCVC97] and [DACTCV00]):

$$\frac{K_{zz}}{w_*\, h} = 0.22\, \Psi^{1/3} \left[1 - \exp\left(-\frac{4z}{h}\right) - 3 \times 10^{-4} \exp\left(\frac{8z}{h}\right)\right],$$

$$\frac{K_{xx}}{w_*\, h} = 0.12\, \Psi^{1/3},$$

where Ψ is the dimensionless dissipation function [DCVC97]:

$$\Psi = \left(\frac{z}{h}\right)\left(1 - \frac{z}{h}\right).$$

For the simulation here, only the vertical diffusion coefficient will be considered. The wind velocity profile can be obtained from a meso-scale meteorological model or from the parameterization [BOT86]

$$u(x,z) = \begin{cases} \ln(z/z_0) - \psi_m(z/L) + \psi_m(z_0/L) & \text{if } z < z_b, \\ u(z_b) & \text{if } z > z_b, \end{cases}$$

where $z_b = \min\,[|L|,\ 0.1h]$, L is the Monin–Obukhov length, $\kappa = 0.4$ is the von Kármán constant, u_* is the friction velocity, z_0 is the roughness length, and ψ_m is the stability function [Pau70]:

$$\psi_m = 2\ln\left(\frac{1+A}{2}\right) + \ln\left(\frac{1+A^2}{2}\right) - 2\tan^{-1}(A) + \frac{\pi}{2},$$
$$A = \left(1 - 16\,\frac{z}{L}\right).$$

The performance of the model with the atmospheric boundary layer parameterization based on Taylor's approach was evaluated using the Copenhagen experiment dataset [GL84]. The experiment dealt with the dispersion of tracer SF6 carried out in the north of Copenhagen. The tracer was released from a tower at 115 m height, and a set of ground-level data-collecting sensors was spread on three crosswind arcs. The sampling units were positioned 2–6 km from the releasing point. The crosswind-integrated concentration values were normalized with the tracer releasing rate from [GHIS87]. The site was placed on a residential area approximately 0.6 m long [TU97]. Table 5.1 shows the mean wind speed, friction velocity, the Monin–Obukhov length, convective velocity scale, boundary layer height, relative pollutant-release height, and relative Monin–Obukhov length.

Table 5.1. Meteorological values for the Copenhagen experiment.

Exp.	$u(z_b)$ (ms^{-1})	u_* (ms^{-1})	L	w_*	h (m)	h_f/h	$h/\|L\|$
1	3.4	0.36	-37	1.8	1980	0.06	53.51
2	10.6	0.73	-292	1.8	1920	0.06	6.57
3	5.0	0.38	-71	1.3	1120	0.10	15.77
4	4.6	0.38	-133	0.7	390	0.29	2.93
5	6.7	0.45	-444	0.7	820	0.14	1.85
6	13.2	1.05	-432	2.0	1300	0.09	3.01
7	7.6	0.64	-104	2.2	1850	0.06	17.78
8	9.4	0.69	-56	2.2	810	0.14	14.46
9	10.5	0.75	-289	1.9	2090	0.06	7.23

The simulation is performed considering $w(x, z) = 0$ for the vertical wind field. For computing the solution, it is necessary to identify the number of terms in expansion (5.9). Figure 5.1 shows the convergence when the number of eigenvalues applied for both directions x and z are taken into account.

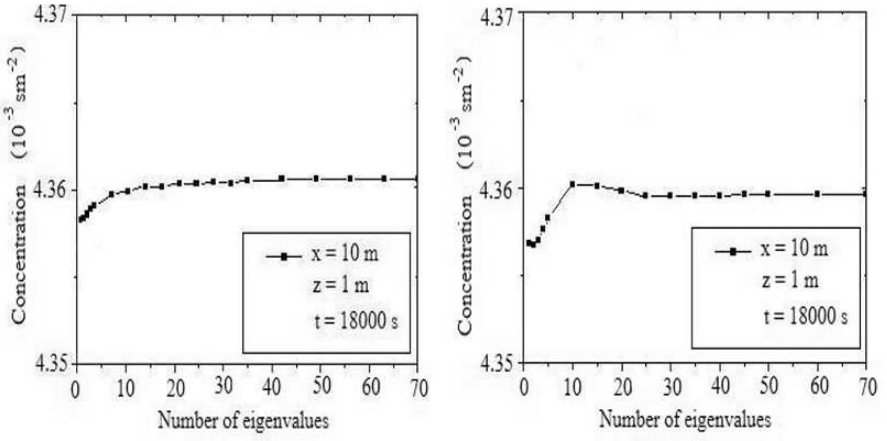

Fig. 5.1. Numerical convergence for the pollutant concentration: (a) direction x (η_x) and (b) direction z (η_z).

The comparison between the experimental (observed) and computed concentrations can be carried out from a scatter diagram, which is shown in Figure 5.2 and indicates good agreement. The comparison can be quantified employing some statistical parameters, presented in Table 5.2. From this table, a strong correlation between the observed and the computed values can be seen. The statistical parameters used in the comparison are

Nmse (normalized mean square error): $(\overline{C^{\mathrm{Exp}} - C})/(\overline{C^{\mathrm{Exp}}\, C})$;

Fa2: fraction of data (%) for $0.5 \leq (C/C^{\mathrm{Exp}}) \leq 2$;

Cor (correlation coefficient): $(\overline{C^{\mathrm{Exp}} - \overline{C^{\mathrm{Exp}}}})\,(\overline{C - \overline{C}})/(\sigma_E\, \sigma_c)$;

Fb (fractional bias): $(\overline{C^{\mathrm{Exp}}} - \overline{C})/[0.5(\overline{C^{\mathrm{Exp}}} + \overline{C})]$;

Fs (fractional standard deviations): $(\sigma_E - \sigma_c)/[0.5(\sigma_E + \sigma_c)]$.

Table 5.2. Model statistical evaluation for ground-level concentration.

Model	Nmse	Cor	Fa2	Fb	Fs
Double GITT	0.04	0.91	1.00	0.06	0.19

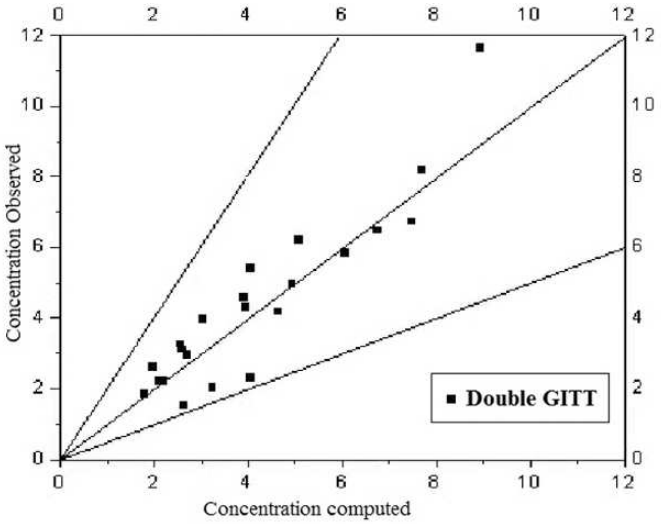

Fig. 5.2. Scatter diagram for crosswind ground-level integrated concentration: observed × computed (lines indicate a factor of two).

A fictitious example can be simulated, where the vertical component of the wind is given by

$$w(x, z) = w_a \cos(w_b\, x);$$

here $w_b = 2\pi/3000$ and w_a ranges from 0 to 4. Figure 5.3 displays the isosurface for the calculated concentration for two w_a values, where the influence of the vertical wind field can clearly be noted.

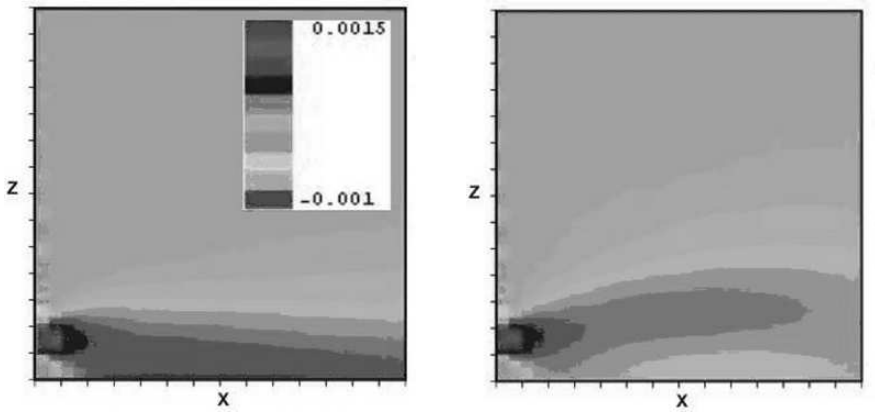

(a) (b)

Fig. 5.3. Iso-concentration lines for (a) $w_a = 0$ and (b) $w_a = 4$.

5.6 Conclusion

The double GITT was derived and applied to the two-dimensional atmospheric pollutant dispersion problem. The computed solution shows good agreement with the experimental data from the Copenhagen experiment [GHIS87], [GL84]. The statistical results indicate small values for the normalized mean-square error (Nmse), fractional bias (Fb), and fractional standard deviation (Fs) (zero is the ideal value). In addition, the correlation coefficient (Cor) and factor of two (Fa2) are close to one.

It should be noted that other GITT schemes can be applied, such as standard GITT [Cot93], [Cot97] or GILTT (generalized integral and Laplace transform technique) [WVCVS05]. However, the latter techniques make it difficult to control the numerical error in the calculated solution. Also, GILTT cannot be applied in the case of variable coefficients. Finally, the truncated numerical error can be controled using the double GITT.

References

[BOT86] Berkowicz, R.R., Olesen, H.R., Torp, U.: The Danish Gaussian air pollution model (OML): Description, test and sensitivity analysis in view of regulatory applications. In: De Wispeleare, C., Schiermeirier, F.A., Gillani, N.V. (eds.), *Air Pollution Modeling and Its Application.* Plenum (1986).

[Cas06] Cassol, M.: Analytical solution to the time dependent two-dimensional atmospheric pollutant dispersion by the Double GITT. Master thesis. Universidade Federal do Rio Grande do Sul, Porto Alegre, Brazil (2006) (Portuguese).

[Cot93] Cotta, R.M.: *Integral Transforms in Computational Heat and Fluid Flow.* CRC Press, Boca Raton, FL (1993).

[Cot97] Cotta, R.M., Mikhaylov, M.: *Heat Conduction Lumped Analysis, Integral Transforms, Symbolic Computation.* Wiley, Chichester (1997).

[DCVC97] Degrazia, G.A., Campos Velho, H.F., Carvalho, J.C., 1997. Nonlocal exchange coefficients for the convective boundary layer derived from spectral properties. *Contrib. Atm. Phys.,* **70**, 57–64 (1997).

[DACTCV00] Degrazia, G.A., Anfossi, D., Carvalho, J.C., Tirabassi, T., Campos Velho, H.F.: Turbulence parameterization for PBL dispersion models in all stability conditions. *Atm. Environ.,* **34**, 3575–3583 (2000).

[GHIS87] Gryning, S.E., Holtslag, A.A.M., Irwin, J.S., Sivertsen, B.: Applied dispersion modeling based on meteorological scaling parameters. *Atmos. Environ.,* **21**, 79–89 (1987).

[GL84] Gryning, S.E., Lyck, E.: Atmospheric dispersion from elevated sources in an urban area: comparison between tracer experiments and model calculations. *Bull. Am. Meteorol. Soc.,* **23**, 651–660 (1984).

[Mor06] Moreira, D.M.: Modelo Euleriano semi-analítico de dispersão turbulenta de contaminantes. D.Sc. Thesis, Universidade Federal do Rio Grande do Sul, Porto Alegre, Brazil (1999).

[Ozi80] Ozişik, M.N.: *Heat Conduction.* Wiley, New York (1980).

[Pau70] Paulson, C.A.: The mathematical representation of wind speed and temperature profiles in unstable atmospheric surface layer. *J. Appl. Meteorol.,* **9**, 857–861 (1970).

[TU97] Tirabassi, T., Rizza, U.: Boundary layer parameterization for a non-Gaussian puff model. *J. Appl. Meteorol.,* **36**, 1031-1037 (1997).

[WVM00] Wortmann, S., Vilhena, M.T., Moura, A.: Analytical solution of the one dimensional transient pollutant problem with variable eddy diffusivity coefficient. National Meeting on Thermal Science (ENCIT), Brazil (2000).

[WVMB05] Wortmann, S., Vilhena, M.T., Moreira, D.M., Buske, D.: A new analytical approach to simulate the pollutant dispersion in the PBL. *Atmos. Environ.,* **39**, 2171–2178 (2005).

[Wo03] Wortmann, S.: Semi-analytical formulation to the transformed equation from GITT application on the adective-diffusive problems. D.Sc. Thesis, Universidade Federal do Rio Grande do Sul, Porto Alegre, Brazil (2003) (Portuguese).

[WVCVS05] Wortmann, S., Vilhena, M.T., Campos Velho, H.F., Segatto, C.F.: The GILTT pollutant simulation in a stable atmosphere. In: Constanda, C., Nashed, Z., Rollins, D. (eds.), *Integral Methods in Science and Engineering.* Birkhäuser-Boston (2005), pp. 300–308.

6

Transient Acoustic Radiation from a Thin Spherical Elastic Shell

D.J. Chappell, P.J. Harris, D. Henwood, and R. Chakrabarti

University of Brighton, UK; d.j.chappell@brighton.ac.uk, p.j.harris@brighton.ac.uk, davidhenwood@talk21.com, r.chakrabarti@brighton.ac.uk

6.1 Introduction

The work presented in this chapter is motivated by the desire to model the transient interaction of a vibrating loudspeaker with the surrounding air. One possible method for solving this problem is to employ a coupled finite element and boundary element procedure, and one such procedure is being developed as part of this work. However, before the method is used to solve the loudspeaker problem, it will be tested on the simpler problem of acoustic radiation from a thin spherical shell as this has an exact solution, the details of which are given here.

Previous work has tended to concentrate on the case of plane wave scattering [CD98], [GY02] and to use the exact solution of Huang [HH68] for comparison with numerical results. This solution uses the Laplace transformation and expresses the transformed values of the quantities sought as sums of Legendre functions multiplied by unknown coefficients. Applying this method to spherical wave radiation simplifies the problem somewhat, since here only the first term of these sums is required. Huang uses an inverse transformation to obtain a solution for the transient shell displacement, but a solution for the pressure is not given due to its complexity in the frequency domain. For our simplified problem, however, a time-domain solution for both the pressure and the velocity potential on the surface of the shell are obtained. This enables us to check the accuracy of both the structural and the acoustic parts of the numerical model.

In loudspeaker modeling, it is often assumed that the effect of the air pressure acting on the loudspeaker cone can be neglected. This assumption is investigated for several different fluid and structure combinations. Results from an uncoupled numerical model will also be compared with both the coupled and the uncoupled exact solution. This will enable us to see how much of the error in the model can be attributed to coupling. A time-domain Burton–Miller-type boundary element method is used for the acoustic model as detailed in [DC06]. The structural data used as input to this is given by an

undamped finite element method for thin shells. This is solved using explicit time integration as detailed in [DH00].

6.2 Mathematical Formulation of the Problem

Consider a thin spherical shell with mid-surface radius a, thickness h, Young's modulus E, Poisson's ratio ν, and density ρ. Suppose that this shell is surrounded by a homogeneous compressible acoustic fluid of density ρ_f and sound wave speed c. The shell is assumed to be radiating a small amplitude acoustic wave permitting the use of linear wave theory to describe its propagation. A spatially-constant pressure-forcing directed into the exterior field is applied to the shell (from the interior) causing the radiation of a spherical wave. The total pressure loading acting on the shell is therefore the sum of this applied pressure and an exterior pressure loading due to the surrounding fluid. The significance of omitting this second component of the pressure will be investigated later in this chapter.

The equation governing the transient motion of the shell due to a spatially-constant pressure-loading may be derived from the Lagrangian equation of motion for the shell as in [HH68]. This is given by

$$\frac{d^2u(t)}{dt^2} + \frac{2E}{\rho(1-\nu)a^2}u(t) = \frac{p(a,t)}{h\rho}, \tag{6.1}$$

where $u(t)$ is the displacement of the shell in the normal direction and $p(a,t)$ is the total pressure loading on the shell, both evaluated at time t. Note that the spherically symmetric pressure is given in spherical polar coordinates, so it only depends on the radial distance from the origin and time. The shell is assumed to be at rest and undisturbed at $t = 0$, which gives rise to the initial conditions

$$u(0) = (d/dt)u(0) = 0.$$

For later use, note that the Laplace transform of (6.1) is given by

$$\left(s^2 + \frac{2E}{\rho(1-\nu)a^2}\right)\tilde{u}(s) = \frac{\tilde{p}(a,s)}{h\rho}, \tag{6.2}$$

where $\tilde{p}(a,s), \tilde{u}(s)$ are the Laplace transforms of $p(a,t), u(t)$, respectively, and s is the transformation parameter.

The applied spherical wave pressure load can be written as $p^f(a,t) = p_0 f(t)$, where p_0 is p_0 is a constant-magnitude term for the applied pressure and $f(t)$ governs the temporal behavior of the applied pressure. The pressure in the surrounding fluid $p^e(r,t)$ at any distance $r \geq a$ from the origin is governed by the wave equation. In spherical polar coordinates with $p^e(r,t)$ assumed to be a spherical wave, this is given by

$$\frac{1}{r^2}\frac{\partial}{\partial r}\left(r^2\frac{\partial p^e}{\partial r}\right) = \frac{1}{c^2}\frac{\partial^2 p^e}{\partial t^2}. \tag{6.3}$$

The initial conditions are

$$p^e(r,0) = (d/dt)p^e(r,0) = 0,$$

as before. The Laplace transform of (6.3) is

$$\frac{1}{r^2}\frac{\partial}{\partial r}\left(r^2\frac{\partial \tilde{p}^e}{\partial r}\right) = \frac{s^2}{c^2}\tilde{p}^e, \tag{6.4}$$

where $\tilde{p}^e$ is the Laplace transform of p^e. Applying the Sommerfeld radiation condition, the solution of (6.4) is simply

$$\tilde{p}^e(r,s) = \frac{\alpha}{r}\left(\sinh(rs/c) - \cosh(rs/c)\right), \tag{6.5}$$

where α is some constant to be determined from the boundary condition at the shell–fluid interface. This enforces the continuity of normal acceleration and is given by

$$\frac{\partial \tilde{p}^e}{\partial r} = -\rho_f s^2 \tilde{u} \quad \text{at} \quad r = a.$$

Applying this boundary condition to (6.5) to determine α and then substituting back in for $\tilde{p}^e$ yields

$$\tilde{p}^e(r,s) = \frac{\rho_f s^2 a^2 c\tilde{u}\left(\sinh(rs/c) - \cosh(rs/c)\right)}{r(as+c)(\sinh(as/c) - \cosh(as/c))}. \tag{6.6}$$

Substituting (6.6) into the transformed structural equation (6.2), noting that $p(a,t) = p^f(a,t) + p^e(a,t)$, and solving for $\tilde{u}$ leads to

$$\tilde{u}(s) = \frac{p_0 a^2(1-\nu)(as+c)\tilde{f}(s)}{\rho h a^3(1-\nu)s^3 + ca^2(1-\nu)(h\rho + a\rho_f)s^2 + 2Ehas + 2Ehc}, \tag{6.7}$$

where $\tilde{f}(s)$ is the Laplace transform of $f(t)$. The inverse Laplace transformation may be applied to (6.7) in order to obtain the transient solution $u(t)$. It is also possible to obtain frequency-domain expressions for the radiated pressure and velocity potential. These expressions are in a form that is easy to invert at points on the shell, i.e., at $r = a$, since the hyperbolic functions cancel. The pressure is obtained by simply substituting (6.7) into (6.6). The velocity potential φ^e may be obtained from the pressure since $p^e = -\rho_f(\partial/\partial t)\varphi^e$, and hence, its Laplace transform is given by $\tilde{\varphi}^e = -\tilde{p}^e/(\rho_f s)$. We arrive at the expression

$$\tilde{\varphi}^e(a,s) = \frac{-cp_0 a^3(1-\nu)s\tilde{f}(s)}{\rho h a^3(1-\nu)s^3 + ca^2(1-\nu)(h\rho + a\rho_f)s^2 + 2Ehas + 2Ehc}. \tag{6.8}$$

The inverse Laplace transforms of (6.7) and (6.8) may be computed in a similar way because they share the same cubic polynomial denominator $q(s)$. Let us define the following common factor of these expressions:

$$\tilde{g}(s) := \frac{p_0 a^2 (1-\nu)}{q(s)}.$$

We denote its inverse Laplace transform by g(t). Applying the convolution and derivative theorems for Laplace transforms, we deduce that the inverse transforms are

$$u(t) = \left(c + a\frac{d}{dt}\right) f(t) * g(t),$$

$$\varphi^e(t) = -ac\frac{df(t)}{dt} * g(t).$$

The calculation of $g(t)$ follows from the Bromwich inversion formula and Cauchy's residue theorem. This yields

$$g(t) = \sum_j \mathrm{Res}(\tilde{g}(s)e^{st}, s_j),$$

where $\mathrm{Res}(F, x)$ denotes the residue of F at x and s_j denotes the values of s that are poles of $\tilde{g}(s)e^{st}$. The values s_j are clearly just the roots of $q(s)$.

The component of the pressure loading on the shell due to the exterior fluid may be omitted by setting $p^e(a,t) = \tilde{p}^{\,e}(a,s) = 0$ in the structural equations (6.1), (6.2). This has the effect of changing the coefficient of s^2 in $q(s)$ to $\rho hca^2(1-\nu)$. In this case, the roots of $q(s)$ are given by $s_1 = -c/a$, $s_2 = \sqrt{2E}/(a\sqrt{\rho(\nu-1)})$, and $s_3 = -s_2$. In the coupled case, these roots do not have such nice expressions but may be calculated easily by computer.

6.3 Example Problems

The numerical calculations are carried out for a spherical shell with $a = 0.1$ m and $h = 0.75$ mm, so the size of the problem is of similar order to the loudspeaker problem. Three different fluid–structure interactions are considered. Air–steel and water–steel are examples in which the coupling would be expected to be insignificant and significant, respectively. The third example considered is air–paper, due to its similarity to the loudspeaker cone problem. The material parameters are summarized in Table 6.1.

The forcing function $f(t)$ is chosen to be a raised cosine, defined by $f(t) = (1 - \cos(2\pi t/t_0))H(t_0 - t)$, where t_0 is the period of the raised cosine pulse and H is the Heaviside step function. The value of the constant p_0 is taken to be 10^5.

Figure 6.1 shows the results of solving both the coupled and the uncoupled systems for the velocity potential φ^e on the surface of the shell, with each row

Table 6.1. Material/fluid parameters.

Structure Materials ρ (kgm^{-3})		E (Pa)	ν
Steel	7800	209×10^9	0.3
Paper	500	3×10^9	0.333
Exterior Fluids	ρ_f (kgm^{-3})	c (ms^{-1})	
Water	1000	1500	
Air	1.21	342.4	

showing one of the three fluid–structure combinations considered. In each case, two values of t_0 are considered: $t_0 = 0.001$ s in the left column and $t_0 = 0.0004$ s in the right. The total duration of the solution in each case is $4t_0$, and the solutions are calculated at 1024 points in this interval. The results show the expected trends of the coupling being most important in the steel–water interaction and least important for steel–air. The coupling also tends to be more significant for the smaller choice of t_0, i.e., for higher frequencies. A Fourier transform shows that for $t_0 = 0.0004$, $f(t)$ is essentially bandlimited at 10000 Hz and for $t_0 = 0.001$, $f(t)$ is essentially bandlimited at 4000 Hz. The coupling is more significant at these higher forcing frequencies as then resonance frequencies of the structure become excited and the coupling acts as a damping force on them.

The error when using an uncoupled numerical scheme to obtain the surface velocity potential solution is now considered. The structural data are calculated using a time-domain finite-element procedure with thin shell elements. The procedure is carried out using explicit time integration and is described in [DH00]. These data are used as input for a time-domain Burton–Miller boundary element method (BEM) to solve the acoustic part of the problem. This technique is employed because of its superior stability properties compared with other time-domain boundary element methods, and is detailed in [DC06]. The error is calculated with respect to both the coupled and the uncoupled exact solutions described above, and is given by

$$\text{Error} = \frac{1}{n} \sum_{i=1}^{n} \sqrt{\frac{\sum_{j=1}^{N} |\varphi^e(a, t_j) - \bar{\varphi}^e(x_i, t_j)|^2}{\sum_{j=1}^{N} |\varphi^e(a, t_j)|^2}}.$$

Here φ^e and $\bar{\varphi}^e$ denote the exact and modeled values of the velocity potential, respectively, x_i, $i = 1, \ldots, n$, denotes the n boundary elements, and t_j, $j = 1, \ldots, N$, denotes the jth time at which the solution is computed. The BEM is a time-marching method with time-step Δt and so $t_j = (j-1)\Delta t$. This error is therefore an L^2-relative error averaged over the n boundary elements. Additional details of the numerical methods are omitted for brevity.

Figure 6.2 shows how the error in the uncoupled numerical method compared with both the coupled and the uncoupled exact solutions varies with

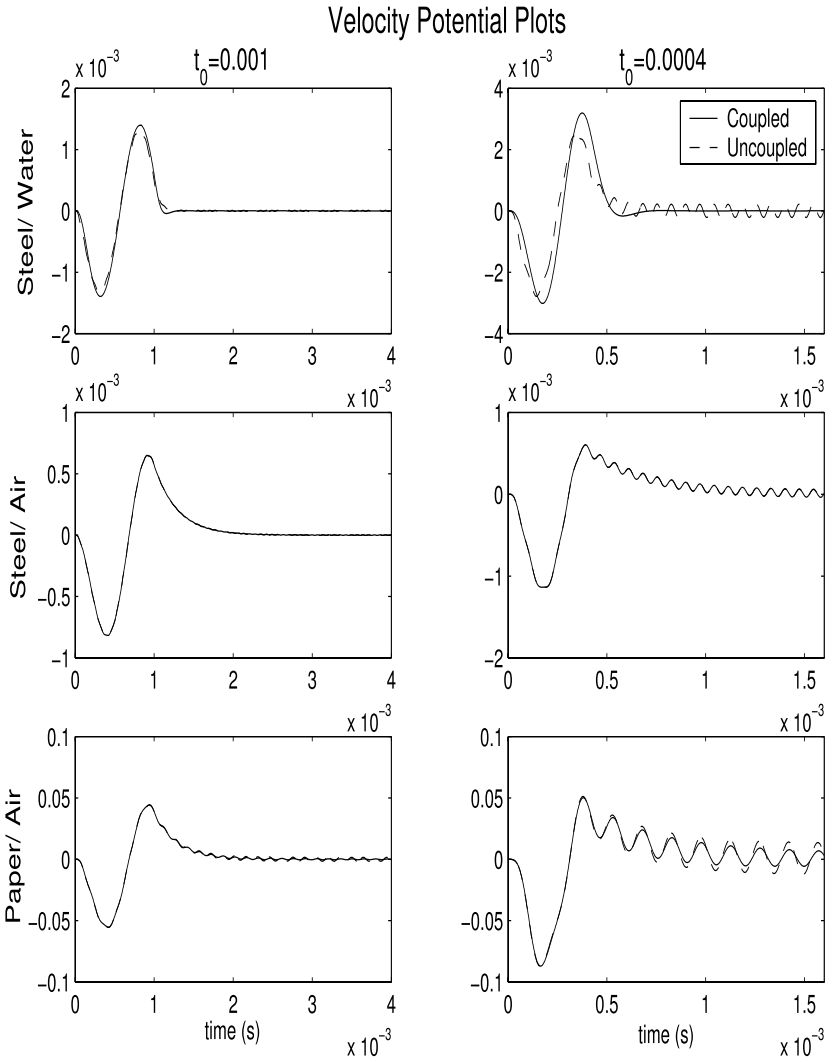

Fig. 6.1. Coupled vs. uncoupled surface velocity potential solution.

the number n of boundary elements. The cases considered are the same as before with the exception of the steel–water interaction, where the error for the coupled exact solution would clearly be very large. The steel–air interaction results are shown in the top row, and the paper–air results are in the second row. The left column shows the errors for the lower frequency case, $t_0 = 0.001$, and the right column shows the higher frequency case, $t_0 = 0.0004$, as before. The solutions were computed at 320 time-points in the interval $[0, 4t_0]$, since this gave a time-step for the BEM whose Nyquist frequency is ten times the

essential band limit of f. Previous work has indicated this solution to be a good choice for accurate results [DC06].

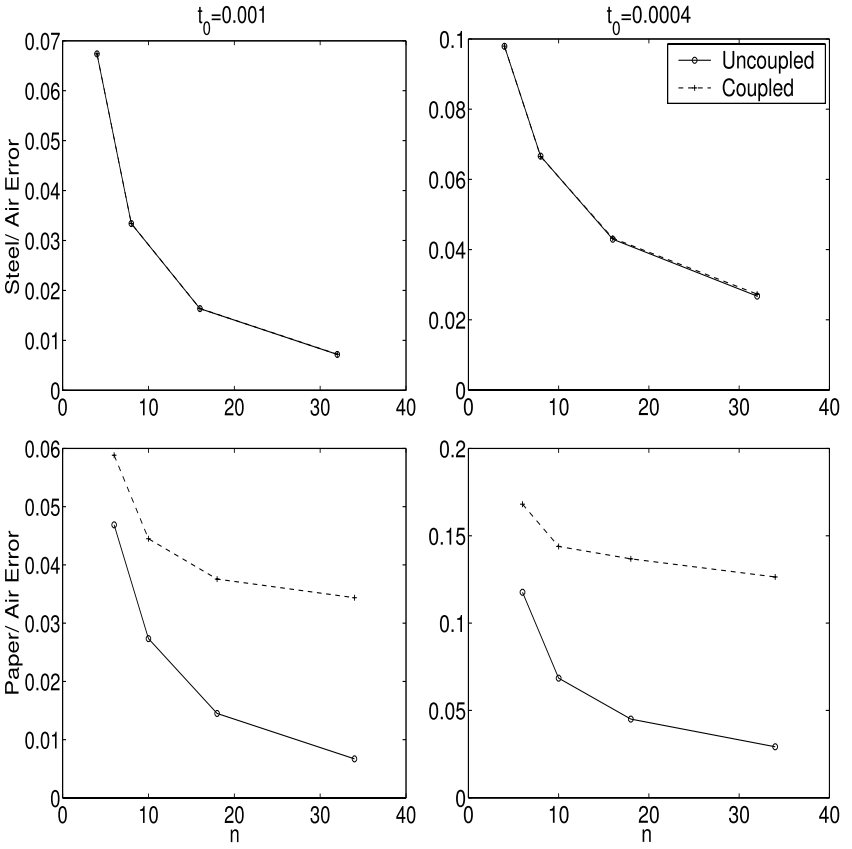

Fig. 6.2. Error in uncoupled modeled solution compared against both coupled and uncoupled exact solutions.

The results show that the error decreases as n is increased and is greater for the higher-frequency case, as expected. The coupling is more significant for the paper–air interaction and as n is increased. The significance of the coupling can be viewed in two ways. First, it can be regarded as the percentage of the error with the coupled solution that arises due to the numerical method being uncoupled, which may be calculated using $(E_c - E_u)/E_c \times 100$, where E_c and E_u are the errors with the coupled and uncoupled exact solutions, respectively. This shows that for the steel–air case, the coupling becomes most significant for the higher-frequency forcing when $n = 32$, where the coupling accounts for just 2.15% of the total error. In contrast, for the paper–air interaction with $n = 34$, the coupling accounts for 80.5% of the total error when $t_0 = 0.001$ and

for 76.9% when $t_0 = 0.0004$. Clearly, the coupling is vastly more significant in the paper–air interaction. Alternatively, the magnitude of the error with the coupled solution may be considered on its own and the coupling may be deemed insignificant if this error is reasonably small. This error is greatest in the high-frequency paper–air case, where for $n = 32$ the error is 0.126, or 12.6%. This may even be regarded as sufficiently accurate in loudspeaker modeling, where errors due to lack of measurement precision and inaccurately estimated material parameters generally dominate.

6.4 Conclusion

An exact solution for modeling transient acoustic radiation from a thin spherical elastic shell has been presented. The effect of omitting the pressure exerted by the exterior fluid back on the shell (or coupling) from the solution has been investigated for several different fluid–structure interactions. A raised cosine-type forcing of varying pulse width has been used. For shorter pulses and thus higher frequencies, the coupling has been shown to have a damping effect on the resonant behavior of the shell. The coupling is therefore more significant in this case than for wider pulses, which do not excite resonances of the shell to the same degree. The effect of the coupling has also been observed to be most pronounced in the steel–water interaction, where the fluid is relatively dense. For lighter fluids like air, the coupling is less significant, although this may vary depending on the material properties of the shell. A comparison with an uncoupled numerical solution showed that the percentage of the error caused by not coupling the numerical method was far greater for the paper–air interaction than the steel–air interaction. However, reasonably accurate results could be obtained in both cases with suitable refinement of the numerical model.

Acknowledgement. The partial funding of this work by B&W Group Limited, Steyning, West Sussex, UK, is gratefully acknowledged.

References

[HH68] Huang, H.: Transient interaction of plane acoustic waves with a spherical elastic shell. *J. Acoust. Soc. Amer.,* **45**, 661–670 (1968).

[CD98] Dyka, C.T., Ingel, R.P.: Transient fluid–structure interaction in naval applications. *Engrg. Anal. Boundary Elements,* **21**, 245–251 (1998).

[DH00] Henwood, D., Moore, J., Geaves, G., Fryer, P.: Towards the transient modelling of loudspeaker diaphragm/surround boundaries. AES 108th Convention Preprints, **5166**, (2000).

[GY02] Yu, G.Y., Lie, S.T., Fan, S.C.: Stable BEM/FEM procedure for dynamic fluid–structure interactions. *J. Engrg. Mech.*, **128**, 909–915 (2002).

[DC06] Chappell, D.J., Harris, P.J., Henwood, D., Chakrabarti, R.: A stable boundary element method for modeling transient acoustic radiation. *J. Acoust. Soc. Amer.,* **120**, 74–80 (2006).

7

The Eigenfrequencies and Mode Shapes of Drilling Masts

S. Chergui

Entreprise Nationale des Travaux aux Puits, Hassi-Messaoud, Algeria;
sadchergui@yahoo.fr

7.1 Introduction

A drilling mast is a thin, metallic spatial structure that generally consists of tubular or straight-shaped uniform bars rigidly assembled together at their ends, called elastic nodes. It can be of one of two types, A or U (see Figure 7.1). The mast, erected above the opening of a well, enables the vertical motion of the traveling block and has the following major functional roles: (i) to sustain—by means of the hoisting system (drawworks, drilling line, crown block, traveling block, hook, and swivel)—the drill string, the casing string, and the tubing string, and to make possible their up-and-down operation; (ii) to store the drill pipes, drill collars, and tubing; and (iii) to facilitate the drilling and tool-running procedures. Consequently, the drilling mast is of vital importance to a drilling rig. When in use, masts undergo strong vibrations, caused by the motion of the tubular string, of the driving equipment of the drilling machines, and of the floating platforms (in an offshore setup), and by winds. Excessive vibrations of these structures can generate undesirable effects and decrease significantly the lifetime of their parts. Such effects may include the wear of pins and their housing or the fatigue and buckling of certain bars. High-performance and economical design, and the rational use of drilling masts, especially of those intended for very deep and ultra-deep wells, require a rigorous theoretical and experimental investigation of their dynamical behavior. The first and most important step in this research is the determination of the eigenfrequencies and of the mode shapes of vibration.

7.2 Proposed Dynamical Model

In practical engineering, the mast strength is calculated by means of simple equivalent patterns of the structures, which allow us to determine the stresses and to compute the dimensions and principal elements of the mast. This type of calculation gives satisfactory results. When performing it, we have to deal

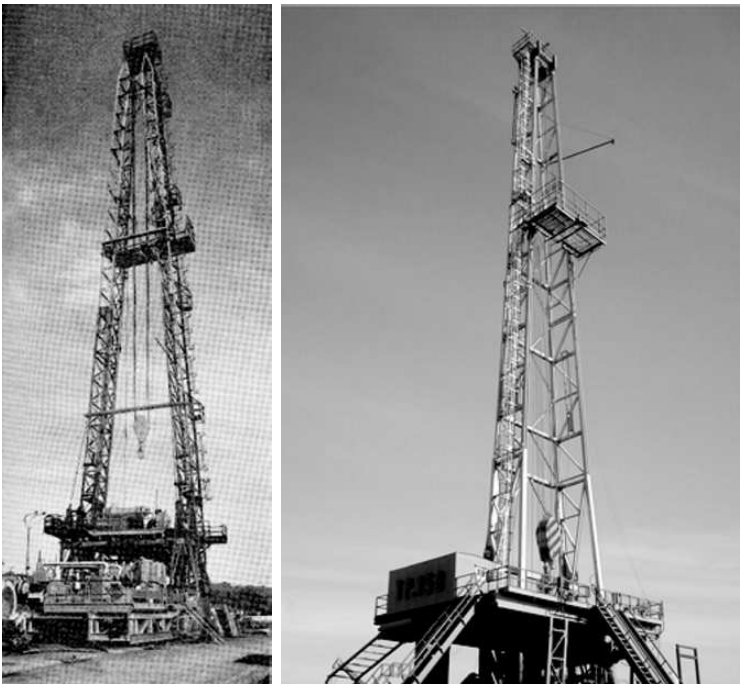

Fig. 7.1. Drilling masts of types A and U.

with the complex structural composition of the masts and of the acting load mode. We must keep in mind that we should use a minimum amount of steel to obtain a mast with a high technical and economic performance. In addition, because of the importance of drilling masts in drilling rigs, the masts must be designed using an adequate dynamical model and a rigorous method of calculation based on the sophisticated software packages currently available.

The proposed dynamical model for a drilling mast is obtained [Ch90] by applying the concentrated masses method. This method makes use of the fact that the distributed masses of the structure bars are concentrated at their junctions, called nodes; therefore, the total concentrated mass at each node is equal to the sum of the nodal contribution of each bar joining at the corresponding node. Those masses are assumed to be connected by a massless link. Figure 7.2 shows the dynamical models for masts of type A and U. Using this model, we can regard a mast as a discrete system with a finite number of degrees of freedom and with the same geometric configuration as the real structure. The number of degrees of freedom is equal to the number of independent parameters specifying the translations and rotations of the nodes. Choosing the node parameters as unknowns, we obtain the displacement method. This method is the most recommended for the static and dynamic computation of bar-assembled structures; hence, it can also be applied to drilling masts.

The assumptions we make for the proposed dynamical model are as follows: (i) the behavior of the structure is linear; (ii) the superposition principle is applicable; (iii) the damping is viscous; and (iv) the translation forces are acting only at the nodes of the mast.

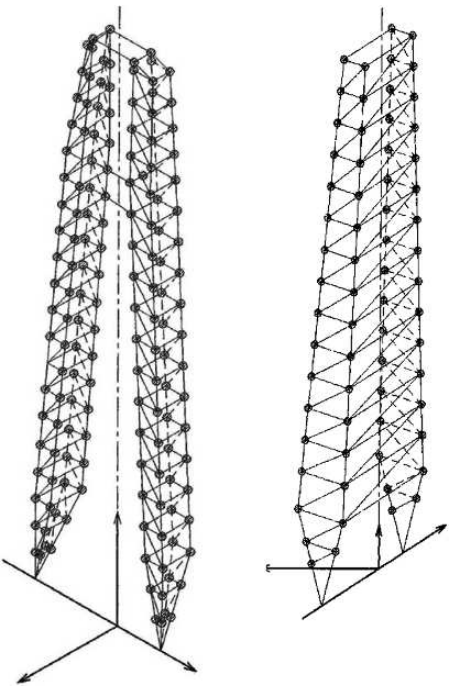

Fig. 7.2. Dynamical models for masts of types A and U.

7.3 Formulation of the Equations of Motion for a Drilling Mast

Each concentrated mass at the nodes of the structure has six unknowns: three translations along the x-, y-, and z-axes and three rotations about the same axes. Those unknowns represent the degrees of freedom for each concentrated mass. The general system of equations is based on six degrees of freedom for each concentrated mass of the mast. Starting from the proposed dynamical model, considering the mast supports to be fixed, using the displacement method, applying the d'Alembert principle to the concentrated mass m_h at node h, and aggregating the dynamic equilibrium for all concentrated masses of the structure, we can write the system of equations governing the motion of a drilling mast in the condensed matrix form

$$[M]\{\ddot{\eta}(t)\} + [B]\{\dot{\eta}(t)\} + [R]\{\eta(t)\} = \{F(t)\},$$

where $[M]$ is the diagonal square matrix of inertia of order N, $[B]$ is the symmetric damping matrix of order N, $[R]$ is the symmetric stiffness matrix of order N, $\{\eta(t)\}$ is the displacement vector of order N, $\{F(t)\}$ is the vector of order N of the excitation forces acting on the concentrated masses, N is the total number of degrees of freedom (translations and rotations) of the dynamical model, and t is the time variable.

This latter system of equations with six unknowns for each node is identical to the well-known classical set of differential equations of second order describing the damped forced vibrations of a linear discrete spatial structure (see [Me67], [Wa76], and [Cl75]). Analytically, this system is decomposed into a set of N second-order differential equations. In the case of drilling masts, where the dimensions of the concentrated masses are lowered, their rotatory inertia may be neglected and the number of unknowns at each node reduces to only three (three translations) instead of six. Hence, the general system of equations of motion for drilling masts becomes

$$[M^{\Delta}]\{\ddot{\Delta}(t)\} + [B^{\Delta}]\{\dot{\Delta}(t)\} + [R^{\Delta}]\{\Delta t\} = \{F^{\Delta}(t)\},$$

where $[M^{\Delta}]$, $[B^{\Delta}]$, and $[R^{\Delta}]$ are the matrices M, B, and R of concentrated masses of order N^{Δ} corresponding to translations only, $\{\Delta(t)\}$ is the displacement vector of order N^{Δ} of the concentrated masses with respect to translations, $\{F^{\Delta(t)}\}$ is the vector of order N^{Δ} of the excitation forces acting on the concentrated masses along the x-, y-, and z-axes, and N^{Δ} is the total number of degrees of freedom (translations only) of the dynamical model.

This system represents the equations of motion for the drilling mast when the rotatory inertia of the concentrated masses is neglected; hence, it contains only half of the unknowns of the general system of equations of motion based on six unknowns for each node. Without any adverse effect on the results, this represents an important reduction of computation time for the dynamical analysis of a drilling mast. Analytically, this system may be decomposed into a set of N^{Δ} second-order differential equations.

7.4 The Eigenfrequencies and Mode Shapes of Vibrations

It is obvious that the equations of free vibrations of a drilling mast when damping is taken into account are

$$[M^{\Delta}]\{\ddot{\Delta}(t)\} + [B^{\Delta}]\{\dot{\Delta}(t)\} + [R^{\Delta}]\{\Delta(t)\} = \{0\},$$

where $\{0\}$ is the zero vector of order N^{Δ}. As the influence of damping on the eigenfrequencies of the vibrations of the structure is negligible, we may

discard the damping effect. Therefore, the eigenfrequencies of a drilling mast can be determined from the set of differential equations for free oscillations

$$[M^{\Delta}]\{\ddot{\Delta}(t)\} + [R^{\Delta}]\{\Delta t\} = \{0\}.$$

This means that the eigenfrequency equation is

$$\left|[R^{\Delta}] - p^2[M^{\Delta}]\right| = 0,$$

that is, an algebraic equation of order N^{Δ} in p^2. The eigenfrequencies p_α of order α and their corresponding mode shapes of vibration can also be determined. Knowing the mode shapes of vibration, we can obtain the free vibrations of the drilling mast as a linear combination of the mode shapes, that is,

$$\begin{aligned}&\left\{\Delta^{\text{free vib.}}(t)\right\}\\ &\quad = \left[\{V_1\}\cos(p_1 t - \theta_1)\ldots\{V_\alpha\}\cos(p_\alpha t - \theta_\alpha)\ldots\right]\left[C_1\ldots C_\alpha\ldots C_N\Delta\right]^T,\end{aligned}$$

where $\left\{\Delta^{\text{free vib.}}(t)\right\}$ is the column vector of the elongations of the discrete masses in free vibration, C_α, θ_α are the constants of the eigenmodes, which can be identified as the amplitudes and phase angles of order α, and $\{V_\alpha\}$ is the column matrix of mode shapes of order α.

7.5 Numerical Application

Using the algorithm proposed in this chapter and the program version SAP 05, we have obtained the eigenfrequencies and mode shapes of vibration of a working drilling mast for a drilling rig of type A designed for very deep wells of up to 7000 m, with drill pipes of $4.5''$. The mast legs have rectangular cross sections and consist of 539 tubular bars and 194 moving nodes. The distributed masses of the bars of the structure are replaced by concentrated masses at the nodes. Neglecting the rotatory inertia of the concentrated masses, we are left to consider a dynamical model with 194×3 degrees of freedom. The dynamical computation of the proposed model by means of the programme SAP 05 needs the following data input: (i) the numerical labeling of the nodes and bars of the mast starting from the base to the top; (ii) the coordinates of the nodes in the Cartesian coordinate system of the dynamical model; (iii) the geometric characteristics: the cross-sectional area and the axial moments of inertia of each bar of the mast; and (iv) the physical characteristics E (longitudinal modulus of elasticity), μ (Poisson ratio), and ρ (density) of the bars.

With this input in SAP 05, the computer calculates the stiffness matrix for each bar of the mast, which is required for the dynamical computation of the eigenfrequencies. In Table 7.1 we present only the values of the first six eigenfrequencies of the mast.

Table 7.1. The first six eigenfrequencies of a working mast.

Eigenfrequency	p_1	p_2	p_3	p_4	p_5	p_6
[rad./s]	4.35	7.72	19.00	21.88	24.79	28.45

7.6 Interpretation of the Results

The analysis of the results obtained in this study allows us to draw several conclusions.

(i) The eigenfrequencies are relatively low and close to each other. This can be explained by the flexibility of the drilling masts. Also, certain eigenfrequencies are included in the domain of angular velocities of the drill string (in the case of rotatory drilling) during drilling operations. This last characteristic is often noticed in the field during drilling for almost all masts, so we should change the rotational speed of the drill string in order to avoid excessive vibrations of the masts.

(ii) The mode shapes of the vibrations are normalized.

(iii) The first four mode shapes, exhibited only by the support leg of the mast and the upper cross section on which the crown block is set, represent bending in the (y, z)-plane, traction in the (x, y)-plane, and torsion about the vertical y-axis.

(iv) Taking into account the energy needed for the excitation of the mast, we assessed that during the tripping operations, which can put the mast outside the elastic equilibrium position, the dynamical deformation of the mast is due to the bending generated by the contribution of the first two oscillation modes.

7.7 Conclusions

(i) The dynamical model adopted here and the corresponding algorithm designed in this chapter can be applied to evaluate the eigenfrequencies of any type of mast.

(ii) It is evident that knowing the eigenfrequencies allows us to avoid the resonance phenomenon in the drilling mast elements and other surface equipment of a drilling rig, by changing the rotational speeds of the drill string. But if the drilling program of a well requires angular velocities of the drill string equal to certain eigenfrequencies of the drilling mast, then we must drill at that speed to reduce the control timing of the drilling mast and of other surface equipment.

(iii) Furthermore, it is easy to see that to determine the eigenfrequencies and mode shapes of vibration of a mast in matrix-calculation theory means

to establish the eigenvalues and eigenvectors of the dynamical stiffness matrix corresponding to the degrees of freedom of the translations of the mast.

References

[Ch90] Chergui, S.: Research concerning the dynamics of a drilling system and mast vibrations. PhD Thesis, Petroleum and Gas Institute, Ploesti, Romania (1990).

[Cl75] Clough, R.W., Penzien, J.: *Dynamics of Structures. Vol. 1. Fundamental Principles.* McGraw-Hill, New York (1975).

[Me67] Meirovitch, L.: *Analytical Methods in Vibrations.* Macmillan, New York (1967).

[Wa76] Warburton, B.G.: *The Dynamical Behavior of Structures.* Pergamon Press, London (1976).

8

Layer Potentials in Dynamic Bending of Thermoelastic Plates

I. Chudinovich and C. Constanda

University of Tulsa, OK, USA; igor-chudinovich@utulsa.edu, christian-constanda@utulsa.edu

8.1 Introduction

The static transverse shear deformation model of elastic plates (see, for example, [Co90], [ChCo00], and [ChCo05]) was generalized to the thermoelastic case in [ScTa93] and [ScTa95]. In this chapter, we solve the time-dependent bending of a thin elastic plate subject to external forces, moments, internal heat sources, homogeneous initial conditions, and Dirichlet or Neumann boundary conditions by reducing the governing equations to time-dependent boundary integral equations with the help of layer potentials and showing the unique solvability of these equations in a variational setting.

A full analysis when thermal effects are not present can be found in [ChCo05] and in [ChCo99], [ChCo00a], [ChCo02], and [ChCo03]. The boundary integral equations arising in the fundamental problems of three-dimensional thermoelasticity [KGBB78] were studied in [ChDu00].

In what follows, we consider a plate with zero initial data. This implies no restriction on generality since homogeneous conditions can easily be achieved by means of an "area" and some "initial" thermoelastic plate potentials (see [ChCo04] and [ChCo06]).

8.2 Preliminaries

We consider a thin elastic plate of thickness $h_0 = \text{const} > 0$, which occupies a region $\bar{S} \times [-h_0/2, h_0/2]$ in $\mathbb{R}^3$, where S is a domain in $\mathbb{R}^2$ with boundary ∂S. The displacement vector at a point x' in this region at $t \geq 0$ is $v(x', t) = (v_1(x', t), v_2(x', t), v_3(x', t))^T$, where the superscript T denotes matrix transposition, and the temperature is $\theta(x', t)$. We write $x' = (x, x_3)$, $x = (x_1, x_2) \in \bar{S}$. We assume [Co90] that

$$v(x', t) = (x_3 u_1(x, t), x_3 u_2(x, t), u_3(x, t))^T.$$

The temperature is best considered through its "moment" (see [ScTa93] and [ScTa95])

$$u_4(x,t) = \frac{1}{h^2 h_0} \int\limits_{-h_0/2}^{h_0/2} x_3 \theta(x, x_3, t)\, dx_3, \quad h^2 = h_0^2/12.$$

Then the vector-valued function

$$U(x,t) = (u(x,t)^T, u_4(x,t))^T, \quad u(x,t) = (u_1(x,t), u_2(x,t), u_3(x,t))^T,$$

satisfies

$$\mathsf{B}_0(\partial_t^2 U)(x,t) + (\mathsf{B}_1 \partial_t U)(x,t) + (\mathsf{A}U)(x,t) = 0, \ \ (x,t) \in G = S \times (0,\infty), \ \ (8.1)$$

where $\mathsf{B}_0 = \operatorname{diag}\{\rho h^2, \rho h^2, \rho, 0\}$, $\partial_t = \partial/\partial t$, $\rho = \text{const} > 0$ is the material density,

$$\mathsf{B}_1 = \begin{pmatrix} 0 & 0 & 0 & 0 \\ 0 & 0 & 0 & 0 \\ 0 & 0 & 0 & 0 \\ \eta\partial_1 & \eta\partial_2 & 0 & \chi^{-1} \end{pmatrix}, \quad \mathsf{A} = \begin{pmatrix} & & & h^2\gamma\partial_1 \\ & A & & h^2\gamma\partial_2 \\ & & & 0 \\ 0 & 0 & 0 & -\triangle \end{pmatrix},$$

$$A = \begin{pmatrix} -h^2\mu\triangle - h^2(\lambda+\mu)\partial_1^2 + \mu & -h^2(\lambda+\mu)\partial_1\partial_2 & \mu\partial_1 \\ -h^2(\lambda+\mu)\partial_1\partial_2 & -h^2\mu\triangle - h^2(\lambda+\mu)\partial_2^2 + \mu & \mu\partial_2 \\ -\mu\partial_1 & -\mu\partial_2 & -\mu\triangle \end{pmatrix},$$

$\partial_\alpha = \partial/\partial x_\alpha$, $\alpha = 1, 2$, η, χ, and γ are positive physical constants, and λ and μ are the Lamé coefficients of the material, satisfying $\lambda + \mu > 0$ and $\mu > 0$.

As explained, the initial conditions are

$$U(x,0) = 0, \quad (\partial_t u)(x,0) = 0, \quad x \in S. \qquad (8.2)$$

Let $\Gamma = \partial S \times (0,\infty)$. In problem (TD) with Dirichlet boundary conditions, the boundary data are

$$U(x,t) = F(x,t) = (f(x,t)^T, f_4(x,t))^T, \quad (x,t) \in \Gamma, \qquad (8.3)$$

where $f(x,t) = (f_1(x,t), f_2(x,t), f_3(x,t))^T$.

We denote by T the boundary moment-stress operator, defined on ∂S by

$$T = \begin{pmatrix} h^2[(\lambda+2\mu)n_1\partial_1 + \mu n_2\partial_2] & h^2(\lambda n_1\partial_2 + \mu n_2\partial_1) & 0 \\ h^2(\mu n_1\partial_2 + \lambda n_2\partial_1) & h^2[(\lambda+2\mu)n_2\partial_2 + \mu n_1\partial_1] & 0 \\ \mu n_1 & \mu n_2 & \mu\partial_n \end{pmatrix}, \qquad (8.4)$$

where $n(x) = (n_1(x), n_2(x))^T$ is the outward unit normal to ∂S and $\partial_n = \partial/\partial n$. In problem (TN) with Neumann boundary conditions, the boundary data are

$$(\mathsf{T}U)(x,t) = G(x,t) = (g(x,t)^T, g_4(x,t))^T, \quad (x,t) \in \Gamma, \qquad (8.5)$$

where $g(x,t) = (g_1(x,t), g_2(x,t), g_3(x,t))^T$ and

$$(\mathsf{T}U)(x,t) = \begin{pmatrix} (Tu)(x,t) - h^2\gamma n(x) u_4(x,t) \\ \partial_n u_4(x,t) \end{pmatrix} = \begin{pmatrix} (\mathsf{T}_e U)(x,t) \\ (\mathsf{T}_\theta U)(x,t) \end{pmatrix}. \tag{8.6}$$

In (8.6) and below, $n(x)$ also stands for the vector $(n_1(x), n_2(x), 0)^T$.

Let S^+ and S^- be the interior and exterior domains bounded by ∂S, and let $G^\pm = S^\pm \times (0,\infty)$. The classical interior and exterior problems $(\mathrm{TD}^\pm)$ consist in finding $U \in C^2(G^\pm) \cap C^1(\bar{G}^\pm)$ that satisfy (8.1) in $G^\pm$, (8.2) in $S^\pm$, and (8.3). The classical interior and exterior problems $(\mathrm{TN}^\pm)$ consist in finding $U \in C^2(G^\pm) \cap C^1(\bar{G}^\pm)$ that satisfy (8.1) in $G^\pm$, (8.2) in $S^\pm$, and (8.5), which we write in the form

$$(\mathsf{T}U)^\pm(x,t) = (\mathsf{T}^\pm U)(x,t) = G(x,t), \quad (x,t) \in \Gamma.$$

The superscripts $\pm$ denote the limiting values of the corresponding functions as $(x,t) \to \Gamma$ from inside $G^\pm$.

To solve the above initial-boundary value problems, we start by considering their Laplace-transformed (with respect to t) versions $(\mathrm{TD}_p^\pm)$ and $(\mathrm{TN}_p^\pm)$.

8.3 The Laplace-Transformed Boundary Value Problems

Let $\mathcal{L}$ and $\mathcal{L}^{-1}$ be the direct and inverse Laplace transformations, and let $\hat{U}(x,p)$ be the Laplace transform of $U(x,t)$, where p is the transformation parameter.

The transformed problems $(\mathrm{TD}_p^\pm)$ consist in finding $\hat{U}(x,p) \in C^2(S^\pm) \cap C^1(\bar{S}^\pm)$ such that

$$\begin{gathered} p^2 \mathsf{B}_0 \hat{U}(x,p) + p\,(\mathsf{B}_1 \hat{U})(x,p) + (\mathsf{A}\hat{U})(x,p) = 0, \quad x \in S^\pm, \\ \hat{U}^\pm(x,p) = \hat{F}(x,p), \quad x \in \partial S. \end{gathered}$$

In problems $(\mathrm{TN}_p^\pm)$, we search for $\hat{U}(x,p) \in C^2(S^\pm) \cap C^1(\bar{S}^\pm)$ such that

$$\begin{gathered} p^2 \mathsf{B}_0 \hat{U}(x,p) + p\,(\mathsf{B}_1 \hat{U})(x,p) + (\mathsf{A}\hat{U})(x,p) = 0, \quad x \in S^\pm, \\ (\mathsf{T}^\pm \hat{U})(x,p) = \hat{G}(x,p), \quad x \in \partial S. \end{gathered}$$

Our analysis requires the introduction of certain function spaces, which we list below. Let $m \in \mathbb{R}$ and $p \in \mathbb{C}$.

$H_m(\mathbb{R}^2)$: the standard Sobolev space of all $\hat{v}_4(x)$, $x \in \mathbb{R}^2$, with norm

$$\|\hat{v}_4\|_m = \left\{ \int_{\mathbb{R}^2} (1 + |\xi|^2)^m |\tilde{v}_4(\xi)|^2 \, d\xi \right\}^{1/2},$$

where $\tilde{v}_4(\xi)$ is the Fourier transform of $\hat{v}_4(x)$.

$\mathbf{H}_{m,p}(\mathbb{R}^2)$: the space of all $\hat{v}(x) = (\hat{v}_1(x), \hat{v}_2(x), \hat{v}_3(x))^T$ in the underlying set of $\left[H_m(\mathbb{R}^2)\right]^3$, with norm

$$\|\hat{v}\|_{m,p} = \left\{ \int\limits_{\mathbb{R}^2} (1 + |\xi|^2 + |p|^2)^m |\tilde{v}(\xi)|^2 \, d\xi \right\}^{1/2}.$$

$\mathcal{H}_{m,p}(\mathbb{R}^2) = \mathbf{H}_{m,p}(\mathbb{R}^2) \times H_m(\mathbb{R}^2)$, with norm $|||\hat{V}|||_{m,p} = \|\hat{v}\|_{m,p} + \|\hat{v}_4\|_m$.

$H_m(S^\pm)$, $\mathbf{H}_{m,p}(S^\pm)$: the spaces of the restrictions to $S^\pm$ of all $\hat{v}_4 \in H_m(\mathbb{R}^2)$, $\hat{v} \in \mathbf{H}_{m,p}(\mathbb{R}^2)$, respectively, with norms

$$\|\hat{u}_4\|_{m;S^\pm} = \inf_{\hat{v}_4 \in H_m(\mathbb{R}^2):\hat{v}_4\big|_{S^\pm} = \hat{u}_4} \|\hat{v}_4\|_m,$$
$$\|\hat{u}\|_{m,p;S^\pm} = \inf_{\hat{v} \in H_{m,p}(\mathbb{R}^2):\hat{v}\big|_{S^\pm} = \hat{u}} \|\hat{v}\|_{m,p}.$$

$\mathcal{H}_{m,p}(S^\pm) = \mathbf{H}_{m,p}(S^\pm) \times H_m(S^\pm)$, with norm

$$|||\hat{U}|||_{m,p;S^\pm} = \|\hat{u}\|_{m,p;S^\pm} + \|\hat{u}_4\|_{m;S^\pm}.$$

$\mathbf{H}_m(\mathbb{R}^2) = \mathbf{H}_{m,0}(\mathbb{R}^2) = \left[H_m(\mathbb{R}^2)\right]^3$, $\mathbf{H}_m(S^\pm) = \mathbf{H}_{m,0}(S^\pm) = \left[H_m(S^\pm)\right]^3$.

$\mathcal{H}_m(\mathbb{R}^2) = \mathbf{H}_m(\mathbb{R}^2) \times H_m(\mathbb{R}^2) = \left[H_m(\mathbb{R}^2)\right]^4$.

$\mathcal{H}_m(S^\pm) = \mathbf{H}_m(S^\pm) \times H_m(S^\pm) = \left[H_m(S^\pm)\right]^4$.

The norms on $\left[H_m(\mathbb{R}^2)\right]^n$ and $\left[H_m(S^\pm)\right]^n$ are denoted by the same symbols $\|\cdot\|_m$ and $\|\cdot\|_{m;S^\pm}$ for all $n = 1, 2, \ldots$.

$\mathring{H}_m(S^\pm)$, $\mathring{\mathbf{H}}_{m,p}(S^\pm)$, $\mathring{\mathcal{H}}_{m,p}(S^\pm) = \mathring{\mathbf{H}}_{m,p}(S^\pm) \times \mathring{H}_m(S^\pm)$: the subspaces of $H_m(\mathbb{R}^2)$, $\mathbf{H}_{m,p}(\mathbb{R}^2)$, $\mathcal{H}_{m,p}(\mathbb{R}^2)$ of all $\hat{v}_4 \in H_m(\mathbb{R}^2)$, $\hat{v} \in \mathbf{H}_{m,p}(\mathbb{R}^2)$, $\hat{V} \in \mathcal{H}_{m,p}(\mathbb{R}^2)$ with $\operatorname{supp} \hat{v}_4 \subset \bar{S}^\pm$, $\operatorname{supp} \hat{v} \subset \bar{S}^\pm$, $\operatorname{supp} \hat{V} \subset \bar{S}^\pm$.

$H_{-m}(S^\pm)$, $\mathbf{H}_{-m,p}(S^\pm)$, $\mathcal{H}_{-m,p}(S^\pm)$: the duals of $\mathring{H}_m(S^\pm)$, $\mathring{\mathbf{H}}_{m,p}(S^\pm)$, $\mathring{\mathcal{H}}_{m,p}(S^\pm)$ with respect to the dualities generated by the inner products in $L^2(S^\pm)$, $\left[L^2(S^\pm)\right]^3$, $\left[L^2(S^\pm)\right]^4$. In what follows, $(\cdot\,,\cdot)_{0;S^\pm}$ is the inner product in $\left[L^2(S^\pm)\right]^n$ for all $n = 1, 2, \ldots$.

We assume that the boundary contour ∂S is a simple, closed, C^2-curve.

$H_{1/2}(\partial S)$, $\mathbf{H}_{1/2,p}(\partial S)$: the spaces of the traces on ∂S of all $\hat{u}_4 \in H_1(S^\pm)$, $\hat{u} \in \mathbf{H}_{1,p}(S^\pm)$, equipped with the norms

$$\|\hat{\varphi}_4\|_{1/2;\partial S} = \inf_{\hat{u}_4 \in H_1(S^+):\hat{u}_4|_{\partial S} = \hat{\varphi}_4} \|\hat{u}_4\|_{1,S^+},$$
$$\|\hat{\varphi}\|_{1/2,p;\partial S} = \inf_{\hat{u} \in \mathbf{H}_{1,p}(S^+):\hat{u}|_{\partial S} = \hat{\varphi}} \|\hat{u}\|_{1,p;S^\pm}.$$

$\mathcal{H}_{1/2,p}(\partial S) = \mathbf{H}_{1/2,p}(\partial S) \times H_{1/2}(\partial S)$, with norm

$$|||\hat{F}|||_{1/2,p;\partial S} = \|\hat{\varphi}\|_{1/2,p;\partial S} + \|\hat{\varphi}_4\|_{1/2;\partial S}.$$

The continuous (uniformly with respect to $p \in \mathbb{C}$) trace operators from $H_1(S^\pm)$ to $H_{1/2}(\partial S)$, from $\mathbf{H}_{1,p}(S^\pm)$ to $\mathbf{H}_{1/2,p}(\partial S)$, and from $\mathcal{H}_{1,p}(S^\pm)$ to $\mathcal{H}_{1/2,p}(\partial S)$, are denoted by the same symbols $\gamma^\pm$.

$H_{-1/2}(\partial S)$, $\mathbf{H}_{-1/2,p}(\partial S)$, $\mathcal{H}_{-1/2,p}(\partial S)$: the duals of $H_{1/2}(\partial S)$, $\mathbf{H}_{1/2,p}(\partial S)$, $\mathcal{H}_{1/2,p}(\partial S)$ with respect to the dualities generated by the inner products in $L^2(\partial S)$, $\big[L^2(\partial S)\big]^3$, $\big[L^2(\partial S)\big]^4$. In what follows, $(\cdot\,,\cdot)_{0;\partial S}$ is the inner product in $\big[L^2(\partial S)\big]^n$ for all $n = 1, 2, \ldots$. The norms of $\hat{g}_4 \in H_{-1/2}(\partial S)$, $\hat{g} \in \mathbf{H}_{-1/2,p}(\partial S)$, $\hat{G} = (\hat{g}^T, \hat{g}_4)^T \in \mathcal{H}_{-1/2,p}(\partial S)$ are denoted by $\|\hat{g}_4\|_{-1/2;\partial S}$, $\|\hat{g}\|_{-1/2,p;\partial S}$, $|||\hat{G}|||_{-1/2,p;\partial S} = \|\hat{g}\|_{-1/2,p;\partial S} + \|\hat{g}_4\|_{-1/2;\partial S}$.

$\mathbf{H}_{\pm1/2}(\partial S) = \mathbf{H}_{\pm1/2,0}(\partial S) = \big[H_{\pm1/2}(\partial S)\big]^3$.

$\mathcal{H}_{\pm1/2}(\partial S) = \mathbf{H}_{\pm1/2}(\partial S) \times H_{\pm1/2}(\partial S) = \big[H_{\pm1/2}(\partial S)\big]^4$.

The norms on $\big[H_{\pm1/2}(\partial S)\big]^n$ are denoted by the same symbols $\|\cdot\|_{\pm1/2;\partial S}$ for all $n = 1, 2, \ldots$.

Let $\hat{U} = (\hat{u}^T, \hat{u}_4)^T$, $\hat{W} = (\hat{w}^T, \hat{w}_4)^T \in \mathcal{H}_{1,p}(S^\pm)$. We write

$$\begin{aligned}\Upsilon_{\pm,p}(\hat{U}, \hat{W}) = a_\pm(\hat{u}, \hat{w}) + (\nabla\hat{u}_4, \nabla\hat{w}_4)_{0;\partial S^\pm} + p^2(B_0^{1/2}\hat{u}, B_0^{1/2}\hat{w})_{0;S^\pm} \\ + \chi^{-1}p\,(\hat{u}_4, \hat{w}_4)_{0;S^\pm} - h^2\gamma(\hat{u}_4, \operatorname{div}\hat{w})_{0;S^\pm} + \eta p\,(\operatorname{div}\hat{u}, \hat{w}_4)_{0,S^\pm},\end{aligned}$$

where $B_0 = \operatorname{diag}\{\rho h^2, \rho h^2, \rho\}$, $a_\pm(\hat{u}, \hat{w}) = 2\int\limits_{S^\pm} E(\hat{u}, \hat{w})\,dx$, and E is the sesquilinear form of the internal static energy density [ChCo00].

$\hat{U} \in \mathcal{H}_{1,p}(S^\pm)$ is called a weak (variational) solution of $(\mathrm{TD}_p^\pm)$ if

$$\Upsilon_{\pm,p}(\hat{U}, \hat{W}) = 0 \quad \forall\hat{W} \in \big[\mathring{H}_1(S^\pm)\big]^4, \quad \gamma^\pm\hat{U} = \hat{F}.$$

Let $\hat{G} \in \mathcal{H}_{-1/2,p}(\partial S)$. For any $\hat{W} \in \mathcal{H}_{1/2,p}(\partial S)$, we write

$$L(\hat{W}) = (\hat{G}, \hat{W})_{0;\partial S} = (\hat{g}, \hat{w})_{0;\partial S} + (\hat{g}_4, \hat{w}_4)_{0;\partial S}.$$

The variational problems $(\mathrm{TN}_p^\pm)$ consist in finding $\hat{U} \in \mathcal{H}_{1,p}(S^\pm)$ such that

$$\Upsilon_{\pm,p}(\hat{U}, \hat{W}) = \pm L(\hat{W}) \quad \forall\hat{W} \in \big[H_1(S^\pm)\big]^4.$$

Let $\mathbb{C}_\kappa = \{p = \sigma + i\zeta \in \mathbb{C} : \sigma > \kappa\}$. Below, we denote by c all positive constants occurring in estimates, which are independent of the functions in those estimates and of $p \in \mathbb{C}_\kappa$ but may depend on κ. Two following assertions were proved in [ChCo05a].

Theorem 1. *For all $\hat{F}(x,p) \in \mathcal{H}_{1/2,p}(\partial S)$, $p \in \mathbb{C}_\kappa$, $\kappa > 0$, problems $(\mathrm{TD}_p^\pm)$ have unique solutions $\hat{U}(x,p) \in \mathcal{H}_{1,p}(S^\pm)$. If the mapping $\hat{F} : \mathbb{C}_\kappa \to \mathcal{H}_{1/2}(\partial S)$ is holomorphic, then so are $\hat{U} : \mathbb{C}_\kappa \to \mathcal{H}_1(S^\pm)$.*

Theorem 2. *For all $\hat{G}(x,p) \in \mathcal{H}_{-1/2,p}(\partial S)$, $p \in \mathbb{C}_\kappa$, $\kappa > 0$, problems $(\mathrm{TN}_p^\pm)$ have unique solutions $\hat{U}(x,p) \in \mathcal{H}_{1,p}(S^\pm)$. If the mapping $\hat{G} : \mathbb{C}_\kappa \to \mathcal{H}_{-1/2}(\partial S)$ is holomorphic, then so are $\hat{U} : \mathbb{C}_\kappa \to \mathcal{H}_1(S^\pm)$.*

8.4 Layer Potentials for the Laplace-Transformed Problems

Let $\mathcal{D}(x,t)$ be a matrix of fundamental solutions for (8.1), which vanishes for $t<0$, and let $\mathcal{A}(x,t) = (\alpha(x,t)^T, \alpha_4(x,t))^T$, where $\alpha(x,t) = (\alpha_1(x,t), \alpha_2(x,t), \alpha_3(x,t))^T$, be a smooth function with compact support in $\partial S \times \mathbb{R}$, which is equal to zero for $t<0$. We define the single-layer thermoelastic plate potential $(\mathcal{V}\mathcal{A})(x,t)$ with density $\mathcal{A}(x,t)$ by

$$(\mathcal{V}\mathcal{A})(x,t) = \int\limits_{\Gamma} \mathcal{D}(x-y,t-\tau)\mathcal{A}(y,\tau)\,ds_y\,d\tau, \quad (x,t)\in\mathbb{R}^3.$$

Its Laplace transform is

$$(\hat{\mathcal{V}}_p\hat{\mathcal{A}})(x,p) = \int\limits_{\partial S} \hat{\mathcal{D}}(x-y,p)\hat{\mathcal{A}}(y,p)\,ds_y, \quad x\in\mathbb{R}^2, \quad p\in\mathbb{C}_0.$$

Let $C^{k,\alpha}(S^{\pm})$ and $C^{k,\alpha}(\partial S)$ be the spaces of functions whose derivatives up to order k are Hölder continuous with index $\alpha\in(0,1]$ in $S^{\pm}$ and on ∂S, respectively. To simplify the notation, we use the symbols C, $C^{k,\alpha}$, and C^m for the appropriate spaces of both scalar and vector-valued functions.

(i) If $\hat{\mathcal{A}}\in C(\partial S)$, then $(\hat{\mathcal{V}}_p\hat{\mathcal{A}})(x,p)$ exists for any $x\in\mathbb{R}^2$, the restrictions of $(\hat{\mathcal{V}}_p\hat{\mathcal{A}})(x,p)$ to $S^{\pm}$ belong to $C^{\infty}(S^{\pm})$, and

$$p^2\mathsf{B}_0(\hat{\mathcal{V}}_p\hat{\mathcal{A}})(x,p) + p\,(\mathsf{B}_1(\hat{\mathcal{V}}_p\hat{\mathcal{A}}))(x,p) + (\mathsf{A}(\hat{\mathcal{V}}_p\hat{\mathcal{A}}))(x,p) = 0, \quad x\in S^{\pm}.$$

Also, $\hat{\mathcal{V}}_p\hat{\mathcal{A}}\in C^{0,\alpha}(\mathbb{R}^2)$ for any $\alpha\in(0,1)$. Thus, the limiting values of $(\hat{\mathcal{V}}_p\hat{\mathcal{A}})(x,p)$, as $x\to\partial S$ from inside $S^{\pm}$, coincide and we write

$$(\hat{\mathcal{V}}_p\hat{\mathcal{A}})^+(x,p) = (\hat{\mathcal{V}}_p\hat{\mathcal{A}})^-(x,p) = (\hat{\mathcal{V}}_p\hat{\mathcal{A}})(x,p), \quad x\in\partial S.$$

Let $\mathcal{V}_p$ be the boundary operator defined by $\hat{\mathcal{A}}(x)\mapsto(\hat{\mathcal{V}}_p\hat{\mathcal{A}})(x,p)$, $x\in\partial S$, which maps $C(\partial S)$ continuously to $C^{0,\alpha}(\partial S)$ for any $\alpha\in(0,1)$.

(ii) If $\hat{\mathcal{A}}\in C^{0,\alpha}(\partial S)$, $\alpha\in(0,1]$, then $\hat{\mathcal{V}}_p\hat{\mathcal{A}}\in C^{1,\beta}(\bar{S}^{\pm})$, with $\beta=\alpha$ for $\alpha\in(0,1)$ and any $\beta\in(0,1)$ for $\alpha=1$.

Let $x_0\in\partial S$, and consider the vector-valued function $(\mathsf{T}(\hat{\mathcal{V}}_p\hat{\mathcal{A}}))(x,p)$, where $x\in S^+$ or $x\in S^-$ and T is defined by (8.4) and (8.6) with $n=n(x_0)$. Then

$$(\mathsf{T}(\hat{\mathcal{V}}_p\hat{\mathcal{A}}))(x,p) = \int\limits_{\partial S} \mathsf{T}\hat{\mathcal{D}}(x-y,p)\hat{\mathcal{A}}(y,p)\,ds_y. \tag{8.7}$$

By (8.7) and the properties of single-layer potentials in static problems [Co90], we find that there exist limiting values $(\mathsf{T}(\hat{\mathcal{V}}_p\hat{\mathcal{A}}))^{\pm}(x_0,p)$, $x_0\in\partial S$, which are connected to the direct value $(\mathsf{T}(\hat{\mathcal{V}}_p\hat{\mathcal{A}}))^{(0)}(x_0,p)$ of the corresponding singular integral by the equalities

$$(\mathsf{T}(\hat{\mathcal{V}}_p\hat{\mathcal{A}}))^{\pm}(x_0,p) = \pm\tfrac{1}{2}\hat{\mathcal{A}}(x_0,p) + (\mathsf{T}(\hat{\mathcal{V}}_p\hat{\mathcal{A}}))^{(0)}(x_0,p), \quad x_0 \in \partial S.$$

Let $\mathcal{B}(x,t) = (\beta(x,t)^T, \beta_4(x,t))^T$, $\beta(x,t) = (\beta_1(x,t), \beta_2(x,t), \beta_3(x,t))^T$, be smooth and with compact support in $\partial S \times \mathbb{R}$, and equal to zero for $t < 0$. We define the double-layer thermoelastic plate potential $(\mathcal{W}\mathcal{B})(x,t)$ with density $\mathcal{B}(x,t)$ by

$$(\mathcal{W}\mathcal{B})(x,t) = \int_{\Gamma} \mathcal{P}(x,y,t-\tau)\mathcal{B}(y,\tau)\, ds_y\, d\tau, \quad (x,t) \in \mathbb{R}^3, \tag{8.8}$$

where $\mathcal{P}(x,y,t) = \left[\mathsf{T}'\mathcal{D}^T(x-y,t)\right]^T$,

$$\mathsf{T}' = \begin{pmatrix} & \eta n_1(y)\partial_t \\ T_y & \eta n_2(y)\partial_t \\ & 0 \\ 0\ 0\ 0 & \partial_{n(y)} \end{pmatrix},$$

and T_y is the boundary differential operator defined by (8.4) in which $n = (n_1(y), n_2(y))^T$ and $\partial_\alpha = \partial/\partial y_\alpha$, $\alpha = 1,2$. Its Laplace transform is

$$(\hat{\mathcal{W}}_p\hat{\mathcal{B}})(x,p) = \int_{\partial S} \hat{\mathcal{P}}(x,y,p)\hat{\mathcal{B}}(y,p)\, ds_y, \quad (x,t) \in \mathbb{R}^2, \quad p \in \mathbb{C}_0, \tag{8.9}$$

where $\hat{\mathcal{B}}(y,p) = (\hat{\beta}(y,p)^T, \hat{\beta}_4(y,p))^T$, $\hat{\mathcal{P}}(x,y,p) = \left[\mathsf{T}'_{\bar{p}}\hat{\mathcal{D}}^T(x-y,p)\right]^T$, and

$$\mathsf{T}'_{\bar{p}} = \begin{pmatrix} & \eta n_1(y)p \\ T_y & \eta n_2(y)p \\ & 0 \\ 0\ 0\ 0 & \partial_{n(y)} \end{pmatrix}.$$

It can be verified that the double-layer potential (8.9) satisfies

$$p^2\mathsf{B}_0(\hat{\mathcal{W}}_p\hat{\mathcal{B}})(x,p) + p\,(\mathsf{B}_1(\hat{\mathcal{W}}_p\hat{\mathcal{B}}))(x,p) + (\mathsf{A}(\hat{\mathcal{W}}_p\hat{\mathcal{B}}))(x,p) = 0, \quad x \in S^+ \cup S_-,$$

and, hence, that its inverse Laplace transform (8.8) satisfies (8.1) in G^+ and G^-.

From the properties of the harmonic double-layer potential and those of the static double-layer potential in the bending of plates with transverse shear deformation [Co90], it follows that there exist limiting values $(\hat{\mathcal{W}}_p\hat{\mathcal{B}})^{\pm}(x_0,p)$, $x_0 \in \partial S$, which are connected to the direct value $(\hat{\mathcal{W}}_p\hat{\mathcal{B}})^{(0)}(x_0,p)$ of the corresponding singular integral by the formulas

$$(\hat{\mathcal{W}}_p\hat{\mathcal{B}})^{\pm}(x_0,p) = \mp\tfrac{1}{2}\,\hat{\mathcal{B}}(x_0,p) + (\hat{\mathcal{W}}_p\hat{\mathcal{B}})^{(0)}(x_0,p), \quad x_0 \in \partial S.$$

The following properties of the double-layer potential follow from the results in [Co90].

(i) If $\hat{\mathcal{B}} \in C^{0,\alpha}(\partial S)$, $\alpha \in (0,1]$, then $\hat{\mathcal{W}}_p\hat{\mathcal{B}} \in C^\infty(S^+ \cup S^-)$.

(ii) In this case, $\hat{\mathcal{W}}_p\hat{\mathcal{B}}$ may be extended from $S^\pm$ to $\bar{S}^\pm$, respectively, and the extended vector-valued functions are of class $C^{0,\beta}(\bar{S}^\pm)$, with $\beta = \alpha$ for $\alpha \in (0,1)$ and any $\beta \in (0,1)$ for $\alpha = 1$.

We define the operators

$$\mathcal{W}_p^\pm : \hat{\mathcal{B}}(x) \to (\hat{\mathcal{W}}_p\hat{\mathcal{B}})^\pm(x,p), \quad x \in \partial S,$$

generated by the limiting values $(\hat{\mathcal{W}}_p\hat{\mathcal{B}})^\pm$ of the double-layer potential.

8.5 Solvability of the Time-Dependent Boundary Integral Equations

A few more function spaces are necessary. Let $\kappa > 0$ and k, $l \in \mathbb{R}$.

$\mathbf{H}^{\mathcal{L}}_{1,k,\kappa}(S^\pm)$, $H^{\mathcal{L}}_{1,k,\kappa}(S^\pm)$ $\mathbf{H}^{\mathcal{L}}_{\pm1/2,k,\kappa}(\partial S)$, $H^{\mathcal{L}}_{\pm1/2,k,\kappa}(\partial S)$: the spaces of all $\hat{u}(x,p)$, $\hat{u}_4(x,p)$, $x \in S^\pm$, $p \in \mathbb{C}_\kappa$, $\hat{e}(x,p), \hat{e}_4(x,p)$, $x \in \partial S$, $p \in \mathbb{C}_\kappa$, which define holomorphic mappings $\mathbb{C}_\kappa \mapsto \mathbf{H}_1(S^\pm)$, $\mathbb{C}_\kappa \mapsto H_1(S^\pm)$ $\mathbb{C}_\kappa \mapsto \mathbf{H}_{\pm1/2}(\partial S)$, $\mathbb{C}_\kappa \mapsto H_{\pm1/2}(\partial S)$, with norms

$$\|\hat{u}\|^2_{1,k,\kappa;S^\pm} = \sup_{\sigma>\kappa} \int_{-\infty}^{\infty} (1+|p|^2)^k \|\hat{u}(x,p)\|^2_{1,p;S^\pm}\, d\zeta,$$

$$\|\hat{u}_4\|^2_{1,k,\kappa;S^\pm} = \sup_{\sigma>\kappa} \int_{-\infty}^{\infty} (1+|p|^2)^k \|\hat{u}_4(x,p)\|^2_{1;S^\pm}\, d\zeta,$$

$$\|\hat{e}\|^2_{\pm1/2,k,\kappa;\partial S} = \sup_{\sigma>\kappa} \int_{-\infty}^{\infty} (1+|p|^2)^k \|\hat{e}(x,p)\|^2_{\pm1/2,p;\partial S}\, d\zeta,$$

$$\|\hat{e}_4\|^2_{\pm1/2,k,\kappa;\partial S} = \sup_{\sigma>\kappa} \int_{-\infty}^{\infty} (1+|p|^2)^k \|\hat{e}_4(x,p)\|^2_{\pm1/2;\partial S}\, d\zeta.$$

$\mathcal{H}^{\mathcal{L}}_{1,k,l,\kappa}(S^\pm) = \mathbf{H}^{\mathcal{L}}_{1,k,\kappa}(S^\pm) \times H^{\mathcal{L}}_{1,l,\kappa}(S^\pm)$, $\mathcal{H}^{\mathcal{L}}_{\pm1/2,k,l,\kappa}(\partial S) = \mathbf{H}^{\mathcal{L}}_{\pm1/2,k,\kappa}(\partial S) \times H^{\mathcal{L}}_{\pm1/2,l,\kappa}(\partial S)$, with norms

$$|||\hat{U}|||_{1,k,l,\kappa;S^\pm} = \|\hat{u}\|_{1,k,\kappa;S^\pm} + \|\hat{u}_4\|_{1,l,\kappa;S^\pm},$$
$$|||\hat{\mathcal{E}}|||_{\pm1/2,k,l,\kappa;\partial S} = \|\hat{e}\|_{\pm1/2,k,\kappa;\partial S} + \|\hat{e}_4\|_{\pm1/2,l,\kappa;\partial S}.$$

Let $\hat{\mathcal{A}} \in \mathcal{H}^{\mathcal{L}}_{-1/2,k,l,\kappa}(\partial S)$, $\hat{F} = (\hat{\varphi}^T, \hat{\varphi}_4)^T \in \mathcal{H}^{\mathcal{L}}_{1/2,k,l,\kappa}(\partial S)$, and $\hat{G} = (\hat{g}^T, \hat{g}_4)^T \in \mathcal{H}^{\mathcal{L}}_{-1/2,k,l,\kappa}(\partial S)$. We define operators $\hat{\mathcal{V}}$ and $\hat{\mathcal{V}}^{-1}$ by setting

$$(\hat{\mathcal{V}}\hat{\mathcal{A}})(x,p) = (\mathcal{V}_p\hat{\mathcal{A}})(x,p), \quad (\hat{\mathcal{V}}^{-1}\hat{F})(x,p) = (\mathcal{V}_p^{-1}\hat{F})(x,p), \quad x \in \partial S, \quad p \in \mathbb{C}_\kappa.$$

We now define operators $\hat{\mathcal{K}}^{\pm}$, $\hat{\mathcal{W}}^{\pm}$, and $\hat{\mathcal{F}}$ and their inverses by setting, for $x \in \partial S$,

$$(\hat{\mathcal{K}}^{\pm}\hat{\mathcal{A}})(x,p) = (\mathcal{K}_p^{\pm}\hat{\mathcal{A}})(x,p), \quad ((\hat{\mathcal{K}}^{\pm})^{-1}\hat{G})(x,p) = ((\mathcal{K}_p^{\pm})^{-1}\hat{G})(x,p),$$
$$(\hat{\mathcal{W}}^{\pm}\hat{\mathcal{B}})(x,p) = (\mathcal{W}_p^{\pm}\hat{\mathcal{B}})(x,p), \quad ((\hat{\mathcal{W}}^{\pm})^{-1}\hat{F})(x,p) = ((\mathcal{W}_p^{\pm})^{-1}\hat{F})(x,p),$$
$$(\hat{\mathcal{F}}\hat{\mathcal{B}})(x,p) = (\mathcal{F}_p\hat{\mathcal{B}})(x,p), \quad (\hat{\mathcal{F}}^{-1}\hat{G})(x,p) = (\mathcal{F}_p^{-1}\hat{G})(x,p).$$

To derive the fundamental results of this chapter, we need to introduce one last batch of function spaces. Again, let $\kappa > 0$ and $k, l \in \mathbb{R}$.

$\mathbf{H}^{\mathcal{L}^{-1}}_{1,k,\kappa}(G^{\pm})$, $H^{\mathcal{L}^{-1}}_{1,l,\kappa}(G^{\pm})$, $\mathcal{H}^{\mathcal{L}^{-1}}_{1,k,l,\kappa}(G^{\pm}) = \mathbf{H}^{\mathcal{L}^{-1}}_{1,k,\kappa}(G^{\pm}) \times H^{\mathcal{L}^{-1}}_{1,l,\kappa}(G^{\pm})$: the spaces of the inverse Laplace transforms of all the elements of $\mathbf{H}^{\mathcal{L}}_{1,k,\kappa}(S^{\pm})$, $H^{\mathcal{L}}_{1,l,\kappa}(S^{\pm})$, $\mathcal{H}^{\mathcal{L}}_{1,k,l,\kappa}(S^{\pm}) = \mathbf{H}^{\mathcal{L}}_{1,k,\kappa}(S^{\pm}) \times H^{\mathcal{L}}_{1,l,\kappa}(S^{\pm})$. The norms of $u(x,t) = \mathcal{L}^{-1}\hat{u}(x,p)$, $u_4(x,t) = \mathcal{L}^{-1}\hat{u}_4(x,p)$, and $U(x,t) = \mathcal{L}^{-1}\hat{U}(x,p) = (u(x,t)^T, u_4(x,t))^T$ are

$$\|u\|_{1,k,\kappa;G^{\pm}} = \|\hat{u}\|_{1,k,\kappa;S^{\pm}}, \quad \|u_4\|_{1,l,\kappa;G^{\pm}} = \|\hat{u}_4\|_{1,l,\kappa;S^{\pm}},$$
$$|||U|||_{1,k,l,\kappa;G^{\pm}} = |||\hat{U}|||_{1,k,l,\kappa;S^{\pm}}.$$

$\mathbf{H}^{\mathcal{L}^{-1}}_{\pm 1/2,k,\kappa}(\Gamma)$, $H^{\mathcal{L}^{-1}}_{\pm 1/2,l,\kappa}(\Gamma)$, $\mathcal{H}^{\mathcal{L}^{-1}}_{\pm 1/2,k,l,\kappa}(\Gamma) = \mathbf{H}^{\mathcal{L}^{-1}}_{\pm 1/2,k,\kappa}(\Gamma) \times H^{\mathcal{L}^{-1}}_{\pm 1/2,l,\kappa}(\Gamma)$: the spaces of the inverse transforms of all the elements of $\mathbf{H}^{\mathcal{L}}_{\pm 1/2,k,\kappa}(\partial S)$, $H^{\mathcal{L}}_{\pm 1/2,l,\kappa}(\partial S)$, $\mathcal{H}^{\mathcal{L}}_{\pm 1/2,k,l,\kappa}(\partial S) = \mathbf{H}^{\mathcal{L}}_{\pm 1/2,k,\kappa}(\partial S) \times H^{\mathcal{L}}_{\pm 1/2,l,\kappa}(\partial S)$. The norms of $e(x,t) = \mathcal{L}^{-1}\hat{e}(x,p)$, $e_4(x,t) = \mathcal{L}^{-1}\hat{e}_4(x,p)$, $\mathcal{E}(x,t) = \mathcal{L}^{-1}\hat{\mathcal{E}}(x,p) = (e(x,t)^T, e_4(x,t))^T$ are

$$\|e\|_{\pm 1/2,k,\kappa;\Gamma} = \|\hat{e}\|_{\pm 1/2,k,\kappa;\partial S}, \quad \|e_4\|_{\pm 1/2,l,\kappa;\Gamma} = \|\hat{u}_4\|_{\pm 1/2,l,\kappa;\partial S},$$
$$|||\mathcal{E}|||_{\pm 1/2,k,l,\kappa;\Gamma} = |||\hat{\mathcal{E}}|||_{\pm 1/2,k,l,\kappa;\partial S}.$$

In what follows, we extend the use of the symbols $\gamma^{\pm}$ to denote also the trace operators from $G^{\pm}$ to Γ.

$U = U(x,t)$, $U = (u^T, u_4)^T \in \mathcal{H}^{\mathcal{L}^{-1}}_{1,0,0,\kappa}(G^{\pm})$, is called a weak solution of the corresponding original problem ($\mathrm{TD}^{\pm}$) if

$$\Upsilon_{\pm}(U,W) = 0, \quad \gamma^{\pm}U = F,$$

where

$$\Upsilon_{\pm}(U,W) = \int_0^{\infty} \{a_{\pm}(u,w) + (\nabla u_4, \nabla w_4)_{0;S^{\pm}} - (B_0^{1/2}\partial_t u, B_0^{1/2}\partial_t w)_{0;S^{\pm}}$$
$$- \chi^{-1}(u_4, \partial_t w_4)_{0;S^{\pm}} - h^2\gamma(u_4, \operatorname{div} w)_{0;S^{\pm}} - \eta(\operatorname{div} u, \partial_t w_4)_{0;S^{\pm}}\}\, dt,$$

for all $W = W(x,t)$, $W = (w^T, w_4)^T \in C_0^{\infty}(\bar{G}^{\pm})$, that is, for all infinitely smooth four-component vector-valued functions with compact support in $\bar{G}^{\pm}$ and satisfying $\gamma^{\pm}W = 0$. Also, $U \in \mathcal{H}^{\mathcal{L}^{-1}}_{1,0,0,\kappa}(G^{\pm})$ is called a weak solution of ($\mathrm{TN}^{\pm}$) if

$$\Upsilon_{\pm}(U,W) = \pm L(W) \quad \forall W \in C_0^{\infty}(\bar{G}^{\pm}),$$

where

$$L(W) = \int_0^{\infty} (G,W)_{0;\partial S}\, dt.$$

The solvability of all these problems was studied in [ChCo05a].

The single-layer and double-layer potentials $(\mathcal{V}\mathcal{A})(x,t)$ and $(\mathcal{W}\mathcal{B})(x,t)$, $(x,t) \in \mathbb{R}^3$, with densities vanishing for $t < 0$, may be defined as the inverse Laplace transforms of $(\hat{\mathcal{V}}\hat{\mathcal{A}})(x,p)$ and $(\hat{\mathcal{W}}\hat{\mathcal{B}})(x,p)$, respectively; that is,

$$(\mathcal{V}\mathcal{A})(x,t) = \mathcal{L}^{-1}((\hat{\mathcal{V}}\hat{\mathcal{A}})(x,p)), \quad (\mathcal{W}\mathcal{B})(x,t) = \mathcal{L}^{-1}((\hat{\mathcal{W}}\hat{\mathcal{B}})(x,p)).$$

These potentials generate boundary operators $\mathcal{V}, \mathcal{W}^{\pm}, \mathcal{K}^{\pm}$, and $\mathcal{F}$ defined by

$$\mathcal{V} = \mathcal{L}^{-1}\hat{\mathcal{V}}\mathcal{L}, \quad \mathcal{W}^{\pm} = \mathcal{L}^{-1}\hat{\mathcal{W}}^{\pm}\mathcal{L}, \quad \mathcal{K}^{\pm} = \mathcal{L}^{-1}\hat{\mathcal{K}}^{\pm}\mathcal{L}, \quad \mathcal{F} = \mathcal{L}^{-1}\hat{\mathcal{F}}\mathcal{L}.$$

We seek the solutions of $(\mathrm{TD}^{\pm})$, in turn, as a single-layer potential and a double-layer potential; in other words,

$$U(x,t) = (\mathcal{V}\mathcal{A})(x,t), \quad U(x,t) = (\mathcal{W}\mathcal{B})(x,t), \quad (x,t) \in G^{\pm},$$

with unknown densities $\mathcal{A}$ and $\mathcal{B}$. After passing to the limit as $(x,t) \to \Gamma$, these representations lead to the systems of boundary integral equations

$$\mathcal{V}\mathcal{A} = F, \quad \mathcal{W}^{\pm}\mathcal{B} = F, \tag{8.10}$$

respectively. The same representations for the solutions of $(\mathrm{TN}^{\pm})$ yield the systems

$$\mathcal{K}^{\pm}\mathcal{A} = G, \quad \mathcal{F}\mathcal{B} = G. \tag{8.11}$$

Theorem 3. *For any $\kappa > 0$ and $k \in \mathbb{R}$, systems* (8.10) *and* (8.11) *have unique solutions.*

Theorem 4. (i) *If $F \in \mathcal{H}^{\mathcal{L}^{-1}}_{1/2,k+1,k+1,\kappa}(\Gamma)$ and $\mathcal{A}$ and $\mathcal{B}$ are the solutions of* (8.10)*, then $U(x,t) = (\mathcal{V}\mathcal{A})(x,t)$ and $U(x,t) = (\mathcal{W}\mathcal{B})(x,t)$ belong to $\mathcal{H}^{\mathcal{L}^{-1}}_{1,k,k,.\kappa}(G^{\pm})$ for any $\kappa > 0$, $k \in \mathbb{R}$, and*

$$|||U|||_{1,k,k,\kappa;G^{\pm}} \le c|||F|||_{1/2,k+1,k+1,\kappa;\Gamma}.$$

(ii) *If $G \in \mathcal{H}^{\mathcal{L}^{-1}}_{-1/2,k+1,k,\kappa}(\Gamma)$ and $\mathcal{A}$ and $\mathcal{B}$ are the solutions of* (8.11)*, then $U(x,t) = (\mathcal{V}\mathcal{A})(x,t)$ and $U(x,t) = (\mathcal{W}\mathcal{B})(x,t)$ belong to $\mathcal{H}^{\mathcal{L}^{-1}}_{1,k,k,\kappa}(G^{\pm})$ for any $\kappa > 0$, $k \in \mathbb{R}$, and*

$$|||U|||_{1,k,k,\kappa;G^{\pm}} \le c|||G|||_{-1/2,k+1,k,\kappa;\Gamma}.$$

(iii) *If $k \ge 0$, then $U(x,t)$ is the weak solution of $(\mathrm{TD}^{\pm})$ or $(\mathrm{TN}^{\pm})$, as appropriate.*

These assertions are proved by using the mapping properties of the boundary operators and Theorems 1 and 2.

References

[ChCo99] Chudinovich, I., Constanda, C.: Nonstationary integral equations for elastic plates. *C.R. Acad. Sci. Paris Sér. I,* **329**, 1115–1120 (1999).

[ChCo00] Chudinovich, I., Constanda, C.: *Variational and Potential Methods in the Theory of Bending of Plates with Transverse Shear Deformation.* Chapman & Hall/CRC, Boca Raton-London-New York-Washington, DC (2000).

[ChCo00a] Chudinovich, I., Constanda, C.: The Cauchy problem in the theory of plates with transverse shear deformation. *Math. Models Methods Appl. Sci.,* **10**, 463–477 (2000).

[ChCo02] Chudinovich, I., Constanda, C.: Boundary integral equations in dynamic problems for elastic plates. *J. Elasticity,* **68**, 73–94 (2002).

[ChCo03] Chudinovich, I., Constanda, C.: Time-dependent boundary integral equations for multiply connected plates. *IMA J. Appl. Math.,* **68**, 507–522 (2003).

[ChCo04] Chudinovich, I., Constanda, C., Colín Venegas, J.: The Cauchy problem in the theory of thermoelastic plates with transverse shear deformation. *J. Integral Equations Appl.,* **16**, 321–342 (2004).

[ChCo05] Chudinovich, I., Constanda, C.: *Variational and Potential Methods for a Class of Linear Hyperbolic Evolutionary Processes.* Springer, London (2005).

[ChCo05a] Chudinovich, I., Constanda, C., Colín Venegas, J.: Solvability of initial-boundary value problems for bending of thermoelasic plates with mixed boundary conditions. *J. Math. Anal. Appl.,* **311**, 357–376 (2005).

[ChCo06] Chudinovich, I., Constanda, C., Colín Venegas, J.: On the Cauchy problem for thermoelastic plates. *Math. Methods Appl. Sci.,* **29**, 625–636 (2006).

[ChDu00] Chudinovich, I., Dumina, O.: Boundary equations in dynamic problems for thermoelastic media. *Visnyk Kharkiv Nat. Univ. Ser. Math. Appl. Math. Mech.,* **475**, 230–240 (2000).

[Co90] Constanda, C.: *A Mathematical Analysis of Bending of Plates with Transverse Shear Deformation.* Longman/Wiley, Harlow-New York (1990).

[KGBB78] Kupradze, V.D., Gegelia, T.G., Basheleishvili, M.O., Burchuladze, T.V.: *Three-dimensional Problems of the Mathematical Theory of Elasticity and Thermoelasticity.* P. Noordhoff, Amsterdam (1978).

[ScTa93] Schiavone, P., Tait, R.J.: Thermal effects in Mindlin-type plates. *Quart. J. Mech. Appl. Math.,* **46**, 27–39 (1993).

[ScTa95] Schiavone, P., Tait, R.J.: Steady time-harmonic oscillations in a linear thermoelastic plate model. *Quart. Appl. Math.,* **53**, 215–233 (1995).

9

Direct Methods in the Theory of Thermoelastic Plates

I. Chudinovich and C. Constanda

University of Tulsa, OK, USA; igor-chudinovich@utulsa.edu, christian-constanda@utulsa.edu

9.1 The Mathematical Model

Consider a plate occupying a region $S \times [-h_0/2,\, h_0/2]$ in $\mathbb{R}^3$, where S is a domain in $\mathbb{R}^2$ with a simple, closed C^2-boundary ∂S and $h_0 = \text{const} > 0$ is the thickness.

We write $G = S \times (0, \infty)$, $\Gamma = \partial S \times (0, \infty)$, and $x = (x_1, x_2)$, and assume that the material is homogeneous and isotropic with Lamé constants λ and μ, density ρ, and heat-related (positive) constants γ, η, and χ.

The displacements and thermal "moment" in the plate are denoted by

$$u(x,t) = \big(x_3 u_1(x,t),\ x_3 u_2(x,t),\ u_3(x,t)\big)^T,$$

$$u_4(x,t) = \frac{1}{h^2 h_0} \int\limits_{-h_0/2}^{h_0/2} x_3 \theta(x, x_3, t)\, dx_3, \quad h^2 = \frac{h_0^2}{12},$$

where $U = (u_1,\, u_2,\, u_3,\, u_4)^T = (u^T, u_4)^T$ and $\theta(x, x_3, t)$ is the temperature.

Applying the procedure of averaging over the thickness, we arrive at the system of governing equations

$$\mathsf{B}_0 \partial_t^2 U(x,t) + \mathsf{B}_1 \partial_t U(x,t) + \mathsf{A} U(x,t) = 0, \quad (x,t) \in G, \tag{9.1}$$

where $\mathsf{B}_0 = \operatorname{diag}\{\rho h^2, \rho h^2, \rho, 0\}$,

$$\mathsf{B}_1 = \begin{pmatrix} 0 & 0 & 0 & 0 \\ 0 & 0 & 0 & 0 \\ 0 & 0 & 0 & 0 \\ \eta\partial_1 & \eta\partial_2 & 0 & \chi^{-1} \end{pmatrix}, \quad \mathsf{A} = \begin{pmatrix} & & & h^2\gamma\partial_1 \\ & A & & h^2\gamma\partial_2 \\ & & & 0 \\ 0 & 0 & 0 & -\Delta \end{pmatrix},$$

$$A = \begin{pmatrix} -h^2\mu\Delta - h^2(\lambda+\mu)\partial_1^2 + \mu & -h^2(\lambda+\mu)\partial_1\partial_2 & \mu\partial_1 \\ -h^2(\lambda+\mu)\partial_1\partial_2 & -h^2\mu\Delta - h^2(\lambda+\mu)\partial_2^2 + \mu & \mu\partial_2 \\ -\mu\partial_1 & -\mu\partial_2 & -\mu\Delta \end{pmatrix},$$

$\partial_t = \partial/\partial t$, and $\partial_\alpha = \partial/\partial x_\alpha$, $\alpha = 1, 2$.

Along with these equations we consider the boundary moment-stress operator

$$T = \begin{pmatrix} h^2[(\lambda+2\mu)n_1\partial_1 + \mu n_2\partial_2] & h^2(\lambda n_1\partial_2 + \mu n_2\partial_1) & 0 \\ h^2(\mu n_1\partial_2 + \lambda n_2\partial_1) & h^2[(\lambda+2\mu)n_2\partial_2 + \mu n_1\partial_1] & 0 \\ \mu n_1 & \mu n_2 & \mu\partial_n \end{pmatrix},$$

where $n = (n_1, n_2)^T$ is the outward unit normal to ∂S and $\partial_n = \partial/\partial n$.

To the governing equations, we adjoin either Dirichlet boundary conditions

$$U = F = (f^T, f_4)^T \quad \text{on } \Gamma \tag{9.2}$$

or Neumann boundary conditions

$$\mathcal{T}U = \begin{pmatrix} Tu - h^2\gamma n u_4 \\ \partial_n u_4 \end{pmatrix} = G = (g^T, g_4)^T \quad \text{on } \Gamma, \tag{9.3}$$

and (without loss of generality) homogeneous initial conditions

$$U(x,0) = 0, \quad (\partial_t u)(x,0) = 0, \quad x \in S. \tag{9.4}$$

For the purpose of this discussion, we distinguish between the interior and exterior domains with respect to the boundary ∂S, denoting the former by S^+ and the latter by S^-. Obviously, we also write $G^\pm = S^\pm \times (0, \infty)$.

Two classical initial-boundary value problems are considered here, as follows:

(TD$^\pm$): find $U \in C^2(G^\pm) \cap C^1(\bar{G}^\pm)$ satisfying (9.1) in $G^\pm$, (9.2) on Γ, and (9.3) in $S^\pm$.

(TN$^\pm$): find $U \in C^2(G^\pm) \cap C^1(\bar{G}^\pm)$ satisfying (9.1) in $G^\pm$, (9.3) on Γ, and (9.4) in $S^\pm$.

9.2 The Laplace-Transformed Problems

With the notation $\mathcal{L}U(x,t) = \hat{U}(x,p)$, we apply the Laplace transformation $\mathcal{L}$ to our initial-value problems and reduce them to corresponding boundary value problems:

(TD$_p^\pm$): Find $\hat{U} \in C^2(S^\pm) \cap C^1(\bar{S}^\pm)$ such that

$$\begin{gathered} p^2\mathsf{B}_0\hat{U} + p\,(\mathsf{B}_1\hat{U}) + (\mathsf{A}\hat{U}) = 0 \quad \text{in } S^\pm, \\ \hat{U} = \hat{F} \quad \text{on } \partial S. \end{gathered}$$

(TN$_p^\pm$): Find $\hat{U} \in C^2(S^\pm) \cap C^1(\bar{S}^\pm)$ such that

$$\begin{gathered} p^2\mathsf{B}_0\hat{U} + p\,(\mathsf{B}_1\hat{U}) + (\mathsf{A}\hat{U}) = 0 \quad \text{in } S^\pm, \\ \mathcal{T}^\pm\hat{U} = \hat{G} \quad \text{on } \partial S. \end{gathered}$$

To study these problems, we adopt all definitions of functions spaces, norms, inner products, and trace operators given in [ChCo1]. We also recall the sesquilinear form for $\hat{U} = (\hat{u}^T, \hat{u}_4)^T$, $\hat{W} = (\hat{w}^T, \hat{w}_4)^T \in \mathcal{H}_{1,p}(S^{\pm})$ defined by

$$\begin{aligned}\Upsilon_{\pm,p}(\hat{U},\hat{W}) = a_{\pm}(\hat{u},\hat{w}) + (\nabla\hat{u}_4, \nabla\hat{w}_4)_{0;\partial S^{\pm}} + p^2(B_0^{1/2}\hat{u}, B_0^{1/2}\hat{w})_{0;S^{\pm}} \\ + \chi^{-1}p\,(\hat{u}_4,\hat{w}_4)_{0;S^{\pm}} - h^2\gamma(\hat{u}_4, \operatorname{div}\hat{w})_{0;S^{\pm}} + \eta p\,(\operatorname{div}\hat{u},\hat{w}_4)_{0,S^{\pm}},\end{aligned}$$

where $B_0 = \operatorname{diag}\{\rho h^2, \rho h^2, \rho\}$, $a_{\pm}(\hat{u},\hat{w}) = 2\int\limits_{S^{\pm}} E(\hat{u},\hat{w})\,dx$, and E is the quadratic form of the internal static energy density.

For $\hat{G} \in \mathcal{H}_{-1/2,p}(\partial S)$ and $\hat{W} \in \mathcal{H}_{1/2,p}(\partial S)$, we define

$$L(\hat{W}) = (\hat{G},\hat{W})_{0;\partial S} = (\hat{g},\hat{w})_{0;\partial S} + (\hat{g}_4,\hat{w}_4)_{0;\partial S}.$$

We can now formulate the variational Laplace-transformed problems.

($\mathrm{TD}_p^{\pm}$): Find $\hat{U} \in \mathcal{H}_{1,p}(S^{\pm})$ such that

$$\Upsilon_{\pm,p}(\hat{U},\hat{W}) = 0 \quad \forall \hat{W} \in \big[\mathring{H}_1(S^{\pm})\big]^4,$$
$$\gamma^{\pm}\hat{U} = \hat{F}.$$

($\mathrm{TN}_p^{\pm}$): Find $\hat{U} \in \mathcal{H}_{1,p}(S^{\pm})$ such that

$$\Upsilon_{\pm,p}(\hat{U},\hat{W}) = \pm L(\hat{W}) \quad \forall \hat{W} \in \big[H_1(S^{\pm})\big]^4.$$

Let $\mathbb{C}_{\kappa} = \{p = \sigma + i\zeta \in \mathbb{C} : \sigma > \kappa\}$.

Theorem 1. (i) *If $\hat{F}(x,p) \in \mathcal{H}_{1/2,p}(\partial S)$, $p \in \mathbb{C}_{\kappa}$, $\kappa > 0$, then ($\mathrm{TD}_p^{\pm}$) have unique solutions $\hat{U}(x,p) \in \mathcal{H}_{1,p}(S^{\pm})$, and if $\hat{F} : \mathbb{C}_{\kappa} \to \mathcal{H}_{1/2}(\partial S)$ is holomorphic, then so are $\hat{U} : \mathbb{C}_{\kappa} \to \mathcal{H}_1(S^{\pm})$.*

(ii) *If $\hat{G}(x,p) \in \mathcal{H}_{-1/2,p}(\partial S)$, $p \in \mathbb{C}_{\kappa}$, $\kappa > 0$, then ($\mathrm{TN}_p^{\pm}$) have unique solutions $\hat{U}(x,p) \in \mathcal{H}_{1,p}(S^{\pm})$, and if $\hat{G} : \mathbb{C}_{\kappa} \to \mathcal{H}_{-1/2}(\partial S)$ is holomorphic, then so are $\hat{U} : \mathbb{C}_{\kappa} \to \mathcal{H}_1(S^{\pm})$.*

9.3 The Analogs of Green's Formulas in the Transform Domain

Let

$$p \in \mathbb{C}_{\kappa}, \;\; \kappa > 0,$$
$$\mathsf{L}_p = p^2\mathsf{B}_0 + p\mathsf{B}_1 + \mathsf{A},$$
$$\hat{U} \in C^2(S^{\pm}) \cap C^1(\bar{S}^{\pm}), \quad \hat{W} \in C^1(S^{\pm}) \cap C(\bar{S}^{\pm}), \quad \hat{\Phi} = \gamma^{\pm}\hat{W}.$$

In S^-, suppose, for example, that

$$|\hat{U}(x,p)| + \sum_{i=1}^{4} |\nabla \hat{u}_i(x,p)| \le \frac{c}{(1+|x|)^{1+\varepsilon}},$$
$$|\hat{W}(x,p)| + \sum_{i=1}^{4} |\nabla \hat{w}_i(x,p)| \le \frac{c}{(1+|x|)^{1+\varepsilon}},$$

where $c = c(p) > 0$ and $\varepsilon > 0$. Then the analog of Green's first formula (Betti formula) for L_p is written as

$$(\mathsf{L}_p\hat{U}, \hat{W})_{0;S^\pm} = \mp(\mathcal{T}_p^{\pm}\hat{U}, \hat{\Phi})_{0;\partial S} + \Upsilon_{\pm,p}(\hat{U}, \hat{W}).$$

The formal adjoint to L_p is

$$\mathsf{L}_p' = \bar{p}^2\mathsf{B}_0 + \bar{p}\,\mathsf{B}_1' + \mathsf{A}',$$

where

$$\mathsf{B}_1' = \begin{pmatrix} 0 & 0 & 0 & -\eta\partial_1 \\ 0 & 0 & 0 & -\eta\partial_2 \\ 0 & 0 & 0 & 0 \\ 0 & 0 & 0 & \chi^{-1} \end{pmatrix}, \quad \mathsf{A}' = \begin{pmatrix} & & & 0 \\ & A & & 0 \\ & & & 0 \\ 0 & 0 & 0 & -\Delta \end{pmatrix}.$$

Then the analog of Green's second formula (reciprocity relation) takes the form

$$(\mathsf{L}_p\hat{U}, \hat{W})_{0;S^\pm} - (\hat{U}, \mathsf{L}_p'\hat{W})_{0;S^\pm} = \mp\big[(\mathcal{T}_p^{\pm}\hat{U}, \hat{\Phi})_{0;\partial S} - (\hat{F}, (\mathcal{T}_p')^{\pm}\hat{W})_{0;\partial S}\big],$$

where

$$\mathcal{T}_p' = \begin{pmatrix} & & \eta n_1(y)\bar{p} \\ & T_y & \eta n_2(y)\bar{p} \\ & & 0 \\ 0 & 0 & 0 \quad \partial_{n(y)} \end{pmatrix}$$

and $\hat{F} = \gamma^{\pm}\hat{U}$.

Finally, the analog of Green's third formula (Somigliana formula) is

$$\hat{U}(x) = \pm\Big\{ \int_{\partial S} \hat{\mathcal{D}}(x-y,p)(\mathcal{T}_p^{\pm}\hat{U})(y)\,ds_y - \int_{\partial S} \hat{\mathcal{P}}(x,y,p)\hat{U}(y)\,ds_y \Big\} + \int_{S^\pm} \hat{\mathcal{D}}(x-y,p)(\mathsf{L}_p\hat{U})(y)\,dy,$$

where $\hat{\mathcal{P}}(x,y,p) = \big[\mathcal{T}_{\bar{p}}'\hat{\mathcal{D}}^T(x-y,p)\big]^T$ and $\hat{\mathcal{D}}(x,p)$ is the Laplace transform of a matrix $\mathcal{D}(x,t)$ of fundamental solutions for (9.1).

9.4 Layer Potentials

For densities $\mathcal{A}$ and $\mathcal{B}$ that are smooth and have compact support in $\partial S \times \mathbb{R}$ and vanish for $t < 0$, the single-layer and double-layer potentials and their Laplace transforms are defined by

$$(\mathcal{V}\mathcal{A})(x,t) = \int_\Gamma \mathcal{D}(x-y,t-\tau)\mathcal{A}(y,\tau)\,ds_y\,d\tau, \quad (x,t) \in \mathbb{R}^3,$$

$$(\hat{\mathcal{V}}_p\hat{\mathcal{A}})(x,p) = \int_{\partial S} \hat{\mathcal{D}}(x-y,p)\hat{\mathcal{A}}(y,p)\,ds_y, \quad x \in \mathbb{R}^2, \quad p \in \mathbb{C}_0,$$

$$(\mathcal{W}\mathcal{B})(x,t) = \int_\Gamma \mathcal{P}(x,y,t-\tau)\mathcal{B}(y,\tau)\,ds_y\,d\tau, \quad (x,t) \in \mathbb{R}^3,$$

$$(\hat{\mathcal{W}}_p\hat{\mathcal{B}})(x,p) = \int_{\partial S} \hat{\mathcal{P}}(x,y,p)\hat{\mathcal{B}}(y,p)\,ds_y, \quad (x,t) \in \mathbb{R}^2, \quad p \in \mathbb{C}_0.$$

The properties of these potentials in the spaces in the appropriate function spaces are mentioned in [ChCo1].

For the transformed problems, we consider the Poincaré–Steklov operators $\mathcal{T}_p^\pm : \mathcal{H}_{1/2,p}(\partial S) \to \mathcal{H}_{-1/2,p}(\partial S)$ and the additional boundary operators

$\mathcal{V}_p : \mathcal{H}_{-1/2,p}(\partial S) \to \mathcal{H}_{1/2,p}(\partial S)$, defined by

$$\hat{\mathcal{A}}(x) \mapsto (\hat{\mathcal{V}}_p\hat{\mathcal{A}})(x,p), \quad x \in \partial S, \quad p \in \mathbb{C}_0,$$

$\mathcal{K}_p^\pm = \mathcal{T}_p^\pm\mathcal{V}_p : \mathcal{H}_{-1/2,p}(\partial S) \to \mathcal{H}_{-1/2,p}(\partial S),\ p \in \mathbb{C}_0,$
$\mathcal{W}_p^\pm : \mathcal{H}_{1/2,p}(\partial S) \to \mathcal{H}_{1/2,p}(\partial S)$, defined by

$$\hat{\mathcal{B}}(x) \mapsto (\hat{\mathcal{W}}_p\hat{\mathcal{B}})^\pm(x,p), \quad x \in \partial S, \quad p \in \mathbb{C}_0,$$

$\mathcal{F}_p = \mathcal{T}_p^+\mathcal{W}_p^+ = \mathcal{T}_p^-\mathcal{W}_p^- : \mathcal{H}_{1/2,p}(\partial S) \to \mathcal{H}_{-1/2,p}(\partial S),\ p \in \mathbb{C}_0,$
$\hat{\mathcal{V}} : \mathcal{H}^{\mathcal{L}}_{-1/2,k+1,k,\kappa}(\partial S) \to \mathcal{H}^{\mathcal{L}}_{1/2,k,k,\kappa}(\partial S)$, defined by

$$\hat{\mathcal{A}}(x,p) \mapsto (\mathcal{V}_p\hat{\mathcal{A}})(x,p), \quad x \in \partial S,\ p \in \mathbb{C}_\kappa,$$

$\hat{\mathcal{K}}^\pm : \mathcal{H}^{\mathcal{L}}_{-1/2,k+1,k,\kappa}(\partial S) \to \mathcal{H}^{\mathcal{L}}_{-1/2,k-1,k-2,\kappa}(\partial S)$, defined by

$$\hat{\mathcal{A}}(x,p) \mapsto (\mathcal{K}_p^\pm\hat{\mathcal{A}})(x,p), \quad x \in \partial S, \quad \kappa \in \mathbb{C}_0,$$

$\hat{\mathcal{W}}^\pm : \mathcal{H}^{\mathcal{L}}_{1/2,k,k,\kappa}(\partial S) \to \mathcal{H}^{\mathcal{L}}_{1/2,k-2,k-2,\kappa}(\partial S)$, defined by

$$\hat{\mathcal{B}}(x,p) \mapsto (\mathcal{W}_p^{\pm}\hat{\mathcal{B}})(x,p), \quad x \in \partial S, \quad \kappa \in \mathbb{C}_0,$$

$\hat{\mathcal{F}} : \mathcal{H}^{\mathcal{L}}_{1/2,k,k,\kappa}(\partial S) \to \mathcal{H}^{\mathcal{L}}_{-1/2,k-3,k-4,\kappa}(\partial S)$, defined by

$$\hat{\mathcal{B}}(x,p) \mapsto (\mathcal{F}_p\hat{\mathcal{B}})(x,p), \quad x \in \partial S, \quad \kappa \in \mathbb{C}_0.$$

For the original problem, we consider the operators

$$\mathcal{V} = \mathcal{L}^{-1}\hat{\mathcal{V}}\mathcal{L} : \mathcal{H}^{\mathcal{L}^{-1}}_{-1/2,k+1,k,\kappa}(\Gamma) \to \mathcal{H}^{\mathcal{L}^{-1}}_{1/2,k,k,\kappa}(\Gamma),$$
$$\mathcal{W}^{\pm} = \mathcal{L}^{-1}\hat{\mathcal{W}}^{\pm}\mathcal{L} : \mathcal{H}^{\mathcal{L}^{-1}}_{1/2,k,k,\kappa}(\Gamma) \to \mathcal{H}^{\mathcal{L}^{-1}}_{1/2,k-2,k-2,\kappa}(\Gamma),$$
$$\mathcal{K}^{\pm} = \mathcal{L}^{-1}\hat{\mathcal{K}}^{\pm}\mathcal{L} : \mathcal{H}^{\mathcal{L}^{-1}}_{-1/2,k+1,k,\kappa}(\Gamma) \to \mathcal{H}^{\mathcal{L}^{-1}}_{-1/2,k-1,k-2,\kappa}(\Gamma),$$
$$\mathcal{F} = \mathcal{L}^{-1}\hat{\mathcal{F}}\mathcal{L} : \mathcal{H}^{\mathcal{L}^{-1}}_{1/2,k,k,\kappa}(\Gamma) \to \mathcal{H}^{\mathcal{L}^{-1}}_{-1/2,k-3,k-4,\kappa}(\Gamma).$$

9.5 The Variational Time-Dependent Problems

We formulate these problems as follows:

(TD$^{\pm}$): Find $U \in \mathcal{H}^{\mathcal{L}^{-1}}_{1,0,0,\kappa}(G^{\pm})$ such that

$$\Upsilon_{\pm}(U,W) = 0 \quad \forall W \in C_0^{\infty}(\bar{G}^{\pm}),$$
$$\gamma^{\pm}U = F,$$

where

$$\Upsilon_{\pm}(U,W) = \int_0^{\infty} \big\{ a_{\pm}(u,w) + (\nabla u_4, \nabla w_4)_{0;S^{\pm}}$$
$$- (B_0^{1/2}\partial_t u, B_0^{1/2}\partial_t w)_{0;S^{\pm}} - \chi^{-1}(u_4, \partial_t w_4)_{0;S^{\pm}}$$
$$- h^2\gamma(u_4, \operatorname{div} w)_{0;S^{\pm}} - \eta(\operatorname{div} u, \partial_t w_4)_{0;S^{\pm}} \big\}\, dt.$$

(TN$^{\pm}$): Find $U \in \mathcal{H}^{\mathcal{L}^{-1}}_{1,0,0,\kappa}(G^{\pm})$ such that

$$\Upsilon_{\pm}(U,W) = \pm L(W) \quad \forall W \in C_0^{\infty}(\bar{G}^{\pm}),$$
$$L(W) = \int_0^{\infty} (G,W)_{0;\partial S}\, dt.$$

It is now obvious that the analogs of the Somigliana formulas in the original domain can be written as

$$\pm U(x,t) = (\mathcal{V}(\mathcal{T}^{\pm}\gamma^{\pm}U))(x,t) - (\mathcal{W}\gamma^{\pm}U)(x,t), \quad (x,t) \in G^{\pm}.$$

Applying $\gamma^{\pm}$ and $\mathcal{T}^{\pm}$ to these equalities, we arrive at the corresponding boundary integral equations: for (TD$^{\pm}$),

$$\mathcal{V}\mathcal{A} = \mathcal{W}^{\mp}F, \quad \mathcal{A} = \mathcal{T}^{\pm}F, \tag{9.5}$$

and for (TN$^{\pm}$),

$$\mathcal{F}\mathcal{B} = \mathcal{K}^{\mp}G, \quad \mathcal{B} = (\mathcal{T}^{\pm})^{-1}G. \tag{9.6}$$

The main result, obtained by combining the mapping properties of the boundary operators introduced above and Theorem 1, is contained in the next assertion.

Theorem 2. *Systems* (9.5) *and* (9.6) *have unique solutions for any* $\kappa > 0$, $k \in \mathbb{R}$.

(i) *If* $F \in \mathcal{H}^{\mathcal{L}^{-1}}_{1/2,k+1,k+1,\kappa}(\Gamma)$, *then*

$$\pm U = \mathcal{V}\mathcal{A} - \mathcal{W}F \in \mathcal{H}^{\mathcal{L}^{-1}}_{1,k,k,\kappa}(G^{\pm}), \quad \kappa > 0, \ \ k \in \mathbb{R},$$
$$|||U|||_{1,k,k,\kappa;G^{\pm}} \leq c|||F|||_{1/2,k+1,k+1,\kappa;\Gamma}.$$

(ii) *If* $G \in \mathcal{H}^{\mathcal{L}^{-1}}_{-1/2,k+1,k,\kappa}(\Gamma)$, *then*

$$\pm U = \mathcal{V}G - \mathcal{W}\mathcal{B} \in \mathcal{H}^{\mathcal{L}^{-1}}_{1,k,k,\kappa}(G^{\pm}), \quad k > 0, \ \ k \in \mathbb{R},$$
$$|||U|||_{1,k,k,\kappa;G^{\pm}} \leq c|||G|||_{-1/2,k+1,k,\kappa;\Gamma}.$$

(iii) *If* $k \geq 0$, *then* U *is the (unique) weak solution of (TD*$^{\pm}$*) or (TN*$^{\pm}$*), as appropriate.*

References

[ChCo1] Chudinovich, I., Constanda, C.: Layer potentials in dynamic bending of thermoelastic plates. In: Constanda, C., Potapenko, S. (eds.), *Integral Methods in Science and Engineering: Techniques and Applications* (this volume). Birkhäuser, Boston, MA (2007), pp. 67–77.

10

The Dirichlet Problem for the Plane Deformation of a Thin Plate on an Elastic Foundation

I. Chudinovich, C. Constanda, D. Doty, W. Hamill, and S. Pomeranz

University of Tulsa, OK, USA; igor-chudinovich@utulsa.edu, christian-constanda@utulsa.edu, dale-doty@utulsa.edu, william-hamill@utulsa.edu, pomeranz@utulsa.edu

10.1 Prerequisites

We consider an elastic plate that occupies a region $S \subset \mathbb{R}^2$ bounded by a simple, closed, C^2-contour ∂S. The extensional motion of the plate is characterized by a displacement field of the form

$$u(x) = \big(u_1(x), u_2(x)\big)^T,$$

where $x = (x_1, x_2)$ and the superscript T denotes matrix transposition. When the plate lies on an elastic foundation, the response of the latter is modeled by the matrix $K = \operatorname{diag}\{k, k\}$, where $k > 0$ is the foundation's elastic coefficient.

The boundary value problem for prescribed displacements on ∂S in the case of equilibrium under in-plane external forces

$$q(x) = \big(q_1(x), q_2(x)\big)^T$$

consists of the governing equations and Dirichlet boundary conditions:

$$\begin{gathered} Zu = Au - Ku = q \quad \text{in } S, \\ u = f \quad \text{on } \partial S, \end{gathered} \tag{10.1}$$

where

$$A = \begin{pmatrix} \mu\Delta + (\lambda+\mu)\partial_1^2 & (\lambda+\mu)\partial_1\partial_2 \\ (\lambda+\mu)\partial_1\partial_2 & \mu\Delta + (\lambda+\mu)\partial_2^2 \end{pmatrix}$$

and $\partial_\alpha = \partial/\partial x_\alpha$, $\alpha = 1, 2$.

We introduce the Sobolev spaces $H_m(S)$, $\mathring{H}(S)$, and $H_m(\partial S)$, $m \in \mathbb{R}$ [DuLi76]. For $q \in \mathring{H}_{-1}(S)$ and $f \in H_{1/2}(\partial S)$, we can use standard functional analysis methods [DuLi76] to prove that problem (10.1) has a unique weak solution in $H_1(S)$. Without loss of generality, we focus on the case $q = 0$, since

the nonhomogenous equation can be reduced to it by means of a Newtonian potential.

In this chapter, we indicate two boundary integral equation techniques, called direct and indirect, for solving (10.1), which are based, respectively, on the Somigliana representation formula and the a priori choice of the form of the solution as a double-layer potential. Numerical results from both methods are obtained and compared graphically.

We point out that our conclusions remain valid if the conditions on the smoothness of ∂S are relaxed, for example, by assuming that the boundary curve ∂S is Lipschitz (in other words, of class $C^{0,1}$) and consists of finitely many Lyapunov arcs.

The question of unique solvability of a variety of boundary value and initial-boundary value problems for bending of plates with transverse shear deformation has been discussed in great detail in [Co90], [ChCo00], and [ChCo05].

10.2 Layer Potentials

Through straightforward calculation, we find that a matrix $D(x, y)$ of fundamental solutions for the operator Z is given by

$$D(x, y) = (\operatorname{adj} Z)(\partial_x)[t(x, y)I_2],$$

where $(\operatorname{adj} Z)(\partial_x)$ is the adjoint of Z that acts on $t(x, y)$ with respect to x, I_2 is the identity (2×2)-matrix,

$$t(x, y) = -\big[2\pi k(\lambda + \mu)\big]^{-1}\big[K_0(c_1|x - y|) - K_0(c_2|x - y|)\big],$$
$$c_1^2 = \frac{k}{\mu}, \quad c_2^2 = \frac{k}{\lambda + 2\mu},$$

and K_0 is the modified Bessel function of second kind and order zero [Co90]. An important role in what follows is also played by the matrix of singular solutions $P(x, y) = [T(\partial_y)D(y, x)]^T$, where T is the boundary stress operator

$$T = \begin{pmatrix} (\lambda + 2\mu)\nu_1\partial_1 + \mu\nu_2\partial_2 & \mu\nu_2\partial_1 + \lambda\nu_1\partial_2 \\ \lambda\nu_2\partial_1 + \mu\nu_1\partial_2 & \mu\nu_1\partial_1 + (\lambda + 2\mu)\nu_2\partial_2 \end{pmatrix}$$

acting on $D(y, x)$ with respect to y and $\nu = (\nu_1, \nu_2)^T$ is the unit outward normal to ∂S. We construct the single-layer and double-layer potentials with densities φ and ψ defined on ∂S by

$$(V\varphi)(x) = \int_{\partial S} D(x, y)\varphi(y)\, ds(y),$$
$$(W\psi)(x) = \int_{\partial S} P(x, y)\psi(y)\, ds(y).$$

If $\varphi \in H_{-1/2}(\partial S)$ and $\psi \in H_{1/2}(\partial S)$, then $V\varphi$, $W\psi \in H_1(S)$. Let γ be the trace operator that maps $H_1(S)$ continuously onto $H_{1/2}(\partial S)$. We can now define boundary operators V^+ and W^+ by

$$V^+\varphi = \gamma(V\varphi),$$
$$W^+\psi = \gamma(W\psi).$$

It is easily seen that V^+ is an integral operator with a weakly singular kernel, and that

$$W^+ = -\tfrac{1}{2}\, I + W_0,$$

where I is the identity operator and W_0 is an integral operator with a singular kernel, which means that the integral in its definition is understood as principal value.

Theorem 1. *The operators*

$$V^+ : H_{-1/2}(\partial S) \to H_{1/2}(\partial S),$$
$$W^+ : H_{1/2}(\partial S) \to H_{1/2}(\partial S)$$

are bijective.

10.3 Boundary Integral Equations

10.3.1 The Indirect Method

We seek the solution of (10.1) in the form

$$u(x) = (W\psi)(x), \quad x \in S,$$

with an unknown density ψ. As x tends to ∂S, we obtain the system of singular integral equations

$$W^+\psi = f \tag{10.2}$$

or

$$-\tfrac{1}{2}\,\psi + W_0\psi = f.$$

Theorem 2. *If $f \in H_{1/2}(\partial S)$, then* (10.2) *has a unique solution $\psi \in H_{1/2}(\partial S)$. In this case, $u = W\psi \in H_1(S)$ is the weak (variational) solution of* (10.1).

10.3.2 The Direct Method

Adapting the procedure for deriving Green's third formula for the Laplace equation to our case, we obtain the so-called Somigliana formula. If $u \in C^2(S) \cap C^1(\bar{S})$ satisfies $Zu = 0$ in S, then

$$\int_{\partial S} \big[D(x,y)(Tu)(y) - P(x,y)u(y)\big]\, ds(y) = \begin{cases} u(x), & x \in S, \\ \frac{1}{2}\, u(x), & x \in \partial S. \end{cases} \tag{10.3}$$

According to the second equation in (10.1), $\gamma u = f$, so representation (10.3) implies that

$$V^+\varphi - W^+ f = f$$

or

$$V^+\varphi = \big(\tfrac{1}{2}\, I + W_0\big) f, \tag{10.4}$$

where $\varphi = Tu$.

We remark that, in contrast to the indirect method, where the density ψ has no physical significance, here φ is the boundary stress vector computed from the solution of the Dirichlet problem. According to Theorem 1, we can extend the operators in (10.4) by continuity to the corresponding Sobolev spaces.

Theorem 3. *If $f \in H_{1/2}(\partial S)$, then system* (10.4) *has a unique solution $\varphi \in H_{-1/2}(\partial S)$. In this case, $u = V\varphi \in H_1(S)$ is the weak (variational) solution of* (10.1).

10.4 Illustrative Example

We considered a square steel floor that occupies the region $\bar{S} = [0,1] \times [0,1]$, for which

$$\lambda = 1.141 \times 10^8, \quad \mu = 8.262 \times 10^7,$$

with all units given in SI (kg, m, s). We assumed that this floor lies on top of a flat foundation with elastic coefficient

$$k = 4 \times 10^7.$$

We chose the boundary condition $f = \gamma u$ to be

$$\begin{aligned} u(x_1, 0) &= \big(0,\ 0.01 \sin(\pi x_1)\big)^T, \\ u(x_1, 1) &= \big(0,\ -0.01 \sin(\pi x_1)\big)^T, \\ u(0, x_2) &= \big(-0.01 \sin(\pi x_2),\ 0\big)^T, \\ u(1, x_2) &= \big(0.01 \sin(\pi x_2),\ 0\big)^T. \end{aligned}$$

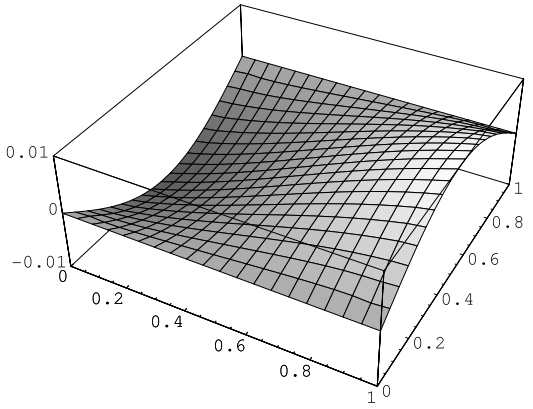

Fig. 10.1. Component u_1 by the indirect method.

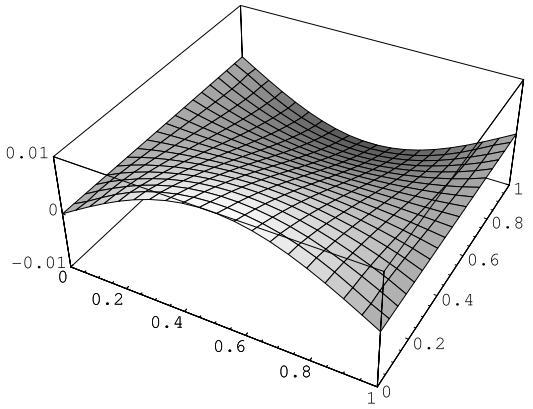

Fig. 10.2. Component u_2 by the indirect method.

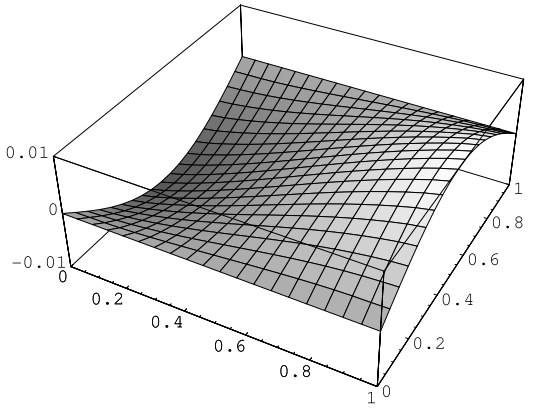

Fig. 10.3. Component u_1 by the direct method.

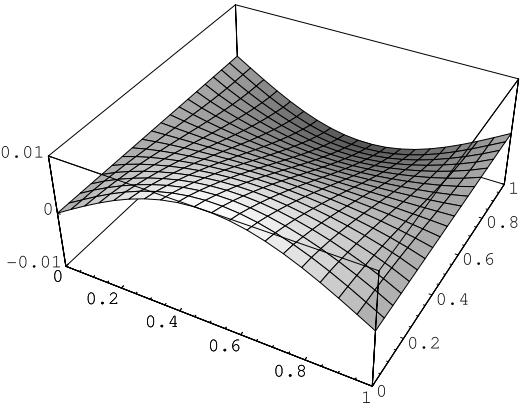

Fig. 10.4. Component u_2 by the direct method.

Using MATEMATICA, we computed $D(x, y)$ and $P(x, y)$ symbolically and employed Gaussian quadrature to calculate the Cauchy principal values, and cubic splines to approximate the solutions of the boundary integral equations.

As Figures 10.1–10.4 show, the results yielded by both the direct and the indirect methods are very good approximations, which means that from a computational viewpoint, the choice of one over the other is not significant. However, the practitioner might prefer the direct method because it is linked to the physics of the model in that the unknown potential density represents the stress vector on the boundary contour.

References

[ChCo00] Chudinovich, I., Constanda, C.: *Variational and Potential Methods in the Theory of Bending of Plates with Transverse Shear Deformation.* Chapman & Hall/CRC, Boca Raton-London-New York-Washington, DC (2000).

[ChCo05] Chudinovich, I., Constanda, C.: *Variational and Potential Methods for a Class of Linear Hyperbolic Evolutionary Processes.* Springer, London (2005).

[Co90] Constanda, C.: *A Mathematical Analysis of Bending of Plates with Transverse Shear Deformation.* Longman/Wiley, Harlow-New York (1990).

[DuLi76] Duvaut, G., Lions, J.-L.: *Inequalities in Mechanics and Physics.* Springer, Berlin (1976).

11

Some Remarks on Homogenization in Perforated Domains

L. Flodén, A. Holmbom, M. Olsson, and J. Silfver[†]

Mittuniversitetet, Östersund, Sweden; lotta.floden@miun.se, anders.holmbom@miun.se, marianne.olsson@miun.se

11.1 Introduction

Mathematical homogenization theory deals with the question of finding effective properties and microvariations in heterogeneous materials. Usually, the difficulty consists in handling the rapid periodic oscillations of coefficients governing some partial differential equation. Sometimes, though, there are also many small periodically arranged holes in the material, i.e., the domain of the equation. In this latter case we have to distinguish between the situations where the holes have Neumann (e.g., isolating holes) and Dirichlet (e.g., constant temperature) boundary conditions. The aim of this chapter is to investigate an intermediate case, where holes with constant zero temperature are coated with a thin layer of a material with low heat-conduction number.

11.2 Some Concepts of Convergence

It is well known that a bounded sequence $\{u_h\}$ in a reflexive Banach space X possesses a subsequence that converges weakly to some $u \in X$, i.e., as $h \to \infty$

$$F(u_h) \to F(u)$$

for every $F \in X'$. Analogously, a bounded sequence $\{F_h\}$ of functionals in X', where X is a separable Banach space, converges weakly* up to subsequence to some $F \in X'$; that is,

$$F_h(u) \to F(u)$$

as $h \to \infty$, for every $u \in X$.

In close connection with these concepts, convergence for operators has been developed. In [Spa68], Spagnolo introduces G-convergence (see also [CD99] and [Mur77]). Consider a sequence of well-posed elliptic equations

$$-\nabla \cdot (A_h(x)\nabla u_h(x)) = f(x) \text{ in } \Omega, \qquad (11.1)$$
$$u_h(x) = 0 \text{ on } \partial\Omega.$$

G-convergence of $\{A_h\}$ to B means that

$$u_h \rightharpoonup u \text{ in } W_0^{1,2}(\Omega)$$

and

$$A_h \nabla u_h \rightharpoonup B\nabla u \text{ in } L^2(\Omega)^N,$$

where u solves

$$-\nabla \cdot (B(x)\nabla u(x)) = f(x) \text{ in } \Omega,$$
$$u(x) = 0 \text{ on } \partial\Omega.$$

For the special case of periodic homogenization we have

$$A_h(x) = A\left(\frac{x}{\varepsilon}\right),$$

where A is a positive definite matrix that is periodic with respect to the unit cube Y and $\varepsilon = \varepsilon(h) \to 0$ for $h \to \infty$. In this case, the limit operator B is a constant matrix that can be computed by solving a partial differential equation defined on a representative unit Y; see [CD99].

All modes of convergence discussed above have the common feature that the limit, whether a function or an operator, is of the same character as the elements in the sequence converging to this limit. In 1986, an important compactness result of a completely different kind was discovered by Nguetseng; see [Ngu89]. He proved that a bounded sequence $\{u_\varepsilon\}$ in $L^2(\Omega)$ possesses a limit in $L^2(\Omega \times Y)$ in a certain weak sense. More precisely, for admissible $v : \Omega \times Y \to R$, that is, sufficiently smooth and periodic in the second variable, and $\{\varepsilon\}$ passing to zero, it holds, up to a subsequence, that

$$\int_\Omega u_\varepsilon(x) v\left(x, \frac{x}{\varepsilon}\right)\, dx \to \int_\Omega \int_Y u_0(x,y)v(x,y)\, dydx. \qquad (11.2)$$

The most frequently used space of admissible test functions is $L^2(\Omega; C_\sharp(Y))$. This compactness result simplifies many homogenization procedures since it enables us to characterize two-scale limits for gradients of bounded sequences in $W^{1,2}(\Omega)$. This means that it is made precise how such two-scale limits depend on the microscale variable y. For $\{u_\varepsilon\}$ a bounded sequence in $W^{1,2}(\Omega)$ and v admissible we get, still up to a subsequence, that, as $\varepsilon \to 0$,

$$\int_\Omega \nabla u_\varepsilon(x) v\left(x, \frac{x}{\varepsilon}\right)\, dx \to \int_\Omega \int_Y (\nabla u(x) + \nabla_y u_1(x,y))v(x,y)\, dydx, \quad (11.3)$$

where u is the weak $W^{1,2}(\Omega)$-limit to $\{u_\varepsilon\}$ and $u_1 \in L^2(\Omega; W_\sharp^{1,2}(Y)/\mathbb{R})$.

In [Ngu89], this result is used to develop a very straightforward homogenization procedure for elliptic equations. The approach is simply to make two suitable choices of test functions in the weak formulation of (11.1) and to apply (11.3). One of the classes of test functions gives us the appropriate homogenized problem and the other the corresponding local problem defined on Y, the solution of which contains the necessary information to compute the homogenized coefficient B.

11.3 Two-Scale Convergence for Perforated Domains

We have already given an example of one of the main difficulties in homogenization theory that consists in the analysis of partial differential equations with rapidly oscillating coefficients. The second most common complication encountered in the study of periodic structures is that of a domain perforated by many small periodically arranged holes. This difficulty is usually overcome by extending functions from the perforated domains, where they are originally defined, to a somewhat larger domain, where the holes have been filled in. To get rid of the irrelevant information provided by the functions' extensions to the holes, we need cutoff functions.

We introduce a class of smooth functions that approaches cutoff functions in the limit. Let Y^H be an open set in $Y \subset \mathbb{R}^2$,

$$Y^\delta = \left\{ y \in Y - Y^H \,\middle|\, d(y, Y^H) < \delta \right\}$$

for fixed $\delta > 0$, and

$$Y^* = Y - Y^H - Y^\delta;$$

see Figure 11.1.

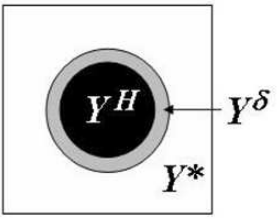

Fig. 11.1. The unit cube Y.

We define a sequence of functions $k_h \in C_\sharp(Y)$ such that

$$\begin{cases} k_h(y) = q_h > 0 & \text{in } Y^H, \\ q_h < k_h(y) < 1 & \text{in } Y^\delta, \\ k_h(y) = 1 & \text{in } Y^*. \end{cases}$$

Furthermore, k_h is strictly increasing with $d(y, Y^H)$; e.g.,

$$k_h(y) = \delta^{-h}(1-q_h)d(y, Y^H)^h + q_h,$$

within Y^δ, and

$$k_h \to \chi_{Y^*} \text{ in } L^p_\sharp(Y)$$

for any $p > 0$ when $h \to \infty$. Finally, we introduce the sets

$$\begin{aligned} \Omega_\varepsilon &= \Omega \cap \left\{ x \in \mathbb{R}^N \,\middle|\, \chi_{Y^*}\left(\frac{x}{\varepsilon}\right) = 1 \right\} \cup P_\varepsilon, \\ \Omega'_\varepsilon &= \Omega \cap \left\{ x \in \mathbb{R}^N \,\middle|\, \chi_{Y^* \cup Y^\delta}\left(\frac{x}{\varepsilon}\right) = 1 \right\} \cup P_\varepsilon, \\ \Omega_{\varepsilon,\delta} &= \Omega'_\varepsilon - \Omega_\varepsilon, \end{aligned} \tag{11.4}$$

where P_ε simply means the part of the perforations $\left\{x \in \mathbb{R}^N \,\middle|\, \chi_{Y^*}\left(\frac{x}{\varepsilon}\right) = 0\right\}$ that cuts $\partial\Omega$ and lies within Ω. This is illustrated in Figure 11.2, where Ω_ε is the white area, Ω'_ε is the white area together with the gray area, and $\Omega_{\varepsilon,\delta}$ is the grey area.

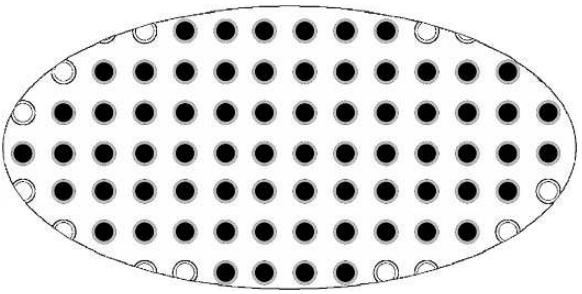

Fig. 11.2. The domain Ω.

Proposition 1. *Let $\{u_\varepsilon\}$ be a sequence in $L^2(\Omega)$ such that $\{\sqrt{k_h(\frac{x}{\varepsilon})}u_\varepsilon(x)\}$ and $\{u_\varepsilon\}$ are bounded in $L^2(\Omega'_\varepsilon)$ and $L^2(\Omega - \Omega'_\varepsilon)$, respectively. Then, up to a subsequence,*

$$\int_{\Omega'_\varepsilon} u_\varepsilon(x) k_h\left(\frac{x}{\varepsilon}\right) v\left(x, \frac{x}{\varepsilon}\right)\, dx \to \int_\Omega \int_{Y^*} u_0(x,y) v(x,y)\, dydx,$$

as $h \to \infty$, for any admissible test function v, where $u_0 \in L^2(\Omega \times Y)$ is the two-scale limit for a sequence of extensions of $u_{\varepsilon|\Omega_\varepsilon}$ to Ω.

Proof. Obviously, $u_{\varepsilon|\Omega_\varepsilon}$ is bounded in $L^2(\Omega_\varepsilon)$, and thus, we can choose a sequence $\{\widetilde{u}_\varepsilon\}$ of extensions that is bounded in $L^2(\Omega)$. Hence, for a suitable subsequence,

$$\int_\Omega u_\varepsilon(x) \chi_{Y^*}\left(\frac{x}{\varepsilon}\right) v\left(x, \frac{x}{\varepsilon}\right)\, dx \to \int_\Omega \int_Y u_0(x,y) \chi_{Y^*}(y) v(x,y)\, dydx,$$

as $\varepsilon \to 0$, for any admissible test function v, where u_0 is the two-scale limit of $\widetilde{u}_\varepsilon$. Moreover, for any $v \in D(\Omega; C^\infty_\sharp(Y))$,

$$\left| \int_{\Omega_{\varepsilon,\delta}} u_\varepsilon(x) k_h\left(\frac{x}{\varepsilon}\right) v\left(x, \frac{x}{\varepsilon}\right)\, dx \right| \leq C \left\| \sqrt{k_h\left(\frac{x}{\varepsilon}\right)} u_\varepsilon(x) \right\|_{L^2(\Omega_{\varepsilon,\delta})} \left\| \sqrt{k_h\left(\frac{x}{\varepsilon}\right)} \right\|_{L^2(\Omega_{\varepsilon,\delta})},$$

and hence, the contribution to

$$\int_\Omega u_\varepsilon(x) k_h\left(\frac{x}{\varepsilon}\right) v\left(x, \frac{x}{\varepsilon}\right)\, dx$$

from $\Omega_{\varepsilon,\delta}$ vanishes. This means that

$$\int_\Omega u_\varepsilon(x) k_h\left(\frac{x}{\varepsilon}\right) v\left(x, \frac{x}{\varepsilon}\right)\, dx \to \int_\Omega \int_Y u_0(x,y) \chi_{Y^*}(y) v(x,y)\, dy dx$$

for any $v \in D(\Omega; C^\infty_\sharp(Y))$, as $h \to \infty$. Since $\{k_h(\frac{x}{\varepsilon}) u_\varepsilon(x)\}$ is bounded in $L^2(\Omega)$, the statement holds for any admissible test function v.

In Section 11.4, we will study sequences of functions defined on sequences of perforated domains Ω_ε like those defined in (11.4). In this connection, we sometimes need to extend the functions from Ω_ε to all of Ω. To be able to apply two-scale convergence, it is necessary that the extended sequence remains bounded in the corresponding Lebesgue and Sobolev spaces of functions defined on Ω. Such techniques have been developed by, e.g., Acerbi et al.; see [ACDP92].

Theorem 1. *Let Ω be some open, connected set with a Lipschitz boundary and E some open, connected periodic subset of $\mathbb{R}^N$ with a Lipschitz boundary. Then, for any $u \in W^{1,p}(\Omega \cap E_\varepsilon)$, there exists an extension $\widetilde{u} \in W^{1,p}_{loc}(\Omega)$ and constants k, C_1 and C_2 such that*

$$\|\widetilde{u}\|_{L^p\left(\Omega_{(\varepsilon k)}\right)} \leq C_1 \|u\|_{L^p(\Omega \cap E_\varepsilon)}, \tag{11.5}$$

$$\|\partial_{x_i} \widetilde{u}\|_{L^p\left(\Omega_{(\varepsilon k)}\right)} \leq C_2 \|\partial_{x_i} u\|_{L^p(\Omega \cap E_\varepsilon)}, \tag{11.6}$$

where k, C_1 and C_2 depend only on E, N, and p but not on ε or u.

The proof can be found in [ACDP92].

Remark 1. For domains like Ω_ε defined in (11.4), where the perforations do not cut the boundary of Ω, it is not necessary to remove a boundary layer close to $\partial\Omega$ and hence $\Omega_{(\varepsilon k)}$ can be replaced with Ω on the left-hand side of (11.5) and (11.6).

Applying these extension techniques to a sequence of functions bounded in $W^{1,2}(\Omega_\varepsilon)$, we obtain the next assertion.

Proposition 2. *Let $\{u_\varepsilon\}$ be a sequence of functions in $W_0^{1,2}(\Omega'_\varepsilon)$ such that $\{\sqrt{k_h(\frac{x}{\varepsilon})}\nabla u_\varepsilon(x)\}$ is bounded in $L^2(\Omega'_\varepsilon)^N$. Then there exists a sequence of functions $\widetilde{u}_\varepsilon$ in $W^{1,2}(\Omega)$ such that $\widetilde{u}_\varepsilon = u_\varepsilon$ in Ω_ε and, up to a subsequence,*

$$\int_\Omega u_\varepsilon(x) k_h\left(\frac{x}{\varepsilon}\right) v\left(x, \frac{x}{\varepsilon}\right) dx \to \int_\Omega \int_Y u(x)\chi_{Y^*}(y)v(x,y)\,dy\,dx \tag{11.7}$$

and

$$\int_\Omega \nabla u_\varepsilon(x) k_h\left(\frac{x}{\varepsilon}\right) v\left(x, \frac{x}{\varepsilon}\right) dx \to \tag{11.8}$$

$$\int_\Omega \int_Y \left(\nabla u(x) + \nabla_y u_1(x,y)\right)\chi_{Y^*}(y)v(x,y)\,dy\,dx,$$

as $h \to \infty$, for any admissible test function v, where u is the weak $W^{1,2}(\Omega)$-limit to $\{\widetilde{u}_\varepsilon\}$ and $u_1 \in L^2(\Omega; W^{1,2}_\sharp(Y)/\mathbb{R})$.

Proof. Let

$$w_h(x) = \sqrt{k_h\left(\frac{x}{\varepsilon}\right)}\nabla u_\varepsilon(x).$$

Then, up to a subsequence,

$$\int_\Omega w_h(x) k_h\left(\frac{x}{\varepsilon}\right) v\left(x, \frac{x}{\varepsilon}\right) dx \to \int_\Omega \int_Y w_0(x,y)\chi_{Y^*}(y)v(x,y)\,dy\,dx,$$

as $h \to \infty$, for any admissible v and some $w_0 \in L^2(\Omega \times Y)^N$. It is obvious that the restriction of w_h to Ω_ε is equal to ∇u_ε and is bounded in $L^2(\Omega_\varepsilon)^N$. By the assumptions on k_h and the Poincaré inequality for periodically perforated domains with homogeneous Dirichlet boundary conditions on the holes, we obtain

$$\|u_\varepsilon\|_{L^2(\Omega)} \le C\varepsilon \|\nabla u_\varepsilon\|_{L^2(\Omega)^N} \le C\frac{\varepsilon}{\sqrt{q_h}} \left\| \sqrt{k_h\left(\frac{x}{\varepsilon}\right)}\nabla u_\varepsilon(x) \right\|_{L^2(\Omega)^N} \le C$$

for $\varepsilon = q_h$, and thus, $\{u_{\varepsilon|\Omega_\varepsilon}\}$ is bounded in $W^{1,2}(\Omega_\varepsilon)$. Hence, Proposition 1 and Theorem 1 are applicable and (11.7) and (11.8) follow. The loss of the second scale in the two-scale limit in (11.7) is due to the strong convergence of $\widetilde{u}_\varepsilon$ in $L^2(\Omega)$.

11.4 Homogenization in Perforated Domains

Our aim in this section is to discuss the connection between homogenization of mixed problems and pure Dirichlet problems in periodically perforated domains. Let us first consider the homogenization of a mixed linear elliptic problem with homogeneous boundary data. This may be considered as a model for

the heat distribution in a piece of a periodic composite material perforated with many small nonconducting holes (Neumann data) and constant temperature (Dirichlet data) on the boundary of Ω. This situation is governed by the mixed problem

$$\begin{aligned} -\nabla \cdot \left(A\left(\frac{x}{\varepsilon}\right) \nabla u_\varepsilon (x) \right) &= f(x) \text{ in } \Omega_\varepsilon, \\ u_\varepsilon (x) &= 0 \text{ on } \partial\Omega, \\ A\left(\frac{x}{\varepsilon}\right) \nabla u_\varepsilon (x) \cdot n &= 0 \text{ on } \partial\Omega_\varepsilon - \partial\Omega; \end{aligned} \tag{11.9}$$

see [AMN93] and [All92]. If we instead imagine that the perforations are kept at a constant zero temperature, we get the pure Dirichlet problem

$$\begin{aligned} -\nabla \cdot \left(A\left(\frac{x}{\varepsilon}\right) \nabla u_\varepsilon (x) \right) &= f(x) \text{ in } \Omega_\varepsilon, \\ u_\varepsilon (x) &= 0 \text{ on } \partial\Omega_\varepsilon. \end{aligned} \tag{11.10}$$

Now let us introduce the coefficient

$$\widetilde{A}_\varepsilon(x) = A\left(\frac{x}{\varepsilon}\right) k_h\left(\frac{x}{\varepsilon}\right)$$

in (11.10) with Ω_ε replaced by Ω'_ε. We obtain

$$\begin{aligned} -\nabla \cdot \left(\widetilde{A}_\varepsilon(x) \nabla u_\varepsilon (x) \right) &= f(x) \text{ in } \Omega'_\varepsilon, \\ u_\varepsilon (x) &= 0 \text{ on } \partial\Omega'_\varepsilon, \end{aligned} \tag{11.11}$$

i.e., an intermediate case, where the cold holes are surrounded by a layer with a low heat-conduction number. Depending on the relation between q_h and ε, we obtain either a limit problem of the same kind as for (11.9) or a temperature distribution that passes to zero in the same way as for problems of the type in (11.10). In mathematical terms, this means that we have found a way to consider a mixed problem as equivalent, in some limiting sense, to certain pure homogeneous Dirichlet problems, where the coefficients $\widetilde{A}_\varepsilon$ are very small close to the perforation. It seems that we have found a natural way to characterize the heat distribution in a material with a thin layer of a material with very low heat conduction number surrounding perforations kept at constant zero temperature. See also [MB04] or [MH04] for a treatment of some related questions.

We carry out a homogenization procedure for (11.11).

Proposition 3. *The solutions u_ε to (11.11) satisfy the a priori estimates*

$$\|u_\varepsilon\|_{L^2(\Omega)} \leq C$$

and

$$\left\| \sqrt{k_h\left(\frac{x}{\varepsilon}\right)} \nabla u_\varepsilon(x) \right\|_{L^2(\Omega)^N} \leq C$$

if $\varepsilon = \sqrt{q_h}$.

Proof. Choosing u_ε as a test function in the weak form of (11.11), we obtain

$$C_1 \left\| \sqrt{k_h\left(\frac{x}{\varepsilon}\right)} \nabla u_\varepsilon(x) \right\|^2_{L^2(\Omega)^N} = \int_\Omega A\left(\frac{x}{\varepsilon}\right) k_h\left(\frac{x}{\varepsilon}\right) \nabla u_\varepsilon(x) \nabla u_\varepsilon(x)\, dx =$$

$$\int_\Omega f(x) u_\varepsilon(x)\, dx \le C_2 \left\| u_\varepsilon \right\|_{L^2(\Omega)}.$$

Hence, applying the Poincaré inequality for periodically perforated domains with homogeneous Dirichlet conditions on the holes, it follows that

$$\left\| \sqrt{k_h\left(\frac{x}{\varepsilon}\right)} \nabla u_\varepsilon(x) \right\|^2_{L^2(\Omega)^N} \le C_3 \varepsilon \left\| \nabla u_\varepsilon \right\|_{L^2(\Omega)^N}$$

$$\le C_3 \frac{\varepsilon}{\sqrt{q_h}} \left\| \sqrt{k_h\left(\frac{x}{\varepsilon}\right)} \nabla u_\varepsilon \right\|_{L^2(\Omega)^N} = C_3 \left\| \sqrt{k_h\left(\frac{x}{\varepsilon}\right)} \nabla u_\varepsilon \right\|_{L^2(\Omega)^N},$$

and the estimates are proven.

With these a priori estimates at hand, we are ready to prove a homogenization result for (11.11).

Theorem 2. *If $\varepsilon = \sqrt{q_h}$, then (11.11) has the same local and homogenized problems as (11.9).*

Proof. For simplicity, we assume that the heat source is zero in $\Omega - \Omega_\varepsilon$, i.e., that it is of the type $f(x)\chi_{Y^*}(\frac{x}{\varepsilon})$. Let $v \in D(\Omega)$. We have

$$\int_\Omega A\left(\frac{x}{\varepsilon}\right) k_h\left(\frac{x}{\varepsilon}\right) \nabla u_\varepsilon(x) \nabla v(x)\, dx \to$$

$$\int_\Omega \int_{Y^*} A(y)(\nabla u(x) + \nabla_y u_1(x,y)) \nabla(x)\, dy dx,$$

as $h \to \infty$, and hence we obtain the homogenized equation

$$\int_\Omega \int_{Y^*} A(y)(\nabla u(x) + \nabla_y u_1(x,y)) \nabla v(x)\, dy dx = \mu(Y^*) \int_\Omega f(x) v(x)\, dx.$$

For the test functions

$$v_\varepsilon(x) = \varepsilon v_1(x) v_2\left(\frac{x}{\varepsilon}\right),$$

where $v_1 \in D(\Omega), v_2 \in C^\infty_\sharp(Y)$, we get in the corresponding way the local problem

$$\int_{Y^*} A(y)(\nabla u(x) + \nabla_y u_1(x,y)) \nabla_y v_2(y)\, dy dx = 0.$$

Both of these equations agree with the corresponding homogenized and local problems for (11.9).

References

[ACDP92] Acerbi, E., Chiadó Piat, V., Dal Maso, G., Percivale, D.: *An Extension Theorem from Connected Sets, and Homogenization in General Periodic Domains.* Pergamon Press, New York (1992).

[All92] Allaire, G.: Homogenization and two-scale convergence. *SIAM J. Math. Anal.*, **23**, 1482–1518 (1992).

[AMN93] Allaire, G., Murat, F., Nandakumaran, A.K.: Homogenization of the Neumann problem with nonisolated holes. *Asympt. Anal.* **7**, 81–95 (1993).

[CD99] Cioranescu, D., Donato, P.: *An Introduction to Homogenization.* Oxford University Press, New York (1999).

[MB04] Mabrouk, M., Boughammoura, A.: Homogenization of a degenerate parabolic problem in a highly heterogeneous medium. *Internat. J. Engrg. Sci.*, **42**, 1061–1096 (2004).

[MH04] Mabrouk, M., Hassan, S.: Homogenization of a composite medium with a thermal barrier. *Math. Methods Appl. Sci.*, **27**, 405–425 (2004).

[Mur77] Murat, F.: H-convergence. Seminaire d'Analyse Fonctionelle et Numérique de l'Université d'Alger (1977).

[Ngu89] Nguetseng, G.: A general convergence result for a functional related to the theory of homogenization. *SIAM J. Math. Anal.*, **20**, 608–623 (1989).

[Spa68] Spagnolo, S.: Sulla convergenza delle soluzioni di equazione paraboliche ed ellittiche. *Ann. Sc. Norm. Sup. Pisa Cl. Sci.,* **22**, 571–597 (1968).

12

Dynamic Response of a Poroelastic Half-Space to Harmonic Line Tractions

V. Gerasik and M. Stastna

University of Waterloo, ON, Canada; vgerasik@uwaterloo.ca, mmstastn@uwaterloo.ca

12.1 Introduction

Studies of acoustic wave processes in porous media are motivated by applications in the fields of seismic prospecting in petrophysics, nondestructive testing of systems such as soils and rocks, concrete, and other porous construction materials, testing of surface coating by nanomaterials, and medicine. Depending on the major practical application involved, frequency bands may differ greatly. For example, low-frequency seismic prospecting focuses on frequencies of around 50 Hz, whereas medical applications allow for frequencies up to approximately 3 MHz, and testing of nanomaterials requires frequencies of approximately 100 MHz.

Modern mathematical approaches to acoustic wave propagation include the classical Biot model [Bio56] or, alternatively, for example, Wilmanski's model [Wil96] and the linearized version of the so-called theory of porous media (TPM) equations [deB05].

Boundary value problems for a poroelastic half-space in the framework of Biot's theory were considered, for example, in [HC86], [DD84], [Phi88], [VTZ95], [STS90], [Mol02], [FJ83], [Pau76], and [MLC05]. Generally speaking, two main types of problems arise: so-called steady-state problems (see [HC86], [DD84], and [VTZ95]), when harmonic time-dependence is assumed for the imposed tractions (and consequently for the stress and displacement fields), and problems of transient response (see [Pau76], [FJ83], [STS90], [Mol02], and [MLC05]), where impulsive tractions are applied. The latter class of problems is more complicated; however, the value of the results obtained can hardly be overestimated for many of the applications mentioned above.

A two-dimensional boundary value problem for a porous half-space, described by the widely recognized Biot's equations of poroelasticity is considered. In this poroelastic version of Lamb's problem [Lam04], the surface of a porous half-space is subjected to a prescribed line traction. A general analytical solution of the problem in the Fourier–Laplace space is obtained by the application of the standard Helmholtz potential decomposition, which reduces

the problem to a system of linear wave equations for three unknown potentials. These potentials correspond to two dilatational waves (one of the first kind, or P1-wave, and Biot's slow wave of the second kind, or P2-wave, which has no counterpart in elastic wave theory) and one shear wave, or S-wave (see [Bio56], [Bou87], and [STS90]). The possibilities of, and procedure for, obtaining analytic solutions in the physical space will be discussed in detail.

12.2 Model Description

Consider Biot's set of equations [Bio56], [Bou87]:

$$(\lambda+\mu)\,\mathbf{grad}\,\mathrm{div}\mathbf{u}+\mu\nabla^2\mathbf{u}+Y\mathbf{grad}\,\mathrm{div}\mathbf{U}=\rho_{11}\ddot{\mathbf{u}}+\rho_{12}\ddot{\mathbf{U}}+b\left(\dot{\mathbf{u}}-\dot{\mathbf{U}}\right), \quad (12.1)$$

$$Y\mathbf{grad}\,\mathrm{div}\mathbf{u}+R\mathbf{grad}\,\mathrm{div}\mathbf{U}=\rho_{12}\ddot{\mathbf{u}}+\rho_{22}\ddot{\mathbf{U}}-b\left(\dot{\mathbf{u}}-\dot{\mathbf{U}}\right), \quad (12.2)$$

where $\mathbf{u}$, $\mathbf{U}$ are the unknown solid and fluid displacement fields, respectively, and

$$\lambda=\lambda_f+M\phi\,(\phi-2\beta)=\lambda_0+M\,(\beta-\phi)^2, \quad Y=M\phi\,(\beta-\phi), \quad R=M\phi^2,$$
$$\rho_{11}=\rho+\phi\rho_f(a-2), \quad \rho_{12}=\phi\rho_f(1-a), \quad \rho_{22}=a\phi\rho_f, \quad b=\eta_f\frac{\phi^2}{k}.$$

In these equations, ρ_{ij} are reference phase densities and λ, Y, and R are generalized poroelastic parameters related to the porosity ϕ, bulk modulus K_s of the solid, bulk modulus K_f of the fluid, bulk modulus K_b of the porous drained matrix, and shear modulus μ of both the drained matrix and the composite through the formulas

$$\lambda=K_b-\frac{2}{3}\mu+\frac{K_f\left(1-\phi-\frac{K_b}{K_s}\right)^2}{\phi_{eff}}, \quad Y=\frac{\phi K_f}{\phi_{eff}}\left(1-\phi-\frac{K_b}{K_s}\right),$$
$$R=\frac{\phi^2K_f}{\phi_{eff}}, \quad \phi_{eff}=\phi+\frac{K_f}{K_s}\left(1-\phi-\frac{K_b}{K_s}\right).$$

An expression for the macroscopic stress tensor can be written in terms of the components of the Cauchy strain tensor ε_{ij}, $\nabla\cdot\mathbf{u}$, and $\nabla\cdot\mathbf{U}$ [Bou87]:

$$\sigma_{ij}=\lambda_f\mathrm{tr}\varepsilon\delta_{ij}+2\mu\varepsilon_{ij}-M\beta\xi\delta_{ij}=\lambda_f\mathrm{tr}\varepsilon\delta_{ij}+2\mu\varepsilon_{ij}+M\beta\phi\left[\nabla\cdot(\mathbf{U}-\mathbf{u})\right]\delta_{ij},$$

which can alternatively be written in the form

$$\begin{aligned}\sigma_{ij}&=(\lambda_f-M\beta\phi)(\nabla\cdot\mathbf{u})\delta_{ij}+2\mu\varepsilon_{ij}+M\beta\phi(\nabla\cdot\mathbf{U})\delta_{ij}\\&=(\lambda+Y)(\nabla\cdot\mathbf{u})\delta_{ij}+2\mu\varepsilon_{ij}+(R+Y)(\nabla\cdot\mathbf{U})\delta_{ij},\end{aligned}$$

where $\lambda=\lambda_f+M\phi\,(\phi-2\beta)=\lambda_0+M\,(\beta-\phi)^2$, $Y=M\phi\,(\beta-\phi)$, $R=M\phi^2$.

12.2.1 Helmholtz Potential Decomposition

Expansion of the displacement field into irrotational and solenoidal parts yields

$$\begin{aligned} \mathbf{u} &= \mathrm{grad}\Phi_1 + \mathrm{curl}\overrightarrow{\mathbf{\Psi}}_1, \qquad \mathrm{curl}\Phi_1 = 0,\ \mathrm{div}\overrightarrow{\mathbf{\Psi}}_1 = 0, \\ \mathbf{U} &= \mathrm{grad}\Phi_2 + \mathrm{curl}\overrightarrow{\mathbf{\Psi}}_2, \qquad \mathrm{curl}\Phi_2 = 0,\ \mathrm{div}\overrightarrow{\mathbf{\Psi}}_2 = 0, \end{aligned} \tag{12.3}$$

and results in the following scalar and vector set of equations in Laplace space:

$$\begin{aligned} (\lambda+2\mu)\nabla^2\Phi_1 + Y\nabla^2\Phi_2 &= \rho_{11}s^2\Phi_1 + \rho_{12}s^2\Phi_2 + bs\,(\Phi_1-\Phi_2)\,, \\ Y\nabla^2\Phi_1 + R\nabla^2\Phi_2 &= \rho_{12}s^2\Phi_1 + \rho_{22}s^2\Phi_2 - bs\,(\Phi_1-\Phi_2)\,, \\ \mu\nabla^2\overrightarrow{\mathbf{\Psi}}_1 &= \rho_{11}s^2\overrightarrow{\mathbf{\Psi}}_1 + \rho_{12}s^2\overrightarrow{\mathbf{\Psi}}_2 + bs\left(\overrightarrow{\mathbf{\Psi}}_1 - \overrightarrow{\mathbf{\Psi}}_2\right), \\ 0 &= \rho_{12}s^2\overrightarrow{\mathbf{\Psi}}_1 + \rho_{22}s^2\overrightarrow{\mathbf{\Psi}}_2 - bs\left(\overrightarrow{\mathbf{\Psi}}_1 - \overrightarrow{\mathbf{\Psi}}_2\right). \end{aligned} \tag{12.4}$$

The first two equations (12.4) may be rewritten in the matrix form

$$\nabla^2\begin{pmatrix}\Phi_1\\ \Phi_2\end{pmatrix} = \tilde{R}^{-1}\tilde{N}\begin{pmatrix}\Phi_1\\ \Phi_2\end{pmatrix}, \tag{12.5}$$

where $\tilde{R}^{-1}$ is the inverse of the rigidity matrix

$$\tilde{R} = \begin{pmatrix}\lambda+2\mu & Y\\ Y & R\end{pmatrix}, \quad \tilde{R}^{-1} = \frac{1}{\det\tilde{R}}\begin{pmatrix}R & -Y\\ -Y & \lambda+2\mu\end{pmatrix}$$

and the components of $\tilde{N}$ are

$$\tilde{N} = s^2\begin{pmatrix}\rho_{11}+b/s & \rho_{12}-b/s\\ \rho_{12}-b/s & \rho_{22}+b/s\end{pmatrix}.$$

Dilatational Waves (P-waves)

It can be shown (a similar approach was used in [HC86] and [STS90]) that (12.5) decouples into two wave equations in an eigenvector reference system:

$$\nabla^2\Phi_1^* = \frac{s^2\bar{z}_1}{c^2}\Phi_1^*, \quad \nabla^2\Phi_2^* = \frac{s^2\bar{z}_2}{c^2}\Phi_2^*,$$

where $\bar{z}_{1,2}$ satisfy the quadratic equation

$$(q_{11}q_{22}-q_{12}^2)\bar{z}^2 - (q_{11}\gamma_{22}+q_{22}\gamma_{11}-2q_{12}\gamma_{12}+b/\rho s)\bar{z} + (\gamma_{11}\gamma_{22}-\gamma_{12}^2+b/\rho s) = 0$$

and the following nondimensional quantities have been introduced:

$$\begin{aligned} &\gamma_{11} = \rho_{11}/\rho, \quad && q_{11} = (\lambda+2\mu)/H, && c^2 = H/\rho, \\ &\gamma_{12} = \rho_{12}/\rho, && q_{12} = Y/H, && \rho = \rho_{11}+\rho_{22}+2\rho_{12}, \\ &\gamma_{22} = \rho_{22}/\rho, && q_{22} = R/H, && H = \lambda+2\mu+R+2Y. \end{aligned}$$

The above equations describe P1-wave and P2-wave behavior, respectively, with phase velocities $\beta_{1,2}$ given by

$$\beta_1 = \frac{c}{\sqrt{\bar{z}_1}}, \quad \beta_2 = \frac{c}{\sqrt{\bar{z}_2}}.$$

The P1-wave corresponds to the case when the solid and liquid displacements are in phase, whereas the P2-wave describes out-of-phase motion (see [Bio56] and [Bou87]). Moreover, the first-kind waves propagate faster and attenuate more slowly than the second-kind wave. The connection between the reference systems is given by the eigenvector matrix $\tilde{V}$:

$$\begin{pmatrix} \Phi_1 \\ \Phi_2 \end{pmatrix} = \tilde{V} \begin{pmatrix} \Phi_1^* \\ \Phi_2^* \end{pmatrix}, \quad \tilde{V} = \begin{pmatrix} v_1^1 & v_1^2 \\ v_2^1 & v_2^2 \end{pmatrix} = \begin{pmatrix} 1 & 1 \\ M_1 & M_2 \end{pmatrix},$$

where the components $M_{1,2}$ can be found straightforwardly as

$$M_{1,2} = \frac{q_{22}\gamma_{11} - q_{12}\gamma_{12} - (q_{11}q_{22} - q_{12}^2)\bar{z}_{1,2} + (q_{22} + q_{12})b/\rho s}{q_{12}\gamma_{22} - q_{22}\gamma_{12} + (q_{22} + q_{12})b/\rho s},$$

so that, finally,

$$\Phi_1 = \Phi_1^* + \Phi_2^*, \quad \Phi_2 = M_1\Phi_1^* + M_2\Phi_2^*. \tag{12.6}$$

Shear Waves (S-waves)

The last two equations in (12.4) can be rewritten [STS90] using Biot's nondimensional parameters:

$$\overrightarrow{\mathbf{\Psi}}_2 = -\frac{\rho_{12} - b/s}{\rho_{22} + b/s}\overrightarrow{\mathbf{\Psi}}_1 = -\frac{\gamma_{12} - b/\rho s}{\gamma_{22} + b/\rho s}\overrightarrow{\mathbf{\Psi}}_1 = -M_3\overrightarrow{\mathbf{\Psi}}_1,$$
$$\overrightarrow{\nabla}^2\overrightarrow{\mathbf{\Psi}}_1 = \frac{1}{\mu}\left[\rho_{11} - \rho_{12}M_3 + (1 + M_3)\, b/s\right] s^2\overrightarrow{\mathbf{\Psi}}_1,$$

where $M_3 = \frac{\gamma_{12} - b/\rho s}{\gamma_{22} + b/\rho s}$.

In the end, we arrive at the wave equation

$$\overrightarrow{\nabla}^2\overrightarrow{\mathbf{\Psi}}_1 = s^2\frac{H}{\mu c^2}\left[\gamma_{11} - \gamma_{12}M_3 + (1 + M_3)\, b/s\right]\overrightarrow{\Psi}_1,$$

which defines the shear wave phase velocity β_3 in the following way [STS90]:

$$\beta_3 = \sqrt{\frac{\mu}{\rho_{11} - \rho_{12}M_3 + (1 + M_3)\, b/s}} = \sqrt{\frac{\mu}{\rho}}\sqrt{\frac{1}{\gamma_{11} - \gamma_{12}M_3 + (1 + M_3)\, b/\rho s}}.$$

12.3 General Solution of the 2D Problem

Consider a poroelastic half-space with an open boundary occupying the region $z < 0$. At time $t = 0$, the porous half-space is subjected to an impulsive external line traction $-P(x)\delta(t)$ at the surface (instantaneous compression). The boundary conditions for the governing equations (12.1),(12.2) and stress–strain relation can be represented in the form ($z = 0$)

$$\begin{aligned} \sigma_{zz}(x,0,t) &= -P(x)\delta(t), \\ \sigma_{xz}(x,0,t) &= 0, \\ p(x,0,t) &= 0. \end{aligned} \tag{12.7}$$

For the 2D problem, the introduction of the four scalar potentials Φ_1, Φ_2 and Ψ_1, Ψ_2 (Ψ_1 and Ψ_2 are linearly dependent) is sufficient, so the 2D problem reduces to the solution of the wave equations in Laplace space:

$$\beta_1^2\nabla^2\Phi_1^* = s^2\Phi_1^*,\ \beta_2^2\nabla^2\Phi_2^* = s^2\Phi_2^*,\ \beta_3^2\nabla^2\Psi_1 = s^2\Psi_1. \tag{12.8}$$

Equations (12.8), written in Fourier space, become (here and below, transformed solutions will be indicated by the arguments)

$$\frac{\partial^2\Phi_{1,2}^*(k,z,s)}{\partial z^2} = \left(k^2 + \frac{s^2}{\beta_{1,2}^2}\right)\Phi_{1,2}^*(k,z,s),\ \frac{\partial^2\Psi_1(k,z,s)}{\partial z^2} = \left(k^2 + \frac{s^2}{\beta_3^2}\right)\Psi_1.$$

Taking into account the far-field conditions (at infinity), the solutions of the above wave equations can be expressed in the form

$$\begin{aligned} \Phi_{1,2}^*(k,z,s) &= A_{1,2}(k,s)\exp\left[-z\cdot\xi_{1,2}(k,s)\right], \\ \Psi_1(k,z,s) &= B(k,s)\exp\left[-z\cdot\xi_3(k,s)\right], \end{aligned} \tag{12.9}$$

where $\xi_i(k,s) = \sqrt{k^2 + \frac{s^2}{\beta_i^2}}$ ($i = 1,2,3$) and $A_{1,2}(k,s)$ and $B(k,s)$ are unknown coefficients to be determined from the boundary conditions (12.7).

In the Laplace–Fourier space, the expressions for the stress tensor and the pressure in terms of the potentials (12.8) can be written as

$$\begin{aligned} \sigma_{zz}(k,z,s) &= (\lambda+Y)\left[-k^2\Phi_1^* - k^2\Phi_2^* + \xi_1^2(k,s)\Phi_1^* + \xi_2^2(k,s)\Phi_2^*\right] \\ &\quad -(R+Y)\left[k^2M_1\Phi_1^* + k^2M_2\Phi_2^* - M_1\xi_1^2(k,s)\Phi_1^* - M_2\xi_2^2(k,s)\Phi_2^*\right] \\ &\quad +2\mu\left[\xi_1^2(k,s)\Phi_1^* + \xi_2^2(k,s)\Phi_2^* + ik\xi_3(k,s)\Psi_1\right], \\ \sigma_{xz}(k,z,s) &= \mu\left(-2ik\xi_1(k,s)\Phi_1^* - 2ik\xi_2(k,s)\Phi_2^* + \xi_3^2(k,s)\Psi_1 + k^2\Psi_1\right), \\ p(k,z,s) &= -\frac{1}{\phi}Y\left[-k^2\Phi_1^* - k^2\Phi_2^* + \xi_1^2(k,s)\Phi_1^* + \xi_2^2(k,s)\Phi_2^*\right] \\ &\quad -\frac{1}{\phi}R\left[-k^2M_1\Phi_1^* - k^2M_2\Phi_2^* + M_1\xi_1^2(k,s)\Phi_1^* + M_2\xi_2^2(k,s)\Phi_2^*\right]. \end{aligned} \tag{12.10}$$

Application of the boundary conditions (12.7) to the expressions (12.10) yields a linear algebraic system that determines the three unknown coefficients $A_{1,2}(k,s)$ and $B(k,s)$ as

$$A_1(k,s) = \frac{P(k)}{2\mu}\frac{n_2\left(2k^2+\frac{s^2}{\beta_3^2}\right)}{F(k,s)}, \quad A_2(k,s) = -\frac{P(k)}{2\mu}\frac{n_1\left(2k^2+\frac{s^2}{\beta_3^2}\right)}{F(k,s)},$$
$$B(k,s) = -2ik\frac{P(k)}{2\mu}\frac{n_1\xi_2(k,s)-n_2\xi_1(k,s)}{F(k,s)}, \tag{12.11}$$

where

$$m_{1,2} = \frac{\lambda+2\mu+YM_{1,2}}{2\mu\beta_{1,2}^2}, \quad n_{1,2} = \frac{Y+RM_{1,2}}{2\mu\beta_{1,2}^2},$$

and $F(k,s)$ is the dispersion relation of the surface (Rayleigh) waves (see [DR62], [HC86], and [STS90])

$$F(k,s) = \left(2k^2+\frac{s^2}{\beta_3^2}\right)\left[n_1(m_2s^2+k^2)-n_2(m_1s^2+k^2)\right]-2k^2\xi_3(n_1\xi_2-n_2\xi_1). \tag{12.12}$$

As an example, consider the vertical component of solid displacement u_z. From (12.3) and (12.6) it follows that

$$u_z = \frac{\partial\Phi_1}{\partial z}-\frac{\partial\Psi_1}{\partial x} = \frac{\partial\Phi_1^*}{\partial z}+\frac{\partial\Phi_2^*}{\partial z}-\frac{\partial\Psi_1}{\partial x},$$

Using (12.9) and (12.11), we bring the above expression to the form

$$\begin{aligned} u_z(k,z,s) = &-\xi_1(k,s)A_1(k,s)e^{-z\cdot\xi_1(k,s)}-\xi_2(k,s)A_2(k,s)e^{-z\cdot\xi_2(k,s)} \\ &-ikB(k,s)e^{-z\cdot\xi_3(k,s)}, \end{aligned}$$

so that, finally, we get the solution in the Laplace space

$$\begin{aligned} u_z(x,z,s) = -\tfrac{1}{2\mu\sqrt{2\pi}}\int\limits_{-\infty}^{+\infty}\tfrac{P(k)}{F(k,s)}\Bigg\{&\left(2k^2+\tfrac{s^2}{\beta_3^2}\right)\big[n_2\xi_1(k,s)e^{-z\cdot\xi_1(k,s)} \\ &-n_1\xi_2(k,s)e^{-z\cdot\xi_2(k,s)}\big] \\ &+2k^2\big[n_1\xi_2(k,s)-n_2\xi_1(k,s)\big]e^{-z\cdot\xi_3(k,s)}\Bigg\}e^{ikx}dk. \end{aligned} \tag{12.13}$$

The solution of Lamb's problem for the perfectly elastic medium (see [Lam04] and [STS90]) can be used as a benchmark solution: One can show that the limiting case of the solution (12.13) recovers the perfectly elastic case. Similarly, it is possible to obtain the exact analytical solutions for the stress tensor components, as well as for the pressure and displacement fields.

12.3.1 Harmonic Response

Despite the different form of the time dependence, it can be shown that the solution (12.13) can be used to describe the solution for a harmonic line source. In this particular case, we assume harmonic time-dependence for the displacements as well as for the components of the total stress tensor and pore pressure. Thus, the first equation in (12.7) reads as $\sigma_{zz}(x,0,t) = -P(x)e^{i\omega t}$ and one gets, for example, the following expression for the normal solid-phase displacement at the surface ($z = 0$) in the physical domain:

$$u_z(x,t,\omega) = \frac{1}{\mu\sqrt{2\pi}}\mathrm{Re}\left\{ e^{i\omega t} \int_{-\infty}^{+\infty} \frac{P(k)\omega^2}{\beta_3^2} \frac{n_2\xi_1(k,\omega) - n_1\xi_2(k,\omega)}{F(k,\omega)} e^{ikx} dk \right\}, \tag{12.14}$$

where $\xi_i(k,\omega) = \sqrt{k^2 - \frac{\omega^2}{\beta_i^2}}$ $(i = 1,2,3)$ and $F(k,\omega)$ is obtained from the Rayleigh wave secular equation $F(k,s)$ (12.12) by the substitution $s = i\omega$.

In the case of line traction, $P(x) = P\delta(x)$, where P is a constant, so in Fourier space we have $P(k) = \frac{P}{\sqrt{2\pi}}$ (P has the dimensions of force per unit length).

The change of variable $k = \frac{\omega p}{\beta_S}$ in (12.14), where

$$\beta_S = \sqrt{\frac{\mu}{\rho}} \sqrt{\frac{1}{\gamma_{11} - \frac{\gamma_{12}^2}{\gamma_{22}}}},$$

and the introduction of the nondimensional quantities

$$\tilde{x} = \frac{\omega x}{\beta_S}, \quad \tilde{z} = \frac{\omega z}{\beta_S}, \quad \tilde{t} = \omega t, \quad \tilde{\omega} = \frac{\rho\omega}{b} = \frac{\omega}{\omega_c}, \quad \tilde{\beta}_i = \frac{\beta_S}{\beta_i} \quad (i = 1,2,3),$$

$$\tilde{u}_z = \frac{4\pi\mu}{P} u_z, \quad \tilde{U}_z = \frac{4\pi\mu}{P} U_z, \quad \tilde{m}_{1,2} = m_{1,2}\beta_S^2, \quad \tilde{n}_{1,2} = n_{1,2}\beta_S^2,$$

leads to expressions for the nondimensional vertical displacements in the form (from now on we omit the tilde)

$$u_z(x,t,\omega) = \mathrm{Re} \int_{-\infty}^{+\infty} \beta_3^2 \frac{n_2\xi_1(p) - n_1\xi_2(p)}{F(p,\omega)} e^{i(px+t)} dp, \tag{12.15}$$

$$U_z(x,t,\omega) = -\mathrm{Re} \int_{-\infty}^{+\infty} \frac{1}{F(p,\omega)} \left\{ n_2\xi_1(p) \left[2p^2(M_1 + M_3) - \beta_3^2 M_1\right] - \right.$$
$$\left. -n_1\xi_2(p) \left[2p^2(M_2 + M_3) - \beta_3^2 M_2\right] \right\} e^{i(px+t)} dp, \tag{12.16}$$

where $\xi_i(p) = \sqrt{p^2 - \beta_i^2}$ $(i = 1,2,3)$ and $F(p,\omega)$ is the nondimensionalized surface wave equation (12.12) [STS90]; that is,

$$F(p,\omega) = \left(2p^2 - \beta_3^2\right) \left[n_1\left(p^2 - m_2\right) - n_2(p^2 - m_1)\right] - 2p^2\xi_3\left(n_1\xi_2 - n_2\xi_1\right).$$

12.3.2 Numerical Example

Expressions (12.15) and (12.16) represent multivalued, slowly decaying, and highly oscillating convergent integrals, so that special care is required in their numerical evaluation. Numerical results for the vertical solid and fluid displacements according to (12.15) and (12.16) are presented in Figures 12.1–12.3 for the poroelastic parameters of the Berea sandstone [CSD06] (see Table 12.1). At the point $x = 0$, where the traction is applied, an integrable singularity can be observed; it can be shown that it will disappear in the case of a uniformly distributed traction. The following frequencies are used in calculations: $\omega = 0.1\omega_c,\ 1.0\omega_c,\ 10\omega_c$, where ω_c is the characteristic (or roll-over) frequency [Bio56] (see Table 12.1). Additional increase of the source frequency gives results similar to Figure 12.3.

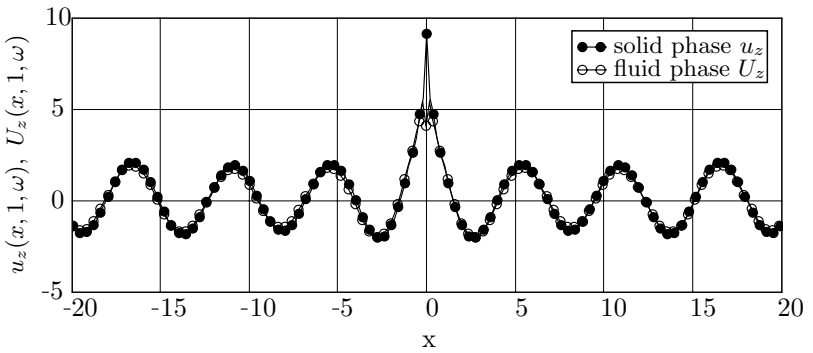

Fig. 12.1. Normalized fluid and solid displacements. Source frequency $\omega = 0.1\omega_c$.

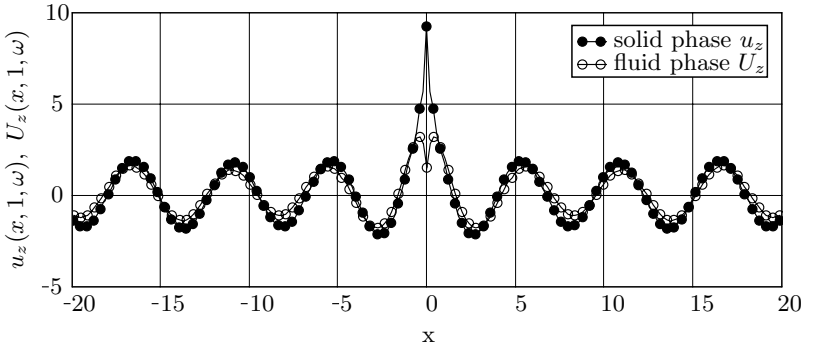

Fig. 12.2. Normalized fluid and solid displacements. Source frequency $\omega = \omega_c$.

Table 12.1. Physical properties of the Berea sandstone and the saturating fluid (water).

Porosity	ϕ	0.20
Permeability (mD)	k	360.0
Tortuosity	a	2.4
Frame bulk modulus (GPa)	K_b	10.37
Shear modulus (GPa)	μ	7.02
Grain bulk modulus (GPa)	K_s	36.5
Liquid bulk modulus (GPa)	K_f	2.25
Solid density (kg m^{-3})	ρ_s	2644.0
Liquid density (kg m^{-3})	ρ_f	1000.0
Liquid viscosity (mPa s)	η_f	1.0
Characteristic frequency (kHz)	ω_c	48.0

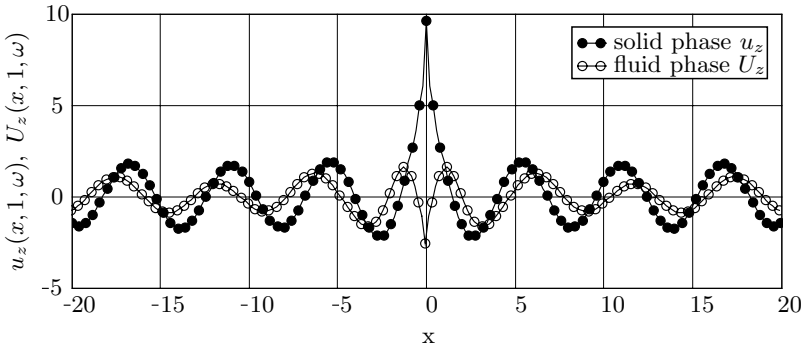

Fig. 12.3. Normalized fluid and solid displacements. Source frequency $\omega = 10\omega_c$.

12.4 Conclusions

Unlike in previous studies (for example, [VTZ95] and [HC86]), the main focus in this chapter is on the response at different source frequencies. Numerical results demonstrate that the character of spatial oscillations is dependent on the source frequency. For relatively low frequencies, displacements are observed to be in phase, with approximately the same amplitudes (see Figure 12.1). Increasing the source frequency leads to a weakening of the viscous coupling effect, and as a consequence, solid and fluid displacements can be of different amplitude and phase, or, in fact, nearly out of phase in the high-frequency range for certain materials. The numerical results are in agreement with Biot's conclusion [Bio56] that when the characteristic frequency lies near unity (see Figure 12.2), the inertia and viscous forces are approximately of the same order. Furthermore, our solution is in agreement with the results for solid-phase displacements and filtration amplitudes obtained in [VTZ95] by means of separation of variables and the fast Fourier transformation. We have extended our analysis to include the decomposition of the surface response into

wave-train contour integrals for P1, P2, and S waves and a residue for the Rayleigh wave response. In the far field, an asymptotic analysis analogous to that in [Lam04] can subsequently be carried out. The results will be presented elsewhere.

References

[Bio56] Biot, M.A.: The theory of propagation of elastic waves in a fluid-saturated porous solid. *J. Acous. Soc. Amer.,* **28**, 168–191 (1956).

[Bou87] Bourbie, T., Coussy, O., Zinzner, B.: *Acoustics of Porous Media.* Gulf Publishing Company, Paris (1987).

[CSD06] Chao, G., Smeulders, D.M.J., van Dongen, M.E.H.: Dispersive surface waves along partially saturated porous media. *J. Acous. Soc. Amer.,* **119**, 1348–1355 (2006).

[deB05] de Boer, R.: *Trends in Continuum Mechanics of Porous Media.* Springer, Dordrecht (2005).

[DR62] Deresiewicz, H., Rice, J.T.: The effect of the boundaries on wave propagation in a liquid filed porous solid. *Bull. Seism. Soc. Amer.,* **52**, 627–638 (1962).

[DD84] Dey, S., De, R.K.: Stresses in fluid-saturated porous half-space due to the normal and tangential loadings. *Indian J. Pure Appl. Math.,* **15**, 1375–1397 (1984).

[FJ83] Feng, S., Johnson, D.L.: High-frequency acoustic properties of a fluid/porous solid interface. II. The 2D reflection Green's function. *J. Acous. Soc. Amer.,* **74**, 915–924, (1983).

[HC86] Halpern, M., Christiano, P.: Response of poroelastic halfspace to steady-state harmonic surface tractions. *Internat. J. Numer. Anal. Geomech.,* **6**, 609–632 (1986).

[Lam04] Lamb, H.: On the propagation of tremors over the surface of an elastic solid. *Phil. Trans. Roy. Soc. London,* **A203**, 1–42 (1904).

[MLC05] Mesgouez, A., Lefeuve-Mesgouez, G., Chambarel, A.: Transient mechanical wave propagation in semi-infinite porous media using a finite element approach. *Soil Dynamics Earth Engng.,* **25**, 421–430 (2005).

[Mol02] Molotkov, L.A.: Sources acting on the free boundary of a porous Biot medium and reflection on this boundary. *J. Math. Sci.,* **5**, 3750–3762 (2002).

[Pau76] Paul, S.: On the displacements produced in a porous elastic half-space by an impulsive line load (no dissipative case). *Pure Appl. Geophys.,* **4**, 605–614 (1976).

[Phi88] Philippacoupoulos, A.J.: Lamb's problem for fluid saturated porous media. *Bull. Seism. Soc. Amer.,* **78**, 908–923 (1988).

[STS90] Seimov, V.M., Trofimchuk, A.N., Savitsky, O.A.: *Oscillations and Waves in Layered Media.* Naukova Dumka, Kiev (1990) (Russian).

[VTZ95] Valiappan, S., Tabatabaie, J., Zhao, C.: Analytical solution for two-dimensional dynamic consolidation in frequency domain. *Internat. J. Numer. Anal. Geomech.,* **19**, 663–682 (1995).

[Wil96] Wilmanski, K.: Porous media at finite strains. The new model with the balance equation for porosity. *Arch. Mech.,* **4**, 591–628 (1996).

13

Convexity Conditions and Uniqueness and Regularity of Equilibria in Nonlinear Elasticity

S.M. Haidar

Grand Valley State University, Allendale, MI, USA; haidars@gvsu.edu

13.1 Introduction: Formulation of the Problem

In this chapter, we consider a nonhomogeneous, isotropic, hyperelastic body that, in its reference configuration, occupies the open bounded subset Ω of $\mathbb{R}^3$ and has a stored-energy function

$$W : \Omega \times M^{3\times 3}_{+} \to [0, \infty).$$

We assume W to be frame-indifferent and isotropic. That is, W satisfies, respectively [TN65],

$$W(x, RF) = W(x, F) \quad \text{and} \quad W(x, FR) = W(x, F)$$

for all $x \in \Omega$, $F \in M^{3\times 3}_{+}$, and R proper orthogonal. With W satisfying additional plausible growth and convexity conditions, we aim to study the uniqueness and regularity of solutions to the equilibrium equations of nonlinear elasticity in which the boundary of the elastic body under consideration is subjected to homogeneous deformations. Our study is partly motivated by the work of Ball [Bal82] and that of Knops and Stuart [KS84] regarding the uniqueness and regularity of solutions to the pure displacement boundary value problem of nonlinear elastostatics.

In the absence of external forces, the total stored energy associated with a deformation $u(\cdot)$ of the body is given by

$$u \to J(u, \Omega) := \int_{\Omega} W(x, \nabla u(x))dx, \tag{13.1}$$

and the equilibrium equations are given by the Euler–Lagrange equations

$$\operatorname{div}\left[\frac{\partial W}{\partial F}(x, F)\right] = 0, \quad x \in \Omega,$$

where $F \equiv \nabla u(x)$. For a given positive real number λ, we mainly[1] consider the questions of uniqueness and regularity of solutions of

$$\operatorname{div}\left[\frac{\partial W}{\partial F}(x,F)\right] = 0 \ \text{ in } \Omega, \tag{13.2}$$

$$u(x) = \lambda x \ \text{ on } \ \partial\Omega. \tag{13.3}$$

In what follows, we use the abbreviation (DBVP) to refer to the problem consisting of equations (13.2) and (13.3). Generally, for the pure displacement boundary value problem of nonlinear elasticity, it is sufficient [AB78] to consider only those deformations for which the condition

$$\det[\nabla u(x)] > 0$$

holds for each x in Ω. Following the terminology in [Bal82] and [Ada75], we say that $u \in W^{1,1}(\Omega;\mathbb{R}^3)$ is a weak solution of (DBVP) if

$$\det(\nabla u(x)) > 0 \text{ for a.e. } x \in \Omega$$

$$\frac{\partial W}{\partial F}(\cdot, \nabla u(\cdot)) \in L'(\Omega;\mathbb{R}^9), \ \text{ and}$$

$$\int_\Omega \frac{\partial W}{\partial u^i_{,\alpha}}\, \phi^i_{,\alpha} dx = 0 \ \text{ for all } \ \phi \in C_0^\infty(\Omega;\mathbb{R}^3).$$

In Section 13.2, the main section of this chapter, we present an answer to the question posed by Ball [Bal82] of whether strong ellipticity of W implies the existence of *nontrivial* equilibrium solutions passing through the origin O and having *finite* energy. We also describe a class of stored-energy functions to show that the uniqueness results of [Bal82] and [Hil57] do not carry over to the nonhomogeneous case.

In the general theory of nonlinear elasticity, there are plenty of situations when uniqueness of solutions to the equilibrium equations of elasticity cannot be expected (see, for example, [Bal77a], [Hil57], [Joh72], and [TN65]). Of course, a stored-energy function W that is strictly convex in F ensures uniqueness. Such a property, however, is completely unrealistic [TN65] as, among many other reasons, it violates the principle of frame-indifference. The class of admissible stored-energy functions has been modified to ensure to some extent the existence, uniqueness, and regularity of solutions for some problems of nonlinear elasticity (more details are given in [Bal77b], [BM84], [Eri83], [Mor52], and [Mor66]). This modification pertains to the generalization of the (traditional) notion of convexity to such concepts as polyconvexity (p.c.), quasiconvexity (q.c.), rank-one-convexity (r.1.c), etc. For homogeneous materials and in the case of the pure displacement boundary value problem, the first general uniqueness result that employs some of the above-mentioned (weaker) notions of convexity is due to [KS84]. We remark that this result does not require W to be isotropic.

[1] Haidar [Hai00] presented a theorem of existence of energy-minimizing deformations for the variational problems associated with (13.2) and (13.3).

Theorem 1 (Knops and Stuart [KS84]). *Let $\Omega \subset \mathbb{R}^3$ be an open bounded domain that is star-shaped with respect to the point $x_0 \in \Omega$, and whose boundary $\partial\Omega$ is piecewise continuously differentiable. For any given F in $M^{3\times 3}_+$ and c in $\mathbb{R}^3$, let u and ψ be solutions of (13.2) with $u(x) = \psi(x) = Fx + c$ for $x \in \partial\Omega$, let $W \in C^2(M^{3\times 3}_+, \mathbb{R})$, and assume that W is rank-one-convex and strictly quasiconvex at F. Then $u(x) = \psi(x) = F(x) + c$ for all $x \in \Omega$.*

By restricting the geometrical structure of Ω to be the unit ball in $\mathbb{R}^3$, Ball [Bal82] discussed conditions other than rank-one-convexity and quasiconvexity to ensure the uniqueness of homogeneous radial equilibria. In this case, the admissible deformations are considered to be of the form

$$u(x) = \frac{r(R)}{R}\, x, \tag{13.4}$$

where $R = |x|$. Before we state Ball's uniqueness result, let us recall the following well-known representation theorem due to [RE55] (see, also, [TN65], pp. 28 and 317).

Theorem 2. *W is isotropic and frame-indifferent if and only if there exists a function $\phi : \Omega_x(0,\infty)^3 \to \mathbb{R}$ such that $\phi(x,\cdot,\cdot,\cdot)$ is symmetric and*

$$W(x,F) = \phi(x, v_1, v_2, v_3), \quad \textit{for all} \quad F \in M^{3\times 3}_+,$$

where the principal stretches v_1, v_2, v_3 of F are the singular values of F.

For $u \in W^{1,1}(\Omega;\mathbb{R}^3)$, the weak derivatives of u in (13.4) are given by

$$\nabla u(x) = \frac{r(R)}{R}\, 1 + \frac{x\otimes x}{R^2}\left[r'(R) - \frac{r(R)}{R}\right], \quad \text{for a.e. } x \in \Omega. \tag{13.5}$$

Equation (13.5) implies that

$$v_1 = r', \; v_2 = v_3 = r/R.$$

The total energy functional $J(u;\Omega)$ in (13.1) now becomes $J(u;\Omega) = 4\pi I(r)$, where

$$I(r) := \int_0^1 R^2 \phi(R; r', r/R, r/R) dR. \tag{13.6}$$

It is known ([Bal82], Theorem 4.2) that $u(x) = (r/R)x \in W^{1,1}(\Omega;\mathbb{R}^3)$ is a weak equilibrium solution if and only if $r'(R) > 0$ a.e. in $(0,1)$, $R^2\phi_{,1}(R)$ and $R^2\phi_{,2}(R) \in L^1(0,1)$, and $R^2\phi_{,1}(R) = 2\displaystyle\int_1^R \rho\phi_{,2}(\rho)d\rho$ + const., a.e. in $(0,1)$, where $\phi_{,i}(R) = \phi_{,i}\left(R; r', \dfrac{r(R)}{R}, \dfrac{r(R)}{R}\right)$ for $i = 1, 2$.

Theorem 3 (for homogeneous materials, Ball [Bal82]). *Assume that*
(H1) $\phi \in C^3((0,\infty)^3)$,
(H2) ϕ *satisfies the Baker–Ericksen inequalities*

$$\frac{v_i\phi_{,i} - v_j\phi_{,j}}{v_i - v_j} > 0,\ i \neq j,\ v_i \neq v_j, \quad \textit{and} \quad \phi_{,i} = \phi_{,i}\,(v_1, v_2, v_3);\ i, j = 1, 2, 3,$$

(H3) $\dfrac{\phi_{,1}\,(v_1, v_2, v_2)}{v_2^2} \to -\infty$ *as* $v_1, v_2 \to 0^+$, *with* $v_1 > v_2$,
(H4) $\dfrac{\phi_{,1}\,(v_1, v_2, v_2)}{v_2^2} \to +\infty$ *as* $v_1, v_2 \to +\infty$, *with* $v_1 < v_2$,
(H5) $r \in C^1(0,1)$ *is a solution of the equilibrium equations associated with* $I(r)$ *with* $r' > 0$ *for all* $R \in (0,1]$ *and* $r(0) = \lim_{R\to 0^+} r(R) = 0$.
Then $r(R) = \lambda R, R \in [0,1]$ *for some* $\lambda > 0$.

This result guarantees that the only radial equilibrium solutions with $r(0) = 0$ are the trivial ones. In that work, Ball argued that the growth hypotheses (H3) and (H4) are essential for every weak solution with $r(0) = 0$ to be trivial (i.e., homogeneous) by giving an example showing that strong ellipticity is not a sufficient condition for the uniqueness of such solutions. He considered

$$W(F) = \phi(v_1, v_2) = g(\eta, \delta) = \eta^a \delta^{-b}, \tag{13.7}$$

where $\eta = v_1 + v_2, \delta = v_1 v_2$, and $a, b \in \mathbb{R}^+$, and showed the existence of solutions of the form $r(R) = \lambda R^\gamma$ for some positive real number $\gamma \neq 1$. But the total energy associated with such a solution is always *infinite*. Ball then posed the following open question:

(BQ) "Does strong ellipticity imply that all solutions of the equilibrium equations which pass through the origin and have *finite* energy are trivial?" (see Remark 2.2).

13.2 Uniqueness and Regularity of Radial Equilibria

To effect an extreme deformation, that is, to compress the body to zero volume or to expand it to infinite volume, we require an infinite amount of energy. This natural observation amounts to having the stored-energy function W obey the following growth behavior[2]:

$$W(x, F) \to +\infty \quad \text{as} \quad \det F \to 0^+ \quad \text{or} \quad +\infty. \tag{13.8}$$

In terms of ϕ, (13.8) is equivalent to the following property:

[2] Note that one cannot expect a convex function to be finite and yet exhibit this type of singular behavior.

$$\lim_{v_i \to 0^+} \phi = \lim_{v_i \to +\infty} \phi = +\infty, \ i = 1, 2, 3. \tag{13.9}$$

From the preceding discussion we see that the smooth stored-energy function ϕ must be chosen so that $\phi \geq 0$, $\phi(R; \cdot, \cdot, \cdot)$ is symmetric in v_1, v_2, and v_3, and satisfies properties (13.8) and (13.10).

Our first model shows that Theorem 1 and Theorem 3 do not carry over to the nonhomogeneous case. Indeed, let $f(R, r, r')$ denote the integrand of $I(r)$ in (13.10), namely,

$$f(R, r, r') = R^2 \phi\left(R; r', \frac{r}{R}, \frac{r}{R}\right). \tag{13.10}$$

For some $\gamma \in (0, 1)$ and for every $\varepsilon > 0$, we assume that f satisfies the constitutive property

$$f(\varepsilon R, \varepsilon^{\gamma} r, \varepsilon^{\gamma - 1} r') = \varepsilon^{-1} f(R, r, r'). \tag{13.11}$$

This homogeneity property was used by [BM85] to study the regularity of minimizers for one-dimensional variational problems in the calculus of variations. We have successfully applied it [Hai00] in modeling the onset of fracture in nonhomogeneous elastic materials where we presented, for the first time, a physical interpretation of this scale-invariance property (see Remark 2.2 below). Setting $\varepsilon = \frac{1}{R}$ in (13.11) yields

$$f(R, r, r') = R^{-1} f(1, rR^{-\gamma}, r' R^{1-\gamma}). \tag{13.12}$$

Let

$$P(R, r') = r' R^{1-\gamma} \text{ and } X(R, r) = rR^{-\gamma}.$$

Relation (13.12) may now be rewritten as

$$f(R, r, r') := R^{-1} e(P, X), \tag{13.13}$$

where

$$e(P, X) = f(1, X, P).$$

Due to the symmetry property of $\phi(R; \cdot, \cdot, \cdot)$ in v_1, v_2, and v_3, we observe that $\phi(R; r', r/R, r/R)$ is the restriction of $\phi(R; v_1, v_2, v_3)$ to the plane $v_2 = v_3 = r/R$. Equivalently, $e(P, X)$ is the restriction to the plane $X_1 = X_2 = X$ of the symmetric quantity $E(P, X_1, X_2)$ associated with $\phi(R; v_1, v_2, v_3)$, where $X_i = v_{i+1} R^{1-\gamma}$ for $i = 1, 2$. Moreover, the condition $\phi_{,11}(R; r', r/R, r/R) \geq 0$ is equivalent to $e_{,pp}(P, X) \geq 0$.

For some $\lambda \in (0, +\infty)$, we observe that an $r(\cdot)$ of the form $r(R) = \lambda R^{\gamma}$ must be an absolute minimizer for $I(\cdot)$ in (13.10) because along such $r(\cdot)$ and in the light of (13.13), one has

$$I(r) = \int_0^1 R^{-1} \ c(\lambda\gamma, \lambda) dR,$$

which will yield the value zero only if there is a zero of c of the form $(\lambda\gamma, \lambda)$ in the PX-plane. So an $r(\cdot)$ of the form $r(R) = \lambda R^\gamma$ corresponds to a point along the line $P = \gamma X$ in the PX-plane or, equivalently, to an admissible solution of the ordinary differential equation $P = \gamma X$. We are now in a position to present the first model. We must say that one generally would not expect that solutions in the nonhomogeneous case are trivial. Nevertheless, the interesting special feature of this model is to illustrate that (even) when W satisfies favorable constitutive hypotheses such as those given in Theorems 1 and 3, (DBVP) may still have nontrivial solutions.

Theorem 4 (Model 1). *There exist positive numbers λ and C such that the equilibrium equations associated with the total energy functional $I(r)$ for*

$$e(P, X) := (PX^2)^{5/3} - 2(PX^2)^{2/3} + (PX^2)^{-1/3} + (P - C)^2(X - C)^4 \quad (13.14)$$

admit nontrivial solutions of the form $r(R) = \lambda R^\gamma, R \in [0, 1]$.

Proof. By direct computation, one can easily verify that $e_{,pp} > 0$ for all P and $X > 0$. The function e satisfies the natural growth condition (13.9). From the discussion that preceded the statement of this theorem, it is also clear that e is the restriction to the plane $X_1 = X_2 = X$ of the symmetric function E given by

$$E(P, X_1, X_2) = (PX_1X_2 - 1)^2(PX_1X_2)^{-1/3} + (P - C)^2(X_1 - C)^2(X_2 - C)^2.$$

More importantly, e satisfies the hypotheses of the uniqueness Theorem 3 for the following reason:

$$e_{,p} = X^{2/3}(PX^2 - 1)(PX^2)^{-4/3}(5PX^2 + 1) + 2(P - C)(X - C)^4.$$

As $P, X \to 0^+$, $e_{,p}/X^2$ behaves like $-(PX^2)^{-4/3}$. Thus, $e_{,p}/X^2 \to -\infty$ as $P, X \to 0^+$. On the other hand, as $P, X \to +\infty$, $e_{,p}/X^2$ behaves like $\frac{5}{3}(PX^2)^{1/3}$. Hence, $e_{,p}/X^2 \to +\infty$ as $P, X \to +\infty$. We have, therefore, established the admissibility of e or, equivalently, that of ϕ. It remains for us to establish the existence of solutions of the form $r(R) = \lambda R^\gamma$ for some $\lambda \in (0, +\infty)$.

Put $X = t$ and $P = \gamma t$. We want to show that for appropriate choices of the numbers λ and C, there exists $t_0 > 0$ such that $e(\gamma t_0, t_0) = 0$. By (13.14),

$$e(\gamma t, t) = \gamma t^3 - 1)^2(\gamma t^3)^{-1/3} + (\gamma t - C)^2(t - C)^4.$$

It is not difficult to see that for $t_0 = \lambda = C = \gamma^{-1/3}$, one obtains $e(\gamma t_0, t_0) = 0$. That is, $\phi(R; r_0(R), \frac{r_0(R)}{R}, \frac{r_0(R)}{R}) = 0$, where

$$r_0(R) = \gamma^{-1/3} R^\gamma, \ R \in [0, 1]. \quad (13.15)$$

Remark 1. By considering the first three terms of e of (13.14), namely,

$$\hat{e}(P, X) = (PX^2 - 1)^2 (PX^2)^{-1/3}, \tag{13.16}$$

one obtains a model that also satisfies the conditions of the uniqueness Theorem 1. Note that the stored-energy function W corresponding to $\hat{e}$ is polyconvex as $\hat{e}$ is convex in the quantity PX^2. On the other hand, it is clear that the unit ball Ω is star-shaped with respect to every point $x_0 \in \Omega$. However, for each $\gamma \in (0, 1)$, the equilibrium equation associated with $\hat{e}$ has a solution of the form given by (13.15). It is worth mentioning that, although $\hat{e}$ of (13.16) takes the value zero along the curve $PX^2 = 1$, e vanishes at only one point of the PX-plane.

Theorem 4 with e as in (13.14) or (13.16) is easily seen to remain valid in the case of n-dimensional elasticity.

Remark 2. Equation (13.7), which represents Ball's example ([Bal82], p. 591), crucially depends on n, the number of elasticity dimensions. This dependence is not so much in reference to the obvious difficulty of testing for the convexity of W, especially for $n > 2$, but rather to the conclusion of the example. According to Ball [Bal82], that example yields solutions of the form $r(R) = R^\alpha$ with $\alpha > 0$ if either $\alpha = 1$ or

$$a \notin [2b, 2(b + 1)], \ \alpha = [a - 2(b + 1)]/(1 - 2b)(1 - b - 1). \tag{13.17}$$

In n-dimensional elasticity with

$$\phi(v_1, \ldots, v_n) = (\eta)^a (\delta)^{-b},$$

one can simply verify by direct computation that the homogeneous deformation $r(R) = \lambda R$ is an equilibrium solution if and only if $n = 3$ or $a = nb$. In terms of (13.17), this says that the case $\alpha = 1$ is not possible, and consequently, the deformations $r(R) = \lambda R$ and $r(R) = \lambda R^\alpha$ with $\alpha > 0$ and $\neq 1$ do not coexist as solutions of the equilibrium equations of (13.7).

Our next result provides a strongly elliptic model in which both the trivial and nontrivial equilibria coexist. Furthermore, the energy associated with each of these solutions is *finite*. In fact, a slight modification of this model yields an example of genuine nonuniqueness in which these different solutions have the *same finite* energy. This homogeneous model, which is the main result of this chapter, represents an answer to (BQ). We now give the statement in the case of plane elasticity.

Theorem 5 (Model 2-H). *Let the positive odd integer a and the positive real number b be given so that*

$$1 + 2b \leq a \leq 2 + 2b. \tag{13.18}$$

Then (i) the function ϕ given by

$$\phi(r', r/R) = |r' - r/R|^a (r'r/R)^{-b} \tag{13.19}$$

is strongly elliptic, and (ii) the equilibrium equations associated with (13.19) have nontrivial solutions of the form $r_0(R) = \lambda R^\gamma$, $R \in [0,1]$, *with* $I(r) < +\infty$.

Proof. The proof of Theorem 5(i) is simply a verification by direct computation of a set of conditions on ϕ, which were developed by [AT80] and are equivalent to the requirement that W be strongly elliptic (see [Hai89], Ch. 3).

The equilibrium equation associated with (13.19) is

$$\frac{d}{dR}\left[R^2 \frac{\partial \phi}{\partial r'}\right] = R^2 \frac{\partial \phi}{\partial r}$$

or, equivalently,

$$Rr''\phi_{,11} + (v_1 - v_2)\phi_{,12} = \phi_{,2} - 2\phi_{,1}\,, \tag{13.20}$$

where $\phi_{,ij} = \dfrac{\partial \phi_{,i}}{\partial v_j}$, $i = 1, 2$, $v_1 = r'$, $v_2 = \dfrac{r}{R}$.

Equation (13.20) has nontrivial weak solutions of the form $r_0(R) = \lambda R^\gamma, \gamma \in (0,1)$, as long as a and b are chosen so that

$$a - 2b - 3(1-\gamma)^{-1} < 0. \tag{13.21}$$

However, this condition is automatically satisfied by hypothesis (13.18) of the above theorem.

For example, taking $a = 7$, $b = 3$, and $\gamma = (135 \pm \sqrt{5553}/132)$ gives rise to weak equilibrium solutions of the form $r_0(R) = \lambda R^\gamma$. Furthermore, the energy associated with such solutions is $I(r_0) = [3 - (1-\gamma)(1-2b)]^{-1}$, which, by (13.21), is finite.

This model shows that strong ellipticity is not sufficient for solutions passing through the origin and having (13.19), and constructs weak equilibrium solutions of the form $r(R) = \lambda R^\gamma$ having the *same* energy value as the trivial solution. In n-dimensional elasticity, the above model still corresponds to a natural state and also yields nontrivial equilibrium solutions exactly like in the case $n = 2$. The corresponding model (13.10) becomes

$$(n-1)|r' - r/R|^a [r'(r/R)^{n-1}]^{-b}.$$

In the nonhomogeneous case, the answer to the analogous question to (BQ) is also negative as can be seen from Theorem 4 and the discussion leading to it. It is interesting to note that the nonhomogeneous version of model (refeqn:hai-19) by itself does not yield the same conclusion as above. More specifically, the function e given by

$$e(P, X) := |P - X|^1 (PX)^{-b} \tag{13.22}$$

is strongly elliptic for $1 + b < a \leq 2 + 2b$. Moreover, the equilibrium equation associated with (13.22), namely,

$$e_{,1} + R\left[e_{,22}\ \frac{dP}{dR} + e_{,12}\,\frac{dX}{dR}\right] = e_{,2}\,,$$

has nontrivial weak solutions of the form $r_0(R) = \lambda R^\gamma,\ \gamma \in (0,1)$, as long as $a = 2b$. The value of the energy associated with such a solution, however, is always *infinite*. While keeping it strongly elliptic, it is possible to modify e in (13.22) in such a way that the corresponding value of the energy associated with r_0 is *finite* (in fact, equal to zero).

Additional results that supplement this work will be forthcoming in another paper to be submitted to *J. Nonlinear Anal.* They have to do with the fundamental question of regularity and with obtaining formulations of the problem that are amenable to successful numerical treatments.

Acknowledgement. This work was partially supported by a grant from the office of Research and Development under Dean P. Kimboko, Grand Valley State University.

References

[Ada75] Adams, R.A.: *Sobolev Spaces.* Academic Press, New York (1975).

[AB78] Antman, S.S., Brezis, H.: The existence of orientation-preserving deformations in nonlinear elasticity. In: Knops, R.J. (ed.), *Nonlinear Analysis and Mechanics,* vol. II. Pitman, London (1978).

[AT80] Aubert, G., Tahroui, R.: Sur la faible fermeture des certains ensembles de constraintes en élasticité nonlinéaire plane. *C.R. Acad. Sci. Paris Sér. I,* **290**, 537–540 (1980).

[Bal77a] Ball, J.M.: Constitutive inequalities and existence theorems in nonlinear elastostatics. In: Knops, R.J. (ed.), *Nonlinear Analysis and Mechanics,* vol. I. Pitman, London, 187–241 (1977).

[Bal77b] Ball, J.M.: Convexity conditions and existence theorems in nonlinear elasticity. *Arch. Rational Mech. Anal.,* **63**, 337–403 (1977).

[Bal82] Ball, J.M.: Discontinuous equilibrium solutions and cavitation in nonlinear elasticity. *Phil. Trans. Roy. Soc. London,* **306**, 557–611 (1982).

[BM84] Ball, J.M., Murat, F.: $W^{1,P}$-quasiconvexity and variational problems for multiple integrals. *J. Functional Anal.,* **58**, 225–253 (1984).

[BM85] Ball, J.M., Mizel, J.V.: One-dimensional variational problems whose minimizers do not satisfy the Euler-Lagrange equation. *Arch. Rational Mech. Anal.,* **90**, 325–388 (1985).

[Eri83] Ericksen, J.L.: Ill-posed problems in thermoelasticity theory. In: Ball, J.M. (ed.), *Systems of Nonlinear Partial Differential Equations,* Reidel, Dordrecht (1983).

[Hai00] Haidar, S.M.: Existence and regularity of weak solutions to the displacement boundary value problem of nonlinear elastostatics. In: Bertram, B., Constanda, C., Struthers, A. (eds.), *Integral Methods in Science and Engineering.* Chapman & Hall/CRC, Boca Raton, FL (2000), pp. 161–166.

[Hai89] Haidar, S.M.: The Lavrentiev phenomenon in nonlinear elasticity. Ph.D. Thesis, Department of Mathematics, Carnegie-Mellon University, Pittsburgh, PA (1989).

[Hil57] Hill, R.: On uniqueness and stability in the theory of finite elastic strains. *J. Mech. Phys. Solids,* **5**, 229–241 (1957).

[Joh72] John, F.: Uniqueness of non-linear elastic equilibrium for prescribed boundary displacements and sufficiently small strains. *Comm. Pure Appl. Math.,* **25**, 617–634 (1972).

[KS84] Knops, R.J., Stuart, C.A.: Quasi-convexity and uniqueness of equilibrium solutions in nonlinear elasticity. *Arch. Rational Mech. Anal.,* **86**, 223–249 (1984).

[Mor52] Morrey, C.B.: Quasi-convexity and the lower semi-continuity of multiple integrals. *Pacific J. Math.,* **2**, 25–53 (1952).

[Mor66] Morrey, C.B.: *Multiple Integrals in the Calculus of Variations.* Springer, Berlin (1966).

[RE55] Rivlin, R.S., Ericksen, J.L.: Stress–deformation relations for isotropic materials. *J. Rational Mech. Anal.,* **4**, 323–425 (1955).

[TN65] Truesdell, C., Noll, W.: The nonlinear field theories of mechanics. In: Flugge, S. (ed.), *Handbuch der Physik,* vol. III/3. Springer, Berlin (1965).

14

The Mathematical Modeling of Syringomyelia

P.J. Harris[1] and C. Hardwidge[2]

[1] University of Brighton, UK; p.j.harris@brighton.ac.uk
[2] Princess Royal Hospital, Haywards Heath, UK; carl.hardwidge@bsuh.nhs.uk

14.1 Introduction

The work presented in this chapter is concerned with constructing a mathematical model of the medical condition syringomyelia. This condition is characterized by the formation of voids or cavities in the spinal cord. An MRI scan of a typical patient is shown in Figure 14.1, where the void in the cord is clearly visible. Although the condition is in its early stages, the patients may not be aware of it, but as it worsens, they can progressively lose the feeling in one or more limbs and may ultimately become paralyzed in the affected limbs. Once a patient has the condition, it is often impossible to treat it, but there are established surgical procedures that help with preventing the condition from getting worse. However, why these procedures are so successful is not fully understood. It is hoped that by mathematically modeling what is happening in the spine, it will be possible to get some insight into the physical processes that lead to the formation and worsening of the voids in the spinal cord. In this study, we have devised a simple model of the spinal cord that can be solved using the finite element method. Our initial studies were with a simple linearly elastic model, but additional studies have been conducted with a viscoelastic model that may prove to give a more realistic response of biologic-type materials under different levels of external loading.

14.2 Description of Syringomyelia

The mechanics of syringomyelia formation and development has been the subject of considerable debate. One hypothesis is that the formation and growth of these voids in the spinal cord is primarily due to the forces that result from the changes in pressure in the fluid surrounding the spinal cord. It is known that changes in the abdominal pressure cause a compression of the spinal dural sac and its contents. In turn, this causes both an increase in the pressure of the spinal fluid and a flow of the fluid from the spine into the fluid-filled

sac that surrounds the brain inside the skull. In most people, when the abdominal pressure relaxes and the spinal cord decompresses, the fluid can flow back from the skull into the spine and the pressure levels return to normal. However, in some people, who either have a malformation of the bones at the back of the skull or have had some traumatic damage to the spine, the fluid is prevented from flowing from the skull back into the spine, and so, when the abdominal pressure relaxes, the pressure in the spinal fluid drops below its equilibrium level. In turn, this allows the spinal cord to expand, and if the resulting tensions in the spinal cord are large enough, then voids may form, or get worse if they are already there.

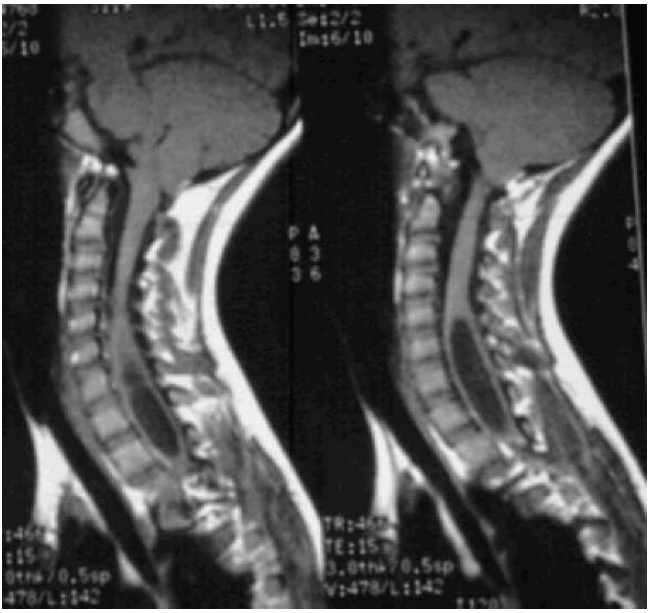

Fig. 14.1. An MRI scan of a patient with syringomyelia.

14.3 Mathematical Model

The geometry of the human spine can be essentially considered as a number of concentric circular cylinders (see Figure 14.2). The innermost cylinder is the spinal cord itself, which can be considered as an elastic or viscoelastic solid. It is surrounded by a layer of cerebral-spinal fluid, which is essentially water. This layer, in turn, is surrounded by a relatively thin layer of soft tissue containing the blood vessels and other elements that the spine needs.

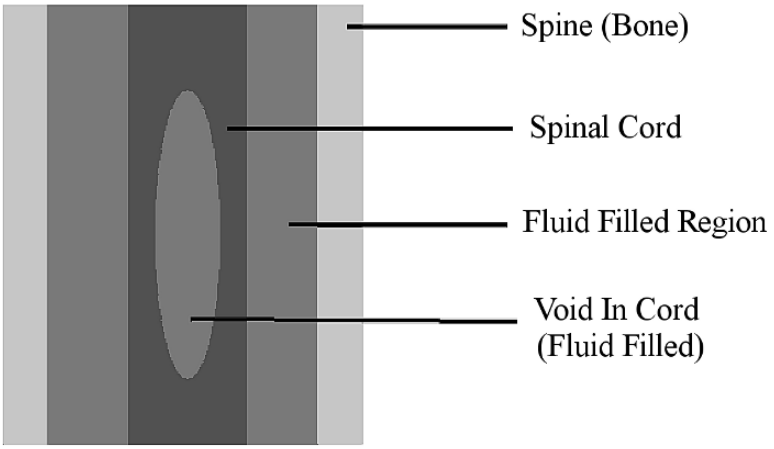

Fig. 14.2. Vertical cross section of the spine.

This layer also acts as the seal that keeps the cerebral-spinal fluid in place. Finally, on the outside are the bones that make up the spine and can be considered as rigid. Whilst the spinal cord is not exactly a circular cylinder (it is not exactly circular in cross section, and the human spine is curved), this is a good approximation and means that the cord can be modeled using an axisymmetric model that greatly simplifies the analysis and reduces the size of the computer model needed to solve the problem.

The initial model proposed here will consider only the spinal cord itself, and assumes that the changes in the pressure in the fluid surrounding the cord are a known function of time. The principal causes of pressure changes in the fluid are the motion of various muscles in the lower abdomen and changes in blood pressure in the soft tissues due to the heart pulse. The changes in pressure due to either of these can be determined from experimental data.

The finite element method has become established as one of the main mathematical tools for modeling the motion of a finite elastic structure. Discretizing the equations of motion of an elastic body using the finite element method yields a matrix equation of the form

$$M\underline{\ddot{u}} + K\underline{u} = \underline{f}, \tag{14.1}$$

where K and M are the stiffness and mass matrices, respectively, $\underline{u}$ is the vector of nodal displacements, $\underline{f}$ is the consistent load vector, and a superposed dot denotes differentiation with respect to time. The derivation of (14.1) can be found in numerous textbooks, such as [OCZ91], and is not repeated here. Given suitable initial conditions, it is possible to integrate this equation through time.

An alternative to the linear elastic model is the use of a viscoelastic model, as this type of model can give a more realistic response of a biologic material to external forces. In the work presented here, a viscoelastic stress–strain relationship of the form

$$\sigma(\mathbf{x},t) = D\varepsilon(\mathbf{x},t) - \sum_{j=1}^{n} \int_0^t \frac{\phi_j}{\tau_j} D e^{(s-t)/\tau_j} \varepsilon(\mathbf{x},s)\, ds$$

is used, where $\sigma(\mathbf{x},t)$ is the vector of the nonzero components of the stress tensor at the point $\mathbf{x}$ and time t, ε is the vector of the nonzero components of the strain tensor, and D is the linear stress–strain matrix. Applying the standard finite element method using this stress–strain relationship leads to

$$\begin{aligned}\int_V B^T \sigma(\mathbf{x},t)\, dV_{\mathbf{x}} &= \int_V B^T D B\, dV_{\mathbf{x}}\, \underline{u}(t) \\ &\quad - \sum_{j=1}^{n} \frac{\phi_j}{\tau_j} \int_V B^T D B\, dV_{\mathbf{x}} \times \int_0^t e^{(s-t)/\tau_j} \underline{u}(s)\, ds \\ &= K\underline{u}(t) - \sum_{j=1}^{n} \frac{\phi_j}{\tau_j} \int_0^t e^{(s-t)/\tau_j} K\underline{u}(s)\, ds,\end{aligned}$$

and hence, the finite element equations are

$$K\underline{u}(t) - \sum_{j=1}^{n} \frac{\phi_j}{\tau_j} \int_0^t e^{(s-t)/\tau_j} K\underline{u}(s)\, ds + M\ddot{\underline{u}}(t) = \underline{f}(t), \tag{14.2}$$

where K and M are the usual elastic stiffness and mass matrices. The integrals appearing in (14.2) can now be evaluated using a quadrature rule of the form

$$\int_0^t e^{(s-t)/\tau_j} f(s)\, ds = \int_0^t e^{-u/\tau_j} f(t-u)\, du \approx \sum_{i=0}^{N} w_{ji} f(t-ih). \tag{14.3}$$

We note that the integral in (14.2) can be truncated at an upper limit $\max(t,t_0)$ since for $u > t_0$, e^{-u/τ_j} becomes small enough that its contribution to the integral can be neglected. By using the quadrature rule given in (14.3), we can write the finite element equations (14.2) as

$$\left(1 - \sum_{j=1}^{n} \frac{\phi_j}{\tau_j} w_{j0}\right) K\underline{u}(t) + M\ddot{\underline{u}}(t) = \underline{f}(t) + K \sum_{i=1}^{N} \left(\sum_{j=1}^{n} \frac{\phi_j}{\tau_j} w_{ji} \underline{u}(t-ih) \right). \tag{14.4}$$

The final finite element equation (14.4) can now be integrated through time using any suitable numerical scheme. Here the trapezium method has been used since it is known to be neutrally stable for solving elasticity and related problems [KEA89].

Once the nodal displacements have been computed, it is possible to compute the stresses in the cord. These will give an indication of where possible future damage may occur.

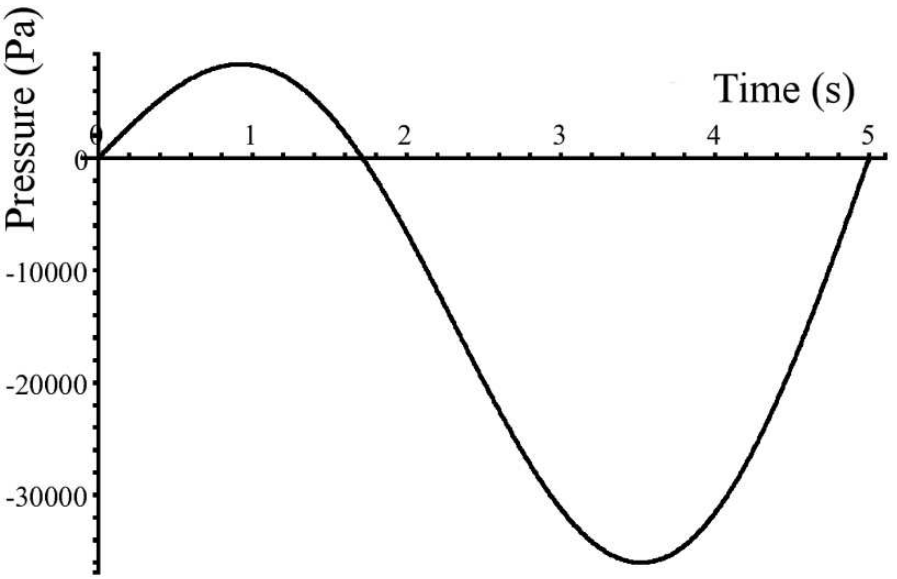

Fig. 14.3. Excess pressure in fluid surrounding the spinal cord.

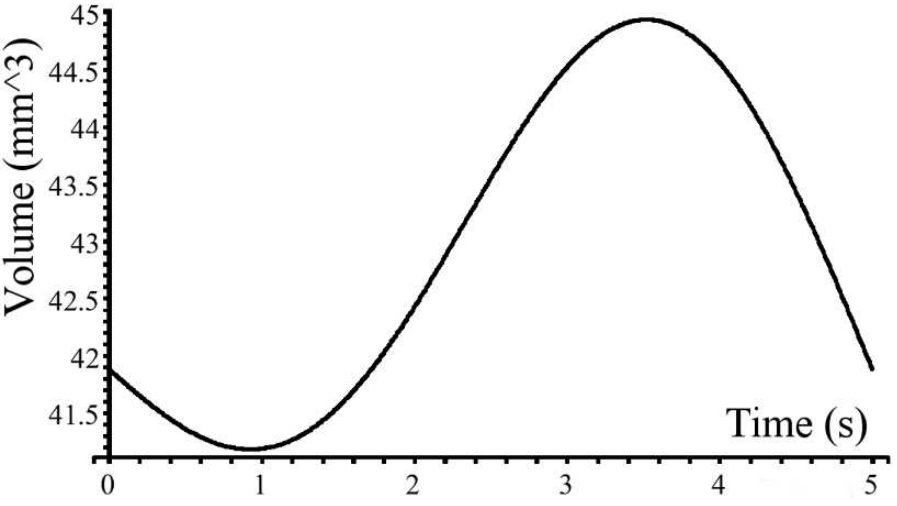

Fig. 14.4. Volume of the void in the spinal cord.

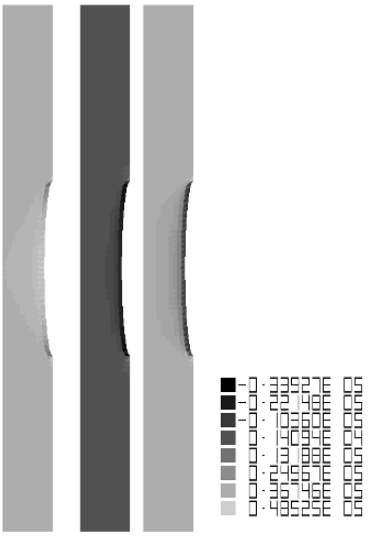

Fig. 14.5. Principal stress components in the spinal cord when the excess pressure is at its minimum.

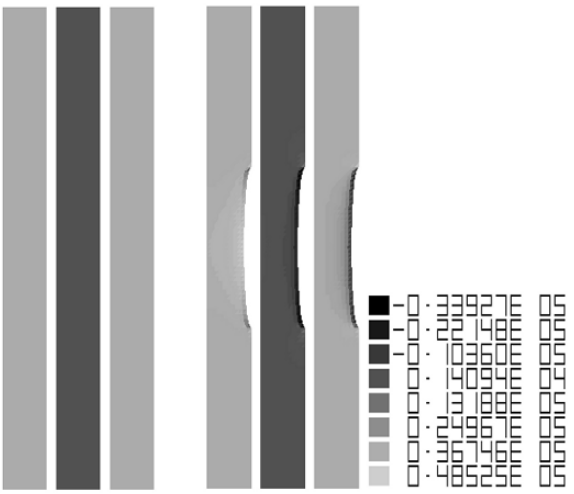

Fig. 14.6. A comparison of the principal stresses in a solid cord and a cord with a void when the excess pressure is at its minimum value.

14.4 Numerical Results

The results below are for computing the displacements in part of the spinal cord using a simple linearly elastic model. Typically, the human spinal cord is approximately 6 mm in radius, and the results are for a section of the cord 60 mm long. The cord section considered here has a single ellipsoidal void of radius 1 mm and length 10 mm located at the center of the cord. The material parameters for the spinal cord are Young's modulus of 1.5×10^6 N m^{-2}, Poisson's ratio of 0.49 (almost incompressible), and density 1500 Kg m^{-3} (see [LEB96] for further details).

Figure 14.3 shows the pressure values in the fluid surrounding the spinal cord which are typical of the levels observed in a patient with syringomyelia. Figure 14.4 shows the corresponding volume of the void in the cord.

Figure 14.5 shows the principal stress components in the spinal cord when the excess pressure is at its lowest value. It can be seen that there are regions of high tensile stresses around the ends of the hole, indicating that if damage were to occur, then it is likely to be at the ends of the hole (i.e., the hole will get bigger). Furthermore, the results in Figure 14.6 show that tensile stresses occurring in a spinal cord that already has a void are greater than those occurring in a solid cord under the same loading. These results seem to indicate that the condition is more likely to get worse in a patient who already has the condition rather than developing in an unaffected patient.

14.5 Conclusions

The work presented in this chapter shows how to use the finite element method to model the deformations of the human spinal cord due to the pressure changes in the surrounding fluid. Furthermore, the results of this early work seem to support the hypothesis that it is the changes in the fluid pressure that are responsible for development and/or worsening of syringomyelia in a patient. Future work will develop the model further, to include crack or void formation and growth effects so that it should be possible to fully simulate what is happening in the spinal cord.

References

[KEA89] Atkinson, K.E.: *An Introduction to Numerical Analysis,* 2nd ed. Wiley, New York (1989).

[LEB96] Bilston, L.E., Thibault L.E.: The mechanical properties of the human cervical spinal cord in vitro. *Biomed. Engng. Soc.,* **24**, 67–74 (1996).

[OCZ91] Zienkiewicz, O.C., Taylor, R.L.: *The Finite Element Method,* vols. 1 and 2. McGraw-Hill, London, (1991).

15

A System Iterative Method for Solving First-Kind, Degraded Identity Operator Equations

J. Hilgers[1,2], B. Bertram[1], and W. Reynolds[2]

[1] Michigan Technological University, Houghton, MI, USA; jwhilger@mtu.edu, bertram@mtu.edu
[2] Signature Research Inc., Calumet, MI, USA; reynolds@signatureresearchinc.com

15.1 Introduction

A class of first-kind integral equations that arise, for example, in problems of image enhancement, feature kernels, or point spread functions (PSFs), which are degraded versions of the Dirac delta function. Such PSFs depend on one or more parameters whose value(s) derive from aperture size, incident wavelength, and sensor geometry.

In problems $Kf = g$ of this type, with f the unknown object, the image g and any approximate regularized solution f_α are blurred forms of the same function f. It then makes sense to view f_α as the image of a higher quality sensor of similar type whose PSF has parameters altered to produce a narrower width. This leads to the problem $K_2 f = f_\alpha$, which is approximately solved, thereby defining one system iteration.

In this chapter, this idea is introduced and a possible improvement is demonstrated. The parameter-choice problem is more complicated and occurs in both directions. In the inverse direction, the parameter α controls the amount of regularization. In the forward direction, the PSF parameter(s) control PSF width, or sensor quality.

A class of first-kind integral equations of the form

$$\int_0^1 K_B(x-y)f(y)dy = g(y), \quad 0 \le x \le 1, \tag{15.1}$$

which arise in image enhancement, feature kernels, or PSFs, that are degraded, or smoothed, versions of the Dirac δ-function. Two examples are considered in this chapter: a Gaussian kernel and a sinc kernel. Formulas and graphs of these are displayed in Section 15.2. A positive parameter controls the width of the PSF. As B increases, the width of the PSF, and so the degree of image

blur, decreases. As $B \to \infty$, $K_B \to \delta$ (in some sense), implying that the sensor becomes perfect since (15.1) then is

$$g(x) = \int_0^1 \delta(x-y) f(y) dy = f(x).$$

In problems of this type, the image $g(x)$ and any regularized approximate solution f_α of (15.1) are both blurred forms of the object function $f_0(y)$. The function f_α is then viewed as the image of a higher quality sensor of similar type, meaning the same PSF with a larger value of B, $B_2 > B$.

The new equation,

$$K_{B_2} f = f_\alpha, \tag{15.2}$$

is then approximately solved in an effort to obtain an improved reconstruction of the true object function $f_0(y)$.

To make this more precise, soppose that the PSF satisfies

$$\begin{aligned} &\text{(i)} \quad K_B : L_2 \to L_2 \ \text{ is completely continuous } \ \forall B > 0, \\ &\text{(ii)} \quad ||K_B f - f|| \to 0 \ \text{ as } \ B \to \infty \ \ \forall f \in L_2. \end{aligned} \tag{15.3}$$

The regularized solution to (15.1) will be taken as

$$f_{B,\alpha} = (K_B^* K_B + \alpha L^* L)^{-1} K_B^* \bar{g}, \tag{15.4}$$

where $\bar{g} = K_B f_0 + \epsilon$ and ϵ is an additive noise vector. Equation (15.4) is the least square solution to (15.1) with Tikhonov regularization applied. L is the regularization operator.

Then the algorithm represented by (15.2) is as follows:

$$\begin{aligned} &\text{(i)} \quad \text{Input } \ B, f_0, \bar{g}, L. \text{ Let } R = \bar{g}. \\ &\text{(ii)} \quad \text{Compute } \ f_{B,\alpha} \ \text{ via (15.4) (with } \bar{g} = R). \text{ Choose} \\ &\qquad \alpha = \alpha_{\text{opt}} \ \text{ to minimize } \ ||f_{B,\alpha} - f_0||. \\ &\text{(iii)} \quad \text{Choose } \ \gamma = C \ \text{ to minimize } \ ||K_\gamma f_0 - f_{B,\alpha_{\text{opt}}}||. \\ &\text{(iv)} \quad R \leftarrow f_{B,\alpha_{\text{opt}}}, B \leftarrow C, \ \text{ go to (ii) (i.e., solve } \ K_C f = f_{B,\alpha_{\text{opt}}}). \end{aligned} \tag{15.5}$$

It is well known (see, for example, [Gro77], [HBR00], [HB04], [Mor84], [Tik63], and [TA77]) that (15.5) exists when

$$\frac{||\epsilon||}{||g||} = \frac{||\epsilon||}{||K_B f_0||} < 1. \tag{15.6}$$

Inequality (15.6) defines the condition for just the first iteration. Thereafter, (15.6) becomes

$$\frac{||\epsilon_{\text{eff}}||}{||K_C f_0||} < 1, \tag{15.7}$$

where ϵ_{eff} is the effective error when the right-hand side R, which is initially ϵ, is set to $f_{B,\alpha_{\text{opt}}}$. Thus, $R = K_C f_0 + \epsilon_{\text{eff}} = f_{B,\alpha_{\text{opt}}}$ so that

$$\epsilon_{\text{eff}} = f_{B,\alpha_{\text{opt}}} - K_C f_0. \tag{15.8}$$

Using the triangle inequality, we find from (15.8) that

$$||\epsilon_{\text{eff}}|| \leq ||f_{B,\alpha_{\text{opt}}} - f_0|| + ||f_0 - K_C f_0||. \tag{15.9}$$

The first term on the right-hand side of (15.9) is just the minimum error achieved by the previous iterate. The second term should decrease to zero due to (15.5(ii)). Thus, if (15.6) is true, it is very likely that (15.7) will follow in subsequent iterations. This merely means that (15.5(ii)) can continue to be executed, and it says nothing as to whether $||f_{B,\alpha_{\text{opt}}} - f_0||$ really does decrease with successive iterations. This will be discussed below. The norm in (15.5(iii)) may or may not have a finite minimum, and the infimum may occur as $\gamma \to \infty$, meaning that $C = \infty$ is possible. Define $Q = ||K_\gamma f_0 - f_{B,\alpha_{\text{opt}}}||$, and assume that $K|_{\gamma \to 0^+} f_0 = 0$ and that $K|_{\gamma \to \infty} f_0 = f_0$. Then a plot of Q versus γ may, in the expected case where $||f_0 - f_{B,\alpha_{\text{opt}}}|| < ||f_{B,\alpha_{\text{opt}}}||$, appear as in Figure 15.1.

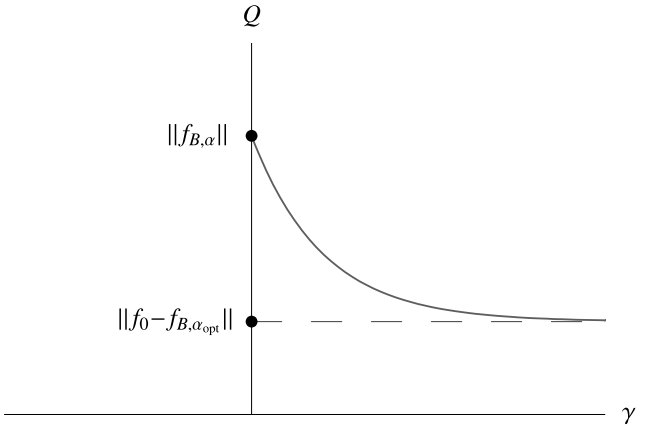

Fig. 15.1. inf Q obtained at $C = \infty$.

The value $C = \infty$ means, as above and in (15.3), that $K_C = I$, in which case, the next iterate by (15.4) belongs to the class

$$f_{\infty,\alpha} = (I + \alpha L^* L)^{-1} \, f_{B,\alpha_{\text{opt}}}.$$

Observe that $f_{\infty,0} = f_{B,\alpha_{\text{opt}}}$, and so the algorithm reaches the fixed point $f_{\infty,0} = f_{B,\alpha_{\text{opt}}}$. Note that if $L = I$, then $\alpha = 0$ may indeed give the minimizer in (15.5(i)). If $f_{\infty,\alpha}$ for $\alpha > 0$ gives a minimizer in (15.5(ii)), then continue the algorithm as defined. In the examples run to date, $C = \infty$ never occurred.

15.2 Numerical Examples

We include four numerical examples featuring two kernels. The first of these is a Gaussian kernel used in the first two cases: $K_B = \frac{B}{\sqrt{\pi}} e^{-B^2(x^2-y^2)}$, with $B = 1$ and $N = 100$ subintervals on $[-2, 2]$. This kernel is shown in Figure 15.2.

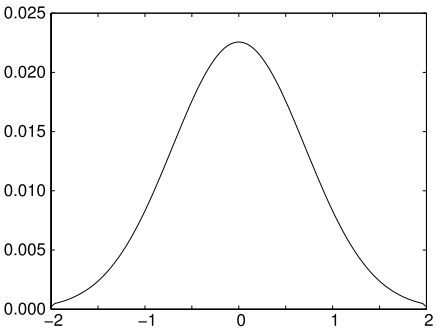

Fig. 15.2. Kernel for Examples 1 and 2.

15.2.1 Example 1

For this example, f_0 (the true answer) is a polynomial, $||\epsilon||/||g||$ (the noise-to-signal ratio) is 0.085, and L (the regularization operator) is the Laplacian. Figure 15.3(a) shows the forcing function with and without noise. Figure 15.3(b) contains the true solution, the Tikhonov solution, and one iteration of the new method.

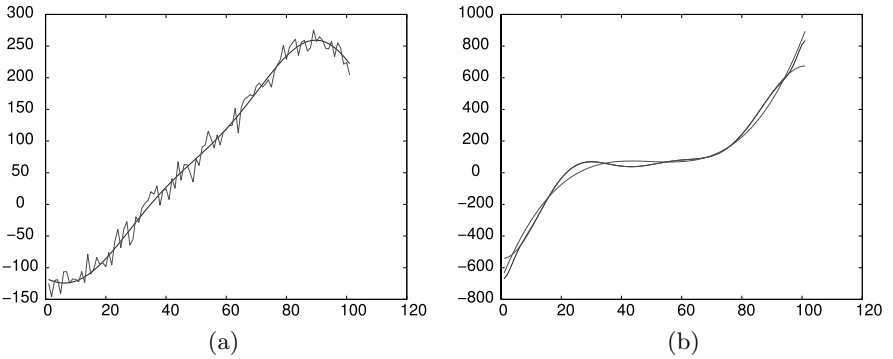

Fig. 15.3. (a) g and $\bar{g}$. (b) f_0, $f_{\alpha_{\text{opt}}}$, and $f_{2,\alpha_{\text{opt}}}$.

Comparison of results:

$$||f_{\alpha_{\text{opt}}} - f_0|| = 448 \quad \text{for} \quad \alpha_{\text{opt}} = 0.5,$$
$$||f_{2,\alpha_{\text{opt}}} - f_0|| = 315 \quad \text{for} \quad \alpha_{\text{opt}} = 8.0, \;\; B_2 = 18.$$

The improvement is 30%.

15.2.2 Example 2

In this example, the Gaussian kernel is used, and the Laplacian is the regularizer. Here, the true solution f_0 is two rectangles of different heights, and the noise-to-signal ratio is $||\epsilon||/||g|| = 0.068$.

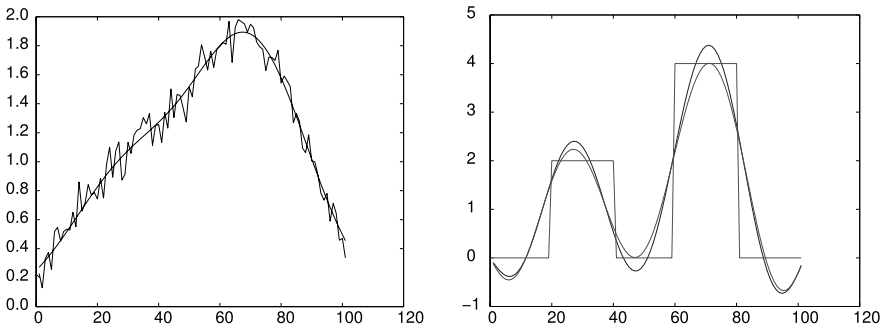

Fig. 15.4. (a) g and $\bar{g}$. (b) f_0, $f_{\alpha_{\text{opt}}}$, and $f_{2,\alpha_{opt}}$.

Comparison of results:

$$||f_{\alpha_{\text{opt}}} - f_0|| = 7.79 \quad \text{for} \quad \alpha_{\text{opt}} = 0.8,$$
$$||f_{2,\beta_{\text{opt}}} - f_0|| = 7.53 \quad \text{for} \quad \beta_{\text{opt}} = 256.0, \;\; B_2 = 18.$$

The improvement is 3.3%.

The second kernel is the sinc kernel used in the last two cases:

$$K_B = \begin{cases} \frac{\sin B(x-y)}{\pi(x-y)} & x \neq y, \\ \frac{B}{\pi} & x = y, \end{cases}$$

with $B = 1$ and $N = 100$ subintervals on $[-4, 4]$. This kernel is shown in Figure 15.5.

15.2.3 Example 3

In this example, the sinc kernel is used, and the Laplacian is the regularizer. Here, the true solution f_0 is two rectangles of different heights, and the noise-to-signal ratio is $||\epsilon||/||g|| = 0.081$.

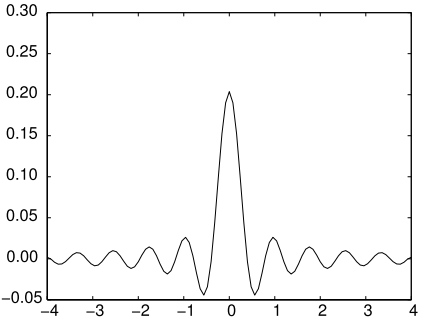

Fig. 15.5. Kernel for Examples 3 and 4.

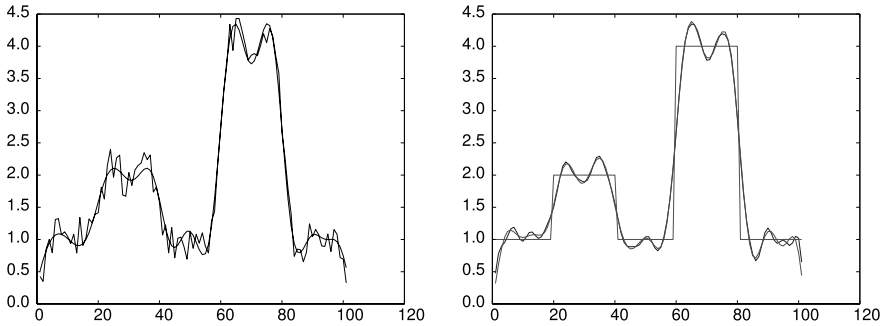

Fig. 15.6. (a) g and $\bar{g}$. (b) f_0, $_{\alpha_{\rm opt}}$, and $f_{2,\alpha_{\rm opt}}$.

Comparison of results:

$$||f_{\alpha_{\rm opt}} - f_0|| = 3.38 \quad \text{for} \quad \alpha_{\rm opt} = 0.4,$$
$$||f_{2,\beta_{\rm opt}} - f_0|| = 3.28 \quad \text{for} \quad \beta_{\rm opt} = 2^{-8},\ \ B_2 = 14.$$

The improvement is 3%.

15.2.4 Example 4

In this example, the sinc kernel is used, and the derivative operator is the regularizer. Here, the true solution f_0 is a polynomial, and the noise-to-signal ratio is $||\epsilon||/||g|| = 0.019$.

$$||f_{\alpha_{\rm opt}} - f_0|| = 12864 \quad \text{for} \quad \alpha_{\rm opt} = 4 \times 10^{-3},$$
$$||f_{2,\beta_{\rm opt}} - f_0|| = 7982 \quad \text{for} \quad \beta_{\rm opt} = 2^{-6},\ \ B_2 = 50.$$

The improvement is 38%.

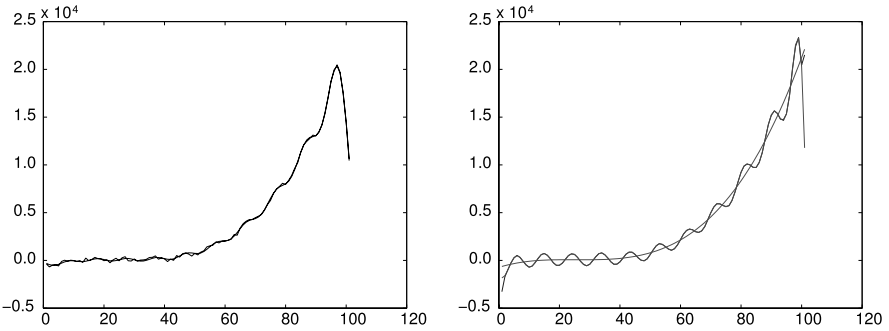

Fig. 15.7. (a) g and $\bar{g}$. (b) f_0, $f_{\alpha_{\text{opt}}}$, and $f_{2,\alpha_{\text{opt}}}$.

15.3 Remarks and Conclusions

1. An algorithm is defined that can significantly improve the quality of regularized solutions to certain first-kind integral equations. In this chapter, the true solution f_0 is used in the computations. Approximating algorithm (15.5) in real computations that do not reference f_0 is left for future work.
2. In this chapter, all examples illustrate just a single iteration of (15.5). Other cases run previously have shown improvements through three or four iterations, after which a fixed point of (15.5) is achieved.
3. The method of this chapter is most effective when $||\epsilon||/||g||$ is large and/or when f_0 does not satisfy boundary conditions forced on f_α by the regularization operator L. In these cases, significant improvement in f_α is possible, and as the examples show, (15.5) can achieve this improvement.
4. In the examples, the second iteration always used the same regularization operator L as the first. But the original error ϵ and the subsequent ϵ_{eff} are quite different, both in norm and in composition. ϵ_{eff} is very smooth with none of the randomness inherent in ϵ. Very different α_{opt} values result, and different L operators should be tried. This is left for future work [HBR00].

References

[Gro77] Groetsch, C.W.: *The Theory of Tikhonov Regularization for Fredholm Equations of the First Kind.* Pitman, London (1977).

[HBR00] Hilgers, J.W., Bertram, B.S., Reynolds, W.R.: Use of cross-referencing for solving the parameter choice problem in generalized CLS. In: Schiavone, P., Constanda, C., Midouchowski, A. (eds.), *Integral Methods in Science and Engineering.* Birkhäuser, Boston (2002), pp. 105–110.

[HB04] Hilgers, J.W., Bertram, B.S.: Comparing different types of approximators for choosing the parameters in the regularization of ill-posed problems. *Computers Math. Appl.,* **48**, 1779–1790 (2004).

[Mor84] Morozov, V.A.: *Methods for Solving Incorrectly Posed Problems.* Springer, Berlin-Heidelberg-New York (1984).

[Tik63] Tikhonov, A.N.: Solution of incorrectly formulated problems and the regularization method. *Soviet Math. Dokl.* (1963), pp. 1035–1038.

[TA77] Tikhonov, A.N., Arsenin, V.Y.: *Solutions of Ill-Posed Problems.* Winston, Washington, DC (1977).

16

Fast Numerical Integration Method Using Taylor Series

H. Hirayama

Kanagawa Institute of Technology, Japan; hirayama@sd.kanagawa-it.ac.jp

16.1 Introduction

We consider the following integral over the finite range [a,b]:

$$I = \int_a^b f(x)dx,$$

where $f(x)$ is a given smooth function.

The arithmetic operations and functions of Taylor series can be defined in Fortran 90, C++ [ES90], and C# programming languages. In addition, functions that consist of arithmetic operations, predefined functions, and conditional statements can quickly be expanded in Taylor series.

Using this procedure, we can expand $f(x)$ at $x = c$ as follows:

$$f(x) = f_0 + f_1(x-c) + f_2(x-c)^2 + f_3(x-c)^3 + \cdots + f_n(x-c)^n. \quad (16.1)$$

If we integrate the Taylor series in (16.1), that is,

$$F(x) = f_0(x-c) + \frac{f_1}{2}(x-c)^2 + \frac{f_2}{3}(x-c)^3 + \cdots + \frac{f_n}{n+1}(x-c)^{n+1}, \quad (16.2)$$

then the integral over the interval [a,b] near $x = c$ may be evaluated using (16.2).

The method outlined above provides us with an effective and fast numerical integration technique.

16.2 Arithmetic of Taylor Series

In this section, we briefly explain the basic idea of how to expand functions into Taylor series. The reader is referred to Rall [Ral81], Henrici [Hen74], and Hirayama [Hir02] for more details.

The arithmetic program for Taylor series can be developed without any difficulty. The following relations are valid not only at the origin but also at any point of the interval [a,b]. The series can be defined in the form

$$f(x) = f_0 + f_1 x + f_2 x^2 + f_3 x^3 + f_4 x^4 + \cdots , \tag{16.3}$$

$$g(x) = g_0 + g_1 x + g_2 x^2 + g_3 x^3 + g_4 x^4 + \cdots , \tag{16.4}$$

$$h(x) = h_0 + h_1 x + h_2 x^2 + h_3 x^3 + h_4 x^4 + \cdots \tag{16.5}$$

and possess the following important properties.

(i) *Addition and subtraction.* If $h(x) = f(x) \pm g(x)$, then the coefficients of f, g, and h satisfy

$$h_i = f_i \pm g_i.$$

(ii) *Multiplication.* If $h(x) = f(x)g(x)$, then the coefficients of f, g, and h satisfy

$$h_n = \sum_{k=0}^{n} f_i g_{n-i}.$$

(iii) *Division.* If $h(x) = f(x)/g(x)$, then the coefficients of f, g, and h satisfy

$$h_0 = \frac{f_0}{g_0}, \quad h_n = \frac{1}{g_0}\left(f_n - \sum_{k=0}^{n-1} h_k g_{n-k}\right), \quad (n \geq 1).$$

(iv) *Exponential function.* If $h(x) = e^{f(x)}$, then $dh/dx = hdf/dx$. Substituting (16.3)–(16.5) into this differential equation and comparing the coefficients of the Taylor series, we arrive at the relations

$$h_0 = e^{f_0}, \quad h_n = \frac{1}{n}\sum_{k=1}^{n} k h_{n-k} f_k, \quad (n \geq 1).$$

We can get similar differential equations and similar relations between the coefficients of the Taylor series for any other elementary transcendental function.

16.3 Numerical Integration Method

In this section, we explain a numerical integration method using Taylor series. We consider the following integral over a finite interval $[a, b]$:

$$I = \int_a^b f(x)dx, \tag{16.6}$$

where $f(x)$ is a given smooth function. We expand the function $f(x)$ at $x = c$ in a Taylor series as

$$f(x) = f_0 + f_1(x-c) + f_2(x-c)^2 + f_3(x-c)^3 + \cdots + f_n(x-c)^n. \quad (16.7)$$

The indefinite integral $F(x)$ can be obtained by integrating the Taylor series derived in (16.7) as

$$F(x) = f_0(x-c) + \frac{f_1}{2}(x-c)^2 + \frac{f_2}{3}(x-c)^3 + \cdots + \frac{f_n}{n+1}(x-c)^{n+1}. \quad (16.8)$$

If $F(x)$ obtained in (16.8) converges sufficiently fast, then we can obtain the value of the integral by computing $F(b) - F(a)$. If this is not the case, then we introduce the function $h = x - c$ and from (16.8) we have

$$F(c+h) = f_0 h + \frac{f_1}{2}h^2 + \frac{f_2}{3}h^3 + \cdots + \frac{f_n}{n+1}h^{n+1}. \quad (16.9)$$

Letting h be sufficiently small, the series in (16.9) becomes a fast convergent Taylor series.

The function h should be chosen so that the absolute value of the last term in (16.9) is less than the error ϵ of computation; i.e.,

$$\left| \frac{f_n}{n+1} h^{n+1} \right| \leq \epsilon. \quad (16.10)$$

From (16.10) we have

$$h \leq \sqrt[n+1]{\frac{(n+1)\epsilon}{|f_n|}}. \quad (16.11)$$

If h satisfies inequality (16.11), we can compute the numerical value of the integral with error ϵ in the interval $[c-h, c+h]$. As the degree of the Taylor series increases, the error of the computation tends to zero.

The numerical integral method described above can be summarized as follows.

(i) Expand $f(x)$ at the center c of the interval $[a, b]$ into a Taylor series.

(ii) Integrate the series.

(iii) Compute h using (16.10) and divide the integral (16.6) into three integrals:

$$\int_a^b f(x)dx = \int_a^{c-h} f(x)dx + \int_{c-h}^{c+h} f(x)dx + \int_{c+h}^b f(x)dx.$$

(iv) The integral over $[c-h, c+h]$ can be computed using the Taylor series. The other integrals can be computed using this integration method recursively.

16.4 Numerical Example

Let us consider a numerical example.

16.4.1 Simple Example

We consider the following simple integral with tolerance $\epsilon = 10^{-10}$:

$$I = \int_0^1 e^x dx = 1.71828182845904523\cdots . \tag{16.12}$$

We expand e^x at $x = 0.5$ into a Taylor series up to degree 9 and integrate it:

$$\begin{aligned}\int e^x dx &= 1.64872(x-0.5) + 0.824361(x-0.5)^2 \\ &+ 0.274787(x-0.5)^3 + 0.0686967(x-0.5)^4 \\ &+ 0.0137393(x-0.5)^5 + 0.00228989(x-0.5)^6 \\ &+ 0.000327127(x-0.5)^7 + 4.08909\times 10^{-5}(x-0.5)^8 \\ &+ 4.54343\times 10^{-6}(x-0.5)^9 + 4.54343\times 10^{-7}(x-0.5)^{10}.\end{aligned} \tag{16.13}$$

We have $h = 0.387707$ from the above Taylor series. Therefore, the integral can be divided into

$$I = \int_0^1 e^x dx = \int_0^{0.112293} e^x dx + \int_{0.112293}^{0.887707} e^x dx + \int_{0.887707}^1 e^x dx. \tag{16.14}$$

The second integral on the right-hand side of (16.14) is obtained by evaluating the Taylor series in (16.13), and is equal to 1.310713. The first and third integrals on the right-hand side of (16.14) can be evaluated similarly. This first integral can be expanded at $x = 0.0561465$ as follows:

$$\begin{aligned}\int e^x dx &= 1.05775(x-0.0561465) + 0.528876(x-0.0561465)^2 \\ &+ 0.176292(x-0.0561465)^3 + 0.044073(x-0.0561465)^4 \\ &+ 0.0088146(x-0.0561465)^5 + 0.0014691(x-0.0561465)^6 \\ &+ 0.000209872(x-0.0561465)^7 \\ &+ 2.62339\times 10^{-5}(x-0.0561465)^8 \\ &+ 2.91488\times 10^{-6}(x-0.0561465)^9 \\ &+ 2.91488\times 10^{-7}(x-0.0561465)^{10}.\end{aligned} \tag{16.15}$$

From the above Taylor series, we have $h = 0.405304$. Because h is greater than the length of the interval of integration in the first integral in (16.14), we can evaluate the first integral by substituting lower and upper limits into (16.15). Applying this method to the third integral, we obtain the values of the first and the third integrals as the follows:

$$\int_0^{0.112293} e^x dx = 0.118840, \quad \int_{0.887707}^1 e^x dx = 0.288729.$$

Evaluating the right-hand side of (16.15) gives

$$I = \int_0^1 e^x dx = 1.718281828456585.$$

The first 12 digits of this result agree with the exact value in (16.12). If we use a Taylor series of order higher than 13, we can compute this integral without a split of the interval of integration.

16.4.2 Kahaner's Test Problems

Kahaner-type test problems [HH03] are usually considered to illustrate the effectiveness of a computational method. These problems deal with discontinuous and singular functions, but in this chapter, we use a slightly different approach to validate our method.

In this work, the calculation times of the numerical integration using Taylor series and AQE11D are compared. The integral routine AQE11D is coded based on the eleventh order adaptive Newton–Cotes method [EU96], which is one of the fastest numerical integration routines.

The comparison performance on a Pentium 4 2.0 GHz is shown in Table 16.1.

Table 16.1. Comparison of performance on Pentium 4 2.0 GHz of the quadrature routine based on Taylor series with error tolerance 1.0E-09.

No.	a	b	Integrand	Taylor μs	AQE11D μs	Ratio
1	0.0	1.0	e^x	1.02	3.06	3.40
4	-1.0	1.0	$0.92\cosh x - \cos x$	3.52	7.50	2.40
5	-1.0	1.0	$1/(x^4 + x^2 + 0.9)$	5.70	8.54	1.70
8	0.0	1.0	$1/(x^4 + 1)$	4.57	6.25	1.50
9	0.0	1.0	$2/(2 + \sin 3.14159x)$	99.60	86.70	0.98
10	0.0	1.0	$1/(1 + x)$	1.60	3.12	2.20
11	0.0	1.0	$1/(e^x + 1)$	1.77	4.23	2.70
12	0.0	1.0	$1/(e^x - 1)$	1.44	7.53	5.90
13	0.0	1.0	$\sin(314.1592x)/(3.141592x)$	185.81	255.00	1.60
14	0.0	10.0	$\sqrt{(50)}e^{50\dot{3}.14159x^2}$	656.20	59.60	0.09
15	0.0	10.0	$25e^{-25x}$	63.90	26.20	0.47
16	0.0	10.0	$50/(3.14159(2500x^2 + 1))$	23.24	29.80	1.40
17	0.01	1.0	$\sin(50\dot{3}.14159x)/(50(50\dot{3}.14159x)^2)$	103.751	227.00	2.40
18	0.0	π	$\cos(\cos x + 3\sin x + 2\cos 2x + 3\sin 2x + 3\cos 3x)$	156.08	81.80	2.40
20	0.0	-1.0	$1/(x^2 + 1.005)$	2.38	9.06	4.30
21	0.0	1.0	$\frac{1}{\cosh^2(10(x-0.2))} + \frac{1}{\cosh^4(100(x-0.4))} + \frac{1}{\cosh^6(1000(x-0.6))}$	11927.20	-	N/A

It may be observed from Table 1 that the method introduced in this chapter gives better results than AQE11D for many test problems, except for the case when the integrated function decays rapidly or oscillates at high frequency. Lower-order Taylor series cannot give a good approximation for rapidly decaying functions over a wide range because, by (16.11), the error of integration in this case is large. For such functions, a polynomial bounded at both ends of the interval gives a better approximation than the Taylor series method.

16.5 Conclusion

The numerical integration method based on Taylor series is one of the fastest for most functions. However, this method does not give good results for rapidly decaying and high-frequency oscillating functions. The method can easily be applied using the C++, C#, or Fortran 90 programming languages.

This method can also be applied, with slight modifications, to the integration of singular and discontinuous functions.

References

[ES90] Ellis, M.A., Stroustrup, B.: *The Annotated C++ Reference Manual.* Addison-Wesley, New York (1990).

[EU96] Engeln-Müllges, G., Uhlig, F.: *Numerical Algorithms with C.* Springer, Berlin-Heidelberg-New York (1996).

[Hen74] Henrici, P.: *Applied Computational Complex Analysis,* vol. 1. Wiley, New York (1974).

[HH03] Hibino, S., Hasegawa, T., Ninomiya, I., Hosoda, Y., Sato, Y.: A doubly adaptive quadrature method based on the combination of the Ninomiya and the FLR schemes. *Trans. IPSJ,* **44**, 2419–2427 (2003) (Japanese).

[Hir02] Hirayama, H.: Numerical method for solving ordinary differential equation by Picard's method. In: Schiavone, P., Constanda, C., Mioduchowski, A. (eds.), *Integral Methods in Science and Engineering.* Birkhäuser, Boston (2002) pp. 111–116.

[Ral81] Rall, L.B.: *Automatic Differentiation-Technique and Applications.* Springer, Berlin-Heidelberg-New York (1981).

17

Boundary Integral Solution of the Two-Dimensional Fractional Diffusion Equation

J. Kemppainen and K. Ruotsalainen

University of Oulu, Finland; jukemppa@oulu.fi, keijo.ruotsalainen@ee.oulu.fi

17.1 Introduction

In this chapter, we discuss the boundary integral solution of the fractional diffusion equation

$$\begin{aligned} \partial_t^\alpha \Phi - \Delta \Phi &= 0 \quad \text{in } Q_T = \Omega \times (0,T), \\ B(\Phi) &= g \quad \text{on } \Sigma_T = \Omega \times (0,T), \\ \Phi(x,0) &= 0 \quad x \in \Omega, \end{aligned} \tag{17.1}$$

where the boundary operator $B(\Phi) = \Phi_{\Sigma_T}$ and ∂_t^α is the Caputo time derivative of the fractional order $0 < \alpha \leq 1$. For $\alpha = 1$, we get the ordinary diffusion equation, and for $\alpha = 0$, we have the Helmholtz equation.

Hilbert space methods to study the initial boundary value problems are well known for the heat and wave equations (see [LM721] and [LM722]).

The boundary integral equation method for elliptic, parabolic, and hyberbolic equations has been extensively studied by several authors (see [Cos92] and the references therein). The idea to represent the solution of these equations as boundary potentials has been used for decades (centuries). This method converts the problem to an equivalent integral equation on the boundary of the domain. The method has been well studied, for example, in [Cos92], [Cos04], and [HS89]. The functional framework has been the interpretation of the boundary integral operators as anisotropic pseudodifferential operators acting on anisotropic Sobolev spaces[Cos01]. In this way, the boundary integral method is closely connected with the Hilbert space approach to the initial boundary value problems studied in [LM721] and [LM722].

In this chapter, we construct a fundamental solution by means of the Fox H-functions and represent the solution of (17.1) as a single-layer potential. Using the jump relations of the potential, we derive the appropriate boundary integral operator and compute its principal symbol. By analyzing the properties of the principal symbol, we can then give the detailed mapping properties of the single-layer operator in anisotropic Sobolev spaces, which

yield the unique solvability of the boundary integral equation, and thus, also the unique solvability of the initial-boundary value problem.

17.2 Boundary Integral Formulation of the Problem

17.2.1 The Fundamental Solution

The fundamental solution $E(x,t)$ of the fractional diffusion equation is constructed by taking the Laplace transform in the time variable and the Fourier transform in the spatial variable of the fractional diffusion equation

$$(\partial_t^\alpha - \Delta)E(x,t) = \delta(x,t),$$

where $\delta(x,t)$ is the Dirac delta distribution. The transformed equation is then

$$(|\xi|^2 + s^\alpha)\widehat{\widetilde{E}}(\xi,s) = 1,$$

where the two-dimensional Fourier transform is defined by

$$\widehat{u}(\xi,t) = \int_{\mathbb{R}^2} e^{-i\langle x,\xi\rangle} u(x,t)dx$$

and the Laplace transform by

$$\widetilde{u}(x,s) = \int_0^\infty e^{-st} u(x,t)dt.$$

Hence, the Fourier–Laplace transform of the fundamental solution is

$$\widehat{\widetilde{E}}(\xi,s) = \frac{1}{|\xi|^2 + s^\alpha}.$$

Using the Laplace transform of the Mittag–Leffler functions [KS04]

$$\int_0^\infty e^{-st} t^{\mu k+\beta-1} E_{\mu,\beta}^{(k)}(-at^\mu)dt = \frac{k!s^{\mu-\beta}}{a+s^\mu},$$

we find out that the Fourier transform of the fundamental solution is

$$\widehat{E}(\xi,t) = \mathcal{F}(E)(\xi,t) = t^\alpha E_{\alpha,\alpha}^{(0)}(-|\xi|^2 t^\alpha).$$

By computing the inverse Fourier transform of the Mittag–Leffler function, we notice that the fundamental solution is the Fox H-function (see [KS04] and [PBM90])

$$E(x,t) = t^{\alpha-1}|x|^{-2} H_{12}^{20}(|x|^2 t^{-\alpha}|_{(1,1),(1,1)}^{\alpha,\alpha}).$$

For later use, we need to compute the Laplace transform of the fundamental solution. We have

$$\widetilde{E}(x,s) = \int_0^\infty e^{-st} E(x,t)dt = \frac{1}{2\pi}\int_{\mathbb{R}^2} e^{i\langle \xi, x\rangle} \frac{1}{|\xi|^2 + s^\alpha} d\xi.$$

Since the Fourier–Laplace transform of the fundamental solution is radial, i.e., $\widehat{\widetilde{E}}(\xi,t) = \widehat{\widetilde{E}}(|\xi|,t)$, its inverse transform is radial as well:

$$\widetilde{E}(x,s) = \widetilde{E}(|x|,s).$$

On the other hand, the Fourier transform of $\widetilde{E}(|x|,s)$ can be written as

$$\widehat{\widetilde{E}}(\xi,s) = \int_0^\infty r\Big[\int_{-\pi}^{\pi} e^{-ir|\xi|\cos(\phi)} d\phi\Big]\widetilde{E}(r,s)dr = 2\pi\int_0^\infty r J_0(r|\xi|)\widetilde{E}(r,s)dr,$$

by changing integration to polar coordinates. Now, by formula 6.576 (7) in [GR96] for the Bessel functions, we have

$$\int_0^\infty r J_0(|\xi|r) K_0(s^{\frac{\alpha}{2}} r)dr = \frac{1}{|\xi|^2 + s^\alpha},\ \mathrm{Re}(s) > 0.$$

Hence, the Laplace transform of the fundamental solution $E(x,t)$ is

$$\widetilde{E}(x,s) = 2\pi K_0(|x| s^{\frac{\alpha}{2}}). \tag{17.2}$$

17.2.2 The Boundary Integral Equation

We now define the boundary potential

$$\Phi(x,t) = S\sigma(x,t) = \int_\Gamma \int_0^t \sigma(y,\tau) E(x-y, t-\tau) ds_y d\tau,\ x \in \Omega,\ t \in (0,T)$$

for a given boundary distribution $\sigma(x,t) \in C^\infty(\Sigma_T)$. The potential is the solution of the fractional diffusion equation both in the interior domain $\Omega \times (0,T)$ and in the exterior domain $[\mathbb{R}^n \setminus \Omega] \times (0,T)$, with the zero initial condition. We denote the direct value of $S\sigma$ on the boundary by $V\sigma$.

The single-layer potential $S\sigma(x,t)$ is continuous up to the boundary due to the asymptotic properties of the fundamental solution. This leads to the boundary relation

$$\gamma(S\sigma) = \gamma(\Phi) = V\sigma(x,t),$$

where $\gamma :\ u \to u|_\Gamma$ is the trace operator. In other words, we have converted the initial-boundary value problem for the fractional diffusion equation (17.1) to the boundary integral equation

$$V\sigma(x,t) = \gamma(\Phi)(x,t) = g(x,t),\ (x,t) \in \Sigma_T.$$

Furthermore, the normal derivative of the single-layer potential experiences a jump across the boundary [KR]:

$$[\partial_n S\sigma]_{\Sigma_T} = \sigma.$$

17.3 Function Spaces

Let $s \in \mathbb{R}$ and $m \geq 1$. The anisotropic Sobolev space $H^s_m(\mathbb{R}^{n+1})$ contains those distributions $u \in S'(\mathbb{R}^{n+1})$ for which the norm

$$\|u\|_{s,m} = (2\pi)^{-\frac{n+1}{2}} \Big(\int_{\mathbb{R}^{n+1}} [(1+|\xi|^2)^m + |\eta|^2]^{\frac{s}{m}} |\widehat{u}(\xi,\eta)|^2 d\xi d\eta \Big)^{\frac{1}{2}}$$

is finite [Cos01]. Here the length of the vector $\xi = (\xi_1, \xi_2, \ldots, \xi_n)$ is denoted as usual by $|\xi|^2 = \xi_1^2 + \xi_2^2 + \cdots + \xi_n^2$.

Anisotropic Sobolev spaces on the cylinder $\mathbb{T}^n \times \mathbb{R}$ are defined in the same way as the anisotropic Sobolev spaces on $\mathbb{R}^{n+1}$:

$$\|u\|_{s,m} = (2\pi)^{-\frac{n}{2}} \Big(\sum_{k\in\mathbb{Z}^n} \int_{\mathbb{R}_\eta} \big((1+|2\pi k|^2)^m + |\eta|^2\big)^{\frac{s}{m}} |\underline{\widehat{u}}(k,\eta)|^2 d\eta \Big)^{\frac{1}{2}}$$

Here $\underline{\widehat{u}}(k,\eta)$ for $(k,\eta) \in \mathbb{Z}^n \times \mathbb{R}$ are defined as the Fourier coefficients in the space variables and the Fourier transform in the time variable, i.e.,

$$\underline{\widehat{u}}(k,\eta) = \int_{[0,1]^n} \int_{\mathbb{R}} e^{-i(2\pi(k,x)+t\eta)} u(x,t) dx\, dt,$$

with the scalar product $(k,x) = \sum_{l=1}^n k_l x_l$.

Finally, let us introduce the anisotropic Sobolev space $\tilde{H}^s_m(\mathbb{R}^{n+1})$, which takes the vanishing initial condition at $t = 0$ into account; that is,

$$\tilde{H}^s_m(\mathbb{R}^{n+1}) = \{u \in H^s_m(\mathbb{R}^{n+1} : \ \mathrm{supp}(u) \subset \mathbb{R}_x \times [0,\infty[\}.$$

For a finite time-interval, we write $\mathbb{R}^{n+1}_T = \mathbb{R}^n_x \times (0,T)$, $T > 0$, and set

$$\tilde{H}^s_m(\mathbb{R}^{n+1}_T) = \{u = U|_{\mathbb{R}^n_x \times (-\infty,T)} : U \in \tilde{H}^s_m(\mathbb{R}^{n+1})\},$$

equipped with the norm

$$\|u\|_{s,m;T} = \inf\{\|U\|_{s,m} : \ u = U|_{\mathbb{R}^n_x \times (-\infty,T)}\}.$$

As above, we define $\tilde{H}^s_m(\mathbb{T}^n \times \mathbb{R})$ as the space of functions vanishing on the negative time-axis and $\tilde{H}^s_m(\Sigma_T)$ as the space of the restrictions to $\Sigma_T = \Gamma \times (0,T)$.

17.4 The Mapping Properties

In this section, we present the main results concerning the mapping properties of the single-layer operator

$$V_\Gamma u_\Gamma(x,t) = \int_\Gamma \int_0^T E(x-y, t-\tau) u(y,\tau) ds_y d\tau.$$

Since, by our assumption, the boundary curve Γ has a smooth parametric representation $\theta \to x(\theta)$, we may identify every boundary distribution with the 1-periodic distribution in the space variable $u(\theta, t) = u_\Gamma(x(\theta), t)$. Hence, the single-layer operator can be written as

$$Vu(\theta, t) = \int_0^t \int_0^1 E(x(\theta) - x(\phi), t - \tau) u(\phi, \tau) d\phi d\tau. \tag{17.3}$$

We will see from the properties of the fundamental solution that the single-layer operator is of Volterra type [KR]; i.e., if $u(\theta, \tau) = 0$ for $\tau < t$, then $Vu(\theta, \tau) = 0$.

We will consider the single-layer operator as an anisotropic pseudodifferential operator, and compute its principal symbol, whose properties yield the mapping properties in the anisotropic Sobolev spaces defined above.

Applying the Laplace transformation and using (17.2), we get

$$\mathcal{L}(Vu)(x, s) = \frac{1}{2\pi} \int_0^1 \widetilde{u}(\phi, s) K_0(|x(\theta) - x(\phi)| s^{\frac{\alpha}{2}}) |x'(\phi)| d\phi.$$

Since we assumed that $u(\phi, t) = 0$, $t < 0$, we obtain the Fourier transform by putting $s = i\eta$:

$$\widehat{Vu}(\theta, \eta) = \frac{1}{2\pi} \int_0^1 \widehat{u}(\phi, \eta) K_0(|x(\theta) - x(\phi)| (i\eta)^{\frac{\alpha}{2}}) |x'(\phi)| d\eta.$$

We define the function $\kappa(\theta, \phi)$ by setting

$$\kappa(\theta, \phi) = \frac{|x(\theta) - x(\phi)|}{2 \sin(\pi(\theta - \phi))}.$$

Hence, the kernel of the integral operator V can be written as

$$K_0(|x(\theta) - x(\phi)| (i\eta)^{\frac{\alpha}{2}}) = K_0(2\kappa(\theta, \phi)(i\eta)^{\frac{\alpha}{2}} \sin(\theta - \phi)),$$

which is 1-periodic in $\theta - \phi$ and has the Fourier series representation ([Obe73], (4.32))

$$K_0(|x(\theta) - x(\phi)| (i\eta)^{\frac{\alpha}{2}}) = \sum_{p \in \mathbb{Z}} I_{|p|}(\kappa(\theta, \phi)(i\eta)^{\frac{\alpha}{2}}) K_{|p|}(\kappa(\theta, \phi)(i\eta)^{\frac{\alpha}{2}}) e^{2\pi p i(\theta - \phi)}.$$

Replacing the kernel of the single-layer operator by the Fourier series, we obtain the following representation of the operator:

$$Vu(\theta, t) = \frac{1}{2\pi} \sum_{p \in \mathbb{Z}} \int_0^1 \int_{\mathbb{R}_\eta} a(\theta, \phi, p, \eta) \widehat{u}(\phi, \eta) e^{2\pi p i(\theta - \phi) + i\eta t} d\phi d\eta,$$

where the amplitude of the pseudodifferential operator is

$$a(\theta,\phi,p,\eta)=\frac{1}{2\pi}I_{|p|}(\kappa(\theta,\phi)(i\eta)^{\frac{\alpha}{2}})K_{|p|}(\kappa(\theta,\phi)(i\eta)^{\frac{\alpha}{2}})|x'(\phi)|.$$

As in [Cos01] (Theorems 3.4 and 4.3), from the asymptotic expansion of the amplitude we now get the leading term by inserting $\phi=\theta$:

$$a(\theta,p,\eta)=a(\theta,\theta,p,\eta)=\frac{1}{2\pi}I_{|p|}(\kappa(\theta)(i\eta)^{\frac{\alpha}{2}})K_{|p|}(\kappa(\theta)(i\eta)^{\frac{\alpha}{2}})|x'(\theta)|,$$

where $\kappa(\theta)=\frac{|x'(\theta)|}{2\pi}$.

From the asymptotic properties of the Bessel functions ([AS71], (9.7.7), (9.3.9), and (9.7.8)), we find (for $p\neq 0$) the asymptotic behavior

$$I_{|p|}(\kappa(\theta)(i\eta)^{\frac{\alpha}{2}})K_{|p|}(\kappa(\theta)(i\eta)^{\frac{\alpha}{2}})\sim\frac{1}{2\sqrt{|p|^2+\kappa(\theta)(i\eta)^{\alpha}}}.$$

Hence, the single-layer operator admits the Fourier representation

$$\begin{aligned}Vu(\theta,t)&=\frac{1}{2\pi}\sum_{p\in\mathbb{Z}}\int_{\mathbb{R}_\eta}a(\theta,p,\eta)\widehat{u}(p,\eta)e^{i2\pi p\theta+i\eta t}d\eta+Bu(\theta,t)\\&=V_0u(\theta,t)+Bu(\theta,t),\end{aligned}$$

where B is an operator of Volterra type, which is a bounded operator between the anisotropic Sobolev spaces $\tilde{H}^s_\gamma(Q_T)$ and $\tilde{H}^{s+2}_\gamma(Q_T)$, $\gamma=\frac{2}{\alpha}$. The principal part V_0 has the the anisotropic symbol

$$a(\theta,p,\eta)=\frac{1}{2}([\frac{2\pi p}{|x'(\theta)|}]^2+(i\eta)^{\alpha})^{-\frac{1}{2}}.$$

Here and in the sequel we set $\gamma=\frac{2}{\alpha}$, $0<\alpha\leq 1$. The principal symbol satisfies the following conditions when the anisotropic distance is

$$\rho(m,\eta)=|m|+|\eta|^{\frac{1}{\gamma}}\geq\rho_0>0.$$

1. $a\in C^\infty(\mathbb{R}^3)$, and it is 1-periodic in θ.
2. The symbol is quasi-homogeneous of order $\beta=-1$:

$$a(\theta,\lambda p,\lambda^{\frac{2}{\alpha}}\eta)=\lambda^{-1}a(\theta,p,\eta),\ \lambda\geq 1.$$

3. The mapping $\eta\to a(\theta,p,\eta)$ has a polynomially-bounded analytic continuation into the domain $\{z\in\mathbb{C}|\ z=\eta-i\sigma,\ \sigma>0\}$ and is continuous for $\sigma\geq 0$.

From the previous properties, we deduce the next assertion.

Theorem 1. *The single-layer operator $V:\tilde{H}^s_\gamma(\Sigma_T)\to\tilde{H}^{s+1}_\gamma(\Sigma_T)$ is bounded for all $s\in\mathbb{R}$.*

Proof. The statement follows directly from the estimate

$$|a(\theta, m, \eta)| \leq C(|m| + |\eta|^{\frac{\alpha}{2}})^{-1},$$

whenever $|m| + |\eta|^{\frac{\alpha}{2}} \geq \rho_0 > 0$, and the definition of the anisotropic Sobolev spaces.

To discuss whether the operator is positive, we need the following lemma, which is proved by elementary complex analysis.

Lemma 1. *For all $0 < \alpha \leq 1$, there exists a positive constant $C(\rho, \alpha) > 0$ such that*

$$Re\{\frac{1}{\sqrt{|m|^2 + (i\eta)^\alpha}}\} \geq C(|m| + |\eta|^{\frac{\alpha}{2}})^{-1}$$

whenever $|m|^2 + |\eta|^\alpha \geq \rho > 0$.

With this lemma we can prove the Gårding inequality [KR].

Theorem 2. *For the single-layer operator, there exist positive constants C_0 and C_1 such that*

$$Re(Vu, u) \geq C_o \|u\|^2_{-\frac{1}{2},\gamma;T} - \|u\|^2_{-\frac{3}{2},\gamma;T}$$

for all $u \in \tilde{H}_m^{-\frac{1}{2}}(\Sigma_T)$.

Coerciveness follows from the following assertion [KR]:

Lemma 2. *For all $\sigma \in \tilde{H}^{-\frac{1}{2},\gamma}(\Sigma_T)$, we have*

$$Re(V\sigma, \sigma) > 0, \quad \text{if } \sigma \neq 0.$$

As in [HS89], we obtain the strong coerciveness of the single-layer operator and can state our main result [KR].

Theorem 3. *The single-layer operator $V : \tilde{H}_\gamma^{-\frac{1}{2}}(\Sigma_T) \to \tilde{H}_\gamma^{\frac{1}{2}}(\Sigma_T)$ is an isomorphism. Furthermore, it is coercive; i.e., there exists a positive constant c such that*

$$Re(V\sigma, \sigma) \geq c\|\sigma\|^2_{-\frac{1}{2},\gamma}$$

for all $\sigma \in \tilde{H}_\gamma^{-\frac{1}{2}}(\Sigma_T)$.

Corollary 1. *For every $g \in \tilde{H}_\gamma^{\frac{1}{2}}(\Sigma_T)$, the fractional diffusion equation admits a unique solution $\Phi(x,t) \in \tilde{H}_\gamma^1(\Omega \times (0,T))$, which is given by the single-layer potential*

$$\Phi(x,t) = S\sigma(x,t),$$

where $\sigma \in \tilde{H}_\gamma^{-\frac{1}{2}}(\Sigma_T)$ is the unique solution of the boundary integral equation

$$V\sigma = g.$$

References

[AS71] Abramowitz, M., Stegun, I.A. (eds.): *Handbook of Mathematical Functions with Formulas, Graphs, and Mathematical Tables.* U.S. Government Printing Office, Washington, DC (1971).

[Cos92] Costabel, M.: Boundary integral operators for the heat equation. *Integral Equations Oper. Theory,* **13**, 498–552 (1992).

[Cos04] Costabel, M.: Time-dependent problems with the boundary integral equation method. In: Stein E., Borst R., Hughes, T.J.R. (eds.), *Encyclopedia of Computational Mechanics.* Wiley, New York (2004).

[Cos01] Costabel, M., Saranen, J., Parabolic boundary integral operators, symbolic representations and basic properties. *Integral Equations Oper. Theory,* **40**, 185–211 (2001).

[GR96] Gradshteyn, I.S., Ryzhik, I.M.: *Table of Integrals, Series and Products.* Academic Press, New York (1996).

[HS89] Hsiao, G.C., Saranen J.: Coercivity of the single layer heat operator. Report 89-2, Center for Mathematics and Waves, University of Delaware, Newark, DE (1989).

[KR] Kemppainen, J., Ruotsalainen, K.: Boundary integral operators for two-dimensional fractional diffusion equations (in press).

[KS04] Kilbas, A.A., Saigo, M.: *H-transforms: Theory and Applications.* CRC Press, Boca Raton, FL (2004).

[LM721] Lions, J.-L., Magenes, E.: *Non-homogeneous Boundary Value Problems and Applications,* vol. I. Springer, Berlin (1972).

[LM722] Lions, J.-L., Magenes, E.: *Non-homogeneous Boundary Value Problems and Applications,* vol. II. Springer, Berlin (1972).

[Obe73] Oberhettinger, F.: *Fourier Expansions.* Academic Press, New York-London (1973).

[PBM90] Prudnikov, A.P., Brychkov, Y.A., Marichev, O.I.: *Integrals and Series, vol. 3. More Special Functions.* Overseas Publishers Association, Amsterdam (1990).

18

About Traces, Extensions, and Co-Normal Derivative Operators on Lipschitz Domains

S.E. Mikhailov

Brunel University West London, Uxbridge, UK; sergey.mikhailov@brunel.ac.uk

18.1 Introduction

For a second-order partial differential equation (PDE)

$$Lu(x) := L(x, \partial_x)\, u(x) := \sum_{i=1}^{n} \frac{\partial}{\partial x_i} \Big(a(x) \frac{\partial u(x)}{\partial x_i} \Big) = f(x), \quad x \in \Omega,$$

acting on a function u from the Sobolev space $H^s(\Omega)$, $\frac{1}{2} < s < \frac{3}{2}$, the function derivatives do not generally exist on the boundary in the trace sense, but a co-normal *generalized* derivative operator can be defined with the help of the first Green identity. However, this definition is related to an extension of the PDE operator and the PDE right-hand side from the domain Ω, where they are prescribed, to the domain boundary, where they are not. Since the extensions are not unique, the generalized co-normal derivative appears to be a nonunique operator, which is also nonlinear in u unless a linear relation between u and the PDE right-hand side extension is enforced. However, for functions u from $H^s(\Omega)$, $\frac{1}{2} < s < \frac{3}{2}$, that are mapped by the PDE operator into the space $\widetilde{H}^t(\Omega)$, $t \geq -\frac{1}{2}$, one can define a *canonical* co-normal derivative operator, which is unique, linear in u, and coincides with the co-normal derivative in the trace sense if the latter exists. These notions were developed in [Mik05] and [Mik06] for a PDE with an infinitely smooth coefficient on a domain with an infinitely smooth boundary, and a right-hand side from $H^{s-2}(\Omega)$, $1 \leq s < \frac{3}{2}$, or extendable to $\widetilde{H}^t(\Omega)$, $t \geq -1/2$.

In Section 18.3 of this chapter, we generalize the above analysis to the co-normal derivative operators on Lipschitz domains for a PDE with a Hölder coefficient and right-hand side from $\widetilde{H}^{s-2}(\Omega)$, $\frac{1}{2} < s < \frac{3}{2}$. This needs a number of auxiliary facts provided in Section 18.2, some of which might be new for Lipschitz domains. Particularly, we prove Lemma 1 on unboundedness of the trace operator, Lemma 2 on boundedness of extension operators from boundary to the domain, Theorem 1 on characterization of the Sobolev space

$H_0^s(\Omega) = \widetilde{H}^s(\Omega)$ on the (larger than usual) interval $\frac{1}{2} < s < \frac{3}{2}$, Lemma 4 on characterization of the space $H^t_{\partial\Omega}$, $t > -\frac{3}{2}$, and Lemma 5 on existence of a bounded linear extension operator $\widetilde{E}^s : H^s(\Omega) \to \widetilde{H}^s(\Omega)$, $-\frac{3}{2} < s < \frac{1}{2}$, $s \neq -\frac{1}{2}$.

An analysis of boundary–domain integral and integro-differential equations extending the corresponding results of [Mik05] and [Mik06] to Lipschitz domains, Hölder coefficients, and a wider range of Sobolev spaces, and based on the results of this chapter, will be published elsewhere.

18.2 Sobolev Spaces, Trace Operators, and Extensions

Suppose that Ω is a bounded, open, n-dimensional region of $\mathbb{R}^n$, $n \geq 2$, whose boundary $\partial\Omega$ is a simply connected, closed, Lipschitz surface.

In what follows, $\mathcal{D}(\Omega) = C^\infty_{\rm comp}(\Omega)$ denotes the space of Schwartz test functions and $\mathcal{D}^*(\Omega)$ the space of Schwartz distributions; $H^s(\mathbb{R}^n) = H^s_2(\mathbb{R}^n)$, $H^s(\partial\Omega) = H^s_2(\partial\Omega)$ are the Bessel potential spaces, where $s \in \mathbb{R}$ is an arbitrary real number. We denote by $\widetilde{H}^s(\Omega)$ the subspace of $H^s(\mathbb{R}^n)$, $\widetilde{H}^s(\Omega) := \{g : g \in H^s(\mathbb{R}^n),\ \text{supp}\ g \subset \overline{\Omega}\}$, and by $H^s(\Omega)$ the space of restrictions to Ω of distributions from $H^s(\mathbb{R}^n)$, $H^s(\Omega) := \{g|_\Omega :\ g \in H^s(\mathbb{R}^n)\}$, where $g|_\Omega$ denotes restriction to Ω and $H^s_0(\Omega)$ is the closure of $\mathcal{D}(\Omega)$ in $H^s(\Omega)$. We recall that H^s coincide with the Sobolev–Slobodetski spaces W^s_2 for any nonnegative s. We denote by $H^s_{\partial\Omega}$ the subspace of $H^s(\mathbb{R}^n)$ (and $\widetilde{H}^s(\Omega)$) whose elements have compact support on $\partial\Omega$; i.e., $H^s_{\partial\Omega} := \{g :\ g \in H^s(\mathbb{R}^n),\ \text{supp}\ g \subset \partial\Omega\}$.

To introduce generalized co-normal derivatives in the next section, we will need several facts about traces and extensions in Sobolev spaces on a Lipschitz domain. First of all, it is well known [Cos88, Lemma 3.7] that the trace operators $\tau : H^s(\mathbb{R}^n) \to H^{s-\frac{1}{2}}(\partial\Omega)$ and $\tau^+ : H^s(\Omega) \to H^{s-\frac{1}{2}}(\partial\Omega)$ are continuous for $\frac{1}{2} < s < \frac{3}{2}$ on any Lipschitz domain Ω. We will also use the notation $u^+ := \tau^+ u$.

Since the space $H^s(\mathbb{R}^n)$ is dense in $H^{\frac{1}{2}}(\mathbb{R}^n)$ for $s > \frac{1}{2}$, the trace operator is well defined on the set $D = \bigcup_{\frac{1}{2}<s\leq 1} H^s(\mathbb{R}^n)$, which is dense in $H^{\frac{1}{2}}(\mathbb{R}^n)$.

Lemma 1. *For a Lipschitz domain Ω, the norm of the trace operator $\tau : H^s(\mathbb{R}^n) \to H^{s-\frac{1}{2}}(\partial\Omega)$ tends to infinity as $s \to \frac{1}{2}$, $s > \frac{1}{2}$, whereas the operator $\tau : H^{\frac{1}{2}}(\mathbb{R}^n) \to L_2(\partial\Omega)$ is unbounded.*

Proof. It suffices to show that there exists a function $v \in L_2(\partial\Omega)$ and a sequence $w'_k \in D$ such that $\|w'_k\|_{H^{\frac{1}{2}}(\mathbb{R}^n)} \leq C < \infty$, but

$$|\langle v, \tau w'_k\rangle| \to \infty, \quad k \to \infty. \tag{18.1}$$

Let us first find such a sequence for the half-space $\Omega = \mathbb{R}^n_+ = \{x \in \mathbb{R}^n : x_n > 0\}$, where $x = \{x', x_n\}$. For a nonzero function $v \in L_2(\partial\Omega)$ and $w \in D$, we have

$$\langle v, \tau w\rangle = \langle v, \delta_n w\rangle = \langle v \otimes \delta_n, w\rangle,$$

where $\delta_n = \delta(x_n)$ is the one-dimensional Dirac distribution. However, the Fourier transform satisfies $\mathcal{F}_{x\to\xi}\{v(x')\delta(x_n)\} = \hat{v}(\xi') := \mathcal{F}_{x'\to\xi'}\{v(x')\}$, and for $s > \frac{1}{2}$ we have (see the proof of Theorem 3.39 in [McL00])

$$\|v \otimes \delta(x_n)\|_{H^{-s}(\mathbb{R}^n)} = \int_{\mathbb{R}^n} (1+|\xi|^2)^{-s} |\hat{v}(\xi')|^2 d\xi = C_s \|v\|^2_{H^{\frac{1}{2}-s}(\mathbb{R}^{n-1})},$$

where $C_s = \int_{-\infty}^{\infty}(1+\eta^2)^{-s}d\eta$ and the substitution $\xi_n = (1+|\xi'|^2)^{\frac{1}{2}}\eta$ was used. Since $\|v\|^2_{H^{\frac{1}{2}-s}(\mathbb{R}^{n-1})} \to \|v\|^2_{L_2(\mathbb{R}^{n-1})} \neq 0$ and $C_s \to \infty$ as $s \to \frac{1}{2}$, we have

$$\sup_{\|w\|_{H^s(\Omega)}=1} |\langle v \otimes \delta_n, w\rangle| = \|v \otimes \delta(x_n)\|_{H^{-s}(\mathbb{R}^n)} \to \infty, \quad s \to \frac{1}{2}\,.$$

This implies that there exists a sequence $w_k \in D$ such that $\|w_k\|_{H^{-\frac{1}{2}}(\mathbb{R}^n)} \leq 1$, but $|\langle v \otimes \delta(x_n), w_k\rangle| \to \infty$ as $k \to \infty$, which proves the lemma for $\Omega = \mathbb{R}^n_+$ if we take $w'_k = w_k$.

Let now Ω be a half-space bounded by a Lipschitz hypograph, $\Omega = \{x \in \mathbb{R}^n : x_n > \zeta(x')\}$, where ζ is a Lipschitz function. Then the sequence $w'_k(x) = w_k(x', x_n - \zeta(x'))$ will have the necessary properties since $H^s(\mathbb{R}^n)$ is invariant under a Lipschitz change of coordinates if $0 \leq s \leq 1$.

If Ω is a general Lipschitz domain, then (generally after a rigid rotation of coordinates) it has a part of the boundary $\Gamma_1 \subset \partial\Omega$ that is a Lipschitz hypograph and can be extended to the boundary of a half-space. Choosing v so that $v = 0$ on $\partial\Omega\backslash\Gamma_1$, $\|v\|_{L_2(\Gamma_1)} \neq 0$, and then w'_k as in the previous paragraph, we obtain property (18.1), which completes the proof.

Lemma 2. *For a bounded Lipschitz domain Ω, there exists a linear bounded extension operator $e : H^{s-\frac{1}{2}}(\partial\Omega) \to H^s(\mathbb{R}^n)$, $\frac{1}{2} \leq s \leq \frac{3}{2}$, which is the right inverse to the trace operators $\tau^{\pm}$; i.e., $\tau^{\pm} e g = g$ for any $g \in H^{s-\frac{1}{2}}(\partial\Omega)$. Moreover, $\|e\|_{H^{s-\frac{1}{2}}(\partial\Omega)\to H^s(\mathbb{R}^n)} \leq C$, where C is independent of s.*

Proof. For Lipschitz domains and $\frac{1}{2} < s \leq 1$, the boundedness of the extension operator is well known (see, e.g., [McL00, Theorem 3.37]).

To prove it for the whole range $\frac{1}{2} \leq s \leq \frac{3}{2}$, let us consider the classical single-layer potential $V_\Delta \varphi$ with a density $\varphi = \mathcal{V}_\Delta^{-1} g \in H^{s-\frac{3}{2}}(\partial\Omega)$, solving the Laplace equation in Ω^+ with the Dirichlet boundary data g, where $\mathcal{V}_\Delta$ is the direct value of the operator V_Δ on the boundary. The operators $\mathcal{V}_\Delta^{-1} : H^{s-\frac{1}{2}}(\partial\Omega) \to H^{s-\frac{3}{2}}(\partial\Omega)$ and $V_\Delta : H^{s-\frac{3}{2}}(\partial\Omega) \to H^s_{loc}(\mathbb{R}^n)$ are continuous for $\frac{1}{2} \leq s \leq \frac{3}{2}$, as stated in [JK81b], [JK81a], [JK82], [Ver84], and[Cos88]. Thus, it suffices to take $e = \chi V_\Delta \mathcal{V}_\Delta^{-1}$, where $\chi \in \mathcal{D}(\mathbb{R}^n)$ is a cutoff function such that $\chi = 1$ in $\bar{\Omega}^+$. The estimate $\|e\|_{H^{s-\frac{1}{2}}(\partial\Omega)\to H^s(\mathbb{R}^n)} \leq C$, where C is independent of s, then follows by interpolation.

Note that for $s = \frac{1}{2}$, the trace operator τ^+ is understood in the nontangential sense, and that the continuity of the operators $\tau^{\pm}$ was not needed in the proof.

To characterize the space $H_0^s(\Omega) = \widetilde{H}^s(\Omega)$ for $\frac{1}{2} < s < \frac{3}{2}$, we will need the following statement.

Lemma 3. *If Ω is a Lipschitz domain and $u \in H^s(\Omega)$, $0 < s < \frac{1}{2}$, then*

$$\int_\Omega \operatorname{dist}(x, \partial\Omega)^{-2s} |u(x)|^2 dx \le C \|u\|^2_{H^s(\Omega)}. \tag{18.2}$$

Proof. Note first that the lemma claim holds true for $u \in \mathcal{D}(\overline{\Omega})$ (see [McL00, Lemma 3.32]). To prove it for $u \in H^s(\Omega)$, let first the domain Ω be such that

$$\operatorname{dist}(x, \partial\Omega) < C_0 < \infty \tag{18.3}$$

for all $x \in \Omega$, which holds true particularly for bounded domains. Let $\phi_k \in \mathcal{D}(\overline{\Omega})$ be a sequence converging to u in $H^s(\Omega)$. If we write $w(x) = \operatorname{dist}(x, \partial\Omega)^{-2s}$, then $w(x) > C_0^{-2s} > 0$. Since (18.2) holds for functions from $\mathcal{D}(\overline{\Omega})$, the sequence $\phi_k \in \mathcal{D}(\overline{\Omega})$ is fundamental in the weighted space $L^2(\Omega, w)$, which is complete, implying that $\phi_k \in \mathcal{D}(\overline{\Omega})$ converges in this space to a function $u' \in L^2(\Omega, w)$. Since both $L^2(\Omega, w)$ and $H^s(\Omega)$ are continuously imbedded in the nonweighted space $L^2(\Omega)$, the sequence ϕ_k converges in $L^2(\Omega)$, implying that the limiting functions u and u' belong to this space and thus coincide.

If condition (18.3) is not satisfied, let $\chi(x) \in \mathcal{D}(\mathbb{R}^n)$ be a cutoff function such that $0 \le \chi(x) \le 1$ for all x, $\chi(x) = 1$ near $\partial\Omega$, and $w(x) < 1$ for $x \in \operatorname{supp}(1 - \chi)$. Then (18.3) is satisfied in $\Omega \bigcap \operatorname{supp} \chi(x)$ and

$$\begin{aligned}\int_\Omega w(x)|u(x)|^2 dx &= \int_\Omega (1 - \chi(x)) w(x) |u(x)|^2 dx + \int_\Omega \chi(x) w(x) |u(x)|^2 dx \\ &\le \|u\|^2_{L_2(\Omega)} + \int_\Omega w(x) |\sqrt{\chi(x)} u(x)|^2 dx \\ &\le \|u\|^2_{H^s(\Omega)} + C \|\sqrt{\chi(x)} u\|^2_{H^s(\Omega)} \le C_1 \|u\|^2_{H^s(\Omega)},\end{aligned}$$

due to the previous paragraph.

Lemma 3 allows us to extend the following statement, known for $\frac{1}{2} < s \le 1$ [McL00, Theorem 3.40(i)], to a wider range of s.

Theorem 1. *If Ω is a Lipschitz domain and $\frac{1}{2} < s < \frac{3}{2}$, then $H_0^s(\Omega) = \widetilde{H}^s(\Omega) = \{u \in H^s(\Omega) : \tau^+ u = 0\}$.*

Proof. The first equality, $H_0^s(\Omega) = \widetilde{H}^s(\Omega)$, is well known for $\frac{1}{2} < s < \frac{3}{2}$ (see, e.g., [McL00, Theorem 3.33]). The theorem claim for $\frac{1}{2} < s \le 1$ is stated in [McL00, Theorem 3.40(i)]. If $u \in \widetilde{H}^s(\Omega)$, then evidently $\tau^+ u = 0$, since

$\mathcal{D}$ is dense in $\widetilde{H}^s(\Omega)$ and the trace operator τ^+ is bounded in $H^s(\mathbb{R}^n)$ for $\frac{1}{2} < s < \frac{3}{2}$. To prove the theorem for $1 < s < \frac{3}{2}$, it remains to prove that the extension of any $u \in \widetilde{H}^s(\Omega)$ by zero outside Ω, $\tilde{u}$, belongs to $H^s(\mathbb{R}^n)$. To do this, we remark first of all that $\tilde{u} \in H^1(\mathbb{R}^n)$, due to [McL00, Theorem 3.40(i)], and then make estimates similar to those in the proof there; that is,

$$\begin{aligned}\|u\|^2_{\widetilde{H}^s(\Omega)} = \|\tilde{u}\|^2_{H^s(\mathbb{R}^n)} \sim \|\tilde{u}\|^2_{W_2^1(\mathbb{R}^n)} + \int_{\mathbb{R}^n}\int_{\mathbb{R}^n} \frac{|\nabla\tilde{u}(x) - \nabla\tilde{u}(y)|^2}{|x-y|^{2(s-1)+n}}\, dx\, dy \\ = \|u\|^2_{W_2^1(\Omega)} + \int_\Omega\int_\Omega \frac{|\nabla u(x) - \nabla u(y)|^2}{|x-y|^{2(s-1)+n}}\, dx\, dy \\ + \int_{\mathbb{R}^n\setminus\Omega}\int_\Omega \frac{|\nabla u(x)|^2}{|x-y|^{2(s-1)+n}}\, dx\, dy + \int_\Omega\int_{\mathbb{R}^n\setminus\Omega} \frac{|\nabla u(y)|^2}{|x-y|^{2(s-1)+n}}\, dx\, dy \\ = \|u\|^2_{W_2^s(\Omega)} + 2\int_\Omega |w_{s-1}(x)\nabla u(x)|^2\, dx,\end{aligned}$$

where

$$w_{s-1}(x) := \int_{\mathbb{R}^n\setminus\Omega} \frac{dy}{|x-y|^{2(s-1)+n}}, \quad x \in \Omega,$$

and $W_2^s(\Omega)$ is the Sobolev–Slobodetski space. Introducing polar coordinates with x as an origin, we obtain, $w_{s-1}(x) \le C\ \mathrm{dist}(x, \partial\Omega)^{-2(s-1)}$ for $x \in \Omega$. Then, taking into account that $\nabla u \in H^{s-1}(\Omega)$ and $\|\nabla u\|_{H^{s-1}(\Omega)} \le \|u\|_{H^s(\Omega)}$, we have by Lemma 3,

$$\|u\|^2_{\widetilde{H}^s(\Omega)} \le \|u\|^2_{W_2^s(\Omega)} + 2C\|u\|^2_{H^s(\Omega)} \le C_s\|u\|^2_{H^s(\Omega)}\ .$$

Lemma 4. *Let Ω be a Lipschitz domain in $\mathbb{R}^n$.*

(i) If $t \ge -\frac{1}{2}$, then $H^t_{\partial\Omega} = \{0\}$.

(ii) If $-\frac{3}{2} < t < -\frac{1}{2}$, then $H^t_{\partial\Omega}$ is the set of distributions g on $\mathbb{R}^n$ of the form

$$\langle g, w\rangle_{\mathbb{R}^n} = \langle v, \tau w\rangle_{\partial\Omega} \quad \forall\ w \in H^{-t}(\mathbb{R}^n), \tag{18.4}$$

where τ is the trace operator, $v \in H^{t+\frac{1}{2}}(\partial\Omega)$, and $\|v\|_{H^{t+\frac{1}{2}}(\partial\Omega)} \le C\|g\|_{H^t(\mathbb{R}^n)}$ with C independent of t.

Proof. We will follow an idea in the proof of Lemma 3.39 in [McL00], extending it from a half-space to a Lipschitz domain Ω.

Let $\Omega^+ = \Omega$ and $\Omega^- = \mathbb{R}^n\setminus\bar{\Omega}$. For any $\phi \in \mathcal{D}(\mathbb{R}^n)$, let us define

$$\phi_\pm(x) = \begin{cases}\phi(x) & \text{if } x \in \Omega^\pm,\\ 0 & \text{otherwise.}\end{cases}$$

Let $t > -\frac{1}{2}$. Then $\phi^\pm \in \widetilde{H}^{-t}(\Omega^\pm)$ (see, e.g., [McL00, Theorems 3.33, 3.40] for $-\frac{1}{2} < t \le 0$; for greater t, it then follows by embedding), $\|\phi - \phi^+ - \phi^-\|_{H^{-t}(\mathbb{R}^n)} = 0$, and there exist sequences $\phi^\pm_k \in \mathcal{D}(\Omega^\pm)$ converging to $\phi^\pm$

in $\widetilde{H}^{-t}(\Omega^{\pm})$ as $k \to \infty$. Hence, $\langle g, \phi \rangle = \lim_{k\to\infty} \langle g, \phi_k^+ + \phi_k^- \rangle = 0$ for any $g \in H^t_{\partial\Omega}$, $t > -\frac{1}{2}$, proving (i) for such t.

Let us prove (ii). For $g \in H^t_{\partial\Omega}$, $-\frac{3}{2} < t < -\frac{1}{2}$, let us define $v \in H^{t+\frac{1}{2}}(\partial\Omega)$ by

$$\langle v, \phi \rangle_{\partial\Omega} := \langle g, e\phi \rangle_{\mathbb{R}^n} \quad \forall\ \phi \in H^{-t-\frac{1}{2}}(\partial\Omega),$$

where $e : H^{-t-\frac{1}{2}}(\partial\Omega) \to H^{-t}(\Omega)$ is a bounded extension operator whose existence is proved in Lemma 2. Observe that

$$|\langle v, \phi \rangle| \le \|g\|_{H^t(\mathbb{R}^n)} \|\phi\|_{H^{-t-\frac{1}{2}}(\partial\Omega)} \|e\|_{H^{-t-\frac{1}{2}}(\partial\Omega)\to H^{-t}(\mathbb{R}^n)},$$

so $\|v\|_{H^{t+\frac{1}{2}}(\partial\Omega)} \le \|e\|_{H^{-t-\frac{1}{2}}(\partial\Omega)\to H^{-t}(\mathbb{R}^n)} \|g\|_{H^t(\mathbb{R}^n)} \le C\|g\|_{H^t(\mathbb{R}^n)}$, where, by Lemma 2, C is independent of t. We also have that

$$\langle g, w \rangle_{\mathbb{R}^n} - \langle v, \tau w \rangle_{\partial\Omega} = \langle g, \rho \rangle_{\mathbb{R}^n} \quad \forall\ w \in H^{-t}(\mathbb{R}^n),$$

where

$$\rho = w - e\tau w \in H^{-t}(\mathbb{R}^n).$$

Then we have $\tau\rho = 0$, which, by Theorem 1, means that $\rho \in \widetilde{H}^{-t}(\Omega^{\pm})$; thus, there exist sequences $\phi_k^{\pm} \in \mathcal{D}(\Omega^{\pm})$ converging to ρ in $\widetilde{H}^{-t}(\Omega^{\pm})$, implying that $\langle g, \rho \rangle_{\mathbb{R}^n} = 0$, since $g \in H^t_{\partial\Omega}$, and, hence, confirming ansatz (18.4).

It remains for us to deal with the case $t = -\frac{1}{2}$ in (i). Let $g \in H^{-\frac{1}{2}}_{\partial\Omega}$. Since $H^{-\frac{1}{2}}_{\partial\Omega} \subset H^t_{\partial\Omega}$ for $t < -\frac{1}{2}$, ansatz (18.4) is valid for g. However, owing to Lemma 1, the norm of the trace operator $\tau : H^{-t}(\mathbb{R}^n) \to H^{-t-\frac{1}{2}}(\partial\Omega)$ tends to infinity as $t \to -\frac{1}{2}$, which means that v should be zero.

Lemma 5. *Let Ω be a Lipschitz domain, and let $-\frac{3}{2} < s < \frac{1}{2}$, $s \ne -\frac{1}{2}$. There exists a bounded linear extension operator $\widetilde{E}^s : H^s(\Omega) \to \widetilde{H}^s(\Omega)$.*

Proof. If $0 \le s < \frac{1}{2}$, then $\widetilde{H}^s(\Omega) = H^s(\Omega)$ (see, e.g., [McL00, Theorems 3.33 and 3.40]), which implies that $\widetilde{E}^s$ can be taken as the identity operator.

Let $-\frac{1}{2} < s < 0$. Since $\widetilde{H}^{-s}(\Omega) = H^{-s}(\Omega)$ as in the above paragraph, we have $H^s(\Omega) = [\widetilde{H}^{-s}(\Omega)]^* = [H^{-s}(\Omega)]^* = \widetilde{H}^s(\Omega)$. The asterisk denotes the dual space. This implies that $\widetilde{E}^s$ can be taken as the identity operator.

Let now $-\frac{3}{2} < s < -\frac{1}{2}$. For s in this range, by [Cos88, Lemma 3.6] (see also [McL00, Theorem 3.38]), the trace operator $\tau^+ : H^{-s}(\Omega) \to H^{-s-\frac{1}{2}}(\partial\Omega)$ is bounded and there exists a bounded extension operator $e : H^{-s-\frac{1}{2}}(\partial\Omega) \to H^{-s}(\Omega)$ (see Lemma 2). Then, by Theorem 1, $(I - e\tau^+)$ is a bounded projector from $H^{-s}(\Omega)$ to $H_0^{-s}(\Omega) = \widetilde{H}^{-s}(\Omega)$. Thus, any functional $v \in H^s(\Omega)$ can be mapped continuously to a functional $\tilde{v} \in \widetilde{H}^s(\Omega)$ such that $\tilde{v}u = v(I - e\tau^+)u$ for any $u \in H^{-s}(\Omega)$. Since $\tilde{v}u = vu$ for any $u \in \widetilde{H}^{-s}(\Omega)$, we conclude that $\widetilde{E}^s = (I - e\tau^+)^* : H^s(\Omega) \to \widetilde{H}^s(\Omega)$ is a bounded extension operator.

Note that Lemma 4 implies uniqueness of the extension operator $\widetilde{E}^s : H^s(\Omega) \to \widetilde{H}^s(\Omega)$ for $-\frac{1}{2} < s < \frac{1}{2}$, which coincides in this case with the identity operator and will be called the *canonical extension operator*. For $-\frac{3}{2} < s < -\frac{1}{2}$, on the other hand, the extension operator $e : H^{-s-\frac{1}{2}}(\partial\Omega) \to H^{-s}(\Omega)$ in the proof of Lemma 5 is not unique, implying nonuniqueness of $\widetilde{E}^s : H^s(\Omega) \to \widetilde{H}^s(\Omega)$.

18.3 Partial Differential Operator Extensions and Co-Normal Derivatives

For $u \in H^s(\Omega)$, $s > \frac{3}{2}$, and $a \in C^{0,\alpha}(\overline{\Omega})$, $\alpha > \frac{1}{2}$, we can denote by T^+ the corresponding co-normal derivative operator on $\partial\Omega$ in the sense of traces, that is,

$$T^+(x, n^+(x), \partial_x)\, u(x) := \sum_{i=1}^{n} a^+(x)\, n_i^+(x) \left(\frac{\partial u(x)}{\partial x_i} \right)^+ ,$$

where $n^+(x)$ is the outward (to Ω) unit normal vector at the point $x \in \partial\Omega$, $\partial_x = (\partial_1, \partial_2, ..., \partial_n)$, and $\partial_j := \partial/\partial x_j$ $(j = 1, 2, ..., n)$.

For simplicity, from now on we will consider only bounded Lipschitz domains. We will need the following particular case of a statement from [Gri85, Theorem 1.4.1.1].

Theorem 2. *Let Ω be a bounded Lipschitz domain and $v \in C^{k,\alpha}(\overline{\Omega})$ with $k+\alpha \geq |s|$ when s is an integer, and $k+\alpha > |s|$ when s is not an integer. Then $vu \in H^s(\Omega)$ for every $u \in H^s(\Omega)$, and there exists a constant $K = K(v, s)$ such that*

$$\|vu\|_{H^s(\Omega)} \leq K \|u\|_{H^s(\Omega)}.$$

For $u \in H^s(\Omega)$ and $v \in H^{2-s}(\Omega)$, $\frac{1}{2} < s < \frac{3}{2}$, $a \in C^{0,\alpha}(\overline{\Omega})$, $\alpha > |s-1|$ if $s \neq 1$ and $\alpha = 0$ if $s = 1$, we define the bilinear form

$$\mathcal{E}(u, v) := \sum_{i=1}^{3} \langle a \partial_i u, \partial_i v \rangle_\Omega ,$$

where $\langle \cdot\,, \cdot \rangle_\Omega$ denotes the duality brackets between the spaces $H^{s-1}(\Omega)$ and $H^{1-s}(\Omega)$.

Let $u \in H^s(\Omega)$, $\frac{1}{2} < s < \frac{3}{2}$. Then Lu is understood as the distribution

$$\langle Lu, v \rangle_\Omega := -\mathcal{E}(u, v) \quad \forall v \in \mathcal{D}(\Omega). \tag{18.5}$$

Since the set $\mathcal{D}(\Omega)$ is dense in $\widetilde{H}^{2-s}(\Omega)$, the above formula defines a bounded operator $L : H^s(\Omega) \to H^{s-2}(\Omega) = [\widetilde{H}^{2-s}(\Omega)]^*$, $\frac{1}{2} < s < \frac{3}{2}$,

$$\langle Lu, v \rangle_\Omega := -\mathcal{E}(u, v) \quad \forall v \in \widetilde{H}^{2-s}(\Omega).$$

Let us consider also the operator $\hat{L} : H^s(\Omega) \to \widetilde{H}^{s-2}(\Omega) = [H^{2-s}(\Omega)]^*$, $\frac{1}{2} < s < \frac{3}{2}$, defined by

$$\langle \hat{L}u, v\rangle_\Omega := -\mathcal{E}(u, v) \quad \forall v \in H^{2-s}(\Omega),$$

which is evidently bounded. For any $u \in H^s(\Omega)$, the functional $\hat{L}u$ belongs to $\widetilde{H}^{s-2}(\Omega)$ and is an extension of the functional $Lu \in H^{s-2}(\Omega)$ from the domain of definition $\widetilde{H}^{2-s}(\Omega)$ to the domain of definition $H^{2-s}(\Omega)$.

The extension is not unique, and any functional of the form

$$\hat{L}u + g, \quad g \in H^{2-s}_{\partial\Omega} \tag{18.6}$$

provides another extension. On the other hand, any extension of the domain of definition of the functional Lu from $\widetilde{H}^{2-s}(\Omega)$ to $H^{2-s}(\Omega)$ has evidently the form (18.6). The existence of such extensions is provided by Lemma 5.

Now we can extend the definition from [McL00, Lemma 4.3] of the generalized co-normal derivative to a range of Sobolev spaces.

Lemma 6. *Let Ω be a bounded Lipschitz domain, $\frac{1}{2} < s < \frac{3}{2}$, $a \in C^{0,\alpha}(\overline{\Omega})$, $\alpha > |s-1|$ if $s \neq 1$ and $\alpha = 0$ if $s = 1$, $u \in H^s(\Omega)$, and $Lu = \tilde{f}|_\Omega$ in Ω for some $\tilde{f} \in \widetilde{H}^{s-2}(\Omega)$. Let us define* the generalized co-normal derivative $\widetilde{T}^+(\tilde{f}, u) \in H^{s-\frac{3}{2}}(\partial\Omega)$ *as*

$$\begin{aligned}\left\langle \widetilde{T}^+(\tilde{f}, u)\,,\, w \right\rangle_{\partial\Omega} &:= \langle \tilde{f}, e^+ w\rangle_\Omega + \mathcal{E}(u, e^+ w) \\ &= \langle \tilde{f} - \hat{L}u, e^+ w\rangle_\Omega \qquad \forall\ w \in H^{\frac{3}{2}-s}(\partial\Omega),\end{aligned} \tag{18.7}$$

where $e^+ : H^{\frac{3}{2}-s}(\partial\Omega) \to H^{2-s}(\Omega)$ is a bounded extension operator. Then $\widetilde{T}^+(\tilde{f}, u)$ is independent of e^+,

$$\|\widetilde{T}^+(\tilde{f}, u)\|_{H^{s-\frac{3}{2}}(\partial\Omega)} \le C_1 \|u\|_{H^s(\Omega)} + C_2 \|\tilde{f}\|_{\widetilde{H}^{s-2}(\Omega)},$$

and the first Green identity holds in the form

$$\left\langle \widetilde{T}^+(\tilde{f}, u)\,,\, v^+ \right\rangle_{\partial\Omega} = \langle \tilde{f}, v\rangle_\Omega + \mathcal{E}(u, v) = \langle \tilde{f} - \hat{L}u, v\rangle_\Omega \quad \forall\ v \in H^{2-s}(\Omega). \tag{18.8}$$

The proof of this lemma can be found in [McL00, Lemma 4.3] for $s = 1$. Taking into account that Lemma 2 provides existence of a bounded extension operator $e^+ : H^{\frac{3}{2}-s}(\partial\Omega) \to H^{2-s}(\Omega)$ in the whole range $\frac{1}{2} < s < \frac{3}{2}$, the proof from [McL00, Lemma 4.3] works verbatim (with the appropriate change of the Sobolev space indices and invoking Theorem 1 and Lemma 4) for all s in this range.

Note that because of the involvement of $\tilde{f}$, the generalized co-normal derivative $\widetilde{T}^+(\tilde{f}, u)$ is generally *nonlinear* in u. It becomes linear if a linear

relation is imposed between u and $\tilde{f}$ (including behavior of the latter on the boundary $\partial\Omega$), thus fixing an extension of $\tilde{f}|_{\Omega}$ into $\widetilde{H}^{s-2}(\Omega)$. For example, $\tilde{f}|_{\Omega}$ can be extended as $\hat{f} = \hat{L}u \neq \tilde{f}$. Then, obviously, $\widetilde{T}^{+}(\hat{f}, u) = \widetilde{T}^{+}(\hat{L}u, u) = 0$.

In fact, for a given function $u \in H^{s}(\Omega)$, $\frac{1}{2} < s < \frac{3}{2}$, any distribution $t^{+} \in H^{s-\frac{3}{2}}(\partial\Omega)$ may be nominated as a co-normal derivative of u through an appropriate extension $\tilde{f}$ of the distribution $Lu \in H^{s-2}(\Omega)$ into $\widetilde{H}^{s-2}(\Omega)$. This extension is again given by the second Green formula (18.8) rewritten as

$$\langle \tilde{f}, v\rangle_{\Omega} := \left\langle t^{+}, \tau^{+}v\right\rangle_{\partial\Omega} - \mathcal{E}(u, v) = \langle \tau^{+*}t^{+} + \hat{L}u, v\rangle_{\Omega} \quad \forall\, v \in H^{2-s}(\Omega). \tag{18.9}$$

Here the operator $\tau^{+*} : H^{s-\frac{3}{2}}(\partial\Omega) \to \widetilde{H}^{s-2}(\Omega)$ is dual to the trace operator, $\langle \tau^{+*}t^{+}, v\rangle_{\Omega} := \langle t^{+}, \tau^{+}v\rangle_{\partial\Omega}$ for all $t^{+} \in H^{s-\frac{3}{2}}(\partial\Omega)$ and $v \in H^{2-s}(\Omega)$. Evidently, the distribution $\tilde{f}$ defined by (18.9) belongs to $\widetilde{H}^{s-2}(\Omega)$ and is an extension of the distribution Lu into $\widetilde{H}^{s-2}(\Omega)$ since $\tau^{+}v = 0$ for $v \in \widetilde{H}^{2-s}(\Omega)$.

To analyze another case, different from $\widetilde{T}^{+}(\hat{L}u, u)$, where the co-normal derivative operator becomes linear, let us consider a subspace $H^{s,t}(\Omega; L_{*})$ of $H^{s}(\Omega)$.

Definition 1. *Let $s \in \mathbb{R}$, and let $L_{*} : H^{s}(\Omega) \to \mathcal{D}^{*}(\Omega)$ be a linear operator. For $t \geq -\frac{1}{2}$, we introduce the space $H^{s,t}(\Omega; L_{*}) := \{g : \ g \in H^{s}(\Omega),\ L_{*}g|_{\Omega} = \tilde{f}_{g}|_{\Omega},\ \tilde{f}_{g} \in \widetilde{H}^{t}(\Omega)\}$ endowed with the norm $\|g\|_{H^{s,t}(\Omega;L_{*})} := \|g\|_{H^{s}(\Omega)} + \|\tilde{f}_{g}\|_{\widetilde{H}^{t}(\Omega)}$.*

The distribution $\tilde{f}_{g} \in \widetilde{H}^{t}(\Omega)$, $t \geq -\frac{1}{2}$, in the above definition is an extension of the distribution $L_{*}g|_{\Omega} \in H^{t}(\Omega)$, and the extension is unique (if it does exist), due to Lemma 4. The uniqueness implies that the norm $\|g\|_{H^{s,t}(\Omega;L_{*})}$ is well defined. Note that another subspace of this kind, where $L_{*}g|_{\Omega}$ belongs to $L_{p}(\Omega)$ instead of $H^{t}(\Omega)$, was presented in [Gri85, p. 59].

If $s, p \in \mathbb{R}$, $L_{*} : H^{s}(\Omega) \to H^{p}(\Omega)$ is a bounded linear operator, $t \leq p$, and $-\frac{1}{2} < t < \frac{1}{2}$, then, evidently, $H^{s,t}(\Omega; L_{*}) = H^{s}(\Omega)$ since $H^{p}(\Omega) \subset H^{t}(\Omega)$ and $\widetilde{H}^{t}(\Omega) = H^{t}(\Omega)$.

Lemma 7. *Let $s, p \in \mathbb{R}$. If the linear operator $L_{*} : H^{s}(\Omega) \to H^{p}(\Omega)$ is continuous, then the space $H^{s,t}(\Omega; L_{*})$ is complete for any $t \geq -\frac{1}{2}$.*

Proof. Let g_{k} be a Cauchy sequence in $H^{s,t}(\Omega; L_{*})$. Then there exists a Cauchy sequence $\tilde{f}_{g_{k}}$ in $\widetilde{H}^{t}(\Omega)$ such that $\tilde{f}_{g_{k}}|_{\Omega} = L_{*}g_{k}|_{\Omega}$. Since $H^{s}(\Omega)$ and $\widetilde{H}^{t}(\Omega)$ are complete, there exist elements $g_{0} \in H^{s}(\Omega)$ and $\tilde{f}_{0} \in \widetilde{H}^{t}(\Omega)$ such that $\|g_{k} - g_{0}\|_{H^{s}(\Omega)} \to 0$, $\|\tilde{f}_{g_{k}} - \tilde{f}_{0}\|_{\widetilde{H}^{t}(\Omega)} \to 0$ as $k \to \infty$. On the other hand, $\|L_{*}g_{k} - L_{*}g_{0}\|_{H^{p}(\Omega)} \to 0$, since L_{*} is continuous. Taking into account that $L_{*}g_{k}|_{\Omega} = \tilde{f}_{g_{k}}|_{\Omega}$, we obtain

$$\|\tilde{f}_{0} - L_{*}g_{0}\|_{H^{p}(\Omega)} \leq \|\tilde{f}_{0} - \tilde{f}_{g_{k}}\|_{H^{t}(\Omega)} + \|\tilde{f}_{g_{k}} - L_{*}g_{0}\|_{H^{p}(\Omega)} \to 0 \ \ k \to \infty$$

if $p \leq t$, and

$$\|\tilde{f}_0 - L_* g_0\|_{H^t(\Omega)} \le \|\tilde{f}_0 - \tilde{f}_{g_k}\|_{H^t(\Omega)} + \|\tilde{f}_{g_k} - L_* g_0\|_{H^p(\Omega)} \to 0 \quad k \to \infty$$

if $t \le p$. That is, $L_* g_0|_\Omega = \tilde{f}_0|_\Omega \in H^t(\Omega)$ in both cases, which implies that $g_0 \in H^{s,t}(\Omega; L_*)$.

We return to the operator L from (18.5) and define the *canonical (or internal)* co-normal derivative operator (cf. [Cos88, Lemma 3.2], where a co-normal derivative operator acting on functions from $H^{1,0}(\Omega; L)$ was defined).

Definition 2. *Let $u \in H^{s,t}(\Omega; L)$, $s \in \mathbb{R}$, $t \ge -\frac{1}{2}$. Then the distribution $Lu \in H^t(\Omega)$ can be extended uniquely to a distribution in $\widetilde{H}^t(\Omega)$, which we will call* the canonical extension *and denote by $L^0 u$ or still use the notation Lu if this will not lead to confusion.*

Definition 3. *For $u \in H^{s,-\frac{1}{2}}(\Omega; L)$, $\frac{1}{2} < s < \frac{3}{2}$; $a \in C^{0,\alpha}(\overline{\Omega})$, $\alpha > |s-1|$ if $s \ne 1$ and $\alpha = 0$ if $s = 1$, we define the* canonical (or internal) co-normal derivative $T^+ u \in H^{s-\frac{3}{2}}(\partial\Omega)$ *by*

$$\begin{aligned}\left\langle T^+ u\,,\, w\right\rangle_{\partial\Omega} &:= \langle L^0 u, e^+ w\rangle_\Omega + \mathcal{E}(u, e^+ w)\\ &= \langle L^0 u - \hat{L} u, e^+ w\rangle_\Omega \quad \forall\, w \in H^{\frac{3}{2}-s}(\partial\Omega), \quad (18.10)\end{aligned}$$

where $e^+ : H^{s-\frac{1}{2}}(\partial\Omega) \to H^s(\Omega)$ is a bounded extension operator. The canonical co-normal derivative $T^+ u$ is independent of e^+, the operator $T^+ : H^{s,-\frac{1}{2}}(\Omega; L) \to H^{s-\frac{3}{2}}(\partial\Omega)$ is continuous, and the first Green identity holds in the form

$$\begin{aligned}\left\langle T^+ u\,,\, v^+\right\rangle_{\partial\Omega} = \left\langle \widetilde{T}^+(L^0 u, u)\,,\, v^+\right\rangle_{\partial\Omega} &= \langle L^0 u, v\rangle_\Omega \;+\; \mathcal{E}(u, v)\\ &= \langle L^0 u - \hat{L} u, v\rangle_\Omega \quad \forall\, v \in H^{2-s}(\Omega). \quad (18.11)\end{aligned}$$

The independence of e^+ and the continuity of the operator T^+, as well as identity (18.11), are implied by the definition of the generalized co-normal derivative in Lemma 6 and Definition 1. Unlike the generalized co-normal derivative, the canonical co-normal derivative is defined uniquely by the function u and operator L only, uniquely fixing an extension of the latter on the boundary.

Definitions (18.7) and (18.10) imply that the generalized co-normal derivative of $u \in H^{s,-\frac{1}{2}}(\Omega; L)$, $\frac{1}{2} < s < \frac{3}{2}$, for any other extension $\tilde{f} \in \widetilde{H}^{s-2}(\Omega)$ of the distribution $Lu|_\Omega \in H^t(\Omega)$ can be expressed as

$$\left\langle \widetilde{T}^+(\tilde{f}, u)\,,\, w\right\rangle_{\partial\Omega} = \left\langle T^+ u\,,\, w\right\rangle_{\partial\Omega} + \langle \tilde{f} - L^0 u, e^+ w\rangle_\Omega \quad \forall\, w \in H^{\frac{3}{2}-s}(\partial\Omega).$$

Note that the distributions $\tilde{f} - \hat{L}u$, $L^0 u - \hat{L}u$ and $\tilde{f} - L^0$ belong to $H^{2-s}_{\partial\Omega}$, since $L^0 u, \hat{L}u, \tilde{f} \in \widetilde{H}^{2-s}(\Omega)$, whereas $L^0 u|_\Omega = \hat{L}u|_\Omega = \tilde{f}|_\Omega = Lu|_\Omega \in H^{s-2}(\Omega)$.

The following lemma and corollary give conditions when the canonical co-normal derivative coincides with the classical co-normal derivative $T^+ u = a^+ (\frac{\partial u}{\partial n})^+$ if the latter exists in the trace sense.

Lemma 8. *Let* $a \in C^{0,\alpha}(\overline{\Omega})$, $\alpha > \frac{1}{2}$, $u \in H^{s,-\frac{1}{2}}(\Omega; L)$, $\frac{1}{2} < s < \frac{3}{2}$, *and* $u_k \in H^2(\Omega)$ *be a sequence such that* $\|u_k - u\|_{H^{s,-\frac{1}{2}}(\Omega;L)} \to 0$. *Then* $\|\sum_{j=1}^n (a\partial_j u_k)^+ n_j - T^+ u\|_{H^{s-\frac{3}{2}}(\partial\Omega)} \to 0$ *as* $k \to \infty$.

Proof. Using the canonical first Green identity (18.11) for u and the classical first Green identity (which follows, e.g., from Lemma 4.1 in [McL00]) for u_k, we deduce that for any $w \in H^{\frac{3}{2}-s}(\partial\Omega)$,

$$\begin{aligned}
\left\langle T^+ u, w \right\rangle_{\partial\Omega} &= \mathcal{E}(u, e^+ w) + \langle L^0 u, e^+ w\rangle_\Omega \\
&= \mathcal{E}(u - u_k, e^+ w) + \mathcal{E}(u_k, e^+ w) + \langle L^0 u, e^+ w\rangle_\Omega \\
= \mathcal{E}(u - u_k, e^+ w) &+ \int_{\partial\Omega} \sum_{j=1}^n (a\partial_j u_k)^+ n_j w d\Gamma - \langle L^0 u_k, e^+ w\rangle_\Omega + \langle L^0 u, e^+ w\rangle_\Omega \\
= \mathcal{E}(u - u_k, e^+ w) &+ \left\langle \sum_{j=1}^n (a\partial_j u_k)^+ n_j, w \right\rangle_{\partial\Omega} + \langle L^0(u - u_k), e^+ w\rangle_\Omega \\
&\to \left\langle \sum_{j=1}^n (a\partial_j u_k)^+ n_j, w \right\rangle_{\partial\Omega},
\end{aligned}$$

as $k \to \infty$. We took into account that $a\partial_j u_k \in H^p(\Omega)$, $\frac{1}{2} < p < \alpha$, $p \le \frac{3}{2}$, by Lemma 2. Since $T^+ u$ is uniquely determined by u, this implies the existence of the limit on the right-hand side and its independence of the sequence u_k.

The sequence u_k mentioned in Lemma 8 always exists, due to the following statement.

Lemma 9. $\mathcal{D}(\overline{\Omega})$ *is dense in* $H^{s,t}(\Omega; L)$, $s \in \mathbb{R}$, $-\frac{1}{2} < t < \frac{1}{2}$.

Proof. We modify appropriately the proof from [Gri85, L. 1.5.3.9] given for another space of this kind.

For every continuous linear functional l on $H^{s,t}(\Omega; L)$, there exist $\tilde{f} \in \widetilde{H}^{-s}(\Omega)$ and $g \in H^{-t}(\Omega)$ such that

$$l(u) = \langle \tilde{f}, u\rangle_\Omega + \langle g, Lu\rangle_\Omega.$$

To prove the lemma claim, it suffices to show that any l vanishing on $\mathcal{D}(\overline{\Omega})$ will also vanish on any $u \in H^{s,t}(\Omega; L)$. Indeed, if $l(\phi) = 0$ for any $\phi \in \mathcal{D}(\overline{\Omega})$, then

$$\langle \tilde{f}, \phi\rangle_\Omega + \langle g, L\phi\rangle_\Omega = 0. \tag{18.12}$$

Extending g outside $\overline{\Omega}$ by zero to $\tilde{g} \in \widetilde{H}^{-t}(\Omega)$ (see the proof of Lemma 5), equation (18.12) can be rewritten as

$$\langle \tilde{f}, \phi\rangle_{\mathbb{R}^n} + \langle \tilde{g}, L\phi\rangle_{\mathbb{R}^n} = 0.$$

This means that $L\tilde{g} = -\tilde{f}$ in $\mathbb{R}^n$ in the sense of distributions. Then the ellipticity of L implies that $\tilde{g} \in H^{2-s}(\mathbb{R}^n)$, and, consequently, $\tilde{g} \in \widetilde{H}^{2-s}(\Omega)$.

Let now $g_k \in \mathcal{D}(\Omega)$ be a sequence converging to $\tilde{g}$ in $\widetilde{H}^q(\Omega)$, $q = \max\{-t, s-2\}$, and thus in $\widetilde{H}^{-t}(\Omega)$ and $\widetilde{H}^{s-2}(\Omega)$, as $k \to \infty$. Then for any $u \in H^{s,t}(\Omega; L)$,

$$l(u) = \lim_{k\to\infty} \{\langle -Lg_k, u\rangle_\Omega + \langle g_k, Lu\rangle_\Omega\} = 0.$$

Thus, l is identically zero.

Corollary 1. *If $a \in C^{0,\alpha}(\overline{\Omega})$, $\alpha > \frac{1}{2}$, and $u \in H^q(\Omega)$, $q > \frac{3}{2}$, then $T^+u = (a\partial_j u)^+ n_j$.*

Proof. If $u \in H^q(\Omega)$, $q > \frac{3}{2}$, then $u \in H^{q,t}(\Omega) \subset H^{s,t}(\Omega; L) \subset H^{s,-\frac{1}{2}}(\Omega; L)$ for any $t \in (-\frac{1}{2}, \min\{\alpha, q-1\} - 1)$ and any $s \in (\frac{1}{2}, \frac{3}{2})$. Hence, a sequence $u_k \in \mathcal{D}(\overline{\Omega})$ such that $\|u_k - u\|_{H^q(\Omega)} \to 0$ as $k \to \infty$ satisfies the hypothesis of Lemma 8 for any $s \in (\frac{1}{2}, \frac{3}{2})$. On the other hand, by Theorem 2,

$$\|\sum_{j=1}^n [a\partial_j(u_k - u)]^+ n_j\|_{H^{s-\frac{3}{2}}(\partial\Omega)} \le \|\sum_{j=1}^n [a\partial_j(u_k - u)]^+ n_j\|_{L_2}(\partial\Omega)$$
$$\le \max|a|\ \|(u_k - u)\|_{H^p(\Omega)} \le \max|a|\ \|(u_k - u)\|_{H^q(\Omega)} \to 0, \quad k \to \infty.$$

References

[Cos88] Costabel, M.: Boundary integral operators on Lipschitz domains: elementary results. *SIAM J. Math. Anal.,* **19**, 613–626 (1988).

[Gri85] Grisvard, P.: *Elliptic Problems in Nonsmooth Domains.* Pitman, Boston-London-Melbourne (1985).

[JK81a] Jerison, D.S., Kenig, C.: The Dirichlet problem in non-smooth domains. *Ann. Math.,* **113**, 367–382 (1981).

[JK81b] Jerison, D.S., Kenig, C.: The Neumann problem on Lipschitz domains. *Bull. Amer. Math. Soc.,* **4**, 203–207 (1981).

[JK82] Jerison, D., Kenig, C.: Boundary value problems on Lipschitz domains. In: Littman, W. (ed.), *Studies in Partial Differential Equations,* MAA (1982), pp. 1–68.

[McL00] McLean, W.: *Strongly Elliptic Systems and Boundary Integral Equations.* Cambridge University Press, Cambridge (2000).

[Mik05] Mikhailov, S.E.: Analysis of extended boundary-domain integral and integro-differential equations of some variable-coefficient BVP. In: Chen, K. (ed.), *Advances in Boundary Integral Methods.* University of Liverpool Publications, Liverpool (2005), pp. 106–125.

[Mik06] Mikhailov, S.E.: Analysis of united boundary-domain integro-differential and integral equations for a mixed BVP with variable coefficient. *Math. Methods Appl. Sci.,* **29**, 715–739 (2006).

[Ver84] Verchota, G.: Layer potentials and regularity for the Dirichlet problem for Laplace's equation in Lipschitz domains. *J. Functional Anal.,* **59**, 572–611 (1984).

19

On the Extension of Divergence-Free Vector Fields Across Lipschitz Interfaces

D. Mitrea

University of Missouri, Columbia, MO, USA; dorina@math.missouri.edu

19.1 Statement of the Problem

A function $\varphi : \mathbb{R}^2 \to \mathbb{R}$ is called Lipschitz if there exists $M > 0$ such that $|\varphi(x) - \varphi(y)| \leq M|x - y|$ for all x, $y \in \mathbb{R}^2$. We say that a bounded open set $\Omega \subset \mathbb{R}^3$ is Lipschitz provided $\partial\Omega$ locally coincides with the graph of a Lipschitz function after an appropriate rotation and translation. By $B_s^{p,q}(\mathbb{R}^2)$, $0 < p, q \leq \infty$, $s \in \mathbb{R}$, we shall denote the scale of Besov spaces in $\mathbb{R}^2$, whose definition can be found in, e.g., [Tr92] and [RS96].

Assume next that $0 < s < 1$ and that $1 < p, q < \infty$. In this context, the Besov space $B_s^{p,q}(\partial\Omega)$ is defined as the collection of all functions $f : \partial\Omega \to \mathbb{R}$ with the property that, locally,

$$\mathbb{R}^2 \ni x \mapsto f(x, \varphi(x)) \in \mathbb{R} \quad \text{belongs to} \quad B_s^{p,q}(\mathbb{R}^2)$$

whenever $\varphi : \mathbb{R}^2 \to \mathbb{R}$ is a Lipschitz function that describes $\partial\Omega$. Furthermore, we let $W^{s,p}(\Omega)$ denote the scale of L^p-based Sobolev spaces of smoothness $s \in \mathbb{R}$ in Ω. Recall that for $s \in \mathbb{R}$ and $1 < p < \infty$,

$$\begin{aligned} W^{s,p}(\mathbb{R}^3) &= (I - \Delta)^{-s/2} L^p(\mathbb{R}^3), \\ W^{s,p}(\Omega) &= \{u|_\Omega : u \in W^{s,p}(\mathbb{R}^3)\}. \end{aligned} \tag{19.1}$$

As is well known, if k is a nonnegative integer, then

$$W^{k,p}(\Omega) := \{u \in L^p(\Omega) : \partial^\alpha u \in L^p(\Omega), \forall\, |\alpha| \leq k\},$$

where $\alpha = (\alpha_1, \alpha_2, \alpha_3)$ with $\alpha_j \in \mathbb{N} \cup \{0\}$ and $|\alpha| := \alpha_1 + \alpha_2 + \alpha_3$.

For a bounded Lipschitz domain Ω, the trace operator

$$\mathrm{Tr}_{\partial\Omega} : W^{s,p}(\Omega) \to B^{p,p}_{s-1/p}(\partial\Omega)$$

is bounded whenever $1 < p < \infty$ and $\frac{1}{p} < s < 1 + \frac{1}{p}$.

The main result in this chapter addresses the issue of extending a divergence-free vector field defined in a Lipschitz domain Ω and exhibiting a certain amount of smoothness (measured on the Sobolev scale) and whose trace is zero on a portion $\Gamma \subseteq \partial\Omega$, across $\partial\Omega \setminus \Gamma$, to a larger bounded domain while retaining the smoothness condition, the divergence-free property, and demanding that the extension has zero trace on the boundary of the larger domain. The precise statement is as follows.

Theorem 1. *Let Ω_1, Ω_2 be two bounded, disjoint, relatively compact Lipschitz domains in $\mathbb{R}^3$ and such that the domain $\Omega := \Omega_1 \cup \Omega_2 \cup \Gamma$ is a relatively compact bounded Lipschitz domain in $\mathbb{R}^3$, where $\Gamma := \partial\Omega_1 \cap \partial\Omega_2$. Then for each $1 < p < \infty$ and each vector field*

$$\begin{cases} \vec{u} \in W^{1,p}(\Omega_1, \mathbb{R}^3), & \\ \operatorname{div} \tilde{\mathrm{u}} = 0 & \text{in } \Omega_1, \\ \operatorname{Tr}_{\partial\Omega_1} \vec{u} = 0 & \text{on } \partial\Omega_1 \setminus \Gamma, \end{cases} \tag{19.2}$$

there exists an extension $\vec{U}$ satisfying

$$\begin{cases} \vec{U} \in W^{1,p}(\Omega, \mathbb{R}^3), & \\ \operatorname{div} \tilde{\mathrm{U}} = 0 & \text{in } \Omega, \\ \operatorname{Tr}_{\partial\Omega} \vec{U} = 0 & \text{on } \partial\Omega, \\ \vec{U} = \vec{u} & \text{in } \Omega_1, \end{cases} \tag{19.3}$$

plus a natural estimate.

The existence of an extension as stated in Theorem 1 is important for numerical applications. For example, in [CCF06], a Gelfan frame is constructed for the space

$$V^1(\Omega) := \{\vec{v} \in W^{1,2}(\Omega, \mathbb{R}^3),\ \operatorname{div} \tilde{\mathrm{v}} = 0,\ \operatorname{Tr}_{\partial\Omega} \tilde{\mathrm{v}} = 0\}.$$

This is done by starting with divergence-free wavelet bases $\{\Psi_i\}$ for $V^1(\Omega_i)$, where Ω_i, $i = 1, \ldots, M$, are overlapping Lipschitz subdomains of Ω such that $\Omega = \cup_{i=1}^{M} \Omega_i$. The collection of extensions of each wavelet in $\{\Psi_i\}$ to a vector field in $V^1(\Omega)$ then proves to be a Gelfan frame for $V^1(\Omega)$.

The proof of Theorem 1 is given in Section 19.3. One main ingredient in the proof is a result from [MMM06], which is stated in Section 19.2 as Theorem 2. Given its potential for applications, the version of Theorem 2 corresponding to the higher smoothness case is also stated in Section 19.2 as Theorem 3. One more application of Theorem 2 is discussed in Section 19.4. This latter application relates to Maxwell's equations. Even though in this chapter we state Theorem 1 for the case when the domains considered are in $\mathbb{R}^n$ with $n = 3$, a similar result is actually valid when $n \geq 2$.

19.2 The Poisson Problem for the Divergence, the Curl, and the Gradient Operators

Fix Ω, a bounded Lipschitz domain in $\mathbb{R}^3$ with arbitrary topology and outward unit normal $\vec{\nu} = (\nu_1, \nu_2, \nu_3)$ that is well defined almost everywhere with respect to the surface measure $d\sigma$ on $\partial\Omega$. Consider the Poisson problem with Dirichlet boundary condition:

$$\begin{cases} Du = f & \text{in } \Omega, \\ \mathrm{Tr}_{\partial\Omega}\, u = g & \text{on } \partial\Omega, \end{cases} \tag{19.4}$$

where D is one of the following first-order differential operators: divergence, curl, or gradient.

In [MMM06], we have identified the natural context in which problem (19.4) has a solution satisfying an appropriate estimate. This was done by using scales of Sobolev and Besov spaces. Recall the Sobolev spaces $W^{s,p}(\Omega)$ from (19.1). The Besov scale $B^{p,p}_s(\Omega)$ can be obtained from Sobolev spaces via real interpolation; that is,

$$B^{p,p}_s(\Omega) := (W^{s_0,p}(\Omega), W^{s_1,p}(\Omega))_{\theta,p},$$

for $s = (1-\theta)s_0 + \theta s_1$ and $1 < p < \infty$. Since in this section we shall work with both Besov and Sobolev scales, as a way of referring to them simultaneously, the notation A^p_s will be used, with the understanding that

$$A^p_s(\Omega) := \begin{cases} W^{s,p}(\Omega) & \text{if } A = W, \\ B^{p,p}_s(\Omega) & \text{if } A = B. \end{cases}$$

There are two types of issues associated with the problem (19.4): issues of analytical nature, such as those due to the low regularity assumptions on the domain and the compatibility conditions the data must satisfy, and issues of a topological nature. As seen in Theorems 2 and 3, in order to ensure the solvability of (19.4), one is led to considering the Betti numbers of the domain Ω. Denote by $b_\ell(\Omega) = 0$ the ℓ-th Betti number of Ω, where $\ell \in \{0, 1, 2, 3\}$. It is known that $b_0(\Omega)$, $b_1(\Omega)$, and $b_2(\Omega)$ equal the number of connected components, of holes, and of handles, respectively, of the domain Ω.

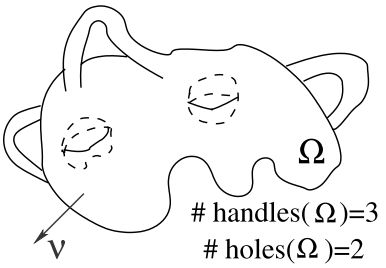

Let $\nabla_{\tan}$ denote the tangential gradient on $\partial\Omega$, and let Div, the surface divergence, denote its formal adjoint. Then the result concerning the solvability of (19.4) when the smoothness index s is close to zero is stated as follows.

Theorem 2. *[MMM06] Suppose that Ω is a bounded Lipschitz domain in $\mathbb{R}^3$ and that $1 < p < \infty$, $-1 + \frac{1}{p} < s < \frac{1}{p}$. Then the following are true.*

(a) For all $f \in A^p_s(\Omega)$ and $\vec{g} \in B^{p,p}_{s+1-1/p}(\partial\Omega, \mathbb{R}^3)$ verifying the compatibility condition

$$(CC1) \quad \int_G f\,dx = \int_{\partial G} \vec{\nu}\cdot\vec{g}\,d\sigma$$

for each connected component G of Ω, there exist $\vec{u} \in A^p_{s+1}(\Omega, \mathbb{R}^3)$ and $C > 0$ (independent of $\vec{u}$, f, $\vec{g}$) such that

$$(P1) \quad \begin{cases} \operatorname{div} \tilde{\mathrm{u}} = \mathrm{f} & \text{in } \Omega, \\ \operatorname{Tr}_{\partial\Omega}\vec{u} = \vec{g} & \text{on } \partial\Omega, \end{cases}$$

and

$$\|\vec{u}\|_{A^p_{s+1}(\Omega,\mathbb{R}^3)} \leq C\|f\|_{A^p_s(\Omega)} + C\|\vec{g}\|_{B^{p,p}_{s+1-1/p}(\partial\Omega,\mathbb{R}^3)}.$$

(b) $b_1(\Omega) = 0$ if and only if for all $\vec{f} \in A^p_s(\Omega, \mathbb{R}^3)$ and $\vec{g} \in B^{p,p}_{s+1-1/p}(\partial\Omega, \mathbb{R}^3)$ verifying the compatibility conditions

$$(CC2) \quad \begin{cases} \operatorname{div} \tilde{\mathrm{f}} = 0 & \text{in } \Omega, \\ \vec{\nu}\cdot\vec{f} = -\operatorname{Div}(\tilde{\nu}\times\tilde{\mathrm{g}}) & \text{on } \partial\Omega, \end{cases}$$

there exist $\vec{u} \in A^p_{s+1}(\Omega, \mathbb{R}^3)$ and $C > 0$ (independent of $\vec{u}$, $\vec{f}$, $\vec{g}$) such that

$$(P2) \quad \begin{cases} \operatorname{curl} \tilde{\mathrm{u}} = \tilde{\mathrm{f}} & \text{in } \Omega, \\ \operatorname{Tr}_{\partial\Omega}\vec{u} = \vec{g} & \text{on } \partial\Omega, \end{cases}$$

and

$$\|\vec{u}\|_{A^p_{s+1}(\Omega,\mathbb{R}^3)} \leq C\|\vec{f}\|_{A^p_s(\Omega,\mathbb{R}^3)} + C\|\vec{g}\|_{B^{p,p}_{s+1-1/p}(\partial\Omega,\mathbb{R}^3)}.$$

(c) $b_2(\Omega) = 0$ if and only if for all $\vec{f} \in A^p_s(\Omega, \mathbb{R}^3)$ and $g \in B^{p,p}_{s+1-1/p}(\partial\Omega)$ verifying the compatibility conditions

$$(CC3) \quad \begin{cases} \operatorname{curl} \tilde{\mathrm{f}} = 0 & \text{in } \Omega, \\ \vec{\nu}\times\vec{f} = \vec{\nu}\times(\nabla_{\tan} g) & \text{on } \partial\Omega, \end{cases}$$

there exist $u \in A^p_{s+1}(\Omega)$ and $C > 0$ (independent of u, $\vec{f}$, g) such that

$$(P3) \quad \begin{cases} \nabla u = \vec{f} & \text{in } \Omega, \\ \operatorname{Tr}_{\partial\Omega} u = g & \text{on } \partial\Omega, \end{cases}$$

and

$$\|u\|_{A^p_{s+1}(\Omega)} \leq C\|\vec{f}\|_{A^p_s(\Omega,\mathbb{R}^3)} + C\|g\|_{B^{p,p}_{s+1-1/p}(\partial\Omega)}.$$

Next we state the analog of Theorem 2 when the smoothness index s is away from zero. The special triplets $(0,0,0)$, $(1,0,0)$, $(0,1,0)$, $(0,0,1)$ will be denoted by (0), e_1, e_2, and e_3, respectively.

Theorem 3. *[MMM06] Suppose Ω is a bounded Lipschitz domain in $\mathbb{R}^3$ and $1 < p < \infty$, $-1+\frac{1}{p} < s-k < \frac{1}{p}$, for some $k \in \mathbb{N}$. Then the following are true.*

(a) For each $f \in A^p_s(\Omega)$ and each family $\vec{g}_\alpha \in B^{p,p}_{s+1-1/p}(\partial\Omega, \mathbb{R}^3)$, $\alpha \in \mathbb{N}_0$ with $|\alpha| \le k$, verifying the compatibility conditions

$$(CC4)\quad \begin{cases} (\nu_j \partial_l - \nu_l \partial_j)\vec{g}_\alpha = \nu_j \vec{g}_{\alpha+e_l} - \nu_l \vec{g}_{\alpha+e_j} \\ \forall\, \alpha : \ |\alpha| \le k-1, \quad \forall j,l = 1,2,3 \\ \int_G f\, dx = \int_{\partial G} \vec{\nu} \cdot \vec{g}_{(0)}\, d\sigma, \end{cases}$$

for each connected component G of Ω, there exist $\vec{u} \in A^p_{s+1}(\Omega, \mathbb{R}^3)$ and $C > 0$ (independent of $\vec{u}$, $\vec{f}$, $\vec{g}_\alpha$) such that

$$(P4)\quad \begin{cases} \operatorname{div} \tilde{\mathrm{u}} = \mathrm{f} & \text{in } \Omega, \\ \operatorname{Tr}_{\partial\Omega}[\partial^\alpha \vec{u}] = \vec{g}_\alpha & \text{on } \partial\Omega, \ \forall\, |\alpha| \le k, \end{cases}$$

and

$$\|\vec{u}\|_{A^p_{s+1}(\Omega,\mathbb{R}^3)} \le C\|f\|_{A^p_s(\Omega)} + C \sum_{|\alpha|\le k} \|\vec{g}_\alpha\|_{B^{p,p}_{s+1-1/p}(\partial\Omega,\mathbb{R}^3)}.$$

(b) $b_1(\Omega) = 0$ if and only if for each $\vec{f} \in A^p_s(\Omega, \mathbb{R}^3)$ and each family $\vec{g}_\alpha \in B^{p,p}_{s+1-1/p}(\partial\Omega, \mathbb{R}^3)$, $\alpha \in \mathbb{N}_0$ with $|\alpha| \le k$, verifying the compatibility conditions

$$(CC5)\quad \begin{cases} \operatorname{div} \tilde{\mathrm{f}} = 0 \quad \text{in } \Omega, \\ (\nu_j \partial_l - \nu_l \partial_j)\vec{g}_\alpha = \nu_j \vec{g}_{\alpha+e_l} - \nu_l \vec{g}_{\alpha+e_j} \\ \forall\, \alpha : \ |\alpha| \le k-1, \quad \forall\, j,l = 1,2,3 \\ \operatorname{Tr}_{\partial\Omega}[\partial^\alpha \vec{f}] = -\sum_{j=1}^{3} \vec{g}_{\alpha+e_j} \times e_j, \ \forall\, |\alpha| \le k-1, \end{cases}$$

there exist $\vec{u} \in A^p_{s+1}(\Omega, \mathbb{R}^3)$ and $C > 0$ (independent of $\vec{u}$, $\vec{f}$, $\vec{g}_\alpha$) such that

$$(P5)\quad \begin{cases} \operatorname{curl} \tilde{\mathrm{u}} = \tilde{\mathrm{f}} & \text{in } \Omega, \\ \operatorname{Tr}_{\partial\Omega}[\partial^\alpha \vec{u}] = \vec{g}_\alpha & \text{on } \partial\Omega, \quad \forall\, |\alpha| \le k, \end{cases}$$

and

$$\|\vec{u}\|_{A^p_{s+1}(\Omega,\mathbb{R}^3)} \le C\|\vec{f}\|_{A^p_s(\Omega,\mathbb{R}^3)} + C \sum_{|\alpha|\le k} \|\vec{g}_\alpha\|_{B^{p,p}_{s+1-1/p}(\partial\Omega,\mathbb{R}^3)}.$$

(c) $b_2(\Omega) = 0$ *if and only if for each* $\vec{f} \in A^p_s(\Omega, \mathbb{R}^3)$ *and each family* $g_\alpha \in B^{p,p}_{s+1-1/p}(\partial\Omega)$, $\alpha \in \mathbb{N}_0$ *with* $|\alpha| \leq k$, *verifying the compatibility conditions*

$$(CC6)\quad \begin{cases} \operatorname{curl} \tilde{\mathrm{f}} = 0 \quad \text{in } \Omega, \\ (\nu_j \partial_l - \nu_l \partial_j) g_\alpha = \nu_j g_{\alpha+e_l} - \nu_l g_{\alpha+e_j} \\ \forall\, \alpha : |\alpha| \leq k-1, \ \ \forall\, j, l = 1, 2, 3 \\ \operatorname{Tr}_{\partial\Omega}[\partial^\alpha f_j] = g_{\alpha+e_j}, \ \ \forall\, j = 1, 2, 3, \ \ \forall\, |\alpha| \leq k-1, \end{cases}$$

there exist $u \in A^p_{s+1}(\Omega)$ *and* $C > 0$ *(independent of* u, $\vec{f}$, g_α*) such that*

$$(P6)\quad \begin{cases} \nabla u = \vec{f} & \text{in } \Omega, \\ \operatorname{Tr}_{\partial\Omega}[\partial^\alpha u] = g_\alpha & \text{on } \partial\Omega, \ \ \forall\, |\alpha| \leq k, \end{cases}$$

and

$$\|u\|_{A^p_{s+1}(\Omega)} \leq C \|\vec{f}\|_{A^p_s(\Omega,\mathbb{R}^3)} + C \sum_{|\alpha|\leq k} \|g_\alpha\|_{B^{p,p}_{s+1-1/p}(\partial\Omega)}.$$

Theorems 2 and 3 are particular cases of the more general setting of the Poisson problem for the exterior derivative operator with Dirichlet boundary condition on Lipschitz subdomains of a manifold M, considered in [MMM06]. For proofs, see [MMM06].

19.3 Proof of Theorem 1

Fix $\vec{u}$ as in (19.2), and define $\vec{w}$ by

$$\vec{w} = \begin{cases} \vec{u} & \text{in } \Omega_1, \\ 0 & \text{in } \mathbb{R}^3 \setminus \bar{\Omega}. \end{cases}$$

Then clearly $\vec{w} \in L^p(\mathbb{R}^3 \setminus \bar{\Omega}_2, \mathbb{R}^3)$ and $\operatorname{supp} \vec{w} \subseteq \bar{\Omega}_1$. In addition, $\vec{w} \in W^{1,p}(\mathbb{R}^3 \setminus \bar{\Omega}_2, \mathbb{R}^3)$ and for each $1 \leq j \leq n$,

$$\partial_j \vec{w} = \begin{cases} \partial_j \vec{u} & \text{in } \Omega_1, \\ 0 & \text{in } \mathbb{R}^3 \setminus \bar{\Omega}, \end{cases}$$

where the derivatives are taken in the distributional sense. Indeed, if $\langle \cdot, \cdot \rangle$ denotes the pairing between a distribution and a test function, for each $\vec{\varphi} \in C^\infty_0(\mathbb{R}^3 \setminus \bar{\Omega}_2, \mathbb{R}^3)$, the properties of $\vec{u}$ and integration by parts imply that

$$\begin{aligned} \langle \partial_j \vec{w}, \vec{\varphi} \rangle &= -\langle \vec{w}, \partial_j \varphi \rangle = -\int_{\mathbb{R}^3 \setminus \bar{\Omega}_2} \vec{w} \cdot \partial_j \vec{\varphi} = -\int_{\Omega_1} \vec{u} \cdot \partial_j \vec{\varphi} \\ &= \int_{\Omega_1} (\partial_j \vec{u}) \cdot \vec{\varphi} - \int_{\partial\Omega_1} \operatorname{Tr}_{\partial\Omega_1} \vec{u} \cdot \vec{\varphi}\, \nu^1_j \, d\sigma = \int_{\Omega_1} (\partial_j \vec{u}) \cdot \vec{\varphi}, \quad (19.5) \end{aligned}$$

where ν_j^1 is the jth component of the outward unit normal ν^1 to Ω_1. The last equality in (19.5) is true since $\operatorname{supp}(\operatorname{Tr}_{\partial\Omega_1}\vec{u}) \subseteq \Gamma$ and $\operatorname{supp}\vec{\varphi} \cap \Gamma = \emptyset$.

Next, define $\vec{f} := \operatorname{Tr}_{\partial(\mathbb{R}^3\setminus\bar{\Omega}_2)}\vec{w}$. From the properties of $\vec{w}$ we can conclude that $\vec{f} \in B^{p,p}_{1-\frac{1}{p}}(\partial\Omega_2, \mathbb{R}^3)$, $\operatorname{supp}\vec{f} \subseteq \Gamma$ and $\operatorname{Tr}_{\partial(\mathbb{R}^3\setminus\bar{\Omega}_2)}\vec{f} = \operatorname{Tr}_{\partial\Omega_1}\vec{u}$ on Γ. Hence, if ν^2 denotes the outward unit normal to Ω_2, it follows that

$$\begin{aligned}\int_{\partial\Omega_2} \nu^2 \cdot \vec{f}\, d\sigma &= -\int_{\Gamma} \nu^1 \cdot \vec{f}\, d\sigma = -\int_{\partial\Omega_1} \nu^1 \cdot \operatorname{Tr}_{\partial\Omega_1}\vec{u}\, d\sigma \\ &= -\int_{\Omega_1} \operatorname{div}\tilde{\mathrm{u}} = 0.\end{aligned}$$

An application of part (a) in Theorem 2 gives the existence of a vector field

$$\begin{cases} \vec{v} \in W^{1,p}(\Omega_2, \mathbb{R}^3), \\ \operatorname{div}\tilde{\mathrm{v}} = 0 \quad \text{in } \Omega_2, \\ \operatorname{Tr}_{\partial\Omega_2}\vec{v} = \vec{f} \in B^{p,p}_{1-\frac{1}{p}}(\partial\Omega_2, \mathbb{R}^3). \end{cases}$$

The claim we make is that the vector field

$$\vec{U} := \begin{cases} \vec{u} \text{ in } \Omega_1, \\ \vec{v} \text{ in } \Omega_2, \end{cases}$$

verifies (19.3). Clearly, $\vec{U} \in L^p(\Omega, \mathbb{R}^3)$. Fix $\vec{\varphi} \in C_0^\infty(\Omega, \mathbb{R}^3)$ and $1 \le j \le n$. Then, the properties of $\vec{U}$ and integration by parts yield

$$\begin{aligned}\langle \partial_j\vec{U}, \vec{\varphi}\rangle &= -\langle \vec{U}, \partial_j\vec{\varphi}\rangle = -\int_{\Omega} \vec{U} \cdot \partial_j\vec{\varphi} = -\int_{\Omega_1} \vec{u} \cdot \partial_j\vec{\varphi} - \int_{\Omega_2} \vec{v} \cdot \partial_j\vec{\varphi} \\ &= \int_{\Omega_1} (\partial_j\vec{u}) \cdot \vec{\varphi} - \int_{\partial\Omega_1} \operatorname{Tr}_{\partial\Omega_1}\vec{u} \cdot \vec{\varphi}\, \nu_j^1\, d\sigma \\ &\quad + \int_{\Omega_2} (\partial_j\vec{v}) \cdot \vec{\varphi} - \int_{\partial\Omega_2} \operatorname{Tr}_{\partial\Omega_2}\vec{v} \cdot \vec{\varphi}\, \nu_j^2\, d\sigma \\ &= \int_{\Omega_1} (\partial_j\vec{u}) \cdot \vec{\varphi} + \int_{\Omega_2} (\partial_j\vec{v}) \cdot \vec{\varphi}. \end{aligned} \tag{19.6}$$

The last equality in (19.6) is a consequence of the fact that the two boundary integrals cancel each other since $\nu_j^1 = -\nu_j^2$ on Γ and $\operatorname{Tr}_{\partial\Omega_1}\vec{u} = \operatorname{Tr}_{\partial\Omega_2}\vec{v}$ on Γ while being zero on the rest of their domains. The conclusion is that, $\forall\, j$,

$$\partial_j\vec{U} := \begin{cases} \partial_j\vec{u} \text{ in } \Omega_1, \\ \partial_j\vec{v} \text{ in } \Omega_2, \end{cases}$$

and hence, $\vec{U} \in W^{1,p}(\Omega, \mathbb{R}^3)$. Furthermore,

$$(\operatorname{div}\vec{U})|_{\Omega_1} = \operatorname{div}(\vec{U}|_{\Omega_1}) = \operatorname{div}\vec{u} = 0,$$
$$(\operatorname{div}\vec{U})|_{\Omega_2} = \operatorname{div}(\vec{U}|_{\Omega_2}) = \operatorname{div}\vec{v} = 0,$$

so $\operatorname{div}\tilde{\mathrm{U}} = 0$ in Ω. We are left with checking that $\mathrm{Tr}_{\partial\Omega}\vec{U} = 0$. This, however, is true since

$$(\mathrm{Tr}_{\partial\Omega}\vec{U})|_{\partial\Omega_2\setminus\Gamma} = (\mathrm{Tr}_{\partial\Omega_2}\vec{v})|_{\partial\Omega_2\setminus\Gamma} = \vec{f}|_{\partial\Omega_2\setminus\Gamma} = 0,$$
$$(\mathrm{Tr}_{\partial\Omega}\vec{U})|_{\partial\Omega_1\setminus\Gamma} = (\mathrm{Tr}_{\partial\Omega_1}\vec{u})|_{\partial\Omega_1\setminus\Gamma} = \vec{f}|_{\partial\Omega_1\setminus\Gamma} = 0.$$

Finally, that $\vec{U}$ satisfies a natural estimate is implicit in the above construction.

19.4 Another Application of Theorem 2

In this section, we discuss the structure of vector fields that play an important role in Maxwell's equations.

Theorem 4. *Let Ω be a bounded, convex, Lipschitz domain in $\mathbb{R}^3$. Then, for any $1 < p \leq 2$, and any vector field $\vec{u} \in L^p(\Omega, \mathbb{R}^3)$ satisfying* $\operatorname{curl}\tilde{\mathrm{u}} \in \mathrm{L}^{\mathrm{p}}(\Omega, \mathbb{R}^3)$, $\operatorname{div}\tilde{\mathrm{u}} \in \mathrm{L}^{\mathrm{p}}(\Omega)$ *and $\vec{\nu}\cdot\vec{u} = 0$ on $\partial\Omega$ can be written in the form*

$$\vec{u} = \vec{v} + \operatorname{curl}\tilde{\omega}, \tag{19.7}$$
$$\vec{v} \in W^{1,p}(\Omega, \mathbb{R}^3), \quad \mathrm{Tr}_{\partial\Omega}\vec{v} = 0, \quad \vec{\omega} \in W^{1,p}(\Omega, \mathbb{R}^3), \tag{19.8}$$
$$\operatorname{div}\tilde{\omega} = 0 \ \text{ in } \Omega, \quad \Delta\tilde{\omega} \in \mathrm{L}^{\mathrm{p}}(\Omega, \mathbb{R}^3), \quad \text{and} \quad \tilde{\nu}\times\tilde{\omega} = 0 \ \text{ on } \partial\Omega. \tag{19.9}$$

Moreover, for some $C = C(\Omega, p) > 0$,

$$\|\vec{v}\|_{W^{1,p}(\Omega,\mathbb{R}^3)} + \|\Delta\vec{\omega}\|_{L^p(\Omega,\mathbb{R}^3)} + \|\vec{\omega}\|_{W^{1,p}(\Omega,\mathbb{R}^3)}$$
$$\leq C\Big(\|\vec{u}\|_{L^p(\Omega,\mathbb{R}^3)} + \|\operatorname{curl}\vec{u}\|_{L^p(\Omega,\mathbb{R}^3)} + \|\operatorname{div}\vec{u}\|_{L^p(\Omega)}\Big).$$

Proof. Since $\vec{\nu}\cdot\vec{u} = 0$, by the Divergence Theorem, the compatibility condition $(CC1)$ is satisfied for $f := \operatorname{div}\tilde{\mathrm{u}}$ and $\vec{g} = 0$. Hence, by Theorem 2 part (a), there exists $\vec{v} \in W^{1,p}_0(\Omega, \mathbb{R}^3)$, with $\operatorname{div}\tilde{\mathrm{v}} = \operatorname{div}\tilde{\mathrm{u}}$ in Ω. Thus, if we set $\vec{w} := \vec{u} - \vec{v}$, then

$$\vec{w} \in L^p(\Omega, \mathbb{R}^3), \ \operatorname{div}\tilde{\mathrm{w}} = 0 \ \text{ in } \Omega, \quad \text{and} \quad \tilde{\nu}\cdot\tilde{\mathrm{w}} = 0 \ \text{ on } \partial\Omega.$$

Apply part (b) in Theorem 2 to obtain

$$\vec{\omega}' \in W^{1,p}_0(\Omega, \mathbb{R}^3), \ \operatorname{curl}\tilde{\omega}' = \tilde{\mathrm{w}} \ \text{ in } \Omega.$$

At this point, we recall a result contained in [Ad93], to the effect that there exists $\varphi \in W^{2,p}(\Omega) \cap W^{1,p}_0(\Omega)$, such that $\Delta\varphi = \operatorname{div}\tilde{\omega}'$. With this

function at hand, define $\vec{\omega} := \vec{\omega}' - \nabla\varphi$. Clearly, $\vec{\omega} \in W^{1,p}(\Omega, \mathbb{R}^3)$. Also, $\operatorname{div}\tilde{\omega} = \operatorname{div}\tilde{\omega}' - \Delta\,\varphi = 0$ in Ω. In addition, $\vec{\nu} \times \vec{\omega} = 0$. The latter follows if we prove that $\vec{\nu} \times \vec{\omega}' = 0$ and $\vec{\nu} \times \nabla\varphi = 0$.

Fix an arbitrary, smooth, compactly supported vector field $\vec{\xi}$ in Ω. By the definition of $\vec{\nu}\times$, write

$$\langle \vec{\nu} \times \vec{\omega}', \vec{\xi}|_{\partial\Omega} \rangle = \int_\Omega \langle \operatorname{curl}(\tilde{\omega}'), \tilde{\xi} \rangle - \int_\Omega \langle \tilde{\omega}', \operatorname{curl}\tilde{\xi} \rangle, \tag{19.10}$$

$$\begin{aligned} \langle \vec{\nu} \times \nabla\varphi, \vec{\xi}|_{\partial\Omega} \rangle &= \int_\Omega \langle \operatorname{curl}(\nabla\varphi), \vec{\xi} \rangle - \int_\Omega \langle \nabla\varphi, curl\,\vec{\xi} \rangle \\ &= -\int_\Omega \langle \nabla\varphi, \operatorname{curl}\tilde{\xi} \rangle \end{aligned} \tag{19.11}$$

Moreover, since $\vec{\omega}' \in W_0^{1,p}(\Omega, \mathbb{R}^3)$ and $\varphi \in W_0^{1,p}(\Omega)$, there exist two sequences $\{\vec{\psi}_j\}_j$ and $\{\varphi_j\}_j$ of smooth, compactly supported vector fields and functions, respectively, such that, as $j \to \infty$, $\vec{\psi}_j \to \vec{\omega}'$ in $W^{1,p}(\Omega, \mathbb{R}^3)$ and $\varphi_j \to \varphi$ in $W^{1,p}(\Omega)$. As such, also using integration by parts, we have that

$$\int_\Omega \langle \operatorname{curl}(\vec{\omega}'), \vec{\xi} \rangle = \lim_{j\to\infty} \int_\Omega \langle \operatorname{curl}(\vec{\psi}_j), \vec{\xi} \rangle = \lim_{j\to\infty} \int_\Omega \langle \vec{\psi}_j, \operatorname{curl}\vec{\xi} \rangle \tag{19.12}$$

$$= \int_\Omega \langle \vec{\omega}', \operatorname{curl}\tilde{\xi} \rangle, \tag{19.13}$$

$$\int_\Omega \langle \nabla\varphi, \operatorname{curl}\vec{\xi} \rangle = \lim_{j\to\infty} \int_\Omega \langle \nabla\varphi_j, \operatorname{curl}\vec{\xi} \rangle = 0. \tag{19.14}$$

A combination of (19.10)–(19.14) now yields $\vec{\nu} \times \vec{\omega} = 0$.

The vectors $\vec{v}$ and $\vec{\omega}$ constructed so far satisfy (19.7)–(19.9). Indeed, $\vec{u} = \vec{v} + \vec{w} = \vec{v} + \operatorname{curl}\tilde{\omega}' = \tilde{\mathrm{v}} + \operatorname{curl}\tilde{\omega}$ in Ω; thus, (19.7) holds. The only condition from (19.9) left to check is that $\Delta\vec{\omega} \in L^p(\Omega, \mathbb{R}^3)$. Observe that since $\operatorname{div}\tilde{\omega} = 0$, the decomposition of $\vec{u}$ from (19.7) implies that $-\Delta\vec{\omega} = \operatorname{curl}\operatorname{curl}\tilde{\omega} = \operatorname{curl}\tilde{\mathrm{v}} - \operatorname{curl}\tilde{\mathrm{u}}$, which, based on the properties of $\vec{u}$ and $\vec{v}$, is indeed in $L^p(\Omega, \mathbb{R}^3)$. This concludes the proof of Theorem 4.

Acknowledgement. This work has been partially supported by NSF-FRG grant 0456306.

References

[Ad93] Adolfsson, V.: L^p-integrability of the second order derivatives of Green potentials in convex domains. *Pacific J. Math.,* **159**, 201–225 (1993).

[CCF06] Charina, M., Conti, C., Fornasier, M.: Adaptive frame methods for nonlinear variational problems. *Numer. Math.* (in press).

[MMM06] Mitrea, D., Mitrea, M., Monniaux, S.: The Poisson problem for the exterior derivative operator with Dirichlet boundary condition on nonsmooth domains. Preprint (2006).

[RS96] Runst, T., Sickel, W.: *Sobolev Spaces of Fractional Order, Nemytskij Operators, and Nonlinear Partial Differential Operators.* de Gruyter, Berlin-New York (1996).

[Tr92] Triebel, H.: *Theory of Function Spaces II.* Birkhäuser, Basel (1992).

20

Solutions of the Atmospheric Advection–Diffusion Equation by the Laplace Transformation

D.M. Moreira[1], M.T. de Vilhena[2], T. Tirabassi[3], and B.E.J. Bodmann[2]

[1] Universidade Federal de Pelotas, Bagé, RS, Brazil;
davidson@mecanica.ufrgs.br
[2] Universidade Federal do Rio Grande do Sul, Porto Alegre, RS, Brazil;
vilhena@mat.ufrgs.br, bardo.bodmann@ufrgs.br
[3] Istituto di Scienze dell'Atmosfera e del Clima, Bologna, Italy;
t.tirabassi@isac.cnr.it

20.1 Introduction

Transport and diffusion models of air pollution are based either on simple techniques, such as the Gaussian approach, or on more complex dynamics, such as the K-theory. The Gaussian equation is an easy method that cannot properly simulate complex non homogeneous conditions, whereas the K-theory can accept any complex meteorological input, but in general requires tedious numerical integration. Gaussian models are still widely used by the environmental agencies all over the world for regulatory applications. Because of their well-known intrinsic limits, the reliability of a Gaussian model depends strongly on the determination of dispersion parameters based on the turbulence structure of the PBL. The Gaussian model needs completion by empirically determined standard deviations, whereas some commonly measurable turbulent exchange coefficient has to be introduced into the advection–diffusion equation. Analytical solutions to the complete advection–diffusion equation cannot be given but in a few specialized cases [Tir03], and numerical solutions cannot be easily "interpreted" as the simple Gaussian model. As a consequence, the major part of applications to practical problems are currently done by using the Gaussian model, and a great deal of empirical work has been done do determine the sigmas appropriate for the PBL under various meteorological conditions and to extend the basic formulation of this model and its range of applicability [Zan90].

The advection–diffusion equation is believed to give a better representation of the effects due to the vertical stratification of the atmosphere. To relate to previous types of models, we employ an analytical solution of the advection–diffusion equation that accepts height-independent wind and eddy diffusivity

coefficients, and subdivide the PBL into several layers, in which the eddy diffusivity and wind speed are considered with their average values. The hybrid model then represents conditions of a height-structured PBL [Vil98].

20.2 The Advection–Diffusion Equation

The advection–diffusion equation for air pollution in the atmosphere is essentially a statement of conservation of the suspended material:

$$\frac{\partial C}{\partial t} + u\frac{\partial C}{\partial x} + v\frac{\partial C}{\partial y} + w\frac{\partial C}{\partial z} = -\frac{\partial \overline{u'c'}}{\partial x} - \frac{\partial \overline{v'c'}}{\partial y} - \frac{\partial \overline{w'c'}}{\partial z} + S,$$

where C denotes the average concentration, u, v, w are the Cartesian components of the wind, and S is the source term. The terms $\overline{u'c'}$, $\overline{v'c'}$, and $\overline{w'c'}$ represent the turbulent fluxes of contaminants in the longitudinal, crosswind, and vertical directions. The concentration turbulent fluxes are assumed to be proportional to the mean concentration gradient, which is known as Fick theory $\overline{u'c'} = -K_x \frac{\partial C}{\partial x}$, $\overline{v'c'} = -K_y \frac{\partial C}{\partial y}$, $\overline{w'c'} = -K_z \frac{\partial C}{\partial z}$, where K_x, K_y, K_z are the Cartesian components of eddy diffusivity and z is the height. This assumption, combined with the continuity equation, leads to the advection–diffusion equation. The crosswind integration yields with $\bar{C} = \int_{-\infty}^{\infty} C(x, y, z)\, dy$ the crosswind integrated concentration

$$\frac{\partial \bar{C}}{\partial t} + u\frac{\partial \bar{C}}{\partial x} + w\frac{\partial \bar{C}}{\partial z} = \frac{\partial}{\partial x}\left(K_x \frac{\partial \bar{C}}{\partial x}\right) + \frac{\partial}{\partial z}\left(K_z \frac{\partial \bar{C}}{\partial z}\right) + S.$$

Before applying the Laplace transformation, we perform a stepwise approximation of these coefficients. To this end, we discretize the height z_i of the PBL into N subintervals such that inside each subregion, K and u assume average values given by $K_n = (z_{n+1} - z_n)^{-1} \int_{z_n}^{z_{n+1}} K_z(z)\, dz$ and $u_n = (z_{n+1} - z_n)^{-1} \int_{z_n}^{z_{n+1}} u_z(z)\, dz$ for $n = 1, \ldots, N$. In scenarios where the vertical eddy diffusivity depends on x and z, one proceeds in a similar fashion, first determining the average in z followed by averaging in x, so that $K_{m,n}$ is double-indexed with n for the vertical segments and $m = 1, \ldots, M$ for the longitudinal ones. The solution may now be determined for each segment.

20.3 The Laplace Transformation Solution

The one-dimensional time-dependent advection–diffusion equation is $\frac{\partial \bar{C}}{\partial t} = \frac{\partial}{\partial z}\left(K_z \frac{\partial \bar{C}}{\partial z}\right)$ for $0 < z < z_i$ and $t > 0$, subject to the boundary conditions $K_z \frac{\partial \bar{C}}{\partial z} = 0$ at $z = 0, z_i$ and with initial condition $\bar{C}(z, 0) = Q\delta(z - H_s)$ at $t = 0$, where H_s is the source height and Q is the emission rate. Assuming that the nonhomogeneous turbulence is modeled by an eddy diffusivity depending

on the z-variable, the Laplace transformation is applied, which changes the advection-diffusion equation $\frac{\partial \bar{C}_n}{\partial t} = K_{zn}\frac{\partial^2 \bar{C}_n}{\partial z^2}$ for each interval $z_i < z < z_{i+1}$ and $n = 1, \ldots, N$ to the form

$$\frac{\partial^2}{\partial z^2}\tilde{C}_n(z,s) - \frac{s}{K_z n}\tilde{C}(z,s) = -\frac{1}{K_{zn}}\bar{C}_n(z,0).$$

Here $\tilde{C}_n(z,s) = \mathcal{L}\{\bar{C}_n(z,t); t \to s\}$ denotes the Laplace transform of $\bar{C}_n(z,t)$ with respect to the t-variable, which has the well-known solution

$$\tilde{C}_n(z,s) = A_n e^{-R_n z} + B_n e^{R_n z} - \frac{Q}{R_a}\cosh\left(R_n(z-H_s)\right)H(z-H_s), \quad (20.1)$$

where $H(z-H_s)$ is the Heaviside function, $R_n = \sqrt{s/K_{zn}}$, and $R_a = \sqrt{K_{zn}s}$. Note that at this stage there are $2N$ integration constants, which are reduced by the $(2N-2)$ interface conditions, namely, the continuity of concentration $\bar{C}_n = \bar{C}_{n+1}$ and flux concentration at the interface: $K_{zn}\frac{\partial \bar{c}_n}{\partial z} = K_{zn+1}\frac{\partial \bar{c}_{n+1}}{\partial z}$, for $n = 1, \ldots, N-1$. Then, by (20.1), we obtain the system

$$\begin{pmatrix}
M_{11} & M_{12} & 0 & 0 & 0 & 0 & \ldots & 0 \\
M_{21} & M_{22} & M_{23} & M_{24} & 0 & 0 & \ldots & 0 \\
M_{31} & M_{32} & M_{33} & M_{34} & 0 & 0 & \ldots & 0 \\
0 & 0 & M_{43} & M_{44} & M_{45} & M_{46} & \ldots & 0 \\
0 & 0 & M_{53} & M_{54} & M_{55} & M_{56} & \ldots & 0 \\
\vdots & \vdots & \vdots & \vdots & \vdots & \vdots & \vdots & \vdots \\
0 & 0 & 0 & \ldots & M_{n-1,n-3} & M_{n-1,n-2} & M_{n-1,n-1} & M_{n-1,n} \\
0 & 0 & 0 & 0 & 0 & \ldots & M_{n,n-1} & M_{n,n}
\end{pmatrix}
\begin{pmatrix} A_1 \\ B_1 \\ A_2 \\ B_2 \\ \vdots \\ \vdots \\ A_n \\ B_n \end{pmatrix}
=
\begin{pmatrix} 0 \\ \vdots \\ 0 \\ D_{n^*} \\ D'_{n^*} \\ 0 \\ \vdots \\ 0 \end{pmatrix},$$

where the M_{ij} are given by

$$\begin{array}{lll}
M_{11}=R_1, & M_{2n,2n+1}=-e^{R_n z_n}, & M_{2n+1,2n+1}=-K_{n+1}R_{n+1}e^{R_{n+1}z_n}, \\
M_{12}=-R_1, & M_{2n,2n+2}=-e^{-R_n z_n}, & M_{2n+1,2n+2}=K_{n+1}R_{n+1}e^{-R_{n+1}z_n}, \\
M_{2n,2n-1}=e^{R_n z_n}, & M_{2n+1,2n-1}=K_n R_n e^{R_n z_n}, & M_{n,n-1}=R_N e^{R_N z_N}, \\
M_{2n,2n}=e^{-R_n z_n}, & M_{2n+1,2n}=-K_n R_n e^{-R_n z_n}, & M_{n,n}=-R_N e^{-R_N z_N},
\end{array}$$

and in the sublayer of contaminant emission, $D_{n^*} = -\frac{Q}{R_a}\cosh\left(R_n(z-H_s)\right)$ and $D'_{n^*} = -Q\cosh\left(R_n(z-H_s)\right)$. Solving this linear system and inverting the transformed concentration by the Gaussian quadrature scheme, we finally get the solution

$$\bar{C}_n(z,t) = \sum_{i=1}^{k} a_i \frac{p_i}{t}\left[A_n e^{-R_n z} + B_n e^{R_n z} - \frac{Q}{R_a}\cosh\left(R_n(z-H_s)\right)H(z-H_s)\right], \quad (20.2)$$

where k is the number of quadrature points, $R_n = \sqrt{p_i/(tK_{zn})}$, and $R_a = \sqrt{K_{zn}p_i/t}$. Here a_i and p_i are the Gaussian quadrature parameters (see [Str66]).

The two-dimensional steady-state advection–diffusion equation is of the form $u\frac{\partial \bar{C}}{\partial x} = \frac{\partial}{\partial z}\left(K_z\frac{\partial \bar{C}}{\partial z}\right)$ for $0 < z < z_i$ and $x > 0$, subject to the

boundary conditions $K_z \frac{\partial \bar{C}}{\partial z} = 0$ at $z = 0, z_i$ and the source condition $\bar{C}(0,z) = \frac{Q}{u}\delta(z - H_s)$ at $x = 0$. Here H_s is the height source and Q is the continuous contaminant emission rate. Proceeding as in the previous section, we perform the stepwise approximation of the parameters, apply the Laplace transformation with respect to the x-variable, solve the resulting set of ordinary differential equations, and apply the boundary and interface conditions to determine the integration constants. This procedure leads to the solution

$$\bar{C}_n(x,z) = \sum_{i=1}^{m} a_i \frac{p_i}{x} \left[A_n e^{-R_n z} + B_n e^{R_n z} - \frac{Q}{R_a} \cosh\left(R_n(z - H_s)\right) H(z - H_s) \right], \tag{20.3}$$

where m is the number of quadrature points, $R_n = \sqrt{\frac{u_n p_i}{K_{zn} x}}$, and $R_a = \sqrt{u_n K_{zn} \frac{p_i}{x}}$.

The two-dimensional steady-state equation with longitudinal diffusion is $u\frac{\partial \bar{C}}{\partial x} = \frac{\partial}{\partial x}\left(K_x \frac{\partial \bar{C}}{\partial x}\right) + \frac{\partial}{\partial z}\left(K_z \frac{\partial \bar{C}}{\partial z}\right)$ for $0 < z < z_i$ and $x > 0$, subject to the boundary conditions $K_z \frac{\partial \bar{C}}{\partial z} = 0$ at $z = 0, z_i$ and the source condition $\bar{C}(0,z) = \frac{Q}{u}\delta(z - H_s)$ at $x = 0$. A procedure similar to the one above yields solution (20.3) if this time we substitute $\frac{Q}{R_a} \rightarrow \frac{QR_b}{R_a}$, where $R_n = \sqrt{R_b p_i u_n/(xK_{zn})}$, $R_a = \sqrt{u_n K_{zn} p_i/x}$, and $R_b = 1 - p_i/P_e$. Here $P_e = u_n x/K_{xn}$ is the Peclet number, which essentially represents the ratio between the advective and diffusive transport terms. Small values of this number are related to a weak wind, which turns the downwind diffusion important and the region of interest (i.e., region of height concentrations) remains close to the source. On the other hand, for large values of the Peclet number, the downwind diffusion may be neglected when compared with the transport advective term. This corresponds to a large distance to the source. The solution reduces to (20.3) when the longitudinal eddy diffusivity tends to zero ($K_x \rightarrow 0$).

The two-dimensional time-dependent advection–diffusion equation is $\frac{\partial \bar{C}}{\partial t} + u\frac{\partial \bar{C}}{\partial x} = \frac{\partial}{\partial z}\left(K_z \frac{\partial \bar{C}}{\partial z}\right)$ for $0 < z < z_i$, $x > 0$, and $t > 0$, subject to the boundary conditions $K_z \frac{\partial \bar{C}}{\partial z} = 0$ at $z = 0, z_i$, the source condition $\bar{C}(0,z,t) = \frac{Q}{u}\delta(z - H_s)$ at $x = 0$, and the initial condition $\bar{C}(x,z,0) = 0$ at $t = 0$. The solution of this system is

$$\bar{C}_n = \sum_{i=1}^{k} a_i \frac{p_i}{t} \sum_{j=1}^{m} a_j \frac{p_j}{x} \left[A_n e^{-R_n z} + B_n e^{R_n z} - \frac{QR_b}{R_a} \cosh\left(R_n(z - H_s)\right) H(z - H_s) \right], \tag{20.4}$$

where $R_n = \sqrt{\frac{p_i}{tK_{zn}} + \frac{u_n p_j}{K_{zn} x}}$ and $R_a = \sqrt{\frac{p_i}{t} K_{zn} + u_n K_{zn} \frac{p_j}{x}}$. Solution (20.4) reduces to (20.3) as time tends to infinity.

Consider the advection–diffusion equation including a decaying contaminant (i.e., a radioactive contaminant) emission as source term ($S = -\lambda \bar{C}$).

The dynamical equation is

$$\frac{\partial \bar{C}}{\partial t} + u\frac{\partial \bar{C}}{\partial x} + w\frac{\partial \bar{C}}{\partial z} = \frac{\partial}{\partial x}\left(K_x \frac{\partial \bar{C}}{\partial x}\right) + \frac{\partial}{\partial z}\left(K_z \frac{\partial \bar{C}}{\partial z}\right) - \lambda \bar{C}$$

for $0 < z < z_i$, $x > 0$, and $t > 0$, with λ the decay constant, and subject to the boundary conditions $K_z \frac{\partial \bar{C}}{\partial z} = 0$ at $z = 0, z_i$, the source condition $\bar{C}(0, z, t) = \frac{Q}{u}\delta(z - H_s)$ at $x = 0$, and the initial condition $\bar{C}(x, z, 0) = 0$ at $t = 0$. Application of the previous procedure leads to solution (20.4), but with $R_n = \frac{w_n}{2K_{zn}} \pm \frac{1}{2}\sqrt{\left(\frac{w_n}{2K_{zn}}\right)^2 + \frac{4}{K_{zn}}\left[p - \alpha + su_n\left(1 - \frac{K_{xn}s}{u_n}\right)\right]}$, $R_b = 1 - \frac{p_j}{P_e}$, and $R_a = \sqrt{w_n^2 + 4K_{zn}\left[p - \alpha + su_n\left(1 - \frac{K_{xn}s}{u_n}\right)\right]}$. This solution reduces to (20.3) as $K_x \to 0$, $t \to \infty$, and $\alpha = w = 0$.

20.4 Advection–Diffusion Considering Non-Fickian Turbulence Closure

The downgradient transport hypothesis is often inconsistent with observed features of turbulent diffusion in the upper portion of the mixed layer, where countergradient material fluxes are known to occur [Dea75]. In the sequel, we report the solution of the advection–diffusion equation considering nonlocal effects in the turbulence closure.

The one-dimensional time-dependent equation reads as $\frac{\partial \bar{C}}{\partial t} = -\frac{\partial \overline{w'c'}}{\partial z}$ for $0 < z < z_i$ and $t > 0$, assuming the non-Fickian closure of turbulence $\left[1 + \left(\frac{S_k T_{L_w} \sigma_w}{2}\right)\frac{\partial}{\partial z} + \tau\frac{\partial}{\partial t}\right]\overline{w'c'} = -K_z \frac{\partial \bar{C}}{\partial z}$ proposed by van Dop and Verver [Van03]. Here S_k is the skewness, T_{L_w} is the vertical Lagrangian time scale, σ_w is the vertical turbulent velocity variance, and τ is the relaxation time. Then the resulting dynamics is

$$\tau\frac{\partial^2 \bar{C}}{\partial t^2} + \frac{\partial \bar{C}}{\partial t} + \left(\frac{S_k T_{L_w} \sigma_w}{2}\right)\frac{\partial^2 \bar{C}}{\partial t \partial z} = \frac{\partial}{\partial z}\left(K_z \frac{\partial \bar{C}}{\partial z}\right),$$

subject to the boundary conditions $K_z \frac{\partial \bar{C}}{\partial z} = 0$ at $z = 0, z_i$ and the initial condition $\bar{C}(z, 0) = Q\delta(z - H_s)$ at $t = 0$. The solution of this system uses $H = H(z - H_s)$ and is given by

$$\bar{C}_n = \sum_{i=1}^{k} a_j \frac{p_i}{t} e^{F_N^*(z - H_s)}\left[A_n e^{R_n^* z} + B_n e^{-R_n^* z} - \frac{\tau P_j Q}{R_a^*}\cosh\left(R_n^*(z - H_s)\right) H\right], \tag{20.5}$$

where $R_n^* = \frac{\sqrt{\beta_n^2 p_i^2 + 4K_{zn} p_i(\tau p_i + t)}}{2K_{zn} t}$, $R_a^* = \sqrt{\beta_n^2 p_i^2 + 4K_{zn} p_i(\tau p_i + t)}$, $F_n^* = \frac{\beta p_i}{2K_{zn} t}$, and $\beta_n = \frac{S_k \sigma_w T_{L_w}}{2}$. Solution (20.5) reduces to (20.2) as β_n and τ tend to zero.

Finally, we analyze the solution of $u\frac{\partial \bar{C}}{\partial x} = -\frac{\partial \overline{w'c'}}{\partial z}$, assuming the non-Fickian closure of turbulence as in the preceding case but with $\tau = 0$:

$$u\frac{\partial \bar{C}}{\partial x} + \frac{\partial}{\partial z}\left(\frac{uS_kT_{L_w}}{2}\frac{\partial \bar{C}}{\partial x}\right) = \frac{\partial}{\partial z}\left(K_z\frac{\partial \bar{C}}{\partial z}\right)$$

for $0 < z < z_i$ and $x > 0$, subject to the boundary conditions $K_z\frac{\partial \bar{C}}{\partial z} = 0$ at $z = 0, z_i$ and the source condition $\bar{C}(0,z) = \frac{Q}{u}\delta(z - H_s)$ at $x = 0$. The solution is

$$\bar{C}_n = \sum_{i=1}^{m} a_i \frac{p_i}{x} e^{F_n^* z}\left[A_n e^{R_n^* z} + B_n e^{-R_n^* z} - \frac{Q}{R_a^*}\cosh\left(R_n^*(z - H_s)\right) H(z - H_s)\right], \tag{20.6}$$

where $R_n^* = \frac{1}{2}\sqrt{\left(\frac{\beta_n p_i}{K_{zn}x}\right)^2 + \frac{4u_n p_i}{K_{zn}x}}$, $R_a^* = \sqrt{\beta_n^2 p_i^2 + 4K_{zn}p_i(\tau p_i + t)}$, $F_n^* = \frac{\beta p_i}{2K_{zn}t}$, and $\beta_n = \frac{u_n S_k \sigma_w T_{L_w}}{2}$. Here solution (20.6) reduces to (20.3) as $\beta_n \to 0$.

20.5 Model Performance Evaluation Against Experimental Data

In order to illustrate the aptness of the discussed formulation to simulate contaminant dispersion in the PBL, we evaluate the performance of solution (20.4) against experimental crosswind ground-level concentration using tracer SF6 data from two different dispersion experiments. The first one, carried out in the northern part of Copenhagen, is described in [Gry87]. The tracer was released without buoyancy from a tower at a height of 115 m and was collected at the ground-level positions at a maximum of three crosswind arcs of tracer sampling units. The sampling units were positioned at 2 to 6 km from the point of release. The site was mainly residential with a roughness length of 0.6 m. The PBL was parameterized assuming the eddy diffusivity proposed by [Deg01], that is, $K_z = 0.55\sigma_w z/(4(f_m^*)_w)$, where $(f_m^*)_w$ is the vertical normalized frequency of spectral peak and σ_w is the vertical wind velocity variance. The wind speed profile has been parameterized following the similarity theory of Monin–Obukhov [Ber86]: $u(z) = \frac{u^*}{k}\left[\ln(z/z_0) - \Psi_m(z/L) + \Psi_m(z_0/L)\right]$ if $z \le z_b$, $u(z) = u(z_b)$ if $z > z_b$, where $z_b = \min[|L|, 0.1h]$, Ψ_m is a stability function given by $\Psi_m = 2\ln((1+A)/2) + \ln((1+A^2)/2) - 2\tan^{-1}A + \pi/2$ with $A = (1 - 16z/L)^{1/4}$, $k = 0.4$ is the Von Karman constant, z_0 is the roughness length, u_* is the friction velocity, and L is the Monin–Obukhov length.

Figure 20.1 (left) shows the scatter diagrams between the measured and predicted crosswind integrated concentrations using the above parameterizations for wind and eddy diffusivities profiles. A good agreement is observed between the results.

The modulus of the real part of the root of the Gaussian quadrature scheme for the Laplace transform inversion increases with N (the order of

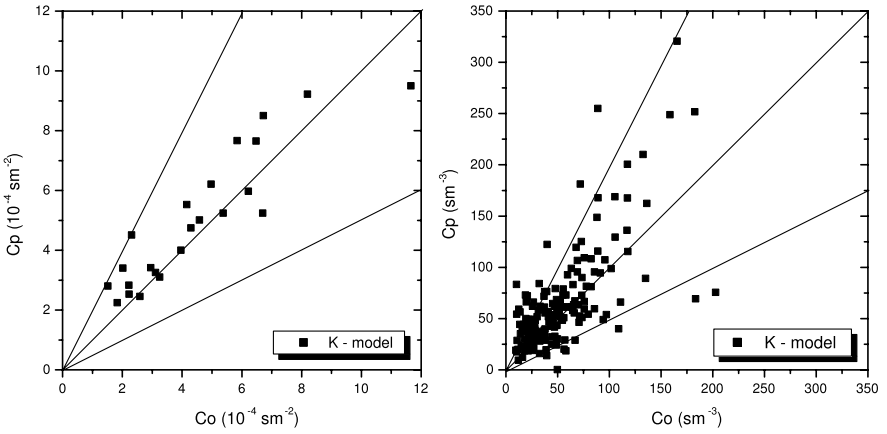

Fig. 20.1. The scatter diagram for the semi-analytical solution (20.4) for the Copenhagen experiment (left) and the Kinkaid experiment (right): observed (Co) and predicted (Cp) crosswind ground-level integrated concentration ($k = 2, m = 8, \Delta z = 40$ m). Points between lines diverge by less than a factor of 2.

the approximation). The solution for the Laplace-transformed concentration has exponential terms; we observed from numerical simulation the appearance of overflows for a positive argument of the exponential and underflow for a negative argument when k and m assume values larger than 8 (on a PC with 32-bit precision). With this restriction, we get results with good statistical accuracy.

One observes that the curves for concentrations in Figure 20.2, especially for the lower time values with the increase of the quadrature points, present a nonphysical oscillatory behavior except for $k = 2$. In Figure 20.3, we show the dimensionless ground-level concentration $C = \bar{C}uz_i/Q$ as a function of the dimensionless time $t^* = tw_*/z_i$ for the source distances $x = 1000$ m and $x = 3000$ m, considering $k = 2$ and $m = 8$; we observed that the steady-state concentration field is obtained as t^* tends to infinity.

In Figure 20.4, we present an analysis of the influence of the number of quadrature points on the solution. Figure 20.4(a) shows the result for the stationary problem (20.3) as a function of the number of quadrature points with its numerical convergence of the results encountered for dimensionless ground-level concentration as a function of the quadrature points m. In Figure 20.4(b), we display the results for problem (20.4) for a steady-state condition. Finally, note the small oscillations of the concentration in Figure 20.4(b), caused by overflow and underflow. The behavior of the solution can be improved by using multiple precision methods.

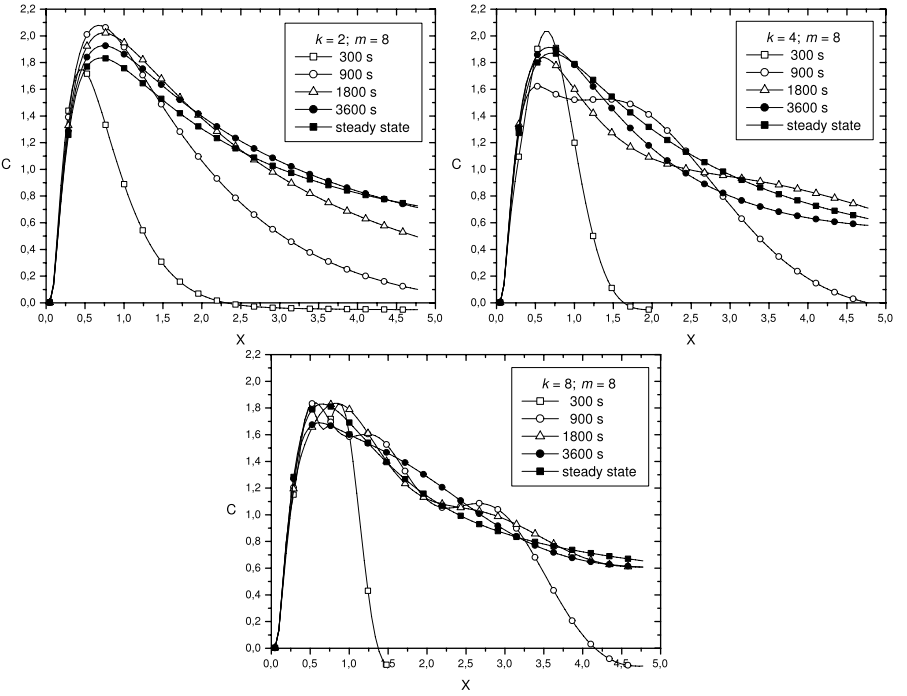

Fig. 20.2. Analysis of the number of quadrature points for the time-dependent equation (20.4). Concentration as a function of source distance $C = Cuz_i/Q$, $X = xw_*/uz_i$.

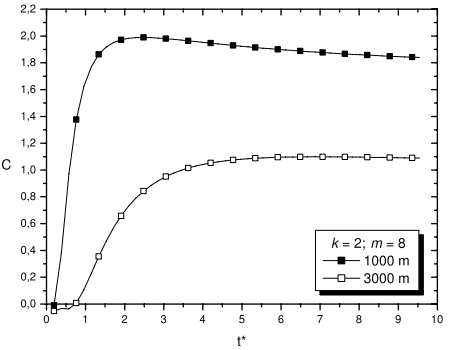

Fig. 20.3. Plot of nondimensional concentration as a function of dimensionless time ($C = \bar{C}uz_i/Q$, $t^* = tw_*/z_i$).

20.6 Conclusions

We semi-analytically solved the Eulerian advection–diffusion equation in the PBL using the Laplace transformation technique. No approximation is made

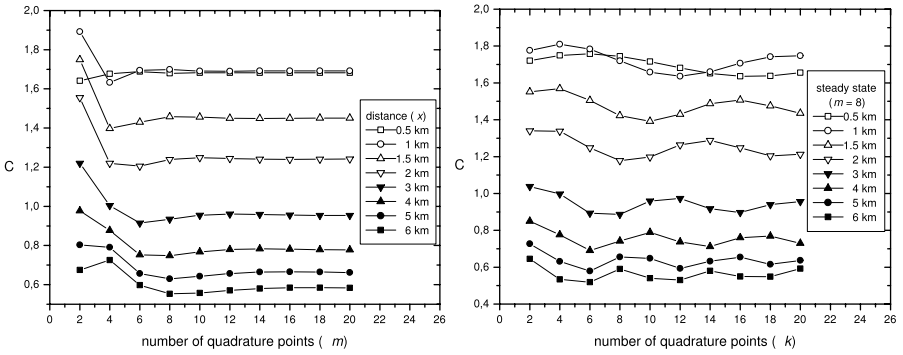

Fig. 20.4. Analysis of the number of quadrature points: (a) for (20.3); (b) steady-state condition in (20.4).

in its derivation except for the stepwise approximation of the parameters and the Laplace numerical inversion by the Gaussian quadrature scheme. It is well known that the results obtained by the Gaussian quadrature scheme of order N are exact when the transformed function is a polynomial of degree $2N-1$. On the other hand, from the Weierstrass approximation theorem, it is known that a continuous function can be approximated by a polynomial, and that the approximation improves with the increase of the degree of the polynomial. This means that increasing k and m in the Gaussian quadrature schemes for the concentration solution, one expects the numerical results to converge to the exact result. The error estimation from numerical results with $k+1$ and k points of quadrature and for $m+1$ and m points permits us to control the error in the Gaussian quadrature scheme by properly choosing k and m, in order to reach a prescribed accuracy.

According to the Lax equivalence theorem for linear problems [Kyt97], the convergence of the numerical schemes demands stability and consistency. To accomplish the stability conditions, the numerical methods impose a large number of step calculations, performing the time integration for most times. Our solution allows us to perform the calculation at any time. This fact justifies the smaller computational time as well as the smaller round-off error influence in the accuracy of the results when compared with the numerical ones. The above arguments and the good agreement between the semi-analytical results and experimental data make us confident that our hybrid method is a robust approach for simulating the pollutant dispersion in the PBL.

Acknowledgement. The authors thank CNPq and FAPERGS for the partial financial support of this work.

References

[Ber86] Berkovicz, R.R., Olesen, H.R., Torp, U.: The Danish Gaussian air pollution model (OML). In: *Proceedings 15th Internat. Tech. Meeting on Air Pollution Modeling and Its Applications V,* Plenum, St. Louis, MO (1986).

[Dea75] Deardoff, J.W., Willis, G.E.: A parameterization of diffusion into the mixed layer. *J. Appl. Meteorol.,* **14**, 1451–1458 (1975).

[Deg01] Degrazia, G.A., Moreira, D.M., Vilhena, M.T.: Derivation of an eddy diffusivity depending on source distance for vertically inhomogeneous turbulence in a Convective Boundary Layer. *J. Appl. Meteorol.,* **40**, 1233–1240 (2001).

[Gry87] Gryning, S.E., Holtslag, A.A.M., Irwin, J.S., Siversteen, B.: Applied dispersion modelling based on meteorologing scaling parameters. *Atmos. Environ.,* **21**, 79–89 (1987).

[Han89] Hanna, S.R., Paine, R.J.: Hibrid plume dispersion model (HPDM) development and evaluation, *J. Appl. Meteorol.,* **28**, 206–224 (1989).

[Kyt97] Kythe, P.K., Puri, P., Schferkotter, M.R.: *Partial Differential Equations and Mathematics.* CRC Press, Boca Raton, FL (1997).

[Mor99] Moreira, D.M., Degrazia, G.A., Vilhena, M.T.: Dispersion from low sources in a convective boundary layer: an analytical model. *Il Nuovo Cimento,* **22C**, 685–691 (1999).

[Str66] Stroud, A.H., Secrest, D.: *Gaussian Quadrature Formulas.* Prentice Hall, Englewood Cliffs, NJ (1966).

[Tir03] Tirabassi, T.: Operational advanced air pollution modeling. *Pure Appl. Geophys.,* **160**, 5–16 (2003).

[Van03] van Dop, H., Verver, G.: Countergradient transport revisited. *J. Atmos. Sci.,* **58**, 2240–2247 (2001).

[Vil98] Vilhena, M.T., Rizza, U., Degrazia, G.A., Mangia, C., Moreira, D.M., Tirabassi, T.: An analytical air pollution model: development and evaluation. *Control Atmos. Phys.,* **71**, 315–320 (1998).

[Zan90] Zanetti, P.: *Air Pollution Modeling.* Computational Mechanics Publications, Southampton (1990).

21

On Quasimodes for Spectral Problems Arising in Vibrating Systems with Concentrated Masses

E. Pérez

Universidad de Cantabria, Santander, Spain; meperez@unican.es

21.1 Introduction

*Q*uasimodes for positive, symmetric, and compact operators on Hilbert spaces arise often in the literature in the description of behavior at high-frequency vibrations (see, for example, [Arn72], [BB91], [Laz99], and [Per03]). Roughly speaking, the quasimodes u can be defined as functions approaching a certain linear combination of eigenfunctions associated with eigenvalues in "small intervals" $[\lambda - r, \lambda + r]$. Their usefulness in describing asymptotics for low frequency vibrations in certain singularly-perturbed spectral problems has been made clear recently in many papers (see [LP03], [Per04], [Per05], [Per06], and [Per07]).

In this chapter, we consider a vibrating system with concentrated masses. Namely, we consider the vibrations of a body occupying a domain Ω of $\mathbb{R}^n$, $n = 2, 3$, that contains many small regions (B^ε) of high density—so-called *concentrated masses*—near the boundary. The small parameter ε deals with the size of the masses, their number, and their densities. The asymptotic behavior, as $\varepsilon \to 0$, of the eigenelements $(\lambda^\varepsilon, u^\varepsilon)$ of the corresponding spectral problem, namely problem (21.3), when $\lambda^\varepsilon = O(\varepsilon^{m-2})$, has been treated in [Per04] (see [LP03] for a substantial list of references on the subject). Here, considering the hyperbolic problem (21.15), we provide estimates for the time t in which certain *standing waves* approach time-dependent solutions when the initial data are quasimodes. Also, precise bounds for the discrepancies between the solutions and standing waves in suitable Hilbert spaces are provided. The results can be extended to high-frequency vibrations.

It should be mentioned that in certain problems arising in spectral perturbation theory, the eigenfunctions associated with low frequencies give rise to vibrations of the system that are concentrated asymptotically in a certain region, and that it is possible to construct quasimodes associated with high frequencies that give rise to other kinds of vibrations. This is the case, for instance, with spectral stiff problems [LP97] or vibrating systems with a single concentrated mass (see [GLP99] and [Per03]).

Nevertheless, when the low frequencies converge toward the same positive value μ (see [LP03], [Per05], and [Per07]), it can be difficult to describe the asymptotic behavior, as $\varepsilon \to 0$, of the individual eigenfunctions and to obtain asymptotics for the first eigenfunction. In some of these problems, quasimodes $\widetilde{u}^\varepsilon$ that provide an approach to linear combinations of eigenfunctions associated with all the eigenvalues in intervals $[\mu - \delta^\varepsilon, \mu + \delta^\varepsilon]$, with $\delta^\varepsilon \to 0$ as $\varepsilon \to 0$, can be constructed. These quasimodes could concentrate asymptotically their support or their energy at points or thin layers. This happens, for example, when describing vibrations of systems with many concentrated masses near the boundary (see [LP03], [Per05], and [Per06]), or in models from geophysics ([BI06] and [Per07]).

For these vibrating systems, given the quasimode as an initial data, the solution of the evolution problem behaves as a standing wave affecting only small regions for a long period of time, which we determine in this chapter. Here we prove that, when considering the evolution problem (21.15), for a long time, namely, for $t \in [0, O((\delta^\varepsilon)^{-\delta})]$ with some positive δ, the solutions of (21.15) are approached through standing waves of the type $e^{\mathrm{i}\sqrt{\mu}t}\widetilde{u}^\varepsilon$. It turns out that the results hold for any eigenvalue μ of the local problem (21.4).

We emphasize that the results in this chapter can be stated in a more general abstract framework and extend to low-frequency and high-frequency vibrations of other vibrating systems (see [LP01], [LP03], [Per03], [Per04], and [Per06]). We also note that these results are very different from those in [LP93] and [LP95b], where the evolution problem (21.15) is used to derive results on spectral convergence for low frequencies, which are much weaker than those in Theorem 2.

Section 21.2 contains preliminary results on quasimodes for problem (21.3). Proofs of these results can be found in [Per04], [Per05], and [Per06]. Section 21.3 contains new results on the ε-dependent evolution problem (21.15) (see Theorem 3 and Remark 1). For brevity, we sketch only an idea of the proof.

21.2 The Spectral Problem

Let $\mathcal{A} : \mathbf{H} \longrightarrow \mathbf{H}$ be a linear, self-adjoint, positive, and compact operator on a separable Hilbert space $\mathbf{H}$. Let $\{\lambda_i^{-1}\}_{i=1}^\infty$ be the set of positive eigenvalues with the usual convention for repeated eigenvalues, $\lambda_i \to \infty$ as $i \to \infty$. Let $\{u_i\}_{i=1}^\infty$ be the set of eigenfunctions, which form an orthonormal basis for $\mathbf{H}$.

A *quasimode with remainder* $r > 0$ *for the operator* $\mathcal{A}$ is a pair $(u, \mu) \in \mathbf{H} \times \mathbb{R}$, with $||u||_H = 1$ and $\mu > 0$, such that $||\mathcal{A}u - \mu u||_{\mathbf{H}} \leq r$. If there is no ambiguity, u is also referred to as a quasimode.

The following result establishes the closeness in the space $\mathbf{H} \times \mathbb{R}$ of the eigenelements of the operator $\mathcal{A}$ to a given quasimode of $\mathcal{A}$ (see, for example, [OSY92] for a proof, and [Laz99] for a more general statement).

Theorem 1. *Given a quasimode (u, μ) with remainder r for $\mathcal{A}$, in each interval $[\mu - r^*, \mu + r^*]$ containing $[\mu - r, \mu + r]$, there are eigenvalues of the operator $\mathcal{A}$, $\{\lambda^{-1}_{i(r^*)+k}\}_{k=1,2,\ldots,I(r^*)}$ for some index $i(r^*)$ and number $I(r^*) \geq 1$. In addition, there is $u^* \in \mathbf{H}$, $\|u^*\|_{\mathbf{H}} = 1$, $u^* = \sum_{k=1}^{I(r^*)} \alpha_k u_{i(r^*)+k}$ for certain constants α_k, and satisfying*

$$\|u - u^*\|_{\mathbf{H}} = \|u - \sum_{k=1}^{I(r^*)} \alpha_k u_{i(r^*)+k}\|_{\mathbf{H}} \leq \frac{2r}{r^*}. \tag{21.1}$$

From the literature on spectral perturbation problems it appears that, when Theorem 1 is applied, the spaces and operators under consideration often depend on a small parameter ε that converges to 0. Also, the function u and the numbers λ and r arising in the definition of a quasimode depend on this parameter. This is the case of the operators associated with vibrating systems with concentrated masses, namely, problem (21.3), which we study in this chapter. For the sake of completeness, in Subsection 21.2.1 we gather certain results on quasimodes for this problem (21.3), used subsequently in the proof of the results in Section 21.3.

21.2.1 The Spectral Perturbation Problem

Let Ω be a bounded domain of $\mathbb{R}^n$, $n = 2, 3$, with a Lipschitz boundary $\partial\Omega$. Let Σ and Γ_Ω be nonempty parts of the boundary such that $\partial\Omega = \bar{\Sigma} \cup \bar{\Gamma}_\Omega$; Σ is assumed to be in contact with $\{x_n = 0\}$. Let ε and η be two small parameters such that $\varepsilon \ll \eta$ and $\eta = \eta(\varepsilon) \to 0$ as $\varepsilon \to 0$.

For $n = 2$, let B be the semicircle $B = \{(y_1, y_2) \ / \ y_1^2 + y_2^2 < 1, y_2 < 0\}$ in the auxiliary space $\mathbb{R}^2$ with coordinates y_1, y_2. For $n = 3$, let B be the half-ball $B = \{(y_1, y_2, y_3) \ / \ y_1^2 + y_2^2 + y_3^2 < 1, y_3 < 0\}$ in the auxiliary space $\mathbb{R}^3$ with coordinates y_1, y_2, y_3. Let ∂B be the boundary of B, $\partial B = \bar{T} \cup \bar{\Gamma}$, where T is the part lying on $\{y_n = 0\}$. Let B^ε (and, similarly, T^ε, Γ^ε) denote its homothetic εB (εT, $\varepsilon\Gamma$). Let B_k^ε (and, similarly, T_k^ε, Γ_k^ε) denote the domain obtained by the translation of the previous B^ε (T^ε, Γ^ε) centered at the point $\tilde{x}_k$ of Σ at distance η between them. Here k is a parameter ranging from 1 to $N(\varepsilon)$, $k \in \mathbf{N}$. $N(\varepsilon)$ denotes the number of B_k^ε contained in Ω; $N(\varepsilon)$ is $O(\eta^{-1})$ for $n = 2$ and $O(\eta^{-2})$ for $n = 3$. The parameter α denotes the value

$$\alpha = \lim_{\varepsilon \to 0} \frac{-1}{\eta \ln \varepsilon} \text{ for } n = 2 \text{ and } \alpha = \lim_{\varepsilon \to 0} \frac{\varepsilon}{\eta^2} \text{ for } n = 3. \tag{21.2}$$

We consider the eigenvalue problem

$$\begin{cases} -\Delta u^\varepsilon = \rho^\varepsilon \lambda^\varepsilon u^\varepsilon & \text{in } \Omega, \\ u^\varepsilon = 0 & \text{on } \Gamma_\Omega \cup \bigcup T^\varepsilon, \\ \frac{\partial u^\varepsilon}{\partial n} = 0 & \text{on } \Sigma - \overline{\bigcup T^\varepsilon}, \end{cases} \tag{21.3}$$

where $\rho^\varepsilon = \rho^\varepsilon(x)$ is the density function defined by

$$\rho^\varepsilon(x) = \frac{1}{\varepsilon^m} \text{ if } x \in \bigcup B^\varepsilon, \quad \rho^\varepsilon(x) = 1 \text{ if } x \in \Omega - \overline{\bigcup B^\varepsilon},$$

the symbol $\bigcup$ is extended, for fixed ε, to all the regions B_k^ε contained in Ω, and the parameter m is a real number, $m > 2$ (see [LP93]–[LP95b] for different values of the parameter m, boundary conditions, and domain shapes).

As is well known, problem (21.3) has a discrete spectrum. For fixed ε, let $\{\lambda_i^\varepsilon\}_{i=1}^\infty$ be the sequence of eigenvalues of (21.3), converging to ∞, with the classical convention for repeated eigenvalues. It has been proved (see [LP93]–[LP95b]) that they satisfy the estimates $C\varepsilon^{m-2} \le \lambda_i^\varepsilon \le C_i\varepsilon^{m-2}$, where C is a constant independent of ε and i and C_i is a constant independent of ε. Let $\{u_i^\varepsilon\}_{i=1}^\infty$ be the corresponding sequence of eigenfunctions, which is an orthogonal basis for the space $\mathbf{V}^\varepsilon$, where $\mathbf{V}^\varepsilon$ is the completion of $\{u \in \mathcal{D}(\bar{\Omega}) \,/\, u = 0 \text{ on } \Gamma_\Omega \cup \bigcup T^\varepsilon\}$ in the topology of $H^1(\Omega)$.

Convergence results for *the low frequencies*, the eigenvalues of order $O(\varepsilon^{m-2})$ of (21.3), and the associated eigenfunctions can be found in [Per04], [Per05], and [Per06]. Also, the limit behavior of the eigenelements for sequences of eigenvalues of order $O(1)$, the so-called *high frequencies*, is in [LP93], [LP95a], [LP95b], and [LP01]. As in the case of a single concentrated mass, in general, low frequencies are associated with *the local vibrations* of the concentrated masses, each one independent of the others. We have found only one exception: For $n = 3$ and $\alpha > 0$, these frequencies also give rise to *global vibrations* affecting the whole structure ([LP03]). Apart from this exception, the low frequencies and the corresponding eigenfunctions are asymptotically described, in a certain way, by a so-called *local eigenvalue problem* (21.4).

The local problem is posed in $\mathbb{R}^{n-} = \{y \in \mathbb{R}^n \,/\, y_n < 0\}$ as follows:

$$\begin{cases} -\Delta_y U = \lambda U \text{ in } B, \\ -\Delta_y U = 0 \text{ in } \mathbb{R}^{n-} - \bar{B}, \\ [U] = [\frac{\partial U}{\partial n_y}] = 0 \text{ on } \Gamma, \\ U = 0 \text{ on } T \ , \ \frac{\partial U}{\partial y_n} = 0 \text{ on } \{y_n = 0\} - \bar{T}, \\ U(y) \to c, \text{ as } |y| \to \infty \ , \ y_n < 0 \text{ when } n = 2, \\ U(y) \to 0, \text{ as } |y| \to \infty \ , \ y_n < 0 \text{ when } n = 3\,, \end{cases} \tag{21.4}$$

where the brackets denote the jump across Γ, $\bar{n}_y$ is the unit outward normal to Γ, and c is some unknown but well-defined constant. The variable y is the *local variable*:

$$y = \frac{x - \tilde{x}_k}{\varepsilon}.$$

Problem (21.4) can be written as a standard eigenvalue problem with a discrete spectrum in the space $\widetilde{\mathcal{V}}$, where $\widetilde{\mathcal{V}}$ is the completion of $\{U \in \mathcal{D}(\overline{\mathbb{R}^{n-}}) \,/\, U = 0 \text{ on } T\}$ in the Dirichlet norm $\|\nabla_y U\|_{L^2(\mathbb{R}^{n-})}$ (see [LP93] and [LP95b]).

Theorem 2 allows us to assert that there are at least $l_0 N(\varepsilon)$ values $\lambda^\varepsilon_{i(\varepsilon)}/\varepsilon^{m-2}$ converging to each eigenvalue λ^0 of (21.4), with l_0 being the multiplicity of λ^0. The corresponding eigenfunctions U^ε [cf. (21.5)] are approached in the space $\widetilde{\mathbf{V}}^\varepsilon$ by the eigenfunctions of (21.4) associated with λ^0, concentrating their support asymptotically in neighborhoods of the concentrated masses as stated in Theorem 2.

Also, the results in Theorem 2 along with the results on comparison of spectra for perturbed domains in [Per05] allow us to obtain an important difference for the asymptotic behavior of the low frequencies between the dimensions $n = 2$ and $n = 3$ of the space. Namely, for $n = 2$, and for each $i = 1, 2, \ldots$, $\lambda^\varepsilon_i/\varepsilon^{m-2} \to \lambda^0_1$, as $\varepsilon \to 0$, where λ^0_1 is the first eigenvalue of (21.4). This does not hold for $n = 3$ and the value of α in (21.2) strictly positive (see [Per05] and [Per06] for further explanations). Let us refer to [GLP99], [OSY92], and [SS89] to compare with the stronger results on the approach for the eigenfunctions in the case of a single concentrated mass, the case where the convergence of the rescaled spectrum of (21.3) to that of (21.4) with conservation of multiplicity holds.

Let us change the variable in (21.3) by setting $y = x/\varepsilon$. We obtain:

$$\int_{\Omega_\varepsilon} \nabla_y U^\varepsilon . \nabla_y V^\varepsilon \, dy = \frac{\lambda^\varepsilon}{\varepsilon^{m-2}} \int_{\Omega_\varepsilon} \beta^\varepsilon(y) U^\varepsilon V^\varepsilon \, dy, \quad \forall\, V^\varepsilon \in \widetilde{\mathbf{V}}^\varepsilon, \tag{21.5}$$

with Ω_ε being the domain $\{\, y \,/\, \varepsilon y \in \Omega \,\}$ and $\beta^\varepsilon(y)$ in (21.5) defined as

$$\beta^\varepsilon(y) = 1 \text{ if } y \in \bigcup \tau_y B^\varepsilon, \quad \text{and } \beta^\varepsilon(y) = \varepsilon^m \text{ if } y \in \Omega_\varepsilon - \overline{\bigcup \tau_y B^\varepsilon}, \tag{21.6}$$

where $\tau_y B^\varepsilon$ denote the transformed domains of the regions B^ε to the y variable. $\widetilde{\mathbf{V}}^\varepsilon$ is the functional space $\{U = U(y) \,/\, U(\varepsilon y) \in \mathbf{V}^\varepsilon\}$. We assume that the eigenfunctions $\{U^\varepsilon_i\}_{i=1}^\infty$, in the local variable, satisfy $\|U^\varepsilon\|_{\widetilde{\mathbf{V}}^\varepsilon} = 1$.

Let us introduce the self-adjoint positive and compact operator $\mathcal{A}^\varepsilon$ on $\widetilde{\mathbf{V}}^\varepsilon$, $\mathcal{A}^\varepsilon$ defined by the right-hand side of (21.5), namely,

$$\langle \mathcal{A}^\varepsilon U, V \rangle_{\widetilde{\mathbf{V}}^\varepsilon} = \int_{\bigcup \tau_y B^\varepsilon} UV \, dy + \varepsilon^m \int_{\Omega_\varepsilon - \overline{\bigcup \tau_y B^\varepsilon}} UV \, dy, \; \forall U, V \in \widetilde{\mathbf{V}}^\varepsilon, \tag{21.7}$$

with eigenelements $\{(\varepsilon^{m-2}/\lambda^\varepsilon_i, U^\varepsilon_i)\}_{i=1}^\infty$.

Let us consider λ^0 an eigenvalue of (21.4) of multiplicity l_0, and let U^0_1, $U^0_2, \ldots, U^0_{l_0}$ be the corresponding eigenfunctions, orthogonal in $\widetilde{\mathcal{V}}$ and satisfying $\|\nabla_y U^0_i\|_{L^2(\mathbb{R}^{n-})} = 1$.

Let us introduce a function $\widetilde{\varphi}^\varepsilon(y)$ that depends on n. For $n = 2$, we consider $R_\varepsilon = \sqrt{\frac{\varepsilon + \eta/4}{\varepsilon}}$ and define $\widetilde{\varphi}^\varepsilon(y) = 0$ if $|y| \geq R^2_\varepsilon$,

$$\widetilde{\varphi}^\varepsilon(y) = 1 \;\text{ if }\; |y| \leq R_\varepsilon, \;\; \widetilde{\varphi}^\varepsilon(y) = 1 - \frac{\ln|y| - \ln R_\varepsilon}{\ln R_\varepsilon} \;\text{ if }\; R_\varepsilon \leq |y| \leq R^2_\varepsilon. \tag{21.8}$$

For $n = 3$, we consider $\tilde{\varphi}^\varepsilon$ as a smooth function that takes the value 1 in the semi-ball of radius $((\varepsilon+\eta/8)/\varepsilon)$, $B((\varepsilon+\eta/8)/\varepsilon)$, and is 0 outside the semi-ball of radius $((\varepsilon+\eta/4)/\varepsilon)$, $B((\varepsilon+\eta/4)/\varepsilon)$:

$$\tilde{\varphi}^\varepsilon(y) = \varphi\left(2\frac{|\varepsilon y| - \varepsilon}{\eta}\right), \tag{21.9}$$

where $\varphi \in C^\infty[0,1]$, $0 \le \varphi \le 1$, $\varphi = 1$ in $[0,1/4]$, and $Supp(\varphi) \subset [0,1/2]$.

Obviously, the elements of $\widetilde{\mathbf{V}}^\varepsilon$ extended by zero in $\mathbb{R}^{n-} - \overline{\Omega_\varepsilon}$ are elements of $\widetilde{\mathcal{V}}$. Moreover, we have (see [LP93] and [LP95b]) that $U_p^0\widetilde{\varphi}^\varepsilon \in \widetilde{\mathbf{V}}^\varepsilon$, and, as $\varepsilon \to 0$, $U_p^0\widetilde{\varphi}^\varepsilon \longrightarrow U_p^0$ in $\widetilde{\mathcal{V}}$.

For each $k = 1, 2, \ldots, N(\varepsilon)$, $p = 1, 2, \ldots, l_0$, we introduce the function

$$Z_{k,p}^\varepsilon(y) = \frac{U_p^0(y - \frac{\tilde{x}_k}{\varepsilon})\tilde{\varphi}^\varepsilon(y - \frac{\tilde{x}_k}{\varepsilon})}{\|\nabla_y(U_p^0\tilde{\varphi}^\varepsilon)\|_{L^2(\mathbb{R}^{n-})}}. \tag{21.10}$$

The following estimates hold (see [Per04] and [Per06] for a proof):

$$\|\mathcal{A}^\varepsilon Z_{k,p}^\varepsilon - \frac{1}{\lambda^0} Z_{k,p}^\varepsilon\|_{\widetilde{\mathbf{V}}^\varepsilon} \le o_\varepsilon\,, \quad \forall k, p, \tag{21.11}$$

where o_ε does not depend on k and p and tends to 0 as $\varepsilon \to 0$,

$$o_\varepsilon = C\left(\ln\frac{\varepsilon+\eta/4}{\varepsilon}\right)^{-1/2} \quad \text{for } n = 2, \tag{21.12}$$

$$o_\varepsilon = C\max\{\left(\frac{\varepsilon}{\eta}\right)^{1/2}, \varepsilon^{m-2}\} \text{ for } n = 3, \tag{21.13}$$

with the constant C independent of ε.

Theorem 2. *Let us consider λ^0 an eigenvalue of (21.4) of multiplicity l_0, and let $U_1^0, U_2^0, \ldots, U_{l_0}^0$ be the corresponding eigenfunctions, assumed to be orthonormal in $\widetilde{\mathcal{V}}$. For any $K > 0$, there is $\varepsilon^*(K)$ such that, for $\varepsilon < \varepsilon^*(K)$, $K < l_0 N(\varepsilon)$, and the interval $[\lambda^0 - d^\varepsilon, \lambda^0 + d^\varepsilon]$ contains eigenvalues of (21.5), $\lambda_{i(\varepsilon)}^\varepsilon/\varepsilon^{m-2}$, with total multiplicity greater than, or equal to, K; d^ε is a certain sequence, $d^\varepsilon \to 0$ as $\varepsilon \to 0$ and the interval $[\lambda^0 - d^\varepsilon, \lambda^0 + d^\varepsilon]$ does not contain other eigenvalues of (21.4) different from λ^0.*

In addition, for any β such $0 < \beta < 1$, and for $d^\varepsilon = (o_\varepsilon)^\beta$, there are $l_0 N(\varepsilon)$ functions, $\{U_{k,p}^\varepsilon\}_{k=1,N(\varepsilon)}^{p=1,l_0}$, $U_{k,p}^\varepsilon \in \widetilde{\mathbf{V}}^\varepsilon$, such that $\|U_{k,p}^\varepsilon\|_{\widetilde{\mathbf{V}}^\varepsilon} = 1$, $U_{k,p}^\varepsilon$ belongs to the eigenspace associated with all the eigenvalues in $[\lambda^0 - d^\varepsilon, \lambda^0 + d^\varepsilon]$, and

$$\|U_{k,p}^\varepsilon - Z_{k,p}^\varepsilon\|_{\widetilde{\mathbf{V}}^\varepsilon} \le 2(o_\varepsilon)^{1-\beta}\,. \tag{21.14}$$

In (21.14), $o_\varepsilon(1)$ is given by (21.12) when $n = 2$ ((21.13) when $n = 3$), $Z_{k,p}^\varepsilon$ is defined by (21.10), and $\widetilde{\varphi}^\varepsilon(y)$ is defined by (21.8) when $n = 2$ ((21.9) when $n = 3$). These functions, $\{U_{k,p}^\varepsilon\}_{k=1,N(\varepsilon)}^{p=1,l_0}$, satisfy the property that for any extracted subset of K functions $\{U_{j_1}^\varepsilon, U_{j_2}^\varepsilon, \ldots, U_{j_K}^\varepsilon\}$, they are linearly independent.

Let us observe that formula (21.11) shows that $(Z^\varepsilon_{k,p}, 1/\lambda^0)$ is a quasimode of remainder o_ε for the operator $\mathcal{A}^\varepsilon$ defined in (21.5)–(21.7). In the same way, according to (21.1), the width of the interval $d^\varepsilon = (o_\varepsilon)^\beta$ in Theorem 2 and the bound in (21.14) provide the closeness of these quasimodes and eigenlements of $\mathcal{A}^\varepsilon$. Theorem 2 has been proved in [Per04] (see also [Per06]) by applying Theorem 1 and results on *almost orthogonality* for the quasimodes.

21.3 The Evolution Problem

Let us consider the set of functional spaces $\widetilde{\mathbf{V}}^\varepsilon$ and $\mathbf{H}^\varepsilon$, where $\widetilde{\mathbf{V}}^\varepsilon$ is introduced in Subsection 21.2.1 with the norm $\|\nabla_y u\|_{L^2(\varepsilon^{-1}\Omega)}$ and $\mathbf{H}^\varepsilon = \{U(y)\,/U(\varepsilon y) \in L^2(\Omega)$ with the norm $\|(\beta^\varepsilon)^{1/2}u\|_{L^2(\varepsilon^{-1}\Omega)}$, β^ε being defined by (21.6). Let A^ε be the operator associated with the form on $\widetilde{\mathbf{V}}^\varepsilon$ arising on the left-hand side of (21.5). Let $(Z^\varepsilon_{k,p}, 1/\lambda^0)$ be the quasimodes constructed in Subsection 21.2.1, for $k = 1, 2, \ldots, N(\varepsilon)$, $p = 1, 2, \ldots, l_0$, from the eigenelement (λ^0, U^0_p) of the local problem (21.4).

Let us consider the hyperbolic problem associated with (21.5):

$$\begin{cases} \dfrac{d^2\mathbf{U}^\varepsilon}{dt^2} + A^\varepsilon \mathbf{U}^\varepsilon = 0 \\ \mathbf{U}^\varepsilon(0) = \varphi^\varepsilon \\ \dfrac{d\mathbf{U}^\varepsilon}{dt}(0) = \psi^\varepsilon \end{cases} \tag{21.15}$$

For initial data $(\varphi^\varepsilon, \psi^\varepsilon) \in \widetilde{\mathbf{V}}^\varepsilon \times \mathbf{H}^\varepsilon$, problem (21.15) has a unique solution, $\mathbf{U}^\varepsilon \in L^\infty(0,\infty,\widetilde{\mathbf{V}}^\varepsilon)$, $\frac{d\mathbf{U}^\varepsilon}{dt} \in L^\infty(0,\infty,\mathbf{H}^\varepsilon)$, satisfying $\mathbf{U}^\varepsilon(0) = \varphi^\varepsilon$, and, for any fixed $T > 0$,

$$\int_0^T \left(\int_{\varepsilon^{-1}\Omega} \nabla_y \mathbf{U}^\varepsilon . \nabla_y \mathbf{\Phi}\, dy - \int_{\varepsilon^{-1}\Omega} \beta^\varepsilon(y) \frac{d\mathbf{U}^\varepsilon}{dt}\, \frac{d\mathbf{\Phi}}{dt}\, dy \right) dt =$$

$$\int_{\varepsilon^{-1}\Omega} \beta^\varepsilon(y) \psi^\varepsilon \mathbf{\Phi}(0)\, dy$$

for any test function $\mathbf{\Phi}$ of the form $\mathbf{\Phi} = \phi(t)V$, where $V \in \widetilde{\mathbf{V}}^\varepsilon$, and $\phi \in C^1([0,T])\,/\,\phi(T) = 0$ (cf. [SS89] and [S80], for instance).

Because of the conservation of energy, for each $t \in R$ we have

$$\|\mathbf{U}^\varepsilon(t)\|_{\widetilde{\mathbf{V}}^\varepsilon} + \left\| \frac{d\mathbf{U}^\varepsilon}{dt}(t) \right\|_{\mathbf{H}^\varepsilon} = \|\varphi^\varepsilon\|_{\widetilde{\mathbf{V}}^\varepsilon} + \|\psi^\varepsilon\|_{\mathbf{H}^\varepsilon}. \tag{21.16}$$

According to the Fourier expansion of $\mathbf{U}^\varepsilon(t)$ in terms of the eigenfunctions of (21.5), for a given $\varphi^\varepsilon = aU^\varepsilon_{i(\varepsilon)}$ and $\psi^\varepsilon = bU^\varepsilon_{i(\varepsilon)}$, with a and b any constants and $U^\varepsilon_{i(\varepsilon)}$ any eigenfunction of (21.5) associated with the eigenvalue $\lambda^\varepsilon_{i(\varepsilon)}/\varepsilon^{m-2}$, the solution of (21.15) is the standing wave

$$\mathbf{U}^\varepsilon(t) = \left(a\,\cos\left(\sqrt{\frac{\lambda^\varepsilon_{i(\varepsilon)}}{\varepsilon^{m-2}}}\,t\right) + b\,\sqrt{\frac{\varepsilon^{m-2}}{\lambda^\varepsilon_{i(\varepsilon)}}}\,\sin\left(\sqrt{\frac{\lambda^\varepsilon_{i(\varepsilon)}}{\varepsilon^{m-2}}}\,t\right)\right) U^\varepsilon_{i(\varepsilon)}.$$

Similarly, for any given data, the functions $U^\varepsilon_{k,p}$ arising in Theorem 2, namely, $\varphi^\varepsilon = \sum_{j=1}^{l_0 N(\varepsilon)} a_j\, U^\varepsilon_{i(\varepsilon)+j}$ and $\psi^\varepsilon = \sum_{j=1}^{l_0 N(\varepsilon)} b_j\, U^\varepsilon_{i(\varepsilon)+k}$ with a_j and b_j constants, the solution of (21.15) is

$$\mathbf{U}^\varepsilon(t) = \sum_{j=1}^{l_0 N(\varepsilon)} \left(a_j \cos\left(\sqrt{\frac{\lambda^\varepsilon_{i(\varepsilon)+j}}{\varepsilon^{m-2}}}\,t\right) + b_j\,\sqrt{\frac{\varepsilon^{m-2}}{\lambda^\varepsilon_{i(\varepsilon)+j}}}\,\sin\left(\sqrt{\frac{\lambda^\varepsilon_{i(\varepsilon)+j}}{\varepsilon^{m-2}}}\,t\right)\right) U^\varepsilon_{i(\varepsilon)+j}.$$

By contrast, in the case where the initial data are the quasimodes of the operator $\mathcal{A}^\varepsilon$ arising in Theorem 2, namely, the $Z^\varepsilon_{k,p}$ associated with the eigenelement (λ^0, U^0_p) of (21.4), for $k = 1, 2, \ldots, N(\varepsilon)$ and $p = 1, 2, \ldots, l_0$, approaching the functions $U^\varepsilon_{k,p}$ (see (21.14)), the solutions of the evolution problem (21.15) are not standing waves or sums of standing waves.

Nevertheless, the following theorem establishes the range of t where the standing wave $\cos(\sqrt{\lambda^0}\,t) Z^\varepsilon_{k,p}$ ($\sqrt{(\lambda^0)^{-1}}\sin(\sqrt{\lambda^0}\,t) Z^\varepsilon_{k,p}$, respectively) approaches the solution $\mathbf{U}^\varepsilon(t)$ of (21.15) for the initial data $(\varphi^\varepsilon, \psi^\varepsilon) = (Z^\varepsilon_{k,p}, 0)$ ($(\varphi^\varepsilon, \psi^\varepsilon) = (0, Z^\varepsilon_{k,p})$, respectively).

Theorem 3. *Let (λ^0, U^0_p) be an eigenelement of (21.4), and let $Z^\varepsilon_{k,p}$ be defined by (21.10) for $k = 1, 2, \ldots, N(\varepsilon)$ and $p = 1, 2, \ldots, l_0$. Let us consider problem (21.15) for $(\varphi^\varepsilon, \psi^\varepsilon) = (Z^\varepsilon_{k,p}, 0)$. Then, for $t > 0$ and sufficiently small ε (namely, $\varepsilon < \varepsilon_0$ with ε_0 independent of t), the unique solution $\mathbf{U}^\varepsilon(t)$ of (21.15) satisfies*

$$\left\| \cos(\sqrt{\lambda^0}\,t) Z^\varepsilon_{k,p} - \mathbf{U}^\varepsilon(t) \right\|_{\widetilde{\mathbf{V}}^\varepsilon} \le C_1\, \max\left((o_\varepsilon)^{1-\beta},\, (o_\varepsilon)^{\beta/2} t \right), \tag{21.17}$$

$$\left\| \sqrt{\lambda^0}\sin(\sqrt{\lambda^0}\,t) Z^\varepsilon_{k,p} + \frac{d\mathbf{U}^\varepsilon}{dt}(t) \right\|_{\mathbf{H}^\varepsilon} \le C_2\, \max\left((o_\varepsilon)^{1-\beta},\, \left((o_\varepsilon)^{\beta/2} t + (o_\varepsilon)^{\beta/2} \right) \right), \tag{21.18}$$

where C_1 and C_2 are constants that may depend on λ^0 but are independent of ε and t, o_ε is defined by (21.12) when $n = 2$ and by (21.13) when $n = 3$, and β is the constant appearing in (21.14), $0 < \beta < 1$.

In the same way, for $(\varphi^\varepsilon, \psi^\varepsilon) = (0, Z^\varepsilon_{k,p})$, the following estimates hold:

$$\left\| \frac{\sin(\sqrt{\lambda^0}\,t)}{\sqrt{\lambda^0}} Z^\varepsilon_{k,p} - \mathbf{U}^\varepsilon(t) \right\|_{\widetilde{\mathbf{V}}^\varepsilon} \le C_1\, \max\left((o_\varepsilon)^{1-\beta},\, (o_\varepsilon)^{\beta/2} t \right), \tag{21.19}$$

$$\left\| \cos(\sqrt{\lambda^0}\,t) Z^\varepsilon_{k,p} - \frac{d\mathbf{U}^\varepsilon}{dt}(t) \right\|_{\mathbf{H}^\varepsilon} \le C_2\, \max\left((o_\varepsilon)^{1-\beta},\, \left((o_\varepsilon)^{\beta/2} t + (o_\varepsilon)^{\beta/2} \right) \right). \tag{21.20}$$

The proof of Theorem 3 is based on (21.16), on the precise bounds (21.11)–(21.14), and on the inequality $\|u\|_{\mathbf{H}^\varepsilon} \leq C\|u\|_{\widetilde{\mathbf{V}}^\varepsilon}\ \forall u \in \mathbf{V}^\varepsilon$, where C is a constant independent of u and ε. For the sake of brevity, we omit the proof, which will be provided in a future publication.

Remark 1. In fact, approaches (21.17)–(21.20) in Theorem 3 hold uniformly for $t \in [0, (o_\varepsilon)^{-\beta\beta'/2}]$ for any constant β' satisfying $0 < \beta' < 1$. Then the bounds on the right-hand side of (21.17)–(21.20) are $C^*(o_\varepsilon)^{\min(1-\beta,\, \beta(1-\beta')/2)}$, where C^* is a constant independent of ε.

Acknowledgement. This work has been partially supported by MEC: MTM2002-07720.

References

[Arn72] Arnold, V.I.: Modes and quasimodes. *Functional Anal. Appl.,* **6(2)**, 94–101 (1972).

[BB91] Babich, V.M., Buldyrev, V.S.: *Short-Wavelength Diffraction Theory. Asymptotic Methods.* Springer, Berlin (1991).

[BI06] Bucur, D., Ionescu, I.: Asymptotic analysis and scaling of friction parameters. *Z. Angew. Math. Phys.,* **57**, 1–15 (2006).

[GLP99] Gómez, D., Lobo, M., Pérez, E.: On the eigenfunctions associated with the high frequencies in systems with a concentrated mass. *J. Math. Pures Appl.,* **78**, 841–865 (1999).

[Laz99] Lazutkin, V.F.: Semiclassical asymptotics of eigenfunctions. In: Fedoryuk, M.V. (ed.), *Partial Differential Equations.* Springer, Heidelberg (1999), pp. 133–171.

[LP93] Lobo, M., Pérez, E.: On vibrations of a body with many concentrated masses near the boundary. *Math. Models Methods Appl. Sci.,* **3**, 249–273 (1993).

[LP95a] Lobo, M., Pérez, E.: Vibrations of a body with many concentrated masses near the boundary: high frequency vibrations. In: Sanchez-Palencia, E. (ed.), *Spectral Analysis of Complex Structures.* Hermann, Paris (1995), pp. 85–101.

[LP95b] Lobo, M., Pérez, E.: Vibrations of a membrane with many concentrated masses near the boundary. *Math. Models Methods Appl. Sci.,* **5**, 565–585 (1995).

[LP97] Lobo, M., Pérez, E.: High frequency vibrations in a stiff problem. *Math. Models Methods Appl. Sci.,* **7**, 291–311 (1997).

[LP01] Lobo, M., Pérez, E.: The skin effect in vibrating systems with many concentrated masses. *Math. Methods Appl. Sci.,* **24**, 59–80 (2001).

[LP03] Lobo, M., Pérez, E.: Local problems for vibrating systems with concentrated masses: a review. *C.R. Mécanique,* **331**, 303–317 (2003).

[OSY92] Oleinik, O.A., Shamaev, A.S., Yosifian, G.A.: *Mathematical Problems in Elasticity and Homogenization.* North-Holland, Amsterdam (1992).

[Per03] Pérez, E.: On the whispering gallery modes on the interfaces of membranes composed of two materials with very different densities. *Math. Models Methods Appl. Sci.,* **13**, 75–98 (2003).

[Per04] Pérez, E.: Vibrating systems with concentrated masses: on the local problem and the low frequencies. In: Constanda, C., Ahues, M., Largillier, A. (eds.), *Integral Methods in Sciences and Engineering: Analytic and Numerical Techniques.* Birkhäuser, Boston (2004), pp. 187–192.

[Per05] Pérez, E.: Spectral convergence for vibrating systems containing a part with negligible mass. *Math. Methods Appl. Sci.,* **28**, 1173–1200 (2005).

[Per06] Pérez, E.: Remarks on vibrating systems with many concentrated masses and vibrating systems with parts of negligible mass. In: Damlamian, A., Lukkasen, D., Meidell, A., Piatnitski, A. (eds.), *Proceedigns of Midnight Sun Narvik Conference on Multiscale Problems and Asymptotic Analysis.* Gakkuto Internat. Ser. Math. Sci. Appl., **20**, pp. 311–323, Gakkotosho, Tokyo (2006).

[Per07] Pérez, E.: On periodic Steklov type eigenvalue problems on half-bands and the spectral homogenization problem. *Discrete Contin. Dyn. Syst. Ser. B,* **7**, 859–883 (2007).

[SS89] Sanchez-Hubert, J., Sanchez-Palencia, E.: *Vibration and Coupling of Continuous Systems. Asymptotic Methods,* Springer, Heidelberg (1989).

[S80] Sanchez-Palencia, E.: *Non-Homogeneous Media and Vibration Theory.* Springer, New York (1980).

22

Two-Sided Estimates for Local Minimizers in Compressible Elasticity

G. Del Piero and R. Rizzoni

Università di Ferrara; dlpgpt@unife.it, rzzrfl@unife.it

22.1 Introduction

In this communication we anticipate some results of a research in progress [DR07], whose purpose is to find necessary conditions and sufficient conditions for local energy minima in finite elasticity. Although our analysis includes both compressible and incompressible continua, this account is restricted to the compressible case.

Consider a three-dimensional continuous body, occupying a region Ω in the reference configuration. Assume that the body is hyperelastic and homogeneous; in other words, assume that there is a strain energy density w which is the same at all points of Ω. The function w is assumed to be frame-indifferent

$$w(F) = w(QF) \quad \text{for all orthogonal } Q \in \mathbb{R}^{3\times 3}, \tag{22.1}$$

and to satisfy the growth conditions

$$\lim_{\det F \to 0^+} w(F) \;=\; \lim_{\|F\|\to+\infty} w(F) \;=\; +\infty\,. \tag{22.2}$$

It is also assumed that there are no body forces, and that no surface tractions act on the free portion $\partial_2\Omega$ of the boundary. Then the strain energy

$$\mathcal{E}(f) \;=\; \int_\Omega w(\nabla f(X))\, dX\,.$$

is in fact the total energy of the body subject to a deformation f. On the constrained portion $\partial_1\Omega$ of the boundary, we prescribe a continuous family $t \mapsto \hat{f}_t$ of boundary conditions, and we consider continuous families $t \mapsto f_t$ of deformations of Ω, such that each f_t satisfies the corresponding boundary condition

$$f_t(X) \;=\; \hat{f}_t(X) \qquad \forall X \in \partial_1\Omega. \tag{22.3}$$

We say that f_t is an *equilibrium configuration* if it is a stationary point for the energy over the set of all deformations that obey the boundary condition

(22.3), and that it is a *minimizing configuration* if it is a local energy minimizer over the same set. Continuous paths made of equilibrium configurations are called *equilibrium paths*, and continuous paths made of minimizing configurations are called *minimizing paths*. The largest minimizing path containing a given minimizing configuration f_t is the *minimizing path from* f_t.

In the paper [DR07] we look for necessary and sufficient conditions for a local minimum, with the purpose of establishing two-sided estimates for minimizing paths. For the specific problem of the axial stretching of an isotropic cylinder made of a Blatz–Ko material, we indeed obtain good improvements of the existing estimates.

Preliminary to our analysis are the choice of a function space as the domain of definition for $\mathcal{E}$, and the choice of a metric giving a precise meaning to the notions of a *continuous path* and of a *local minimum*. A natural regularity assumption for the deformations of a continuum seems to be Lipschitz continuity, which requires that the ratio between the distance before and after deformation be bounded in Ω. The same requirement imposed on the inverse deformation leads to the additional condition that the same ratio be bounded from below by a positive number c_1, and the two conditions together result in the double inequality

$$c_1\,|X_2 - X_1| \;\le\; |f(X_2) - f(X_1)| \;\le\; c_2\,|X_2 - X_1| \qquad \forall X_1, X_2 \in \Omega\,,$$

which defines the set of all *bi-Lipschitz* functions from Ω. This set is denoted by $\mathrm{BLip}(\Omega)$ and is a proper subset of the Sobolev space $W^{1,\infty}(\Omega)$. It is proved in [DR07] that $\mathrm{BLip}(\Omega)$ is open in the topology of $W^{1,\infty}(\Omega)$; this allows one to use a basic tool of the calculus of variations, that is, the expansion of a functional along line segments in $W^{1,\infty}(\Omega)$, to obtain conditions for a minimum. It also suggests as a natural norm the $W^{1,\infty}$-norm

$$\|f\|_{W^{1,\infty}} \;=\; \sup_{X\in\Omega} \,|\, f(X) \,|\, + \;\sup_{X\in\Omega} \,|\, \nabla f(X) \,|\,,$$

with the suprema taken to within sets of measure zero. This norm defines the *weak* minima in the standard sense of the calculus of variations.

22.2 Two-Sided Estimates for a Minimizing Path

Consider a deformation f_0 in $\mathrm{BLip}(\Omega)$ obeying the boundary condition (22.3), and let F_0 be the gradient of f_0. The first and second derivatives of the energy density w at F_0 define the Piola stress tensor $S(F_0)$ and the elasticity tensor $\mathbb{A}(F_0)$, respectively. It is known that necessary conditions for a (local or global) minimum are the vanishing of the first variation of $\mathcal{E}$ and the non-negativeness of the second variation

$$\int_\Omega S(F_0)\cdot\nabla v \; dX \;=\; 0\,, \qquad \int_\Omega \mathbb{A}(F_0)\nabla v\cdot\nabla v\, dX \;\ge\; 0\,, \tag{22.4}$$

for all v in $W^{1,\infty}(\Omega)$ with $v(X) = 0$ on $\partial_1\Omega$, whereas the vanishing of the first variation and the *uniform* Hadamard inequality

$$\int_\Omega \mathbb{A}(F_0)\,\nabla v \cdot \nabla v\, dX \;\geq\; \varepsilon \int_\Omega |\nabla v|^2\, dX\,, \quad \varepsilon > 0\,, \tag{22.5}$$

form a sufficient condition for a local minimum.[1]

In our study, we found it convenient to write the expression of the energy in the current configuration $\omega = f_0(\Omega)$. To do this, we set

$$x = f_0(X)\,, \quad v(X) \;=\; u(f_0(X)) \;=\; u(x)\,,$$

and we use the stress tensor and the elasticity tensor in the current configuration

$$T(F_0) = (\det F_0)^{-1}\,(I \boxtimes F_0)\,S(F_0),$$
$$\mathbb{B}(F_0) = (\det F_0)^{-1}(I \boxtimes F_0)\,\mathbb{A}(F_0)\,(I \boxtimes F_0^T),$$

where $A \boxtimes B$ is the fourth-order tensor such that $(A \boxtimes B)\,H \;=\; AHB^T$ for all second-order tensors H, and $T(F_0)$ is the Cauchy stress tensor. Conditions (22.4) and (22.5) then take the form

$$\int_\omega T(F_0) \cdot \nabla u\; dx \;=\; 0\,, \quad \int_\omega \mathbb{B}(F_0)\nabla u \cdot \nabla u\, dx \geq\; c \int_\omega |\nabla u|^2\, dx\,. \tag{22.6}$$

The equation defines an equilibrium configuration, and the inequality with $c = 0$ is a necessary condition for a minimum. Therefore, an equilibrium configuration F_0 is a local minimizer only if all roots of the eigenvalue problem

$$u \in W^{1,\infty}(\omega): \quad u\big|_{\partial_1\omega} = 0, \quad \int_\omega \mathbb{B}(F_0)\nabla u \cdot \nabla u\, dx \;=\; 0$$

are nonnegative. Using the Gauss–Green formula

$$\int_\omega \mathbb{B}(F_0)\nabla u \cdot \nabla u\, dx = -\int_\omega \operatorname{div}\big(\mathbb{B}(F_0)\nabla u\big) \cdot u\, dx + \int_{\partial\omega} \big(\mathbb{B}(F_0)\nabla u\big) n \cdot u\, dx$$

we transform the problem into

$$u \in W^{1,\infty}(\omega): \;\; u\big|_{\partial_1\omega} = 0, \;\; \operatorname{div}\big(\mathbb{B}(F_0)\big) = 0\,, \;\; \int_{\partial_2\omega} \big(\mathbb{B}(F_0)\nabla u\big) n \cdot u\, dx = 0\,. \tag{22.7}$$

Necessary conditions and sufficient conditions for a minimum are then obtained from upper and lower estimates of the smallest eigenvalue of problem (22.7), respectively. Namely, upper bounds are obtained by restricting the problem to properly chosen classes of functions,[2] and lower bounds are obtained from any inequality that implies $(22.6)_2$ for some positive c.

One possible way to get a lower bound inequality is to exploit the restrictions on the derivatives of w induced by the indifference assumption (22.1).[3]

[1] See, e.g., [GH95], Section 4.1.1.

[2] Simpson and Spector [SS84a, SS84b].

[3] A procedure based on this fact was introduced by Holden [Ho64] and systematically used by Beatty [Be71].

The consequences of this assumption are that $T(F_0)$ is symmetric and that the fourth-order tensor $\mathbb{B}(F_0)$ admits the decomposition

$$\mathbb{B}(F_0) = \mathbb{C}(F_0) + I \boxtimes T(F_0)\,,$$

with $I \boxtimes T(F_0)$ a tensor with the major symmetry and $\mathbb{C}(F_0)$ a tensor with the two minor symmetries. If we denote by $c_C^s(F_0)$ the smallest eigenvalue of $\mathbb{C}(F_0)$ *restricted to the symmetric tensors* and by $c_T(F_0)$ the smallest eigenvalue of $I \boxtimes T(F_0)$,[4] we have that

$$\mathbb{B}(F_0)H \cdot H \;\geq\; c_C^s(F_0)\,|H^s|^2 + c_T(F_0)\,|H|^2\,,$$

where H^s is the symmetric part of H. After setting

$$\bar{c}_C^s \;=\; \inf_{X\in\Omega} c_C^s(F_0(X))\,, \qquad \bar{c}_T \;=\; \inf_{X\in\Omega} c_T(F_0(X))\,,$$

we see that inequality $(22.6)_2$ is satisfied if

$$\bar{c}_C^s \int_\omega |\nabla^s u|^2\,dx \;+\; \bar{c}_T \int_\omega |\nabla u|^2\,dx \;\geq\; c \int_\omega |\nabla u|^2\,dx\,. \tag{22.8}$$

Making use of the algebraic inequality $|H^s| \leq |H|$ and of Korn's inequality

$$c_K \int_\omega |\nabla^s u|^2\,dx \;\geq\; \int_\omega |\nabla u|^2 dx\,,$$

we see that (22.8) holds if $\bar{c}_T \geq 0$ and $\bar{c}_C^s + \bar{c}_T > 0$, and if $\bar{c}_T < 0$ and $\bar{c}_C^s + c_K \bar{c}_T > 0$. The two conditions can be collected in the single inequality

$$\bar{c}_C^s > -\bar{c}_T^+ + c_K\,\bar{c}_T^-\,, \tag{22.9}$$

with $\bar{c}_T^+ = \max\{0, \bar{c}_T\}$ and $\bar{c}_T^- = \max\{0, -\bar{c}_T\}$.

Condition (22.9) has a global character, since $\bar{c}_C^s$ and $\bar{c}_T$ are obtained by minimization over the whole body. A more efficient local condition proposed in [Ho64] has the form

$$c_C^s(F_0(X)) + c_{KT}(F_0(X)) \;\geq\; c \qquad \text{for a.e. } X \text{ in } \Omega\,, \tag{22.10}$$

with the constant c_{KT} depending on the punctual values of $T(F_0)$ and on the Korn constant c_K. The expression of c_{KT} given in [Ho64] was improved in [Dp80], and an additional improvement obtained in [DR07] yields

$$c_{KT}(F_0) = \min_{i\in\{1,2,3\}} \sup_{\eta\in\mathcal{A}} \left\{ 2\,T_i(F_0) - (c_K - 1)\,\eta^+ - \frac{(\tau_i(F_0)\,(2\,T_i(F_0) + \eta))^+}{2T_i(F_0) - \tau_i(F_0) + \eta} \right\}, \tag{22.11}$$

where T_i are the eigenvalues of $T(F_0)$, τ_i are the differences

$$T_1 - T_2,\;\; T_2 - T_3,\;\; T_3 - T_1\,,$$

[4] The eigenvalues of $I \boxtimes T(F_0)$ coincide with those of $T(F_0)$; see [DR07], Appendix B.

and $\mathcal{A}$ is the set of all η such that

$$2\,T_i(F_0(X)) - \tau_i(F_0(X)) + \eta \;>\; 0$$

for all i in $\{1,2,3\}$ and for a.e. X in Ω. In what follows, explicit necessary conditions based on restrictions of the eigenvalue problem (22.7) and sufficient condition based on inequality (22.10) are given for the problem of the stretching of an isotropic cylinder.

22.3 Stretching of an Isotropic Cylinder

Let Ω be a cylinder of arbitrary cross section. At all points X located on the bases, we prescribe the normal displacements

$$(\hat{f}_t(X) - X)\cdot e \;=\; (t-1)\,(X - X_0)\cdot e\,, \quad t>0\,, \tag{22.12}$$

where e is the direction of the axis, X_0 is a fixed point, and the parameter t measures the stretch of the cylinder, with $t>1$ corresponding to extension and $t<1$ corresponding to contraction. We focus our attention on the two-parameter family of deformations

$$f_{t,\lambda}(X) = X_0 + \big(t\,e\otimes e + \lambda(I - e\otimes e)\big)(X - X_0)\,,$$

where t is again the stretch, and λ is a uniform dilatation of the cross section if $\lambda>1$ and a uniform contraction if $\lambda<1$. Each $f_{t,\lambda}$ is a homogeneous deformation, with deformation gradient

$$F_{t,\lambda} \;=\; t\,e\otimes e + \lambda\,(I - e\otimes e)\,, \tag{22.13}$$

and obeys the boundary condition (22.12) for the corresponding t.

From this family it is possible to extract an equilibrium path if, for each t, there is a $\lambda(t)$ such that $f_{t,\lambda(t)}$ is an equilibrium configuration. We recall that if the cylinder is isotropic and if the deformation gradient is as in (22.13), the Cauchy stress is a linear combination of $e\otimes e$ and I

$$T_{t,\lambda} \;=\; \sigma_{t,\lambda}\,e\otimes e + \tau_{t,\lambda} I\,,$$

with constant coefficients $\sigma_{t,\lambda}, \tau_{t,\lambda}$. [5] It is easy to verify that $T_{t,\lambda}$ is equilibrated with null body forces, null surface tractions on the lateral surface, and null tangential tractions on the bases, if and only if $\tau_{t,\lambda}=0$. Moreover, it is known that, if the energy density satisfies the growth conditions (22.2), for each $t>0$ there is a unique $\lambda(t)$ for which $\tau_{t,\lambda(t)}=0$. [6] The deformations $f_t = f_{t,\lambda(t)}$ then form an equilibrium path, with deformation gradient $F_t = F_{t,\lambda(t)}$ and Cauchy stress

[5] See [TN65], Sect. 47.

[6] Simpson and Spector [SS84a], Theorem 3.1.

$$T_t = \sigma_t\, e\otimes e\,, \qquad \sigma_t = \sigma_{t,\lambda(t)}\,. \tag{22.14}$$

Assume that the configuration f_t with $t = 1$ is a local minimizer. Then the the minimizing interval from f_t is the largest interval (t_a, t_b) with $t_a \le 1 \le t_b$, in which all eigenvalues of problem (22.7) are positive. An upper bound for t_a and a lower bound for t_b are obtained from inequality (22.9), where now $\bar{c}_T = \min\{\sigma_t, 0\} = -\sigma_t^-$ due to (22.14), and $\bar{c}_C^s = c_C^s(F_t)$ due to the fact that the deformation is homogeneous. The inequality then takes the form

$$c_C^s(F_t) \;>\; c_{K,t}\,\sigma_t^-. \tag{22.15}$$

For the local condition (22.10), it is proved in [DR07] that it takes the same form as (22.15), with c_{KT} replaced by

$$c_{K,t}^* \;=\; \tfrac{1}{2}\,c_{K,t} + (c_{K,t}-1)^{1/2}.$$

In particular, all configurations F_t with $\sigma_t^-= 0$ are minimizing configurations if $\mathbb{C}^s(F_t)$ is positive definite. The *absence of bifurcation in tension* observed by several authors in various circumstances[7] is then, in fact, a property of all materials for which $\mathbb{C}^s$ is positive definite.

As a specific example, we consider a Blatz–Ko material, whose energy density is

$$w(F) \;=\; \alpha\left(\tfrac{1}{2}\,(F\cdot F - 3) + \gamma^{-1}((\det F)^{-\gamma} - 1)\right),$$

with α and γ positive constants. For it, we find that the equilibrium condition $\tau_{t,\lambda(t)} = 0$ is satisfied by

$$\lambda(t) = t^{1-\delta/2}\,, \qquad \delta \;=\; \tfrac{2+3\gamma}{1+\gamma}\,. \tag{22.16}$$

For $f_t = f_{t,\lambda(t)}$, we have

$$F_t \;=\; t\,e\otimes e + t^{1-\delta/2}(I - e\otimes e)\,, \qquad \det F_t \;=\; t^{3-\delta}\,, \tag{22.17}$$

and after some computation, we find that

$$\sigma_t \;=\; \alpha\,t^{-1}\big(t^\delta - 1\big)\,, \qquad c_C^s(F_t) = 2\,\alpha\,t^{-1}.$$

We observe that σ_t is positive for $t > 1$ and negative for $t < 1$, and that $c_C^s(F_t)$ is positive for all $t > 0$. Then inequality (22.15) is always verified in tension, and the upper extreme of the minimizing interval is $t_b = +\infty$. In compression, the same inequality takes the form $2 > c_{K,t}\,(1 - t^\delta)$. An upper bound for the lower extreme t_a of the minimizing interval is then provided by the equation

$$c_{K,t}\,(1 - t^\delta) = 2\,. \tag{22.18}$$

This equation always admits solutions in (0,1). Indeed, it is generally true that $c_{K,t} \ge 2$, the value 2 being attained only if $\partial_1\Omega = \partial\Omega$. Then the left-hand

[7] See [Sp84] and the papers cited therein.

side of (22.18) is not less than 2 for $t = 0$ and is zero for $t = 1$. Because $c_{K,t}$ depends continuously on t, the value 2 must be attained somewhere in (0,1).

The same equation with $c_{K,t}$ replaced by $c^*_{K,t}$ provides the upper bound for t_a according to the local condition (22.10). Since $c^*_{K,t} > c_{K,t}$ for all $c_{K,t} > 2$, one sees that the new bound improves the one provided by equation (22.18).

22.4 Numerical Results for Circular Cylinders

In this section, we give some estimates for circular cylinders made of a Blatz–Ko material. Since for such a material the minimizing intervals are of the form $(t_a, +\infty)$, our task reduces to finding upper and lower bounds for t_a.

Let Ω be a circular cylinder of height H_1 and radius R_1, and let $t \mapsto f_t$ be the equilibrium path (22.17). Then every f_t is a map of Ω into the cylinder ω_t of height $H_t = tH_1$ and radius $R_t = t^{1-\delta/2}R_1$. To get a lower bound for t_a, for each t we evaluate the smallest eigenvalue of problem (22.7) restricted to suitable subspaces of $W^{1,\infty}(\omega_t)$. In particular, we take two subspaces made of all functions u of the form [8]

$$u = \begin{Bmatrix} x_1\varphi(r)\cos\frac{n\pi x_3}{H_t} \\ x_2\varphi(r)\cos\frac{n\pi x_3}{H_t} \\ \psi(r)\sin\frac{n\pi x_3}{H_t} \end{Bmatrix}, \qquad u = \begin{Bmatrix} 0 \\ \varphi(x_2)\cos\frac{n\pi x_3}{H_t} \\ \psi(x_2)\sin\frac{n\pi x_3}{H_t} \end{Bmatrix}, \tag{22.19}$$

where n is an integer, $\{O, x_1, x_2, x_3\}$ is a Cartesian coordinate system with origin O at the center of one of the bases of the cylinder, x_3 is the direction of the axis, $r = (x_1^2 + x_2^2)^{1/2}$ is the distance from the axis, and φ and ψ are functions in $W^{1,\infty}(-R_t, R_t)$. The functions u in the first subspace represent displacements of the *barreling type*, whereas those in the second subspace represent displacements of the *buckling type* in the (x_2, x_3) plane. The functions of the first type are required to obey the regularity conditions at the origin

$$\varphi(0) \,=\, 0\,, \qquad (r\varphi')(0) \,=\, 0\,,$$

and those of the second type are restricted by the normalization conditions

$$\varphi(0) \,=\, 1\,, \qquad \psi(0) \,=\, 0\,.$$

Both satisfy the boundary condition (22.12). The condition $\operatorname{div}\big(\mathbb{B}(F_0)\big) = 0$ reduces to the system of differential equations

$$\begin{aligned} (2+\gamma)(r\varphi'' + 3\varphi') + (1+\gamma)\tfrac{n\pi}{H_t}\,\psi' - t^\delta \tfrac{n^2\pi^2}{H_t^2}\, r\varphi \,&=\, 0, \\ r\psi'' + \psi' - (1+\gamma)\tfrac{n\pi}{H_t}\,(r^2\varphi' + 2\,r\varphi) - (1+\gamma+t^\delta)\,\tfrac{n^2\pi^2}{H_t^2}\, r\psi \,&=\, 0 \end{aligned} \tag{22.20}$$

[8] The lower bounds corresponding to functions of the barreling type were determined in [SS84a] and [SS84b], and those corresponding to functions of the buckling type were determined in [DR07].

for the functions of the first type, and to the system

$$\begin{aligned} (2+\gamma)\,\varphi'' + (1+\gamma)\,\psi' - t^{\delta}\,\tfrac{n^2\pi^2}{H_t^2}\,\varphi \;=\; 0\,, \\ \psi'' - (1+\gamma)\,\tfrac{n\pi}{H_t}\,\varphi' - (1+\gamma+t^{\delta})\,\tfrac{n^2\pi^2}{H_t^2}\,\psi \;=\; 0 \end{aligned} \tag{22.21}$$

for the functions of the second type. The solutions of system (22.20) are the linear combinations of the modified Bessel functions of the first kind

$$I_0\big(\frac{n\pi r t^{\delta/2}}{H_t}\big)\,,\quad I_0\big(\frac{n\pi r t_*^{\delta/2}}{H_t}\big)\,,\quad I_1\big(\frac{n\pi r t^{\delta/2}}{H_t}\big)\,,\quad I_1\big(\frac{n\pi r t_*^{\delta/2}}{H_t}\big)\,,$$

where γ and δ are the constants in (22.16), and

$$t_*^{\delta} \;=\; \frac{\gamma+1+t^{\delta}}{\gamma+2}\,.$$

The eigenvalues of (22.7) are the roots of the equation

$$4\,\nu(n\pi/\rho_1^*) - \frac{(1+t^{\delta})^2}{t_*^{\delta}}\,\nu(n\pi/\rho_1) + 2\,t^{\delta} \;=\; 2\,, \tag{22.22}$$

where $\rho_1 = H_1/R_1$ is the *slenderness ratio* in the reference configuration $t = 1$, and

$$\rho_1^* \;=\; \Big(\frac{t}{t_*}\Big)^{\delta/2}\rho_1\,, \qquad \nu(z) \;=\; z\frac{I_0(z)}{I_1(z)}\,.$$

For displacements of the buckling type, the solutions of system (22.21) are the linear combinations of the exponentials

$$\exp\big(\frac{n\pi x_2 t^{\delta/2}}{H_t}\big)\,,\;\; \exp\big(-\frac{n\pi x_2 t^{\delta/2}}{H_t}\big)\,,\;\; \exp\big(\frac{n\pi x_2 t_*^{\delta/2}}{H_t}\big)\,,\;\; \exp\big(-\frac{n\pi x_2 t_*^{\delta/2}}{H_t}\big)\,,$$

and the corresponding eigenvalues are the roots of the equation

$$\begin{aligned} &(3+t^{\delta})^2\big(\frac{t}{t_*}\big)^{\delta/2} I_1\big(\frac{2\,n\pi}{\rho_1}\big)\; I_1\big(\frac{2\,n\pi}{\rho_1^*}\big) \\ &= \Big(\big(2\,t^{\delta/2} + \frac{1+t^{\delta}}{t_*^{\delta/2}}\big)\, I_1\big(\frac{n\pi}{\rho_1} + \frac{n\pi}{\rho_1^*}\big) - \big(2\,t^{\delta/2} - \frac{1+t^{\delta}}{t_*^{\delta/2}}\big)\, I_1\big(\frac{n\pi}{\rho_1} - \frac{n\pi}{\rho_1^*}\big)\Big)^2. \end{aligned} \tag{22.23}$$

The lower bounds for t_a obtained from the solutions of (22.22) and (22.23) are plotted in Figure 22.1 as functions of the slenderness ratio ρ_1 at $t = 1$. The barreling modes provide better bounds for small ρ_1, and the buckling modes provide better bounds for large ρ_1. The optimal value of n is n=1 for the buckling modes, whereas for the barreling modes the optimal n increases with ρ_1. The figure also shows the lower bound given by the Euler–Bernoulli buckling displacement field, obtained from $(22.19)_2$ by approximating $\varphi(x_2)$ and $\psi(x_2)$ with $1 - \pi^2 x_2^2/2H_t^2$ and $\pi x_2/H_t$, respectively. As expected, this approximation is accurate only for large values of ρ_1. An upper bound for t_a

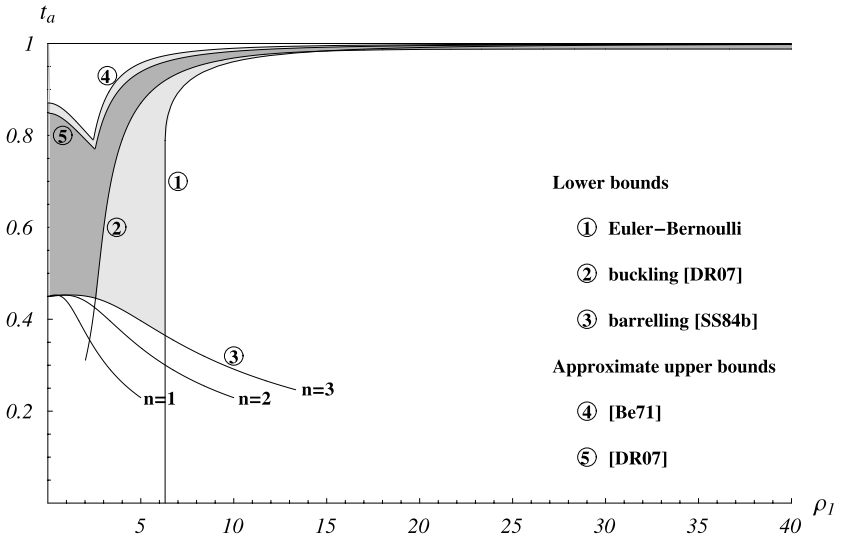

Fig. 22.1. Upper and lower bounds for the compressive stretching t_a for circular cylinders made of a Blatz–Ko material.

is provided by (22.18) with $c_{K,t}$ replaced by $c^*_{K,t}$. In it, a major problem is the determination of the exact value, or at least of an upper bound, for the Korn constant c_K appearing in the expression (22.11) of $c_{K,t}$. This is still an open problem. We use Bernstein and Toupin's approximated formula [BT60][9]

$$c_K \approx 2 + \frac{4\,J_{\max}}{J_{\mathrm{med}} + J_{\min}}\ ,$$

in which $J_{\max} \geq J_{\mathrm{med}} \geq J_{\min}$ are the principal moments of inertia of the cylinder. For a circular cylinder with slenderness ratio $\rho_t = H_t/R_t = t^{\delta/2}\rho_1$, one has

$$c_{K,t} \approx 2 + \max\left\{ \frac{12}{3 + t^\delta \rho_1^2}\ ,\ \frac{2}{3}\, t^\delta \rho_1^2 \right\},$$

and substituting into (22.18), one finds that an approximate upper bound for t_a is provided by the solutions of

$$\rho_1^2\, t^{\,2\delta} + 9\, t^{\,\delta} = 6 \quad \text{for } \rho_1^2 < 6\,, \qquad \rho_1^2\,(1 - t^{\,\delta}) = 3 \quad \text{for } \rho_1^2 > 6\,,$$

the approximation being due to the uncertainty about the expression used for the Korn constant. This bound is represented by a curve in Figure 22.1. For comparison, the same figure also shows the estimate given in [Be71], obtained

[9] This is neither an upper bound nor a lower bound for c_K. It is not an upper bound because it is obtained solving a minimum problem over a strict subclass of the admissible deformation gradient fields, and it is not a lower bound because it refers to boundary conditions less restrictive than (22.12).

using the Bernstein and Toupin approximation for the Korn constant, and a less refined expression for the constant $c_{K,t}$.

We see that the two curves representing the overall upper and (approximate) lower bounds are similar in shape, since both consist of two segments, one corresponding, roughly, to deformations of the buckling type and one corresponding to deformations of the barreling type. The gap between the two curves, as it comes from the results available in the literature (light gray area in Figure 22.1) has been substantially reduced by the present study (dark gray area). The gap is narrow for large values of ρ_1 but still important for small values. This reveals the need for a deeper study of the minimizing displacement modes for thick cylinders.

Acknowledgement. This work has been supported by PRIN 2005 "Modelli Matematici per la Scienza dei Materiali" and by the Research Project "Nano & Nano" of the University of Ferrara.

References

[Be71] Beatty, M.F.: Estimation of ultimate safe loads in elastic stability theory. *J. Elasticity,* **1**, 95–120 (1971).

[BT60] Bernstein, B., Toupin, R.A.: Korn inequalities for the sphere and the circle. *Arch. Rational Mech. Anal.,* **6**, 51–64 (1960).

[Dp80] Del Piero, G.: Lower bounds for the critical loads of elastic bodies, *J. Elasticity,* **10**, 135–143 (1980).

[DR07] Del Piero, G., Rizzoni, R.: Weak local minimizers in finite elasticity (in preparation).

[GH95] Giaquinta, M., Hildebrandt, S.: *Calculus of Variations.* Springer, Berlin-Heidelberg (1996).

[Ho64] Holden, J.T.: Estimation of critical loads in elastic stability theory. *Arch. Rational Mech. Anal.,* **17**, 171–183 (1964).

[SS84a] Simpson, H.C., Spector, S.J.: On barrelling instabilities in finite elasticity, *J. Elasticity,* **14**, 103–125 (1984).

[SS84b] Simpson, H.C., Spector, S.J.: On barrelling for a special material in finite elasticity. *Quart. Appl. Math.,* **42**, 99–111 (1984).

[Sp84] Spector, S.J.: On the absence of bifurcation for elastic bars under tension. *Arch. Rational Mech. Anal.,* **85**, 171–199 (1984).

[TN65] Truesdell, C., Noll, W.: The Non-Linear Field Theories of Mechanics. In: Flügge, S. (ed.), *Handbuch der Physik, III/3.* Springer, Berlin-Heidelberg-New York (1965).

23

Harmonic Oscillations in a Linear Theory of Antiplane Elasticity with Microstructure

S. Potapenko

University of Waterloo, ON, Canada; spotapen@uwaterloo.ca

23.1 Introduction

The theory of micropolar (Cosserat) elasticity [Er66] has been developed to account for discrepancies between the classical theory and experiments when the effects of material microstructure were known to affect significantly the body's overall deformation, for example, in the case of granular bodies with large molecules (e.g., polymers) or human bones (see [Lak95], [Lak91], and [Lak82]). Significant progress has been achieved in this direction for the last 30 years (see [Now86] for a review of works in this area and an extensive bibliography), but investigations have been confined mainly to the problems of elastostatics. A dynamic problem of wave propagation in the three-dimensional elastic micropolar space was formulated by Kupradze in [Kup79]. However, a rigorous treatment of the corresponding boundary value problems in the antiplane case when waves propagate in an infinite cylinder of any arbitrary cross section in the direction of the generators of the cylinder or in the unbounded antiplane space is, to the author's knowledge, still absent from the literature. The main difficulties arising here are when we try to apply Helmholtz's theorem to a solution of the governing equations in the exterior domain. The decomposition is not as straightforward as in classical elasticity. Only one part satisfies a Helmholtz equation, and so we can impose only one Sommerfeld-type radiation condition.

In this chapter, we introduce time dependency into the theory of antiplane micropolar elasticity presented in [PSM05] by considering the case where all applied forces, and hence, displacement, strain, and stress components are periodic functions of time. Furthermore, we find that uniqueness is guaranteed, provided that the frequency of oscillation is greater than a fixed constant multiple of the speed of longitudinal waves in an infinite micropolar medium.

23.2 Preliminaries

In what follows, Greek and Latin indices take the values 1,2 and 1,2,3, respectively, the convention of summation over repeated indices is understood, and a superscript T indicates matrix transposition.

Let S be a domain in $\mathbb{R}^2$ bounded by a closed C^2-curve ∂S and occupied by a homogeneous and isotropic linearly elastic micropolar material with elastic constants $\lambda, \mu, \alpha, \beta$, γ, and κ. The state of micropolar antiplane shear is characterized by a displacement field $U(x',t) = (U_1(x',t), U_2(x',t), U_3(x',t))^T$ and a microrotation field $\phi(x',t) = (\phi_1(x',t), \phi_2(x',t), \phi_3(x',t))^T$ of the form $U_\alpha(x',t) = 0$, $U_3(x',t) = U_3(x,t)$, $\phi_3(x',t) = 0$, $\phi_\alpha(x',t) = \phi_\alpha(x,t)$, where $x' = (x_1, x_2, x_3)$ and $x = (x_1, x_2)$ are generic points in $\mathbb{R}^3$ and $\mathbb{R}^2$, respectively. In the absence of body forces and moments, we find that the equations of motion of micropolar antiplane shear written in terms of displacements and microrotations are

$$L(\partial_x)U(x,t) = F(x,t), \quad x \in S, \tag{23.1}$$

Here $U(x,t) = (U_1(x,t), U_2(x,t), U_3(x,t))^T$, where the U_α have replaced the ϕ_α, and the matrix partial differential operator $L(\partial x) = L(\partial/\partial x_\alpha)$ is defined by

$$L(\xi) = L(\xi_\alpha)$$

$$= \begin{pmatrix} (\gamma+\kappa)\Delta - 4\alpha + (\beta+\gamma-\kappa)\xi_1^2 & (\beta+\gamma-\kappa)\xi_1\xi_2 & 2\alpha\xi_2 \\ (\beta+\gamma-\kappa)\xi_1\xi_2 & (\gamma+\kappa)\Delta - 4\alpha + (\beta+\gamma-\kappa)\xi_2^2 & -2\alpha\xi_1 \\ -2\alpha\xi_2 & 2\alpha\xi_1 & (\mu+\alpha)\Delta \end{pmatrix},$$

with $\Delta = \xi_\alpha\xi_\alpha$.

Together with L, we consider the boundary stress operator $T(\partial x) = T(\partial/\partial x_\alpha)$ defined by

$$T(\xi) = T(\xi_\alpha)$$

$$= \begin{pmatrix} (2\gamma+\beta)\xi_1 n_1 + (\gamma+\kappa)\xi_2 n_2 & (\gamma-\kappa)\xi_2 n_1 + \beta\xi_1 n_2 & 2\alpha n_2 \\ (\gamma-\kappa)\xi_1 n_2 + \beta\xi_2 n_1 & (\gamma+\kappa)\xi_1 n_1 + (2\gamma+\beta)\xi_2 n_2 & 2\alpha n_1 \\ 0 & 0 & (\mu+\alpha)\xi_\alpha n_\alpha \end{pmatrix},$$

where $n = (n_1, n_2)^T$ is the unit outward normal to ∂S,

$$F(x,t) = \left(J\frac{\partial^2 U_1}{\partial t^2},\ J\frac{\partial^2 U_2}{\partial t^2},\ \rho\frac{\partial^2 U_3}{\partial t^2} \right)^T,$$

ρ is the mass density, and J is the moment of inertia.

Furthermore, we assume that the time dependency is periodic, that is, the waves are monochromatic; consequently, $U(x,t)$ may be represented in the form

$$U(x,t) = Re[u(x)e^{-i\omega t}], \tag{23.2}$$

where $\omega \in R$ is the frequency of oscillation and $u(x) = (u_1(x), u_2(x), u_3(x))^T$ is some real-valued function.

Substituting (23.2) in (23.1), we find that in terms of $u(x) = (u_1, u_2, u_3)^T$, system (23.1) becomes

$$\left[L(\partial x) + \begin{pmatrix} J\omega^2 & 0 & 0 \\ 0 & J\omega^2 & 0 \\ 0 & 0 & \rho\omega^2 \end{pmatrix} \right] u(x) = 0. \tag{23.3}$$

Throughout what follows, we assume the following restrictions on the elastic constants of the material [PSM05]:

$$2\gamma + \beta > 0, \quad \kappa, \alpha, \gamma, \mu > 0. \tag{23.4}$$

23.3 Expansion of a Regular Solution

To obtain the analytical solution of (23.3), we have to prove the following theorem.

Theorem 1. *Any regular solution of system (23.3) admits in the domain of regularity a representation*

$$u(x) = \left(\frac{\partial \Phi}{\partial x_1} - \frac{\partial \Psi}{\partial x_2}, \frac{\partial \Phi}{\partial x_2} + \frac{\partial \Psi}{\partial x_1}, u_3 \right)$$

such that

$$\begin{aligned} (\Delta + k_1^2)(\Delta + k_2^2)\Psi = 0 \quad &(i), \\ (\Delta + k_1^2)(\Delta + k_2^2)u_3 = 0 \quad &(ii), \\ (\Delta + k_3^2)\Phi = 0 \quad &(iii), \end{aligned}$$

where

$$\begin{aligned} k_1^2 + k_2^2 &= \tfrac{4\alpha^2 + J\omega^2 - 4\alpha + \rho\omega^2(\gamma+\varepsilon)}{(\mu+\alpha)(\gamma+\varepsilon)}, \\ k_1^2 k_2^2 &= \tfrac{\rho\omega^2(J\omega^2 - 4\alpha)}{(\mu+\alpha)(\gamma+\varepsilon)}, \quad k_3^2 = \tfrac{(J\omega^2 - 4\alpha)}{2\gamma+\beta}. \end{aligned}$$

This assertion can be proved by direct verification, following the procedure discussed in [SC93].

23.4 Radiation Conditions

Let $S^+ \equiv S$ and $S^- \equiv R^2 \backslash (S^+ \cup \partial S)$. We now consider solutions of (23.3) in the domain S^-. Clearly, since the domain of interest now extends to infinity, we must consider the behavior of any solution of (23.3) at infinity.

In the history of uniqueness theorems for oscillation problems, a important role was played by the Sommerfeld-type radiation conditions for the

Helmholtz equation. They were later generalized for the elastodynamic problem by Kupradze [Kup65]. To proceed, we establish suitable radiation conditions and asymptotic estimates for the functions $\Psi(x)$, $\Phi(x)$, and $u_3(x)$.

Definition 1. *Let $x \in S^-$. If, as $|x| = R \to \infty$,*

$$\Psi(x) = o(R^{-1/2}), \quad \frac{\partial \Psi}{\partial x_\alpha}(x) = O(R^{-1}), \tag{23.5}$$

$$\Phi(x) = O(R^{-1/2}), \quad \frac{\partial \Phi}{\partial R}(x) - ik_3\Phi(x) = o(R^{-1/2}), \tag{23.6}$$

$$u_3(x) = o(R^{-1/2}), \quad \frac{\partial u_3}{\partial x_\alpha}(x) = O(R^{-1}), \tag{23.7}$$

we say that the regular solution $u(x) = (\frac{\partial \Phi}{\partial x_1} - \frac{\partial \Psi}{\partial x_2}, \frac{\partial \Phi}{\partial x_2} + \frac{\partial \Psi}{\partial x_1}, u_3)$ satisfies the radiation conditions.

23.5 Boundary Value Problems

Let f and g be continuous (3×1) matrices prescribed on ∂S. Consider the following Dirichlet and Neumann boundary value problems in the exterior domain S^-.

(D^-) Find a regular solution u of (23.3) in the domain S^-, satisfying the radiation conditions (23.5)–(23.7) and the boundary condition

$$u(x) = f(x), \quad x \in \partial S.$$

(N^-) Find a regular solution u of (23.3) in the domain S^- satisfying the radiation conditions (23.5)–(23.7) and the boundary condition

$$T(\partial x, n)u(x) = g(x), \quad x \in \partial S,$$

where n is the unit outward normal to ∂S.

23.6 Uniqueness Theorem

Theorem 2. *If $\omega^2 > 4\alpha/J$, then (D^-) and (N^-) have at most one solution.*

Proof. To verify this, it is enough to show that in the case of homogeneous Dirichlet or Neumann boundary conditions the solution is identically zero. Consider system (23.3). As stated above, it is clear that finding an analytical solution to (23.3) is equivalent to determining functions Φ and Ψ that satisfy (23.4).

Let $\Omega = (\Delta + k_2^2)\Psi$. Then, by Theorem 1(i), $(\Delta + k_1^2)\Psi = 0$ in S^-. Consider the integral

$$\int_{\partial K_R} |\Omega|^2 \, dS,$$

where ∂K_R is the circumference of a circle, radius R, sufficiently large to enclose ∂S. Using the asymptotic estimates (23.5) for Ψ, it is a straightforward exercise to show that

$$\lim_{R\to\infty} \int_{\partial K_R} |\Omega|^2 \, dS = 0. \tag{23.8}$$

Since Ω solves a Helmholtz equation with $k_1^2 > 0$, we can use (23.8) and Rellich's lemma citeKupradze2 to deduce that $\Omega = 0$ in S^-; that is,

$$(\Delta + k_2^2)\Psi = 0 \text{ in } S^-.$$

As above, (23.5) gives us that

$$\lim_{R\to\infty} \int_{\partial K_R} |\Psi|^2 \, dS = 0.$$

Rellich's Lemma with $k_2^2 > 0$ then leads us to

$$\Psi = 0 \text{ in } S^-. \tag{23.9}$$

Similarly, starting from (ii), we obtain

$$u_3 = 0 \text{ in } S^-. \tag{23.10}$$

Applying the reciprocity relation for the elastostatic antiplane shear deformations of Cosserat solids [PSM05] to a regular solution of (23.3) in the bounded region $S^- \cap K_R$, we obtain

$$\int_{\partial S + K_R} \left[\overline{u}^T T u - u^T T \overline{u}\right] dS = 0. \tag{23.11}$$

Next, following standard procedures for uniqueness proofs in the theory of boundary value problems, we impose zero Dirichlet or Neumann conditions on ∂S, so that (23.11) becomes

$$\int_{K_R} \left[\overline{u}^T T u - u^T T \overline{u}\right] dS = 0. \tag{23.12}$$

Furthermore, substituting the representation of $u(x)$ given in Theorem 1 into (23.12), taking into account (23.6) and the conditions (23.4) imposed on the elastic constants, and following exactly the procedure described in [SC93] to prove the uniqueness theorems for oscillations of plates, we obtain, as $R \to \infty$,

$$\lim_{R\to\infty} \int_{\partial K_R} |\Phi|^2 \, dS = 0. \tag{23.13}$$

Theorem 1(ii), (23.13), and Rellich's lemma now imply that

$$\Phi = 0 \quad \text{in } S^-. \tag{23.14}$$

Hence, in view of (23.9), (23.10), and (23.14),

$$u(x) = 0 \quad \text{in } S^-,$$

which completes the proof.

Remark 1. The condition $\omega^2 > 4\alpha/J$ is necessary to ensure that $\mathrm{k}_i^2 > 0$ and hence the use of Rellich's Lemma.

References

[Er66] Eringen, A.C.: Linear theory of micropolar elasticity. *J. Math. Mech.,* **15**, 909–923 (1966).

[Kup65] Kupradze, V.D.: *Potential Methods in the Theory of Elasticity.* Israel Program for Scientific Translations, Jerusalem (1965).

[Kup79] Kupradze, V.D., Gegelia, T.G., Basheleishvili, M.O., Burchuladze, T.V.: *Three-Dimensional Problems of the Mathematical Theory of Elasticity and Thermoelasticity.* North-Holland, Amsterdam (1979).

[Lak82] Lakes, R.: Dynamical study of couple stress effects in human compact bone. *J. Biomedical Engng.,* **104**, 6–11 (1982).

[Lak91] Lakes, R.: Experimental micromechanics methods for conventional and negative Poisson's ratio cellular solids as Cosserat continua. *J. Engng. Materials Tech.,* **113**, 148–155 (1991).

[Lak95] Lakes, R.: Experimental methods for study of Cosserat elastic solids and other generalized elastic continua. In: Muhlhaus, H-B. (ed.), *Continuum Models for Materials with Microstructure.* Wiley, New York (1995), pp. 1–22.

[Now86] Nowacki, W.: *Theory of Asymmetric Elasticity.* Polish Scientific Publishers, Warszawa (1986).

[PSM05] Potapenko, S., Schiavone, P., Mioduchowski, A.: Anti-plane shear deformations in a linear theory of elasticity with microstructure. *J. Appl. Math. Phys. (ZAMP),* **56**, 516–528 (2005).

[SC93] Schiavone, P., Constanda, C.: Oscillation problems in thin plates with transverse shear deformation. *SIAM J. Appl. Math.,* **53**, 1253–1263 (1993).

24

Exterior Dirichlet and Neumann Problems for the Helmholtz Equation as Limits of Transmission Problems

M.-L. Rapún[1] and F.-J. Sayas[2]

[1] Universidad Politécnica de Madrid, Spain; marialuisa.rapun@upm.es
[2] Universidad de Zaragoza, Spain; jsayas@unizar.es

24.1 Statement of the Problems

In this chapter, we propose a new way of understanding the classical exterior Dirichlet and Neumann problems for the Helmholtz equation as limiting situations of transmission problems, and study the stability of this limiting process under discretization. This kind of problems appear in the study of the scattering of time-harmonic acoustic and thermal waves.

We assume that $\Omega_{\rm int} \subset \mathbb{R}^d$, $d = 2$ or 3, is a bounded, simply connected, open set with smooth boundary Γ. If the obstacle is impenetrable, then the scattering amplitude of a time-harmonic wave with wavenumber λ^2 solves an exterior Dirichlet or Neumann problem for the Helmholtz equation $\Delta u + \lambda^2 u = 0$ in $\Omega_{\rm ext} := \mathbb{R}^d \setminus \overline{\Omega}_{\rm int}$. It satisfies the Sommerfeld radiation condition at infinity

$$\lim_{r\to\infty} r^{\frac{d-1}{2}} (\partial_r u - \imath\lambda u) = 0,$$

uniformly in all directions $\mathbf{x}/|\mathbf{x}| \in \mathbb{R}^d$, $r := |\mathbf{x}|$ (see [CK83]). When waves can propagate through Γ, that is, when the obstacle is penetrable, and the physical properties in both media are different, the problem in $\Omega_{\rm int}$ is modeled by $\Delta u + \mu^2 u = 0$. Both Helmholtz equations are coupled through two continuity conditions of the form

$$\begin{aligned} u^{\rm int} - u^{\rm ext} &= f, && \text{on } \Gamma, \\ \alpha\, \partial_n u^{\rm int} - \beta\, \partial_n u^{\rm ext} &= \beta\, g, && \text{on } \Gamma. \end{aligned}$$

Typically, $f = u_{\rm inc}$ and $g = \partial_n u_{\rm inc}$ are the Cauchy data on Γ of an incident wave, a known solution to the exterior Helmholtz equation. In acoustics, μ^2 is proportional to ρ/α^2, where ρ is the density and α the velocity of transmission in $\Omega_{\rm int}$. For thermal waves, μ^2 is proportional to $\imath\rho/\alpha$, where ρ is the density multiplied by the specific heat capacity and α is the conductivity. General conditions on the parameters λ, μ, α, and β guaranteeing uniqueness can be found in [RS06a] and the references therein.

Dirichlet, Neumann, and transmission problems have been studied successfully from both the analytical and the numerical points of view in a wide number of works with a special emphasis on the study of acoustic waves (see for instance [CK83], [CS85], [KM88], [KR78], and [TW93]). More recently, Helmholtz transmission problems have also appeared in the study of scattering of thermal waves (see [Man01], [RS06a], and [TSS02]).

When studying the behavior of the solution to the transmission problem depending on the interior parameters, physical experiments as well as numerical simulations seem to point out that, for a fixed interior wave number, when the parameter α tends to zero, the solution to

$$(P_\alpha)\quad \left|\begin{array}{ll} \Delta u_\alpha + \lambda^2 u_\alpha = 0, & \text{in } \Omega_{\text{ext}},\\ \Delta u_\alpha + \mu^2 u_\alpha = 0, & \text{in } \Omega_{\text{int}},\\ u_\alpha^{\text{int}} - u_\alpha^{\text{ext}} = f, & \text{on } \Gamma,\\ \alpha\, \partial_n u_\alpha^{\text{int}} - \beta\, \partial_n u_\alpha^{\text{ext}} = \beta\, g,, & \text{on } \Gamma,\\ \lim\limits_{r\to\infty} r^{\frac{d-1}{2}}(\partial_r u_\alpha - \imath\lambda u_\alpha) = 0, & \end{array}\right.$$

tends to the solution to the exterior Neumann problem

$$(P_N)\quad \left|\begin{array}{ll} \Delta u_N + \lambda^2 u_N = 0, & \text{in } \Omega_{\text{ext}},\\ \partial_n u_N = -g, & \text{on } \Gamma,\\ \lim\limits_{r\to\infty} r^{\frac{d-1}{2}}(\partial_r u_N - \imath\lambda u_N) = 0, & \end{array}\right.$$

whereas if α goes to infinity, the solution (P_α) converges to the solution of the exterior Dirichlet problem

$$(P_D)\quad \left|\begin{array}{ll} \Delta u_D + \lambda^2 u_D = 0, & \text{in } \Omega_{\text{ext}},\\ u_D = -f, & \text{on } \Gamma,\\ \lim\limits_{r\to\infty} r^{\frac{d-1}{2}}(\partial_r u_D - \imath\lambda u_D) = 0. & \end{array}\right.$$

This can also be seen by taking limits formally. The aim of this work is to give a rigorous proof of these facts, providing the corresponding convergence rates. We want to point out that we are restricting ourselves to a particular family of transmission problems where only one of the two interior parameters varies. In this case we will show linear convergence. To improve our estimates, both interior parameters would have to converge to zero in the Neumann case or to infinity in the Dirichlet one. In view of numerical experiments in the two-dimensional setting, we believe that for the case of the Dirichlet problem, the faster the modulus of the interior wavenumber increases, the higher the convergence rate is, although we cannot predict any rate in terms of it. On the other hand, for the Neumann problem, we have not observed any substantial improvement by making the interior wavenumber tend to zero. At the current

stage of our research, we cannot prove the results when both parameters vary, since our study is based on the very simple fact that all the integral operators involved in the boundary formulation do not depend on α. Taking into account that the fundamental solution depends on the wavenumber, our study cannot be adapted easily to the case of a family of transmission problems depending on both interior parameters.

24.2 Boundary Integral Formulations

Since we are dealing with exterior problems, a suitable way of inspecting them is by using boundary integral formulations. We introduce the fundamental solution to the Helmholtz equation $\Delta u + \rho^2 u = 0$,

$$\phi_\rho(\mathbf{x},\mathbf{y}) := \begin{cases} \imath\, H_0^{(1)}(\rho\,|\mathbf{x}-\mathbf{y}|)/4, & \text{if } d=2,\\ \exp(\imath\,\rho|\mathbf{x}-\mathbf{y}|)/(4\pi|\mathbf{x}-\mathbf{y}|), & \text{if } d=3, \end{cases}$$

and the single-layer potential

$$\mathcal{S}^\rho\varphi \;:=\; \textstyle\int_\Gamma \phi_\rho(\,\cdot\,,\mathbf{y})\,\varphi(\mathbf{y})\,d\gamma_{\mathbf{y}} \;:\; \mathbb{R}^d \longrightarrow \mathbb{C}.$$

We also define the boundary integral operators

$$V^\rho\varphi := \textstyle\int_\Gamma \phi_\rho(\,\cdot\,,\mathbf{y})\,\varphi(\mathbf{y})\,d\gamma_{\mathbf{y}} \;:\; \Gamma \longrightarrow \mathbb{C},$$

$$J^\rho\varphi := \textstyle\int_\Gamma \partial_{n(\,\cdot\,)}\phi_\rho(\,\cdot\,,\mathbf{y})\,\varphi(\mathbf{y})\,d\gamma_{\mathbf{y}} \;:\; \Gamma \longrightarrow \mathbb{C}.$$

We recall some well-known properties of the integral operators above (see [McL00]): (i) the bounded operator $V^\rho : H^{-1/2}(\Gamma) \to H^{1/2}(\Gamma)$ is invertible if and only if $-\rho^2$ is not a Dirichlet eigenvalue of the Laplace operator in $\Omega_{\rm int}$; (ii) the bounded operator $-\frac{1}{2}I + J^\rho : H^{-1/2}(\Gamma) \to H^{-1/2}(\Gamma)$ is invertible; and (iii) the bounded operator $\frac{1}{2}I + J^\rho : H^{-1/2}(\Gamma) \to H^{-1/2}(\Gamma)$ is invertible if and only if $-\rho^2$ is not a Neumann eigenvalue of the Laplace operator in $\Omega_{\rm int}$.

We will use indirect formulations in terms of single-layer potentials that can fail if either $-\mu^2$ or $-\lambda^2$ are Dirichlet eigenvalues of the Laplace operator in $\Omega_{\rm int}$ and if $-\mu^2$ is a Neumann eigenvalue of the Laplacian in $\Omega_{\rm int}$. To avoid these particular cases, we can adapt our results to the indirect formulation proposed in [RS06b] and based on Brakhage–Werner potentials.

The solution to the Dirichlet problem (P_D) can be represented as $u_D = \mathcal{S}^\lambda\psi_D$, where ψ_D is the unique solution to

$$V^\lambda\psi_D = -f. \tag{24.1}$$

The solution to the Neumann problem (P_N) is $u_N = \mathcal{S}^\lambda\psi_N$, where ψ_N is the unique solution to

$$(\tfrac{1}{2}I - J^{\lambda})\psi_N = g. \tag{24.2}$$

Finally, the solution to the transmission problem (P_α) can be obtained as $u_\alpha = \mathcal{S}^{\lambda}\psi_\alpha$ in $\Omega_{\rm ext}$ and $u_\alpha = \mathcal{S}^{\mu}\varphi_\alpha$ in $\Omega_{\rm int}$, with $(\psi_\alpha, \varphi_\alpha)$ solving

$$\mathcal{H}_\alpha \begin{bmatrix} \varphi_\alpha \\ \psi_\alpha \end{bmatrix} := \begin{bmatrix} V^{\mu} & -V^{\lambda} \\ \alpha(\frac{1}{2}I + J^{\mu}) & \beta(\frac{1}{2}I - J^{\lambda}) \end{bmatrix} \begin{bmatrix} \varphi_\alpha \\ \psi_\alpha \end{bmatrix} = \begin{bmatrix} f \\ \beta\, g \end{bmatrix}. \tag{24.3}$$

The proof of these results can be found in [CZ92, Chap. 7] and [RS06a].

24.3 Convergence Analysis

We start by noticing that if $\mathbf{x} \in \Omega_{\rm ext}$, then

$$|u_\alpha(\mathbf{x}) - u_*(\mathbf{x})| = |\mathcal{S}^{\lambda}(\psi_\alpha - \psi_*)(\mathbf{x})| = |\langle \psi_\alpha - \psi_*, \phi_\lambda(\mathbf{x}, \cdot)\rangle| \leq C_{\mathbf{x}} \|\psi_\alpha - \psi_*\|_{-1/2},$$

where the subscript "$*$" stands for either D or N. Therefore, the study of pointwise convergence in $\Omega_{\rm ext}$ can be carried out by analyzing the convergence of the densities in $H^{-1/2}(\Gamma)$. Indeed, here we use the natural $H^{-1/2}(\Gamma)$-norm, but when using a weaker or stronger norm, one obtains the same convergence rate in terms of α. The only difference is the constant appearing in the estimate. In any case, it does not depend on α, but depends on $\mathbf{x}$. It only blows up when we are close to Γ and it is uniformly bounded in the exterior of any ball containing Γ when $\lambda \notin \mathbb{R}$, whereas for $\lambda \in \mathbb{R}$, uniform boundedness is only assured in compact sets.

Proposition 1. *Consider the operators*

$$A := (\tfrac{1}{2}I + J^{\mu})(V^{\mu})^{-1} : H^{1/2}(\Gamma) \to H^{-1/2}(\Gamma),$$
$$D := \beta^{-1}(\tfrac{1}{2}I - J^{\lambda})^{-1} A V^{\lambda} : H^{-1/2}(\Gamma) \to H^{-1/2}(\Gamma),$$
$$H_\alpha := \beta(\tfrac{1}{2}I - J^{\lambda}) + \alpha A V^{\lambda} : H^{-1/2}(\Gamma) \to H^{-1/2}(\Gamma).$$

Then

(a) *If* $|\alpha| < \|D\|^{-1}$, *then* H_α *is invertible. Moreover,*

$$\|H_\alpha^{-1}\| \leq C, \qquad \forall\, |\alpha| \leq \alpha_0 < \|D\|^{-1}.$$

(b) *If* $|\alpha| > \|D^{-1}\|$, *then* H_α *is invertible. Moreover,*

$$\|H_\alpha^{-1}\| \leq C\, |\alpha|^{-1}, \qquad \forall\, |\alpha| \geq \alpha_0 > \|D^{-1}\|.$$

(c) *If either* $|\alpha| < \|D\|^{-1}$ *or* $|\alpha| > \|D^{-1}\|$, *then*

$$\psi_\alpha = H_\alpha^{-1}\,(-\alpha A f + \beta\, g)\,. \tag{24.4}$$

Proof. First, we assume that $|\alpha| < \|D\|^{-1}$ and decompose

$$H_\alpha \;=\; \beta(\tfrac{1}{2}I - J^\lambda)(I + \alpha D). \tag{24.5}$$

Applying the geometric series theorem (see [AH01, Theorem 2.3.1]), we deduce that H_α is invertible. Furthermore, for all $|\alpha| \le \alpha_0 < \|D\|^{-1}$,

$$\|H_\alpha^{-1}\| \;\le\; \|\beta^{-1}(\tfrac{1}{2}I - J^\lambda)^{-1}\|\|(I + \alpha D)^{-1}\| \;\le\; \frac{C}{1 - |\alpha|\|D\|} \;\le\; C'.$$

For $|\alpha| > \|D^{-1}\|$, the proof is completely analogous: We now decompose

$$H_\alpha \;=\; \alpha A V^\lambda (I + \alpha^{-1} D^{-1}), \tag{24.6}$$

to deduce the invertibility of H_α and the uniform bound

$$\|H_\alpha^{-1}\| \le |\alpha|^{-1}\|(V^\lambda)^{-1}A^{-1}\|\|(I + \alpha^{-1}D^{-1})^{-1}\| \le \frac{C\,|\alpha|^{-1}}{1 - |\alpha|^{-1}\|D^{-1}\|} \le C'|\alpha|^{-1},$$

for all $|\alpha| \ge \alpha_0 > \|D^{-1}\|$. Finally, to show (c), we remark that

$$\mathcal{H}_\alpha = \begin{bmatrix} I & 0 \\ \alpha A & I \end{bmatrix} \begin{bmatrix} V^\mu & -V^\lambda \\ 0 & H_\alpha \end{bmatrix},$$

with $\mathcal{H}_\alpha$ being the operator introduced in (24.3). By (a) and (b), the operator H_α is invertible for the considered values of α, and

$$\begin{aligned} \mathcal{H}_\alpha^{-1} &= \begin{bmatrix} (V^\mu)^{-1} & (V^\mu)^{-1}V^\lambda H_\alpha^{-1} \\ 0 & H_\alpha^{-1} \end{bmatrix} \begin{bmatrix} I & 0 \\ -\alpha A & I \end{bmatrix} \\ &= \begin{bmatrix} (V^\mu)^{-1}(I - \alpha V^\lambda H_\alpha^{-1} A) & (V^\mu)^{-1}V^\lambda\, H_\alpha^{-1} \\ -\alpha\, H_\alpha^{-1} A & H_\alpha^{-1} \end{bmatrix}. \end{aligned}$$

Finally, the result follows readily from (24.3).

Proposition 2. (a) *For all* $|\alpha| \le \alpha_0 < \|D\|^{-1}$,

$$\|\psi_\alpha - \psi_N\|_{-1/2} \;\le\; C\,|\alpha|.$$

(b) *For all* $|\alpha| \ge \alpha_0 > \|D^{-1}\|$,

$$\|\psi_\alpha - \psi_D\|_{-1/2} \;\le\; C\,|\alpha|^{-1}.$$

Proof. (a) From (24.2) and (24.4) it follows that

$$\psi_\alpha - \psi_N = -\alpha\, H_\alpha^{-1} A f + \left(\beta\, H_\alpha^{-1} - (\tfrac{1}{2}I - J^\lambda)^{-1}\right) g,$$

and, by (24.5), we can write

$$\beta\, H_\alpha^{-1} - (\tfrac{1}{2} I - J^\lambda)^{-1} \;=\; \beta\, H_\alpha^{-1} - \beta(I + \alpha D) H_\alpha^{-1} \;=\; -\alpha\beta D H_\alpha^{-1}.$$

Applying Proposition1(a), we now easily deduce the result. To prove (b), we proceed likewise: by direct computation using (24.1) and (24.4), we see that

$$\psi_\alpha - \psi_D = \left(-\alpha H_\alpha^{-1} A + (V^\lambda)^{-1}\right) f + \beta H_\alpha^{-1} g,$$

and, by (24.6), we have

$$-\alpha H_\alpha^{-1} A + (V^\lambda)^{-1} \;=\; -\alpha H_\alpha^{-1} A + (\alpha\, I + D^{-1}) H_\alpha^{-1} A \;=\; D^{-1} H_\alpha^{-1} A.$$

The result is now a consequence of Proposition1(b).

Corollary 1. (a) *The solution of* (P_α) *converges to the solution of* (P_N) *in* Ω_{ext} *as* $\alpha \to 0$. *Moreover, for all* $|\alpha| \leq \alpha_0 < 1/\|D\|$,

$$|u_\alpha(\mathbf{x}) - u_N(\mathbf{x})| \leq C_{\mathbf{x}} |\alpha|, \qquad \mathbf{x} \in \Omega_{\text{ext}}.$$

(b) *The solution of* (P_α) *converges to the solution of* (P_D) *in* Ω_{ext} *as* $\alpha \to \infty$. *Moreover, for all* $|\alpha| \geq \alpha_0 > \|D^{-1}\|$,

$$|u_\alpha(\mathbf{x}) - u_D(\mathbf{x})| \leq C_{\mathbf{x}} |\alpha|^{-1}, \qquad \mathbf{x} \in \Omega_{\text{ext}}.$$

24.4 Convergence at the Discrete Level

In this section, we describe briefly how the previous study applies when dealing with numerical approximations to (P_D), (P_N), and (P_α) obtained by an abstract class of discretizations sharing some common features. The hypotheses we will specify shortly are satisfied by a wide number of numerical methods; in particular, all the abstract Petrov–Galerkin schemes analyzed in [RS06a] fall into that setting, along with the quadrature methods studied in [DRS06].

We will assume that all the densities involved in the numerical solution to the corresponding boundary integral equations are approximated in a discrete space X_m of dimension m. In principle, X_m could not be a subspace of $H^{-1/2}(\Gamma)$ as happens when using quadrature methods where the discrete space is formed by Dirac delta distributions. As in the continuous case, the considered norm does not add any difficulty as indicated at the beginning of Section 24.3. We also assume that in order to compute the coordinates of the approximate densities in a basis of X_m, one has to solve linear systems of equations of the form

$$V_m^\lambda \psi_D^m = -f_m, \tag{24.7}$$

$$(\tfrac{1}{2} I_m - J_m^\lambda)\psi_N^m = g_m, \tag{24.8}$$

$$\begin{bmatrix} V_m^\mu & -V_m^\lambda \\ \alpha(\frac{1}{2} I_m + J_m^\mu) & \beta(\frac{1}{2} I_m - J_m^\lambda) \end{bmatrix} \begin{bmatrix} \varphi_\alpha^m \\ \psi_\alpha^m \end{bmatrix} = \begin{bmatrix} f_m \\ \beta\, g_m \end{bmatrix}, \tag{24.9}$$

for (P_D), (P_N), and (P_α), respectively, where the matrices V_m^λ, I_m, J_m^λ, V_m^μ, and J_m^μ do not depend on α. Obviously, to have a unique solution in (24.7)–(24.9), the corresponding matrices have to be invertible. Then, with the same arguments as in Propositions 1 and 2, the following bounds can be proven:

$$\|\psi_\alpha - \psi_N\| \leq C\,|\alpha|, \qquad \forall\, |\alpha| \leq \alpha_0,$$
$$\|\psi_\alpha - \psi_D\| \leq C\,|\alpha|^{-1}, \qquad \forall\, |\alpha| \geq \alpha_1,$$

where $\|\cdot\|$ is any norm in $\mathbb{C}^m$. From here one deduces the same kind of bounds for the densities in the norm of X_m. If the approximate solutions to (P_D), (P_N), and (P_α) are defined by simply introducing the discrete densities obtained in (24.7)–(24.9) in the definition of the single-layer potentials, then results analogous to those in Corollary 1 can be derived straightforwardly.

24.5 Numerical Examples

This last section is devoted to numerical illustrations in the two-dimensional setting. The numerical method we use here is an easy-to-implement quadrature method proposed in [DRS06].

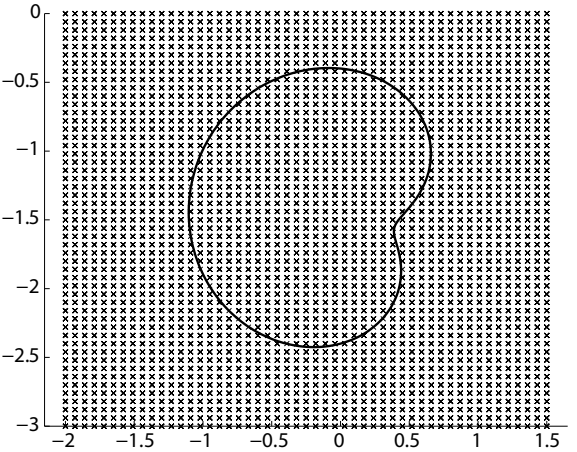

Fig. 24.1. Geometry of the problem.

We have considered the nonconvex domain represented in Figure 24.1, whose boundary is smooth. The physical parameters are $\lambda = \mu = 1 + \imath$ and $\beta = 1$, which correspond to a problem of scattering of thermal waves. We have taken $u_{\rm inc}(x_1, x_2) := \exp(-\imath\lambda x_2)$ as incident wave and have computed the total wave

$$u_{\rm inc} + u_\alpha \quad \text{in } \Omega_{\rm ext}, \qquad u_\alpha \quad \text{in } \Omega_{\rm int},$$

for some different values of α. In Figure 24.2, we represent the modulus of the total wave for five transmission problems with decreasing values of α as well as the modulus of the total wave that solves the exterior Neumann problem. Notice that the solution for $\alpha = 1$ is the planar incident wave.

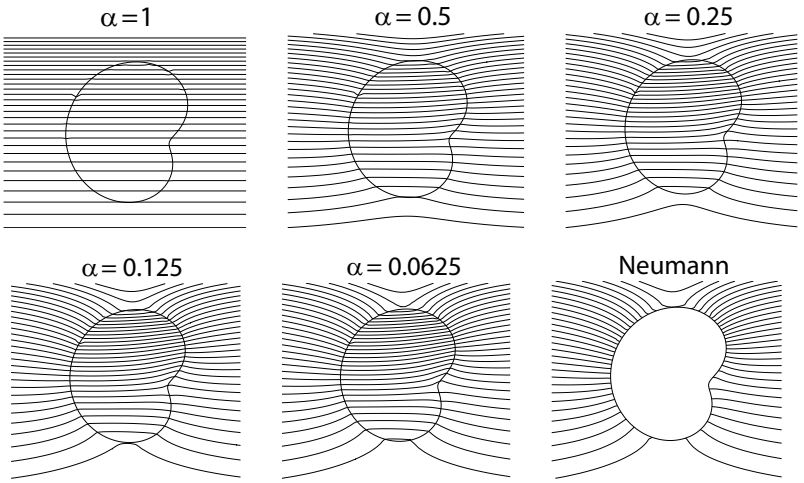

Fig. 24.2. $\alpha = 1,\ 1/2,\ 1/4,\ 1/8,\ 1/16$, and the Neumann exterior problem.

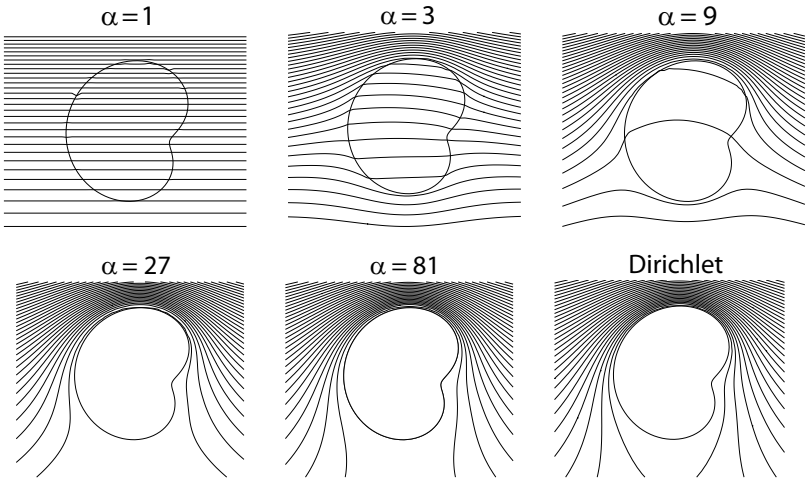

Fig. 24.3. $\alpha = 1,\ 3,\ 9,\ 27,\ 81$, and the Dirichlet exterior problem.

In Table 24.1, we write the errors $E^N_{\text{abs}} := \max_i |u_\alpha(\mathbf{x}_i) - u_N(\mathbf{x}_i)|$ and $E^N_{\text{rel}} := \max_i (|u_\alpha(\mathbf{x}_i) - u_N(\mathbf{x}_i)|/|u_N(\mathbf{x}_i)|)$, where $\mathbf{x}_i$ are the 50×50 points in the rectangle $[-2, 1.5] \times [-3, 0]$ represented in Figure 24.1. The corresponding estimated convergence rates (ecr) are computed by comparing errors for consecutive values of α in the usual way. It is clear that these numerical results fit with the theoretical ones.

We now solve the same problem for increasing values of α. In Figure 24.3, we represent the modulus of the total wave solution for the transmission and Dirichlet problems. Relative and absolute errors at the points $\mathbf{x}_i$ are written on the right of Table 24.1. Notice that in this case, although absolute errors have almost the same size as in the Neumann case, relative errors are now really large. This is not surprising, since the total wave in the Dirichlet problem is almost zero in the shadow of the obstacle.

Acknowledgement. The authors are partially supported by MEC/FEDER Project MTM-2004-01905, Gobierno de Navarra Project Ref. 18/2005, and by DGA-Grupo Consolidado PDIE.

Table 24.1. Absolute and relative errors for the Neumann and Dirichlet problems.

α	E^N_{abs}	ecr	E^N_{rel}	ecr
10^{-1}	$5.95 \cdot 10^{-2}$		$1.24 \cdot 10^{-1}$	
10^{-2}	$6.33 \cdot 10^{-3}$	0.97	$1.34 \cdot 10^{-2}$	0.96
10^{-3}	$6.37 \cdot 10^{-4}$	0.99	$1.35 \cdot 10^{-3}$	0.99
10^{-4}	$6.37 \cdot 10^{-5}$	0.99	$1.35 \cdot 10^{-4}$	0.99
10^{-5}	$6.37 \cdot 10^{-6}$	0.99	$1.35 \cdot 10^{-5}$	0.99

α	E^D_{abs}	ecr	E^D_{rel}	ecr
10^{1}	$2.30 \cdot 10^{-1}$		$5.00 \cdot 10^{2}$	
10^{2}	$2.77 \cdot 10^{-2}$	-0.91	$7.01 \cdot 10$	-0.85
10^{3}	$2.82 \cdot 10^{-3}$	-0.99	7.25	-0.98
10^{4}	$2.82 \cdot 10^{-4}$	-0.99	$7.28 \cdot 10^{-1}$	-0.99
10^{5}	$2.82 \cdot 10^{-5}$	-0.99	$7.28 \cdot 10^{-2}$	-0.99

References

[AH01] Atkinson, K., Han, W.: *Theoretical Numerical Analysis: A Functional Analysis Framework.* Springer, New York (2001).

[CZ92] Chen, G., Zhou, J.: *Boundary Element Methods.* Academic Press, London (1992).

[CK83] Colton, D.L., Kress, R.: *Integral Equation Methods in Scattering Theory.* Wiley, New York (1983).

[CS85] Costabel, M., Stephan, E.: A direct boundary integral equation method for transmission problems. *J. Math. Anal. Appl.,* **106**, 367–413 (1985).

[DRS06] Domínguez, V., Rapún, M.–L., Sayas, F.–J.: Dirac delta methods for Helmholtz transmission problems. *Adv. Comput. Math.* (in press).

[KM88] Kleinman, R.E., Martin, P.A.: On single integral equations for the transmission problem of acoustics. *SIAM J. Appl. Math.,* **48**, 307–325 (1988).

[KR78] Kress, R., Roach, G.F.: Transmission problems for the Helmholtz equation. *J. Math. Phys.,* **19**, 1433–1437 (1978).

[Man01] Mandelis, A.: *Diffusion–Wave Fields. Mathematical Methods and Green Functions*. Springer, New York (2001).

[McL00] McLean, W.: *Strongly Elliptic Systems and Boundary Integral Equations.* Cambridge University Press, Cambridge (2000).

[RS06a] Rapún, M.-L., Sayas, F.-J.: Boundary integral approximation of a heat diffusion problem in time-harmonic regime. *Numer. Algorithms,* **41**, 127–160 (2006).

[RS06b] Rapún, M.-L., Sayas, F.-J.: Indirect methods with Brakhage–Werner potentials for Helmholtz transmission problems. In: *Proceedings of ENUMATH 2005*. Springer, New York (2006), pp. 1146–1154.

[TSS02] Terrón, J.M., Salazar, A., Sánchez–Lavega, A.: General solution for the thermal wave scattering in fiber composites. *J. Appl. Phys.,* **91**, 1087–1098 (2002).

[TW93] Torres, R.H., Welland, G.V.: The Helmholtz equation and transmission problems with Lipschitz interfaces. *Indiana Univ. Math. J.,* **42**, 1457–1485 (1993).

25

Direct Boundary Element Method with Discretization of All Integral Operators

F.-J. Sayas

Universidad de Zaragoza, Spain; jsayas@unizar.es

25.1 Introduction

The history of boundary element methods (BEMs) for elliptic boundary value problems is the result of a combination of many different approaches. The origins of the method, from a purely theoretical point of view, can be traced back to the first studies of integral equations and, hence, to the birth of functional analysis. It was the development of Fredholm theory that first gave an impulse to numerical methods that reformulate a boundary value problem (BVP) on the boundary of the domain and then solve an integral equation by any method available. These first essays are centered on the use of integral equations of the second kind. Later on, when the ellipticity of some important boundary integral operators was proved, the type of boundary integral equation of interest changed drastically to integral equations of the first kind. In addition, the ellipticity of the equations proved the adequacy of using Galerkin methods. It was back then that a main bifurcation happened between the mathematical and the engineering literature on BEM. The gap is now much deeper than the well-known duplication of efforts in the finite element world.

A priori, theorists in the mathematical community and some practitioners in the realm of physics have preferred boundary integral formulations that lead to equations where Galerkin methods can be employed. In part because of the additional integration process that Galerkin methods impose, there has been a preference for indirect formulations. In these, a potential is proposed as a solution of the partial differential equation. Imposition of boundary conditions leads to boundary integral equations. The unknown is a density without a clear physical meaning, if it has any at all. On the side of advantages, equations are simpler, data do not appear under the action of integral operators and there is a clear knowledge of how the numerical methods converge, with some well-understood superconvergence phenomena in weak norms. However, in addition to the fact that we are computing something that has no physical interpretation (it is the numerical input of a function that gives the approx-

imate solution of the BVP), these equations fail to be well posed in some relevant situations.

It has been advocated by the more practically-oriented community of boundary element developers to insist in using direct formulations. These arise from taking Green's third formula (actually, its adaptation to the particular elliptic operator) and substituting the data in it. Then the unknowns are the remaining Cauchy data. Even when the operator involved in the equation is not invertible, the equation is always solvable and all possible solutions are valid from the point of view of reconstructing the solution of the BVP. We are nevertheless faced with having the data under the action of an integral operator. Typically, practitioners have preferred collocation methods to partially compensate for this problem, even though there is no strong theoretical support for their general convergence.

There is, however, an additional aspect of the practical literature on BEM that is usually ignored by theorists. Even the most elementary texts treat the equations as if all the boundary data were unknown and discretizing all the integral operators. Only in a final step, data are plugged into the equation. This approach further simplifies the need of approximating integrals in the practical implementation of the method and makes these implementations more reusable for different boundary value problems.

In this paper we are going to explain, with a collection of very simple examples, how to profit from this idea in the context of Galerkin or Petrov-Galerkin methods. In some cases, we will construct methods that preprocess data before inputting them in the discrete equations. In some other cases, we will develop methods based on the theory of a mixed finite element method (FEM), where this projection of data and the computation of the unknowns are done simultaneously.

To fix the language of Petrov-Galerkin methods for operator equations (or variational problems), we refer to Section 25.4, where we will shortly review some important results. Proofs thereof, albeit in a very different language, can be found in [K99]. Results on inf-sup conditions and problems with mixed structure can be found in [BF91]. For theoretical aspects on boundary integral operators, we refer the reader to [M00] and its extensive bibliography. A very thorough exposition of the basic theory of Sobolev spaces on Lipschitz boundaries can be found in the same monograph.

From among the many, and sometimes conflicting, notations for potentials and integral operators, we will be using those of George Hsiao (see Section 25.2 and [GH95], for example). The angled bracket $\langle \cdot\,, \cdot \rangle$ will be used to denote the $H^{-1/2}(\Gamma) \times H^{1/2}(\Gamma)$-duality product that arises from identifying $L^2(\Gamma)$ with its dual space. The norm on $H^r(\Gamma)$ will be denoted simply by $\| \cdot \|_r$.

25.2 Model Problem, Potentials, and Operators

As a very simple model problem, where we can concentrate on the boundary operators avoiding some unimportant technicalities, we will consider Yukawa's equation in an exterior domain. Let then Γ be the boundary of a Lipschitz domain (connectedness of this domain is not necessary), and let Ω be the exterior of this domain. We then consider the problem

$$u \in H^1(\Omega), \quad -\Delta u + u = 0 \text{ in } \Omega, \tag{25.1}$$

together with Dirichlet or Neumann boundary conditions on Γ. The domain Ω being unbounded, the hypothesis $u \in H^1(\Omega)$ requires a certain behavior at infinity. Because of the ellipticity of the problem, we do not need to impose any kind of radiation condition.

Let Φ be the fundamental solution (Green's function in free space) of the Yukawa operator:

$$\Phi(\mathbf{x},\mathbf{y}) := \begin{cases} \frac{1}{2\pi} K_0(|\mathbf{x}-\mathbf{y}|) & \text{in two dimensions,} \\ \dfrac{\exp(-|\mathbf{x}-\mathbf{y}|)}{4\pi|\mathbf{x}-\mathbf{y}|} & \text{in three dimensions.} \end{cases}$$

In connection with it, we define the single-layer and double-layer potentials on Γ by

$$\mathcal{S}\lambda := \int_\Gamma \Phi(\,\cdot\,, y)\lambda(y)\mathrm{d}\gamma(y),$$
$$\mathcal{D}\varphi := \int_\Gamma \partial_{\nu(y)}\Phi(\,\cdot\,, y)\varphi(y)\mathrm{d}\gamma(y).$$

The four (generalized) integral operators

$$V\lambda := \int_\Gamma \Phi(\,\cdot\,, y)\lambda(y)\mathrm{d}\gamma(y),$$
$$K^t\lambda := \int_\Gamma \partial_{\nu(\,\cdot\,)}\Phi(\,\cdot\,, y)\lambda(y)\mathrm{d}\gamma(y),$$
$$K\varphi := \int_\Gamma \partial_{\nu(y)}\Phi(\,\cdot\,, y)\varphi(y)\mathrm{d}\gamma(y),$$
$$W\varphi := -\partial_{\nu(\,\cdot\,)}\int_\Gamma \partial_{\nu(y)}\Phi(\,\cdot\,, y)\varphi(y)\mathrm{d}\gamma(y)$$

enable us to write the trace and normal derivative of these potentials (see [M00] for these limits and the corresponding mapping properties in Sobolev spaces). We recall that compactness of $K : H^{1/2}(\Gamma) \to H^{1/2}(\Gamma)$ requires some degree of smoothness of Γ: It is sufficient to assume Lyapunov regularity, which excludes polygonal or polyhedral boundaries.

Green's third formula states that any solution of (25.1) satisfies

$$u = \mathcal{D}\varphi - \mathcal{S}\lambda \ \text{ in } \Omega, \quad \text{where } \varphi := \gamma u, \ \ \lambda := \partial_\nu u. \tag{25.2}$$

Because of the expression for the limits of the layer potentials (they are sometimes referred to as the jump properties of the potentials), the Cauchy data $(\varphi, \lambda) \in H^{1/2}(\Gamma) \times H^{-1/2}(\Gamma)$ of any solution of (25.1) satisfy

$$V\lambda + (\tfrac{1}{2}I - K)\varphi = 0, \tag{25.3}$$
$$(\tfrac{1}{2}I + K')\lambda + W\varphi = 0. \tag{25.4}$$

The operators V and W are elliptic; i.e., there exist positive constants C_V and C_W such that

$$\langle \lambda, V\lambda \rangle \geq C_V \|\lambda\|^2_{-1/2} \quad \forall \lambda \in H^{-1/2}(\Gamma),$$
$$\langle W\varphi, \varphi \rangle \geq C_W \|\varphi\|^2_{1/2} \quad \forall \varphi \in H^{1/2}(\Gamma).$$

25.3 Exterior Boundary Value Problems

25.3.1 The Dirichlet Problem and the First Formula

Consider the Dirichlet problem, composed by joining (25.1) and

$$u = g_0 \quad \text{in } \Gamma. \tag{25.5}$$

Recall the representation formula (25.2) for u in terms of its Cauchy data. A direct boundary integral formulation for (25.1), (25.5) can be deduced by considering (25.3) as an integral equation with $\lambda \in H^{-1/2}(\Gamma)$ as unknown, after plugging g_0 in place of φ and moving that term to the right-hand side. This is obviously equivalent to the following integral system with a trivial upper triangular structure:

$$\begin{cases} (\lambda, \varphi) \in H^{-1/2}(\Gamma) \times H^{1/2}(\Gamma), \\ V\lambda + (\tfrac{1}{2}I - K)\varphi = 0, \\ \varphi = g_0. \end{cases}$$

Now take three sequences of finite-dimensional spaces

$$X_h^{-1/2}, Z_h^{-1/2} \subset H^{-1/2}(\Gamma), \quad Y_h^{1/2} \subset H^{1/2}(\Gamma)$$

(henceforth the numerical superscript $\pm 1/2$ will be used to recall in which of $H^{\pm 1/2}(\Gamma)$ the discrete space is imbedded). We then consider the Petrov–Galerkin scheme

$$\begin{cases} (\lambda_h, \varphi_h) \in X_h^{-1/2} \times Y_h^{1/2}, \\ \langle \mu_h, V\lambda_h \rangle + \langle \mu_h, (\frac{1}{2}I - K)\varphi_h \rangle = 0 \quad \forall \mu_h \in X_h^{-1/2}, \\ \langle \xi_h, \varphi_h \rangle = \langle \xi_h, g_0 \rangle \quad \forall \xi_h \in Z_h^{-1/2}. \end{cases} \tag{25.6}$$

Note that testing the first equation with the same space where we look for the first unknown is suggested by the ellipticity of V. Then, to square the system, we need that $\dim Z_h^{-1/2} = \dim Y_h^{1/2}$. The second group of equations is equivalent to preprocessing the datum g_0 before substituting it under the action of the integral operator K. From a practical point of view, this operation is done beforehand. The following result follows from some standard manipulations at the discrete level. For the language on stability and convergence, as well as to see the meaning of the symbol $\gtrsim$, see Section 25.4.

Theorem 1. *Stability of the method is equivalent to*

$$\sup_{0 \neq \xi_h \in Z_h^{-1/2}} \frac{|\langle \xi_h, \varphi_h \rangle|}{\|\xi_h\|_{-1/2}} \gtrsim \|\varphi_h\|_{1/2} \quad \forall \varphi_h \in Y_h^{1/2}. \tag{25.7}$$

For instance, if $Y_h^{1/2} \subset H^1(\Gamma)$ and the following conditions hold:

$$\sup_{0 \neq \xi_h \in Z_h^{-1/2}} \frac{|\langle \xi_h, \varphi_h \rangle|}{\|\xi_h\|_{-r}} \gtrsim \|\varphi_h\|_r \quad \forall \varphi_h \in Y_h^{1/2}, \quad r \in \{0, 1\}$$

(these ones are a priori simpler to verify, since they do not involve fractional Sobolev norms), then (25.7) follows by interpolation.

The simplest example is taking $Z_h^{-1/2} := TY_h^{1/2}$, where $T : H^{1/2}(\Gamma) \to H^{-1/2}(\Gamma)$ is the operator associated with the Riesz–Fréchet representation of the dual of $H^{1/2}(\Gamma)$ as itself; that is, for $\xi \in H^{1/2}(\Gamma)$, $\langle T\xi, \cdot \rangle := \langle \xi, \cdot \rangle_{1/2}$. This is equivalent to using the nonlocal $H^{1/2}(\Gamma)-$inner product in the preprocessing step of (25.6). A second simple option is taking $Z_h^{-1/2} = Y_h^{1/2}$. Then (25.7) is the $H^{1/2}(\Gamma)$-stability of the $L^2(\Gamma)$-orthogonal projection onto $Y_h^{1/2}$, which is related to some traditional problems in the field of parabolic problems. This property is satisfied by spectral-type spaces, like trigonometric polynomials in two dimensions and spherical harmonics in three, or by piecewise polynomial spaces on quasiuniform meshes. In fact, in all those cases, the result is a consequence of the following lemma.

Lemma 1. *Assume that there exists* $\varepsilon(h)$ *such that* $\lim_{h \to 0} \varepsilon(h) = 0$ *and*

$$\inf_{\varphi_h \in Y_h^{1/2}} \big(\varepsilon(h) \|\varphi - \varphi_h\|_{1/2} + \|\varphi - \varphi_h\|_0 \big) \lesssim \varepsilon(h) \|\varphi\|_{1/2} \quad \forall \varphi \in H^{1/2}(\Gamma),$$

$$\|\varphi_h\|_{1/2} \lesssim \varepsilon(h)^{-1} \|\varphi_h\|_0 \quad \forall \varphi_h \in Y_h^{1/2}.$$

Then (25.7) *holds with* $Z_h^{-1/2} = Y_h^{1/2}$.

More general choices of spaces satisfying (25.7) usually involve the use of dual/staggered meshes as in [S03] or [RS06].

25.3.2 The Neumann Problem and the First Formula

The Neumann problem, i.e., (25.1) and

$$\partial_\nu u = g_1 \quad \text{in } \Gamma,$$

can be approached with the same formula (25.3), using φ as unknown. However, the situation is very different. The equation is formally one of the second kind, but Fredholm theory works if K is compact, which calls for additional regularity of Γ. Note that $\frac{1}{2}I - K$ is a Fredholm operator even for Lipschitz boundaries, but its principal part is not $\frac{1}{2}I$ but something else, when Γ is not Lyapunov. We thus restrict our attention to these boundaries. The boundary integral formulation is

$$\begin{cases} (\lambda, \varphi) \in H^{-1/2}(\Gamma) \times H^{1/2}(\Gamma), \\ V\lambda + (\frac{1}{2}I - K)\varphi = 0, \\ \lambda = g_1. \end{cases} \tag{25.8}$$

The approach of Subsection 25.3.1 can be applied here. Although we do not need to use the ellipticity of V, the reasonable thing to do is still to use a Galerkin scheme for it. A possibility is then to take two subspaces, with $\dim X_h^{-1/2} = \dim Y_h^{1/2}$, and do as follows:

$$\begin{cases} (\lambda_h, \varphi_h) \in X_h^{-1/2} \times Y_h^{1/2}, \\ \langle \mu_h, V\lambda_h \rangle + \langle \mu_h, (\frac{1}{2}I - K)\varphi_h \rangle = 0 \quad \forall \mu_h \in X_h^{-1/2}, \\ \langle \lambda_h, \rho_h \rangle = \langle g_1, \rho_h \rangle \quad \forall \xi_h \in Y_h^{1/2}. \end{cases} \tag{25.9}$$

If we wrote the second group of discrete equations in the first place, we would easily notice the lower-triangular structure of the system: The data are preprocessed to create a discrete copy λ_h and are then plugged into the discretization of (25.3).

Theorem 2. *Assuming compactness of K, convergence of* (25.9) *is attained provided that*

$$\sup_{0 \neq \mu_h \in X_h^{-1/2}} \frac{|\langle \mu_h, \varphi_h \rangle|}{\|\mu_h\|_{-1/2}} \gtrsim \|\varphi_h\|_{1/2} \quad \forall \varphi_h \in Y_h^{1/2}, \tag{25.10}$$

and that the sequences $X_h^{-1/2}$ and $Y_h^{1/2}$ are approximating in $H^{-1/2}(\Gamma)$ and $H^{1/2}(\Gamma)$, respectively.

The structure of (25.9), as we have written it, recalls, however, also the theory of mixed problems. Apart from the compact perturbation K and a factor $1/2$ in the first equation, the operator equation (25.8) is one of mixed

type with elliptic diagonal operator. We can then try (25.9) by dropping the condition of equality of dimensions of the subspaces. Theorem 2 still holds. For (25.10), it is necessary that $\dim X_h^{-1/2} \geq \dim Y_h^{1/2}$. The system cannot be understood anymore as preprocessing the data and substituting, although Uzawa-type iterations can be applied to avoid working with the full system. These methods can be rewritten as a sequence of preprocesses for the data and substitutions, only in reverse order (solving a sequence of Dirichlet problems instead of the Neumann one).

25.3.3 Use of the Second Formula

The use of (25.4) as the basic boundary integral equation reverses the roles of the unknowns in the considerations above. The Neumann problem is now an elliptic one (W is the associated operator) and works with a simple preprocessing of the incoming datum, not needing the hypothesis on compactness of K. The Dirichlet problem now leads to an equation of the second kind, and everything works as above, assuming that K is compact.

25.3.4 Mixed Boundary Conditions

A similar approach can easily be applied to the mixed BVP. We will simply sketch how the method works. Assume that Γ is subdivided into two nonoverlapping, nontrivial parts Γ_D and Γ_N, and that we have the boundary conditions

$$u = g_0 \quad \text{in } \Gamma_D, \qquad \partial_\nu u = g_1 \quad \text{in } \Gamma_N,$$

for (25.1). We first create any extension of g_0 to $H^{1/2}(\Gamma)$, say $\widetilde{g}_0$. Let $H := \{\rho \in H^{1/2}(\Gamma) \,|\, \rho \equiv 0, \quad \text{in } \Gamma_D\}$. Using (25.3), we can deal with the problem by writing the system

$$\begin{cases} (\lambda, \varphi_0, \rho) \in H^{-1/2}(\Gamma) \times H \times H^{1/2}(\Gamma), \\ V\lambda + (\frac{1}{2}I - K)\varphi_0 + (\frac{1}{2}I - K)\rho = 0, \\ \langle \lambda, \chi \rangle = \langle g_1, \chi \rangle \quad \forall \chi \in H, \\ \rho = \widetilde{g}_0. \end{cases}$$

Then $\varphi = \varphi_0 + \widetilde{g}_0$ is the full Dirichlet datum and λ is the full Neumann datum. The compactness of K becomes relevant again at the numerical level. We can use two spaces $X_h^{-1/2}$ and $Y_h^{1/2}$, assuming that $\dim X_h^{-1/2} = \dim Y_h^{1/2}$, and a third space $H_h := Y_h^{1/2} \cap H$. The associated Petrov–Galerkin method

$$\begin{cases} (\lambda_h, \varphi_h^0, \rho_h) \in X_h^{-1/2} \times H_h \times Y_h^{1/2}, \\ \langle \mu_h, V\lambda_h \rangle + \langle \mu_h, (\frac{1}{2}I - K)\varphi_h^0 \rangle + \langle \mu_h, (\frac{1}{2}I - K)\rho_h \rangle = 0 \quad \forall \mu_h \in X_h^{-1/2}, \\ \langle \lambda_h, \chi_h \rangle = \langle g_1, \chi_h \rangle \quad \forall \chi_h \in H_h, \\ \langle \eta_h, \rho_h \rangle = \langle \eta_h, \widetilde{g}_0 \rangle \quad \forall \eta_h \in X_h^{-1/2}, \end{cases}$$

preprocesses the extended Dirichlet datum and then works the whole method in the sense of Subsection 25.3.2.

Theorem 3. *Assuming the compactness of K, approximation properties for all the discrete spaces, and the* inf-sup *condition*

$$\sup_{0\neq\xi_h\in H_h} \frac{|\langle\lambda_h,\chi_h\rangle|}{\|\chi_h\|_{1/2}} \gtrsim \|\lambda_h\|_{-1/2} \quad \forall\lambda_h\in X_h^{-1/2},$$

the above method converges.

25.3.5 Other

Very similar ideas apply very naturally in transmission problems, be they treated with systems of boundary integral operators or with coupled interior-boundary problems, ready for the application of BEM–FEM coupling techniques. Such ideas appear in the background of the analytical and computational tools developed in [RS06], [RS07], and related work.

25.4 Appendix: Petrov–Galerkin Methods

Consider two Hilbert spaces H_1 and H_2 and a linear variational problem

$$\begin{cases} u\in H_1, \\ a(u,v)=\ell(v) \quad \forall v\in H_2, \end{cases} \tag{25.11}$$

where $a : H_1\times H_2\to\mathbb{R}$ is a continuous bilinear form and ℓ is any element of the dual of H_2. The well posedness of the problem is characterized by the invertibility of the operator $A : H_1\to H_2'$

$$Au := a(u,\,\cdot\,) : H_2\to\mathbb{R},$$

and means that (25.11) is uniquely solvable for any ℓ, and that the solution operator is bounded. Let $H_\alpha^h\subset H_\alpha$ ($\alpha\in\{1,2\}$) be two sequences of finite-dimensional spaces, directed on the parameter $h\to 0$, with the restriction $\dim H_1^h = \dim H_2^h$. A Petrov–Galerkin method for (25.11), associated with the spaces H_1^h and H_2^h, is a scheme of the form

$$\begin{cases} u_h\in H_1^h, \\ a(u_h,v_h)=\ell(v_h) \quad \forall v_h\in H_2^h. \end{cases} \tag{25.12}$$

Equations (25.12) are equivalent to a square linear system with the same dimension as that of the discrete spaces. The concept of stability of the scheme is that of unique solvability of the equations together with a uniform bound (for all h and all u)

$$\|u_h\| \lesssim \|u\|,$$

where the expression $a_h \lesssim b_h$ (we will also use the reversed symbol $\gtrsim$) means that there exists a positive constant $C > 0$, independent of h and of the quantities it multiplies, such that $a_h \leq C\, b_h$. Stability is equivalent to a uniform Babuška–Brezzi condition

$$\sup_{0 \neq v_h \in H_2^h} \frac{|a(u_h, v_h)|}{\|v_h\|} \gtrsim \|u_h\| \quad \forall u_h \in H_1^h. \tag{25.13}$$

Notice that (25.13) already implies unique solvability of the associated system. Because of the Céa–Polski estimate, convergence (i.e., convergence for arbitrary right-hand sides) is equivalent to stability plus the approximation property

$$\inf_{\chi_h \in H_1^h} \|u - \chi_h\| \xrightarrow{h \to 0} 0 \quad \forall u \in H_1. \tag{25.14}$$

The sequence of spaces H_1^h is said to be approximating in H_1 if (25.14) holds. Sometimes stability is only considered in an asymptotic way, that is, beginning with h small enough. The sense of this is the fact that the equations could be noninvertible for h large, or that the inherent constant in (25.13) could evolve to a stable regime as h decreases and the values for h large are nonoptimal.

Proposition 1 (Discrete Fredholm property). *Convergence is preserved under compact perturbations of the operator A; namely, if K is compact, $A+K$ is one-to-one, and the Petrov–Galerkin method with spaces H_1^h and H_2^h is convergent for A, then the method is convergent for $A + K$.*

Finally, note that if $\dim H_1^h = \dim H_2^h$, as we have assumed, then the role of these spaces in condition (25.13) can be reversed. When the dimensions do not coincide, the condition ceases to be symmetrical. It is then equivalent to the injectivity of the discrete operator $A_h : H_1^h \to (H_2^h)'$ defined by

$$A_h u_h := a(u_h, \cdot\,) : H_2^h \to \mathbb{R},$$

together with the uniform boundedness of its Moore–Penrose pseudoinverse.

References

[BF91] Brezzi, F., Fortin, M.: *Mixed and Hybrid Finite Element Methods.* Springer, New York (1991).

[GH95] Gatica, G.N., Hsiao, G.C.: *Boundary-Field Equation Methods for a Class of Nonlinear Problems.* Longman, Harlow (1995).

[K99] Kress, R.: *Linear Integral Equations,* 2nd ed. Springer, New York (1999).

[M00] McLean, W.: *Strongly Elliptic Systems and Boundary Integral Equations.* Cambridge University Press, Cambridge (2000).

[RS06] Rapún, M.-L., Sayas, F.-J.: Boundary integral approximation of a heat-diffusion problem in time-harmonic regime. *Numer. Algorithms,* **41**, 127–160 (2006).

[RS07] Rapún, M.-L., Sayas, F.-J.: Boundary element simulation of thermal waves. *Arch. Comput. Methods Engrg,* **14**, 3–46 (2007).

[S03] Steinbach, O.: *Stability Estimates for Hybrid Coupled Domain Decomposition Methods.* Springer, Berlin (2003).

26

Reciprocity in Elastomechanics: Development of Explicit Results for Mixed Boundary Value Problems

A.P.S. Selvadurai

McGill University, Montreal, QC, Canada; patrick.selvadurai@mcgill.ca

26.1 Introduction

The reciprocity principle put forward in 1864 by Maxwell [Max64] essentially dealt with the application of the principle to structural systems that involved forces, moments, and their kinematic counterparts. In 1872, Enrico Betti [Bet72] put forward a more general statement of the theorem of reciprocity, which is recognized as one of the most significant results in the classical theory of elasticity. An important discussion of Betti's reciprocal theorem given by Truesdell [Tr63] shows that reciprocity in elastomechanics is consistent with the *existence of a strain energy function*. The most important feature of the reciprocity property is the ability to link two states through their corresponding traction and displacement fields governing analogous boundary value problems. This presents a significant advantage; Betti's reciprocal theorem continues to be the key identity in development of the boundary element method in elasticity. The theorem can also be applied successfully in situations where results of global interest are sought. Examples of these situations include contact, inclusion, and crack problems in elasticity, where compliances, stiffness, and stress intensity factors are of interest. Shield [Sh67] and Shield and Anderson [Sh66] have applied the reciprocal theorem to determine load–displacement relationships, and examples of the application of the principle to contact and inclusion problems are given by Selvadurai [Sel00, Sel07].

Here we illustrate the use of Betti's reciprocal theorem to examine a contact problem, where the conventional formulations of the associated mixed boundary value problems in elasticity yield a class of integral equations that are amenable to solution only through numerical techniques. The application of Betti's reciprocal theorem on the other hand leads to the development of either *exact closed form* solutions or much simpler integral results for estimates of engineering interest.

26.2 A Contact Problem for a Half-Space

The problem involving the direct axisymmetric loading of the rigid circular punch was examined by Boussinesq [Bou85] using the analogy with potential theory and later by Harding and Sneddon [Har45], who formulated the mixed boundary value problem as a set of dual integral equations, reducing them to a single integral equation of the Abel-type, which was solved in an exact fashion. As a special case, we restrict attention to the situation where the contact between a rigid circular indentor with a flat smooth base initiated by the load P is perturbed by a concentrated normal load Q^* that acts at an exterior location on the surface of the half-space (Figure 26.1(a)). The objective is

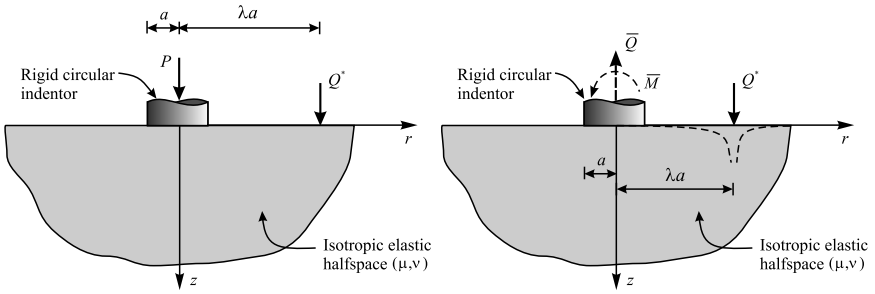

Fig. 26.1. Interaction of a rigid indentor and an externally placed load. (a) The contact problem. (b) The reduced mixed boundary value problem.

to determine the additional axial displacement and rotation of the smooth indentor as a result of this external load. Since the classical elasticity problem is linear, we can superimpose the effects of P and Q^*, provided there is no separation at the smoothly indenting interface. We restrict attention to the analysis of the interaction between a smoothly interacting rigid indentor with a flat base with a bilateral contact (i.e., capable of sustaining tensile tractions) and the externally placed force Q^*. If the contact is bilateral, the smooth indentor will experience a rigid body translation and a rigid body rotation during the application of the external load Q^*. We now apply corrective force resultants in the form of an axial force $\bar{Q}$ and a moment $\bar{M}$, such that the displacement of the indentor is suppressed (Figure 26.1(b)). The resulting mixed boundary value problem can be formulated in relation to the half-space region $z \geq 0$, as follows:

$$u_z(r,\theta,0) = 0, \qquad 0 \leq \theta \leq 2\pi, \quad 0 \leq r \leq a, \tag{26.1}$$

$$\sigma_{zz}(r,\theta,0) = -p(r,\theta), \qquad 0 \leq \theta \leq 2\pi, \quad a < r < \infty, \tag{26.2}$$

$$\sigma_{rz}(r,\theta,0) = 0, \qquad 0 \leq \theta \leq 2\pi, \quad 0 < r < \infty, \tag{26.3}$$

where $p(r,\theta)$ is an even function of θ.

To solve the mixed boundary value problem, we make use of the Hankel transformation-based solutions of the equations of elasticity presented by Muki [M60]. It can be shown that when the condition (26.3) pertaining to zero shear tractions is satisfied on $z=0$, the displacement $u_z(r,\theta,0)$ and the normal stress $\sigma_{zz}(r,\theta,0)$ can be expressed in the following forms:

$$[c]u_z(r,\theta,0) = 2(1-\nu)\sum_{m=0}^{\infty} \mathrm{H}_m[\xi^{-2}\,\Psi_m(\xi);r]\,\cos m\theta,$$

$$\sigma_{zz}(r,\theta,0) = -2\mu\sum_{m=0}^{\infty} \mathrm{H}_m[\xi^{-1}\,\Psi_m(\xi);r]\,\cos m\theta,$$

where

$$\mathrm{H}_m[\Phi(r);\xi] = \int_0^{\infty} r\,\Phi(r)\,J_m(\xi r)\,\mathrm{d}r$$

is the mth order Hankel operator and $\Psi_m(\xi)$ are unknown functions to be determined by satisfying the mixed boundary conditions (26.1) and (26.2). Assuming that $p(r,\theta)$ admits a representation of the form

$$p(r,\theta) = 2\mu\sum_{m=0}^{\infty} g_m(r)\,\cos m\theta,$$

we see that the mixed boundary conditions (26.1) and (26.2) yield the following sets of dual integral equations for the unknown functions $\Psi_m(\xi)$:

$$\mathrm{H}_m[\xi^{-2}\,\Psi_m(\xi);r] = 0, \qquad 0 \le r \le a, \tag{26.4}$$

$$\mathrm{H}_m[\xi^{-1}\,\Psi_m(\xi);r] = g_m(r), \qquad a < r < \infty. \tag{26.5}$$

The solution of the dual systems indicated by (26.4) and (26.5) is given by several authors including Noble [N58] and Sneddon and Lowengrub [Sn69], and the details will not be repeated. It is sufficient to note that for the concentrated external loading of the half-space

$$[g_0(r);g_m(r)] = \frac{Q^*\,a\,\delta(r-\lambda a)}{8\,\pi^2\,\mu\,r}\,[1;2],$$

where $\delta(r-\lambda a)$ is the Dirac delta distribution and the contact stress distribution at the interface region $0 \le r \le a$ is given by

$$\sigma_{zz}(r,\theta,0) = \frac{2Q^*}{\pi^2}\sum_{m=0}^{\infty}\left(\frac{r}{\lambda a}\right)^m \cos m\theta \int_a^{\infty} \frac{t\,H(\lambda a - t)\,\mathrm{d}t}{\sqrt{\lambda^2 a^2 - t^2}\,(t^2-r^2)^{3/2}}$$

and $H(\lambda a - t)$ is the Heaviside step function. The explicit expression for σ_{zz} in the contact region of the indentor is given by

$$\sigma_{zz}(r,\theta,0) = \frac{Q^*\sqrt{\lambda^2-1}}{a^2\pi^2\sqrt{\rho^2-1}\,[\lambda^2+\rho^2-2\lambda\rho\cos\theta]}, \tag{26.6}$$

where $\rho = r/a$. The result (26.6) can be used to determine the force $\bar{Q}$ and the resultant moment $\bar{M}$ that should be applied to the indentor in order to maintain the axial displacements zero within the indentor region. It can be shown that

$$\bar{Q} = \frac{2Q^*}{\pi}\,\sin^{-1}\left(\frac{1}{\lambda}\right), \quad \bar{M} = Q^*\lambda a\left[1-\frac{2}{\pi}\left\{\tan^{-1}\sqrt{\lambda^2-1}+\frac{\sqrt{\lambda^2-1}}{\lambda^2}\right\}\right].$$

It remains now to apply equal and opposite force resultants directly to the rigid punch to render the rigid punch free of force resultants. This aspect will be discussed in detail in the next section, but it is sufficient to note here that the displacement of the rigid punch in bilateral smooth contact with the elastic half-space region under the action of an external surface load Q^* is given by

$$u_z(r,\theta,0) = \frac{Q^*(1-\nu)}{4\mu a}\left[\frac{2}{\pi}\,\sin^{-1}\left(\frac{1}{\lambda}\right) + \frac{3}{2}\lambda\,\rho\,\cos\theta\left\{1-\frac{2}{\pi}\,\tan^{-1}\sqrt{\lambda^2-1}-\frac{2}{\pi}\frac{\sqrt{\lambda^2-1}}{\lambda^2}\right\}\right], \quad 0\le r\le a.$$

26.3 Solution of the Contact Problem via Betti's Reciprocal Theorem

We now apply Betti's reciprocal theorem of the solution to the nonclassical contact problem shown in Figure 26.2(a). The auxiliary solution required to apply Betti's theorem relates to the problem of a smoothly indenting circular punch with a flat base, which is subjected to an eccentric load Q^* acting at a distance ζa from the center of the indentor (Figure 26.2(b)). The eccentric loading induces a rigid body displacement w_0 at the center of the circular punch and a rotation ϑ_0 within the indentor area. If there is no separation within the contact region, the displacement boundary conditions associated with the eccentric loading are

$$u_z(r,\theta,0) = w_0, \qquad 0\le r\le a, \tag{26.7}$$

$$u_z(r,\theta,0) = \vartheta_0 r\cos\theta, \qquad 0\le r\le a. \tag{26.8}$$

In addition, the traction boundary conditions applicable to problems are

$$\sigma_{zz}(r,\theta,0) = 0, \qquad 0\le\theta\le 2\pi, \quad a<r<\infty, \tag{26.9}$$

$$\sigma_{rz}(r,\theta,0) = 0, \qquad 0\le\theta\le 2\pi, \quad 0\le r<\infty. \tag{26.10}$$

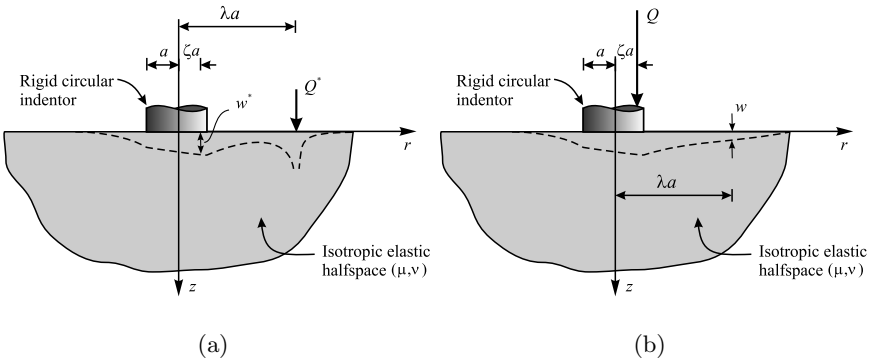

Fig. 26.2. The reciprocal states. (a) The contact problem. (b) The auxiliary solution.

Considering a Hankel transformation development of the governing equations, the conditions (26.7)–(26.10) yield a set of dual integral equations of the forms

$$\begin{aligned} &\mathrm{H}_0[\xi^{-1} A_1(\xi); r] = w_0, && 0 \le r \le a, \\ &\mathrm{H}_0[A_1(\xi); r] = 0, && a < r < \infty, \end{aligned}$$

and

$$\begin{aligned} &\mathrm{H}_1[\xi^{-1} A_2(\xi); r] = \vartheta_0, && 0 \le r \le a, \\ &\mathrm{H}_1[A_2(\xi); r] = 0, && a < r < \infty, \end{aligned}$$

where $A_1(\xi)$ and $A_2(\xi)$ are unknown functions.

The solution of these dual systems is standard, and details are given by Sneddon [Sn75]. The result of interest to the application of the reciprocal theorem involves the displacements of the indentor and the region exterior to the indentor due to the eccentric loading; these can be expressed as follows:

$$u_z(r,\theta,0) = \frac{Q(1-\nu)}{4\mu a}\left[1 + \frac{3\zeta r\cos\theta}{2a}\right], \quad 0 \le r \le a, \tag{26.11}$$

$$\begin{aligned} u_z(r,\theta,0) = \frac{Q(1-\nu)}{4\mu a}&\left[\frac{2}{\pi}\sin^{-1}\left(\frac{a}{r}\right) + \frac{3\zeta r\cos\theta}{2a}\right. \\ &\left.\times\left\{1 - \frac{2}{\pi}\tan^{-1}\left(\frac{\sqrt{r^2-a^2}}{a}\right) - \frac{2a}{\pi}\frac{\sqrt{r^2-a^2}}{r^2}\right\}\right], \quad a \le r \le \infty. \end{aligned} \tag{26.12}$$

Consider now the following reciprocal states. The first involves the eccentric displacement w^* of the rigid circular indentor at a point within it $(\zeta a, 0, 0)$, due to the action of an external normal load Q^* acting at the location $(\lambda a, 0, 0)$ (Figure 26.2(a)). The value of w^* can be obtained from (26.11). The second considers the displacement w at an external point on the surface of the

traction-free half-space $(\lambda a, 0, 0)$ due to the application of an eccentric load that acts at a point $(\zeta a, 0, 0)$ within the indentor region (Figure 26.2(b)). The value of w^* can be obtained from (26.12). In both cases, the smooth contact is assumed to be bilateral and it is assumed that no separation takes place at the contact zone. Furthermore, the choice of $\theta = 0$ is simply to illustrate the reciprocity relationship and the result can be generalized to include any arbitrary location both within the indentor region and exterior to it. By comparing these results, we clearly see that

$$Q^* \, w = Q \, w^*.$$

We can generalize the result to include the point of application of Q^* as $(\lambda a, \phi, 0)$ and the point within the rigid indentor where the displacement is sought by $(\rho a, 0, 0)$. The reciprocal relationship gives the result

$$w_0 = \frac{Q^*(1-\nu)}{4\mu a} \left[\frac{2}{\pi} \sin^{-1}\left(\frac{1}{\lambda}\right) + \frac{3\lambda\rho}{2} \cos(\theta - \phi) \times \left(1 - \frac{2}{\pi} \left\{ \tan^{-1}\sqrt{\lambda^2 - 1} + \frac{\sqrt{\lambda^2 - 1}}{\lambda^2} \right\} \right) \right].$$

26.4 The Cable Jacking Test

The cable jacking test refers to an indentation problem where a test plate resting on the surface of a geologic medium is subjected to loading via a self-stressing system of reaction points located within the medium. The interpretation of the test results is made through the results of a Boussinesq indentation problem applicable to the test configuration, void of any influences of the reaction forces located within the geologic medium. The conventional method of providing a reaction is to consider an axisymmetric load that is located along the axis of the indenting plate. (See, e.g., Zienkiewicz and Stagg [Z67].) The studies by Selvadurai [Sel78], [Sel79] extended the axisymmetric problem in the theory of elasticity to explicitly evaluate the influence of the location of the internal axisymmetric equilibrating force. The solution for the displacement of a smoothly indenting rigid circular plate of radius a that is subjected to an external axial force and an internal axial force located at a distance from the rigid plate and acting in a direction opposite to a is given by

$$w_0 = \frac{P(1-\nu)}{4a\mu} \left(1 - \frac{P_M}{P} \left\{ \frac{2}{\pi} \tan^{-1}\left(\frac{a}{c}\right) + \frac{ac}{\pi(1-\nu)(a^2 + c^2)} \right\} \right).$$

The extension of the analysis of the cable jacking test to include other forms of internal load distributions is nonroutine. Consider the test arrangement shown in Figure 26.3, where the reactive loads are provided by concentrated equilibrating forces that are located at the interior of the half-space region.

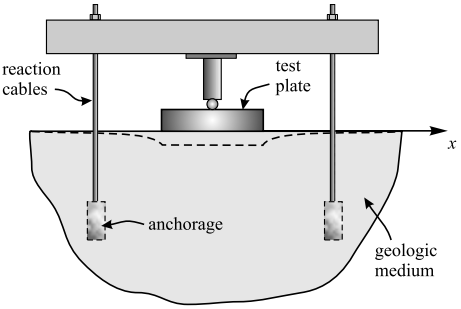

Fig. 26.3. The cable jacking test in geomechanics.

In this case, the direct formulation of the problem can be performed by making use of the general approach presented in Section 26.2, except that the function $p(r, \theta)$ is a much more complicated function, associated with the interior loading of the half-space region by a pair of symmetrically placed concentrated forces. In contrast, Betti's reciprocal theorem can be applied quite conveniently to determine the resulting displacement of the test plate under the self-stressing loading system shown in Figure 26.3.

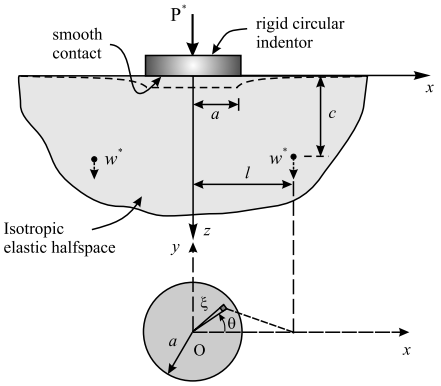

Fig. 26.4. Indentation of the half-space by a smooth rigid indentor.

The contact stress distribution at the interface of a rigid smooth plate of radius a resting on the surface of a half-space and subjected to an axisymmetric load P^* is given by

$$\sigma_{zz}(r, 0) = \frac{P^*}{\pi a \sqrt{a^2 - r^2}}.$$

Integrating this result (see Figure 26.4), we can determine the axial displacement at the interior of the half-space region due to the indentor as follows:

$$w^*(l, c) = \frac{P^*(1-\nu)}{4\mu a} \left[\frac{1}{\pi^2} \int_0^a \left[\int_0^{2\pi} \frac{1}{\phi \sqrt{a^2 - r^2}} \left\{ 1 + \frac{c^2}{2(1-\nu)\phi^2} \right\} \mathrm{d}\theta \right] \xi \mathrm{d}\xi \right],$$

where

$$\phi = [c^2 + l^2 + \xi^2 - 2c\xi\cos\theta]^{1/2}.$$

The required solution is the axial displacement $\tilde{w}$ of the rigid circular indentor due to the action of the reactive concentrated forces $\tilde{P}$ acting at the interior of the half-space region (Figure 26.5). If smooth bilateral contact is main-

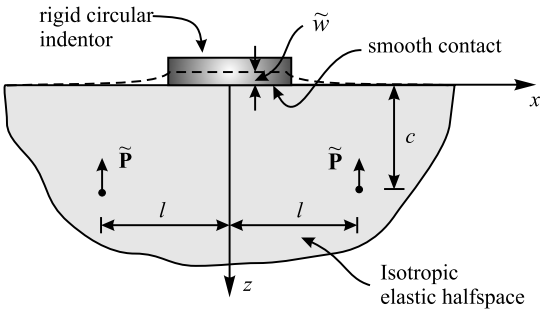

Fig. 26.5. Displacement of the rigid punch in bilateral contact-action of internal loads.

tained during the application of the reactive loads, then we can apply Betti's reciprocal theorem to the two states indicated in Figures 26.4 and 26.5, which gives $\tilde{w}\,P^* = 2\tilde{P}\,w^*$. The net axial displacement of the rigid circular plate of radius a due to a directly applied load of magnitude P and internal loads of magnitude $P/2$ located at the Cartesian coordinate distances $(l, 0, c)$ and $(-l, 0, c)$ is given by

$$w = \frac{P(1-\nu)}{4\mu a}\left(1 - \left[\frac{2}{\pi^2}\int_0^a \left[\int_0^{2\pi} \frac{1}{\phi\sqrt{a^2-\xi^2}}\left\{1 + \frac{c^2}{2(1-\nu)\phi^2}\right\}\mathrm{d}\theta\right]\xi\mathrm{d}\xi\right]\right). \tag{26.13}$$

The result (26.13) for the net displacement of the rigid indentor is in an explicit form that can be evaluated through a numerical integration technique.

26.5 Conclusions

The reciprocity principle proposed by Betti is a powerful tool for the development of compact results for problems in classical elasticity. The examples provided in this chapter deal with specific contact problems. The direct formulation of the contact problems usually involve integral equations that are difficult to solve analytically; recourse must invariably be made to computational techniques for their solution. Consequently, using the direct approach, the result for the load–displacement relationship for a nonclassical contact problem can be evaluated only as a numerical result. The application of the reciprocal

theorem, however, enables the development of the load-displacement result in either a *compact integral form* or in an *exact closed form.* In the above examples, where the external load is located at the surface of the half-space, the systems of dual integral equations governing the problem involving the direct formulation can be solved in a convenient way. If the external loading is located at an arbitrary point within the half-space region, the solution is not as straightforward and can be developed only through the numerical technique that converts the dual integral equations to either an Abel-type or a Fredholm-type integral equation of the second kind. The application of the reciprocal theorem is a more convenient way of developing solutions to the external load-rigid indentor interaction problem. The main reason for the ease of application of Betti's reciprocal theorem stems from the fact that the auxiliary solutions associated with these problems can be obtained in compact forms through the solution of a set of dual integral equations. The methodologies described in this chapter can be extended to include other classes of reciprocal relationships associated with inhomogeneous media, elastodynamic problems, and poroelasticity problems.

Acknowledgement. This work was supported through the *2003 Max Planck Forschungspreis in the Engineering Sciences* awarded by the Max Planck Gesellschaft, Germany.

References

[Bet72] Betti, E.: *Teoria dell'Elasticità,* Nuovo Cimento Ser. II, VII, VIII (1872).

[Bou85] Boussinesq, J.: *Application des Potentiels à l'Étude de l'Equilibre et du Mouvement des Solides.* Gauthier-Villars, Paris (1885).

[Har45] Harding, J.W., Sneddon, I.N.: The elastic stresses produced by the indentation of the plane surface of a semi-infinite solid by a rigid punch. *Camb. Phil. Soc.,* **41**, 16–26 (1945).

[M60] Muki, R.: Asymmetric problems in the theory of elasticity for a semi-infinite solid and a thick plate. In: Sneddon, I.N., Hill, R. (eds.), *Progress in Solid Mechanics,* vol. 1. North-Holland, Amsterdam (1960), pp. 339–349.

[Max64] Maxwell, J.C.: On the calculation of equilibrium and stiffness of frames. *Phil. Mag.,* **27**, 294–299 (1864).

[N58] Noble, B.: Certain dual integral equations. *J. Math. Phys.,* **37**, 128–136 (1958).

[Sel78] Selvadurai, A.P.S.: The interaction between a rigid circular punch on an elastic halfspace and a Mindlin force. *Mech. Res. Comm.,* **5**, 57–64 (1978).

[Sel79] Selvadurai, A.P.S.: The displacement of a rigid circular foundation anchored to an isotropic elastic halfspace. *Geotechnique,* **29**, 195–202 (1979).

[Sel00] Selvadurai, A.P.S.: On the mathematical modelling of certain fundamental elastostatic contact problems in geomechanics. In: Zaman, M., Gioda, G., Booker, J.R. (eds.), *Modelling in Geomechanics.* Wiley, New York (2000).

[Sel07] Selvadurai, A.P.S.: The analytical method in geomechanics. *Appl. Mech. Reviews,* **60**, 87–106 (2007).

[Sh66] Shield, R.T., Anderson, C.A.: Some least work principles for elastic bodies. *Z. Angew. Math. Phys.,* **17**, 663–676 (1966).

[Sh67] Shield, R.T.: Load–displacement relations for elastic bodies. *Z. Angew. Math. Phys.,* **18**, 682–693 (1967).

[Sn69] Sneddon, I.N., Lowengrub, M.: *Crack Problems in the Classical Theory of Elasticity.* Wiley, New York (1969).

[Sn75] Sneddon, I.N.: *Application of Integral Transforms in the Theory of Elasticity.* Springer, Wien (1975).

[Tr63] Truesdell, C.: The meaning of Betti's reciprocal theorem. *J. Research Nat. Bur. Standards,* **67B**, 85–86 (1963).

[Z67] Zienkiewicz, O.C., Stagg, K.G.: Cable method of in-situ rock testing. *Int. J. Rock Mech. Min. Sci.,* **4**, 273–300 (1967).

27

Integral Equation Modeling of Electrostatic Interactions in Atomic Force Microscopy

Y. Shen, D.M. Barnett, and P.M. Pinsky

Stanford University, CA, USA; shenyx@stanford.edu, barnett@stanford.edu, pinsky@stanford.edu

27.1 Introduction

Since its invention in 1986 [BQG86], the atomic force microscope (AFM) has evolved as a major tool for characterizing materials. Of the several operational modes of the AFM, the noncontact mode is normally used to determine the sample surface charge distribution. In this range of tip–sample separation, the Coulombic interaction between the tip and the sample dominates over magnetic and van der Waal forces. Despite the simple and explicit expression of Coulomb's law, mapping AFM images to sample charge distributions cannot be done in a straightforward way because of the finite size of the AFM tip and the roughness of the sample. Thus, researchers have been approaching this inverse problem from the opposite direction by making efforts to predict AFM measurements based on assumed sample properties. Numerous models have been proposed to tackle this electrostatic problem.

For the case in which both the tip and the sample are conductors, some previous approaches treat the surfaces of these two objects as two equipotentials due to an assumed distribution of source and image charges relative to the sample surface, for example, a single charge [HXOS95], a series of point charges [BGL97], or a uniformly charged line [HBS91]. Another approach replaces the tip with a geometrical object and either solves the Laplace equation in a closed form (e.g., the spherical-tip model [TSRM89] and the hyperboloidal-tip model [PSPCM94]) or approximates the electric field lines using circular arcs and straight lines (e.g., the models that treat the tip as a cone with a spherical apex [HJGB98] or a parabolic apex [CGB01]). In all of these models, a geometrical approximation error of the tip is introduced.

On the other hand, numerical schemes have also been developed to compute the tip–sample interaction in which the tip shape information is fully taken into account (up to the mesh error). Belaidi et al. [BLGLP98] proposed a finite element setup for this external Dirichlet problem in which the infinite domain (the vacuum outside the tip and the sample) was truncated to a finitely large cylindrical domain, but this truncated domain still required

a three-dimensional mesh. In contrast, Strassburg et al. [SBR05] employed a boundary element method to reconstruct the images of a conductive sample in which only the tip surface had to be meshed, while the sample surface with vanishing boundary value was accommodated by an image term in the Green's function. However, in [SBR05], the sample is restricted to be conductive.

Independently, we have developed a boundary integral equation approach similar to that of [SBR05], but our formulation applies not only to conductive samples but also to dielectric ones, with arbitrary distributions of surface and/or volumetric charges that can be taken into account; thus, our work is applicable to a wider range of problems.

27.2 Conductive Sample

27.2.1 Boundary Value Problem

In our model, only the Coulombic interaction between the AFM tip and the sample is taken into account, whereas both the van der Waal and the magnetic interactions are ignored, resulting in a classical electrostatic problem. Because the AFM cantilever only contributes a constant shift to the tip–sample interaction (see, e.g., [CGB01]), and the interpretation of AFM images primarily relies only on the *contrast* between regions rather than on the actual *magnitudes* of interactions, it seems reasonable that the cantilever not be included in our model. Furthermore, the tip is truncated to have a height of 100 nm, assuming that such a height is enough to capture the *variation* in tip–sample interaction relative to a homogeneous sample, as the tip scans the sample while maintaining a constant separation.

The AFM tip is almost always manufactured to be conductive, whereas the sample may be either conductive or dielectric. If the sample is also conductive, the electrostatic problem becomes an exterior Dirichlet problem with a single homogeneous domain Ω (the vacuum or air between the tip and the sample), over which Laplace's equation ($\nabla^2\phi = 0$) holds, as shown in Figure 27.1. Dirichlet boundary conditions are imposed on both the tip surface S_{tip} ($\phi = \phi_0$) and the sample surface $S_{\text{sam}}(\phi = 0)$. For simplicity, throughout this chapter, the sample is assumed to be *flat* and *semi-infinite*.

27.2.2 Boundary Integral Equation

Classical potential theory (see, e.g., [JS77]) yields the boundary integral equation

$$\int_{S_{\text{tip}}} G(\vec{r};\vec{r'})\sigma(\vec{r})dS(\vec{r}) = \phi_0, \quad \forall \vec{r'} \in S_{\text{tip}}, \tag{27.1}$$

where

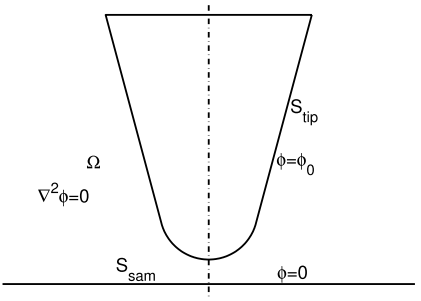

Fig. 27.1. Schematic of the exterior Dirichlet problem that describes the electrostatic interaction between an AFM tip and a conductive sample.

$$G(\vec{r};\vec{r'}) := \Phi(\vec{r}-\vec{r'}) - \Phi(\vec{r}-\vec{r'}^{\,\mathrm{im}}),$$

which is the Green's function that vanishes at the sample surface, $\Phi(\vec{r}-\vec{r'}) := (4\pi\epsilon_0|\vec{r}-\vec{r'}|)^{-1}$ being the fundamental solution to the Laplace equation in free space ($\epsilon_0 = 8.854\times10^{-12}$ F/m is the permittivity of vacuum). $\vec{r'}^{\,\mathrm{im}}$ is the image position of the source point $\vec{r'}$ with respect to the sample plane; and

$$\sigma(\vec{r}) := \epsilon_0 \frac{\partial\phi(\vec{r})}{\partial\vec{n}_{\vec{r}}},$$

which is the unknown charge density on the tip surface; $\vec{n_r}$ is the unit outward normal of Ω, thus pointing *inward* on the tip.

27.2.3 Numerical Analysis and Postprocessing

Equation (27.1) is a Fredholm boundary integral equation of the first kind, the unknown of which is the moment of a single-layer potential. The boundary element method was employed to solve it. First, the tip surface was meshed into either four-node quadrilaterals or eight-node serendipity elements [Beer01, Chapter 3], and the associated interpolation functions were used to represent the unknown surface charge density $\sigma(\vec{r})$ on the tip. Then, the point collocation approach was used to deduce the matrix equation, the unknowns of which are all the nodal σ values. Thereafter, a biconjugate gradient solver was employed to solve for these unknowns. We adopted the boundary element code given in [Beer01] for the assembly and equation-solving processes.

Upon obtaining $\sigma(\vec{r})$, the tip–sample capacitance C is, by definition, ready to compute as

$$C = \frac{1}{\phi_0}\int\limits_{S_{\mathrm{tip}}} \sigma(\vec{r})dS(\vec{r}).$$

To calculate the net tip–sample force $\vec{f}$, we integrate the traction associated with the Maxwell stress over the tip surface as

$$f_i = -\int\limits_{S_{\text{tip}}} \frac{\sigma(\vec{r})^2}{2\epsilon_0} n_{\vec{r}i} dS(\vec{r}), \tag{27.2}$$

where $i = 1, 2, 3$, denoting the axial directions in the Cartesian coordinate frame, of which x_3 is chosen so as to parallel the tip axis and to point outward from the flat sample.

To compute the force gradient component $\partial f_i / \partial x_j^{\text{tip}}$, where $\vec{x}^{\text{tip}}$ denotes the tip apex position, we take the derivative of (27.2) with respect to x_j^{tip} and have

$$\frac{\partial f_i}{\partial x_j^{\text{tip}}} = -\int\limits_{S_{\text{tip}}} \frac{\sigma(\vec{r})}{\epsilon_0} \frac{\partial \sigma(\vec{r})}{\partial x_j^{\text{tip}}} n_i dS(\vec{r}), \tag{27.3}$$

where $\partial \sigma(\vec{r}) / \partial x_j^{\text{tip}}$ can be computed by taking the derivative of (27.1) with respect to x_j^{tip} and rearranging the terms to have

$$\int\limits_{S_{\text{tip}}} G(\vec{r}; \vec{r'}) \frac{\partial \sigma(\vec{r})}{\partial x_j^{\text{tip}}} dS(\vec{r}) = -\int\limits_{S_{\text{tip}}} \frac{\partial G(\vec{r}; \vec{r'})}{\partial x_j^{\text{tip}}} \sigma(\vec{r}) dS(\vec{r}), \quad \forall \vec{r'} \in S_{\text{tip}}. \tag{27.4}$$

The matrix equation associated with (27.4) has the same coefficient matrix as that for (27.1) since they have the same integral operator on the unknowns.

27.2.4 Convergence Study

To verify the numerical scheme proposed above, a benchmark problem with an exact analytical solution is useful. We chose the sphere–plane capacitance system, and looked up and completed the solution by [Smythe68, Chapter V]. The complete solution is also provided in the Appendix.

We applied the boundary element method to a sphere–plane capacitance problem corresponding to a typical experimental setup: a sphere with a radius of 20 nm and a sphere-plane separation of 5 nm. The potential difference between the sphere and the plane is set to 1 V.

The absolute errors for the different mesh types and mesh sizes in terms of nodal σ values, capacitance, force, and force gradient are listed in Table 27.1. The exact solutions for those global quantities are provided in the last row of Table 27.1. Thus, the relative errors can be obtained by dividing the absolute errors by the corresponding exact solutions. The average number of iterations was obtained by averaging the number of iterations in solving the matrix equations associated with (27.1) and (27.4) using the biconjugate gradient solver. The convergence criterion was that the elemental *relative* difference between two successive steps is less than 10^{-4}. If the resolution of the force is 1 pN, we can deduce the critical mesh parameters to be 2 nm for four-node quadrilaterals and 8 nm for eight-node serendipity elements. The serendipity element is favored for less cost in assembly time and better approximation to the curved tip surface.

Subsequent results for the tip-sample interaction are, accordingly, based on the 8 nm serendipity element.

Table 27.1. Convergence study of the sphere–plane capacitance system.

Mesh type	A	B	C	D	E	F	G	H
Four-node quadrilateral	10	76	10	5×10^{-1}	1×10^{2}	5	1	2
	8	108	9.5	3×10^{-1}	8×10	4	6×10^{-1}	2
	6	165	11.5	2×10^{-1}	5×10	2	1×10^{-1}	1
	4	370	10	1×10^{-1}	2×10	1	9×10^{-2}	5×10^{-1}
	2	1406	12	3×10^{-2}	6	3×10^{-1}	1×10^{-2}	1×10^{-1}
	1	5480	13.5	7×10^{-3}	2	8×10^{-2}	2×10^{-3}	3×10^{-2}
Eight-node serendipity	20	44	11	1	9×10	7	1	3
	10	86	11.5	3×10^{-1}	2×10	1	8×10^{-1}	6×10^{-1}
	8	323	14.5	5×10^{-2}	2	5×10^{-2}	2×10^{-2}	5×10^{-2}
	6	485	10	7×10^{-2}	8×10^{-1}	3×10^{-3}	1×10^{-2}	2×10^{-2}
	4	1124	12.5	5×10^{-2}	1×10^{-1}	8×10^{-3}	1×10^{-3}	3×10^{-3}
	2	4136	16.5	4×10^{-2}	4×10^{-2}	6×10^{-3}	3×10^{-4}	1×10^{-3}
Exact solutions	–	–	–	–	3957.47	−84.683	0	46.080

The designation of the columns in Table 27.1 is as follows:

A: Mesh size (nm).
B: Number of degrees of freedom.
C: Average number of iterations.
D: Nodal L^2-error (10^{-3} C/m^2).
E: Error in C (10^{-21} F).
F: Error in f_3 (pN).
G: Error in f_{12} (pN).
H: Error in $\partial f_3/\partial x_3^{\text{tip}}$ (pN/nm).

27.3 Dielectric Sample with Arbitrary Surface and/or Volumetric Charges

27.3.1 Formulation

A dielectric sample is generally no longer an equipotential. It may also have distributions of surface charge $s(\vec{r})$ and volumetric charge $\rho(\vec{r})$. The partial differential equations that govern the problem are Laplace's equation in the air Ω and Poisson's equation in the interior of the sample Ω_{sam}, namely:

$$\nabla^2\phi(\vec{r}) = \begin{cases} 0, & \text{if} \quad \vec{r} \in \Omega, \\ -\rho(\vec{r})/K, & \text{if} \quad \vec{r} \in \Omega_{\text{sam}}, \end{cases}$$

where K denotes the sample's dielectric constant.

The continuity equation for the sample surface is

$$\left.\frac{\partial\phi}{\partial\vec{n}}(\vec{r})\right|_{\Omega} - K\left.\frac{\partial\phi}{\partial\vec{n}}(\vec{r})\right|_{\Omega_{\text{sam}}} = s(\vec{r}) \quad \forall\vec{r}\in S_{\text{sam}},$$

where $\vec{n}$ points *inward* of the sample.

Now, the counterpart of the boundary integral equation (27.1) is

$$\begin{aligned}\int\limits_{S_{\text{tip}}} \bar{G}(\vec{r};\vec{r'})\sigma(\vec{r})dS(\vec{r}) = \phi_0 - \frac{2}{1+K}\int\limits_{S_{\text{sam}}} \Phi(\vec{r}-\vec{r'})s(\vec{r})dS(\vec{r}) \\ - \frac{2}{1+K}\int\limits_{\Omega_{\text{sam}}} \Phi(\vec{r}-\vec{r'})\rho(\vec{r})dV(\vec{r}), \quad \forall\vec{r'}\in S_{\text{tip}},\end{aligned} \tag{27.5}$$

where

$$\bar{G}(\vec{r};\vec{r'}) := \Phi(\vec{r}-\vec{r'}) - \frac{K-1}{K+1}\Phi(\vec{r}-\vec{r'}^{\text{im}}) \quad \forall\vec{r},\vec{r'}\in\bar{\Omega},$$

which is the Green's function for the dielectric sample.

27.3.2 Predicted Images for a Test Case

If both $s(\vec{r})$ and $\rho(\vec{r})$ are known, (27.5) can also be solved using the boundary element method, as in the case for a conductive sample. Furthermore, the tip-sample forces and their gradients can be obtained via (27.2) and (27.3), respectively.

Thus, using this framework, we can predict AFM images as the tip scans a sample with a constant separation. To exemplify this capability, we use zirconia as a model sample material with a dielectric constant $K = 40$. This sample is assumed to have no volumetric charge ($\rho(\vec{r}) = 0$), but only a surface charge of density

$$s(\vec{r}) = s(x,y) = \frac{s_0}{3}\left\{\cos\left[k\left(x-\frac{y}{\sqrt{3}}\right)\right] + \cos\frac{2ky}{\sqrt{3}} + \cos\left[k\left(x+\frac{y}{\sqrt{3}}\right)\right]\right\},$$

where $2\pi/k = 20$ nm, the periodicity of the surface charge and $s_0 = 17.49$ e/nm^2, corresponding to the maximum surface charge density of a (111) oxygen lattice plane of zirconia. Such a surface charge may be due to surface segregation of ions. A contour plot of $s(\vec{r})$ is presented in Figure 27.2. The AFM tip is assumed to be a cone (with a total cone angle of 30°) with a spherical apex (with a radius of 20 nm). The height of the cone is truncated to be 100 nm. Here we use sizes of serendipity elements finer than 8 nm to better resolve the sample spatial charge variation (2 nm for the apex and 6 nm for the rest of the tip). In the case of zero DC bias between the tip and the sample, predicted images in terms of force and force gradient at the separation of 5 nm are plotted in Figures 27.3 and 27.4, respectively. If the resolution of the force difference as the tip scans the sample is 1 pN, we can conclude that such variation in surface charge can be detected by the AFM.

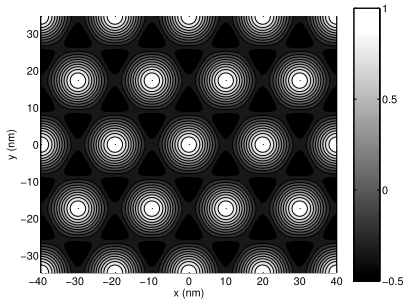

Fig. 27.2. Assumed sample surface charge density relative to s_0.

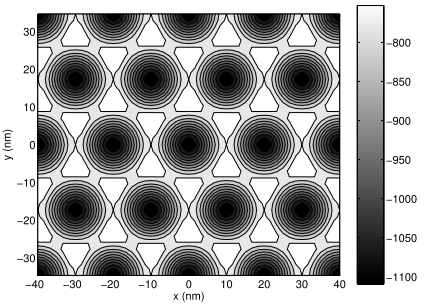

Fig. 27.3. Predicted image in terms of force component f_3 (in pN).

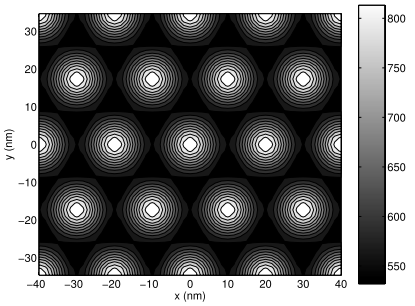

Fig. 27.4. Predicted image in terms of force gradient component $\partial f_3/\partial x_3^{\text{tip}}$ (in pN/nm).

27.4 Conclusions

A unified formulation for the AFM tip–sample electrostatic interaction has been developed in terms of boundary integral equations. To the authors' knowledge, these are the first such computations for dielectric samples with charge distributions. The sample in this chapter is restricted to be semi-infinite

and with a flat surface; however, the extension to a finite-sized, nonflat sample is not difficult to achieve.

With the Maxwell stress tensor, the AFM image due to electrostatic interaction can be predicted based on the knowledge of the sample and the experimental condition.

Acknowledgement. This work has been funded by the Global Climate & Energy Project, Grant No. 33453.

Appendix: Exact Solution for the Sphere–Plane Capacitance System

In the sphere–plane capacitance system, we assume that the plane (and thus also the semi-infinite conductor) is grounded and that the sphere of radius a is at potential ϕ_0. The distance between the sphere center and the plane is denoted by d.

According to Smythe [Smythe68], the electric field between the sphere and the plane can be represented by two sets of image charges, one set of which located inside the spherical conductor and the other set inside the semi-infinite conductor.

If we establish a Cartesian coordinate frame so that the origin coincides with the sphere center and the z-axis is normal to the plane, then the equation of the plane is given by $z = -d$, without loss of generality.

Smythe's two sets of image charges are $\{q_n\}$ at $\{(0, 0, -s_n)\}$ and $\{-q_n\}$ at $\{(0, 0, -2d + s_n)\}$, $n = 1, 2, 3, ...$, where

$$q_n := 4\pi\epsilon_0\phi_0 a \sinh\alpha \operatorname{csch} n\alpha, \quad s_n := a \sinh(n-1)\alpha \operatorname{csch} n\alpha,$$

and $\alpha := \cosh^{-1}(d/a)$.

Thus, the axisymmetric potential outside the two conductors, $\phi(\rho, z)$, where $\rho := (x^2 + y^2)^{1/2}$, is given by

$$\phi(\rho, z) = \frac{1}{4\pi\epsilon_0} \sum_{n=1}^{\infty} \left\{ \frac{q_n}{[\rho^2 + (z + s_n)^2]^{1/2}} - \frac{q_n}{[\rho^2 + (z + 2d - s_n)^2]^{1/2}} \right\}.$$

And the surface charge density *on the sphere* follows as

$$\sigma(\rho, z) = \epsilon_0 \sinh\alpha \sum_{n=1}^{\infty} \operatorname{csch} n\alpha \left\{ \frac{a^2 + z s_n}{[a^2 + 2z s_n + s_n^2]^{3/2}} - \frac{a^2 + 2zd - z s_n}{[a^2 + 2z(2d - s_n) + (2d - s_n)^2]^{3/2}} \right\}.$$

The capacitance can be obtained by summing one set of the charges as

$$C = \frac{1}{\phi_0} \sum_{n=1}^{\infty} q_n = 4\pi\epsilon_0 a \sinh\alpha \sum_{n=1}^{\infty} \operatorname{csch} n\alpha.$$

The force component f_z and force gradient component $\partial f_z/\partial d$ can be evaluated by taking the first and second derivatives of the capacitance with respect to d, respectively, as

$$f_z = -\frac{1}{2}\phi_0^2 \frac{\partial C}{\partial d} = 2\pi\epsilon_0\phi_0^2 \sum_{n=1}^{\infty} \operatorname{csch} n\alpha(\coth\alpha - n\coth n\alpha)$$

and

$$\frac{\partial f_z}{\partial d} = \frac{2\pi\epsilon_0\phi_0^2 \sinh\alpha}{a} \times \sum_{n=1}^{\infty} \operatorname{csch} n\alpha\big\{n^2 \operatorname{csch}^2 n\alpha - \operatorname{csch}^2\alpha + n\coth n\alpha(n\coth n\alpha - \coth\alpha)\big\}.$$

References

[Beer01] Beer, G.: *Programming the Boundary Element Method: An Introduction for Engineers.* Wiley, New York (2001).

[BGL97] Belaidi, S., Girard, P., Leveque, G.: Electrostatic forces acting on the tip in atomic force microscopy: modelization and comparison with analytic expressions. *J. Appl. Phys.,* **81**, 1023–1030 (1997).

[BLGLP98] Belaidi, S., Lebon, E., Girard, P., Leveque, G., Pagano, S.: Finite element simulations of the resolution in electrostatic force microscopy. *Appl. Phys. A,* **66**, S239–S243 (1998).

[BQG86] Binnig, G., Quate, C.F., Gerber, Ch.: Atomic force microscope. *Phys. Rev. Lett.,* **56**, 930–933 (1986).

[CGB01] Colchero, J., Gil, A., Baró, A.M.: Resolution enhancement and improved data interpretation in electrostatic force microscopy. *Phys. Rev. B,* **64**, 245403 (2001).

[HBS91] Hao, H.W., Baró, A.M., Sáenz, J.J.: Electrostatic and contact forces in force microscopy. *J. Vac. Sci. Tech. B,* **9**, 1323–1328 (1991).

[HJGB98] Hudlet, S., Saint Jean, M., Guthmann, C., Berger, J.: Evaluation of the capacitive force between an atomic force microscopy tip and a metallic surface. *Eur. Phys. J. B,* **2**, 5–10 (1998).

[HXOS95] Hu, J., Xiao, X.-D., Ogletree, D.F., Salmerón, M.: Imaging the condensation and evaporation of molecularly thin films of water with nanometer resolution. *Science,* **268**, 267–269 (1995).

[JS77] Jaswon, M.A., Symm, G.T.: *Integral Equation Methods in Potential Theory and Elastostatics.* Academic Press, London-New York (1977).

[PSPCM94] Pan, L.H., Sullivan, T.E., Peridier, V.J., Cutler, P.H., Miskovsky, N.M.: Three-dimensional electrostatic potential, and potential-energy barrier, near a tip–base junction. *Appl. Phys. Lett.,* **65**, 2151–2153 (1994).

[SBR05] Strassburg, E., Boag, A., Rosenwaks, Y.: Reconstruction of electrostatic force microscopy images. *Rev. Scientif. Instrum.,* **76**, 083705 (2005).

[Smythe68] Smythe, W.R.: *Static and Dynamic Electricity,* 3rd ed. McGraw-Hill, New York (1968).

[TSRM89] Terris, B.D., Stern J.E., Rugar, D., Mamin, H.J.: Contact electrification using force microscopy. *Phys. Rev. Lett.,* **63**, 2669–2672 (1989).

28

Integral Representation for the Solution of a Crack Problem Under Stretching Pressure in Plane Asymmetric Elasticity

E. Shmoylova[1], S. Potapenko[2], and L. Rothenburg[2]

[1] Tufts University, Medford, MA, USA; elena.shmoylova@tufts.edu
[2] University of Waterloo, ON, Canada; spotapen@uwaterloo.ca, leoroth@uwaterloo.ca

28.1 Introduction

The theory of micropolar elasticity (also known as *Cosserat* or *asymmetric* theory of elasticity) was introduced by Eringen [Er66], to eliminate discrepancies between the classical theory of elasticity and experiments in cases when effects of material microstructure were known to contribute significantly to the body's overall deformation, for example, materials with granular microstructure such as polymers or human bones (see Lakes [Lak95], [Lak82], Lakes et al. [LNB90], and Nakamura and Lakes [NL88]). These cases are becoming increasingly important in the design and manufacture of modern-day advanced materials as small-scale effects become very important in the prediction of the overall mechanical behavior of these materials.

Several studies relating to investigations of stress distributions around a crack have been undertaken under assumptions of a simplified theory of plane Cosserat elasticity by Mühlhaus and Pasternak [MP02], Atkinson and Leppington [AtL02], experimentally by Lakes et al. [LNB90], and using the finite element method (see Nakamura and Lakes [NL88]).

Recently, Chudinovich and Constanda [CC00] used the boundary integral equation method in a weak (Sobolev) space setting to obtain the solution for fundamental boundary value problems in a theory of bending of classical elastic plates. This approach has wide practical applicability because it also covers domains with reduced boundary smoothness. In addition, it provides an answer to the fundamental question of existence and uniqueness of the solution, and gives an opportunity to employ an effective numerical procedure for constructing a numerical solution, which can be very useful for practical purposes. Furthermore, Chudinovich and Constanda [CC00] extended their method to accommodate several problems relating to the investigation of stress concentrations around a crack in classical plates.

In several very recent works by Shmoylova et al. (see [SPR06], [SPRa], and [SPRb]), the authors performed a rigorous analysis of interior and exterior Dirichlet and Neumann boundary value problems in plane Cosserat elasticity and obtained the solution to the crack problem arising in this theory in the form of modified integral potentials with unknown distributional densities. Unfortunately, it is very difficult, if not impossible, to find these densities analytically. In this work we apply the boundary element method to obtain a numerical approximation of the solution. This method has been developed by Brebbia [Br78] and has become very popular among researchers in different areas, including fracture mechanics (see, for example, [AlB93] for references on applications of the boundary element method in science and engineering).

In this chapter, we use the boundary element method to find the solution for an infinite domain weakened by a crack in plane Cosserat elasticity, when stresses and couple stresses are prescribed along both sides of the crack (Neumann boundary value problem). To illustrate the effectiveness of the method for applications, we consider a crack in a human bone that is modeled under assumptions of plane micropolar elasticity. We find the numerical solution for the stresses around the crack and show that the solution may be reduced to the classical one if we set all micropolar elastic constants equal to zero. We come to the conclusion that there could be up to a 26% difference in the quantitative characteristics of the stress around a crack in the micropolar case by comparison with the model when microstructure is ignored (the classical case; see, for example, [Sn69]).

28.2 Preliminaries

In what follows Greek and Latin indices take the values 1, 2 and 1, 2, 3, respectively, the convention of summation over repeated indices is understood, $\mathcal{M}_{m\times n}$ is the space of $(m \times n)$-matrices, and a superscript T indicates matrix transposition.

Let S be a domain in $\mathbb{R}^2$ occupied by a homogeneous and isotropic, linearly elastic micropolar material with elastic constants $\lambda, \mu, \alpha, \gamma$, and ε. We use the notation $\|\cdot\|_{0;S}$ and $\langle\cdot,\cdot\rangle_{0;S}$ for the norm and inner product in $L^2(S)\cap\mathcal{M}_{m\times 1}$ for any $m \in \mathbb{N}$. When $S = \mathbb{R}^2$, we write $\|\cdot\|_0$ and $\langle\cdot,\cdot\rangle_0$.

The state of plane micropolar strain is characterized by a displacement field $u(x') = (u_1(x'), u_2(x'), u_3(x'))^T$ and a microrotation field $\phi(x') = (\phi_1(x'), \phi_2(x'), \phi_3(x'))^T$ of the form

$$\begin{aligned} u_\alpha(x') &= u_\alpha(x), \qquad u_3(x') = 0, \\ \phi_\alpha(x') &= 0, \qquad \phi_3(x') = \phi_3(x), \end{aligned}$$

where $x' = (x_1, x_2, x_3)$ and $x = (x_1, x_2)$ are generic points in $\mathbb{R}^3$ and $\mathbb{R}^2$, respectively.

The internal energy density is given by [Sch96]

$$2E(u,v) = 2E_0(u,v) + \mu(u_{1,2}+u_{2,1})(v_{1,2}+v_{2,1}) \\ +\alpha(u_{1,2}-u_{2,1}+2u_3)(v_{1,2}-v_{2,1}+2v_3) \\ +(\gamma+\varepsilon)(u_{3,1}v_{3,1}+u_{3,2}v_{3,2}),$$

$$2E_0(u,v) = (\lambda+2\mu)(u_{1,1}v_{1,1}+u_{2,2}v_{2,2}) + \lambda(u_{1,1}v_{2,2}+u_{2,2}v_{1,1}).$$

In what follows we assume that

$$\lambda+\mu>0, \quad \mu>0, \quad \gamma+\varepsilon>0, \quad \alpha>0.$$

Clearly, $E(u,u)$ is a positive quadratic form.

We consider the boundary stress operator $T(\partial_x) = T(\partial/\partial x_\alpha)$ defined by

$$T(\xi) = T(\xi_\alpha)$$

$$= \begin{pmatrix} (\lambda+2\mu)\xi_1 n_1 + (\mu+\alpha)\xi_2 n_2 & (\mu-\alpha)\xi_1 n_2 + \lambda\xi_2 n_1 & 2\alpha n_2 \\ (\mu-\alpha)\xi_2 n_1 + \lambda\xi_1 n_2 & (\lambda+2\mu)\xi_2 n_2 + (\mu+\alpha)\xi_1 n_1 & -2\alpha n_1 \\ 0 & 0 & (\gamma+\varepsilon)\xi_\alpha n_\alpha \end{pmatrix},$$

where $n = (n_1, n_2)^T$ is the unit outward normal to ∂S.

The space of rigid displacements and microrotations $\mathcal{F}$ is spanned by the vectors $z^{(1)} = (1,0,0)^T$, $z^{(2)} = (0,1,0)^T$, and $z^{(3)} = (-x_2, x_1, 1)^T$.

We consider the matrix of fundamental solutions $D(x,y)$ and the matrix of singular solutions $P(x,y) = (T(\partial y)D(y,x))^T$.

We consider an infinite domain with a crack modeled by an open arc Γ_0 and assume that Γ_0 is a part of a simple closed C^2-curve Γ that divides $\mathbb{R}^2$ into interior and exterior domains Ω^+ and Ω^-. In what follows, we denote by the superscripts $+$ and $-$ the limiting values of functions as $x \to \Gamma$ from within Ω^+ or Ω^-. Furthermore, we define $\Omega = \mathbb{R}^2 \backslash \overline{\Gamma_0}$ and $\Gamma_1 = \Gamma \backslash \overline{\Gamma_0}$. We introduce the restriction operators $\pi^\pm$ to $\Omega^\pm$ and the trace operators $\gamma_0^\pm$ on Γ_0 and $\gamma_1^\pm$ on Γ_1 from within $\Omega^\pm$, respectively. Let $H_{1,\omega}(\Omega)$ be the space of all $u = \{u_+, u_-\}$ such that $u_+ \in H_1(\Omega^+)$, $u_- \in H_{1,\omega}(\Omega^-)$, and $\gamma_1^+ u_+ = \gamma_1^- u_-$. The space $H_1(\Omega^+)$ is a standard Sobolev space and $H_{1,\omega}(\Omega^-)$ is a weighted Sobolev space defined in [21].

Next, we introduce the corresponding single-layer and double-layer potentials, respectively, by

$$(V\varphi)(x) = \int_{\Gamma_0} D(x,y)\varphi(y)\, ds(y),$$

$$(W\varphi)(x) = \int_{\Gamma_0} P(x,y)\varphi(y)\, ds(y),$$

where $\varphi \in \mathcal{M}_{3\times 1}$ is an unknown density matrix.

28.3 Boundary Value Problem

Let us consider the Neumann boundary value problem with the boundary conditions

$$(Tu)^+(x) = g^+(x), \quad (Tu)^-(x) = g^-(x), \quad x \in \Gamma_0,$$

where g^+ and g^- are prescribed on Γ_0. We write δg for the jump of these quantities across the crack.

The variational formulation of the boundary value problem is as follows. We seek $u \in H_{1,\omega}(\Omega)$ such that

$$b(u,v) = \left\langle \delta g, \gamma_0^+ v_+ \right\rangle_{0;\Gamma_0} + \left\langle g^-, \delta v \right\rangle_{0;\Gamma_0} \quad \forall v \in H_{1,\omega}(\Omega), \tag{28.1}$$

where $b(u,v) = 2\int_{\Omega^-} E(u_-, v_-)\, dx + 2\int_{\Omega^+} E(u_+, v_+)\, dx$. Note that (28.1) is solvable only if

$$\langle z, \delta g \rangle_{0;\Gamma_0} = 0 \ \forall z \in \mathcal{F}.$$

We define the modified single-layer potential $\mathcal{V}$ of density φ by

$$(\mathcal{V}\varphi)(x) = (V\varphi)(x) - \left\langle (V\varphi)_0, \widetilde{z}^{(i)} \right\rangle_{0;\Gamma_0} \widetilde{z}^{(i)}(x), \quad x \in \mathbb{R}^2,$$

where $V\varphi$ is the single-layer potential, V_0 is the boundary operator defined by $(V\varphi)_0 = \gamma_0^{\pm}\pi^{\pm} V\varphi$, and $\{\widetilde{z}^{(i)}\}_{i=1}^3$ is an $L^2(\Gamma_0)$-orthonormal basis for $\mathcal{F}$.

Also, we introduce the modified double-layer potential $\mathcal{W}$ of density ψ

$$(\mathcal{W}\psi)(x) = (W\psi)(x) - \left\langle \pi_0 W^+ \psi, \widetilde{z}^{(i)} \right\rangle_{0;\Gamma_0} \widetilde{z}^{(i)}(x), \quad x \in \Omega,$$

where π_0 is the operator of restriction to Γ_0.

The solution of problem (28.1) may be represented in the form

$$u = (\mathcal{V}\varphi)_\Omega + \mathcal{W}\psi + z, \tag{28.2}$$

where φ and ψ are unknown densities and $z \in \mathcal{F}$ is arbitrary. The detailed procedure for obtaining solution (28.2) has been developed by Shmoylova et al. in [SPRb].

28.4 Boundary Element Method

Consider problem (28.1). As shown in [SPRb], the solution to this problem may be represented in the form (28.2), and the corresponding boundary integral equations are uniquely solvable with respect to distributional densities φ and ψ. As stated above, these densities cannot be found analytically. To approximate them numerically, we use the boundary element method [GKW03], which makes use of the following classical result.

Lemma 1. *(Somigliana formula If $u \in H_{1,\omega}(\Omega)$ is a solution of (28.1) in Ω, then*

$$\int_{\Gamma_0} \left[D(x,y)\delta\left(T(\partial_y)u(y)\right) - P(x,y)\delta u(y) \right] ds(y) = \frac{1}{2}\delta u(x), \quad x \in \Gamma_0, \tag{28.3}$$

where $\delta(\cdot)$ denotes the jump of $(\cdot)$ across the crack.

It has been shown in [SPRb] that the density of the modified single-layer potential may be found in the form $\varphi = \delta\,(T(\partial_y)u(y)) = \delta g$. Now we need to find the density of the modified double-layer potential $\psi = -\delta u$. To achieve this goal, we divide Γ_0 into n elements $\Gamma_0^{(k)}$, each of which possesses one node $\xi^{(k)}$ located in the middle of the element. The values of δg and δu are constant throughout the element and correspond to the value at the node $\delta g(\xi^{(k)})$ and $\delta u(\xi^{(k)})$. Then (28.3) becomes

$$\sum_{k=1}^{n} \int_{\Gamma_0^{(k)}} \left[D(x,y)\delta g(\xi^{(k)}) - P(x,y)\delta u(\xi^{(k)}) \right] \, ds(y) = \frac{1}{2}\delta u(x), \quad x \in \Gamma_0.$$

Placing x sequentially at all nodes, we obtain the linear algebraic system of equations

$$\sum_{k=1}^{n} \left(\int_{\Gamma_0^{(k)}} D(\xi^{(i)}, y) \, ds(y) \right) \delta g(\xi^{(k)}) - \sum_{k=1}^{n} \left(\int_{\Gamma_0^{(k)}} P(\xi^{(i)}, y) \, ds(y) \right) \delta u(\xi^{(k)}) = \frac{1}{2}\delta u(\xi^{(i)}), \qquad i,k = \overline{1,n} \tag{28.4}$$

with respect to $\delta u(\xi_i)$.

We note that $\int_{\Gamma_0^{(k)}} D(\xi^{(i)}, y) \, ds(y)$ are defined for any i and k, as in [Sch96].

Solving (28.4), we construct an approximation to ψ. If we introduce the shape function $\Phi_k(x)$ by

$$\Phi_k(x) = \begin{cases} 1, \, x \in \Gamma_0^{(k)}, \\ 0, \, x \in \Gamma_0 \backslash \Gamma_0^{(k)}, \end{cases}$$

then the approximate densities φ and ψ are $\varphi^{(n)}(x) = \sum_{k=1}^{n} \Phi_k(x)\delta g(\xi^{(k)})$ and $\psi^{(n)}(x) = -\sum_{k=1}^{n} \Phi_k(x)\delta u(\xi^{(k)})$, and the approximate solution takes the form $u^{(n)} = (\mathcal{V}\varphi^{(n)})_\Omega + \mathcal{W}\psi^{(n)} + z$, where z is arbitrary. It is easy to check that $u^{(n)} \to u$ as $n \to \infty$.

28.5 Example

As an example, we consider a longitudinal crack inside a human bone in the case when constant normal stretching pressure of magnitude p is applied on both sides of the crack. If we consider a typical transversal cross section of the bone and assume that this cross section is small enough, then the deformation of each cross section under the prescribed load will be the same throughout the length of the bone and will develop in the plane of the cross section. Consequently, such deformations may be considered under assumptions of plane micropolar elasticity. Such a model is not an idealization that lies far from reality, as it may seem at first, but, as shown, for example, in [BJ01] and

[JS04], it can describe actual cracks in bones very closely, since orthopedic biomechanics usually deals with cracks of a very small size.

We model a crack as an open arc of the circle given by $x_1 = a\cos\theta$ and $x_2 = a\sin\theta$, $\theta \in (0, \pi/6)$. Changing the radius a of the circle, we will change the length of the crack. We are interested in how the normal traction distributes at a distance from the crack tip along the line $x_1 = a$, $x_2 < 0$. Clearly, this problem can be considered as the Neumann problem described above.

Elastic constants for a human bone have been measured in [Lak95] and take the following values: $\alpha = 4000$ MPa, $\gamma = 193.6$ N, $\varepsilon = 3047$ N, $\lambda = 5332$ GPa, $\mu = 4000$ MPa. In our example, we construct solutions for cracks of lengths equal to 0.26 mm, 0.52 mm, 0.75 mm, and 10 mm to show good agreement of our results with those presented in the experimental study by Nakamura and Lakes [NL88], performed on human bone cracks of the same lengths. We also assume that the normal stretching pressure p takes the value 2 MPa.

Let the distance from the tip of the crack be $\rho = |x_2|$. The numerical solution for boundary tractions and moments has been found to coincide with the exact solution to five decimal places for $n = 52$ elements of Γ_0.

Let us now compare the results for the normal traction in the micropolar case with the results of the classical theory. The classical case may be obtained from the solution for micropolar elasticity by setting the micropolar elastic constants equal to zero. In Figures 28.1–28.3 there is a graphical representation for the distribution of the normal traction at a distance from the lower crack tip for crack lengths equal to 0.26 mm, 0.52 mm, and 0.75 mm, respectively. The traction is divided by the applied load p to represent the data in nondimensional values. The bold curve characterizes the stress distribution in the micropolar case, whereas the classical case is plotted by the ordinary curve. The distance between the first point, in which we compute the normal traction, and the tip of the crack is equal to one fifth of the length of the crack.

We see that the normal traction is significantly higher in the vicinity of the crack tip in the micropolar case in comparison with the case when microstructure is ignored (classical theory). In the case when the length of the crack is equal to 0.75 mm, we can observe that the normal traction in the vicinity of the crack tip is 26.8% higher under the assumptions of Cosserat elasticity in comparison with the classical case.

When it comes to the consideration of stresses at a distance from the crack tip, we can conclude that the traction in the micropolar case decays faster than in the classical case, and at a distance of approximately one crack length, the values of the normal traction in both cases become equal to each other. Farther from the crack tip, the traction in the micropolar case becomes lower than in the classical case, especially when we consider the crack of length 0.26 mm, for which, as may be seen from Figure 28.1, the difference is drastic and may be up to 19.8%. Additionally, it may be observed that at a distance

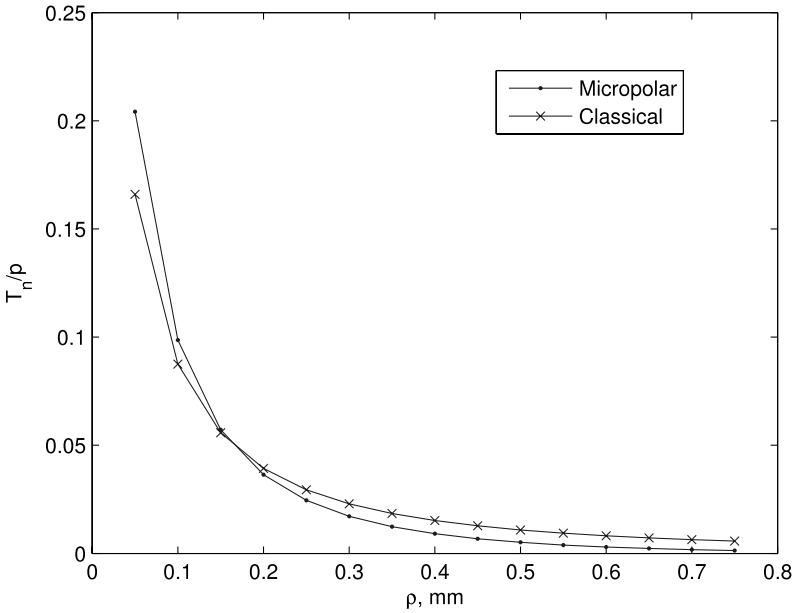

Fig. 28.1. Normal traction on the edge of a crack of length 0.26 mm.

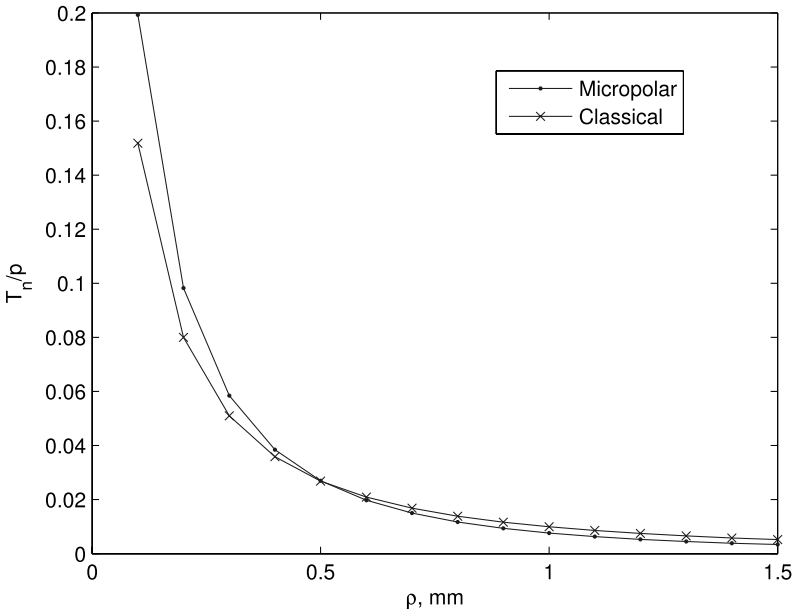

Fig. 28.2. Normal traction on the edge of a crack of length 0.52 mm.

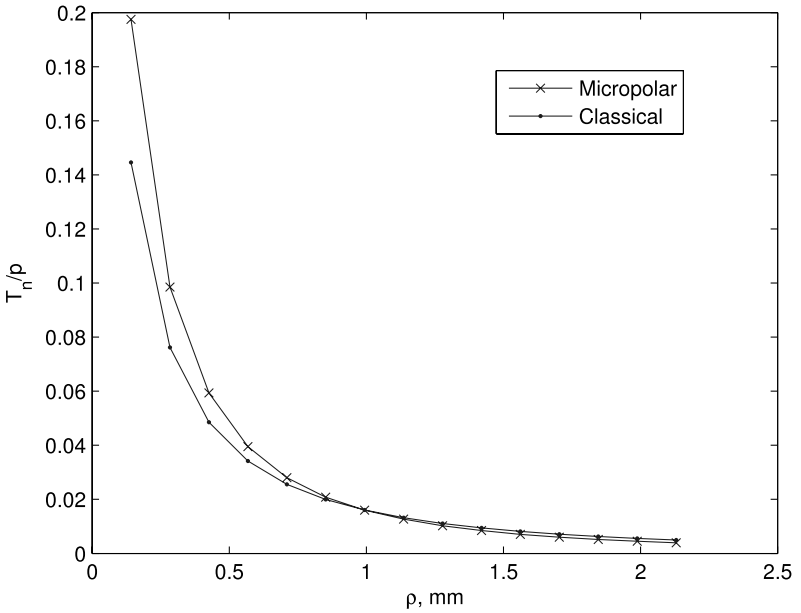

Fig. 28.3. Normal traction on the edge of a crack of length 0.75 mm.

of approximately three crack lengths from the tip of the crack, the effect of the crack on stresses is negligible, in agreement with Saint-Venant's principle.

The results presented in Figures 28.1–28.3 may be compared with earlier investigations undertaken in the area of Cosserat solids. Nakamura and Lakes [NL88] performed an experimental study on stress concentrations around cracks in a human bone. They considered the same crack lengths as in this chapter. Later, Lakes et al. validated their results presented in [NL88] using the finite element method [LNB90]. However, it should be noted that a direct comparison with the results presented in [NL88] and [LNB90] does not seem feasible since our formulation of the crack problem is different from that adopted in [NL88] and [LNB90], where a crack is considered to be a "blunt" notch, as in the approach of classical fracture mechanics [Sn69], in which a crack is usually modeled as a "squashed" ellipse of small eccentricity. The tip of the crack considered in [NL88] and [LNB90], therefore, is smooth, whereas in our study, the crack is represented by a piece of a plane curve whose edges have sharp corners. It has been found in [LNB90] that the difference in stress concentrations near the crack edge between the classical and micropolar case for a crack with a "blunt" tip may be up to 30% in the case when the crack length is equal to 0.26 mm, and that for longer cracks, this difference is almost negligible. The order of difference is in agreement with our results, but in [LNB90], the stress concentration near the crack tip in the micropolar case

is lower than in the classical case. At a distance from the crack tip, the results obtained in [LNB90] are almost identical to the results of this investigation.

The explanation of discrepancies between our results and those presented in [LNB90] in the vicinity of a crack tip lies in the crack geometry. If we consider a smooth contour such as an ellipse of small eccentricity as in [LNB90], then material particles can rotate under the applied load and generate couple stresses. Consequently, a part of the applied load is compensated by couple stresses and the resultant traction is reduced in comparison with the classical case. When we consider a crack with a sharp tip, material particles get trapped in the corner and cannot rotate; however, the load accumulated by the couple stresses (due to continuity) is still present. Hence, the resultant stress in the vicinity of a sharp edge grows. When we move away from the corner, the particles gain back their ability to rotate and the load is redistributed between the stresses and the couple stresses, so the resultant traction starts decreasing.

Indirect confirmation of our explanation may be found in [PL86] and [PSM04]. In [PL86], Park and Lakes performed an experimental investigation of the torsion of a rectangular micropolar beam. The boundary of any typical cross section of such a beam by a plane perpendicular to the generators contains sharp corners. It has been found that the stress distribution on the boundary of the beam cross section is significantly higher than in the case when microstructure is ignored. At the same time, the study by Potapenko et al. [PSM04], performed for an elliptic micropolar bar (in this case any typical cross section of the bar is bounded by a smooth curve), shows that stress concentrations on the boundary of the bar cross section may be up 15% lower than in the classical case. Similar conclusions may be drawn when we compare cracks with sharp and "blunt" tips in a micropolar medium.

28.6 Summary

In this chapter, we have shown that the method introduced by Shmoylova et al. in [SPRb] may be applied to the investigation of stress distribution around a crack with a sharp tip in a micropolar medium. We came to the conclusion that material microstructure has a significant effect on the stress distribution around a crack, and demonstrated it by using the example of a crack in a human bone. The effect of material microstructure depends on the crack length and crack geometry, and exercises the strongest influence in the vicinity of the crack tip.

References

[AlB93] Aliabadi, M.H., Brebbia, C.A.: *Advances in Boundary Element Methods for Fracture Mechanics.* Computational Mechanics Publ., Southampton, Boston; Elsevier, London-New York (1993).

[AtL02] Atkinson, C., Leppington, F.G.: The effect of couple stresses on the tip of a crack. *Internat. J. Solids Structures,* **13**, 1103–1122 (1977).

[BJ01] Bouyge, F., Jasiuk, I., Ostoja-Starzewski, M.: A micromechanically based couple-stress model of an elastic two-phase composite. *Internat. J. Solids Structures,* **38**, 1721–1735 (2001).

[Br78] Brebbia, C.A.: *The Boundary Element Method for Engineers.* Pentech Press, London (1978).

[CC00] Chudinovich, I., Constanda, C.: *Variational and Potential Methods in the Theory of Bending of Plates with Transverse Shear Deformation.* Chapman & Hall/CRC, Boca Raton-London-New York-Washington, DC (2000).

[Er66] Eringen, A.C.: Linear theory of micropolar elasticity. *J. Math. Mech.,* **15**, 909–923 (1966).

[GKW03] Gaul, L., Kögl, M., Wagner, M.: *Boundary Element Methods for Engineers and Scientists.* Springer, Berlin-Heidelberg-New York (2003).

[JS04] Jasiuk, I., Ostoja-Starzewski, M.: Modeling of bone at a single lamella level. *Biomech. Model. Mechanobiology,* **3**, 67–74 (2004).

[Lak82] Lakes, R.: Dynamical study of couple stress effects in human compact bone. *J. Biomedical Engng.,* **104**, 6–11 (1982).

[Lak95] Lakes, R.: Experimental methods for study of Cosserat elastic solids and other generalized elastic continua. In: Muhlhaus, H-B. (ed.), *Continuum Models for Materials with Microstructure.* Wiley, New York (1995), pp. 1–22.

[LNB90] Lakes, R., Nakamura, S., Behiri, J., Bonfield, W.: Fracture mechanics of bone with short cracks. *J. Biomech.,* **23**, 967–975 (1990).

[MP02] Mühlhaus, H.-B., Pasternak, E.: Path independent integrals for Cosserat continua and application to crack problems. *Internat. J. Fracture,* **113**, 21–26 (2002).

[NL88] Nakamura, S., Lakes, R.: Finite element analysis of stress concentration around a blunt crack in a Cosserat elastic solid. *Comput. Methods Appl. Mech. Engng.,* **66**, 257–266 (1988).

[PL86] Park, H., Lakes, R.: Cosserat micromechanics of human bone: strain redistribution by a hydration sensitive constituent. *J. Biomechanics,* **19**, 385–397 (1986).

[PSM04] Potapenko, S., Schiavone, P., Mioduchowski, A.: Generalized Fourier series solution of torsion of an elliptic beam with microstructure. *Appl. Math. Lett.,* **17**, 189–192 (2004).

[Sch96] Schiavone, P.: Integral equation methods in plane asymmetric elasticity. *J. Elasticity,* **43**, 31–43 (1996).

[SPR06] Shmoylova, E., Potapenko, S., Rothenburg, L.: Weak solutions of the interior boundary value problems of plane Cosserat elasticity. *Z. Angew. Math. Phys.,* **57**, 506–522 (2006).

[SPRa] Shmoylova, E., Potapenko, S., Rothenburg, L.: Weak solutions of the exterior boundary value problems of plane Cosserat elasticity. *J. Integral Equations Appl.* (in press).

[SPRb] Shmoylova, E., Potapenko, S., Rothenburg, L.: Stress distribution around a crack in plane micropolar elasticity. *J. Elasticity* (in press).

[Sn69] Sneddon, I.: *Crack Problems in the Classical Theory of Elasticity.* Wiley, New York (1969).

29

Euler–Bernoulli Beam with Energy Dissipation: Spectral Properties and Control

M. Shubov

University of New Hampshire, Durham, NH, USA;
marianna.shubov@euclid.unh.edu

29.1 Statement of the Problem

We present several results on the problems associated with the Euler–Bernoulli beam model with dynamical nonconservative boundary conditions. A forcing term, treated as a distributed control, is introduced into the equation governing small transverse vibrations of a beam. The main question is the following: *Can one provide an explicit formula for the control law in order to steer an initial state to zero in a prescribed time interval of length* $T > 0$*?* As we show, the answer is affirmative for any $T > 0$ if certain conditions on the initial state and force distribution function are satisfied; if these conditions are not satisfied, then one has an approximate controllability (Theorems 6 and 7 below). However, to give explicit formulas for the control laws, one needs the following information: (i) detailed asymptotic and spectral results on the dynamics generator governing beam vibrations; (ii) facts about completeness, minimality (linear independence for an infinite number of vectors), and the Riesz basis property of the generalized eigenvectors of the dynamics generator (recall that a *Riesz basis* is a linear isomorphic image of an orthonormal basis, i.e., it is the mildest modification of an orthonormal basis); and (iii) results on solvability of the corresponding moment problem that, in turn, requires some information on the basis property of *nonharmonic exponentials* in $L^2(0, T)$.

We also present an interesting result on the nature of a semigroup for which the main operator, the dynamics generator, is an infinitesimal generator. It is found that this semigroup is of a Gevrey class; i.e., differentiability of such a semigroup is slightly weaker than that of an analytic semigroup (see [T89] and [TC90]).

Extensive research exists on the Euler–Bernoulli beam model in traditional areas such as control, stability, and optimization for the model involving both undamped and damped cases (see [CR82], [CKM87], [CLL98], [GWY05], and [R73]). However, one of the contemporary research directions is developing in the field of unmanned aerial vehicles (UAV) in aeronautics. In particular, a long-span, very light, flexible object in flight (high aspect-ratio "flying wing"

configuration) can be considered as an elastic beam with both ends free, and boundary feedback stabilization of such a beam could be of great interest both in control theory and in engineering practice (see [H90], [PHC00], and [PH04]).

Consider a linear model of the Euler–Bernoulli beam with a forcing term

$$\rho(x)h_{tt}(x.t) + (EI(x)h_{xx}(x,t))_{xx} = g(x)f(t), \quad (x,t) \in (0,L) \times R^+, \quad (29.1)$$

where h is the transverse displacement, ρ is the mass density, and EI is the flexural rigidity:

$$\rho \in C^1[0,L], \quad EI \in C^2[0,L], \quad \rho(x) > 0, \quad EI(x) > 0, \quad x \in [0,L]. \quad (29.2)$$

We assume that the beam is clamped at the left end; i.e.,

$$h(0,t) = h_x(0,t) = 0, \quad t \geqslant 0. \quad (29.3)$$

The right-end conditions reflect shear feedback design for vibration suppression [GWY05]

$$h_{xx}(L) = 0, \quad (EI(x)h_{xx}(x,t))_x|_{x=L} = kh_{xt}(x,t)|_{x=L}, \quad (29.4)$$

with k being a positive parameter that can be changed in practice.

The initial conditions are standard:

$$h(x,0) = h_0(x), \quad h_t(x,0) = h_1(x). \quad (29.5)$$

In what follows, we assume that the force distribution function is $g \in L^2(0,L)$; f will be called an *admissible* control function on the interval $[0,T]$ if $f \in L^2(0,T)$.

29.1.1 Exact Controllability Problem

Let initial conditions (29.5) and $T > 0$ be given. *Does there exist an admissible control $f(t)$ on the interval $[0,T]$ such that the solution of problem (29.1)–(29.5) also satisfies the additional conditions at $t = T$*

$$h(x,T) = 0, \quad h_t(x,T) = 0, \quad x \in [0,L]? \quad (29.6)$$

From now on, we will consider the case of a uniform beam with $x \in [0,1]$. Even though the asymptotic analysis of a differential equation with variable coefficients is lengthy, the main results of this chapter remain essentially the same in the nonuniform case.

Let $\mathcal{H}$ be the state space of the system; i.e., $\mathcal{H}$ is a Hilbert space of two-component vector-valued functions $(h(x,t), \ h_t(x,t))^T$ obtained as a closure of the set of smooth, compactly supported functions $U(x) = (u_0(x), u_1(x))^T$ in the norm (the superscript T means transposition)

$$\|U\|_{\mathcal{H}}^2 = \int_0^1 [|u_0''(x)|^2 + |u_1(x)|^2]dx.$$

Evidently, if $U \in \mathcal{H}$, then $u_0(0) = u_0'(0) = 0$. Equation (29.1) and conditions (29.2)–(29.5) (without a forcing term) define the following first order (in time) evolution problem:

$$U_t(x,t) = (\mathcal{L}_k U)(x,t), \quad U|_{t=0} = (u_0^0(x), u_1^0(x))^T, \quad 0 \leqslant x \leqslant 1, \ \ t \geqslant 0,$$

where the dynamics generator $\mathcal{L}_k$ is given by the matrix differential expression

$$\mathcal{L}_k = -i \begin{pmatrix} 0 & 1 \\ -\frac{d^4}{dx^4} & 0 \end{pmatrix} \tag{29.7}$$

defined on the domain

$$\mathcal{D}(\mathcal{L}_k) = \big\{U \in \mathcal{H} : \quad u_0 \in H^4(0,1), \ \ u_1 \in H^2(0,1), \quad u_1(0) = u_1'(0) = 0, \\ u_0(0) = u_0'(0) = u_1''(1) = 0, \quad u_0'''(1) = k u_1'(1)\big\},$$

where $H^s(0,1), \ \ s = 2, 4$, are the standard Sobolev spaces [A75]. The adjoint operator $\mathcal{L}_k^*$ can be given by the same differential expression as (29.7), with the following change in the domain:

$$\mathcal{D}(\mathcal{L}_k^*) = \big\{U \in \mathcal{H} : \quad u_0 \in H^4(0,1), \ \ u_1 \in H^2(0,1), \quad u_1(0) = u_1'(0) = 0, \\ u_0(0) = u_0'(0) = u_1'''(1) = 0, \quad u_0''(1) = k u_1(1)\big\}.$$

29.2 Asymptotic and Spectral Properties of Operator $\mathcal{L}_k$

29.2.1 Asymptotic Distribution of the Eigenvalues

Theorem 1. *(i) $\mathcal{L}_k$ is an unbounded non-self-adjoint operator with a compact resolvent. Therefore, the spectrum of $\mathcal{L}_k$ consists of a countable set of normal eigenvalues (i.e., isolated eigenvalues, each of a finite algebraic multiplicity [GK96]) that can accumulate only at infinity.*

(ii) (a) When $k > 1$, the following asymptotic representation holds for the eigenvalues as the number n of an eigenvalue tends to infinity:

$$\lambda_n = (\pi n)^2 + i\pi n \ln\frac{k+1}{k-1} - \frac{1}{4}\ln^2\frac{k+1}{k-1} + O(e^{-\gamma n}), \ \ n > 0,$$

where $\gamma > 0$ is an absolute constant. The spectrum is symmetric with respect to the imaginary axis; i.e., $\lambda_{-|n|} = -\bar{\lambda}_n$.

(b) When $0 < k < 1$, the following asymptotic representation holds for the eigenvalues as the number n of an eigenvalue tends to infinity:

$$\lambda_n = \pi^2\left(n - \frac{1}{2}\right)^2 + i\pi\left(n - \frac{1}{2}\right)\ln\frac{1-k}{1+k} - \frac{1}{4}\ln^2\frac{1-k}{1+k} + O(e^{-\gamma n}), \quad n > 0.$$

29.2.2 Riesz Basis Property of the Generalized Eigenvectors

The set of the almost-normalized eigenvectors can be written in the form

$$\Phi_n(x) = \begin{pmatrix} \frac{1}{\mu_n^2}\varphi_n(x) \\ \varphi_n(x) \end{pmatrix}_{n\in\mathbb{Z}}, \quad \|\Phi_n\|_{\mathcal{H}} \asymp 1, \tag{29.8}$$

where φ_n is an eigenfunction of the Sturm–Liouville problem that is equivalent to the spectral problem for $\mathcal{L}_k$. The following approximation is valid as $n \to \infty$ $(\mu_n = \sqrt{\lambda_n})$:

$$\varphi_n(x) = \sin \mu_n x - \cos \mu_n x + e^{-\mu_n x} + O(e^{-|n|}).$$

Taking into account that $\mu_{-|n|} = i\bar{\mu}_{|n|}$, as $n \to -\infty$, we obtain the approximation

$$\varphi_{-|n|}(x) = i(-\sin(\bar{\mu}_{|n|}x) + \cos(\bar{\mu}_{|n|}x)) - ie^{-\bar{\mu}_{|n|}x} + O(e^{-|n|}).$$

As we know, the non-self-adjoint operator $\mathcal{L}_k$ may have a finite number of multiple eigenvalues that could lead to a finite number of the associate vectors.

Theorem 2. *The set of the generalized eigenvectors (eigenvectors and associate vectors together) of the operator $\mathcal{L}_k$ forms a Riesz basis for $\mathcal{H}$. The set of the generalized eigenvectors of the adjoint operator $\mathcal{L}_k^*$ forms a biorthogonal Riesz basis (see [GK96], [S96], and [S00]).*

29.2.3 Generation of a Gevrey-Class Semigroup

We now discuss the properties of a semigroup for which the operator $(i\mathcal{L}_k)$ is an infinitesimal generator. This operator generates a strongly continuous semigroup. Indeed, $(i\mathcal{L}_k)$ is closed and its domain $\mathcal{D}(i\mathcal{L}_k)$ is dense in $\mathcal{H}$. The only fact to be proved is that the resolvent $\mathbb{R}(\lambda, i\mathcal{L}_k)$ satisfies the estimate $\|\mathbb{R}(\lambda, i\mathcal{L}_k)^n\| \leqslant M/(\lambda - \omega)^n$, where M is an absolute constant and $\lambda > \omega$ with some $\omega > 0$ (see [P83] and [S06]). This estimate can be proved by using the spectral asymptotics and the spectral decomposition for the resolvent operator.

We now turn to the fact that the semigroup is of a Gevrey class. (The relevant definition can be found in [T89], [TC90], and [S06].)

Theorem 3. *A strongly continuous semigroup $T(t)$ is of Gevrey class δ for $t > t_0$ if it is infinitely differentiable for $t \in (t_0, \infty)$ and if for every compact set $\mathcal{K} \subset (t_0, \infty)$ and each $\theta > 0$, there exists a constant $\mathcal{B} = \mathcal{B}(\theta, \mathcal{K})$ such that $\|T^{(n)}(t)\| \leqslant \mathcal{B}\theta^n(n!)^\delta$ for all $t \in \mathcal{K}$ and $n = 0, 1, 2, \ldots$.*

As one can see, "Gevrey regularity" involves bounds on the nth-order derivatives, which are similar to (but somewhat weaker than) the bounds on the nth-order derivatives for the case of an analytic semigroup [P83]. The main result of this section is included in the next assertion.

Theorem 4. *The semigroup generated by the operator $\mathcal{L}_k$ is of Gevrey class $\delta > 1/2$.*

The detailed proof can be found in [S06].

29.3 Moment Problem and Controllability Results

29.3.1 Some Known Results on Nonharmonic Exponentials

To formulate the solution of the control problem , we need some information on the properties of nonharmonic exponentials (see [HNP81], [Y80], and [AI95]). Let

$$\mathfrak{P} = \left\{\exp\left(i\bar{\lambda}_n\, t\right)\right\}_{n\in\mathbb{Z}},$$

where $\{\lambda_n\}_{n\in\mathbb{Z}}$ is the spectrum of $\mathcal{L}_k$. The following statement is valid for $\mathfrak{P}$:

Theorem 5. *For any $T > 0$, (i) the set of nonharmonic exponentials $\mathfrak{P}$ is not complete in $L^2(0,T)$, and (ii) this set forms a Riesz basis for its closed linear span in $L^2(0,T)$.*

Let $T > 0$, and let $E(\mathfrak{P}, T)$ denote the smallest closed subspace in $L^2(0,T)$ containing $\mathfrak{P}$. As is well known [FR71], $E(\mathfrak{P}, T)$ is a proper subspace of $L^2(0,T)$ if and only if $\sum\limits_{n\in\mathbb{Z}} \frac{1}{|\lambda_n|} < \infty$, which is our case. It is also known that if $\mathfrak{P}^n \equiv \left\{\bar{\lambda}_n \;\; |k \neq n\right\}$, then $E(\mathfrak{P}^n, T)$, then the smallest closed subspace in $L^2(0,T)$ containing $\mathfrak{P}^n$does not include $\exp(i\bar{\lambda}_n t)$. In this case, using standard arguments from Hilbert space theory, one can show that there is a unique function $\tau_n(t) \in E(\mathfrak{P}^n, T)$ that is closest to the function $\exp(i\bar{\lambda}_n t)$ in the $L^2(0,T)$-norm. If

$$(d_n(T))^2 = \int_0^T (e^{i\bar{\lambda}_n t} - \tau(t))^2 dt,$$

then the set

$$\psi_n(t) = \frac{e^{i\bar{\lambda}_n t} - \tau_n(t)}{(d_n(T))^2}, \quad n \in \mathbb{Z},$$

is a biorthogonal set for $\mathfrak{P}$ in $L^2(0,T)$. Obviously, since the set $\mathfrak{P}$ is *not complete* in $L^2(0,T)$, the biorthogonal set is *not unique*. However, the set $\{\psi_n\}_{n\in\mathbb{Z}}$ is called the *optimal* biorthogonal set for $\mathfrak{P}$. Suppose that $\{\widetilde{\psi}_n\}_{n\in\mathbb{Z}}$ is any other biorthogonal vector for $\mathfrak{P}$ in $L^2(0,T)$. It is easily verified that $\widetilde{\psi}_n = \psi_n + \varphi_n$ and $\varphi_n \in E(\mathfrak{P}, T)^{\perp}$, $n \in \mathbb{Z}$; hence, $\|\psi_n\|_{L^2(0,T)} \leqslant \|\widetilde{\psi}_n\|_{L^2(0,T)}$, $n \in \mathbb{Z}$, which yields $\|\psi_n\|_{L^2(0,T)} = (d_n\,(T))^{-1}$.

Since $\mathfrak{P}$ is a Riesz basis for $E(\mathfrak{P}, T)$, the biorthogonal family $\{\psi_n\}_{n\in\mathbb{Z}}$ is also a Riesz basis for $E(\mathfrak{P}, T)$.

29.3.2 Moment Problem

Let $G(x) = (0, g(x), 0, 0)^T \in \mathcal{H}$, where $g(x)$ is the force profile function from (29.1). Then, from (29.1)–(29.5), we obtain the following representation of the initial problem:

$$U_t(x) = i(\mathcal{L}_k U)(x) + f(t)G(x), \quad U(x,0) = \mathcal{F}_0(x). \tag{29.9}$$

Let us expand the solution of (29.9) with respect to the Riesz basis of the generalized eigenvectors of the operator $\mathcal{L}_k$ (29.8):

$$U(x,t) = \sum_{n\in\mathbb{Z}} a_n(t)\, \Phi_n(x), \quad x \in (0,1), \;\; t \geqslant 0. \tag{29.10}$$

We use through numeration for the generalized eigenvectors making no difference between the eigenvectors and associate vectors of $\mathcal{L}_k$. We also expand the functions $G(\cdot)$ and $\mathcal{F}_0(\cdot)$ with respect to the same Riesz basis:

$$G(x) = \sum_{n\in\mathbb{Z}} g_n\, \Phi_n(x), \quad \mathcal{F}_0(x) = \sum_{n\in\mathbb{Z}} \varphi_n\, \Phi_n(x), \quad \sum_{n\in\mathbb{Z}} \left(|g_n|^2 + |\varphi_n|^2\right) < \infty. \tag{29.11}$$

Substituting (29.10) and (29.11) into (29.9), we obtain an infinite sequence of the initial-value problems

$$(a_n(t))_t = i\lambda_n a_n(t) + g_n f(t), \quad a_n(0) = \varphi_n, \quad n \in \mathbb{Z}. \tag{29.12}$$

Solving problems (29.12) for $a_n(t)$, we rewrite representation (29.10) in the form

$$U(x,t) = \sum_{n\in\mathbb{Z}} \left[\varphi_n\, e^{i\lambda_n t} + g_n \int_0^t e^{i\lambda_n (t-\tau)} f(\tau) d\tau \right] \Phi_n(x). \tag{29.13}$$

Our main question is the following: *Is there a moment $T > 0$ such that $U(x,T) = 0$?* From (29.13) and the Riesz basis property of $\{\Phi_n\}_{n\in\mathbb{Z}}$, we find that $U(x,T) = 0$ if and only if the following infinite system of equations has a solution $f \in L^2(0,T)$:

$$\varphi_n + g_n \int_0^T e^{-i\lambda_n \tau}\, f(\tau) d\tau = 0, \quad n \in \mathbb{Z}. \tag{29.14}$$

The problem of finding a solution of (29.14) is known as *the moment problem* (see [Y80] and [Z91]). To solve it, we will use the properties of nonharmonic exponentials.

29.3.3 Exact and Approximate Controllability

We are now in a position to present our results on exact controllability [S07].

Theorem 6. *(i) Suppose that*

$$g_n \neq 0 \qquad \text{for all } n \in \mathbb{Z}. \tag{29.15}$$

The following statements are valid.

(a) System (29.9) is controllable on the time interval $[0,T]$ *with any* $T>0$ *if and only if*

$$\{\gamma_n \equiv \varphi_n/g_n\}_{n\in\mathbb{Z}} \in \ell^2(\mathbb{Z}), \quad \textit{i.e.,} \quad \sum_{n\in\mathbb{Z}} |\gamma_n|^2 < \infty. \tag{29.16}$$

(b) The desired control function f*, which brings the system to the zero state on the time interval* $[0,T]$*,* $T>0$*, can be defined by the formula*

$$f(t) = -\sum_{n\in\mathbb{Z}} \gamma_n\, \psi_n(t), \tag{29.17}$$

where ψ_n *are the functions biorthogonal to the corresponding nonharmonic exponentials. There exist infinitely many control functions from* $L^2(0,T)$*. However,* f *defined by (29.17) has the minimal norm; i.e., if another function* $\widetilde{f}$ *brings the system to rest in the same time* T*, then*

$$\|f\|_{L^2(0,T)} \leqslant \|\widetilde{f}\|_{L^2(0,T)}.$$

(ii) Assume that (29.15) is not satisfied, and let $R = \{n \in \mathbb{Z} :\ g_n = 0\}$*. Let* γ_n *be defined by (29.16) only for* $n \in \mathbb{Z}\backslash R$*, and let* $S = \{n \in \mathbb{Z} :\ \varphi_n = 0\}$*. Then the following statements hold:*

(a) The system is controllable in time $T>0$ *if and only if* $R \subseteq S$ *and*

$$\sum_{n\in\mathbb{Z}} |\gamma_n|^2 < \infty.$$

(b) The desired control function is not unique and can be given by the formula

$$f(t) = -\Big[\sum_{n\in\mathbb{Z}\backslash S} \gamma_n\, \psi_n(t) + \sum_{m\in R} b_m\, \psi_m(t)\Big],$$

where $b_m \in \mathbb{C}$ *are arbitrary coefficients such that* $\sum\limits_{m\in R} |b_m|^2 < \infty$*.*

(c) If the set $R\backslash(R \bigcap S)$ *is not empty, then the system is not controllable in any time.*

Remark 1. The formulas for the basis functions $\psi_n(t)$ that are biorthogonal to the basis of the nonharmonic exponentials are known to be very complicated and can be given in terms of the truncated Blaschke product.

Theorem 7. *(Approximate Controllability) Suppose that condition (29.16) is not valid, but that*

$$\{\gamma_n\}_{n\in\mathbb{Z}} \in l^q(\mathbb{Z}) \quad \text{for some } q \in (2,\infty], \quad \text{i.e.,}$$
$$\sum_{n\in\mathbb{Z}} |\gamma_n|^q < \infty, \ \ (\text{if } \ 2 < q < \infty) \quad \text{or} \quad \sup_{n\in\mathbb{Z}} |\gamma_n| < \infty \ \ (\text{if } q = \infty).$$

Then for any $\epsilon > 0$, there exists N such that for the control function

$$f_N(t) = \sum_{|n|\leqslant N} \gamma_n \, \psi_n(t),$$

the following estimate is valid:

$$\|U(\cdot,T)\|_{\mathcal{H}} \leqslant \epsilon \quad \text{for } T > 0.$$

However, $\|f_N\|_{L^2(0,T)} \to \infty$ as $N \to \infty$.

Acknowledgement. The author is grateful to Irena Lasiecka for important information on Gevrey-class semigroups. Partial support from the NSF award DMS # 0604842 is highly appreciated.

References

[A75] Adams, R.A.: *Sobolev Spaces.* Academic Press, New York (1975).

[AI95] Avdonin, S.A., Ivanov, S.A.: *Families of Exponentials. The Method of Moments in Controllability Problems for Distributed Parameter Systems.* Cambridge University Press, Cambridge (1995).

[CR82] Chen, G., Russell, D.L.: A mathematical model for linear elastic systems with structural damping. *Quart. Appl. Math.,* **39**, 433–454 (1982).

[CKM87] Chen, G., Krantz, S.G., Ma, D.W., Wayne, C.E., West, H.H.: The Euler-Bernoulli beam equations with boundary energy dissipation. In: *Operator Methods for Optimal Control Problems.* Marcel Dekker, New York (1987), pp. 67–96.

[CLL98] Chen, S., Liu, K., Liu, Z.: Spectrum and stability for elastic systems with global or local Kevin–Voigt damping. *SIAM J. Appl. Math.,* **59**, 651–668 (1998).

[FR71] Fattorini, H.O., Russell, D.L.: Exact controllability theorems for linear parabolic equations in one space dimension, *Arch. Rational Mech. Anal.,* **43**, 272–292 (1971).

[GK96] Gohberg, I.Ts., Krein, M.G.: *Introduction to the Theory of Linear Nonselfadjoint Operators.* AMS, Providence, RI (1996).

[GWY05] Guo, B.–Z., Wang, J.–M., Yung, S.–P.: On the C_0-semigroup generation and exponential stability resulting from a shear force feedback on a rotating beam. *Systems Contr. Lett.,* **54**, 557–574 (2005).

[H90] Hodges, D.H.: A mixed variational foundation based on exact intrinsic equations for dynamics of moving beams. *Internat. J. Solids Structures,* **26**, 1253–1273 (1990).

[HNP81] Hruschev, S.V., Nikol'skii, N.K., Pavlov, B.S.: *Unconditional Bases of Exponentials and Reproducing Kernels.* Springer, Berlin-Heidelberg (1981), pp. 214–335.

[PHC00] Patil, M.J., Hodges, D.H., Cesnik, C.E.S.: Nonlinear aeroelastic analysis of complete aircraft in subsonic flow. *J. Aircraft,* **37**, 753–760 (2000).

[PH04] Patil, M.J., Hodges, D.H.: On the importance of aerodynamic and structural geometrical nonlinearities in aeroelastic behavior of high aspect-ratio wings. *J. Fluids Structures,* **19**, 905–915 (2004).

[P83] Pazy, A.: *Semigroups of Linear Operators and Applications to Partial Differential Equations.* Springer, New York (1983).

[R73] Russel, D.L.: A unified boundary controllability theory for hyperbolic and parabolic partial differential equations. *Stud. Appl. Math.,* **52**, 189–211 (1973).

[S96] Shubov, M.A.: Riesz basis property of eigenfunctions of nonselfadjoint operator pencils generated by the equation of nonhomogeneous damped string. *Integral Equations Oper. Theory,* **25**, 289–328 (1996).

[S00] Shubov, M.A.: Riesz basis property of root vectors of nonselfadjoint operators generated by radial damped wave equations. *Adv. Differential Equations,* **5**, 623–656 (2000).

[S06] Shubov, M.A.: Generation of Gevrey class semigroup by non-selfadjoint Euler–Bernoulli beam model. *Math. Methods Appl. Sci.,* **29**, 2181–2199 (2006).

[S07] Shubov, M.A.: Exact controllability of nonselfadjoint Euler–Bernoulli beam model via spectral decomposition method. *IMA J. Math. Control Inf.* (in press).

[T89] Taylor, S.W.: Gevrey regularity of solutions of evolution equations and boundary controllability. PhD Thesis, University of Minnesota, Minneapolis (1989).

[TC90] Triggiani, R., Chen, S.: Gevrey class semigroups arising from elastic systems with gentle dissipation: the case $0 < \alpha < 1/2$. *Proc. Amer. Math. Soc.,* **110**, 401–415 (1990).

[Y80] Young, R.M.: *Introduction to Nonharmonic Fourier Series.* Academic Press, New York (1980).

[Z91] Zwaan, M.: *Moment Problems in Hilbert Space with Applications to Magnetic Resonance Imaging.* Centrum voor Wiskunde en Informatica, CWI TRACT (1991).

30

Correct Equilibrium Shape Equation of Axisymmetric Vesicles

N.K. Vaidya[1], H. Huang[1], and S. Takagi[2]

[1] York University, Toronto, ON, Canada; nvaidya@mathstat.yorku.ca, hhuang@yorku.ca
[2] University of Tokyo, Japan; takagi@mech.t.u-tokyo.ac.jp

30.1 Introduction

Under favorable conditions, lipid molecules consisting of hydrophobic tail and hydrophilic head groups, self-assemble to form vesicles in an aqueous medium with a lipid bilayer separating the inner and outer solutions [Ino96], [Kom96]. Vesicles have been attracting enormous attentions because of their biological significance with numerous applications such as drug delivery and targeting, medical imaging, catalysis, etc. [KR96], [Zan96]. It is recognized that the equilibrium shape of the vesicle is determined by minimizing a shape energy given by the spontaneous-curvature model of Helfrich [Hel73], [OH89]:

$$F = \frac{1}{2}k_b \oint (c_1 + c_2 - c_0)^2 dA + k_G \oint c_1 c_2 dA + \lambda \oint dA + \Delta P \int dV. \quad (30.1)$$

Here dA, dV, and k_b are the surface area element, volume element, and the bending rigidity, respectively; c_1 and c_2 denote the two principal curvatures and c_0 denotes the spontaneous curvature, which takes the possible asymmetry of the bilayer into account; λ and ΔP are Lagrangian multipliers used to incorporate the constraints of constant area and constant volume, respectively. Physically, λ and ΔP can be interpreted as the tensile stress and pressure difference, respectively. For vesicles with the same topological forms, the Gaussian curvature term $k_G \oint c_1 c_2 dA$ can be dropped from (30.1).

For vesicles with axisymmetric equilibrium shapes, four different approaches have been used to derive the shape equation in the literature.

A1. In Ou-Yang and Helfrich [OH89], a general shape equation was derived by allowing the variation of the functional F only in the normal direction of the membrane surface. The axisymmetric shape equation can be obtained by applying the axisymmetric condition.

A2. This approach is similar to A1, allowing variation only in the normal direction. The difference is that variation is carried out after the axisymmetric condition is applied [HO93].

A3. Again, functional F is written in the axisymmetric form first. The calculus of variation is performed without the restriction in the normal direction [MFR91], [Pet85].

A4. This approach is similar to A3. However, the arc-length is used as the primary variable, instead of the distance to the axis of symmetry [SBL91], [Sef66].

Both A1 and A2 generate the same equation. The shape equations produced by A3 and A4, however, are slightly different, as pointed out in [HO93]. In an attempt to remove the confusion, it was shown in [ZL93] that the shape equations in A1 and A3 are related. However, due to the coordinate singularity, this relationship does not necessarily imply equivalence [BP04], [Poz03]. This was confirmed in [NOO93] with the help of an analytical expression of a circular biconcave discoid (the shape of red blood cells). In addition, by considering the 2D limit, it was shown that the equations derived from A3 and A4 are erroneous since they do not recover the correct equation, whereas the equation from A1 and A2 gives the correct limit [BP04], [Poz03]. Other special solutions have also been used to validate or invalidate the equivalence of the shape equations [HO93], [NOO93]. The most satisfactory discussion about these issues has been presented in [JS94], in which it was shown that the same equation can be obtained by A4 and A1. Their main conclusion is that an additional equation has to be introduced for the Hamiltonian (i.e., constant Hamiltonian), which can be maintained by proper treatment of the boundary conditions. However, this idea of treatment of the boundary condition does not work for fixed integral limits (i.e., constant total contour length) and the validity of the argument was questioned by [BP04], [Poz03]. Therefore, it is still not clear whether it is necessary to restrict the variation in the normal direction, as suggested in [OH89].

In this chapter, we show that the same shape equation in A1 and A2 can be obtained without restricting the variation in the normal direction. We further prove that a slight modification of A3 produces the correct equation. As long as a geometric condition is satisfied (*explicitly* or *implicitly*), the variation does not have to be in the normal direction, contrary to the argument in [HO93]. To show the equivalence of equations by A1 and A4, [JS94] also suggested similar types of geometric conditions. However, they and others following their arguments have not implemented these conditions in their later works [DBS03], [JL96] when attempting to get the axisymmetric shape equations. Our result (correct shape equation by modification of A3) suggests that when A4 is used, apart from the extra Hamiltonian condition, the geometric condition should also be imposed properly to get the correct shape equations.

The rest of the chapter is organized as follows. In Section 30.2, we present the equations obtained using A1–A3 in the literature. In Section 30.3, we show that the correct equation can be obtained by taking the variation in the direction perpendicular to the axis of symmetry. Furthermore, by imposing the geometric condition implicitly in the action form of the energy functional,

we show that A3 can produce exactly the same equation as A1 (and A2). Various topological shapes of vesicles are discussed in Section 30.3.4, and we present our conclusions in Section 30.4.

30.2 Shape Equation

We consider vesicles of axisymmetric shape with the axis of symmetry along the z-axis. We denote the arc length of the contour, the distance to the symmetric axis, and the angle made by the tangent to the contour with the plane perpendicular to the axis of symmetry by s, ρ, and ψ, respectively (see Figure 30.1(a).

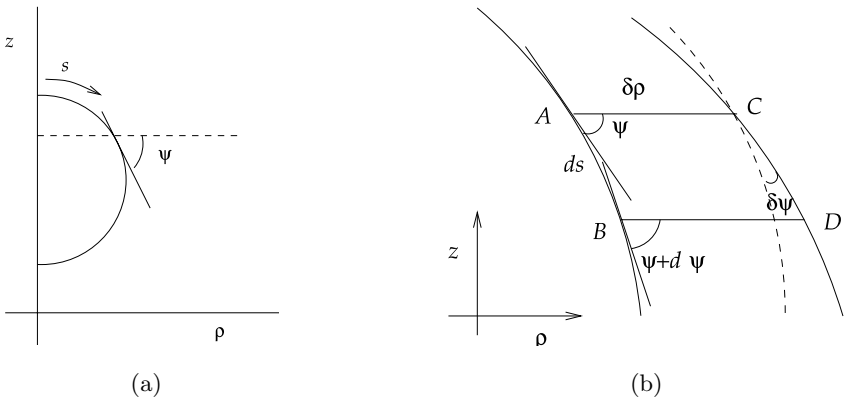

(a) (b)

Fig. 30.1. (a) Schematic diagram of the axisymmetric vesicle. (b) The variation in the direction perpendicular to the axis of symmetry (i.e., in ρ-direction). $AB = ds$ is the segment in the original generating curve, CD is the corresponding segment in the curve deduced by the variation $\delta\rho$ in the ρ-direction, and the dashed curve is the curve deduced by moving the original curve from A to C.

Using A1, that is, substituting the mean curvature

$$H = -(c_1 + c_2)/2 = -(1/2)[\cos\psi(d\psi/d\rho) + \sin\psi/\rho]$$

and the Gaussian curvature

$$K = c_1 c_2 = \cos\psi \sin\psi(1/\rho)(d\psi/d\rho)$$

in the general shape equation derived by Ou-Yang and Helfrich [OH89], we obtain the shape equation as (see [BP04], [HO93], [NOO93], [Poz03], and [ZL93])

$$\cos^3\psi\frac{d^3\psi}{d\rho^3} = 4\sin\psi\cos^2\psi\frac{d^2\psi}{d\rho^2}\frac{d\psi}{d\rho} - \cos\psi(\sin^2\psi - \frac{1}{2}\cos^2\psi)\left(\frac{d\psi}{d\rho}\right)^3 + \frac{7\sin\psi\cos^2\psi}{2\rho}\left(\frac{d\psi}{d\rho}\right)^2 - \frac{2\cos^3\psi}{\rho}\frac{d^2\psi}{d\rho^2} + \left(\frac{c_0^2}{2} - \frac{2c_0\sin\psi}{\rho} + \frac{\sin^2\psi}{2\rho^2} + \frac{\lambda}{k_b} - \frac{\sin^2\psi - \cos^2\psi}{\rho^2}\right)\cos\psi\frac{d\psi}{d\rho} + \frac{\Delta P}{k_b} + \frac{\lambda\sin\psi}{k_b\rho} - \frac{\sin^3\psi}{2\rho^3} + \frac{c_0^2\sin\psi}{2\rho} - \frac{\sin\psi\cos^2\psi}{\rho^3}. \tag{30.2}$$

The axisymmetric shape equation generated by A3, in which axisymmetric expressions for curvatures are used in (30.1) and the Euler–Lagrange equation is obtained, is (see [MFR91] and [Pet85])

$$\mathcal{H} = 0,$$

where

$$\mathcal{H} = \cos^2\psi\frac{d^2\psi}{d\rho^2} - \frac{\sin\psi\cos\psi}{2}\left(\frac{d\psi}{d\rho}\right)^2 - \frac{\sin\psi}{2\rho^2\cos\psi} - \frac{\sin\psi\cos\psi}{2\rho^2} - \frac{c_0^2\sin\psi}{2\cos\psi} + \frac{\cos^2\psi}{\rho}\frac{d\psi}{d\rho} - \frac{c_0\sin^2\psi}{\rho\cos\psi} - \frac{\Delta P\rho}{2k_b\cos\psi} - \frac{\lambda\sin\psi}{k_b\cos\psi}. \tag{30.3}$$

The shape equation based on A4 is obtained in the same way [JS94], [SBL91], [Sef66].

30.3 Equivalence of the Shape Equations

Equation (30.3) has been obtained without any reference to the z-coordinate. Therefore, $\psi(\rho)$ varies over a larger class of functions, and the extremal function, which minimizes the energy functional, may not be admissible. In fact, the coordinates $z(s)$ and $\rho(s)$ have to satisfy the geometric relations $d\rho/ds = \cos\psi$ and $dz/ds = -\sin\psi$, which give the geometric relation in the parameter ρ as

$$\frac{dz}{d\rho}\cos\psi + \sin\psi = 0. \tag{30.4}$$

In what follows, we show that the correct shape equation can be obtained if this geometric condition is imposed explicitly or implicitly. We will demonstrate this fact by using two different approaches.

30.3.1 Variation in the ρ-Direction

We now derive the shape equation for axisymmetric vesicles by taking the variation of the axisymmetric energy functional. The method used here is similar

to A2 [HO93], but the variation is performed along the direction perpendicular to the axis of symmetry (i.e., the ρ-direction) and the corresponding induced variations in ψ and s are obtained by using the geometric relations $d\rho/ds = \cos\psi$ and $dz/ds = -\sin\psi$. The method used here is similar to the method used to find the equation of geodesics in Riemannian geometry by means of the variational method [HO93], [Spi79].

We start with the axisymmetric shape energy functional with parameter s

$$F_s = \pi \int \left[k_b \rho \left(\frac{d\psi}{ds} + \frac{\sin\psi}{\rho} - c_0 \right)^2 + \Delta P \rho^2 \sin\psi + 2\lambda\rho \right] ds$$

and introduce an arbitrary parameter t to get

$$F_s = \pi \int \bar{L} \left(\rho(t), \psi(t), \dot{\psi}(t), \dot{s}(t) \right) dt,$$

where

$$\begin{aligned} \bar{L} \left(\rho(t), \psi(t), \dot{\psi}(t), \dot{s}(t) \right) = \frac{k_b \rho (\dot{\psi})^2}{\dot{s}} + \frac{k_b \dot{s} \sin^2\psi}{\rho} + k_b \rho c_0^2 \dot{s} - 2k_b c_0 \rho \dot{\psi} \\ + 2\lambda\rho\dot{s} + \Delta P \rho^2 \sin\psi \dot{s}. \end{aligned} \tag{30.5}$$

Note that the terms $2k_b\dot{\psi}\sin\psi$ and $-2k_b c_0 \dot{s}\sin\psi$ have been neglected in (30.5) as they do not contribute to the shape equation [HO93].

Let $\delta\rho$ be an infinitesimal variation along the ρ-direction so that the variation along the z-direction is $\delta z = 0$ (see Figure 30.1(b)). The geometric relation $d\rho = \cos\psi ds$ gives

$$-\sin\psi ds(\delta\psi) + \cos\psi \delta ds = \delta d\rho. \tag{30.6}$$

Similarly, the geometric relation $dz = -\sin\psi ds$, given that $d\delta z = \delta dz$ due to the independence of the operators d and δ, yields

$$\cos\psi ds(\delta\psi) + \sin\psi \delta(ds) = 0. \tag{30.7}$$

Solving (30.6) and (30.7) for $\delta\psi$ and $\delta(ds)$, we get

$$\delta\psi = -\frac{\sin\psi \delta d\rho}{ds}, \delta(ds) = \cos\psi \delta d\rho, \delta\dot{\psi} = -\frac{d}{dt}\left(\frac{\sin\psi\delta d\rho}{ds} \right), \delta\dot{s} = \frac{\cos\psi\delta d\rho}{dt}.$$

The shape equation is determined by the variational equation $\delta F_s = 0$, which leads to

$$\int \left[\frac{\partial \bar{L}}{\partial \rho}\delta\rho + \frac{\partial \bar{L}}{\partial \psi}\delta\psi + \frac{\partial \bar{L}}{\partial \dot{\psi}}\delta\dot{\psi} + \frac{\partial \bar{L}}{\partial \dot{s}}\delta\dot{s} \right] dt = 0. \tag{30.8}$$

Using expressions for $\delta\psi$, $\delta\dot{\psi}$, and $\delta\dot{s}$ in (30.8), and performing integration by parts and simplification, we obtain the shape equation

$$\frac{\partial \bar{L}}{\partial \rho} + \frac{d}{dt}\left(\frac{\sin\psi}{\dot{s}}\frac{\partial \bar{L}}{\partial \psi}\right) - \frac{d}{dt}\left(\frac{\sin\psi}{\dot{s}}\frac{d}{dt}\frac{\partial \bar{L}}{\partial \dot{\psi}}\right) - \frac{d}{dt}\left(\cos\psi\frac{\partial \bar{L}}{\partial \dot{s}}\right) = 0. \quad (30.9)$$

We use (30.5) in (30.9) and consider ρ as a parameter by taking $t = \rho$. Then, using $\dot{\psi} = d\psi/d\rho$, $\dot{s} = ds/d\rho = 1/\cos\psi$, and $\dot{\rho} = 1$ along with their higher derivatives in the resulting equation, we obtain (30.2), which is also the shape equation derived in the literature from A2. Therefore, we have shown that the variation does not have to be in the normal direction, and that the variation in other directions can also produce the same shape equation if the induced variations in the other variables are obtained from the geometric relations $d\rho/ds = \cos\psi$ and $dz/ds = -\sin\psi$. We note that the approach outlined here breaks down when the surface is perpendicular to the axis of symmetry. We now move on to a more general approach.

30.3.2 The Method of Lagrange Multiplier

We include the geometric condition (30.4) in the action form of the shape energy functional via an additional Lagrange multiplier η as follows:

$$F = \pi \int \tilde{L}\left(\rho, \psi(\rho), z(\rho), \eta(\rho), \frac{d\psi}{d\rho}, \frac{dz}{d\rho}\right) d\rho,$$

where the Lagrangian $\tilde{L}$ is

$$\tilde{L} = \frac{k_b\rho}{\cos\psi}\left(\frac{d\psi}{d\rho}\cos\psi + \frac{\sin\psi}{\rho} - c_0\right)^2 + \frac{\Delta P\rho^2\sin\psi}{\cos\psi} + \frac{2\lambda\rho}{\cos\psi} + \eta\left(\frac{dz}{d\rho}\cos\psi + \sin\psi\right).$$

This gives the Euler–Lagrange equations

$$\mathcal{H} = \frac{\eta}{2k_b\rho}, \quad (30.10)$$

$$\frac{dz}{d\rho} = -\frac{\sin\psi}{\cos\psi}, \quad (30.11)$$

$$\cos\psi\frac{d\eta}{d\rho} = \eta\sin\psi\frac{d\psi}{d\rho}. \quad (30.12)$$

We rewrite (30.10) as $\eta = \eta\left(\rho, \psi, d\psi/d\rho, d^2\psi/d\rho^2\right)$ and find the expression for $d\eta/d\rho$, then substitute the expressions for η and $d\eta/d\rho$ in (30.12). After lengthy mathematical manipulations, we obtain (30.2), which is the equation generated by A1 (and A2).

This suggests that the discrepancy in the shape equations obtained by different approaches in the literature occurs when the geometric relation (30.4) is not imposed. A3 can produce the same equation as A1 (and A2) as long as the geometric relation (30.4) is preserved when the variation is performed. In

the situation when ψ can vary independently without taking z into consideration, the geometric condition is not necessary. Furthermore, if the variation is with respect to the normal displacement, as in A1 and A2, ρ and z are varied proportionately so that the geometric relation is implicitly preserved.

30.3.3 Relationship Between the Shape Equations

Equation (30.12) can be expressed as $d(\eta\cos\psi)/d\rho = 0$, which, by (30.10), leads to $d(\rho\mathcal{H}\cos\psi)/d\rho = 0$. We note that this relation differs from the equation in [ZL93]; i.e., $(1/\rho)[d(\rho\mathcal{H}\cos\psi)/d\rho] = 0$, which has an extra factor $1/\rho$. Not having $1/\rho$ avoids the singularity at $\rho = 0$, which removes the doubt on the validity of the conclusion in [ZL93], as pointed out in [BP04] and [Poz03]. Integrating once yields $\eta\cos\psi = 2k_b\rho\mathcal{H}\cos\psi = \mathcal{C}$, where $\mathcal{C}$ is an integrating constant. Obviously, $\mathcal{C} = 0$ does not necessarily lead to $\mathcal{H} = 0$ unless $\rho\cos\psi \neq 0$. Therefore, (30.2) and (30.3) are equivalent if and only if $\eta = 0$, which is relatively easy to verify.

30.3.4 Vesicles with Distinct Topological Shapes

It has been pointed out in the literature that the shape equations obtained using different approaches are equivalent only for spherical vesicles. We now demonstrate this by observing the value of the Lagrange multiplier η used in our approach.

Spherical Vesicles

For spherical vesicles, $\rho = r_0\sin\psi$, (30.2) leads to $\Delta P r_0^3 + 2\lambda r_0^2 + k_b c_0^2 r_0^2 - 2k_b c_0 r_0 = 0$ and (30.10)–(30.12) yield

$$\Delta P r_0^3 + 2\lambda r_0^2 + k_b c_0^2 r_0^2 - 2k_b c_0 r_0 + \eta\cot\psi\csc\psi r_0 = 0.$$

Since these two conditions are identical, we have $\eta = 0$. Thus, (30.3) is equivalent to (30.2) for spherical vesicles. This is due to the fact that we do not need to impose any constraint on z and its derivatives, which allows ψ to vary freely.

Cylindrical Vesicles

We now assume that the vesicle is of cylindrical shape, which is given by the equations $\rho = r_0, \psi = \pi/2$. Substituting this in (30.2) and in (30.10)–(30.12), we can verify that for this cylindrical vesicle equation to be a solution of both (30.2) and (30.10)–(30.12), we require that

$$\mathcal{C} = \Delta P r_0\,(2 - r_0) + 2\lambda r_0\left(\frac{1}{r_0} - 1\right) + c_0^2 k_b r_0\left(\frac{1}{r_0} - 1\right) + 2k_b c_0 - \frac{k_b}{r_0}\left(\frac{1}{r_0} + 1\right).$$

Since $\mathcal{C} \neq 0$ and $\cos\psi = 0$, η cannot be zero. To obtain the cylindrical vesicle, we need to have infinite slope $dz/d\rho$ $(= -\sin\psi/\cos\psi)$, which must be maintained when the variation is performed. Hence, (30.3) and (30.2) are not equivalent for cylindrical vesicles.

Toroidal Vesicles

Similarly, a vesicle of perfect torus shape given by $\rho = x + \sin\psi$, where $1/x$ is the ratio of its generating radii, can be a solution of both (30.2) and (30.10)–(30.12) only if $\mathcal{C} = 2k_b(1 + 2c_0)$. Thus, $\eta = 0$ only if $c_0 = -1/2$. However, based on experiments performed in [FMB92], [MBB91], and [MB91] and the theoretical result in [Wil82], in general [HO93] $c_0 \neq -1/2$. Therefore, $\eta \neq 0$ and (30.3) is not equivalent to (30.2) for toroidal vesicles.

As a simple observation, we offer the following explanation. To have a vesicle of perfect torus shape, we need to have vanishing slope of the curve $z = z(\rho)$ at the point $\rho = x$ (i.e., $(dz/d\rho)|_{\rho=x} = 0$). Because of this condition, ψ cannot vary without taking z into consideration.

Circular Biconcave Discoids

In [NOO93], the authors showed that $\psi = \arcsin[\rho(c_0 \ln\rho + b)]$ with a constant b is a solution of (30.2) under the condition $\Delta P = \lambda = 0$. This solution with $c_0 < 0$ represents a circular biconcave discoid, the shape of the red blood cell (RBC). For this vesicle to be a solution of (30.10)–(30.12) under the condition $\Delta P = \lambda = 0$, we require that $\eta = 4k_b c_0/(\sqrt{1 - \rho^2(c_0 \ln\rho + b)^2})$. The nonzero η indicates that (30.3) is not equivalent to (30.2), unless $c_0 = 0$.

When $c_0 \neq 0$, the biconcave vesicle $z = z(\rho)$ has a local extreme value; i.e., $dz/d\rho = 0$ at $\rho = \exp(-b/c_0)$. Thus, ψ cannot vary independently. When $c_0 = 0$, the biconcave vesicle becomes spherical with $b = 1/r_0$; thus, $\eta = 0$, and (30.3) and (30.2) become equivalent.

30.4 Conclusion

We have introduced two new approaches for deriving the equilibrium shape equation for axisymmetric vesicles. We have shown that as long as the geometric relation $dz/d\rho = -\tan\psi$ is maintained in performing the calculus of variations, both approaches produce the correct shape equation. We have also shown that the variation does not have to be in the normal direction. Furthermore, by imposing the geometric condition as a Lagrange multiplier, we established a simple relationship between the two distinct shape equations derived previously in the literature. Using this relationship, it becomes a straightforward exercise to verify the equivalence of the shape equation using explicit shape solutions.

Acknowledgement. Part of this research was supported by the Natural Science and Engineering Research Council (NSERC) of Canada. One of the authors (HH) also wishes to thank Japan Society for the Promotion of Sciences (JSPS) for providing a visiting fellowship that enabled him to carry out a part of this research.

References

[BP04] Blyth, M.G., Pozrikidis, C.: Solution space of axisymmetric capsules enclosed by elastic membranes. *Eur. J. Mech. A/Sol.,* **23**, 877–892 (2004).

[DBS03] Derganc, J., Bozic, B., Svetina, S., Zeks, B.: Equilibrium shape of erythrocytes in rouleau formation. *Biophys. J.,* **84**, 1486–1492 (2003).

[FMB92] Fourcade, B., Mutz, K., Bensimon, D.: Experimental and theoretical study of toroidal vesicles. *Phys. Rev. Lett.,* **68**, 2551–2554 (1992).

[Hel73] Helfrich, W.: Elastic properties of lipid bilayers—theory and possible experiments. *Z. Naturforsch.,* **28c**, 693 (1973).

[HO93] Hu, J.-G., Ou-Yang, Z.-C.: Shape equations of the axisymmetric vesicles. *Phys. Rev. E,* **47**, 461–467 (1993).

[Ino96] Inoue, T.: Interaction of surfactants with phospholipid vesicles. In: *Vesicles.* Marcel Dekker, New York (1996), pp. 152–195.

[JL96] Julicher, F., Lipowsky, R.: Shape transformations of vesicles with intramembrane domains. *Phys. Rev. E,* **53**, 2670–2683 (1996).

[JS94] Julicher, F., Seifert, U.: Shape equations for axisymmetric vesicles: a clarification. *Phys. Rev. E,* **49**, 4728–4731 (1994).

[Kom96] Komura, S.: Shape fluctuations of vesicles. In: *Vesicles.* Marcel Dekker, New York (1996), pp. 198–236.

[KR96] Kunieda, H., Rajagopalan, V.: Formation and structure of reverse vesicles. In: *Vesicles.* Marcel Dekker, New York (1996), pp. 80–103.

[MFR91] Miao, L., Fourcade, B., Rao, M., Wortis, M.: Equillibrium budding and vesiculation in the curvature model of fluid lipid vesicles. *Phys. Rev. A,* **43**, 6843–6856 (1991).

[MBB91] Mutz, M., Bensimon, D., Birenne, M.J.: Wrinkling transition in partially polymerized vesicles. *Phys. Rev. Lett.,* **67**, 923–926 (1991).

[MB91] Mutz, M., Bensimon, D.: Observation of toroidal vesicles. *Phys. Rev. A,* **43**, 4525–4527 (1991).

[NOO93] Naito, H., Okuda, M., Ou-Yang, Z.-C.: Counterexample to some shape equations for axisymmetric vesicles. *Phys. Rev. E,* **48**, 2304–2307 (1993).

[OH89] Ou-Yang, Z.-C., Helfrich, W.: Bending energy of vesicle membranes: general expressions for the first, second and third variation of the shape energy and applications to spheres and cylinders. *Phys. Rev. A,* **39**, 5280–5288 (1989).

[Pet85] Peterson, M.: An instability of the red blood shape. *J. Appl. Phys.,* **57**, 1739–1742 (1985).

[Poz03] Pozrikidis, C.: *Shell Theory for Capsules and Cells. Modeling and Simulation of Capsules and Biological Cells.* Chapman & Hall/CRC, Boca Raton, FL (2003), pp. 35–101.

[SBL91] Seifert, U., Berndl, K., Lipowsky, R.: Shape transformations of vesicles: phase diagram for spontaneous-curvature and bilayer-coupling models. *Phys. Rev. A,* **44**, 1182–1202 (1991).

[Sef66] Seifert, U.: Vesicles of toroidal topology. *Phys. Rev. Lett.,* **66**, 2404–2407 (1991).

[Spi79] Spivak, M.: *A Comprehensive Introduction to Differential Geometry.* Publish or Perish, Berkeley (1997).

[Wil82] Willmore, T.J.: *Total Curvature in Riemannian Geometry.* Horwood, Chichester (1982).

[Zan96] Zanten, Z.H.V.: Characterization of vesicles and vesicular dispersions via scattering techniques. In: *Vesicles.* Marcel Dekker, New York (1996), pp. 240–294.

[ZL93] Zheng, W., Liu, J.: Helfrich shape equation for axisymmetric vesicles as a first integral. *Phys. Rev. E,* **48**, 2856–2860 (1993).

31

Properties of Positive Solutions of the Falkner–Skan Equation Arising in Boundary Layer Theory

G.C. Yang[1], L.L. Shi[1], and K.Q. Lan[2]

[1] Chengdu University of Information Technology, Sichuan, P.R. China; gcyang@cuit.edu.cn, shili119@126.com
[2] Ryerson University, Toronto, ON, Canada; klan@ryerson.ca

31.1 Introduction

We consider the well-known Falkner–Skan equation

$$\begin{cases} f'''(\eta) + f(\eta)f''(\eta) + \lambda[1 - (f')^2(\eta)] = 0 \quad \text{on } \eta \in (0,\infty), \\ f(0) = f'(0) = 0, \quad f'(\infty) = 1, \\ 0 < f'(\eta) < 1 \quad \text{for } \eta \in (0,\infty), \end{cases} \tag{31.1}$$

which is used to describe the steady two-dimensional flow of a slightly viscous incompressible fluid past a wedge-shaped body of angle related to $\lambda\pi/2$, where η is the similarity boundary layer ordinate, $f(\eta)$ is the similarity stream function, and $f'(\eta)$ and $f''(\eta)$ are the velocity and shear stress, respectively. If $\lambda \in [-2, 0]$, the corresponding flow is called a corner flow and if $\lambda \in [0, 2]$, the flow is a wedge flow. We refer to [Na79] and [SG00] for a more detailed physical interpretation of (31.1).

It is well known that there exists $\lambda^* < 0$ such that (31.1) has at least one solution for each $\lambda \geq \lambda^*$ and no solutions for $\lambda < \lambda^*$. Moreover, the condition $0 < f'(\eta) < 1$ for $\eta \in (0,\infty)$ can be replaced by $f''(\eta) > 0$ for $\eta \in (0,\infty)$ (see [LY07] and the references therein). An open problem left in [LY07] is what is exactly λ^*? A well-known numerical result shows that $\lambda^* = -0.1988$ (see [BS66], [LL67], and [RW89]). We refer to [AO02], [Cop60], [Har02], [Har72], [Has71], [Has72], [Tam70], [WG99], [Wey42], [Yan03], and [Yan04] for an analytic study of (31.1). Recently, Lan and Yang [LY07] have proved analytically that $\lambda^* \in [-0.4, -0.12]$. The main idea is to prove that (31.1) is equivalent to a singular integral equation of the form

$$z(t) = \int_t^1 \frac{(1-s)(\lambda + \lambda s + s)}{z(s)}\, ds + (1-t)\int_0^t \frac{s}{z(s)}\, ds \quad \text{for } t \in (0,1), \tag{31.2}$$

and study the properties of the positive solutions of (31.2) and the range of λ^* for (31.2). Many properties of f, f', and f'' have been obtained by Lan

and Yang in [LY07] and [YL07]. For example, f is increasing and concave up on $(0,\infty)$, $f(\eta) < \eta$ for $\eta \in (0,\infty)$, $\lim_{\eta\to\infty} f(\eta)/\eta = 1$, and both the set of velocity functions f' and the set of shear stress functions f'' are compact in $BC(\mathbb{R}_+)$ for each $\lambda \in [\lambda^*, 0]$. It is proved in [LY07] that the norm of f'' satisfies $2/27 \le \|f''\| \le 1$ for $\lambda \in [\lambda^*, 0]$.

In this chapter, we shall prove a better result concerning the above inequalities satisfied by $\|f''\|$. The method is again based on the study of the properties of the positive solutions of (31.2). We provide upper and lower bounds for the positive solutions $z(t)$ of (31.2) and give explicit formulas for these bounds. When $\lambda \in [\lambda^*, 0]$, we prove new inequalities for $\|z\|$, which improve a result in [LY07]. Then we use the equalities $z(t) = f''(\eta)$ and $t = f'(\eta)$, proved in [LY07], to derive properties of f' and f''.

31.2 Properties of the Positive Solutions of (31.2)

Let $z \in C(0,1)$ with $z(t) > 0$ for $t \in (0,1)$. We define

$$Az(t) = \int_t^1 f_z(s)\,ds \quad \text{for } t \in [0,1] \text{ and } Bz(t) = \int_0^t \frac{s}{z(s)}\,ds \quad \text{for } t \in [0,1),$$

where $f_z(s) := \frac{(1-s)(\lambda+\lambda s+s)}{z(s)}$ for $s \in (0,1)$. Let $\delta := \delta(\lambda) = \frac{-\lambda}{1+\lambda}$. Then $\delta \in [0,1)$ if and only if $\lambda \in (-1/2, 0]$. It is shown in [LY07] that if $\delta \in (0,1)$, then

$$f_z(s) \le 0 \quad \text{for } s \in (0,\delta) \text{ and } f_z(s) \ge 0 \text{ for } s \in [\delta, 1) \tag{31.3}$$

and

$$Az \text{ is increasing on } (0,\delta) \text{ and decreasing on } [\delta, 1). \tag{31.4}$$

We denote by $C[0,1]$ the Banach space of continuous functions defined on $[0,1]$ with the maximum norm $\|z\| = \max\{|z(t)| : t \in [0,1]\}$. Let

$$Q = \{z \in C[0,1] : z(t) > 0 \quad \text{for } t \in (0,1)\}.$$

It is known that if $z \in Q$ and the improper integral $Az(t)$ converges for $t \in [0,1)$, then $Az(t)$ is a Lebesuge integral for $t \in [0,1)$ and

$$Az(t) \ge 0 \quad \text{for } t \in [0,1]$$

and if $z \in Q$ is a solution of (31.2), then $Bz(1) = \lim_{t\to 1^-} Bz(t) = \infty$ and $\lim_{t\to 1^-}(1-t)Bz(t) = 0$. If a function $z : [0,1] \to \mathbb{R}_+$ satisfies (31.2), then $z \in C(0,1)$.

The following result obtained in [LY07] gives the values of a positive solution $z(t)$ of (31.2) at $t = 0, 1$.

Lemma 1. *Suppose that* $(\lambda, z) \in (-1/2, \infty) \times Q$ *satisfies* (31.2). *Then* $z(0) = Az(0)$ *and* $z(1) = 0$.

It is showed in [LY07] that (31.2) is equivalent to two differential equations with suitable boundary conditions. We state one of these results, which will be used later.

Lemma 2. *Let $(\lambda, z) \in (-1/2, \infty) \times Q$. Then (λ, z) satisfies* (31.2) *if and only if $z(1) = 0$ and*

$$z'(t) = \frac{-\lambda(1-t^2)}{z(t)} - Bz(t) \quad \text{for } t \in (0,1). \tag{31.5}$$

It is known that (31.1) is equivalent to (31.2) (see Lemma 4 below). The results on (31.1) can be used to derive the results on (31.2) via the equivalence. Hence, the following result is a consequence of Lemma 4.1 in [LY07].

Lemma 3. *There exists $\lambda^* \in [-0.4, -0.12]$ such that* (31.2) *has multiple solutions in Q for each $\lambda \in (\lambda^*, 0)$, has a unique solution for either $\lambda = \lambda^*$ or $\lambda \geq 0$, and has no solutions for $\lambda < \lambda^*$.*

It is difficult to find the explicit expressions of the solutions of (31.2), but we can provide upper and lower bounds for the positive solutions of (31.2) and give the explicit formulas of these bounds in the following theorem.

Theorem 1. *Assume that $(\lambda, z) \in [\lambda^*, \infty) \times Q$ satisfies* (31.2). *Then the following assertions hold:*

(i) If $\lambda \in [\lambda^*, 0)$, then for $t \in [0,1]$,

$$\frac{\sqrt{3}(1+\lambda)(1-t)t^2}{2\sqrt{4\lambda^3+4\lambda^2+2\lambda+1}} \leq z(t) \leq \frac{\sqrt{3[(1+2\lambda)^3 - 2\lambda(1+\lambda)^2 t(3-t^2)]}}{3(1+\lambda)}.$$

(ii) If $\lambda \in [\lambda^*, 0)$, then

$$2/27 < \frac{2\sqrt{9855}}{1971} \leq \|z\| \leq \frac{3(1+\lambda)^2}{4\lambda^3+4\lambda^2+2\lambda+1} \leq \sqrt{9855}/135 < 1.$$

(iii) If $\lambda \geq 0$, then

$$\frac{\sqrt{6}}{6}(1-t)g(t) \leq z(t) \leq \sqrt{6}[z_1(t) + (1-t)z_2(t)] \quad \text{for } t \in [0,1].$$

where $g(t) = \sqrt{2(\lambda+1)t + 4\lambda + 1}$, $z_1(t) = \dfrac{[\lambda - 2 - (1+\lambda)t]g(t)}{3(1+\lambda)^2}$, *and*

$$z_2(t) = \frac{\sqrt{1+4\lambda} - g(t)}{1+\lambda} + \frac{\sqrt{6\lambda+3}}{6\lambda+3} \ln\Big[\frac{5\lambda + 2 + (1+\lambda)t + \sqrt{(6\lambda+3)}g(t)}{(1-t)(5\lambda+2+\sqrt{(6\lambda+3)(1+4\lambda)})}\Big].$$

Proof. (i) We define a function $h : [\lambda^*, 0] \to [0, \infty)$ by

$$h(\lambda) = \int_{\delta(\lambda)}^{1} (1-t)(\lambda + \lambda t + t)\, dt.$$

By computation, we have $h(\lambda) = \dfrac{(1+2\lambda)^3}{6(1+\lambda)^2}$. Assume that $(\lambda, z) \in [\lambda^*, 0) \times Q$ satisfies (31.2). Then $z(t) > 0$ and $z(t) \geq (Az)(t)$ for $t \in (0,1)$. By (31.3), $f_z(t) \geq 0$ for $t \in [\delta, 1)$ and we have for $t \in [\delta, 1)$,

$$-(Az)'(t)(Az)(t) = f_z(t)(Az)(t) \leq f_z(t)z(t) = (1-t)(\lambda + \lambda t + t).$$

Integrating the above inequality from $\delta(= \delta(\lambda))$ to 1 and using $Az(1) = 0$, we have

$$[(Az)(\delta)]^2 \leq 2h(\lambda).$$

By (31.4), we have $(Az)(t) \leq (Az)(\delta)$ for $t \in [0,1]$. This and Lemma 1 imply that

$$[z(0)]^2 = [(Az)(0)]^2 \leq [(Az)(\delta)]^2 \leq 2h(\lambda) = \frac{(1+2\lambda)^3}{3(1+\lambda)^2}.$$

By (31.5) and the continuity of z, we obtain $z(t)z'(t) \leq -\lambda(1-t^2)$ for $t \in [0,1]$. Integrating the inequality from 0 to t implies that

$$\frac{1}{2}[z^2(t) - z^2(0)] \leq -\lambda \int_0^t (1-t^2)dt = (-\lambda)(t - t^3/3).$$

This yields

$$[z(t)]^2 \leq (-2\lambda)(t-t^3/3)+[z(0)]^2 \leq (-2\lambda)(t-t^3/3)+\frac{(1+2\lambda)^3}{3(1+\lambda)^2} \quad \text{for } t \in [0,1], \tag{31.6}$$

and so, the second inequality of (i) holds. Since $z(t) \geq Bz(t) \geq \frac{t^2(1-t)}{2}\|z\|^{-1}$, the first inequality of (i) follows.

(ii) Noting that $g(t) := (t - t^3/3)$ is increasing on $t \in [0,1]$ and (31.6), for $t \in [0,1]$ we have

$$[z(t)]^2 \leq -4\lambda/3 + \frac{(1+2\lambda)^3}{3(1+\lambda)^2} = \frac{4\lambda^3 + 4\lambda^2 + 2\lambda + 1}{3(1+\lambda)^2}.$$

This implies that

$$\|z\| \leq \sqrt{\frac{4\lambda^3 + 4\lambda^2 + 2\lambda + 1}{3(1+\lambda)^2}} := \omega(\lambda). \tag{31.7}$$

Let $\omega_1(\lambda) = \dfrac{4\lambda^3 + 4\lambda^2 + 2\lambda + 1}{(1+\lambda)^2}$ for $\lambda \in [-0.4, 0]$. Then

$$\omega_1'(\lambda) = \frac{4\lambda[(\lambda + 3/2)^2 - 1/4]}{(1+\lambda)^3} < 0 \quad \text{for } \lambda \in [-0.4, 0]$$

and ω_1 is decreasing on $[-0.4, 0]$. Hence, we have

$$\omega(\lambda) \le \omega(-0.4) = \sqrt{9855}/135 \quad \text{for } \lambda \in [-0.4, 0].$$

By (31.7), we have $\|z\| \le \sqrt{9855}/135$. Let $h_1(t) = \frac{1}{2}(1-t)t^2$ for $t \in [0,1]$. Then $h_1(t) \le h_1(2/3) = \|h_1\| = 2/27$ for $t \in [0,1]$. From (i) and (31.7) it follows that $z(t) \ge h_1(t)/\omega(\lambda)$ for $t \in [0,1]$. This implies that

$$\|z\| \ge (135/\sqrt{9855})\|h_1\| = (2/27)(135/\sqrt{9855}) = \frac{2\sqrt{9855}}{1971}.$$

(iii) By (31.5), we have for $t \in (0,1)$, $z'(t) = -\frac{\lambda(1-t^2)}{z(t)} - Bz(t) < 0$ and z is decreasing $[0,1]$. Hence, we have for $t \in [0,1)$,

$$z(t) \ge Az(t) \ge \frac{1}{z(t)} \int_t^1 (1-s)(\lambda + \lambda s + s)ds = \frac{[2(\lambda+1)t + 4\lambda + 1](1-t)^2}{6z(t)}$$

and $[z(t)]^2 \ge [g(t)]^2(1-t)^2/6$. This implies that $z(t) \ge g(t)(1-t)/\sqrt{6}$ for $t \in [0,1]$. By (31.2), we obtain for $t \in (0,1)$,

$$z(t) \le \sqrt{6}(I_1(t) + (1-t)I_2(t)),$$

where $I_1(t) = \int_t^1 \frac{\lambda+\lambda s+s}{g(s)}\,ds$ and $I_2(t) = \int_0^t \frac{s}{\sqrt{(1-s)g(s)}}\,ds$. By substitution $u = g(s)$, we can prove that $I_1(t) = z_1(t)$ and $I_2(t) = z_2(t)$ for $t \in [0,1]$. Hence, (iii) follows.

31.3 Properties of the Solutions of (31.1)

In this section we derive properties of the solutions of (31.1). We need the following known result, which shows that (31.1) is equivalent to (31.2).

Lemma 4. *(i) If $(\lambda, f) \in \mathbb{R} \times C^2(\mathbb{R}_+)$ satisfies* (31.1)*, then (λ, z) satisfies* (31.2)*, where $z : [0,1] \to \mathbb{R}_+$ is defined by*

$$z(t) = \begin{cases} f''((f')^{-1}(t)) & \text{if } t \in [0,1), \\ 0 & \text{if } t = 1. \end{cases}$$

(ii) If $(\lambda, z) \in (-1/2, \infty) \times Q$ satisfies (31.2)*, then $(\lambda, f) \in \mathbb{R} \times C^2(\mathbb{R}_+)$ and satisfies* (31.1)*, where $f : \mathbb{R}_+ \to \mathbb{R}_+$ is defined by*

$$f(\eta) = \int_0^{g^{-1}(\eta)} \frac{s}{z(s)}\,ds$$

and $g : [0,1) \to \mathbb{R}_+$ is defined by $g(t) = \int_0^t \frac{1}{z(s)}\,ds$.

It is shown in [LY07] that there exists $\lambda^* \in [-0.4, -0.12]$ such that (31.1) has at least one solution for $\lambda \in (\lambda^*, 0)$ and has a unique solution for $\lambda \in \{\lambda^*, 0\}$. We denote by Γ the set of solutions of (31.1); that is,

$$\Gamma := \{(\lambda, f) \in [\lambda^*, 0] \times C^2(\mathbb{R}_+) : \quad (\lambda, f) \text{ satisfies (31.1) } \}.$$

We denote by $BC(\mathbb{R}_+)$ the Banach space of continuous bounded functions defined on $\mathbb{R}_+$ with the norm $\|f\| = \sup\{|f(x)| : x \in \mathbb{R}_+\}$. It is shown in [LY07] that if $(\lambda, f) \in \Gamma$, then $2/27 \le \|f''\| \le 1$. Using Theorem 1 and Lemma 4, we obtain the following new result, which improves the inequalities just mentioned.

Theorem 2. *Suppose that* $(\lambda, f) \in [\lambda^*, 0] \in \Gamma$. *Then*

$$2\sqrt{9855}/1971 \le \|f''\| \le \frac{3(1+\lambda)^2}{4\lambda^3 + 4\lambda^2 + 2\lambda + 1} \le \sqrt{9855}/135.$$

Proof. By Lemma 4, $z(t) = f''(\eta)$ and $t = f'(\eta)$. This, together with Theorem 1(ii), implies the required inequalities.

In Theorem 1(i),(iii), one can replace $z(t)$ and t by $f''(\eta)$ and $f'(\eta)$, respectively, to obtain inequality relations between $f''(\eta)$ and $f'(\eta)$. We leave the obvious statements to the reader.

Acknowledgement. The first author was supported in part by the Applied and Fundamental Research Foundation of Sichuan Province, the Sichuan Ministry of Education, and the Scientific Research Funds of Chengdu University of Information Technology. The third author was supported in part by the Natural Sciences and Engineering Research Council of Canada.

References

[AO02] Agarwal, R.P., O'Regan, D.: Singular integral equations arising in Homann flow. *Dynamics of Continuous, Discrete and Impulsive Systems Ser. B: Applications and Algorithms,* **9**, 481–488 (2002).

[BS66] Brown, S.N., Stewartson, K.: On the reversed flow solutions of the Falkner–Skan equations. *Mathematika,* **13**, 1–6 (1966).

[Cop60] Coppel, W.A.: On a differential equation of boundary–layer theory. *Phil. Trans. Roy. Soc. London Ser. A,* **253**, 101–136 (1960).

[Har02] Hartman, P.: *Ordinary Differential Equations.* SIAM, Philadelphia, PA (2002).

[Har72] Hartman, P.: On the existence of similar solutions of some boundary layer problems. *SIAM J. Math. Anal.,* **3**, 120–147 (1972).

[Has71] Hastings, S.P.: An existence theorem for a class of nonlinear boundary value problems including that of Falkner and Skan. *J. Differential Equations,* **9**, 580–590 (1971).

[Has72] Hastings, S.P.: Reversed flow solutions of the Falkner–Skan equations. *SIAM J. Appl. Math.,* **22**, 329–334 (1972).

[LY07] Lan, K.Q., Yang, G.C.: Positive solutions of the Falkner–Skan equation arising in the boundary layer theory, *Canad. Math. Bull.* (in press).

[LL67] Libby, P.A., Liu, T.M.: Further solutions of the Falkner–Skan equation. *AIAA J.,* **5**, 1040–1042 (1967).

[Na79] Na, T.Y.: *Computational Methods in Engineering Boundary Value Problems.* Academic Press (1979).

[RW89] Riley, N., Weidman, P.D.: Multiple solutions of the Falkner–Skan equation for flow past a stretching boundary. *SIAM J. Appl. Math.,* **49**, 1350–1358 (1989).

[SG00] Schlichting, H., Gersten, K.: *Boundary–Layer Theory,* 8th ed. Springer, Berlin (2000).

[Tam70] Tam, K.K.: A note on the existence of a solution of the Falkner–Skan equation. *Canad. Math. Bull.,* **13**, 125–127 (1970).

[WG99] Wang, J., Gao, W., Zhang, Z.: Singular nonlinear boundary value problems arising in boundary layer theory. *J. Math. Anal. Appl.,* **233**, 246–256 (1999).

[Wey42] Weyl, H.: On the differential equations of the simplest boundary–layer problems. *Ann. Math.,* **43**, 381–407 (1942).

[YL07] Yang, G.C., Lan, K.Q.: The velocity and shear stress functions of the Falkner–Skan equation arising in boundary layer theory. *J. Math. Anal. Appl.,* **328**, 1297–1308 (2007).

[Yan03] Yang, G.C.: Existence of solutions to the third-order nonlinear differential equations arising in boundary layer theory. *Appl. Math. Lett.,* **16**, 827–832 (2003).

[Yan04] Yang, G.C.: A note on $f''' + ff'' + \lambda(1 - f'^2) = 0$ with $\lambda \in (-\frac{1}{2}, 0)$ arising in boundary layer theory. *Appl. Math. Lett.,* **17**, 1261–1265 (2004).

32

Stabilization of a Four-Dimensional System under Real Noise Excitation

J. Zhu[1], W.-C. Xie[1], and R.M.C. So[2]

[1] University of Waterloo, ON, Canada; j7zhu@engmail.uwaterloo.ca, xie@uwaterloo.ca
[2] The Hong Kong Polytechnic University, Hong Kong; mmmcso@polyu.edu.hk

32.1 Introduction

The sample or almost-sure stability of a dynamic system is determined by the Lyapunov exponent, which characterizes the average exponential rate of growth of the solutions of a dynamic system for τ large and is defined as

$$\lambda_{q(\tau)} = \lim_{\tau\to\infty} \frac{1}{\tau} \log \|\mathbf{q}(\tau)\|,$$

where $\mathbf{q}(\tau) = \{q(\tau), q'(\tau)\}^T$ and $\|\mathbf{q}\| = \left(\mathbf{q}^T\mathbf{q}\right)^{1/2}$ is the Euclidean norm. If the largest Lyapunov exponent is negative, the dynamic system is stable with probability 1; otherwise, it is unstable almost surely.

On the other hand, the stability of the pth moment $\mathsf{E}\left[\|\mathbf{q}\|^p\right]$ of the solution of the dynamic system is governed by the pth moment Lyapunov exponent defined by

$$\Lambda_{q(\tau)}(p) = \lim_{\tau\to\infty} \frac{1}{\tau} \log \mathsf{E}\left[\|\mathbf{q}\|^p\right],$$

where $\mathsf{E}[\,\cdot\,]$ denotes the expected value. If $\Lambda_{q(\tau)}(p)$ is negative, then the pth moment is stable; otherwise, it is unstable.

The relationship between the sample stability and the moment stability was formulated by Arnold [Arn84]. The pth moment Lyapunov exponent $\Lambda_{q(\tau)}(p)$ is a convex analytic function in p that passes through the origin, and whose slope at the origin is equal to the largest Lyapunov exponent $\lambda_{q(\tau)}$; i.e.,

$$\lambda_{q(\tau)} = \lim_{p\to 0} \frac{\Lambda_{q(\tau)}(p)}{p}.$$

The moment Lyapunov exponents are important in obtaining a complete picture of the dynamic stability of a system. Suppose the largest Lyapunov exponent $\lambda_{q(\tau)}$ is negative, implying that the system is sample stable, the pth moment typically grows exponentially for large enough p, implying that

the pth moment of the trivial solution is unstable. This can be explained by large deviation. Although the solution of the system $\|\mathbf{q}\| \to 0$ as $\tau \to \infty$ with probability one at an exponential rate $\lambda_{q(\tau)}$, there is a small probability that $\|\mathbf{q}\|$ is large, which makes the expected value $\mathsf{E}\big[\|\mathbf{q}\|^p\big]$ of this rare event large for large enough values of p, leading to pth moment instability.

32.2 Formulation

Consider a linear stochastic system governed by the equations of motion

$$\dot{x} = Ax + \varepsilon\xi(t)Bx, \quad x \in \mathbb{R}^4,$$

where

$$A = \begin{bmatrix} -\varepsilon^2\delta_1 & \omega_1 & 0 & 0 \\ -\omega_1 & -\varepsilon^2\delta_1 & 0 & 0 \\ 0 & 0 & -\delta_2 & \omega_2 \\ 0 & 0 & -\omega_2 & -\delta_2 \end{bmatrix}, \quad B = \begin{bmatrix} K_{11} & K_{12} & M_{11} & M_{12} \\ K_{21} & K_{22} & M_{21} & M_{22} \\ N_{11} & N_{12} & L_{11} & L_{12} \\ N_{21} & N_{22} & L_{21} & L_{22} \end{bmatrix}.$$

The quantities δ_1 and δ_2 represent the real part of the eigenvalues of the critical mode and stable mode, respectively.

Applying the transformation

$$x_1 = \mathrm{e}^{\rho}\cos\phi_1\cos\theta, \qquad x_3 = \mathrm{e}^{\rho}\cos\phi_2\sin\theta,$$

$$x_2 = -\mathrm{e}^{\rho}\sin\phi_1\cos\theta, \qquad x_4 = -\mathrm{e}^{\rho}\sin\phi_2\sin\theta,$$

one can obtain the following set of equations for the amplitude ρ, phase variables (ϕ_1, ϕ_2, θ), and noise process ξ:

$$\dot{\rho} = \sum_{j=0}^{2} \varepsilon^j q^j(\phi_1, \phi_2, \theta, \xi), \qquad \dot{\theta} = \sum_{j=0}^{2} \varepsilon^j s^j(\phi_1, \phi_2, \theta, \xi),$$

$$\dot{\phi}_i = \sum_{j=0}^{2} \varepsilon^j h_i^j(\phi_1, \phi_2, \theta, \xi), \qquad \mathrm{d}\xi = -\alpha\xi\mathrm{d}t + \sigma \circ \mathrm{d}W_t.$$

Since the processes $(\phi_1, \phi_2, \theta, \xi)$ do not depend on ρ, it follows that the processes $(\phi_1, \phi_2, \theta, \xi)$ form a Markov process and the associated generator is given by

$$\mathscr{L}(p) = \mathscr{L}_0(p) + \varepsilon\mathscr{L}_1(p) + \varepsilon^2\mathscr{L}_2(p),$$

where

$$\mathscr{L}_0 = \frac{\sigma^2}{2}\frac{\partial^2}{\partial\xi^2} - \alpha\xi\frac{\partial}{\partial\xi} + \sum_{i=1}^{2}\omega_i\frac{\partial}{\partial\phi_i} + s^0\frac{\partial}{\partial\theta},$$

$$\mathscr{L}_1 = s^1\frac{\partial}{\partial\theta} + \sum_{i=1}^{2}h_i^1\frac{\partial}{\partial\phi_i}, \qquad \mathscr{L}_2 = s^2\frac{\partial}{\partial\theta} + \sum_{i=1}^{2}h_i^2\frac{\partial}{\partial\phi_i}.$$

Arnold et al. ([AOP86] and [AKO86]) proved that $\Lambda(p)$ is an isolated simple eigenvalue of $L(p)$ with nonnegative eigenfunction ψ; i.e.,

$$L(p)\psi = \Lambda(p)\psi \quad \forall p \in \mathbb{R}, \tag{32.1}$$

where

$$L(p) = L_0(p) + \varepsilon L_1(p) + \varepsilon^2 L_2(p)$$

and

$$L_0(p) = \mathscr{L}_0 + pq^0, \quad L_1(p) = \mathscr{L}_1 + pq^1, \quad L_2(p) = \mathscr{L}_2 + pq^2.$$

32.3 Moment Lyapunov Exponent

A method of regular perturbation is applied to obtain a weak noise expansion of the moment Lyapunov exponent. Consider an expansion of the moment Lyapunov exponent in powers of ε:

$$\Lambda(p) = \Lambda_0(p) + \varepsilon\Lambda_1(p) + \varepsilon^2\Lambda_2(p) + \mathcal{O}(\varepsilon^2).$$

Substituting the above expansions into equation (32.1), one obtains the equations

$$\big(L_0(p) - \Lambda_0(p)\big)\psi_0 = 0, \tag{32.2}$$

$$\big(L_0(p) - \Lambda_0(p)\big)\psi_1 = \Lambda_1(p)\psi_0 - L_1(p)\psi_0, \tag{32.3}$$

$$\big(L_0(p) - \Lambda_0(p)\big)\psi_2 = \Lambda_2(p)\psi_0 + \Lambda_1(p)\psi_1 - L_2(p)\psi_0 - L_1(p)\psi_1.$$

32.3.1 Zeroth-Order Perturbation

From the definition of $\Lambda(p)$ it follows that $\Lambda_0(p) \equiv 0$ for all possible p. Thus, (32.2) reduces to

$$\big(\mathscr{L}_0 + pq^0\big)\psi_0 = 0.$$

Using the method of separation of variables, one can easily obtain

$$\psi_0(\phi_1, \phi_2, \theta, \xi) = (\cos\theta)^p.$$

Based on the analysis in [PW88], the solution to the associated adjoint equation of (32.2) is

$$\Psi_0^* = \frac{Z_0^*(\xi)\delta_0}{4\pi^2},$$

where δ_0 is the Dirac distribution at 0 and $Z_0^*(\xi)$ is the stationary probability density.

32.3.2 Solution of $\mathscr{L}_0\psi = f(\xi)g(\phi_1, \phi_2, \theta)$

Consider the partial differential equation

$$\mathscr{L}_0\psi_1 = f(\xi)\, g(\phi_1, \phi_2, \theta). \tag{32.4a}$$

Introducing an auxiliary time t in (32.4a) leads to

$$\left(\frac{\partial}{\partial t} + \mathscr{L}_0\right) \Psi(t, \phi_1, \phi_2, \theta, \xi) = f(\xi)\, g(\phi_1, \phi_2, \theta), \tag{32.4b}$$

where

$$\Psi(0, \phi_1, \phi_2, \theta, \xi) = 0.$$

Applying the transformation

$$\tilde{t} = \frac{t}{4} + \frac{\phi_1}{4\omega_1} + \frac{\phi_2}{4\omega_2} - \frac{\ln(\tan\theta)}{4\delta_2}, \qquad \tilde{s} = \frac{t}{4} - \frac{\phi_1}{4\omega_1} - \frac{\phi_2}{4\omega_2} - \frac{\ln(\tan\theta)}{4\delta_2},$$

$$\gamma_1 = \omega_2\phi_1 - \omega_1\phi_2, \qquad \gamma_2 = 2\omega_1\omega_2 t - \omega_2\phi_1 - \omega_1\phi_2,$$

we bring (32.4b) to the form

$$\left(\frac{\partial}{\partial\tilde{t}} + \frac{\sigma^2}{2}\frac{\partial^2}{\partial\xi^2} - \alpha\xi\frac{\partial}{\partial\xi} - p\delta_2\sin^2\theta\right) \tilde{\Psi}(\tilde{t}, \tilde{s}, \gamma_1, \gamma_2, \xi) = f(\xi)\tilde{g}(\tilde{t}, \tilde{s}, \gamma_1, \gamma_2), \tag{32.4c}$$

where

$$\tilde{\Psi}(\tilde{t}, \tilde{s}, \gamma_1, \gamma_2, \xi) = \Psi(t, \phi_1, \phi_2, \theta, \xi), \quad \tilde{g}(\tilde{t}, \tilde{s}, \gamma_1, \gamma_2) = g(\phi_1, \phi_2, \theta).$$

To remove the $\sin^2\theta$ term, we introduce the function $\tilde{\beta}$ defined by

$$\tilde{\beta}(t, \tilde{s}, \gamma_1, \gamma_2) = \tilde{\Psi}\exp\Big\{-\int^t p\delta_2\sin^2\theta(r)\mathrm{d}r\Big\}.$$

Hence, (32.4c) becomes

$$\left(\frac{\partial}{\partial\tilde{t}} + \frac{\sigma^2}{2}\frac{\partial^2}{\partial\xi^2} - \alpha\xi\frac{\partial}{\partial\xi}\right) \tilde{\beta}(\tilde{t}, \tilde{s}, \gamma_1, \gamma_2, \xi) = f(\xi)\tilde{g}(\tilde{t}, \tilde{s}, \gamma_1, \gamma_2) R_{\tilde{\beta}}(\tilde{t}, \tilde{s}, \gamma_1, \gamma_2), \tag{32.4d}$$

where

$$\begin{aligned} R_{\tilde{\beta}}(\tilde{t}, \tilde{s}, \gamma_1, \gamma_2) &= \exp\Big\{-\int^{\tilde{t}} p\delta_2\sin^2\theta(r)\mathrm{d}r\Big\} \\ &= \Big\{1 + \exp\big[2\delta_2\big(\frac{\gamma_2}{2\omega_1\omega_2} - \tilde{t} - 3\tilde{s}\big)\big]\Big\}^{\frac{p}{2}}. \end{aligned}$$

Applying Duhamel's principle (see, for example, [Zau89]), we see that the solution $\tilde{\beta}(\tilde{t}, \tilde{s}, \gamma_1, \gamma_2, \xi)$ to (32.4d) is given by

$$\tilde{\beta}(\tilde{t},\tilde{s},\gamma_1,\gamma_2,\xi)=\int_0^{\tilde{t}} V(\tilde{t},\tilde{s},\gamma_1,\gamma_2,\xi;r)\,\mathrm{d}r, \tag{32.5a}$$

where $V(\tilde{t},\tilde{s},\gamma_1,\gamma_2,\xi;r)$ is the solution of the homogeneous equation

$$\begin{aligned}&\left(\frac{\partial}{\partial\tilde{t}}+\frac{\sigma^2}{2}\frac{\partial^2}{\partial\xi^2}-\alpha\xi\frac{\partial}{\partial\xi}\right)V(\tilde{t},\tilde{s},\gamma_1,\gamma_2,\xi;r)=0, \qquad \text{for } \tilde{t}>r,\\ &V(r,\tilde{s},\gamma_1,\gamma_2,\xi;r)=f(\xi)\tilde{g}(r,\tilde{s},\gamma_1,\gamma_2)R_{\tilde{\beta}}(r,\tilde{s},\gamma_1,\gamma_2), \qquad \text{for } \tilde{t}=r.\end{aligned} \tag{32.5b}$$

To solve (32.5b), consider the equation

$$\begin{aligned}&\left(\frac{\partial}{\partial\tilde{t}}+\frac{\sigma^2}{2}\frac{\partial^2}{\partial\xi^2}-\alpha\xi\frac{\partial}{\partial\xi}\right)P(\tilde{t},\xi;\tau,z)=0, \qquad \tilde{t}<\tau,\\ &P(\tau,\xi;\tau,z)=\lim_{\tilde{t}\uparrow\tau}P(\tilde{t},\xi;\tau,z)=\delta(z-\xi).\end{aligned} \tag{32.6a}$$

Equation (32.6a) is the backward Kolmogorov equation for the transition probability function $P(\tilde{t},\xi;\tau,z)$. It is known that $P(\tilde{t},\xi;\tau,z)$ is also the solution of the forward Kolmogorov or Fokker–Planck equation, i.e., for the initial condition $\tilde{t}$ and ξ fixed,

$$\begin{aligned}&\left[\frac{\partial}{\partial\tau}-\frac{\sigma^2}{2}\frac{\partial^2}{\partial z^2}+\frac{\partial}{\partial z}(-\alpha z)\right]P(\tilde{t},\xi;\tau,z)=0, \quad \tau>\tilde{t},\\ &P(\tilde{t},\xi;\tilde{t},z)=\lim_{\tau\downarrow\tilde{t}}P(\tilde{t},\xi;\tau,z)=\delta(z-\xi).\end{aligned} \tag{32.6b}$$

The solution of (32.6b) is given by

$$P(\tilde{t},\xi;\tau,z)=\frac{1}{\sqrt{2\pi}\sigma_{z(\tau)}}\exp\left\{-\frac{\big[z-\mu_{z(\tau)}\big]^2}{2\sigma^2_{z(\tau)}}\right\}, \tag{32.7}$$

where

$$\mu_{z(\tau)}=\xi\mathrm{e}^{-\alpha(\tau-\tilde{t})}, \qquad \sigma^2_{z(\tau)}=\frac{\sigma^2\big[1-\mathrm{e}^{-2\alpha(\tau-\tilde{t})}\big]}{2\alpha}.$$

By (32.5b) and (32.6a), the solution $V(\tilde{t},\tilde{s},\gamma_1,\gamma_2,\xi;r)$ to (32.5b) is given by

$$V(\tilde{t},\tilde{s},\gamma_1,\gamma_2,\xi;r)=\tilde{g}(r,\tilde{s},\gamma_1,\gamma_2)R_{\beta}(r,\tilde{s},\gamma_1,\gamma_2)\int_{-\infty}^{\infty} f(z)\,P(\tilde{t},\xi;r,z)\,\mathrm{d}r, \tag{32.8}$$

where

$$\mathsf{E}\big[\,f\big(z(r)\big)\big]=\int_{-\infty}^{\infty} f(z)\,P(\tilde{t},\xi;r,z)\,\mathrm{d}z$$

is the expected value of the random variable $f\big(z(r)\big)$, with $z(r)$ being the normally distributed random variable as defined in (32.7).

Combining (32.5a) and (32.8), we see that the solution to (32.4c) is given by

$$\tilde{\beta}(\tilde{t},\tilde{s},\gamma_1,\gamma_2,\xi)=\int_0^{\tilde{t}}\tilde{g}(r,\tilde{s},\gamma_1,\gamma_2)R_\beta(r,\tilde{s},\gamma_1,\gamma_2)\,\mathsf{E}\big[\,f\big(z(r)\big)\big]\,\mathrm{d}r. \tag{32.9}$$

Hence, one has

$$\tilde{\Psi}(\tilde{t},\tilde{s},\gamma_1,\gamma_2,\xi)=\frac{\tilde{\beta}}{R_{\tilde{\beta}}}.$$

The solution $\psi(\phi_1,\phi_2,\theta,\xi)$ to (32.4a) is obtained by using the inverse transformation and passing to the limit as $\tilde{t}\to-\infty$.

32.3.3 First-Order Perturbation

Substituting the above expression for $\psi_0(\theta)$ in (32.3) leads to

$$L_0\psi_1=-s^1(\phi_1,\phi_2,\theta,\xi)\frac{\partial\psi_0}{\partial\theta}+[\Lambda_1(p)-pq^1(\phi_1,\phi_2,\theta,\xi)]\psi_0. \tag{32.10}$$

By the Fredholm Alternative, for equation (32.10) to have a solution, it is required that

$$\langle -s^1\psi_0'+[\Lambda_1(p)-pq^1]\psi_0,\Psi_0^*\rangle=0;$$

i.e.,

$$\Lambda_1(p)=\langle s^1\psi_0'+pq^1\psi_0,\Psi_0^*\rangle=0. \tag{32.11}$$

The last equality in (32.11) results from the fact that q^1 and s^1 are periodic in ϕ_1 and ϕ_2, and ξ is a zero-mean process. Hence, (32.10) reduces to

$$\mathscr{L}_0\psi_1=-\xi g(\phi_1,\phi_2,\theta). \tag{32.12}$$

Equation (32.12) is of the form (32.4a), and its solution is given by (32.9).

32.3.4 Second-Order Perturbation

The equation for the second-order perturbation is

$$L_0(p)\psi_2=[\Lambda_2(p)-L_2(p)]\psi_0-L_1(p)\psi_1.$$

By the Fredholm Alternative,

$$\Lambda_2(p)=\langle L_2\psi_0+L_1\psi_1,\Psi_0^*\rangle.$$

After performing the integration, one obtains

$$\Lambda_2(p)=\big[-8\delta_1+\big(\kappa_2F_0+\kappa_3F_1+\kappa_4F_2+\kappa_5F_3+\kappa_6F_4\big)\big]\frac{p}{8}+\big[\kappa_2F_0+\frac{2\kappa_1}{\alpha}\big]\frac{p^2}{16},$$

where

$$\kappa_1 = (K_{11} + K_{22})^2, \quad \kappa_2 = (K_{12} + K_{21})^2 + (K_{11} - K_{22})^2,$$
$$\kappa_3 = (N_{12} + N_{21})(M_{11} - M_{22}) - (N_{11} - N_{22})(M_{12} + M_{21}),$$
$$\kappa_4 = (N_{12} + N_{21})(M_{12} + M_{21}) + (N_{11} - N_{22})(M_{11} - M_{22}),$$
$$\kappa_5 = (N_{11} + N_{22})(M_{12} - M_{21}) + (N_{12} - N_{21})(M_{11} + M_{22}),$$
$$\kappa_6 = (N_{11} + N_{22})(M_{11} + M_{22}) - (N_{12} - N_{21})(M_{12} - M_{21}),$$

and

$$F_0 = \frac{\sigma^2}{\alpha^2 + 4\omega_1^2},$$

$$F_1 = \frac{\sigma^2(\omega_1 + \omega_2)}{\alpha[(\delta_2 + \alpha)^2 + (\omega_1 + \omega_2)^2]}, \qquad F_2 = \frac{\sigma^2(\delta_2 + \alpha)}{\alpha[(\delta_2 + \alpha)^2 + (\omega_1 + \omega_2)^2]},$$

$$F_3 = \frac{\sigma^2(\omega_1 - \omega_2)}{\alpha[(\delta_2 + \alpha)^2 + (\omega_1 - \omega_2)^2]}, \qquad F_4 = \frac{\sigma^2(\delta_2 + \alpha)}{\alpha[(\delta_2 + \alpha)^2 + (\omega_1 - \omega_2)^2]}.$$

The maximal Lyapunov exponent is given by

$$\lambda = \big[-\delta_1 + \frac{1}{8}\big(\kappa_2 F_0 + \kappa_3 F_1 + \kappa_4 F_2 + \kappa_5 F_3 + \kappa_6 F_4\big)\big].$$

32.4 Numerical Simulation

The Lyapunov exponent and moment Lyapunov exponent can also be obtained by Monte Carlo simulations (see, for example, [Xie06]). Figures 32.1 and 32.2 compare the analytical results with the numerical results, in which the system matrices are given by

$$A_0 = \begin{bmatrix} \delta_1 & 1 & 0 & 0 \\ -1 & \delta_1 & 0 & 0 \\ 0 & 0 & -0.5 & 1.5 \\ 0 & 0 & -1.5 & -0.5 \end{bmatrix}, \quad B = \begin{bmatrix} 1.1 & 1.0 & 1.2 & 1.0 \\ -1.0 & 0.5 & -2.0 & 1.0 \\ 1.0 & 2.0 & -1.5 & 1.0 \\ -2.0 & 1.0 & -1.0 & -1.0 \end{bmatrix}.$$

It is seen from Figure 32.1 that the system can be stabilized by real noise. When α decreases, the effect of stabilization is more significant. The numerical results agree well with the analytical results with larger α. Since a larger α means that the real noise is more flat (wide-band), the perturbation method can achieve better results. This conclusion also applies to the moment Lyapunov exponent (see, for example, Figure 32.2). Figure 32.2 also shows that a smaller ϵ yields better results. However, if only one degree of freedom is considered, the previous equation for the Lyapunov exponent is reduced to include only κ_2 and F_0. Since they are both positive, the system with one degree of freedom cannot be stabilized, which agrees with the results of Xie [Xie02].

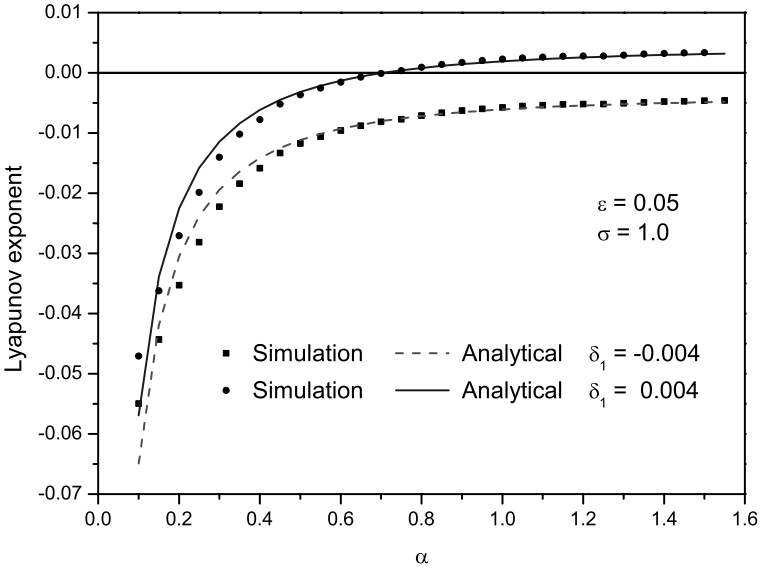

Fig. 32.1. Lyapunov exponent.

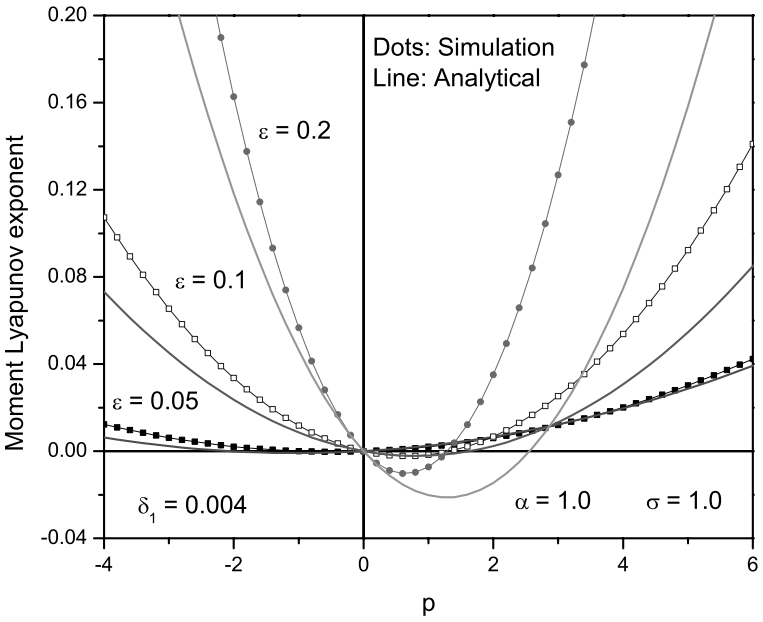

Fig. 32.2. Moment Lyapunov exponent for $\delta_1 = 0.004$.

32.5 Conclusions

In this chapter, the effect of noise on the stability of a parametrically excited four-dimensional system is considered. The dynamic stability of the system is studied by determining the moment Lyapunov exponents and the Lyapunov exponents. For weak noise excitations, a regular perturbation method is employed to obtain second-order expansions of the moment Lyapunov exponents. The Lyapunov exponent is then obtained using the relationship between the moment Lyapunov exponent and the Lyapunov exponent. The correctness and accuracy of the approximate analytical results are validated and assessed by comparing them with the numerical results. It is observed that the system can be stabilized by real noise with proper parameters.

References

[Arn84] Arnold, L.: A formula connecting sample and moment stability of linear stochastic systems. *SIAM J. Appl. Math.,* **44**, 793–802 (1984).

[AKO86] Arnold, L., Kliemann, W., Oeljeklaus, E.: Lyapunov exponents of linear stochastic systems. In: Arnold, L., Wihstutz, V. (eds.), *Lyapunov Exponents.* Springer, Berlin (1986).

[AOP86] Arnold, L., Oeljeklaus, E., Pardoux, E.: Almost sure and moment stability for linear Itô equations. In: Arnold, L., Wihstutz, V. (eds.), *Lyapunov Exponents.* Springer, Berlin (1986).

[PW88] Pardoux, E., Wihstutz, V.: Lyapunov exponent and rotation number of two-dimensional linear stochastic systems with small diffusion. *SIAM J. Appl. Math.,* **48**, 442–457 (1988).

[Xie02] Xie, W.-C.: Moment Lyapunov exponents of a two-dimensional system in wind-induced vibration under real noise excitation. *Chaos, Solitons and Fractals,* **14**, 349–367 (2002).

[Xie06] Xie, W.-C.: *Dynamic Stability of Structures.* Cambridge University Press, New York (2006).

[Zau89] Zauderer, E.: *Partial Differential Equations of Applied Mathematics,* 2nd ed. Wiley, New York (1989).

Index